AUGUST 1977

analytical chemistry

ANCHAM

Near IR Reflectance Spectrophotometry

Analysis of Agricultural Products

Just tell it what you want it to do...

ESA's Model 3040 Charge Transfer Analyzer

- **Operate** as an electrochemical detector for liquid chromatography
- **Determine and quantify** different valence states of toxic metal solutions or effluents
- **Analyze** complex radicals in drugs or bio-chemicals
- **Investigate** electrochemical transitions in research reaction systems
- **Separate** reversible from irreversible chemical reactions
- **Quality control** of plating bath concentrations

We've used it to measure nanogram levels of Vitamin C, Fe^{+2} or Fe^{+3}, Cr^{+3} and Cr^{+6} vanadium, halides and as an LC detector, differential pulsed polaragraph, coulometer or programmed voltammeter.

The ESA Model 3040 Charge Transfer Analyzer is the most exciting advance in electrochemistry in years. Now you can analyze any element or charged species which will undergo a charge transfer or cause a sensor to alter its response to that charged species.

That means you can look at virtually every element in the periodic table (with the exception of the rare earths and certain of the actinides), decide on which valence state you wish to observe, or measure charged radicals quantitatively . . probably without destroying the sample matrix.

If we haven't looked at your application yet it's because the technique offers so many possibilities we cannot get to all of them. Why not develop your own program? We can supply sensors, technical assistance, printers and universal or dedicated accessories.

esa

ENVIRONMENTAL SCIENCES ASSOCIATES, INC.
45 Wiggins Ave., Bedford, MA 01730 Tel (617) 275-0100, Telex 923344

CIRCLE 63 ON READER SERVICE CARD

Don't miss the boat!

(it's ready to analyze your sample for S, N, or X).

Can the Dohrmann® Microcoulometric Titrating System successfully analyze your sample—solid or liquid—for trace amounts of S, N, or X?

Yes, thanks to this tiny platinum sample-handling boat, the MCTS probably can.

The boat is one of several introduction devices that allow the MCTS to analyze an enormous range of samples, including solids, brines, catalysts, and many other difficult materials.

Recently the Dohrmann Applications Laboratory successfully analyzed plastic used for baby bottles and shoe soles for trace chlorine content; analyzed the chlorine level in aviation hydraulic fluid; nitrogen in bee's intestines; N in coal; N in sterile disposable paper products used in operating rooms, and sulfur in gasoline, oil, water, and pure toluene diisocyanate.

Our Applications Lab will be happy to discuss a free feasibility study on *your* sample, whether we need to use a boat or not. Give Mel Carter, Bob Booth, or Madeline Moore a call.

Madeline Moore begins the analysis of a sample sent into the Dohrmann Applications Lab. Five minutes later, the precise amount of the element being analyzed (S, N, or X) will be displayed on the digital readout.

ENVIROTECH® | DOHRMANN

3240 Scott Boulevard
Santa Clara, California 95050
Telephone (408) 249-6000
Telex 346 395

CIRCLE 47 ON READER SERVICE CARD

if you work in...

- *Air Pollution*
- *Wastewater Analysis*
- *Suspended Solids Analysis (EPA)*
- *Stack Sampling*
- *Gas/Liquid Purity Analysis*
- *Cell Harvesting*
- *Biomedical / Biochemical Analysis*
- *Radioimmunoassay*
- *Liquid Scintillation Counting*

you really need

reeve angel brand glass fiber filters and media

because you get

- ***Better Particle Retention***
- ***Higher Temperature Capability***
- ***Better Chemical Resistance***
- ***Higher Filtration Rates***
- ***Higher Loading Capacities***
- ***Better Stability***

Reeve Angel brand Glass Fiber Filters and Media are made of 100% borosilicate glass. They are chemically and biologically inert. For critical sampling you get excellent retention of sub-micron and micron particles. In filtration you get higher flow rates, much better chemical and biological resistance, freedom to work at temperatures to 500 °C, a lower-cost, highly effective substitute for membranes in most applications.

Reeve Angel brand Glass Fiber Filters and Media offer a non-aging material with superior optical properties. Binder-free, they provide an ideal matrix for impregnation with reactive chemicals, enzymes, dyes, etc. and are highly useful as, e.g., paper chromatography, electrophoresis media.

You can get Reeve Angel brand Glass Fiber Filters and Media from selected dealers. WHATMAN INC. —— A member of the Whatman Reeve Angel Group—9 Bridewell Place, Clifton, New Jersey 07014 • (201) 777-4825.

Write today for your Science Folder on Reeve Angel brand Glass Fiber Filters and Media!

Whatman

CIRCLE 232 ON READER SERVICE CARD

Volume 49, No. 9, August 1977
ANCHAM
49(9) 759A–842A/1281–1472 (1977)
ISSN 0003-2700

analytical chemistry

© Copyright 1977
by the American Chemical Society

No part of this publication may be reproduced in any form without written permission from the American Chemical Society

Published monthly with review issue added in April and Laboratory Guide in August by the American Chemical Society, from 20th and Northampton Sts., Easton, Pa. 18042. Executive and Editorial headquarters, American Chemical Society, 1155 16th St., N.W., Washington, D.C. 20036 (202) 872-4600. Second class postage paid at Washington, D.C., and at additional mailing offices.

1977 Subscription rates—including surface postage

	1 yr	2 yr	3 yr
MEMBERS:			
Domestic	$ 9.00	$16.00	$22.00
PUAS	17.00	32.00	46.00
Canada, Foreign	18.00	34.00	49.00
NONMEMBERS:			
Domestic	12.00	21.00	29.00
Canada	21.00	39.00	56.00
PUAS	23.00	43.50	64.00
Foreign	24.00	45.50	67.00

Airmail and air freight rates are available from Membership & Subscription Services, ACS, P.O. 3337, Columbus, Ohio 43210, (614) 421-7230.

New and renewal subscriptions should be sent with payment to the Office of the Controller at the ACS Washington address.

Subscription service inquiries and changes of address (include both old and new addresses with ZIP code and *recent mailing label*) should be directed to the ACS Columbus address noted above. Please allow six weeks for change of address to become effective.

Claims for missing numbers will not be allowed if loss was due to failure of notice of change of address to be received in the specified time: if claim is dated (a) North America: more than 90 days beyond issue date, (b) all other: more than one year beyond issue date; or if the reason given is "missing from files".

Microfiche subscriptions, one year only, are available at the same rates but are mailed first class domestic and airmail foreign.

	Write or call
Microfiche subscriptions, for inquiries and payments	Special Issues Sales American Chemical Society 1155 16th St., N.W. Washington, D.C. 20036 202-872-4364
Single issues, current year, $2.50 except review issue, $4.00	
Back issues and volumes	
Microfilm editions from Vol. 1 to present	

Advertising Management: Centcom, Ltd., 25 Sylvan Road South, Westport, Conn. 06880 (203) 226-7131

CONTENTS

REPORT

Burnaby Munson, University of Delaware, discusses the development of chemical ionization mass spectrometry over the past 10 years **772 A**

INSTRUMENTATION

C. A. Watson, USDA, describes the application of near infrared reflectance spectrophotometry to agricultural products analysis **835 A**

NEWS

Technical programs of interest to analytical chemists at the 174th ACS National Meeting in Chicago, August 28–September 2, 1977, are listed. Alan Walsh, the originator of AA, and Donald Young of NIH are honored. Surveys of papers published in ANALYTICAL CHEMISTRY and of meeting exhibitions are discussed in Analytical Chemistry at Work **783 A**

BOOKS

Books on electrochemical stripping analysis, polarographic oxygen sensors, analytical chemistry, and chemisorption are reviewed by K. W. Hanck, J. J. Lingane, Donald F. Logdson, and W. Henry Weinberg **823 A**

EDITORS' COLUMN

Highlights of ANALYTICAL CHEMISTRY's Advisory Board meeting are presented **833 A**

EDITORIAL

ANALYTICAL CHEMISTRY will launch a new feature, LETTERS TO THE EDITOR **1281**

Technical Contents/Briefs	**762 A**
Author Index	**IBC**
Future Articles	**IBC**
Call for Papers	**802 A**
Meetings	**802 A**
Short Courses	**804 A**
New Products	**812 A**
Chemicals	**816 A**
Manufacturers' Literature	**819 A**

Near infrared reflectance spectrophotometry provides an easy method for analysis of food products

หองสมุด กรมวิทยาศาสตร์
4 ส.ค. 2520

Briefs

Factors Affecting Quantitative Determinations by X-ray Photoelectron Spectroscopy 1282

With single-phase homogeneous system, the main source of error is the variability in shake-up and shake-off processes, especially with transition metals. All other factors cause a standard deviation of about 10%.

C. D. Wagner, Shell Development Company, P.O. Box 1380, Houston, Tex. 77001 *Anal. Chem., 49 (1977)*

Surface Studies of Mammalian Cells Grown in Culture by X-ray Photoelectron Spectroscopy 1290

The surface elemental composition of Balb 3T3 A31 HYF mouse fibroblast cells and transformed MSV/MLV Balb 3T3 A31 HYF cells is obtained with x-ray photoelectron spectroscopy.

Merle M. Millard* and James C. Bartholomew, Western Regional Research Center, U.S. Department of Agriculture, Berkeley, Calif. 94710 and Laboratory of Chemical Biodynamics, Lawrence Berkeley Laboratory, University of California, Berkeley, Calif. 94720 *Anal. Chem., 49 (1977)*

Simultaneous Analysis of Light Elements Using Prompt Nuclear Reaction Gamma Rays 1297

Simultaneous quantitative analysis of Li, B, F, Na, Mg, and Al is demonstrated for a range of different materials. Factors affecting the accuracy of an analysis are discussed.

Robert B. Boulton and George T. Ewan,* Department of Physics, Stirling Hall, Queen's University, Kingston, Ontario, Canada K7L 3N6 *Anal. Chem., 49 (1977)*

Analysis of Thyroid Hormones as Their Heptafluorobutyryl Methyl Ester Derivatives by Gas Chromatography–Mass Spectrometry 1304

The HFB-ME derivatives of thyroid hormones exhibit interpretable mass spectra with well defined molecular ion peaks. Subpicogram detection limits are attained in the analysis of these derivatives with a capillary column GC/MS combination.

B. A. Petersen and Paul Vouros,* Institute of Chemical Analysis, Applications and Forensic Science, Northeastern University, Boston, Mass. 02115 *Anal. Chem., 49 (1977)*

Determination of Mefruside and Its Metabolites in Urine by High Performance Liquid Chromatography 1311

Reliable extraction is achieved from urine and resolution of sulfonamide metabolites from co-extracted material is achieved without interference from paracetamol.

C. J. Little,* A. D. Dale, D. A. Ord, and T. R. Marten, Roche Products Ltd., P.O. Box 8, Welwyn Garden City, Hertfordshire, United Kingdom *Anal. Chem., 49 (1977)*

Determination of Selenium in Blood Serum by Proton-Induced X-ray Emission 1313

Selenium determination in blood serum is tested for thick (dry-ashed) samples with x-ray emission spectra induced by 1.8- to 4-MeV proton beams.

Marina Berti, Giampaolo Buso, Paolo Colautti, Giuliano Moschini,* Bianca Maria Stievano, and Cristina Tregnaghi, Laboratori Nazionali dell' Istituto Nazionale di Fisica Nucleare, Via Romea n. 4, 35020 Legnaro (Padova), Italy
Anal. Chem., 49 (1977)

Optical Multichannel Analyzer for Characterization of Fluorescent Liquid Chromatographic Petroleum Fractions 1316

Real time data acquisition of fluorescence emission spectra of petroleum fractions, separated by HPLC, is accomplished by using an Optical Multichannel Analyzer coupled to a spectrofluorometer.

J. R. Jadamec and W. A. Saner,* U.S. Coast Guard Research and Development Center, Avery Point, Groton, Conn. 06340 and **Y. Talmi,** Princeton Applied Research Corporation, P.O. Box 2565, Princeton, N.J. 08540 *Anal. Chem., 49 (1977)*

Determination of Trace Concentrations of Cobalt(II) and Other Metals by the Chemiluminescent Oxidation of Gallic Acid 1322

A select group of metals enhance this reaction at ppb–ppm levels. Interfering species are examined, and a comparison of three chemiluminescent systems is made.

Scott Stieg and Timothy A. Nieman,* School of Chemical Sciences, University of Illinois, Urbana, Ill. 61801
Anal. Chem., 49 (1977)

Chelex-100 Ion-Exchange Filter Membranes for Preconcentration in X-ray Fluorescence Spectrometric Analysis of Water 1326

Preconcentration of trace metals from water by Chelex-100 chelating ion-exchange filters, combined with x-ray fluorescence constitutes a precise and sensitive analysis technique, but only for water samples with low alkaline earth ion contents.

René E. Van Grieken,* Catharina M. Bresseleers, and Bruno M. Vanderborght, Department of Chemistry, University of Antwerp (U.I.A.), B-2610 Wilrijk, Belgium *Anal. Chem., 49 (1977)*

Determination of Ammonia in Aqueous Solutions by Infrared Spectrometry Following Preconcentration on Zeolite 1331

The method results in a preconcentrated sample matrix which is chemically and physically stable for IR analysis and is, thus, very suitable for field studies of water systems.

O. Yavuz Ataman and Harry B. Mark, Jr.,* Department of Chemistry, University of Cincinnati, Cincinnati, Ohio 45221
Anal. Chem., 49 (1977)

* Corresponding author.

THE ELECTRODE POTENTIAL IS NOW −104.5 MV
(IT WAS −142.7 MV IN THE 1.00 STANDARD SOLUTION.)
AND THE ELECTRODE SLOPE IS +59.16 MV PER DECADE,
AND THE BLANK CORRECTION IS 0.17 PPM, THEN −
THE UNKNOWN
CONCENTRATION IS ... **4.98** PPM!

The Model 901 combines the precision of a research pH/mv meter with the calculation horsepower of a microprocessor. This pre-programmed instrument has eleven operating modes that simplify pH, specific ion, and gas-sensing electrode analyses.

The 901 does away with calibration curves, tables, nomograms, and calculations. It is simple to operate — just dial in the operating mode (pH, concentration, known addition, analate addition, etc.), the standard solution value, and the electrode slope . . . the 901 is ready to go.

Standardization and blank correction are accomplished at the push of a button. Volume corrections, if they apply, are automatically calculated. Results are continuously updated and reported on the floating decimal point LED display.

Price? Not much more than you'd pay for a quality research-grade pH meter. How about a demonstration of the "thinking meter" in your laboratory? Call our toll-free number, (800) 225-1480, in the U.S.A. (except Massachusetts) or (800) 363-9270 in Canada.

ORION RESEARCH

380 Putnam Avenue, Cambridge, Mass. 02139 U.S.A.

CIRCLE 156 ON READER SERVICE CARD

Briefs

Use of Internal Standards for Atomic Absorption Spectrometric Analyses of Samples Atomized by Sputtering 1336

Accurate analyses of alloys and powdered, metallic and nonmetallic samples are made with a single reference sample and an internal standard to correct for variations in sputtering rate.

D. C. McDonald, Division of Chemical Physics, CSIRO, P.O. Box 160, Clayton, Victoria, Australia 3168 *Anal. Chem., 49 (1977)*

Laser-Vaporized Atomic Absorption Spectrometry of Solid Samples 1339

For several elements in brass, steel, and Al alloy, precision is 1.0 to 12%, and the detection limits range from 1.9 to 32 ppm (1.9×10^{-12} to 2.6×10^{-11} g).

Toshio Ishizuka,* Yoshinori Uwamino, and Hiroshi Sunahara, Government Industrial Research Institute, Nagoya 1-1, Hirate-machi, Kita-ku, Nagoya, 462 Japan *Anal. Chem., 49 (1977)*

Spectrophotometric Determination of Vitamin K Compounds 1343

The method uses the formation of highly colored complexes of the vitamin K compounds with titanium(IV) for the spectrophotometric analysis of these compounds in the 10^{-5} M range.

J-C Viré and G. J. Patriarche, Institut de Pharmacie, Université Libre de Bruxelles, Campus Plaine, 205/1 Bruxelles, Belgium, and **Robert J. Nowak and Harry B. Mark, Jr.,*** Department of Chemistry, University of Cincinnati, Cincinnati, Ohio 45221
Anal. Chem., 49 (1977)

Fourier Transform Infrared Spectrometric Determination of Gaseous Performic Acid 1346

The IR spectrum of gaseous performic acid is determined over the range of 600 to 3600 cm^{-1} at 0.1 cm^{-1} resolution with FTIR.

P. D. Maker, Hiromi Niki, C. M. Savage, and L. P. Breitenbach, Research Staff, Ford Motor Company, Dearborn, Mich. 48121 *Anal. Chem., 49 (1977)*

Double Wavelength Spectrophotometry with a Rapid Scanning Instrument 1348

A spectrophotometer with an oscillating mirror is adapted to rapid wavelength selection techniques (20–100 Hz) in the range of 200 to 700 nm. The system is applied to acquiring spectra in turbid solutions containing intact mitochondria.

Robert Szentrimay and Theodore Kuwana,* Department of Chemistry, Ohio State University, Columbus, Ohio 43210
Anal. Chem., 49 (1977)

Effect of Cavity Loading on Analytical Electron Spin Resonance Spectrometry 1353

Cavity loading effects cause a non-linearity of the response for intense samples. The nature of the sample and ESR cavity determine the maximum quantity that should be used.

Ira B. Goldberg* and Harry R. Crowe, Science Center, Rockwell International, Thousand Oaks, Calif. 91360
Anal. Chem., 49 (1977)

Representation-Space Transformation for the Display of Multivariate Chemical Information 1357

A new algorithm for displaying multivariate chemical information of a three-dimensional coordinate system is presented and its applications on pattern recognition treatment, computer retrieval, and spectral signal-shape analysis are shown.

Chi-Hsiung Lin* and Hwa-Fu Chen, Department of Chemistry, National Cheng Kung University, Tainan, Taiwan, Republic of China *Anal. Chem., 49 (1977)*

Buffer Solutions for Testing Glass Electrode Performance in Aqueous Solutions over the pH Range 0–14 at 25 °C 1363

The new method of testing glass electrodes is extended at both ends of the pH scale, with sodium errors determined at constant pH in the range 6.5–14 for up to 1 M Na^+ addition.

Arthur K. Convington* and M. Isabel A. Ferra, Department of Physical Chemistry, University of Newcastle upon Tyne, NE1 7RU, England *Anal. Chem., 49 (1977)*

Application of Pattern Recognition Techniques to the Interpretation of Severely Overlapped Voltammetric Data: Theoretical Studies 1369

Pattern recognition methods are applied to the classification of noisy doublet/singlet voltammetric curves derived from reversible, irreversible, and quasi-reversible theory. Fourier transform features and the k-nearest neighbor algorithm provide the best results.

Q. V. Thomas and S. P. Perone,* Purdue University, Department of Chemistry, West Lafayette, Ind. 47907
Anal. Chem., 49 (1977)

Application of Pattern Recognition Techniques to the Interpretation of Severely Overlapped Voltammetric Data: Studies with Experimental Data 1376

Pattern recognition methods are applied to the classification of real doublet/singlet voltammetric curves. Fourier transform features and the k-nearest neighbor algorithm provide the best results.

Q. V. Thomas, R. A. DePalma, and S. P. Perone,* Department of Chemistry, Purdue University, West Lafayette, Ind. 47907
Anal. Chem., 49 (1977)

Determination of Sulfide and Thiols in the Presence of Vitamin B_{12a} by Pulse Polarography 1380

Cathodic differential pulse polarographic peaks are observed for a mixture of a thiol and vitamin B_{12a} or B_{12r}. The reaction of cysteine and vitamin B_{12a} is studied using these peaks.

Manoutchehr Youssefi and Ronald L. Birke,* City University of New York, Department of Chemistry, The City College, New York, N.Y. 10031 *Anal. Chem., 49 (1977)*

Matheson has

99 Gas Regulators

Engineered for your specific requirements

Specialty Gas Handling Equipment is our business. To handle a gas properly you must have the proper regulating device. Matheson has 99 engineered regulators, each for a specific use. For example:

Corrosion Resistant

Models 11 through 16. The Matheson Catalog lists 21 regulators to handle specific corrosive gases. Our Models 11-14 are designed to withstand gases that attack copper bearing alloys. They have an anodized aluminum body, with AISI 316 internal parts and inert plastics for diaphragm and seat surfaces. Our Models 15 and 16 for acid forming gases (e.g. halogens) have a chemically coated nickel body with internal parts of Monel, Kel-F, and Teflon, with a seat closure for added safety should minor corrosion develop. Delivery pressure ranges of 4-35, 4-50, 4-80 and 50-650 psi are available.

CIRCLE 144

General Purpose

These regulators have earned their excellent reputation in many years of dependable service. They are basic regulators suitable for most laboratory applications. Available in two stage (Series 8 and 9) and single stage (Series 1) models; they provide accurate, stable delivery pressures, and excellent no-flow shut-off capabilities. Delivery pressure ranges of 2-15, 4-50, 10-100, and 20-250 psi are available.

CIRCLE 145

Line Regulators

These versatile regulators are used to eliminate pressure fluctuations in plant lines or to provide pressure control at selected stations. Their large diaphragm areas provide sensitive, accurate low pressure control. Some models can be adopted for use on low pressure gases in cylinders. In all we have 13 regulators in a variety of pressure ranges and construction materials. Delivery pressure ranges of 2"-12" of water, 0.5-5, 0.5-8, 5-10, 5-12, 0-20, 4-25, 4-90, 5-100, and 20-200 psi are available.

CIRCLE 146

High Purity

Designed for the most exacting applications. These regulators prevent the diffusion of atmospheric gases into your system. They have metal diaphragms to eliminate out-gassing of hydrocarbon type compounds. Of our 18 high purity regulators, nine are all stainless steel; nine are brass. All of them can pass a 5 minute helium leak rate test of $<2 \times 10^{-10}$ ccs. Series 3800, 3500, 3100, 19, 3451. Delivery pressure ranges of 0-15, 0-20, 0-25, 4-50, 0-75, 4-90, 4-100 and 10-150 psi are available.

CIRCLE 147

Vacuum Regulator

This vacuum regulator allows gas to bleed into a system under constant evacuation to maintain a desired vacuum (2-655 torr). Maximum inlet pressure 50 psig. Use it with air or any non-corrosive gas. We have not found the vacuum pump that can beat our regulator.

CIRCLE 148

Lecture Bottle Regulators

Matheson created the lecture bottle. These regulators were specifically engineered for use with lecture bottles. They can also be fitted with standard CGA connections for use on larger cylinders. With 3 models for non-corrosive service and 7 for corrosive gases, there is a model for your application. Delivery pressure ranges of 0-18" of water, 1-6, 2-15 and 4-60 psi are available.

CIRCLE 149

Custom Engineered

Some requirements cannot be met by standard regulators. Matheson will review your needs and modify a standard regulator or develop a new one to suit your purpose. Pre-set delivery pressure, tamper-proof adjustments, and special characteristics are only a sample of what we can do. Send us your specifications today.

Matheson

Lyndhurst, N.J. 07071

East Rutherford, N.J. 07073
Morrow, Georgia 30260
Bridgeport, N.J. 08014
Gloucester, Massachusetts 01930
Joliet, Illinois 60434
La Porte, Texas 77571
Cucamonga, California 91730
Newark, California 94560
Hanover, Maryland 21076
Whitby, Ontario, Canada L1N 5R9
Edmonton, Alberta Canada T5B 4K6
B 2431 Oevel, Belgium
6056 Heusenstamm, West Germany

Briefs

Phase-Selective Cathodic Stripping Voltammetry for Determination of Water-Soluble Mercaptans 1386

The method is capable of determining 1 ppb mercaptan in aqueous solution and removal of oxygen from the electrolyte prior to analysis is not necessary.

W. Michael Moore* and V. Frances Gaylor, The Standard Oil Company (Ohio), 4440 Warrensville Center Road, Cleveland, Ohio 44128
Anal. Chem., 49 (1977)

Peak Shapes in Semidifferential Electroanalysis 1390

Predicted features of reversible and irreversible $d^{1/2}i/dt^{1/2}$ vs. E curves are compared with experimental curves obtained using several semidifferentiating circuits.

Penny Dalrymple-Alford, Trent University, Peterborough, Canada, and **Masashi Goto,** Nagoya University, Japan, and **Keith B. Oldham,*** Bristol University, United Kingdom
Anal. Chem., 49 (1977)

Carbon and Mercury–Carbon Optically Transparent Electrodes 1395

Carbon film and mercury–carbon film optically transparent electrodes are characterized and the spectroelectrochemical behavior of cysteine oxidation is studied.

Thomas P. DeAngelis, Roger W. Hurst, Alexander M. Yacynych, Harry B. Mark, Jr., and William R. Heineman,* Department of Chemistry, University of Cincinnati, Ohio 45221, and **James S. Mattson,** Center for Experiment Design and Data Analysis, Environmental Data Service, National Oceanic and Atmospheric Administration, Washington, D.C. 20235
Anal. Chem., 49 (1977)

Evaluation of a Cesium Primary Ion Source on an Ion Microprobe Mass Spectrometer 1399

A Cs^+ primary ion source is used in conjunction with an ion microprobe mass spectrometer to achieve good detection limits for electronegative species.

Peter Williams* and R. K. Lewis, Materials Research Laboratory, University of Illinois, Urbana, Ill. 61801, and **Charles A. Evans, Jr.,** Materials Research Laboratory and School of Chemical Sciences, University of Illinois, Urbana, Ill. 61801, and **P. R. Hanley,** General Ionex Corp., Ipswich, Mass. 01938
Anal. Chem., 49 (1977)

Effect of Matrix Composition on Line Intensity in the Determination of Light Elements in Organic Compounds by X-ray Fluorescence Spectrometry 1403

A method is described to calculate the effect of changes in organic composition on the the x-ray fluorescent intensity of light elements.

G. W. Tindall, Tennessee Eastman Company, Division of Eastman Kodak Company, Kingsport, Tenn. 37662
Anal. Chem., 49 (1977)

Propylene Incorporation in 1-Butene Copolymers by Carbon-13 Nuclear Magnetic Resonance Spectrometry 1405

A method based on ^{13}C NMR spectrometry is described whereby standards are obtained of known propylene content in copolymers with 1-butene.

Michael H. Fisch,* Witco Chemical Corporation, P.O. Box 110, Oakland, N.J. 07436, and **J. J. Dannenberg,** Department of Chemistry, Hunter College, City University of New York, 695 Park Avenue, New York, N.Y. 10021
Anal. Chem., 49 (1977)

Computerized Curve-Fitting to Determine the Equivalence Point in Spectrophotometric Titrations 1408

A nonlinear least squares fit is used to determine the equivalence point of a spectrophotometric titration curve. Accuracy is within 0.3% under most circumstances.

Scott R. Goode, Department of Chemistry, University of South Carolina, Columbia, S.C. 29208
Anal. Chem., 49 (1977)

High Solids Sample Introduction for Flame Atomic Absorption Analysis 1413

Development of a new clog-free Babington principle nebulizer is reported for direct flame spectrochemical analysis of a variety of highly complex materials such as tomato sauce and whole blood.

R. C. Fry and M. B. Denton,* Department of Chemistry, University of Arizona, Tucson, Ariz. 85721
Anal. Chem., 49 (1977)

Comparison of Inorganic Interferences in Atomic Absorption Spectrometric Determination of Arsenic and Selenium 1417

Three techniques of sample preparation/sample atomization for the determination of arsenic and selenium by atomic absorption spectrometry are compared as to interfering effects of several selected anions, cations, and acids.

F. D. Pierce* and H. R. Brown, Utah Biomedical Test Laboratory, 520 Wakara Way, Salt Lake City, Utah 84108
Anal. Chem., 49 (1977)

Performance of the Super Modified Simplex 1422

A new, improved simplex optimization procedure is developed which significantly increases the utility, reliability, and efficiency of current state-of-the-art simplicial methods in the presence of random response fluctuations.

M. W. Routh, P. A. Swartz, and M. B. Denton,* Department of Chemistry, University of Arizona, Tucson, Ariz. 85721
Anal. Chem., 49 (1977)

Determination of pK_a Values of Acid Components in Atmospheric Condensates by Linearization of Segmented Titration Curves 1429

Modified Gran plots are used to determine the concentrations of acid components in a mixture and to identify each of the acids in the mixture. The composition of atmospheric condensates is examined by this method.

M. D. Seymour, J. W. Clayton, and Quintus Fernando,* Department of Chemistry and Toxicology Program, University of Arizona, Tucson, Ariz. 85721
Anal. Chem., 49 (1977)

If You're Into Spectrophotometry, We'll Give You 6 Good Reasons to Standardize on MC/B Spectroquality® Solvents

I

Specifications, including absorbance characteristics, water content, and evaporation residues are more stringent than any published or recommended for the field. Optical purity is unexcelled.

II

Purity, determined by gas liquid chromatography assay on almost all solvents, exceptions are noted, is guaranteed to be over 99%. Similarly, fluorescence for all solvents is guaranteed not to exceed 0.5 ppb (quinine base).

III

The MC/B Spectroquality line is the most comprehensive line offered. Forty four solvents, with a wide choice of polarity and solubility properties are available.

IV

MC/B's Spectroquality packaging is carefully designed to guarantee the integrity of the product and its analysis from its preparation, through stocking and shipping, to your laboratory — ready for use. All packaging is under tight technical supervision.

V

The MC/B Spectroquality catalog contains so much information that it is used as an instructional aid. In addition to spectral characteristics, physical properties including dipole moment — product specifications, and typical uses are offered. Solubility information is extensive.

VI

Not only are MC/B Spectroquality Solvents stocked in our Norwood and Los Angeles plants but they are also stocked by MC/B's large distributor network throughout the U.S. This assures good delivery.

Valuable Free Catalog

Send for our MC/B Spectroquality Solvents Catalog and price list. Use the Reader Service number or contact us directly.

MC/B

MANUFACTURING CHEMISTS

2909 Highland Avenue, Norwood, OH 45212
(513) 631-0445
2121 South Leo Avenue, Los Angeles, CA 90022
(213) 685-5280

Blessed are the pure.

CIRCLE 139 ON READER SERVICE CARD

Briefs

Composition, Treatment Efficiency, and Environmental Significance of Dye Manufacturing Plant Effluents 1433

Over 50 compounds are identified in a dye manufacturing plant wastewater. The concentrations of many of these compounds increase during waste treatment.

Larry M. Games and Ronald A. Hites,* Department of Chemical Engineering, Massachusetts Institute of Technology, Cambridge, Mass. 02139 *Anal. Chem., 49 (1977)*

Correspondence

Performance Prediction and Evaluation of Systems for Computer Identification of Spectra 1441

F. W. McLafferty, Department of Chemistry, Cornell University, Ithaca, N.Y. 14853 *Anal. Chem., 49 (1977)*

Factor Analysis of the Mass Spectra of Oligodeoxyribonucleotides 1444

D. R. Burgard and S. P. Perone,* Department of Chemistry, Purdue University, West Lafayette, Ind. 47907, and **J. L. Wiebers,** Department of Biological Sciences, Purdue University, West Lafayette, Ind. 47907 *Anal. Chem., 49 (1977)*

Atomic Spectrochemical Measurements with a Fourier Transform Spectrometer 1446

W. K. Yuen and Gary Horlick,* Department of Chemistry, University of Alberta, Edmonton, Alberta, Canada T6G 2G2 *Anal. Chem., 49 (1977)*

Stoichiometry of Nitrogen Dioxide Determination in Triethanolamine Trapping Solution 1448

Avram Gold, Occupational Health Program, Harvard School of Public Health, 665 Huntington Avenue, Boston, Mass. 02115 *Anal. Chem., 49 (1977)*

Aids for Analytical Chemists

Modified Inductively Coupled Plasma Arrangement for Easy Ignition and Low Gas Consumption 1450

John L. Genna and Ramon M. Barnes,* Department of Chemistry, University of Massachusetts, Amherst, Mass. 01003, and **Charly D. Allemand,** Jarrell-Ash Division, Fisher Scientific Company, Waltham, Mass. 02154 *Anal. Chem., 49 (1977)*

Evaluation of Tetraphenylporphinatozinc(II) as a Stable Standard for Porphyrin Determinations by Fluorescence Spectrometry 1453

David K. Lavallee* and James T. Norelius, Department of Chemistry, Colorado State University, Fort Collins, Colo. 80523 *Anal. Chem., 49 (1977)*

Low Capacity Codes for Mass Spectra Based on Statistical Moments 1456

C. P. Anese and J. A. Richards,* Department of Electrical Engineering, James Cook University of North Queensland, Townsville, Queensland 4811, Australia *Anal. Chem., 49 (1977)*

Teflon Powders for Near Infrared Spectra of Hydrides 1458

Tryggvi Emilsson and Vakula S. Srinivasan,* Department of Chemistry, Bowling Green State University, Bowling Green, Ohio 43403 *Anal. Chem., 49 (1977)*

Modification of Pulse Polarograph for Rapid Scanning and Its Use with Stationary Electrodes 1459

KeriLyn C. Burrows, Mark P. Brindle, and Michael C. Hughes,* Department of Chemistry, Lehigh University, Seeley G. Mudd Building #6, Bethlehem, Pa. 18015 *Anal. Chem., 49 (1977)*

Dynamically Refreshable Computer Display Controller with Vertical Line Generator for Mass Spectrometry Applications 1462

Philip S. Berger and William F. Holmes,* Department of Biological Chemistry, Division of Biology and Biomedical Sciences, Washington University, St. Louis, Mo. 63110 *Anal. Chem., 49 (1977)*

High-Speed, High-Purity Extraction Apparatus 1465

Walter A. Aue,* Marek M. Daniewski, Jürgen Müller, and John P. Laba, Chemistry Department, Dalhousie University, Halifax, Nova Scotia, Canada *Anal. Chem., 49 (1977)*

Laboratory Real Time Clock Featuring Computer, Experiment, and Manual Interaction 1466

Robert L. Veazey and Timothy A. Nieman,* School of Chemical Sciences, University of Illinois, Urbana, Ill. 61801 *Anal. Chem., 49 (1977)*

Unheated External Column and Inlet Modification of a Gas Chromatograph for Phosphine Determinations 1468

Jerry R. Bean and Robert E. White, U.S. Fish & Wildlife Service, Wildlife Research Center, Denver, Colo. 80255

Optically Transparent Vitreous Carbon Electrode 1470

V. E. Norvell and Gleb Mamantov, Department of Chemistry, University of Tennessee, Knoxville, Tenn. 37916

The perfect balance.

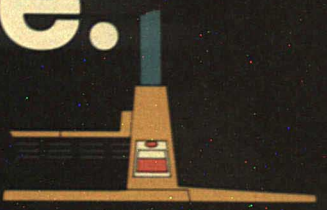

The perfect balance between price and speed, with the accuracy necessary to make speed count... in schools, hospitals, industrial labs:

The Ohaus Cent-O-Gram 311's four-tiered beams have notched and windowed poises for foolproof reading.

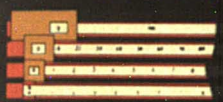

On the comparable Ohaus Dial-O-Gram 310, two beams and poises are replaced by a precision engraved dial and vernier. This dial incorporates a spring that applies torque to the beam at its fulcrum, the torque being equal to the weight indicated on the dial.

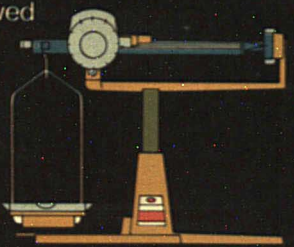

Another of the many features that make these scales invaluable in the laboratory is a self-storing platform for quick and easy specific gravity measurements.

For our illustrated 32-page catalog, write: Ohaus Scale Corporation, 29 Hanover Road, Florham Park, N.J. 07932.

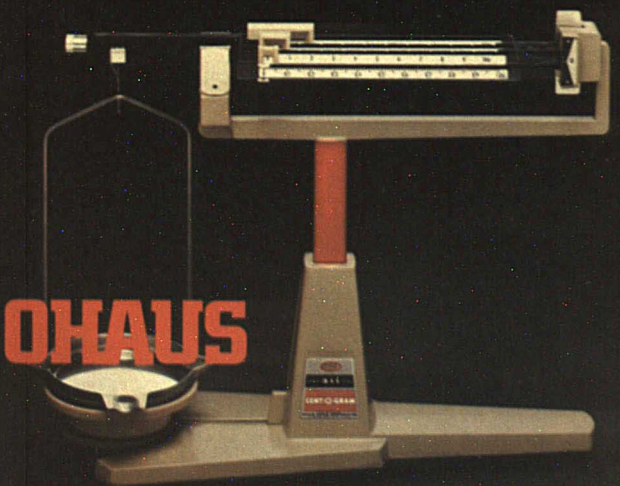

Measuring up since 1907

CIRCLE 157 ON READER SERVICE CARD

LECO®
DEMONSTRATES
ANYWHERE!

CIRCLE 130 ON READER SERVICE CARD

LECO believes that "show" is better than "tell": accordingly we have added a fleet of mobile labs to bring our instruments and our engineers to your plant at your convenience. We require only a place to park, a source of electric power, and you — our interested customer.

Call us for a demonstration — we welcome the opportunity to show you LECO's latest technology.

Products for demonstration include:

INSTRUMENTS
Carbon and Sulfur
Oxygen, Nitrogen, and Hydrogen
Silicon, Manganese, and Phosphorus
Protein and Sugar in Foods & Feeds

THERMOCOUPLES
Instrumentation, Small & Large Diameter Units

EXPENDABLES
Diskpins, Accelerators, and other items

CERAMICS
Shrouds, Nozzles and Melting Crucibles

MICROSCOPES
Olympus, PME, and Vanox

METALLOGRAPHIC
Cut-Off's, Grinders, Polishers, and Mounting Presses

LECO®

LECO CORPORATION
3000 Lakeview Ave.
St. Joseph, MI 49085, U.S.A.
Phone: (616) 983-5531
Telex: 72 9411
Cable: LECO

Burnaby Munson
Department of Chemistry
University of Delaware
Newark, Del. 19711

Chemical Ionization Mass Spectrometry:

Chemical ionization mass spectrometry (CIMS) is an outgrowth of studies of gaseous ion-molecule reactions. Products of ion-molecule reactions were observed early in the history of mass spectrometry. Thomson reported the ionic species H_3^+ by 1913 (*1*). The rare gas hydride ions (HeH^+, NeH^+, ArH^+) were sufficiently common to be used for the precise determination of atomic masses (*2*). Dempster established in 1916 that H_3^+ was formed by secondary processes,

$$H_2^+ + H_2 \rightarrow H_3^+ + H \qquad (1)$$

and this work may be considered as the origin of ion-molecule reaction studies (*3*).

With the advent of better vacuum technology, however, ion-molecule reactions were observed less frequently and received little attention in the development of mass spectrometry. There was perhaps enough work on ion-molecule reactions between 1916–1956 to provide a good genealogical tree; somewhat more realistically, the early work was nearly completely forgotten, and ion-molecule reactions were rediscovered in the 1950's.

About 20 years ago, work was independently reported on ion-molecule reactions by Tal'roze and Lyubimova in the Soviet Union (*4*), by Stevenson and Schissler at the Shell Development Co. (*5*), and by Field et al. at the Humble Oil Co. (now Exxon) (*6*). All of these groups reported the completely unexpected reaction:

$$CH_4^+ + CH_4 \rightarrow CH_5^+ + CH_3 \qquad (2)$$

Coincidentally, CH_4 with its major product ions, CH_5^+ and $C_2H_5^+$, was the first reagent gas used in CIMS.

In 1966 as a direct outgrowth of work on gaseous ion-molecule reactions at high pressures, Munson and Field reported CIMS as an analytical application of ion-molecule reactions by showing the CH_4 CI mass spectra, or the distribution of product ions, from ion-molecule reactions of CH_5^+ and $C_2H_5^+$ with different compounds (*7*). Because of the need for new instruments or modifications to existing instruments, the only work during the next few years was done by these workers. However, by 1969 other instruments had been modified for high-pressure operation, and other workers began to use the technique for analysis (*8, 9*). Since then, many more laboratories have developed CI capabilities, and the technique is now routinely used in analysis. Most of the early work was concerned with the development of the methodology and could be readily recognized by key words in the title. It is now no longer possible to determine the number of papers published annually which use CIMS because in an increasing number of instances the technique is only incidental to the work and is not mentioned even in the abstract of the paper.

Much of the early work was to obtain chemical ionization mass spectra and to compare these spectra with the standard electron ionization (EI) mass spectra to show the utility of the technique. In many instances the CH_4 CI mass spectra were easier to interpret than the EI mass spectra and contained sufficient information for a confirmation of structure. Such studies are still useful and are being done today. For example, the CH_4 and *i*-C_4H_{10} CI spectra of peracetylnitrate (PAN) provide excellent confirmation of the proposed structure and mole-

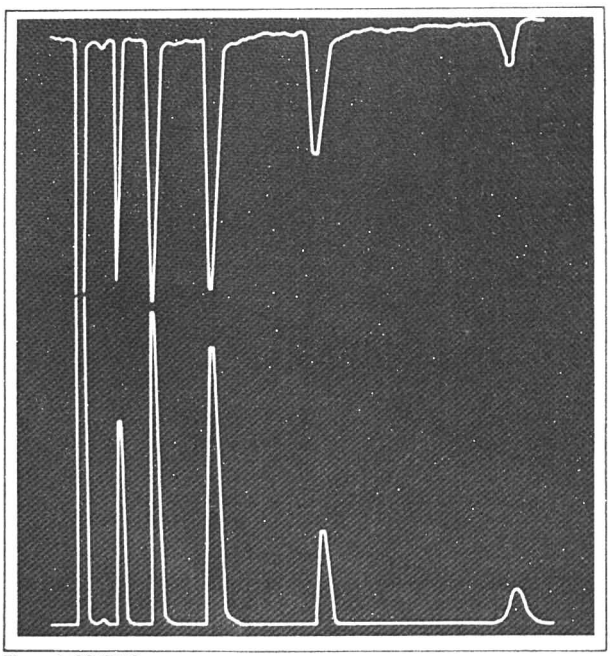

Figure 1. GC/CIMS

Top trace: reactant ion monitoring with CH_5^+, m/e = 17. Bottom trace: flame ionization detector. Peaks (left to right): solvent (diethyl ether), benzyl propionate, 1-phenyl-1-pentanone, 1-phenyl-1-heptanone, 1-phenyl-1-nonanone, methyl stearate

Ten Years Later

cule weight, whereas the EI spectra are not useful (*10*). Other illustrations are the mass spectra of explosives for which the molecular weight and major structural features can be established by CI but not EI mass spectrometry (*11*). Of course, there are the many examples of the CI mass spectra of molecules of biomedical interest which show an enhancement of abundances of ions in the molecular weight region when compared with EI mass spectra (*12*).

One of the advantages of chemical ionization mass spectrometry over electron impact mass spectrometry is the simplification of the spectra—a smaller number of ions per compound in CIMS. In many cases, CI reagent gases are chosen to produce only one or two peaks for each compound. The advantage of this technique for the analysis of mixture is obvious. As one illustration, we can consider the analysis of cholesterol esters of fatty acids. The EI mass spectra of these esters contain essentially no molecular ions, and the spectra of the higher esters are sufficiently complex to mask the characteristic low mass fragment ions of the lower esters; however, the CH_4 or i-C_4H_{10} CI spectra contain essentially only protonated acid ions and ions at 369 $(M + H - RCOOH)^+$ (*13*). Consequently, an analysis of mixtures of these sterol esters can be performed readily by CIMS. The pyrolysis of polymers in the source of a mass spectrometer with a direct insertion probe produces EI spectra that are almost too complex to interpret, but the CI spectra allow ready identification of molecular species. The EI mass spectrum of the pyrolysis of polymethylmethacrylate at 250 °C directly into the source of the mass spectrometer contains essentially every mass from 29 to 250. The characteristic ions of methylmethacrylate are observed, and this compound can be identified in the spectrum. The CH_4 CI mass spectrum obtained under similar conditions contains predominantly $(M + H)^+$ and $(2M + H)^+$ ions of methylmethacrylate, and the presence of the monomer as the dominant pyrolysis product is immediately obvious (*14*).

Table I. Relative Rate Constants, $C_2H_5^+$

Compound	GC/CIMS	Literature
	$k/k(C_2H_5^+, n\text{-}C_6H_{14})$	
n-C_5H_{12}	0.68 ± 0.03	0.69 ± 0.14[a] 0.83 ± 0.04[b]
n-C_6H_{14}	1.00	
n-C_8H_{18}	1.58 ± 0.07	1.56 ± 0.30[a] 1.31 ± 0.07[b] 1.58 ± 0.10[c]
CH_3COCH_3	1.71 ± 0.05	1.64 ± 0.08[d] 3.04 ± 0.14[e]

[a] Ref. 76. [b] Ref. 77. [c] Ref. 78. [d] Ref. 17. [e] Ref. 79.

A simple kinetic analysis shows that the ionization of sample molecules by ion-molecule reactions, and therefore the sensitivity for a given compound, depends upon the time for reaction between the reactant ions and sample molecules, the concentration of sample molecules, and the rate constants for reactions of the reactant ions with the sample molecules (*15*). For CH_4, the following result is obtained:

$$\Sigma I_i = \Delta t(k_{17}I_{17} + k_{29}I_{29})[M] \quad (3)$$

in which $[M]$ = concentration of sample, $k_i = k_i\ (I^+, M)$ = rate constant for reaction of ion I^+ with molecule M, Δt = reaction time, and I_i = ion current at $m/e = i$. Exothermic proton transfer reactions have roughly the same rate constants (within a factor of two), independent of the nature of the reactant ion or sample molecule (*16–19*). For high-energy reactant ions, like CH_5^+ and $C_2H_5^+$, which should react exothermically and rapidly with most organic molecules, one would not expect major variations in rate constants with changes in molecular weights of the compounds. Under similar conditions, one would expect essentially equivalent CI sensitivities with methane for all compounds. In the early work in CI mass spectrometry, essentially the same sensitivities were noted for a series of propionate esters, C_1 to C_7 (*20*). More recently, the same sensitivities were observed for the CI spectra of valerophenone with CH_4 (reactant ions = CH_5^+ and $C_2H_5^+$) as the reagent gas and with CH_4/H_2O mixtures (reactant ion = H_3O^+) as the reagent gas (*21*). For a series of polyamines, similar sensitivities were observed using CH_4, N_2, and i-C_4H_{10} as reagent gases (*22*).

The approximation that exothermic ion-molecule reactions have equal rate constants is only a crude approximation. The theories of ion-molecule reactions predict that the rate constants for reaction will increase with increasing polarizability and increasing dipole moment of the sample molecules (*23–27*), and rate constants differing by factors of 2–3 have been observed for exothermic reactions. Under CI conditions the formation of each product ion requires the loss of a reactant ion. If we monitor the signal of one of the reactant ions during a GC/MS experiment, we can expect to observe a decrease in the ion current of the reactant ions as the sample molecules pass through the source of the mass spectrometer. This decrease in signal depends on the ionic reaction time in the source of the mass spectrometer, the concentration of sample molecules, and the rate constants for reaction. By continuously recording the ion current of one of the reactant ions during a GC/MS run, we can obtain a trace that is the equivalent of the total ion current vs. time in EIGC/MS or the flame ionization detector trace in GC analysis. This technique is called reactant ion monitoring (*28, 29*). Figure 1 shows a comparison of a reactant ion trace with CH_5^+ and the simultaneous trace of the flame ionization detector of the GC for a mixture of oxygenated compounds. It is possible to relate the peak areas in these measurements to the relative rate constants for reactions of the sample ion with different samples to obtain the data shown in Table I (*30*). From these data it is possible to see the expected increase in rate constant and sensitivity with increasing molecular weight and dipole moment of the sample molecules. These data may be used for quantitation in GC/CIMS studies.

If ion-molecule reactions are approximately thermoneutral, then it is

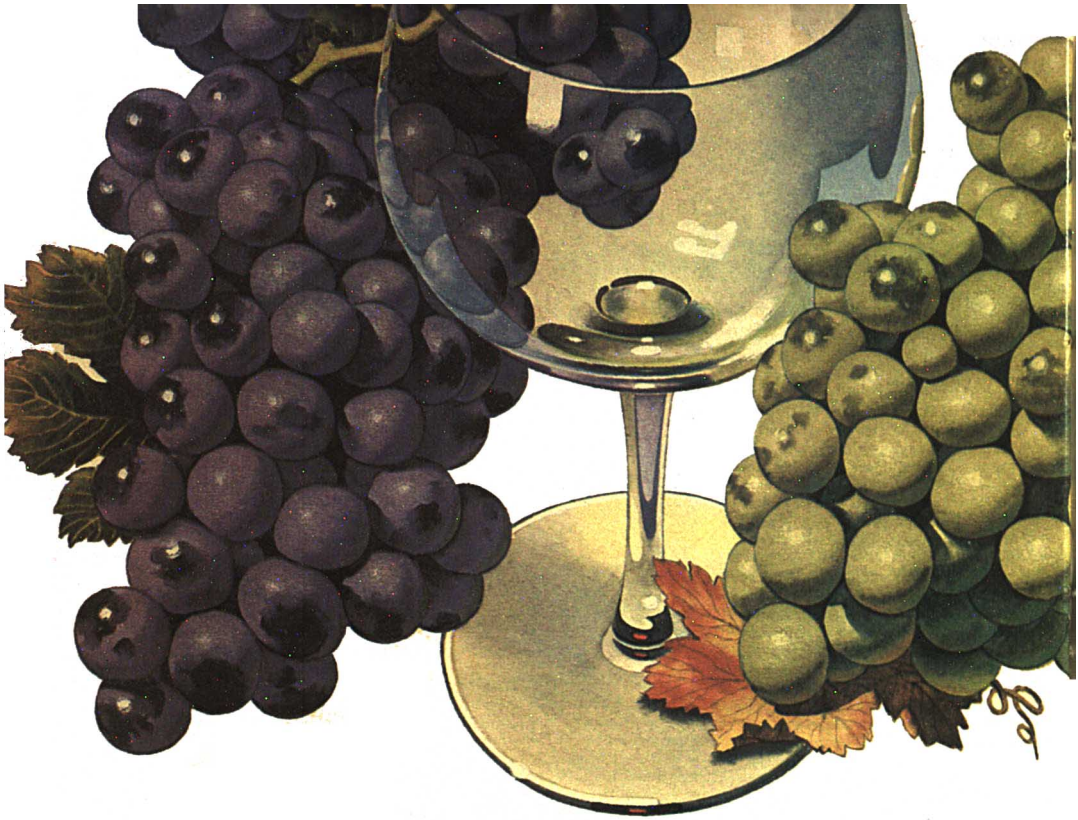

Are they sweet enough to make a fine wine?

For wine-making or for any other reason that you want to determine sugar or other solid concentrations, Mettler/Paar digital density meters can give you the answer. They require only small samples and give results in seconds. They tell you, scientifically, whether the fruit is ready for picking, whether the process is maintaining quality standards, or how sweet the new product should be.

Mettler helps solve problems in analytical laboratories and on the production floors of industry. We market a variety of weighing and measuring instruments. All of them made with world-renowned Mettler craftsmanship. All of them backed by a worldwide team of service specialists who can be there when you need them. Mettler—instruments and people you can depend on. In the U.S., contact Mettler, Box 100, Princeton, NJ 08540. In other countries, contact Anton Paar, KG, Postfach 17, Graz, Austria.

Depend on Mettler for the answer.

Mettler

Electronic balances and weighing systems • Thermal analysis instruments • Titration instruments • Automated laboratory systems.

CIRCLE 142 ON READER SERVICE CARD

very likely that small differences in the structures of the sample molecules will have significant effects on the rate constants for ion-molecule reactions. It has been reported, for example, in the acetylation of the norborneols with $(CH_3CO)_3^+$ that the rate constant for reaction with the less hindered exonorborneol is four times as large as the rate constant for reaction with endonorborneol (*31*). We have also observed that the isobutane CI spectra of endo- and exonorborneol are significantly different in the relative abundances of $(M - H)^+$ ions. The dominant ion in the i-C_4H_{10} spectra of both of these compounds is $(M - OH)^+$, but endonorborneol (for which the α-hydrogen is in the exo-configuration and therefore less hindered for attack) shows about 5% $(M - H)^+$ in its spectrum, whereas, exonorborneol for which the α-hydrogen is in the more hindered endo-position has only about 0.5% $(M - H)^+$ in its spectrum (*32*). These small differences, which we attribute to steric effects, are accentuated by the use of larger, lower energy reactant ions, since the CH_4 CI mass spectra of endo- and exonorborneol are almost identical (32).

In CI mass spectrometry, increasing the exothermicity of ion-molecule reactions (by changing the nature of the reactant ions) increases the extent of fragmentation (*33, 34*). Conversely, decreasing the exothermicity of the ion-molecule reactions will decrease the extent of fragmentation and enhance the abundances of ions in the molecular weight region of the CI mass spectra. When the interest is primarily to determine the molecular weight of a compound or to confirm it as one of a small set of compounds, a low-energy reactant ion such as t-$C_4H_9^+$ (from i-C_4H_{10}) is frequently used. The i-C_4H_{10} CI spectra have been used for identification in drug overdose cases (*35*) and also for the characterization of street drugs (*36*). The t-$C_4H_9^+$ ion may react by OH^- transfer instead of proton transfer; therefore, the i-C_4H_{10} CI spectra of alcohols generally do not contain $(M + H)^+$ ions (*37*). However, if one uses an even weaker protonating agent like NH_4^+, it is possible to obtain $(M + H)^+$ and $(M + NH_4)^+$ ions to characterize polyhydroxy compounds like sugars (*38*).

CI mass spectra can be used to give approximate values for proton affinities of complex molecules. The CI spectra obtained with ammonia, methylamine, dimethylamine, and trimethylamine have been used to determine an approximate order of basicities of several complex amines (*39*). Similarly, the basicities of some phosphine oxides have been estimated from their i-C_4H_{10}, ammonia, pyridine, and trimethylamine spectra (*40*). In these experiments, one expects and observes abundant $(M + H)^+$ ions of the sample if the sample is more basic than the reagent gas and abundant $(M + XH)^+$, where XH^+ = protonated reactant ion, if the sample is less basic than the reagent gas.

Another type of reaction is observed if one uses labeled polar compounds as reagent gases in CIMS experiments. D_2O, for example, has been used to determine the number of replaceable hydrogens in polar compounds by comparing the H_2O CI spectra with D_2O CI spectra. All of the active hydrogens are replaced (*41*). Similar discrimination was demonstrated among primary, secondary, and tertiary amines with ND_3 as a reagent gas (*42*). Recently, GC/CIMS studies have been reported in which a complex mixture of amines was characterized for replaceable hydrogens by comparison of the CH_3OH and CH_3OD CI spectra (*43*).

In the early work on CIMS, the reactions involved heavy particle (H^+, H^-, or X^-) transfer. However, in the past few years, the definition has been expanded to include charge exchange (CE) or electron transfer reactions as well. The term "chemical ionization" is now used to include all types of ion-molecule reactions for the production of spectra of the sample molecules. A wide variety of charge exchange reactant ions are available and have been used. Charge exchange spectra obtained using Ar, N_2, or CO are relatively similar to conventional electron ionization mass spectra (*22, 44*). One advantage of this technique of ion production is in GC/CIMS when one may use N_2 as the carrier-reagent gas and obtain spectra of compounds that may be compared with the compilations of EI mass spectra.

The charge exchange mass spectra (N_2, CO) of many biological molecules contain little or no M^+ for the determination of molecular weights. Consequently, there has been work using low-energy charge exchange ions to produce simplified spectra. The most common low-energy charge exchange reactant ion is NO^+ (*44–46*). NO has been used as a reagent gas, and its utility as a pure reagent gas is extended by using an electric discharge rather than a conventional hot wire filament as the source of electrons (*47*). Dilute mixtures of NO in N_2 can be readily used in conventional CI mass spectrometers, and these mixtures provide significant enhancement of M^+ ions for many compounds, particularly for TMS ethers of biologically important compounds (*46*). NO^+ reacts with compounds by reactions other than charge exchange. Hydride transfer and oxidative addition reactions have been noted for aliphatic compounds for which charge exchange is endothermic (*48, 49*).

Because of its use as a carrier gas in gas chromatography, He has been used as a reagent gas for charge exchange reactions. He^+ has a high recombination energy: $RE(He^+) = 24.6$ eV (*50*). The ionization potentials of most organic molecules will be about 8–10 eV (*50*). Hence, the M^+ ions produced by charge exchange

$$He^+ + M \rightarrow M^{+\bullet} + He \qquad (4)$$

will contain a large amount of internal excitation energy and should decompose almost completely. Experimentally, spectra obtained with high pressures of He still contain reasonable abundances of high mass ions (*28, 51, 52*). Direct ionization with low-energy electrons that are present in the high pressure of He, charge exchange reactions of sample ions or impurity ions in He, or collisional stabilization of the excited $M^{+\bullet}$ ions may be occurring. Although the modes of formation of the sample ions have not been determined, spectra obtained with high pressures of He are analytically useful.

One of the problems that is associated with charge exchange spectra is an incorrect isotope ratio for the molecular ion. In general, the ratio, $(M + 1)^+/M^+$, is always higher than predicted for ^{13}C, etc., and sometimes $(M + 1)^+$ is larger than M^+ (*44*). The high-pressure mass spectrum of the reagent gas contains varying abundances of hydrogen containing ions (HeH^+, N_2H^+, or ArH^+), and H_3O^+ is almost always present. Stable $(M + H)^+$ ions are formed by proton transfer from these impurity ions and/or proton transfer from sample ions to sample molecules. It is virtually impossible to remove all water and other hydrogen containing molecules from the reagent gas; therefore, isotope ratios should not be used from charge exchange mass spectra to estimate the elemental composition of molecular ions. Experiments have been done using mixed charge exchange and proton transfer reagent gases by adding a small amount of H_2O to He or Ar (*53, 54*). Dissociative charge exchange occurs from reactions of He^+ or Ar^+, and $(M + H)^+$ ions or $(M + H_3O)^+$ ions are produced from reactions of H_3O^+. These spectra are routinely used for characterization of compounds.

The CI spectra of polyfunctional compounds are often not directly predictable from the spectra of the monofunctional compounds. The CH_4 CI spectra of alcohols contain essentially no $(M + H)^+$ ions (*7, 55*). The spectra of some steroidal diols in which the hydroxyl groups are widely separated by a rigid nucleus also show essential-

TIRED OF STANDARDIZING THIOSULFATE SOLUTIONS?
TAKE A LOOK AT
PAO
see page 57

in HACH's NEW ANALYTICAL CHEMICALS CATALOG

When frequent normality checks bog down your work, it's time to switch to a more stable titrant. PAO (Phenylarsine Oxide) will effectively replace sodium thiosulfate in any iodometric titration, and it won't break down from bacterial action. Dilute solutions are stable for over one year. Standard solutions available in a range of normalities from 0.00564 to 0.113 N.

PAO is just one of over 400 analytical chemicals featured in Hach's new catalog: 128 pages of high-quality, high-purity chemicals—everything from colorimetric indicators to spectro-grade solvents to ultra-purity standards. Product information, chemical symbols, product applications, too.

CALL BOB DOLLINGER,
PRODUCT MANAGER
TOLL FREE: 800-247-3986
(Iowa residents, call collect: 515-232-2533.)
FOR YOUR FREE COPY

HACH CHEMICAL COMPANY
Fine Chemicals Division
P.O. Box 907-A • Ames, Iowa 50010 U.S.A.

CIRCLE 94 ON READER SERVICE CARD

ly no $(M + H)^+$ ions (*56*). However, the CH_4 CI spectra of some α,ω-aliphatic diols show significant abundances of $(M + H)^+$ ions (*57*). These very obvious differences are attributed to the stabilization of $(M + H)^+$ ions of the diols by internal hydrogen bonding; this internal hydrogen bonding is possible in the case of the flexible aliphatic diols and impossible for the rigid 3,17-steroidal diols.

We have used these internal hydrogen bonding effects of the unambiguous determination of the stereochemistry of 2,5-diendoprotoadamantanediol. Of the four isomeric 2,5-protoadamantanediols, only this isomer can exhibit hydrogen bonding. For this isomer, $(M + H)^+$ is the most abundant ion in the i-C_4H_{10} mass spectrum. $(M + H)^+$ is only a minor ion in the spectra of the other three isomers. These internal hydrogen bonding effects have been used for the differentiation of epimeric compounds, but there is not agreement about the necessary conditions for stabilization of $(M + H)^+$ by internal hydrogen bonding (*58–61*). In some cases, internal hydrogen bonding leads to a decrease in the abundance of $(M + H)^+$ ions by opening a new path for decomposition. The CH_4 CI spectra of long chain aliphatic carboxylic acids and their methyl esters cortain $(M + H)^+$ as the most abundant ion; however, the CH_4 CI spectra of the diacids and diesters of about the same molecular weight contain $(M + H - H_2O)^+$ or $(M + H - CH_3OH)^+$ as the most abundant ions (*62*). Much additional work is needed on the effects of intramolecular interactions on CI spectra.

There has been much discussion about the relative sensitivities of EI and CI mass spectrometry, but few data have been presented on comparisons of the two techniques, and the comparisons are very difficult to make (*63*). Opinions of the sensitivities of the two techniques vary widely: It has been reported that CI with Ar/H_2O mixtures is approximately 50 times more sensitive than EI mass spectrometry (*64*), and also that EI MS is approximately 4 times more sensitive than i-C_4C_{10} mass spectrometry (*65*). We have recently completed a comparison of EI vs. CI sensitivities in a modified CEC (Du Pont) 21-110B mass spectrometer. In this instrument we attempted to optimize the sensitivities of the two modes with different ionization sources. The CI sensitivity strongly depends upon experimental conditions. Our experiments indicated essentially equal sensitivities for the two techniques under the best conditions which we were able to obtain for each technique (*66*). For many complex molecules, however, the abundance of the molecular ion is almost negligible, but $(M + H)^+$ ions are abundant in CI spectra. Selected ion monitoring of these high mass ions will be much more sensitive for CI than for EI mass spectrometry.

A somewhat less precise measure of sensitivity in CIMS is given by sample sizes that are used for analyses or levels of impurities which may be detected. Detection limits of SF_6 in air with GC/charge exchange were estimated at 3×10^{-12} g of sample, and quantitative analyses were obtained at the 20 ppb (v/v) level of SF_6 in air, or on 10^{-10} g of sample. The sensitivity of this analysis was considered to be "substantially better" than the sensitivity of electron ionization and "comparable to" the sensitivity of electron capture (*67*). Also organic compounds in water may be detected at the ppm level (or about 50 ng of sample) using water from the solution as the CI reagent gas (*68*). Our GC/MS is not a particularly sensitive one, and we are able to detect approximately 10^{-10} g of sample with the selected ion monitoring technique (*69*).

The kinetic analysis mentioned before indicates that the extent of conversion of reactant ions to sample ions depends on the number of collisions the reactant ions make in the source of the mass spectrometer. One method of increasing the number of collisions between reactant ions and sample molecules is to increase the pressure within the source. Instrumentation has been developed in which the source of the mass spectrometer is operated at 1 atm, atmospheric pressure ionization mass spectrometry (*70, 71*) It has been reported that 10^{-13} g, or lower, of basic compounds can be detected with this technique. With this extremely high sensitivity, trace levels of impurities are readily detected in almost every sample.

At the other extreme, it is possible to use the "trapped ion mode" of ion cyclotron resonance mass spectrometry to keep the reactant ions within the source chamber for times as long as seconds (compared with milliseconds in high-pressure mass spectrometry). Under these conditions it is possible to observe extensive conversion of reactant ions to sample ions even for very low-pressure (10^{-7} torr) samples. Even though few ions are produced at the low pressures of ICR experiments, essentially all of these ions are detected. Hence, it may be possible to analyze very low-pressure, thermally unstable molecules with this technique (*72*).

All of the preceding discussion has been directed toward the use of positive ions and their reactions for analysis. Many instruments now have the capability of detecting either positive or negative ions, and there are many

What is the indispensable dispenser?

1. Does it hold, store and dispense **all** laboratory reagents, including concentrated acids, alkalies and solvents?
2. Does it have a 100-division scale? Can you set a 10 ml instrument accurately at 50 microliters?
3. Does it have a guaranteed accuracy of 1% full scale?
4. Does it have a **magnifying** indicator that eliminates parallax and minimizes the chances for inaccurate volume setting errors?
5. Does it come in **all** sizes? 0.5, 1, 5, 10, 20, 50, and 100 ml? Does it come with a convenient **two-opening** widemouth container?
6. Can you order a "universal" model that will fit **any reagent container** with a neck opening over 19 mm?
7. Does it save **90%** of the time required for dispensing by manual methods?

8. Does it have a 14-year history of **reliable** performance, back-up **service** from the manufacturer, and a 50% lifetime warranty?

Only Labindustries REPIPET® Dispensers meet ALL these qualifications for the "indispensable dispenser."

ALL THIS FOR UNDER $80!
(Sizes 10 ml and under)

For complete details on REPIPET Dispensers and other unique L/I instruments, request our 1977 catalog "Labindustries Today."

LABINDUSTRIES

1802 Second Street
Berkeley, CA 94710
Phone: (415) 843-0220

CIRCLE 131 ON READER SERVICE CARD

illustrations of negative chemical ionization mass spectrometry for analysis (*73, 74*). Lack of space prevents a discussion of this important area of research in analytical applications of ion-molecule reactions. One of the most recent developments in this area, however, is the development of a quadrupole mass spectrometer with the capability of simultaneous detection of both positive and negative ions (*75*).

Acknowledgment

The author is grateful to Barbara Jelus, Frank Hatch, and Charles Polley for their assistance.

References

(1) Sir J. J. Thomson, "Rays of Positive Electricity and Their Applications to Chemical Analysis", Longmans, Green, London, England, 1913.
(2) F. W. Aston, "Mass Spectra and Isotopes", Longmans, Green, London, England, 1933.
(3) A. J. Dempster, *Philos. Mag.*, **31**, 438 (1916).
(4) V. L. Tal'roze and A. K. Lyubimova, *Dokl. Akad. Nauk SSSR*, **86**, 909 (1952).
(5) D. P. Stevenson and D. O. Schissler, *J. Chem. Phys.*, **23**, 1353 (1955); D. O. Schissler and D. P. Stevenson, *ibid.*, **24**, 926 (1956).
(6) F. H. Field, J. L. Franklin, and F. W. Lampe, *J. Am. Chem. Soc.*, **78**, 5697 (1956).
(7) M.S.B. Munson and F. H. Field, *ibid.*, **88**, 2621 (1966).
(8) G. P. Arsenault, J. R. Althaus, and P. V. Divekar, *Chem. Commun.*, 1414 (1969).
(9) H. M. Fales, G.W.A. Milne, and M. L. Vestal, *J. Am. Chem. Soc.*, **91**, 3682 (1969).
(10) C. T. Pate, J. L. Sprung, and J. N. Pitts, Jr., *Org. Mass. Spectrom.*, **11**, 552 (1976).
(11) R. G. Gillis, M. J. Lacey, and J. S. Shannon, *ibid.*, **9**, 359 (1974).
(12) R. L. Foltz, *Chem. Technol.*, **5**, 39 (1975).
(13) Takeshi Murata, Seiji Takahashi, and Tsunezo Takeda, *Anal. Chem.*, **47**, 577 (1975).
(14) Yukio Shimizu and Burnaby Munson, unpublished data.
(15) Burnaby Munson, in "Interactions Between Ions and Molecules", Pierre Ausloos, Ed., p 505, Plenum, New York, N.Y., 1975.
(16) D. K. Bohme, *ibid.*, p 489.
(17) D. P. Ridge, thesis, California Institute of Technology, Pasadena, Calif., 1972.
(18) Timothy Su and M. T. Bowers, *J. Am. Chem. Soc.*, **95**, 7609 (1973).
(19) Lucette Hellner and L. W. Sieck, *J. Res. Nat. Bur. Stand.*, **75A**, 487 (1971).
(20) M.S.B. Munson and F. H. Field, *J. Am. Chem. Soc.*, **88**, 4337 (1966).
(21) J. Michnowicz and B. Munson, *Org. Mass. Spectrom.*, **6**, 283 (1972).
(22) T. A. Whitney, L. P. Klemann, and F. H. Field, *Anal. Chem.*, **43**, 1048 (1971).
(23) G. Gioumousis and D. P. Stevenson, *J. Chem. Phys.*, **29**, 294 (1958).
(24) T. F. Moran and W. H. Hamill, *ibid.*, **39**, 1413 (1963).
(25) S. K. Gupta, A. G. Jones, A. G. Harrison, and J. J. Myher, *Can. J. Chem.*, **45**, 3107 (1967).
(26) T. Su and M. T. Bowers, *J. Chem. Phys.*, **58**, 3027 (1973).
(27) R. A. Barker and D. P. Ridge, *ibid.*, **64**, 4411 (1976).
(28) Frank Hatch and Burnaby Munson, *Anal. Chem.*, **49**, 169 (1977).
(29) Frank Hatch and Burnaby Munson, *ibid.*, p 731.
(30) Frank Hatch and Burnaby Munson, unpublished data.
(31) M. M. Bursey and M. K. Hoffman, *Can. J. Chem.*, **49**, 3395 (1971).
(32) B. L. Jelus, D. L. Dalrymple, J. Michnowicz, and B. Munson, unpublished work.
(33) Burnaby Munson, *Anal. Chem.*, **43**, 28A (1971).
(34) J. Michnowicz and Burnaby Munson, *Org. Mass. Spectrom.*, **4**, 481 (1970).
(35) G.W.A. Milne, H. M. Fales, and Theodore Axenrod, *Anal. Chem.*, **43**, 1815 (1971).
(36) Jew-Ming Chew, Richard Saferstein, and John Manura, *ibid.*, **46**, 296 (1974).
(37) F. H. Field, *J. Am. Chem. Soc.*, **92**, 2672 (1970).
(38) D. F. Hunt, *Prog. Anal. Chem.*, **6**, 359 (1973).
(39) I. Dzidic, *J. Am. Chem. Soc.*, **94**, 8333 (1972).
(40) S. D. Goff, B. L. Jelus, and E. E. Schweizer, *Org. Mass. Spectrom.*, in press.
(41) D. F. Hunt, C. N. McEwen, and R. A. Upham, *Anal. Chem.*, **44**, 1292 (1972).
(42) D. F. Hunt, C. N. McEwen, and R. A. Upham, *Tetrahedron Lett.*, 4539 (1971).
(43) W. Blum, E. Schlumpf, J. G. Liehr, and W. J. Richter, *ibid.*, 565 (1976).
(44) Noel Einolf and Burnaby Munson, *Int. J. Mass. Spectrom. Ion Phys.*, **9**, 141 (1972).
(45) D. F. Hunt and J. F. Ryan, *J. Chem. Soc. Chem. Commun.*, 620 (1972).
(46) B. L. Jelus, B. Munson, and C. Fenselau, *Biomed. Mass. Spectrom.*, **1**, 96 (1974).
(47) D. F. Hunt, C. N. McEwen, and T. M. Harvey, *Anal. Chem.*, **47**, 1730 (1975).
(48) D. F. Hunt and T. M. Harvey, *ibid.*, p 1965.
(49) D. F. Hunt and T. M. Harvey, *ibid.*, p 2136.
(50) J. L. Franklin, J. G. Dillard, H. M. Rosenstock, J. T.Herron, K. Draxl, and F. H. Field, NSRDS-NBS 26, Dept. Commerce, 1969.
(51) J. P. Hoppesch and R. C. Domingo, *Anal. Lett.*, **8**, 839 (1975).
(52) H. M. Fales, in "Mass Spectrometry, Techniques and Applications", G.W.A. Milne, Ed., p 179, Wiley-Interscience, New York, N.Y., 1971.
(53) G. P. Arsenault, *J. Am. Chem. Soc.*, **94**, 8421 (1972).
(54) D. F. Hunt and J. F. Ryan, *Anal. Chem.*, **44**, 1306 (1972).
(55) F. H. Field, in "Advances in Mass Spectrometry", Vol 4, E. Kendrick, Ed., p 645, Institute of Petroleum, London, England, 1968.
(56) John Michnowicz and Burnaby Munson, *Org. Mass. Spectrom.*, **6**, 765 (1972).
(57) I. Dzidic and J. A. McCloskey, *J. Am. Chem. Soc.*, **93**, 4955 (1971).
(58) B. L. Jelus, Frank Hatch, T. K. Morgan, Jr., R. K. Murray, Jr., and Burnaby Munson, unpublished data.
(59) J. Winkler and F. W. McLafferty, *Tetrahedron*, **30**, 2971 (1974).
(60) P. Longevialle, G.W.A. Milne, and H. M. Fales, *J. Am. Chem. Soc.*, **95**, 6666 (1973).
(61) F. W. Hatch and B. Munson, Paper 23, presented at 9th Middle Atlantic Regional Meeting, Wilkes-Barre, Pa., April 1974.
(62) R. J. Weinkam and Joseph Gal, *Org. Mass. Spectrom.*, **11**, 188 (1976).
(63) F. H. Field, in "Ion Molecule Reactions", Vol 1, J. L. Franklin, Ed., p 261, Plenum, New York, N.Y., 1972.
(64) D. F. Hunt, in "Advances in Mass Spectrometry", Vol 6, A. R. West, Ed., p 517, Applied Science, Essex, England, 1974.
(65) Ian Jardine and Catherine Fenselau, *Anal. Chem.*, **47**, 730 (1975).
(66) Frank Hatch and Burnaby Munson, unpublished data.
(67) J. P. Hoppesch and R. C. Domingo, *Anal. Lett.*, **8**, 839 (1975).
(68) Philip Price, D. P. Martinsen, R. A. Upham, H. S. Swofford, Jr., and S. E. Buttrill, Jr., *Anal. Chem.*, **47**, 190 (1975).
(69) Frank Hatch and Burnaby Munson, unpublished data.
(70) E. C. Horning, M. G. Horning, D. I. Carroll, I. Dzidic, and R. N. Stillwell, *Anal. Chem.*, **45**, 936 (1973).
(71) D. I. Carroll, I. Dzidic, R. N. Stillwell, M. G. Horning, and E. C. Horning, *ibid.*, **46**, 706 (1974).
(72) R. T. McIver, Jr., E. B. Ledford, Jr., and J. S. Miller, *ibid.*, **47**, 692 (1975).
(73) R. C. Dougherty, J. D. Roberts, and F. J. Biros, *ibid.*, p 54.
(74) D. F. Hunt, T. M. Harvey, and J. W. Russell, *J. Am. Chem. Soc. Chem. Commun.*, 151 (1975).
(75) D. F. Hunt, G. C. Stafford, Jr., F. W. Crow, and J. W. Russell, *Anal. Chem.*, **48**, 2098 (1976).
(76) J. W. Long, thesis, University of Delaware, Newark, Del., 1972.
(77) S. G. Lias, J. R. Eyler, and P. Ausloos, *Int. J. Mass Spectrom. Ion Phys.*, **11**, 444 (1975).
(78) C. W. Polley, unpublished data.
(79) A. A. Herod and A. G. Harrison, *Int. J. Mass Spectrom.*, **4**, 415 (1970).

Work partially supported by the National Science Foundation, Grant # GP20231. Presented at the Third Federation of Analytical Chemistry and Spectroscopy Societies Meeting, Philadelphia, Pa., November 1976.

Burnaby Munson is professor of chemistry at the University of Delaware. Dr. Munson earned his BA, MA, and PhD degrees from the University of Texas in 1954, 1956, and 1959, respectively. He was associated with the Esso Research and Engineering Co. from 1959 until 1967 when he joined the faculty at the University of Delaware. Dr. Munson was coinventor with Frank Field of the chemical ionization technique while at Esso. His current research interests are in electron and chemical ionization mass spectrometry, kinetics, and the thermochemistry of ion-molecule reactions.

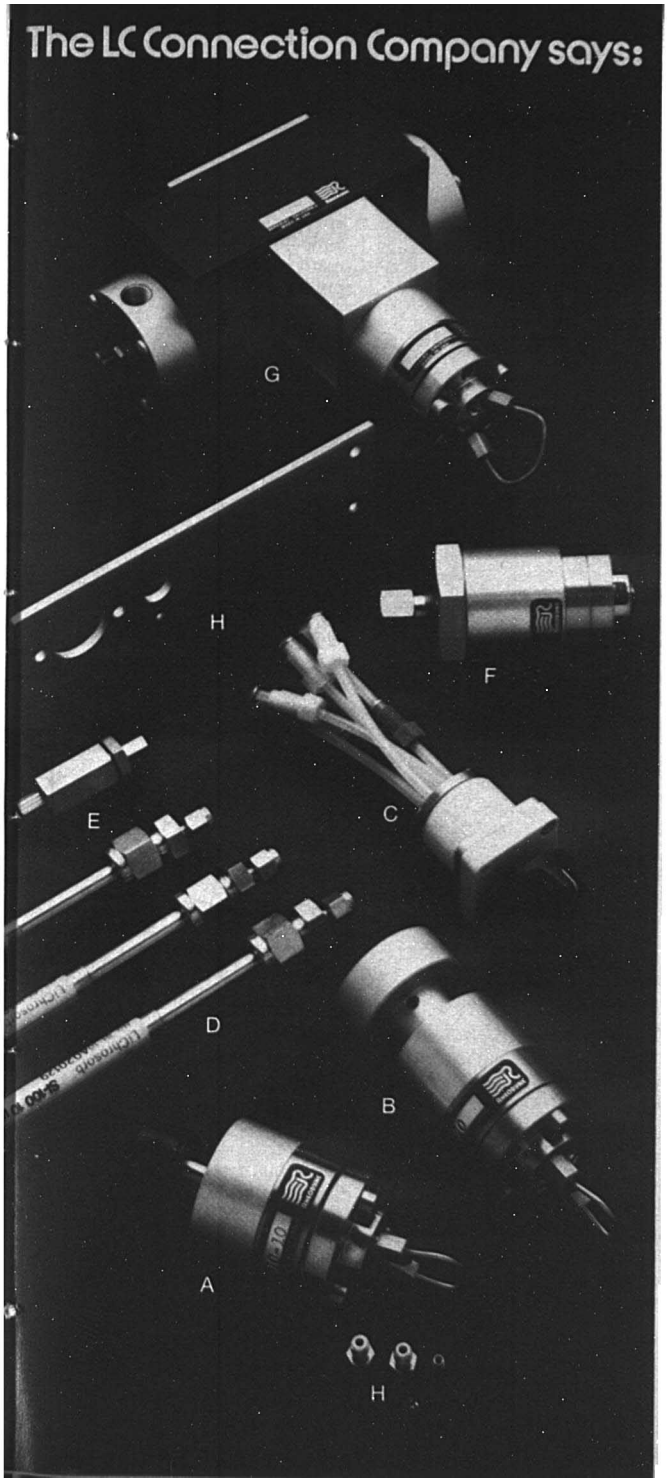

Barebones HPLC doesn't do it.

You need Rheodyne valves, injectors, packed columns, filters, actuators and fittings for better, safer liquid chromatography.

Turn on easy with the 70-10 Sample Injection Valve (A)

For just $290, you can get this 6-port sample injection valve with a removable sample loop and 7000 psi pressure rating. Sample loops from 10 μl to 2.0 ml.

Circle no 181 for more information.

The two way valve (B)

Use the Rheodyne Model 7120 Syringe Loading Sample injector valve to fill loops conventionally or in the partial loop variable volume mode with only 0.5 μl sample loss. Only $490 with 20 μl sample loop.

Circle no 182 for more information.

Teflon Rotary Valves at about half the cost (C)

Three, four and six way valves in 0.8 mm and 1.5 mm bores are priced at $70 to $87. Features zero dead volume, chemical inertness (only Teflon* contacts stream), and 300 psi rating.

Circle no 183 for more information.

*Teflon is a registered T.M. of DuPont.

Well packed HPLC columns (D)

Using the best of American and European technology, Rheodyne gives you guaranteed peak symmetry and minimum plates per meter to doubly assure optimum column performance. Six columns using SI-100, NH_2, DIOL and RP-8 are available at prices from $180 to $240.

Circle no 184 for more information.

Accessories to protect and enhance performance

To protect column inlet frits from plugging, use our filter. **(E)** Sells for $40. Package of five 2 μm replaceable filter element for $20.

Our new pressure relief valve can be set at any point over the range of 2000 to 7000 psi (140 to 500 bar). Connect the relief valve in-line for continuous flushing of the 6 μl chamber. Price for this type 316 stainless steel unit is $250. **(F)**

For automatic operation of Rheodyne sample injection, 3-way and 4-way valves, use our Model 70-01 Pneumatic Actuator. Order separately for $160 or factory assembled in combination at $430 to $450. **(G)**

Also available are high pressure switching valves, tube fittings and valve mounting plates. **(H)**

Circle no 185 for more information.

For even faster data on any of these items, write or call Rheodyne, Inc., 2809 Tenth Street, Berkeley, CA 94710. Phone (415) 548-5374.

CIRCLE 177 ON READER SERVICE CARD

RHEODYNE

THE LC CONNECTION COMPANY

Du Pont Instruments solve tough measurement problems.

Du Pont LC size exclusion system performs polymer characterization 5 times faster than GPC systems.

Du Pont Model 848 High Performance Liquid Chromatograph

The chromatograms at right compare the separation of copolymers containing polystyrene at molecular weights of 100,000 and 200,000. They were obtained by an LC user who found that the Du Pont size exclusion (SEC) system was able to complete the separation in 7 minutes, while a standard gel permeation (GPC) system required 37 minutes.

What's more, in the experiment above, precision was found to be five times higher with the Du Pont system at molecular weight 200,000. And the GPC system required 6 columns (total cost: $3,000), while SEC required only one (total cost: $350).

In many other applications as well, the Du Pont system, consisting of flow-controlled chromatograph and size exclusion columns, can reduce analysis times to a few minutes. And the system's high resolving power means high precision in molecular weight determinations.

Du Pont also offers a system specifically designed for high temperature size exclusion chromatography for materials such as polyolefins. This system—consisting of the Du Pont 830 flow-controlled chromatograph, infrared detector and Du Pont size exclusion columns—overcomes the problems of temperature sensitivity usually associated with gel-type packings and the refractive index detector.

Free Offer: If you have an analysis, characterization or other measurement problem that could be solved by SEC or any other mode of High Performance Liquid Chromatography, we'll be happy to consult with you at no charge. Just write to Du Pont Instruments, Room 25479,Wilmington, DE 19898. Or call our LC Hot Line at (302) 772-5139.

Figure 1

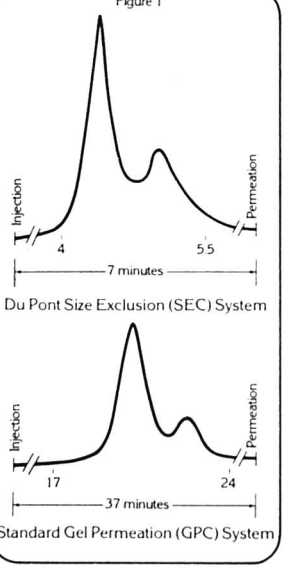

Du Pont Size Exclusion (SEC) System

Standard Gel Permeation (GPC) System

Circle reader service number 48.

Du Pont DMA detects subtle transitions– even in laminated or reinforced materials.

The new Du Pont Dynamic Mechanical Analyzer (DMA), which measures the physical properties of a material, is so sensitive it was able to detect the two glass transitions in an epoxy laminate as shown in the thermogram.

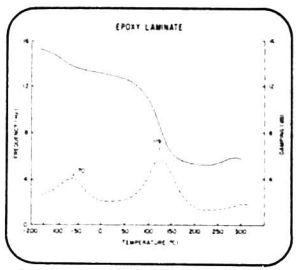

Glass transitions in this epoxy laminate are marked at −70 C and 119 C.

In this experiment, the DMA recorder/console was programmed and the instrument was left to run on its own. It produced the thermogram in just 1-1/2 hours. Other methods would have required a day or more with constant operator attention to measure across the same temperature range.

In addition, the DMA measures modulus accurately across the widest range available. Because of its thermal analysis dimension, it allows very precise linear temperature programming. And it provides direct digital display and continuous recording of resonant frequency (relative modulus) and damping on the X, Y, Y' recorder.

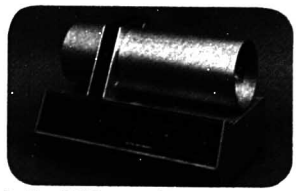

Du Pont 980 Dynamic Mechanical Analyzer

Free Offer: If you have an analysis, characterization or measurement problem that could be solved by physical testing or thermal analysis, we'll be happy to consult with you at no charge. Just write to Du Pont Instruments, Room 25480, Wilmington, DE 19898. Or call our TA Hot Line at (302) 772-5134.

Circle reader service number **49.**

Du Pont MEA measures smaller samples faster than L.O.D. test.

In just 25 minutes, a lyophilized sample of 2-5 mg. was analyzed in the Du Pont Moisture Evolution Analyzer (MEA) and found to contain 1.0% moisture. Using the calibration factor obtained by running a standard of known moisture content, the water level was determined with a standard deviation of 4.5% (rel.). The same analysis done with the loss on drying test (L.O.D.) could have required two days and a sample size of 1 gram.

The L.O.D. test measures sample weight change as water and other volatiles are given off. The coulometric detector in the MEA, on the other hand, automatically measures the actual amount of water volatilized and absorbed from a sample. The amount of current associated with the electrolysis is integrated, scaled and directly displayed by digital read-out as μg. water.

The MEA is highly specific for water and, unlike the Karl Fischer test, does not require the use of toxic chemicals. It is sensitive enough to measure as low as 0.1 μg. water, which makes it particularly well-suited for lyophilized materials where low moisture levels must be measured rapidly.

Free Offer: If you have an analysis or measurement problem that could be solved by Moisture Evolution Analysis, we'll be happy to consult with you at no charge. Just write Du Pont Instruments, Room 25481, Wilmington, DE 19898. Or call our Thermal Analysis Hot Line (302) 772-5134.

Circle reader service number **50.**

Du Pont 902 Moisture Evolution Analyzer

Du Pont Instruments

DU PONT

ห้องสมุด กรมวิทยาศาสตร์

Take a closer look at EASTMAN Organic Chemicals

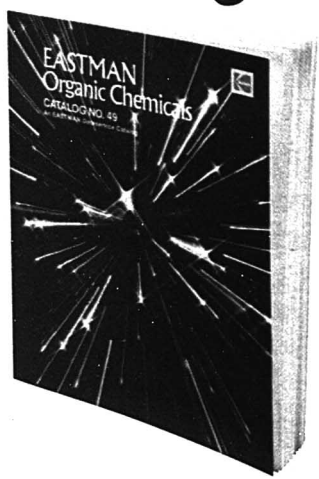

If you haven't received your EASTMAN Organic Chemicals Catalog No. 49, order it now, and take a closer look at:

- thousands of organic chemicals
- structural formulas for more than 1,000 chemicals
- many new chemicals recently added to our line (including general purpose laboratory reagents like Oiive Oil, Beeswax, and Egg Albumin)
- dyes, stains, and indicators; reagents for protein and polypeptide synthesis and analysis; liquid scintillation counting; electrophoresis; and more
- details on the EASTMAN *Dataservice* Publications Program, and guide to distributors and regional offices

Kodak

Worth a close look.

in our free 182-page catalog

Eastman Kodak Company, Eastman Organic Chemicals, Dept. 412L, Rochester, N.Y. 14650 8-40

Gentlemen: I want a closer look. Please send a free copy of EASTMAN Organic Chemicals Catalog No. 49 to:

Name

Affiliation

Address

City State Zip

CIRCLE 65 ON READER SERVICE CARD

1977 ACS National Meeting

August 28–September 2

Chicago, the convention capital of the U.S., will again host an ACS national meeting August 28–September 2, 1977. The 174th Annual Meeting of the American Chemical Society will feature technical sessions and professional and social activities that will attract more than 8 000 attendees. In all, 28 of the Society's 29 divisions and six committees will participate in the five days of technical sessions. The technical program will include over 1500 papers to be presented in about 220 planned symposia.

The Analytical Chemistry Division will hold 16 half-day sessions at which over 100 papers will be presented. These sessions are composed of four symposia of 12 sessions and 4 general sessions. Among the symposia topics are high-resolution gas chromatography, ultratrace metal analysis in biological sciences and environment, the analytical approach in problem solving, and forensic chemistry. Of these, the first two topics with 29 and 21 presentations each at four respective sessions seem to dominate the technical program of the Division. This emphasis is probably a reflection of the current interest in these areas. The general sessions will cover general analytical chemistry topics in two sessions and electrochemistry and chromatography in one session each.

In addition to these programs for which the Analytical Division is the primary sponsor, the Division will participate in two symposia sponsored by the Division of Polymer Chemistry Inc.: novel instrumental methods for probing polymer structures (four sessions) and chromatography of polymers (three sessions). The Analytical Division will also participate in a symposium on the present status of the teaching of analytical chemistry (two sessions) sponsored by the Division of Chemical Education Inc.

Other programs of interest to analytical chemists are those sponsored by the Division of Agricultural & Food Chemistry, the Division of Chemical Health & Safety (probationary), and the Division of Industrial & Engineering Chemistry. The programs of these divisions contain presentations on applications of various analytical techniques to the elucidation of food and beverage constituents or to the monitoring of toxic substances. In addition, the Division of Fuel Chemistry will hold a symposium on new techniques in coal analysis, and the Division of Nuclear Chemistry & Technology will also hold a symposium on nuclear spectroscopy.

All sessions sponsored by the Analytical Chemistry Division and those jointly sponsored with the Division of Polymer Chemistry Inc., will be held in the Palmer House. The symposium sponsored jointly with the Division of Chemical Education Inc., will take place in the Pick-Congress Hotel which is only four blocks away from the Palmer House.

The Analytical Division social hour will be held on Tuesday, August 30, from 6:00 p.m. in the Water Tower Place, Pearson Room, 175 East Chestnut Street. The division dinner and business meeting will follow beginning at 6:45 and 7:45 p.m., respectively.

The ACS Chemical Exposition will be held in the Palmer House, Upper Exhibit Hall (fourth floor), Monday, August 29 through Thursday, September 1. It will include exhibits of the latest chemical instruments, publications, and services and will be sponsored by ACS and the Chicago Section.

Several ACS courses given in conjunction with the meeting prior to Monday will be of interest to analytical chemists also. For more information, see page 804 A.

The detailed technical program given below includes all the Analytical Chemistry sessions and those cosponsored by the Division.

Preregistration forms and housing information are contained in *Chem. Eng. News*, June 13, 1977. The complete technical program for the meeting appears in *Chem. Eng. News*, July 25, 1977.

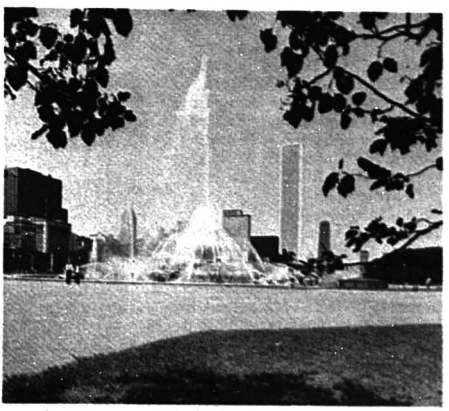

DIVISION OF ANALYTICAL CHEMISTRY

J. W. Miller, *Chairman*
F. A. Guthrie, *Secretary*

MONDAY MORNING

SECTION A

Palmer House, Wabash Parlor (3rd Floor)

Symposium on High Resolution Gas Chromatography: Columns and Analyses

S. P. Cram, Presiding

9:00—Introductory Remarks.
9:10—1. Capillary Gas Chromatography: A Story of Success in Modern Analytical Chemistry. **M. Novotny.**
10:00—2. High Resolution Separations with Metal & Glass Large Bore Open Tubular Columns. **R. Teranishi, R. A. Flath, T. R. Mon.**
10:20—3. Characteristics and Performance of High Resolution Glass Capillary GC Systems. **S. P. Cram, F. J. Yang.**
10:40—4. Twenty Years of Open Tubular (Capillary) Columns—An Overview. **L. S. Ettre.**
11:00—5. Developments in PLOT Column Technology. **J. G. Nikelly, P. C. Uden, D. E. Henderson.**
11:20—6. High Resolution Columns in Gas Chromatography. **W. Bertsch, E. L. Anderson, M. Moskot.**
11:40—7. High Efficiency GC Columns. **J. Clemons, H. McNair.**

SECTION B

Palmer House, Parlor B (6th Floor)

Symposium on Ultratrace Metal Analysis in Biological Sciences and Environment

T. H. Risby, Presiding

9:00—Introductory Remarks.
9:15—8. Trace Element Analysis in Nutrition Research. **W. Mertz.**
9:55—9. Simultaneous Multi-element Analysis of Biologically Related Samples with a RF-ICP. Advantages and Limitations. **F. N. Abercrombie, M. D. Silvester, R. B. Cruz.**
10:15—Intermission.
10:30—10. Health Implications of Trace Metals in the Environment. **K. Bridbord.**
11:10—11. The Analysis of Molybdenum in Biological Materials. **G. E. Bentley, L. Markowitz, R. R. Meglen.**
11:30—12. Analysis for Size-Fractionated Airborne Particulate Matter for Metals by Atomic Absorption Spectroscopy and Neutron Activation Analysis. **G. J. Rosenberger, W. D. Smith, W. W. Miller, T. H. Risby.**

SECTION C

Symposium on Novel Instrumental Methods for Probing Polymer Structures *Joint with Division of Polymer Chemistry Inc.* *(see page 795 A)*

MONDAY AFTERNOON

SECTION A

Palmer House, Wabash Parlor (3rd Floor)

Symposium on High Resolution Gas Chromatography: Columns and Analyses

L. Ettre, Presiding

2:00—13. High Resolution Gas Chromatographic Determination of Organic Compounds in Ozonized Wastewater. **R. E. Sievers, R. H. Shapiro, H. F. Walton, G. A. Eiceman, R. M. Barkley.**
2:20—14. Analyses of Textile Effluent and Tobacco Smoke Condensate Samples by Glass Capillary GC/MS/COM. **M. Gordon.**
2:40—15. High Performance GC—Aspects of Column Design and Selection. **J. R. Jeffs.**
3:00—16. Glass Capillary GC-MS Analysis of Organics in Drinking Water Concentrates and Advanced Waste Treatment Concentrates. **D. C. K. Lin, B. A. Petersen, R. G. Melton, W. E. Coleman.**
3:20—17. Applications of Dexsil and Other PLOT GC Columns to Metal Compound Separations and Pyrolysis. **P. C. Uden, F. P. DiSanzo, D. E. Henderson, R. J. Lloyd, T. Tetu.**
3:40—18. Indirect Evidence of Imprinting of Hepatic Enzyme Systems in the Human Using High Resolution Glass Capillary Gas Chromatography. **C. D. Pfaffenberger.**
4:00—19. Simultaneous Determination of Multiple Testicular Steroids Utilizing High Resolution Glass Capillary Gas Chromatography. **R. H. Wohleb, L. L. Hilton, M. J. Free.**

SECTION B

Palmer House, Parlor B (6th Floor)

Symposium on Ultratrace Metal Analysis in Biological Sciences and Environment

T. H. Risby, Presiding

2:00—Introductory Remarks.
2:05—20. Collection and Analysis of Airborne Metallic Elements. **R. Thompson.**
2:45—21. Ultratrace Quantities of Heteropolycyclic Aromatic Compounds in the Environment. **G. R. Dubay, R. A. Hites.**
3:05—22. Multi-element Characterization of Airborne Particulate Dispersal Patterns—the New Instrumental Technique. **F. N. Abercrombie, M. D. Silvester, A. Murray.**
3:25—23. Ultra-trace Analysis of Metals in Biological Systems. **A. V. Colucci, W. S. Simmons.**
4:20—24. Application of Stable-Isotropically Labelled Organics in Analysis of Environmental Samples Water and Air. Part I. **H. G. Nowicki, R. F. Devine, C. A. Kieda.**

SECTION C

Symposium on Novel Instrumental Methods for Probing Polymer Structures *Joint with Division of Polymer Chemistry, Inc.* *(see page 795 A)*

TUESDAY MORNING

SECTION A

Palmer House, Wabash Parlor (3rd Floor)

Symposium on High Resolution Gas Chromatography: Techniques

S. P. Cram, Presiding

9:00—Introductory Remarks.
9:10—25. Analysis of Complex Natural Samples by High Resolution Gas Chromatography. **W. E. Reed, D. H. Stuermer.**
10:00—26. Fractionation and Characterization of Petroleum Cycloalkanes. **J. S. Warner, D. C. K. Lin.**
10:20—27. A Method for Isolation, Identification and Comparison of Tobacco Essential Oil Components. **R. A. Lloyd, Jr.**
10:40—28. Closed-Loop Headspace Sampling. **C. R. Green, F. A. Thome.**
11:00—29. Photoionization Detection in a High Resolution Glass Capillary System. **W. G/ Jennings.**
11:20—30. Application of High Resolution Capillary Columns to Complex Mixtures. **M. J. Hartigan, B. Welton.**
11:40—31. Moment Theory of Gas-Solid Chromatography. **B. J. McCoy, R. G. Carbonell.**

SECTION B

Palmer House, Parlor B (6th Floor)

Symposium on Ultratrace Metal Analysis in Biological Sciences and Environment

T. H. Risby, Presiding

Varian Introduces the high precision, moderately priced SF-330 SPECTROFLUOROMETER

You can bet that Varian wouldn't enter the spectrofluorometer field except with a sensitive, highly stable, superbly performing instrument. More than that—our SF-330 is moderately priced, giving you top spectrofluorometric value for your instrument dollar. Scan these features!

RATIO PHOTOMETER

Dynode supply voltage is automatically compensated to eliminate effects of source variation, and to assure stability and reproducibility.

CONCAVE GRATING MONOCHROMATOR

Both emission and excitation monochromators are equipped with precision, concave gratings for high light throughput. Zero order excitation and emission studies are routine on the SF-330. The high intensity 150 watt Xenon lamp is designed to minimize the generation of ozone.

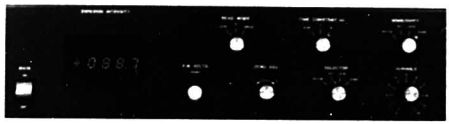

DIGITAL READOUT Analytical results are legibly presented on a four-digit LED display. Read mode options may be selected to display mean values each 0.25 sec or each 5 sec. In the Hold mode, a mean value is presented on the LED display after 5 second integration and the same value is output to an optional printer.

INSTRUMENT VERSATILITY

Selectors provide stepwise variations of the spectral bandwidth isolated by the excitation (3, 5, and 10 nm) and the emission (5, 10, and 20 nm) monochromators. Scan speeds of 25 and 50 nm/min may be selected on a front panel control.

LARGE SAMPLE COMPARTMENT

Voluminous and convenient sample compartment occupies upper left corner of the Model SF-330 chassis. When opened, immediate accessibility is provided to front, side and top. A four-cell sample turret is provided as standard.

Optional accessories offered include a solid sample holder, high pressure liquid chromatography flow cell, micro cell and holder, flow cell adapter, digital printer, recorder, thermostatting hardware and more.

CIRCLE 220 ON READER SERVICE CARD

varian

9:00—Introductory Remarks.
9:05—**32.** Trace Metal Measurements in Assessing Human Disease Processes. **M. A. Evenson.**
9:45—**33.** Metal Carcinogenesis in Tissue Culture. **M. Costa.**
10:25—Intermission.
10:40—**34.** Future Analytical Requirements for the Determination of Trace and Ultratrace Levels of Metals in Bioenvironmental Systems. **G. B. Morgan, E. W. Brethauer.**
11:20—**35.** Simultaneous Determination of Trace Elements in Urine by Inductively Coupled Plasma—Atomic Emission Spectrometry. **W. J. Haas, Jr., V. A. Fassel, R. N. Kniseley, W. L. Sutherland.**
11:40—**36.** Isotope Dilution GCMS for Quantitative Organic Trace Analysis. **B. N. Colby.**

SECTION C

Palmer House, Parlor F (6th Floor)

General

J. D. Carr, Presiding

9:00—37. Opto-Acoustic Spectroscopy with a Pulsed Dye Laser. **R. W. Shaw.**
9:20—38. Results of Multicomponent Fluorescence Studies Using the Video Fluorometer. **D. W. Johnson, C.-N. Ho, J. B. Callis, G. D. Christian.**
9:40—39. Determination of Submicrogram Quantities of Arsenic and Methylarsenicals in Water by Arsine Generation Followed by Graphite Furnace Atomic Absorption Spectrometry. **A. U. Shaikh, D. E. Tallman.**
10:00—40. Determination of Some Trace Metals in Biological Excreta by Atomic Absorption Spectroscopy. **G. W. C. Hung.**
10:20—Intermission.
10:40—41. Lightly Sulfonated Porous Polymers for Gas-Solid Chromatography. **R. F. Hirsch, R. J. Gaydosh.**
11:00—42. Critical Study of Temperature Effects in Stopped-Flow Mixing Systems. **F. J. Holler, C. G. Enke, S. R. Crouch.**
11:20—43. Acidity and Complexation Behavior of Phosphonoacetic Acid. **P.-H. C. Heubel, A. I. Popov.**
11:40—44. Reaction Kinetics of Ferrate(VI) Ion with One-Carbon Compounds. **J. D. Carr, A. R. Tabatabai, C. C. Greenwalt.**

SECTION D

Symposium on Novel Instrumental Methods for Probing Polymer Structures *Joint with Division of Polymer Chemistry, Inc.* *(see page 795 A)*

TUESDAY AFTERNOON

SECTION A

Palmer House, Wabash Parlor (3rd Floor)

Symposium on High Resolution Gas Chromatography: Techniques

R. A. Lloyd, Presiding

2:00—45. Two-Dimensional Gas Chromatography. Selected Applications. **E. L. Anderson, M. M. Thomason, W. Bertsch.**
2:20—46. Analysis of Organic Contaminants in Surface Water Using High Resolution Gas Chromatography and Selective Detectors. **T. A. Rooney, R. R. Freeman.**
2:40—47. Comparison of the GC Detectors in Their Usefulness, Suitability, Sensitivity, and Selectivity in Glass Capillary Gas Chromatography. **F. J. Yang, S. P. Cram, E. Freitas.**
3:00—48. Detailed Analysis of Shale Oil Using Specific Detectors. **C. E. Kennard, S. M. Sonchik, M. P. T. Bradley.**
3:20—49. Investigation of Trace Organic Components in Chlorinated Natural Waters Using Glass WCOT Columns. **R. M. Bean, P. W. Ryan, R. G. Riley.**
3:40—50. Glass Capillary Gas Chromatography and Computerized Mass Spectrometry in Complex Mixture Analyses. **J. Meili, F. C. Walls, R. McPherron, A. L. Burlingame.**
4:00—51. A Dual GC-MS Interface for Packed and Capillary Columns. **J. C. Cook, Jr., R. M. Milberg, L. Brayton.**
4:20—52. High Resolution Gas Chromatography/Mass Spectrometry. **W. A. Wolstenholme, U. Rapp, H. Kaufmann.**
6:00—*Divisional Social Hour.* Water Tower Place, Pearson Room, 175 East Chestnut St.
6:45—*Divisional Dinner/Theatre.* Water Tower Place, Pearson Room, 175 East Chestnut St.
7:45—*Divisional Business Meeting.* Water Tower Place, 175 East Chestnut St.

SECTION B

Palmer House, Parlor B (6th Floor)

Symposium on Ultratrace Metal Analysis in Biological Sciences and Environment

T. H. Risby, Presiding

2:00—Introduction.
2:05—53. Zinc Biochemistry of Normal and Abnormal Growth Processes. **D. S. Auld.**
2:45—54. A Modified Standard Addition Method for Determining Cadmium, Lead, Copper and Iron in Sea Water Samples by Atomic Absorption Spectroscopy. **C. P. Weisel, S. R. Piotrowicz, R. A. Duce, J. L. Fasching.**
3:05—55. Ultratrace Determination of Sulfur Hexafluoride and Perfluorocarbons for Atmospheric Tracing. **R. N. Dietz, E. A. Cote, R. W. Goodrich.**
3:25—Intermission.
3:40—56. Sources of Environmentally Important Metals in the Atmosphere. **R. E. Lee, Jr., F. V. Duffield.**
4:20—57. Saturated Non-Resonant Emission Spectroscopy for Atomic Detection. **J. A. Gelbwachs, C. F. Klein, J. E. Wessel.**
4:40—58. Trace Metal Uptake in *Bacillus Subtilis* 168. **J. J. Dulka, P. E. Kolenbrander, T. H. Risby.**
6:00—*Divisional Social Hour* (see Section A for location).
6:45—*Divisional Dinner/Theatre* (see Section A for location).
7:45—*Divisional Business Meeting* (see Section A for location).

SECTION C

Palmer House, Parlor F (6th Floor)

General: Electrochemistry

A. I. Popov, Presiding

2:00—59. Electrogenerated Chemiluminescence of t-Stilbene Derivatives. **J. R. Wilson, S-M. Park.**
2:20—60. Electrochemical Studies of Dimethyl Benz(a)pyrenes. **S-M. Park, J. J. Michnovicz.**
2:40—61. Complexation of Monovalent Cations by the Antibiotic Ionophore Monensin. **J. G. Hoogerheide, A. I. Popov.**
3:00—62. The Effect of Slow Two-Electron Transfers and Disproportionation on Cyclic Voltammograms. **M. D. Ryan.**
3:20—Intermission.
3:40—63. Potential Dependence of the Transfer Coefficient in the Electrochemical Reduction of tert-Nitrobutane and Interpretation According to Marcus Theory of Electron Transfer Reactions. **D. A. Corrigan, D. H. Evans.**
4:00—64. A Comparison of Differential Pulse Polarographic and Gas Chromatographic Methods for the Analysis of N-nitrosodiethanolamine in Synthetic Cutting Fluids. **M. R. Smyth, P. G. Rowley, J. G. Osteryoung.**
4:20—65. Amperometric Determination of Polyhydroxy Compounds by Means of Metal Oxide Electrodes. **K. G. Schick, C. O. Huber.**
4:40—66. The Application of Twin-Electrode Thin-Layer Voltammetry for the Elimination of Intermetallic

New Varian Model 3700–the greatest gas chromatograph–the one that lets you do better gas chromatography

You can do better gas chromatography with the new Varian 3700 because it brings together all the major chromatographic breakthroughs plus new, applications-oriented design concepts in every component.

It's Modular... And Model 3700 is modular so you can choose just those components that you want in a chromatograph for your specific application. Here are some of the 3700's great new performance features.

New ESP* monitor continuously checks 3700 operating parameters—injectors, column oven, detectors, flows. And its bright self-diagnostic LED display continuously lets you know whether parameters are at their settings.

New digital controls let you set all chromatographic conditions in a few seconds. And there's no resettability error.

Extra-large, 1350 cubic inch, column oven with removable door gives you more room to install columns.

New Automatic Linear Temperature Programmer (ALTP). So good it will even operate the oven at 12°C above room temperature without cryogenic cooling, giving you increased resolution of low boiling components.

New non-contaminating flame ionization detector reduces down time and obtains accurate detection over a wide range of sample concentrations.

New flame-out indicator light and automatic reignite provide extra FID safety protection and help assure trouble-free automatic operation.

New pulsed ^{63}Ni electron capture detector has a linear dynamic range better than 10^4 and an MDQ better than 0.1 pg of lindane.

New highest sensitivity thermal conductivity detector has a built-in amplifier that can amplify the bridge output signal to the recorder up to 10 times—greatly increasing capability to record and measure trace amounts.

New flame photometric detector with dual-flame design provides high selectivity.

New flow control convenience because all pneumatics are arranged in a large compartment planned for operator access.

New carrier gas flow stability and reproducibility because all critical flow control elements are isolated in an independently heated and thermostatted oven within the pneumatics compartment. This minimizes the effect of laboratory temperature changes and improves the precision and reproducibility of the data.

New flow control automation. New dual Automatic Flow Controller lets you dial-in carrier gas flow rates.

New versatile injector system has universal bases and interchangeable injector bodies including capillary.

New applications automation capabilities. The 3700 combines with the AutoSampler and CDS-111 Chromatography Data System to provide complete GC automation.

For full information on the greatest gas chromatograph ever made, circle ***Reader Service No. 218.*** To have a Varian representative call circle ***Reader Service No. 219.***

*Electro Sensor Panel

Varian Instrument Division
611 Hansen Way, Box D-070
Palo Alto, California 94303

varian

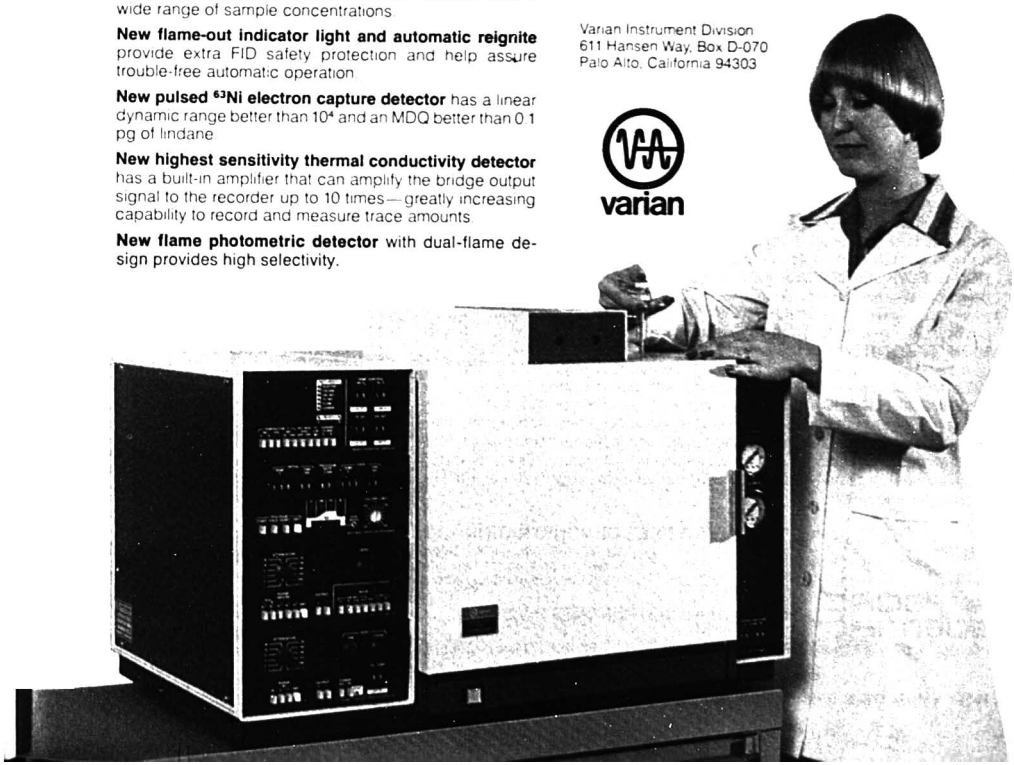

Automatic Sizing Analyzer Plotter

HIAC Model PA-520 ASAP
Automatic Sizing Analyzer Plotter

Measures particle size/volume (weight) distributions with pushbutton simplicity—delivers X-Y plots in 40 seconds!

Just put in the sample, insert a chart and press a button. In less than a minute ASAP measures particle size and computes, in its microprocessor, particle size and volume (weight) distributions. 11" x 17" X-Y plots are automatically delivered in your choice of any or all of six different modes of data presentation, cumulative or differential.

NON-ELECTROLYTIC HIAC® PRINCIPLE/ You don't have to use electrically conductive carrier fluids. You can use water, alcohol, oil, solvents—almost any liquid—even viscous fluids, with HIAC accessories. Standard sensors cover from 1 micron through 1000 microns!

HIGH RESOLUTION PRECISION/ ASAP can analyze up to one million particles per sample, with an accuracy traceable to NBS certified materials. Wide-range sensors analyze broad size distributions quickly, easily.

DIVERSE APPLICATIONS/ Include powdered materials of all kinds—pigments, pharmaceuticals, metals, abrasives, ceramics, sediments, fillers, cement, ash, toners, food products. Liquid applications include emulsions, synthetic fibers, resins, agricultural chemicals, catalysts. Research and Development or Quality Control, ASAP can analyze your material quickly, accurately and easily.

GET A FREE DEMONSTRATION—ASAP!
In your lab on your material—
or send a sample for free analysis
in our Applications Laboratory.

PACIFIC SCIENTIFIC™ HIAC HIAC INSTRUMENTS DIVISION
P.O. Box 3007, 4719 Brooks St., Montclair, Calif. 91763 Phone: (714) 621-3965

CIRCLE 168 ON READER SERVICE CARD

Compound Interferences in Stripping Voltammetry. **E. E. Brooks, W. R. Heineman, D. A. Roston.**

6:00—*Divisional Social Hour* (see Section A for location).

6:45—*Divisional Dinner/Theatre* (see Section A for location).

7:45—*Divisional Business Meeting* (see Section A for location).

SECTION D

Symposium on Novel Instrumental Methods for Probing Polymer Structures *Joint with Division of Polymer Chemistry, Inc.* *(see page 796 A)*

WEDNESDAY MORNING

SECTION A

Palmer House, Wabash Parlor (3rd Floor)

Symposium on Problem Solving: The Analytical Approach

J. T. Vanderberg, Presiding

9:00—67. The Analytical Approach. **C. A. Lucchesi.**

9:15—68. Analytical Problem Solving: Academia's Challenge, Industry's Opportunity. **J. G. Grasselli.**

9:50—Intermission.

10:05—69. An Analysis of the Industrial Analytical Chemist. **J. E. Burroughs.**

10:40—70. Chemical Detectives, The FDA. **C. Meloan.**

11:15—71. Practical Solutions to Circuit Board Production Problems Via Chemical Analysis. **J. W. Mitchell, J. E. Riley.**

SECTION B

Palmer House, Parlor B (6th Floor)

General: Chromatography

P. C. Uden, Presiding

9:00—72. A General Metal Ion LC Detector Using a Copper(II)-Selective Electrode. **R. C. Dorey, P. W. Carr.**

9:20—73. Metal Specific Detection in GC and HPLC with Interfaced DC Plasma Emission Spectrometry. **P. C. Uden, R. M. Barnes, I. E. Bigley, W. G. Elliott, R. J. Lloyd, B. D. Quimby.**

9:40—74. A Novel Two-proton Detector for Liquid Chromatography. **E. S. Yeung, M. J. Sepaniak.**

10:00—75. Silver Nitrate-High Performance Liquid Chromatography of Fatty Methyl Esters. **C. R. Scholfield.**

10:20—Intermission.

10:30—76. Quantitative Stripping of Low Molecular Weight Compounds from a Flowing Air Stream of Porous Polymers and Related Absorbents. **R. J. Sydor, C-H. Chu, D. J. Pietrzyk.**

New...Varian Automatic Liquid Chromatograph

It increases sample throughput, improves reproducibility, and automatically calculates and reports analysis results.

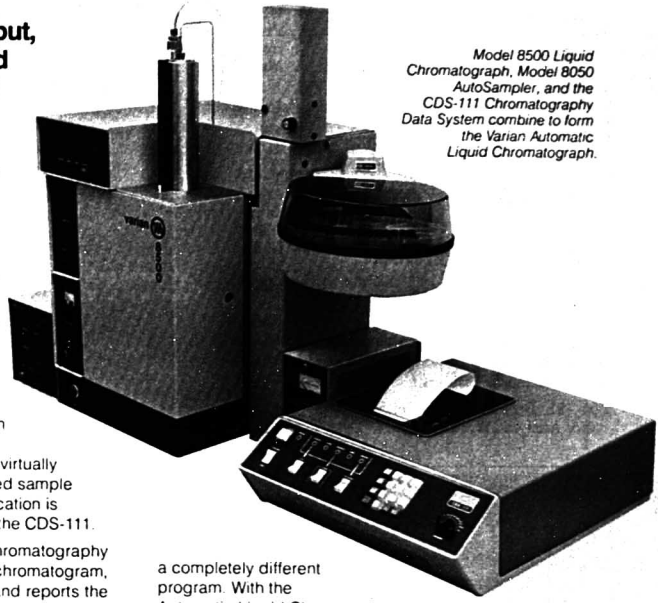

Model 8500 Liquid Chromatograph, Model 8050 AutoSampler, and the CDS-111 Chromatography Data System combine to form the Varian Automatic Liquid Chromatograph.

Varian's new Automatic LC System consists of three high performance components. It is completely automatic from injection through separation, calculations and final report.

The system's Model 8500 positive displacement pump provides the pulseless flow required for good accuracy, reproducibility, detectability and high efficiency.

The reliable 8050 AutoSampler™ obtains injection reproducibilty that sets the standard for automatic liquid chromatography and surpasses the precision of human operation. It can handle up to 60 samples unattended. Sample cross contamination is virtually eliminated because of the dynamic controlled sample purge of all components. All sample identification is encoded for display on the output report of the CDS-111.

The third system component, the CDS-111 Chromatography Data System, automatically integrates the chromatogram, calculates the data by any of six methods and reports the results. Area normalization, internal standard and external standard calculations can be performed, as well as computation of the appropriate response factors needed in these calculations. Up to nine different analytical method files may be stored in memory. On command from the AutoSampler the CDS-111 will automatically change the analytical method file to handle various sample types with a completely different program. With the Automatic Liquid Chromatograph, retention time reproducibilities of better than 1% can commonly be achieved, even with gradient elution analysis. Compositional variances, based on peak area, will be in the range of 1% to 2%.

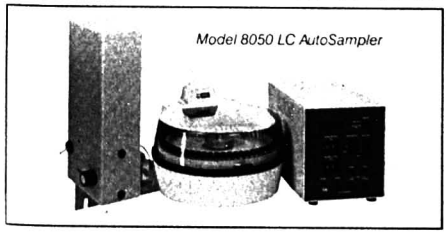

Model 8050 LC AutoSampler

The components of this system: the 8500, the AutoSampler, and the CDS-111, are also available separately. Together, they form the finest automatic LC system available today.

For details, circle the indicated Reader Service Number:	**Reader Service Number**
Automatic Liquid Chromatograph	**125**
Automatic LC System Components:	
Model 8500 Liquid Chromatograph	**126**
CDS-111 Chromatography Data System	**127**
Model 8050 AutoSampler	**128**
To have a representative contact you	**129**

Varian Instrument Division, 611 Hansen Way, Box D-070, Palo Alto, CA 94303

varian

10:50—77. Chemically Modified Surfaces for Normal Phase Chromatography. **R. K. Gilpin, W. R. Sisco.**
11:10—78. The Effect of Crown Ethers on the Ion Exchange Behavior of Selected Mono and Divalent Cations II. **W. H. Delphin, E. P. Horwitz.**
11:30—79. Rapid Liquid Chromatographic Assay of Chloroaniline Isomers. **L. Kesner, S. M. Vratsanos.**
11:40—80. Differential Temperature Programmed Gas Chromatography. **R. Rowan, Jr.**

SECTION C

Symposium on Chromatography of Polymers *Joint with Division of Polymer Chemistry, Inc.* (*see page 796 A*)

WEDNESDAY AFTERNOON

SECTION A

Palmer House, Wabash Parlor (3rd Floor)

Symposium on Problem Solving: The Analytical Approach

D. G. Anderson, Presiding

2:00—81. Problem Solving with Surface Analysis. **W. M. Riggs.**
2:34—82. Water Quality Monitoring—Some Hows and Whys. **J. H. Wiersma.**
3:10—Intermission.
3:25—83. Analytical Chemists at the Launch Pad. **H. D. Bennett.**
4:00—84. The Use of H.P.L.C. to Establish the Optimum Purification Procedure for a Dye Used in Electrophoretic Imaging Devices. **T. I. Martin, P. Macbeth.**

SECTION B

Palmer House, Parlor B (6th Floor)

General

C. L. Wilkins, Presiding

2:00—85. Clinical Profiling with an Ammonia Gas Electrode Based on an Internal Monovalent Cation Glass Electrode. **R. G. Wawro, J. G. Montalvo, Jr.**
2:20—86. Demonstration of Cocaine Metabolite in Human Urine by Thin Layer Chromatography. **A. E. Finkler.**
2:40—87. A Stopped-Flow Clinical Analyzer Which Uses Immobilized Enzyme Reaction Loops. **M. D. Joseph, D. J. Kasprzak, S. R. Crouch.**
3:00—88. A New Enzymatic Method for Measuring Blood Alcohol. **F. S. Cheng, G. D. Christian.**
3:20—Intermission.
3:40—89. Structural Changes of the Chemical Constituents of Petroleum During Biodegradation. **D. M. Jewell, L. Petrakis, J. D. Walker.**
4:00—90. Simultaneous Quantitative Analysis of Prostaglandin $F_{1\alpha}$ and $F_{2\alpha}$ by Mass Fragmentography. **A. Ferretti, V. P. Flanagan.**
4:20—91. The Use of Histograms for Feature Selection in Carbon NMR Pattern Recognition. **T. R. Brunner, C. L. Wilkins.**
4:40—92. A General Instrumental Method for the Measurement of Mercury Vapour in Workroom, Stack and Adjacent Atmospheres. **G. F. Dowd, J. C. Hilborn.**

SECTION C

Symposium on Chromatography of Polymers *Joint with Division of Polymer Chemistry, Inc.* (*see page 796 A*)

THURSDAY MORNING

SECTION A

Palmer House, Wabash Parlor (3rd Floor)

Symposium on Forensic Chemistry

M. J. Camp, Presiding

9:00—Introductory Remarks.
9:05—93. The Mössbauer Spectrometry in the Forensic Characterization of Paint. **F. E. Klink, J. D. Nicol, J. H. Liu, G. V. Smith, M. Saporoschenko.**
9:25—94. X-ray Microanalysis of Physical Evidence. **R. C. Briner, C. R. Longwell, D. E. Smith, T. C. Holt.**
9:45—95. Identification and Differentiation of Raw Micro Marihuana Sample by Standard and Isotope Ratio Mass Spectrometric Techniques. **M. P. Fitzgerald, J. H. Liu, J. D. Nicol, G. V. Smith, R. D. Cole.**
10:05—96. Forensic Characterization of Commercial Bond Papers. **L. A. Wolfe, C. L. Baskin.**
10:25—97. Development of Methods for the Analysis of Some Food Products in Customs Laboratories. **M. J. Prager, M. A. Miskiewicz.**
10:45—98. The Effect of Environmental Factors on Genetic Markers in Human Bloodstains. **H. C. Lee, R. E. Gaensslen, P. R. DeForest, D. Crim.**
11:05—99. Identification of Some Positional and Chemical Analogues of Methaqualone. **S. A. Angelos, T. A. Dal Cason, O. Washington.**

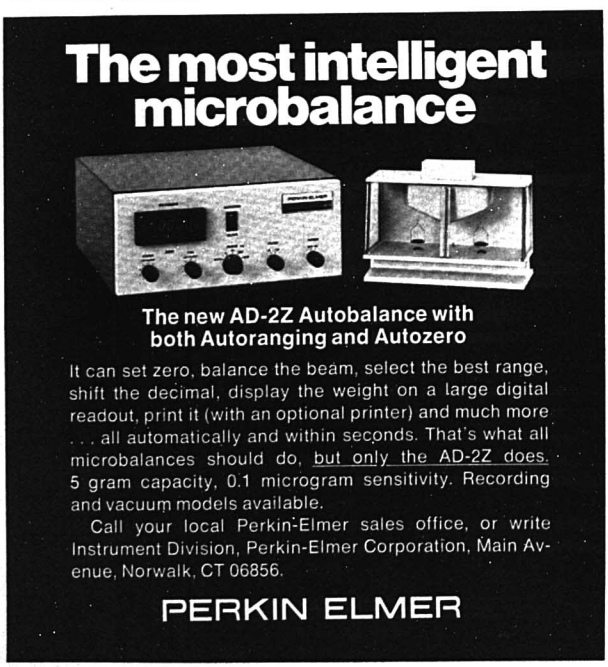

CIRCLE 167 ON READER SERVICE CARD

Compute your sample's

UV absorbance and...

FIRST CLASS
PERMIT NO. 12
NORWALK, CT

BUSINESS REPLY MAIL

NO POSTAGE STAMP NECESSARY IF MAILED IN THE UNITED STATES

POSTAGE WILL BE PAID BY

Perkin-Elmer Corporation
Main Avenue MS 12
Norwalk, CT 06856

Apply micro

Microprocessor Control. Perkin-Elmer's Model 340 is the world's first microprocessor controlled recording UV-VIS-NIR spectrophotometer and heralds a new era of instrument design. The transmission in both the sample and reference beams is directly converted to digital values; their ratio computed and then the resulting sample absorbance or concentration calculated. The microprocessor obsoletes the conventional analog logarithmic amplifier and its associated drift, providing increased stability and eliminating trimpots and correlation controls. The microprocessor also controls the instrument's wavelength drive, providing a digital display of wavelength and automatically selecting the appropriate source, grating and detector.

A major contributor to photometric error, especially at higher absorbance levels, is stray light. The Model 340 employs a prism-grating double monochromator to reduce stray light to negligible levels and can record linearly from 0 - 4A.

Photometric Fidelity. The 57 series incorporate a unique photometric system which ensures that sample and reference measurements are carried out under identical wavelength conditions. As the instrument scans, the

Please send me more information. ANC

Name _____ Title _____

Department _____ (PLEASE PRINT)

Firm _____

Address _____

City _____ State _____ Zip _____

Telephone Number (_____)

INFORMATION REQUESTED: ☐ Model 57 Series ☐ Model 340

☐ Photometric design requirements

☐ Scattered transmission accessory

☐ Second derivative spectroscopy

I intend to purchase in 3 months 6 months 12 months
(CIRCLE ONE)

☐ I would like a representative to call

Please send me a quotation on _____

processor technology to UV spectroscopy and...

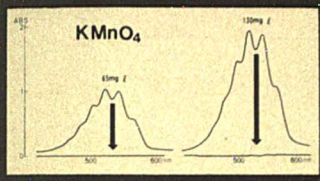

The 340's baseline corrector can compensate spectra up to 2A; even draw a difference spectrum without using the reference beam.

monochromator stops to allow the ratio of transmittance to be measured at successive wavelengths. The result is a series of discrete digital values of transmittance associated with specific wavelengths irrespective of scanning speed or reference absorption.

Each member of the 57 series can be equipped with a digital background corrector which flattens the instrument's baseline to ±0.001A. The flat background aids interpretation of difference spectra and eliminates the need to record a baseline for every quantitative measurement.

Difficult Samples. Turbid and sold samples produce photometric errors due to energy loss by scattering. The 57 series has a scattered transmission accessory where such difficult samples can be placed close to a large, endon-window, photomultiplier. Much of the scattered energy is recollected by the detector and values closer to the time sample absorbance are recorded. The Model 340 can be equipped with a selection of integrating spheres covering its wide UV-VIS-NIR range to allow examination of solid samples by reflection.

If the tear-off card has been used, for further information contact: Instrument Division, Norwalk, CT 06856 USA; Bodenseewerk Perkin-Elmer & Co., GmbH, 7770 Ueberlingen, West Germany

...assure photometric fidelity!

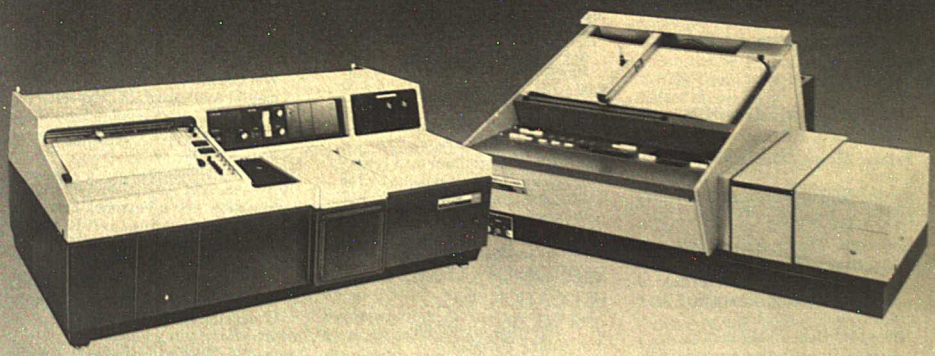

PERKIN-ELMER

CIRCLE 174 ON READER SERVICE CARD

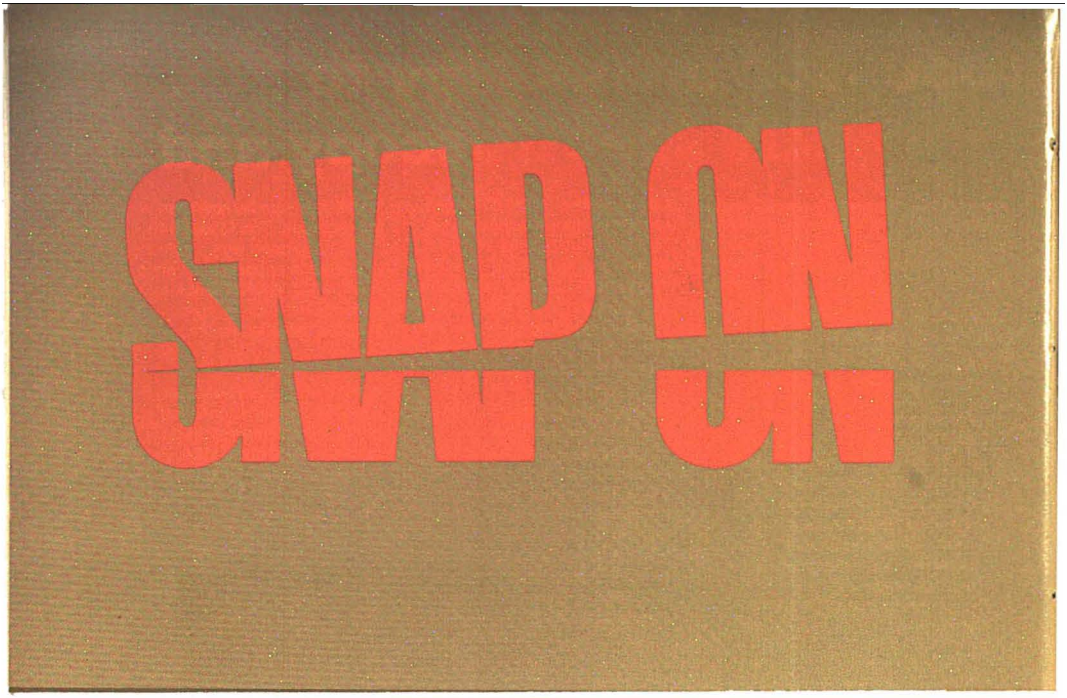

News

SECTION B

Symposium on Chromatography of Polymers *Joint with Division of Polymer Chemistry, Inc.* (*see page 796 A*)

SECTION C

Symposium on the Present Status of the Teaching of Analytical Chemistry *Joint with Division of Chemical Education, Inc.* (*see page 794 A*)

THURSDAY AFTERNOON

SECTION A

Palmer House, Wabash Parlor (3rd Floor)

Symposium on Forensic Chemistry

H. C. Lee, Presiding

2:00—100. The Crystal and Molecular Structure of Two Forensically Important Substances. **D. Canfield, J. C. Barrick, M. J. Camp, B. C. Giessen.**

2:20—101. Genetic Markers in Semen: Quantitative Analysis of Polymorphic Proteins. **G. F. Sensabaugh, E. T. Blake.**

2:40—102. Review of LEAA—AEROSPACE Gunshot Residue Detection Program. **G. M. Wolten.**

SECTION B

Symposium on the Present Status of the Teaching of Analytical Chemistry *Joint with Division of Chemical Education, Inc.* (*see page 794 A*)

General

3:40—103. Computer Controlled Spectropolarimetry. **V. C. Zadnik, J. L. Scott, R. M. Megargle, K. H. Pearson.**

4:00—104. Computer Controlled Spectropolarimetric Titrimetry. **J. L. Scott, V. C. Zadnik, R. M. Megargle, K. H. Pearson.**

4:20—105. Determination of Ionic Species in Engine Coolants by Ion Chromatograph. **E. Chladek, L. C. Westwood.**

DIVISION OF CHEMICAL EDUCATION, INC.

R. W. Ramette, *Chairman*
J. A. Young, *Secretary*

THURSDAY MORNING AND AFTERNOON

Pick Congress, Gold Room (2nd Floor South)

Symposium on the Present Status of the Teaching of Analytical Chemistry *Joint with Division of Analytical Chemistry*

T. R. Williams, Presiding

9:00—Introductory Remarks.

9:10—45. Analytical Chemistry in an Integrated Laboratory Sequence. **K. E. Dolbow.**

9:40—46. Analytical Chemistry at a Community College: A Balance of Wet Chemical Methods and Instrumental Analysis. **J. M. Hayes.**

10:10—47. The Sophomore Level Analytical Laboratory for Non-Majors. **R. A. Pacer.**

10:40—Intermission.

10:50—48. The Analytical Textbook Situation: Can a Textbook Present Analytical Chemistry as It Really Is? **R. H. Bromund, T. R. Williams.**

11:20—49. Industrial Expectations of the Recent Graduate in Analytical Chemistry. **J. C. Abbott.**

11:50—Concluding Remarks.

2:00—50. The Graduate Level Analytical Chemistry Teaching Program at the University of Massachusetts. **R. M. Barnes, D. J. Curran, J. E. Roberts, S. Siggia, P. C. Uden.**

a new head for 10X to 500X better AA sensitivity

the 10^{-10} to 10^{-14} gram range when you replace the burner head of your AA unit with the atomizer head of our **flameless accessory.**

It instantly adapts all Jarrell-Ash atomic absorption spectrophotometers for ultra-trace analysis.

Only the Jarrell-Ash FLA-100 accessory offers you **true air ashing.** Dramatically cuts background by completely burning off carbonaceous materials. (In the picogram neighborhood you're working in, this can make all the difference.)

FLA-100 provides another outstanding capability. **Temperature** complete freedom to select the best operating conditions for a sample.

You also get **flash atomization.** To well over 3000°C. Hence minimum tailing, maximum sharpness — even with elements like Vanadium.

Our accessory internally monitors current to its atomizer head, automatically corrects for deviations. (Comfort in time of brownouts.) Our advanced tube design maintains sensitivity as tube ages. And there's output for a variety of accessories.

Send for brochure. Or phone Dr. Morganthaler at JA to talk ultra-trace **direct.** Number is (617) 890-4300.

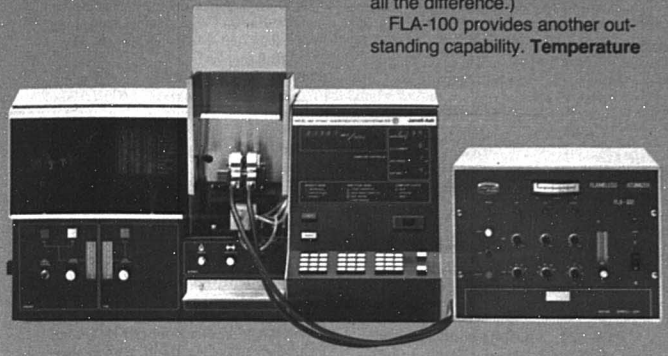

AA problem-solver.

Fisher Scientific Company
711 Forbes Avenue
Pittsburgh, PA 15219
(412) 562-8300

CIRCLE 78 ON READER SERVICE CARD

2:30—51. The Making of the Analytical Chemist—1977. Conflicts in Graduate Education. **L. R. Faulkner.**
3:00—Panel Discussion on the Teaching of Analytical Chemistry. **R. Large, Chairman, L. R. Faulkner, P. C. Uden, J. G. Grasselli, J. C. Abbott.**
4:30—Concluding Remarks.

DIVISION OF POLYMER CHEMISTRY, INC.

V. T. Stannett, *Chairman*
E. J. Vandenberg, *Secretary*

MONDAY MORNING

Palmer House, P.D.R. #14 (Club Floor)

Symposium on Novel Instrumental Methods for Probing Polymer Structures *Joint with Division of Analytical Chemistry*

A. N. Gent, Presiding

9:00—Introductory Remarks.
9:10—7. Noise Phenomena Associated with Flow and Thermal Transitions in Polymeric Systems. **C. Klason, J. Kubát.**
9:30—Discussion.
9:40—8. Acoustic Emission of Crazing Polymers. **A. Peterlin.**
10:00—Discussion.
10:10—9. The Nanotensilometer—An Accurate, Sensitive Tensile Test Instrument. **C. G. Andeen, R. W. Hoffman.**
10:30—Discussion.
10:40—10. An Apparatus and Method for Measurement of Nonlinear Viscoelastic Properties of Polymers in Cyclic Deformation under a Relatively Large Strain Amplitude. **Y. D. Kwon, R. K. Sharma, D. C. Prevorsek.**
11:00—Discussion.
11:10—11. Stress Mass Spectrometry of Polymeric Materials. **M. A. Grayson, C. J. Wolf.**
11:30—Discussion.

MONDAY AFTERNOON

Palmer House, P.D.R. #14 (Club Floor)

Symposium on Novel Instrumental Methods for Probing Polymer Structures *Joint with Division of Analytical Chemistry*

A. M. Jamieson, Presiding

2:00—Introductory Remarks.
2:10—25. The Characterization of Organic Polymers Via Pyrolysis-IR. **W. L. Truett.**
2:30—Discussion.
2:40—26. Thermal Degradation Mechanisms and Structural Differentiation of Polymers by Pyrolysis-Mass Spectrometry. **M. Przybylski, I. Luderwald, H. Ringsdorf.**
3:00—Discussion.
3:10—27. Inelastic Electron Tunneling Spectroscopy of Chemisorbed Substances. **H. T. Chu, N. K. Eib, A. N. Gent, P. N. Henriksen.**
3:30—Discussion.
3:40—28. A Molecular Probe of Mechanical Transitions. **J. L. Koenig, W. W. Hart.**
4:00—Discussion.
4:10—29. ESCA Characterization of Structure and Bonding in Polymers. **D. W. Dwight, J. E. McGrath, J. P. Wightman.**
4:30—Discussion.

TUESDAY MORNING

Palmer House, P.D.R. #14 (Club Floor)

Symposium on Novel Instrumental Methods for Probing Polymer Structures *Joint with Division of Analytical Chemistry*

M. Litt, Presiding

9:00—Introductory Remarks.
9:10—45. Certain Aspects of the Dynamics of Polymers Studied by Neutron Transmission. **L. A. Vinhas.**
9:30—Discussion.
9:40—46. Small Angle Neutron Scattering of High Polymers. **J. S. King, R. Ullman.**
10:00—Discussion.
10:10—47. Brillouin Scattering from Polymers. **G. D. Patterson.**
10:30—Discussion.
10:40—48. Characterization of Polymer Structure in Solution by Quasi-elastic Light Scattering Techniques. **A. M. Jamieson.**
11:00—Discussion.
11:10—49. Studies of Polymer Dynamics by Multipass Fabray Perot Spectroscopy (MPFPS). **S. M. Lindsay, I. W. Shepherd.**
11:30—Discussion.

TUESDAY AFTERNOON

Palmer House, P.D.R. #14 (Club Floor)

Symposium on Novel Instrumental Methods for Probing Polymer Structures *Joint with Division of Analytical Chemistry*

W. L. Truett, Presiding

2:00—Introductory Remarks.
2:10—64. Ion Recombination Luminescence of Heterogeneous Polymer Systems. **G. G. A. Bohm, K. R. Lucas.**
2:30—Discussion.
2:40—65. Study of Polymer Structures and Motions by Electron-Electron Double Resonance. **J. C. W. Chien, H. Yang.**
3:00—Discussion.
3:10—66. Structural Analysis by Diffusion Measurements. **K. T. Chaing, M/ V. Sefton.**
3:30—Discussion.
3:40—67. Use of Mössbauer Spectroscopy in Ion Containing Polymers. **C. T. Meyer, M. H. Pineri.**
4:00—Discussion.
4:10—68. Small Angle Neutron Scattering Studies of Crystalline Isotropic Polypropylene. **D. G. H. Ballard, J. Schelten, G. W. Longman.**
4:30—Discussion.

WEDNESDAY MORNING

Palmer House, P.D.R. #18 (Club Floor)

Symposium on Chromatography of Polymers *Joint with Division of Analytical Chemistry*

E. Drott, Presiding

9:00—Introductory Remarks.
9:05—69. Modern High-Performance GPC in Polymer Analysis. **D. D. Bly.**
10:00—70. Separation of Polymers by Field-Flow Fractionation (One Phase Chromatography). **J. C. Giddings, M. N. Myers, G-C. Lin, S. L. Brimhall, M. Martin, L. K. Smith.**
10:30—71. Crystallizability Distributions in Polymers: A New Analytical Technique. **L. Wild, T. Ryle.**
10:55—72. Application of the Plasma Chromatograph to Polystyrene. **M. Dole, C. V. Gupta, L. L. Mack, K. Nakamae.**
11:25—73. An Overview of Gas-Chromatographic Applications to Analysis of Polymer Microstructure. **S. A. Liebman.**

WEDNESDAY AFTERNOON

Palmer House, P.D.R. #18 (Club Floor)

Symposium on Chromatography of Polymers *Joint with Division of Analytical Chemistry*

J. Harmon, Presiding

2:00—79. Solute-Gel Interactions in GPC with Organic Eluents. **J. V. Dawkins.**
2:35—80. Particle Porosimetry by Inverse Gel Permeation Chromatography. **D. H. Freeman, I. C. Poinescu.**
3:05—81. Recent Advances in Aqueous Gel Permeation Chromatography. **A. R. Cooper, D. S. Van Derveer.**
3:35—82. Some Applications of Modern GPC and Comparison with Liquid Chromatography. **A. Revillon.**
4:05—83. Multidetector System for Gel Permeation Chromatography. **Z. Grubisic-Gallot, H. Benoit.**
4:35—84. GPC Analysis of a Branched Condensation Polymer Incorporating Radiolabeled Branching Agent or Terminator. **S. deKeczer, P. L. Dubin, R. Hale, M. Kronstadt, A. R. Read.**
5:30—*Divisional Social Hour* (Joint with Cellulose, Paper and Textile Division and Division of Organic Coatings and Plastics Chemistry). Palmer House, State Ballroom (4th floor).

THURSDAY MORNING

Palmer House, P.D.R. #18 (Club Floor)

Symposium on Chromatography of Polymers *Joint with Division of Analytical Chemistry*

M. Ezrin, Presiding

9:00—90. Standardization of GPC Techniques. **D. D. Bly, J. V. Dawkins, E. E. Drott, R. F. Kratz, A. Revillon.**
9:40—91. Numerical Treatment of Gel Permeation Chromatography Data. **A. R. Cooper, D. P. Matzinger.**
10:00—92. Influence of Li-Br on the Exclusion Chromatography of Poly-(N-vinylacetamide) on Silanized Porous Glass in DMF. **P. L. Dubin, V. P. Miller.**
10:30—93. Gel Chromatographic Studies on Degradation Reactions in Bisphenol A Polymers. **K. B. Abbâs.**
11:00—94. m-Cresol as a Gel Permeation Chromatography (GPC) Solvent. **H. L. Browning, Jr., J. R. Overton.**
11:30—95. High Performance GPC with Silica Microspheres. **J. V. Dawkins, G. Yeadon.**

Royal Honor for Australian Scientist

Alan Walsh, widely known to analytical chemists for his invention of the atomic absorption spectrophotometer, was recently honored by Queen Elizabeth II of England, who is also Queen of Australia, by being created a Knight Bachelor, one of 38, at the Birthday Celebration and Jubilee.

Sir Alan Walsh

Sir Alan, a native of Lancashire, England, was educated at the University of Manchester. After receiving a Master of Science Degree in x-ray crystallography, he joined the British Non-Ferrous Metals Research Association as a spectroscopist in 1939 and while there, he developed and patented a multi-purpose source unit for emission spectroscopy that is still being manufactured commercially.

In 1947 he went to Australia to join the Chemical Physics Section of the Division of Industrial Chemistry of the Council for Scientific Industrial Research. There he began fundamental studies on emission methods of spectrochemical analysis, but at the

Fast, total surface analysis... all sample types, all fields, monolayers to bulk, trace to gross. That's Analytical Systems' capability.

The kind of capability that lets you solve problems in production, quality control, research and development. Capability that can provide vital information about the elemental makeup of the outermost layers of your sample surface. Capability that 3M can offer in a complete unit or as modular additions to your existing surface analysis equipment.

3M's ion beam technologies (ISS and SIMS) have been combined to provide new dimensions in sensitivity for surface analysis. These user-proven techniques and other significant 3M ion beam developments include the SIMS attachment for SEM, the MiniBeam Ion Gun Systems, and the high-sensitivity ISS/CMA. Data processor and data storage systems are also available for both ISS and SIMS systems to help you solve your specific surface analysis problems.

Applications of 3M ion beam systems are numerous. Consider the following:

Metals—Identification of trace elements (ppm to ppb) including H, D, low Z elements and all isotopes by SIMS and high Z elements by ISS for both surfaces and as thin film depth profiles, for solutions to problems pertaining to grain boundary fracture, adhesion, contamination, friction, oxidation and semiconductor dopants.

Glasses—Eliminate charging problems to routinely obtain reliable analysis for all surface elements without the need for carbon or gold coating, silver paste or other troublesome sample procedures.

Ceramics—Monitor trace additives or contaminations.

Catalysts—Identify undesirable contaminations and poisons, and obtain structural information of volatile absorbants using residual gas analysis.

Polymers—Correlate properties such as bonding, oxidation, hardness, etc., with minor modifications to the surface chemistry of the outermost atomic layers.

Powders—Study thin coatings, contaminations and small segregations of insulating powders directly.

If you're serious about expanding your surface analysis capabilities, you should consider ISS and SIMS technologies as additions to the techniques you are now using. And, if you're starting from scratch, start with 3M Analytical Systems. Whatever the material, whatever the surface analysis problem, 3M can help you solve it. For more information on 3M Brand surface analysis instruments, call 612/733-3909, or write: Analytical Systems, 3M Company, 3M Center, Building 209, St. Paul, MN 55101.

The above ISS spectrum showing the top 4 Å of a salmon fish scale was obtained in 32 seconds using ^3He at 3000 eV and 200 nA beam current. Arsenic was observed at this high concentration only on the outermost 2 to 5 Å. This work contributed to ecology and environmental studies.

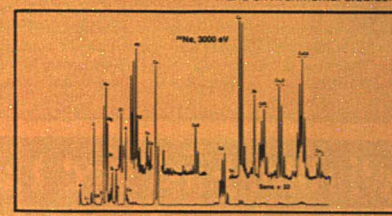

The SIMS spectrum illustrates high detection sensitivity and chemical bonding information routinely obtained during surface studies of solar cell material. A dynamic range of 10^4 to 10^7 is commonly applicable in SIMS studies of trace contaminants.

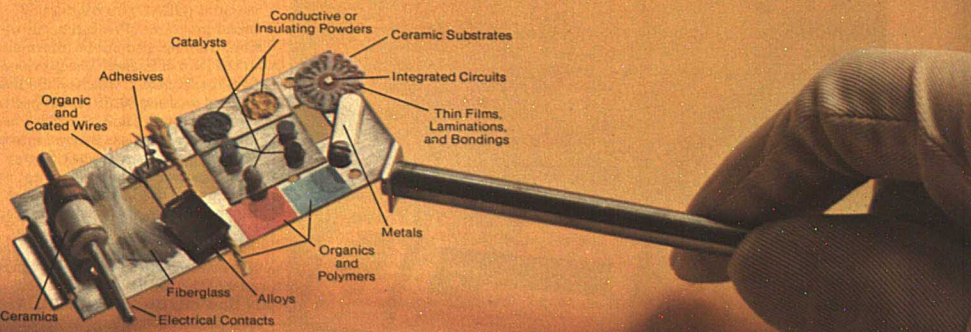

Complete ISS/SIMS System with Data Processor and Storage.

ISS and SIMS Attachment Systems.

3M COMPANY

CIRCLE 141 ON READER SERVICE CARD

same time became interested in the problems of IR. This led him to develop a device for converting a single monochromator to a multiple monochromator. This invention was patented in 1950 and was licensed to The Perkin-Elmer Corporation, who for some years incorporated it in their single-beam infrared spectrometers.

It was in 1952 that he conceived the idea of using measurements of atomic absorption rather than emission for the determination of metals, and in early 1954 a working atomic absorption spectrophotometer was demonstrated at an exhibition held in Melbourne by the Institute of Physics. It created no interest whatsoever, and indeed it was some years before analytical chemists and instrument manufacturers took notice of the new technique, which was to revolutionize the determination of metals in such diverse fields as medicine, agriculture, geochemistry, metallurgy, and environmental studies.

In recent years his research efforts have mainly been in the development of other novel instruments and techniques of potential use in spectrochemical analysis, such as boosted-output hollow cathode lamps, atomization of solid samples by cathodic sputtering, and non-dispersive spectroscopic systems.

Among the many awards he has received may be mentioned the Talanta Gold Medal (1969), the Maurice F. Hasler Award (1972), the Torbern Bergman Medal (1976), and the Royal Medal of the Royal Society of London (1976). He was elected Fellow of the Australian Academy of Science (1959), Honorary Member of the Society for Analytical Chemistry, London (1969), Foreign Member of the Royal Academy of Sciences, Sweden (1969), and Fellow of the Royal Society of London (1969).

Sir Alan retired from the CSIRO Division of Chemical Physics in January 1977.

NIH Chemist Awarded

Donald Young of the National Institutes of Health, Bethesda, Md., has been named to receive the 1977 Award for Outstanding Contributions to Clinical Chemistry by the American Association for Clinical Chemistry. The award, sponsored annually by Ames Co., a Division of Miles Laboratories, will be presented at the Association's 29th Annual Meeting in Chicago, July 17–22, 1977. The award recognizes Dr. Young's achievements in improving laboratory performances, laboratory data handling by computers, and new analytical techniques such as kinetic nephelometry and the miniature centrifugal analyzer. He is also cited for his editorial contributions to *Clinical Chemistry*, the association's monthly journal. Dr. Young is a former review (clinical chemistry) author of ANALYTICAL CHEMISTRY as well.

Donald Young

ERDA Extends Contract with Oak Ridge Associated Universities

The Energy Research and Development Administration (ERDA) has extended for a five-year period its contract with Oak Ridge Associated Universities (ORAU) for conducting broad programs of research, education, training, and public information in the field of energy. The previous five-year contract, which would have expired on June 30, 1977, has been extended through June 30, 1982. The original contract was entered into in 1947 by the former Atomic Energy Commission and the predecessor organization to ORAU, the former Oak Ridge Institute of Nuclear Studies. ORAU is a nonprofit corporation sponsored by 45 colleges and universities primarily in the southeastern region of the U.S.

Under its contract with ERDA, ORAU conducts a large biomedical research program that conducts interrelated research programs in immunology, biochemistry, radiopharmaceuticals, epidemiology, and radiation biology that focus on chemical toxicants and radiation problems related to energy production and development. An important objective is to improve methods of treatment of accidental radiation exposures.

CIRCLE 140 ON READER SERVICE CARD

We stock a broad spectrum of chemicals

Chemicals are just one part of the S/P Responsive System

S/P, a *leading* distributor of chemicals, instrumentation and supplies, offers you a wide choice of acids, inorganics and organics throughout its computerized network of 25 stocking locations. And, if back orders are a problem, your S/P Representative can respond. He carries a microfiche which enables him to quickly determine the availability of all 55,000 items stocked. With an inventory set-up like this, we are able to stock seldom used chemicals and laboratory supplies, *specifically for you.* It's all part of our S/P Responsive System. Call your S/P Representative. He'll respond—in a hurry.

Inventory? $60 million of stock includes 55,000 items and $5 million of chemical inventory.

Back Orders? Microfiche weekly inventory list shows you complete stock and provides alternatives.

Order Processing? Central computerized order system is designed to process orders in one day.

Delivery? A private fleet of S/P trucks provides dependable local delivery...fast!

Economy? Multi locations or single location, large or small, S/P has systems to reduce your inventory and paperwork and thereby your total cost of acquisition.

Personal Contact? Your face-to-face contact is the S/P Representative—a trained business and technical professional. Inside S/P, you are assigned a personal Customer Service Representative who is familiar with your lab's needs.

Our service system works because we have people who care enough to make it work for you.

We're responsive

scientific products
distributor of chemicals, laboratory supplies and scientific instruments

Division of American Hospital Supply Corporation
1430 Waukegan Road, McGaw Park, IL 60085

CIRCLE 190 ON READER SERVICE CARD

Analytical Chemistry at Work

Chromatography Leads in Techniques Reported in ANALYTICAL CHEMISTRY

Approximately 30% of the papers published in ANALYTICAL CHEMISTRY in 1976/77 are concerned with chromatographic techniques. This compares with about 24% ten years ago. Although gas chromatography is still the leading chromatographic technique, the overall increase in chromatography papers is primarily the result of research in liquid chromatography and combined gas chromatography/mass spectrometry methods. The number of papers covering chromatography published in ANALYTICAL CHEMISTRY in the recent 12-month period, 176, tops the number of papers published in this field in the same period in some of the specialized chromatography journals.

These data were accumulated by studying by technique the published papers in ANALYTICAL CHEMISTRY from July 1976 to June 1977 and a like period in 1966/67. Trends in the use of various techniques may be divined, but a heavy reliance cannot be placed on the individual data because of the difficulty in deciding classifications of some papers. For instance, for our purposes we classified GC/MS papers as chromatographic, whereas others might well classify them as mass spectrometric papers. With these limitations in mind, it is still possible to form some tentative conclusions about the use of various analytical methods based on the data.

For instance, about 28% of the research papers in ANALYTICAL CHEMISTRY deal with spectrometric methods. This is the same percentage as 10 years ago. However, the division of papers within this specialization has changed. The number of papers concerned with atomic absorption, fluorescence, mass spectrometry, x-ray fluorescence, and Raman has increased. A decrease has occurred in ultraviolet/visible and infrared spectrometry. The greatest decrease, from 10% in the 1966/67 period to less than 4% in 1976/77, is in UV/VIS spectrometry. This, of course, does not mean these methods are less important—only that there are now fewer research papers dealing with these methods.

The third major specialization, electroanalytical methods, increased slightly. In 1976/77, 15% of the papers were in the electrochemical areas, compared with 13% in the 1966/67 period. Again, the division within the specialization shows a large increase (eight times) in papers dealing with ion selective electrodes with a corresponding decrease in papers in other branches of electroanalytical chemistry.

Also confirming the trend of slower growth rates in activation analysis research papers mentioned by Braun et al. in last month's REPORT, page 682 A, are nuclear methods which are represented by only 4% of the total papers published in 1976/77. This is down from 7% ten years ago. It is well to remember, however, since the total number of papers studied in both time periods is over 550, 4% during 1976/77 is not an insignificant number.

The most noticeable trend observed in delineating the subject matter by technique of papers published in ANALYTICAL CHEMISTRY is the large increase in papers concerned with detection, sampling methods, and the recording, handling, evaluation, and analysis of data. Into these areas fall many of the computer papers. There is a corresponding decrease in papers dealing with limited procedural studies. There is also a greater variety of techniques in the analytical chemist's arsenal today. This shows up as 10% of the total number of papers which are not classifiable under MAJOR technique headings vs. about 7% in that category 10 years ago.

An overwhelming increase in the number of papers concerned with the environment is shown if applied papers in ANALYTICAL CHEMISTRY are examined for the field in which the research is used or proposed for use. Further analysis shows increased numbers of papers in the clinical, biological, and pharmaceutical areas. Nevertheless, many papers, as might be expected, deal with innovations and refinements in analytical techniques that have applications in myriads of fields.

Pittsburgh Conference Scores High as Trade Show

Although not one of the largest trade shows attendance-wise, the Pittsburgh Conference on Analytical Chemistry and Applied Spectroscopy placed first on lists of the 10 shows with highest "buying" scores. In a two-part article (*Industrial Marketing*, April and May 1977 issues) Richard K. Swandby and Jonathan Cox of Exhibit Surveys reported trade show trends resulting from their survey of 31 shows in 1976.

The Pittsburgh Conference was outstripped on attendance by many other shows, such as the Offshore Technology Conference and the National Restaurant Hotel/Motel show. Nevertheless, 71% of the audience at the Pittsburgh Conference indicated they had

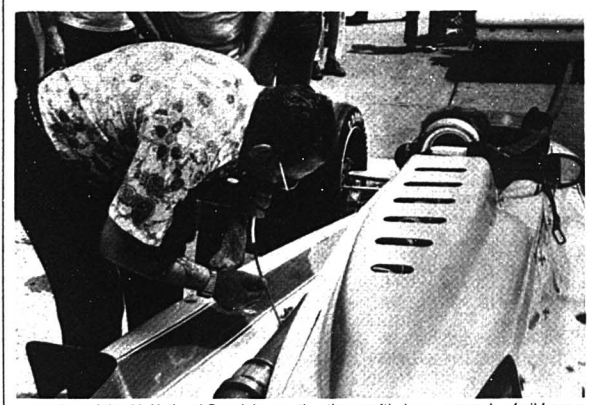

A member of the Air National Guard, in vacation-time mufti, draws a sample of oil from a racing car entered in the Indianapolis Speedway 500 Memorial Day race. The oil is analyzed by atomic absorption for wear metals to determine which parts of the engine are wearing. Other tests given free under the supervision of the U.S. Auto Club include use of an infrared spectrophotometer to test fuels for illegal additive boosters. Substances such as nitromethane or other oxygen-bearing additives that would turn the engines over faster might be added to the cars' methanol fuel prescribed by the rules. The instruments were lent to the speedway by Perkin-Elmer

Analytical results must be correct: on no account should correctness be jeopardized by compromises in optics and electronics or operator errors.

Zeiss rules out such compromises: with the PM 6 spectrophotometer.

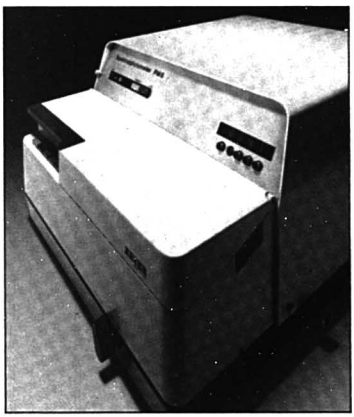

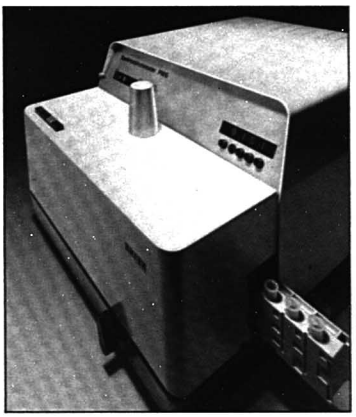

Results provided by any PM 6 spectrophotometer are correct. For:

The double grating monochromator is virtually free from straylight. Any wavelength between 200 and 800 nm can be set and read off to an accuracy of 0.1 nm. No filter and detector change. The band width of 2 nm is narrow enough even for more exacting samples.

Electronics replace controls for gain and exact cell transport. Concentrations or activity data are shown by the digital display with correct decimal point. With autosampler (PM 6P) the photometer analyzes up to 200 samples/hr absolutely unattended. It takes into account sample blanks or common reagent blanks and prints out a concentration report with magazine numbers, sample numbers and other identification data while the next samples are prepared. Photometric perfection without compromises.

Discuss the optimization potential of your lab with us. Even if your budget is tight. Come and see us or write to
Carl Zeiss, D-7082 Oberkochen

ZEISS
West Germany
Focus on the future

CIRCLE 240 ON READER SERVICE CARD

NOW!
LIQUID CHROMATOGRAPHY IS EASY..
..with the Pye Unicam LC3

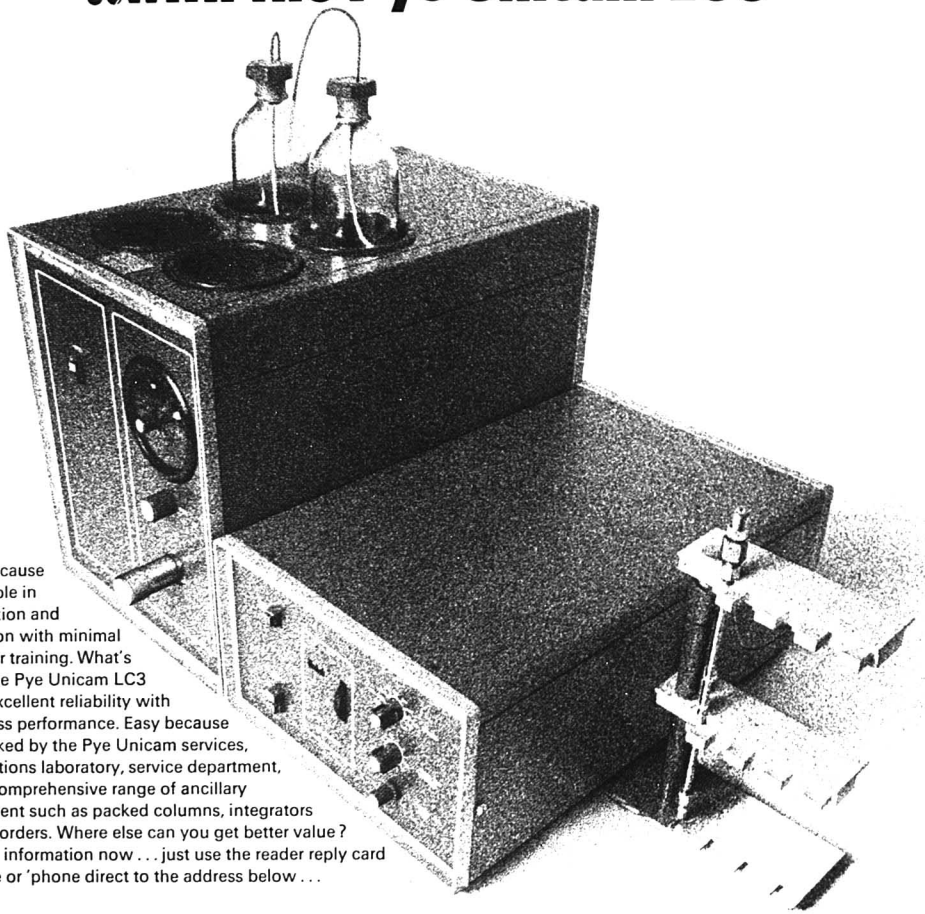

Easy because it's simple in installation and operation with minimal operator training. What's more the Pye Unicam LC3 gives excellent reliability with top-class performance. Easy because it's backed by the Pye Unicam services, applications laboratory, service department, and a comprehensive range of ancillary equipment such as packed columns, integrators and recorders. Where else can you get better value? Get full information now . . . just use the reader reply card or write or 'phone direct to the address below . . .

Pye Unicam Ltd

York Street, Cambridge, England CB1 2PX
Cambridge (0223) 58866. Telex: 817331

A member of the Pye of Cambridge Group

CIRCLE 171 ON READER SERVICE CARD

The Pye Unicam SP 8-100

UV/Visible Spectrophotometer

The Pye Unicam SP8-100 is a major development in the design of precision instrumentation for applications which include scanning and reaction kinetics. High performance is combined with extreme simplicity of operation in a neat and compact package. Bench space is preserved by the built-in recorder and accessories which plug into the control console or fit within the vast sample compartment.

The unique 'Synchroscan' recording principle provides calibrated spectra automatically. 5 bandwidths, 5 chart speeds, 5 scan speeds and 9 recorder ranges from 0.05A give the flexibility required for any sample. High photometric accuracy up to 3A, low noise, fast response and superb stability add up to make the SP8-100 the highest performer in the medium price range.

The very wide selection of accessories includes quick-change attachments for colour measurement, fluorescence, densitometry, column monitoring, turbid samples and automated measurements.

So whatever your application, we're certain that you will discover an SP8-100 system that's Simply the Best for your needs.

Write, phone or use the reader reply service now for full details.

Pye Unicam Ltd

York Street, Cambridge, England CB1 2PX.
Cambridge (0223) 58866. Telex: 817331.

CIRCLE 172 ON READER SERVICE CARD

Flame or Flameless

Pye Unicam AA technology is second to none

The range of Pye Unicam atomic absorption spectrophotometers is now the best ever. With recently-introduced state-of-the-art single and double beam instruments. With an exclusive graphite tube for the SP9-01 that brings new standards of performance to electrothermal atomisation. With a complete range of versatile accessories like the Electrodeless Discharge Lamp System and the automatic Gas Control Unit.
Take time to check the Pye Unicam range against other instruments. Write for our brochures. Only then will you be able to agree that in performance, price, reliability, versatility and ease-of-use Pye Unicam AA spectrophotometers are second to none.

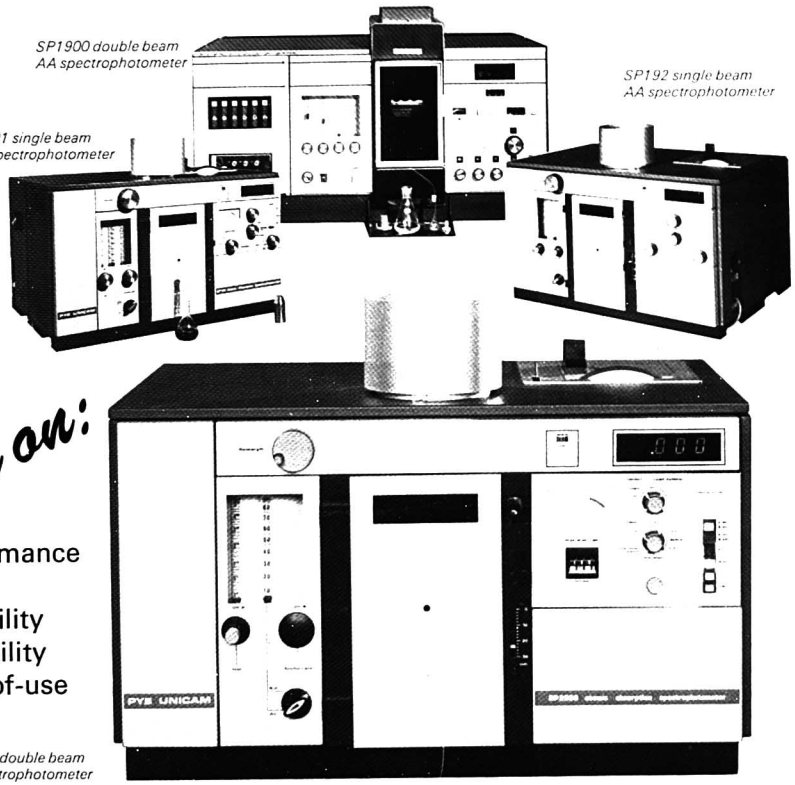

Check on:

- Performance
- Price
- Reliability
- Versatility
- Ease-of-use

SP2900 double beam AA spectrophotometer

Pye Unicam Ltd

York Street Cambridge England CB1 2PX
Telephone: Cambridge (0223) 58866 Telex: 817331

CIRCLE 170 ON READER SERVICE CARD

Why did Varian M.A.T. outsell all competitors in 1976?

Last year, Varian M.A.T.'s high resolution mass spectrometer sales grew to the point where more Varian systems were sold throughout the U.S. than any other brand. Our customers tell us that the primary reason we were selected, time-after-time, is their overall satisfaction with system performance — the result of more than 25 years of unwavering dedication to advancing the state-of-the-art in mass spectrometry.

This dedication has led to developments such as:

- Turbomolecular pumps for exceptionally clean background
- Proven FD/FI/EI ion source
- Temperature-programmable direct probe
- Proven CI/EI source for optimized ion source chamber geometry in both modes, with dual electronic controls
- "DADI" metastable analysis
- Field-regulated magnets

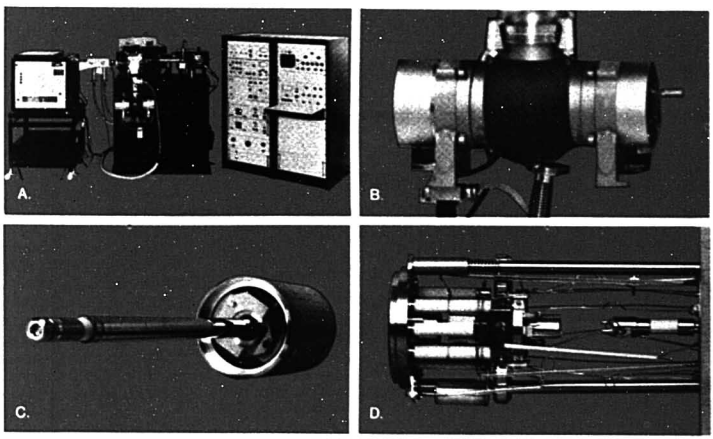

A. Pictured is our Model M.A.T. 311A — one of our most popular high resolution systems. Our other high resolution sector field instruments include the M.A.T. 731 ultra high resolution mass spectrometer with both photographic and electrical recording and the highly flexible M.A.T. 112S reverse geometry GC/MS instrument. CI/EI and FD/FI/EI ion sources are available for all these instruments. **B**. Turbomolecular pumps. **C**. Temperature-programmable direct probe. **D**. FD/FI/EI ion source.

We will continue offering the mass spectrometry community quality without compromise in instruments that provide a significant technological edge.

Give yourself that edge. Send today for our informative new 36-page catalog. Or contact us for a demonstration. Varian M.A.T. Mass Spectrometry, 25 Hanover Road, Florham Park, New Jersey 07932, Telephone (201) 822-3700 •Varian M.A.T. GmbH, Postfach 14 4062, Barkhausenstr. 2, 2800 Bremen 10, West Germany, Tel. (0421) 54931.

varian

CIRCLE 221 ON READER SERVICE CARD

Shown is the interior of one of the five air pollution monitoring trailers delivered to the Du Pont Savannah River Plant in South Carolina. Included in the specially equipped, air conditioned trailer is instrumentation to automatically monitor and record the levels of SO_2, H_2S, and residual sulfurs in air down to the ppb level. All equipment is shock mounted in these trailers assembled by Tracor, Inc. The trailers cost about $20 000 and include special inert sample canes, automatic sulfur gas chromatographs, chart recorders, sulfur calibration systems based on permeation tubes, and hydrogen generators

"buying plans". This was the largest percentage for any show in the survey. Also reported is that 95% of the attendees at the Conference had "buying influence", topping its closest competitive show in this list, the Super Market Institute, which scored 93%.

The "audience interest factor", measured as the average percentage of the audience who stopped to talk or acquire literature at a minimum of 2 out of 10 exhibits from a selected list of 20–25 exhibits included on the survey's questionnaire, also produced a high score for the Conference. Placing second on a list of 10 shows with the highest audience interest factor, the Pittsburgh Conference had 75% and was exceeded in this figure only by the Association of Operating Room Nurses with 83%.

The overall trends in shows for 1976 as determined by the survey indicated that both audience quality and activity indicators equaled the previous all-time highs measured in 1974. Most figures were up, such as attendance, numbers of exhibitors, and net square footage of exhibit space. The article cited above gave details of the survey techniques and the meaning of the results.

In assessing the impact of individual exhibitors, a measure was made of "most remembered" exhibits. In this survey question, attendees were asked to name three of the exhibits that most attracted their attention. The only Conference exhibitor making the list of 10 most remembered exhibits in 1976 was Perkin-Elmer.

Laser Radiation Generated at 38 nm

At the Naval Research Laboratory, optical scientists led by John F. Reintjes have generated coherent laser radiation at a wavelength of 38 nm. This tops the team's earlier achievement, 53.22 nm, reported last fall. The six-member group is seeking improved x-ray laser systems that would provide scientists a new tool for the microscopic study of crystals and giant molecules. These systems could also be used to process and test new materials and provide a new technique for producing super-miniaturized electronic microcircuits.

The coherent radiation was generated in helium at pressures up to 120 torr by seventh harmonic conversion of mode-locked laser pulses at 266.1 nm (the fourth harmonic of a Nd:YAG laser). The radiation was observed photographically with Kodak 101-01 film and photoelectronically with a windowless solarblind photomultiplier.

The pump radiation in the experiment was focused with a 5-cm focal length calcium fluoride lens to a spot size of 5 μm at the center of a 250-μm-diameter aperture, which replaced the entrance slit of a normal incidence vacuum spectrometer. In the earlier experiment last fall, the researchers had used both helium and neon with gas pressures at 40 torr to generate the fifth harmonic of the mode-locked laser pulses at 266.1 nm. The pump radiation was focused with a 10-cm calcium fluoride lens to a spot size of 10 μm at the center of a 500-μm-diameter aperture.

Call for Papers

29th Pittsburgh Conference on Analytical Chemistry and Applied Spectroscopy

Cleveland Convention Center, Cleveland, Ohio. Feb. 27–Mar. 3, 1978. Papers in all aspects of analytical chemistry and spectroscopy are solicited. Symposia are planned on the following topics: recent developments in ion selective electrodes and their biomedical applications, molecular spectroscopy, laboratory systems management, computer information handling in clinical laboratories, automatic analysis comes of age, advances in applied electron spectroscopy, high-performance liquid chromatography in petroleum and synthetic oil characterization, the state-of-the-art in surface analysis, keeping up with computer interfacing and microcomputers, new developments in high-resolution gas chromatography, low and subnanosecond events—IR and UV time-resolved, critical evaluation of procedures for the analysis of nitrogen oxides, analytical chemistry and OSHA, toxicology—emphasis on regulations of FDA, chemical analysis in the steel industry, 1978 awards symposium, Coblentz Award and symposium, and Fourier transform spectroscopy.

Submit three copies of 300-word abstract, not later than Aug. 29, to Robert W. Baudoux, United States Steel Corp., Research Laboratory, MS 57, Monroeville, Pa. 15146.

Meetings

The following meetings are newly listed in ANALYTICAL CHEMISTRY. *The 1977 meetings listed earlier appear in the July issue*

■ **2nd French, American, and Canadian International Congress of Clinical & Analytical Toxicolo-**

5 steps to the easiest Quadrupole GC/MS analysis ever.

. . . now from Varian MAT — the world's first fully-microprocessor-controlled GC/MS.

You won't believe how easy such a sophisticated system can be to operate. Five easy steps make fast work of pollution, drug, pesticide and other chemical analyses.

1 Select E.I. or C.I. operation.

2 Input desired operating parameters via keyboard in response to questions posed and displayed on the TV screen.

3 Inject sample.

4 Press keyboard "space bar" to initiate fully-automated programmed operation. Analysis will be run in its entirety and system will shut down upon completion of run.

5 Readout data via continuous real-time TV screen display of normalized spectra and chromatograms, Or, print-out data on the hardcopy unit. Modify operating parameters as desired during run via keyboard entry.

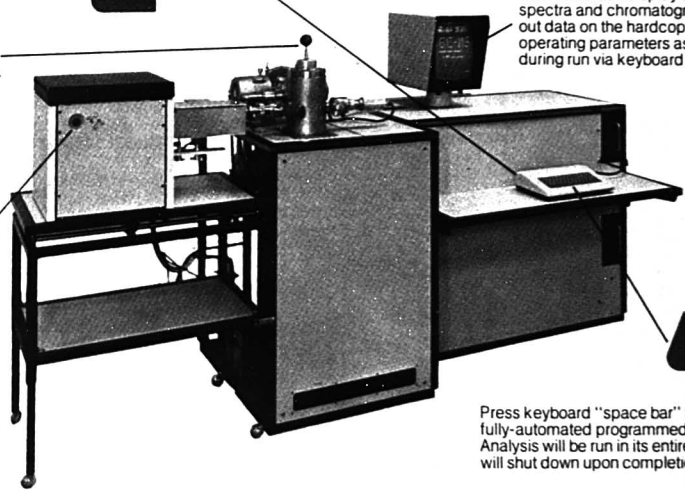

It's that simple to use the Varian MAT-44. It includes all the versatility you need for virtually any type of routine analysis:

- Extended mass range: to 1200
- Oil-free turbomolecular pumps for clean background
- Packed or capillary column GC operation
- Hyperbolic quadrupole analyzer for high sensitivity.
- New SS-200 Data System *simultaneously* acquires and processes data.

Take the first step to seeing this remarkable instrument in action. Call or write today for literature or a demonstration. Telephone (201) 822-3700.

Varian MAT
Mass Spectrometry
25 Hanover Road
Florham Park, N.J. 07932

varian

CIRCLE 222 ON READER SERVICE CARD

gy. Aug. 1–5. St. Adele, Quebec, Canada. *Contact: Yves Lacasse, AMBT (AACT), Santa Cabrini Hospital, Toxicology Unit, 5655 East St. Zotique, Montreal, P.Q., H17 1P7, Canada*

- **Third Symposium on Environmental Aspects of Fuel Conversion Technology.** Sept. 13–16. Diplomat Hotel, Hollywood, Fla. Sponsored by the U.S. Environmental Protection Agency's Industrial Environmental Research Laboratory/RTP. *Contact: Franklin A. Ayer, Research Triangle Institute, P.O. Box 12194, Research Triangle Park, N.C. 27709. 919-541-6260*
- **16th Annual Meeting of ASTM Committee E-19 on the Practice of Chromatography.** Oct. 2–5. San Francisco. *Contact: Gerald Dupre, Bio/dynamics, Inc., Box 43, Mettlers Rd., East Millstone, N.J. 08873*
- **ISA/77 Conference & Exhibit.** Oct. 16–20. International Convention Center, Niagara Falls, N.Y. *Contact: Instrument Society of America/77—Niagara Falls, P.O. Box 34093P, Pittsburgh, Pa. 15230*
- **Advances in Photon-Excited X-ray Fluorescence Analysis.** Nov. 27–Dec. 2. San Francisco. Sponsored by the Isotopes and Radiation Div. of the American Nuclear Society (ANS) and held in conjunction with the ANS winter meeting. *Contact: Enzo Ricci, Analytical Chemistry Div., Oak Ridge National Laboratory, P.O. Box X, Oak Ridge, Tenn. 37830*
- **2nd Annual Toxic Substances Control Conference & Exposition.** Dec. 8–9. Shoreham Americana Hotel, Washington, D.C. *Contact: Government Institutes, Inc., 4733 Bethesda Ave., N.W., Washington, D.C. 20014. 301-657-2922*

Short Courses

ACS Courses. For more information, contact: Department of Educational Activities, American Chemical Society, 1155 16th St., N.W., Washington, D.C. 20036. 202-872-4508

Electroanalytical Chemistry
Chicago. Aug. 26–28. Dennis Evans and Paul Whitson. Given in conjunction with the ACS National Meeting. $255, ACS members; $305, nonmembers

High-Pressure Liquid Chromatography Workshop
Chicago. Aug. 27–28. David Freeman. Given in conjunction with the ACS National Meeting. $245, ACS members; $295, nonmembers

Capillary Gas Chromatography
Chicago. Aug. 27–28. Milos Novotny and Stuart Cram. Given in conjunction with the ACS National Meeting. $245, ACS members; $295, nonmembers

Statistics for Experimental Design
Chicago. Aug. 27–28. John Hromi. Given in conjunction with the ACS National Meeting. $195, ACS members; $235, nonmembers

Thin-Layer Chromatography
Washington, D.C. Sept. 28–29. Victor Rodwell and Donald McNamara. $195, ACS members; $235, nonmembers

Chromatographic Maintenance and Troubleshooting Workshop
San Francisco. Oct. 1–2. John Walker, Minor Jackson, and M.P.T. Bradley. $195, ACS members; $235, nonmembers

Laboratory Safety: Recognition and Management of Hazards
Detroit. Nov. 4–6. Norman Steere and Maurice Golden. Given in conjunction with the FACSS Meeting. $255, ACS members; $305, nonmembers

Column Selection in Gas Chromatography
Detroit. Nov. 10–11. Harold McNair and Walter Supina. Given in conjunction with the FACSS Meeting. $165, ACS members; $205, nonmembers

Thermal Methods of Analysis
Detroit. Nov. 10–11. Wesley Wendlandt and Ilya Sarasohn. Given in conjunction with the FACSS Meeting. $195, ACS members; $235, nonmembers

Electroanalytical Chemistry
New York City. Nov. 17–19. Dennis Evans and Paul Whitson. $255, ACS members; $305, nonmembers

Laboratory Safety: Recognition and Management of Hazards
San Francisco. Dec. 7–9. Norman Steere and Maurice Golden. $255, ACS members; $305, nonmembers

Thin-Layer Chromatography
San Francisco. Dec. 8–9. Victor Rodwell and Donald McNamara. $195, ACS members; $235, nonmembers

Radioimmunoassay
Philadelphia. Aug. 8–20. Jointly sponsored by Philadelphia College of Pharmacy and Science and the Clinical Radioassay Society, Delaware Valley Section. *Contact:* Office of Continuing Education, Philadelphia College of Pharmacy and Science, 43rd St. and Kingsessing Mall, University City, Philadelphia, Pa. 19104

Chemical Analysis of Petroleum Products
Houston, Tex., Aug. 16–18; Edmonton, Alt., Canada, Aug. 30–Sept. 1; Rolling Meadows, Ill., Sept. 20–22. $225. *Contact:* Bill Hart, Hewlett-Packard Co., Route 41, Avondale, Pa. 19311

Applications of Chromatography in Clinical Laboratory
Montreal. Sept. 14–16. $225. *Contact:* Bill Hart, Hewlett-Packard Co., Route 41, Avondale, Pa. 19311

Gas Chromatography/Mass Spectrometry
Chicago. Oct. 6–Nov. 7. Sponsored by the Chicago Section of the Society for Applied Spectroscopy. *Contact:* Paul Bourassa, UOP, Des Plaines, Ill. 60016. 312-391-3380

Modern Techniques in Instrumental Analysis
Texas A&M University, College Station, Tex. Oct. 17–21. Sponsored by the Center for Trace Characterization, Dept. of Chemistry, Texas A&M University, College Station, Tex. $275. *Contact:* Robert Beck Clark, College of Science, Office of the Dean, Texas A&M University, College Station, Tex. 77843

Industrial Hygiene—Recognition, Evaluation, and Control of Occupational Health Hazards
Marriott Inn, Pittsburgh, Pa. Nov. 14–16. $165, IHF members; $225, nonmembers. *Contact:* George Reilly, Industrial Health Foundation, 5231 Centre Ave., Pittsburgh, Pa. 15232. 412-687-2100

For Your Information

The **Environmental Protection Agency (EPA) intends to regulate organic emission** from certain chemical processes as identified by the Agency. In response to EPA's willingness in this connection to consider incorporating valid standard methods of the American Society for Testing and Materials (ASTM) into standard com-

The Gilson Micro-Fractionator:

Compact quality you can carry with one hand— and it doesn't cost you an arm and a leg.

MODEL FC-80
FOR LIQUID CHROMATOGRAPHY
—drop counting or time-actuated fraction collector. Single-unit collector, with base, drop detector, timer and electronic digital counter. Includes two test tube racks. Holds 80 glass test tubes— 13 x 100 mm (9 ml). Size: 29 x 15 cm (11½ x 6 in.)

If you need to collect in larger test tubes, the Model FC-100 holds 100 test tubes, 18 x 150 mm.

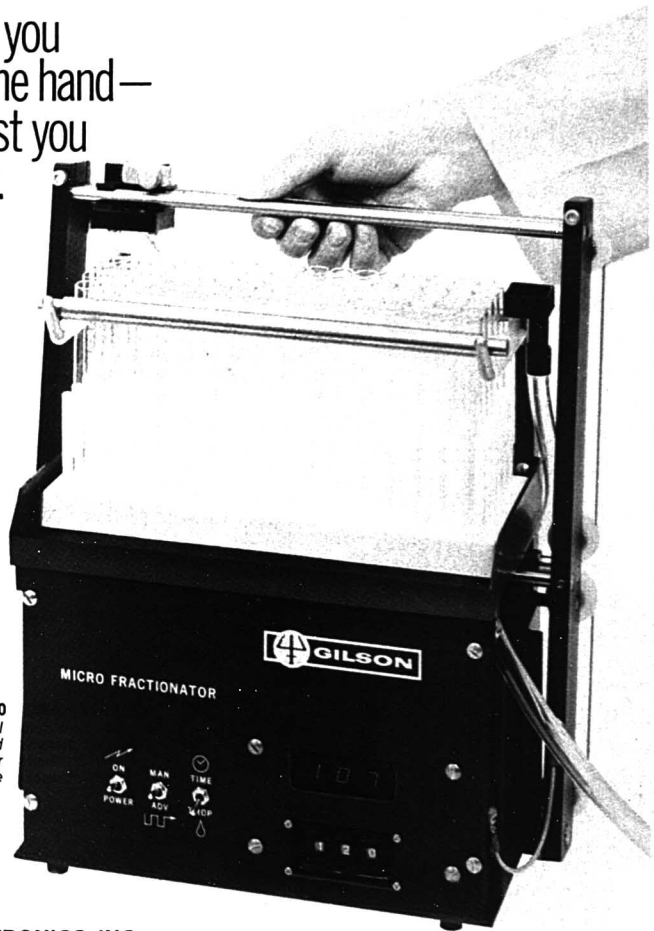

MODEL FC-80
An electronic digital counter indicates elapsed number of drops or elapsed time per tube

Write or phone
U.S.A. MANUFACTURING PLANT:
GILSON MEDICAL ELECTRONICS, INC.
P.O. BOX 27, MIDDLETON, WIS. 53562
Telephone 608/836-1551 • TELEX 26-5478

GILSON®

EUROPEAN MANUFACTURING PLANT:
GILSON MEDICAL ELECTRONICS (FRANCE) S.A.
69, 72 rue Gambetta
VILLIERS-LE-BEL 95400 • ARNOUVILLE-LES-GONESSE, FRANCE
Telephone 990 54-41

CIRCLE 83 ON READER SERVICE CARD

Gas Chromatography

Tracor 700

Hall Electrolytic Conductivity Detector

From the leader in specific G. C. detector technology, the Hall Electrolytic Conductivity Detector can offer expanded capability for any G. C. system. Unexcelled for the selective determination of:

- Chlorinated hydrocarbon pesticides in the presence of PCB's and PCN's
- Nitrosamines in the presence of other nitrogen compounds
- Sulfur without interference of hydrocarbons
- Chloroform in water by direct injection

Tracor Instruments

Tracor, Inc.
6500 Tracor Lane
Austin, Texas 78721
Telephone 512: 926 2800

CIRCLE 201 ON READER SERVICE CARD

pliance test methodology, the Society is organizing a new task force. The task force is inviting interested persons to present their preference or in-house procedures as a first step in the development of full consensus ASTM standards. Everyone interested should contact: Thomas A. Kittleman, E. I. du Pont Co., Environmental Quality Engineering, Service Div., Engineering Dept., Louviers Bldg., Wilmington, Del. 19898.

Materials Research Corp. (Orangeburg, N.Y. 10962, 914-359-4200) announces the availability of a new laboratory facility to perform thin-film sputtering. Located in the MRC plant in Pearl River, N.Y., the laboratory is equipped with a new Model 900 inline magnetron sputtering system and a library of high-purity metal, alloy, and ceramic sputtering targets.

Dexsil Chemical Corp. is a firm newly established with the acquisition of the Dexsil product line from the Olin Chemical Corp. The new company will assume the complete line of Dexsil products such as Dexsil 300GC, 400GC, and 410GC, which are widely used as a gas chromatographic stationary phase. For more information, contact Dexsil Chemical Corp., 295 Treadwell St., Hamden, Conn. 06514 (203-288-3509).

The National Science Foundation (NSF) has awarded **grants totaling $1 660 900 to 20 U.S. colleges and universities** to purchase equipment for use in experimental research in computer science. The grants, intended to help computer scientists by providing special research tools, ranged in size from $10 000 to $150 000. The final selections were based on the scientific quality of the research and the need for the equipment by more than one computer science research activity in the institution.

The manufacturer of the world-famous filter papers, **Whatman Inc.** (9 Bridewell Place, Clifton, N.J. 07014), **has acquired the assets of Quantum Industries.** The addition of the Quantum line of precoated glass TLC plates, prepacked columns, and chromatography accessories will integrate smoothly into Whatman's separations science products areas. Whatman presently supplies products for high-pressure liquid chromatography, paper chromatography and electrophoresis, and column chromatography in addition to its line of filter papers. The Quantum operation will remain at its present location in Fairfield, N.J.

New York State's Department of Environmental Conservation has awarded a contract for 30 carbon monoxide monitoring systems to Beckman Instruments, Inc. The **Model 866 ambient carbon monoxide monitoring system** that Beckman is to deliver under the contract has been designated a reference method by the U.S. Environmental Protection Agency in accordance with Title 40, Code of Federal Regulations, Part 53. For more information on the Model 866, write: Beckman Instruments, Inc., Technical Information Section, Process Instruments Div., P.O. Box 3100, 2500 Harbor Blvd., Fullerton, Calif. 92634.

Employment of scientists and engineers in U.S. private industry decreased 5% from 1970 to 1975, according to a report released by the National Science Foundation (NSF). The decline was in contrast to a 14% gain from 1965 to 1970 and a 19% increase in the 1960–65 period. These and other data, collected for NSF's Science Resources Studies Division by the Bureau of the Census, appear in the NSF publication, **"Science Resources Studies Highlights (NSF 77-312)".** Copies of the publication are available from the Division of Science Resources Studies, National Science Foundation, Washington, D.C. 20550.

A **radioimmunoassay correspondence course** has been developed by Quantimetrix Medical Industries. The course contents include the literature, the mathematics, setting up the radioimmunoassay, antisera and antibodies, radiolabeling, radioimmunoassay kits, specific radioimmunoassays, validation and quality control, review, and final examination. Three booklets entitled "How to Use the Logit Log Plot", "How to Use the Scatchard Plot", and "How to Use the Fernandez Loeb Plot" accompany the course. A series of graded examinations accompanies each assignment, and a final certificate of completion is issued upon completion of the nine-part course which costs $200. For further information contact: Quantimetrix, Radioimmunoassay Educational Div., 5912 Blackwelder St., Culver City, Calif. 90230.

LABORATORY SERVICE CENTER

POLLUTION STUDIES
- AIR, WATER & INDUSTRIAL ENVIRONMENTS
- CONTAMINATION IN FOOD & PACKAGING

Write for Brochure

GOLLOB ANALYTICAL SERVICE CORP.
46 Industrial Road, Berkeley Heights, N. J. 07922
201-464-3331

USE LABORATORY SERVICE CENTER

Allylthiourea • p-Aminohippuric Acid • Ammonium Reineckate • Aurin
1-Benzyl-4-piperidone • Cellobiose • α-Chloralose • Diacetyl Monoxime
Dimethylamine HCl • 2,2′-Dipyridyl • Esculin • Ethyl Levulinate
Fructose • Inulin • o-Iodobenzoic Acid • L-Malic Acid • Maltose
DL-Mandelic Acid • Mercuric Potassium Iodide • o-Nitrobenzaldehyde
Orcinol • Orcein • P.A.N. • pH Indicators • L-Rhamnose • Salicin
Sodium Diethyldithiocarbamate • Sodium Dithionate • Succinimide
Thiosemicarbazide • Triphenylphosphine • o-Vanillin • Xylitol • Xylose

Write for our Products List of over 3000 chemicals

Tel: 516-273-0900 TWX: 510-227-6230

EASTERN CHEMICAL BOX 2500 K
Division of GUARDIAN CHEMICAL CORP. HAUPPAUGE, N. Y. 11787

Laboratory Service Center (Equipment, Materials, Services, Instruments for Leasing), Maximum space — 4 inches per advertisement. Column width, 2-3/16"; two-column width, 4-9/16". Artwork accepted. No combination of directory rates with ROP advertising. Rates based on number of inches used within 12 months from date of first insertion. Per inch: **1" — $58; 12" — $57; 24" — $56; 36" — $55; 48" — $54.**

CALL OR WRITE BARBARA AUFDERHEIDE

ANALYTICAL CHEMISTRY
25 Sylvan Road, So.
Westport, Ct. 06880
203-226-7131

A Century of Chemistry

The Role of Chemists and the American Chemical Society

Herman Skolnik, *Chairman, Editorial Board*
Kenneth M. Reese, *Editor*

An illuminating portrait of the life and times of the world's largest scientific society devoted to a single discipline.

The book portrays the growth and activities of the ACS in the context of a century that saw two World Wars, the Great Depression, the Cold War, the Space Race, the environmental movement, and numerous scientific and engineering advances.

The volume traces the development of chemical science and technology in the framework of the 27 technical divisions of the Society. It includes a compact, 100-year record of ACS people and events.

Part One: Historical Perspectives, Chemical Education, Professionalism, Publications, Impact of Government, Public Affairs, Intersociety Relations, Governance, Headquarters Staff and Operations, ACS Divisions and their Disciplines. Part Two: The Record—a list of past presidents, chairmen, members of the board of directors, editors, award winners, and more.

468 pages (1976) $15.00 clothbound
LC 76-6126 ISBN 0-8412-0307-5

Special Issues Sales
American Chemical Society
1155 Sixteenth St., N.W.
Washington, D.C. 20036

CIRCLE 1 ON READER SERVICE CARD

INDEX TO ADVERTISERS IN THIS ISSUE

CIRCLE INQUIRY NO.	ADVERTISERS	PAGE NO.
xx	**The Aerospace Corporation**	818A
4	**Airco Industrial Gases** Hammond Farrell, Inc.	827A
2	**American Instrument Company** Industrial Advertising Associates	818A
1	**Anderson Laboratories, Inc.** Worrell-Ericson Advertising Agency	824A
5	**Auckland Nuclear Accessory Company Limited**	828A
19,20	***J. T. Baker Chemical Company** Naimark & Barba, Inc.	824A, 830A
23	**Barnes Engineering Company** Jarman, Spitzer & Felix, Inc.	831A
16	***Brinkmann Instruments, Inc.** Blatt Advertising, Inc.	OBC
18	***Bruker Instruments** Schwietzer Advertising	842A
21	**Buchler Instruments** Fletcher-Walker-Gesell, Inc.	821A
22	***Burdick & Jackson Laboratories, Inc.** Studio 5 Advertising, Inc.	816A
32	**Crane Company** Doremus Uptown	819A
47	***Dohrmann** Fred Schott & Associates	759A
48–50	***E. I. DuPont de Nemours & Company, Inc., Photo Products/Instruments** N. W. Ayer ABH International	780A–781
65	***Eastman Kodak** Rumrill-Hoyt, Inc.	782A
64	***EM Laboratories, Inc.** Langeler-Mason Inc.	811A
63	***Environmental Sciences Associates** Marketing Dimensions, Inc.	IFC
74	**Finnigan Corporation** John Feack	841A
75, 76, 78	***Fischer Scientific Company** Tech-Ad Associates	794A–795A, 815A, 829A
82	***Gilford Instrument Laboratories, Inc.** Oberlin Industrial Advertising	839A
83	***Gilson Medical Electronics, Inc.** Towell, Inc. Advertising Marketing	805A
94	***Hach Chemical Company** Wesley Day Advertising	776A
97	***Hacker Instruments, Inc** Ron Carlucci	817A
96	***Hamilton Company** Mealer & Emerson, Inc.	813A
95	**Hewlett-Packard** Dorland Advertising Limited	834A
105	***ICN Pharmaceuticals, Inc.** Bayless-Kerr Company	809A
131	***Labindustries** Fred Schott & Associates	777A
130	***LECO Corporation** FYI	770A–771A
141	**3M New Business Ventures Division** Kerker & Associates	797A
144–149	***Matheson** Kenyon Hoag Associates	765A
139	***MC/B Manufacturing Chemists** Kenyon Hoag Associates	767A
142	***Mettler** Harris D. McKinney, Inc.	774A
143	***MFE Corporation** Letter-Men	833A
140	**Mitsubishi Chemical Industries Ltd.** Global Advertising Company, Ltd.	798A
157	***Ohaus Scale Corporation** Michel-Cather, Inc.	769A
156	***Orion Research, Inc.** OBC Advertising	763A
165	**Pacific Scientific** Allen, Dorsey & Hatfield, Inc.	788A
167	***Perkin-Elmer Corporation** Marquardt & Roche, Inc.	790A
174	**Perkin-Elmer, Coleman Instrument Division**	791A, 792A, 793A
173	***Philips Electronic Instruments, Inc.** Dobbs Advertising Company, Inc.	831A
170, 171, 172	***Pye Unicam, Ltd**	800C, 800D, 800E
179	***Rainin Instrument Company, Inc.** Robert J. Allen	838A
177	***Rheodyne** Bonfield Associates, Inc.	779A
188	***Schoeffel Instrument Corporation** Tek-Mark, Inc.	838A
193	**Scientific Glass Engineering** Arden Advertising Agency	817A
190	**Scientific Products** Mitchel Suttner McPhilliamy Inc. Advertising	799A
191	**Shimadzu Seisakusho Ltd.** General Advertising Agency, Inc.	820A
192	***G. Frederick Smith Chemical Company** Andrew Show Advertising	818A
187	***Spex Industries, Inc.** Seymour Nussenbaum	810A
200, 201	***Tracor Analytical Instruments** Aim Advertising Agency	806A, 832A
125–129, 218–219, 220	***Varian** Ahern Advertising Agency	785A, 787A, 789A
221, 222	**Varian-MAT** Shepherd, Tibball Galog Associates	801A, 803A
235–237	***Waters Associates** Edward W. Fischer & Associates	826A
232	***Whatman, Inc.** J. S. Lanza & Associates	760A
234	***John Wiley & Sons, Inc.** 605 Advertising Group	822A
240	****Carl Zeiss, Inc.** Werbedienst fur Markenwaren GmbH	800B

* *See ad in ACS Laboratory Guide*

** *Company so marked has advertisement in the foreign regional edition only*

Advertising Management for the American Chemical Society Publications

CENTCOM, LTD.

Thomas N. J. Koerwer, President: Clay S. Holden, Vice President: Benjamin W. Jones, Vice President; Robert L. Voepel, Vice President; C. Douglas Wallach, Vice President, 25 Sylvan Rd. South, Westport, Connecticut 08880 (Area Code 203) 226-7131

ADVERTISING SALES MANAGER
James A. Byrne

SALES REPRESENTATIVES

Atlanta, GA . . . Robert E. Kelchner, CENTCOM, Ltd. Telephone: WX2586

Chicago . . . Eugene Eldridge, CENTCOM, LTD., 540 Frontage Rd., Northfield, Ill. 60093. 312-441-6383.

Cleveland . . . Michael Hayes, CENTCOM, LTD., Suite 205, 18615 Detroit Ave., Lakewood, Ohio 44107. 216 228-8050.

Houston . . . Michael Hayes, CENTCOM, LTD., 216-228-8050.

Denver . . . Clay S. Holden, CENTCOM LTD., 213-776-0552.

Los Angeles 90045 . . . Clay S. Holden, CENTCOM, LTD., Newton Pacific Center, 3142 Pacific Coast Highway, Suite 200, Torrance, CA 90505, 213-325-1903

New York 10017 . . . Don Davis, Richard L. Going, CENTCOM LTD., 60 East 42nd St., 212-972-9660

Philadelphia . . . Richard L. Going, CENTCOM LTD., GSB Building, Suite 510 1 Belmont Avenue Bala Cynwyd, Pa. 19004. Telephone: 215-667-9666

San Francisco, CA . . . Robert LaPointe, CENTCOM, LTD., Room 235, 1499 Bayshore Highway, Burlingame, CA 94010. Telephone: (415) 692-0949

Westport 06880 . . . Don Davis, CENTCOM, LTD., 25 Sylvan Rd. So., 203-226-7131.

Manchester, England . . . Jill E. Loney, Technomedia Ltd., 216, Longhurst Lane, Mellor, Stockport, SK6 5PW, Telephone: 061-427-5660

Reading, England . . . Malcolm Thiele, Technomedia Ltd., Wood Cottage, Shurlock Row, Reading, RG10 OOE. Telephone 073-581-302

Paris, France . . . Patric B. Hale, Technomedia Ltd., 18 Rue Gounod, 92 Saint-Cloud, Paris. Telephone: 602-24-79

Tokyo, Japan . . . Haruo Moribayashi, International Media Representatives Ltd., 1, Shibe-Kotohiracho, Minato-ku Tokyo. Telephone: 502-0656

PRODUCTION DEPARTMENT

Production Director
Joseph P. Stenza

Advertising Production Assistant
Barbara Aufderheide

PRODUCT CAPSULES

Scan this list for products of interest. Then, circle the indicated numbers on the adjacent reply card and selected literature from advertisers in the previous issue will be sent to you.

No.	Product Capsules
301	Balances
302	Baths; Circulators
303	Biological Analyzers
304	Books; Periodicals; Catalogs
305	Centrifuge Equipment
306	Chemicals; Reagents; Gases
307	Chromatography, Gas
308	Chromatography, Liquid
309	Chromatography, Thin Layer
310	Computers; Calculators
311	Coolers; Freezers
312	Densitometers
313	Electrical Equip: Amplifiers; Power Supplies; Voltmeters; etc.
314	Electrochemical: pH Meters; Ion Meters; Titrators; Electrodes
315	Electrophoresis
316	Elemental Analyzers
317	Environmental Analyzers
318	Fourier Transform Data Systems
319	Furniture; Fume Hoods
320	Gas Chrom/Mass Spec Systems
321	Labware: Glass; Plastic; Metal
322	Lasers
323	Mechanical Equip: Presses; Mills; etc.
324	Microscopes
325	Mixers; Stirrers; Blenders; Shakers
326	Nuclear Instruments
327	Oscilloscopic Instruments
328	Ovens; Furnaces; Heaters
329	Photometers; Colorimeters
330	Pipets; Samplers; Dispensers
331	Pumps; Flowmeters
332	Recorders; Integrators
333	Services, Analytical; Consultants
334	Signal Averagers
335	Spectro, AA
336	Spectro, Fluorescence
337	Spectro, Infrared
338	Spectro, Mass
339	Spectro, NMR
340	Spectro, UV/Vis
341	Spectro, X-Ray
342	Stills; Demineralizers
343	Supplies: Lubricants; Detergents; etc.
344	Thermal Analyzers
345	Valves; Fittings; Tubing
346	Vacuum Equipment

ICN W-200 ALUMINAS

for quality and reliability there are no equals!

ICN W-200 Neutral, Basic, Acidic Aluminas —

unsurpassed for both chromatographic and non-chromatographic applications

* **Precisely controlled particle size** — ranges from 3-6 um for HPLC to 200 um for classic column Chromatography — **offers the finest separations.**
* Highly standardized initial activity with constant deactivation behavior — results in **extraordinary reproducibility, batch to batch, with no surprises!**
* **The highest purity** — from the smallest package size (500 g) to the largest (50 kg)

Regardless of your application — from laboratory investigation to the largest bulk requirements — there is really **only one product that meets all requirements** ICN W-200 ALUMINAS

Available from stock — delivery in less than 36 hours.

ICN Pharmaceuticals, Inc.
Life Sciences Group
26201 Miles Road
Cleveland, Ohio 44128

For immediate action . . . Call Collect or write, Chromatography Product Manager (216) 831-3000

CIRCLE 105 ON READER SERVICE CARD

FIRST CLASS
Permit No. 25682
Philadelphia, Pa.
19101

BUSINESS REPLY CARD

No postage stamp necessary if mailed in the United States

POSTAGE WILL BE PAID BY

ANALYTICAL CHEMISTRY

P. O. Box #8660

Philadelphia, Pennsylvania 19101

Analytical Chemistry — AUGUST 1977 — Valid through December 1977

NEW PRODUCTS, CHEMICALS, LITERATURE: 401 402 403 404 405 406 407 408 409 410 411 412 413 414 415
416 417 418 419 420 421 422 423 424 425 426 427 428 429 430 431 432 433 434 435 436 437 438 439 440 441 442
443 444 445 446 447 448 449 450 451 452 453 454 455 456 457 458 459 460 461 462 463 464 465 466 467 468 469
470 471 472 473 474 475 476 477 478 479 480 481 482 483 484 485 486 487 488 489 490 491 492 493 494 495 496

ADVERTISED PRODUCTS: 1 2 3 4 5 6 7 8 9 10 11 12 13 14 15 16 17 18 19
20 21 22 23 24 25 26 27 28 29 30 31 32 33 34 35 36 37 38 39 40 41 42 43 44 45 46
47 48 49 50 51 52 53 54 55 56 57 58 59 60 61 62 63 64 65 66 67 68 69 70 71 72 73
74 75 76 77 78 79 80 81 82 83 84 85 86 87 88 89 90 91 92 93 94 95 96 97 98 99 100
101 102 103 104 105 106 107 108 109 110 111 112 113 114 115 116 117 118 119 120 121 122 123 124 125 126 127
128 129 130 131 132 133 134 135 136 137 138 139 140 141 142 143 144 145 146 147 148 149 150 151 152 153 154
155 156 157 158 159 160 161 162 163 164 165 166 167 168 169 170 171 172 173 174 175 176 177 178 179 180 181
182 183 184 185 186 187 188 189 190 191 192 193 194 195 196 197 198 199 200 201 202 203 204 205 206 207 208
209 210 211 212 213 214 215 216 217 218 219 220 221 222 223 224 225 226 227 228 229 230 231 232 233 234 235
236 237 238 239 240 241 242 243 244 245 246 247 248 249 250 251 252 253 254 255 256 257 258 259 260 261 262

PRODUCT CAPSULES: 301 302 303 304 305 306 307 308 309 310 311 312 313 314 315 316 317 318 319 320 321 322 323
324 325 326 327 328 329 330 331 332 333 334 335 336 337 338 339 340 341 342 343 344 345 346

Name_____ Position_____

Company_____

Street_____ City_____

State_____ Zip_____ Telephone_____

99.9 - 99.99999% PURE INORGANICS

SPEX

HI PURE MATERIALS

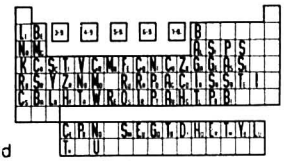

Over 500 high purity metals and compounds, each provided with a semiquantitative spectrographic determination of impurities. Accompanying each compound in addition is a wet chemical assay.

ELEMENT KITS—up to 2g quantities each of
49 Common Elements or 16 Rare Earths
or 10 Noble Metals

SPEX INDUSTRIES, INC. P.O. BOX 798 METUCHEN, N. J. 08840 ☎ (201) 549-7144

CIRCLE 187 ON READER SERVICE CARD

Analytical Chemistry AUGUST 1977 Valid through December 1977

NEW PRODUCTS, CHEMICALS, LITERATURE: 401 402 403 404 405 406 407 408 409 410 411 412 413 414 415 416 417 418 419 420 421 422 423 424 425 426 427 428 429 430 431 432 433 434 435 436 437 438 439 440 441 442 443 444 445 446 447 448 449 450 451 452 453 454 455 456 457 458 459 460 461 462 463 464 465 466 467 468 469 470 471 472 473 474 475 476 477 478 479 480 481 482 483 484 485 486 487 488 489 490 491 492 493 494 495 496

ADVERTISED PRODUCTS: 1 2 3 4 5 6 7 8 9 10 11 12 13 14 15 16 17 18 19 20 21 22 23 24 25 26 27 28 29 30 31 32 33 34 35 36 37 38 39 40 41 42 43 44 45 46 47 48 49 50 51 52 53 54 55 56 57 58 59 60 61 62 63 64 65 66 67 68 69 70 71 72 73 74 75 76 77 78 79 80 81 82 83 84 85 86 87 88 89 90 91 92 93 94 95 96 97 98 99 100 101 102 103 104 105 106 107 108 109 110 111 112 113 114 115 116 117 118 119 120 121 122 123 124 125 126 127 128 129 130 131 132 133 134 135 136 137 138 139 140 141 142 143 144 145 146 147 148 149 150 151 152 153 154 155 156 157 158 159 160 161 162 163 164 165 166 167 168 169 170 171 172 173 174 175 176 177 178 179 180 181 182 183 184 185 186 187 188 189 190 191 192 193 194 195 196 197 198 199 200 201 202 203 204 205 206 207 208 209 210 211 212 213 214 215 216 217 218 219 220 221 222 223 224 225 226 227 228 229 230 231 232 233 234 235 236 237 238 239 240 241 242 243 244 245 246 247 248 249 250 251 252 253 254 255 256 257 258 259 260 261 262

PRODUCT CAPSULES: 301 302 303 304 305 306 307 308 309 310 311 312 313 314 315 316 317 318 319 320 321 322 323 324 325 326 327 328 329 330 331 332 333 334 335 336 337 338 339 340 341 342 343 344 345 346

Name_____ Position_____

Company_____

Street_____ City_____

State_____ Telephone_____

FIRST CLASS
Permit No. 25682
Philadelphia, Pa.
19101

BUSINESS REPLY CARD
No postage stamp necessary if mailed in the United States

POSTAGE WILL BE PAID BY

ANALYTICAL CHEMISTRY
P. O. Box #8660
Philadelphia, Pennsylvania 19101

PRODUCT CAPSULES

Scan this list for products of interest. Then, circle the indicated numbers on the adjacent reply card and selected literature from advertisers in the previous issue will be sent to you.

No.	Product Capsules
301	Balances
302	Baths; Circulators
303	Biological Analyzers
304	Books; Periodicals; Catalogs
305	Centrifuge Equipment
306	Chemicals; Reagents; Gases
307	Chromatography, Gas
308	Chromatography, Liquid
309	Chromatography, Thin Layer
310	Computers; Calculators
311	Coolers; Freezers
312	Densitometers
313	Electrical Equip: Amplifiers; Power Supplies; Voltmeters; etc.
314	Electrochemical: pH Meters; Ion Meters; Titrators; Electrodes
315	Electrophoresis
316	Elemental Analyzers
317	Environmental Analyzers
318	Fourier Transform Data Systems
319	Furniture; Fume Hoods
320	Gas Chrom/Mass Spec Systems
321	Labware: Glass; Plastic; Metal
322	Lasers
323	Mechanical Equip: Presses; Mills; etc.
324	Microscopes
325	Mixers; Stirrers; Blenders; Shakers
326	Nuclear Instruments
327	Oscilloscopic Instruments
328	Ovens; Furnaces; Heaters
329	Photometers; Colorimeters
330	Pipets; Samplers; Dispensers
331	Pumps; Flowmeters
332	Recorders; Integrators
333	Services, Analytical; Consultants
334	Signal Averagers
335	Spectro, AA
336	Spectro, Fluorescence
337	Spectro, Infrared
338	Spectro, Mass
339	Spectro, NMR
340	Spectro, UV/Vis
341	Spectro, X-Ray
342	Stills; Demineralizers
343	Supplies: Lubricants; Detergents; etc.
344	Thermal Analyzers
345	Valves; Fittings; Tubing
346	Vacuum Equipment

New HPLC Column News

EM LABORATORIES VOL. I, NO. 1

NEW HIBAR®-II

ELMSFORD, NY (EM)
EM Laboratories has just introduced a brand new, totally different line of prepacked columns for HPLC – Hibar-II.

BRAND NEW HIBAR®-II HARDWARE

The Hibar-II columns are 25 cm long and have an inside diameter of 4.6 mm. Hibar-II columns are adaptable to all modular or unitized HPLC systems, featuring zero dead volume fittings. Each column contains removable/cleanable frits for extended life.

WIDE RANGE OF PREPACKED SORBENTS

But the best news is that Hibar-II columns are prepacked with the entire line of great sorbents from E. Merck, Darmstadt, Germany. That means convenience and versatility like you've never before enjoyed in HPLC. Sorbents for partition, adsorption, gel permeation, and ion exchange chromatography. Two different particle shapes: irregular shaped, totally porous (LiChrosorb®) and totally spherical shaped porous (LiChrospher®), and two different particle sizes . . . 5 and 10 micron.

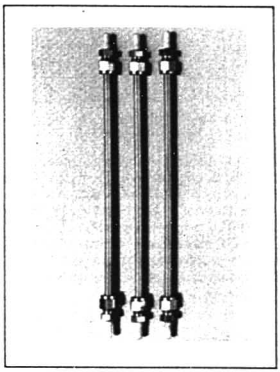

For your price convenience and service, Hibar-II columns are available from selected nationwide scientific supply houses.

You need all the facts on this important development in our industry, so write today for complete technical information and the name of your nearest stocking distributor.

CIRCLE 64 ON READER SERVICE CARD

Pure Consistency...

EM Laboratories, Inc.
associate of
E. Merck, Darmstadt, Germany
500 Executive Boulevard
Elmsford, N.Y. 10523
(914) 592-4660

◆ laboratory reagents and indicator strips ◆ sorbents, plates and columns for chromatography
◆ biochemical specialties ◆ instrumentation chemicals

New Products

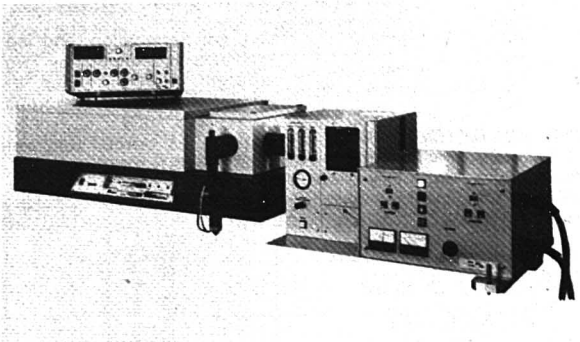

SPS 1000 inductively coupled plasma spectrometer offers sensitivity down to the picogram level and for some elements down to the parts per trillion level with an accuracy and repeatability of over 1%. The dynamic range of 10^6 permits quantitative measurement over a wide concentration range. The separation of elements obtained in the plasma at a temperature in excess of 10 000 K permits an unmatched element separation and minimizes interaction between elements. The instrument is computer compatible and is offered with a computer option including the software for automatic element search, background subtraction, and automatic calibration. J-Y Optical Systems Div., Instruments SA, Inc. **401**

Tunable Substance Specific Detectors

Model GC-33 IR detector and Model GC-55 UV detector for gas chromatography are intended for further qualitative identification of unknown samples or for the confirmation of samples believed to be of a certain type. The GC-33 IR detector is a selectable wavelength, nonscanning spectrometer and is equipped with a heated connecting line and heated flow-through cell. The wavelength range the detector operates in is from 4000 to 800 cm^{-1}. The GC-55 UV detector is based on the Coleman Model 55 UV–VIS spectrometer, modified to accept a heated cell and a heated connecting line from the effluent of the GC. Wavelength is selectable in the range 190–800 nm. Perkin-Elmer Corp. **408**

Double-Beam Spectrophotometer

DM 4 spectrophotometer for the UV, VIS, and near IR regions can be operated for routine concentration analysis and kinetics as well as scanning ratio recording for qualitative determinations. Features include automatic lamp switch-over, push-button operation, precision grating monochromator, wavelength scan, and 6-position sample changer. The DM 4 has a spectral range from 195 to 850 nm, an absorbance range from −0.3 to 2.5 A, and a concentration range from 0 to 10 000. It requires no more than a 0.3-mL sample volume. Digital and analog outputs are provided. Carl Zeiss, Inc. **409**

Cyanide Spill Cleanup Kit

Kit provides a technically correct method to quickly and effectively control both solid and liquid cyanide spills. Included are two chemical formulations, CN-Plex and Liquisorb, that neutralize and absorb cyanide spills. Also included are all of the materials needed to clean up and dispose of spill, including gloves, scoops, a sponge, and a brush. The neutralized spill material is placed in a plastic bag, sealed, and labeled, ready for disposal in accordance with local environmental regulations. J. T. Baker Chemical Co. **410**

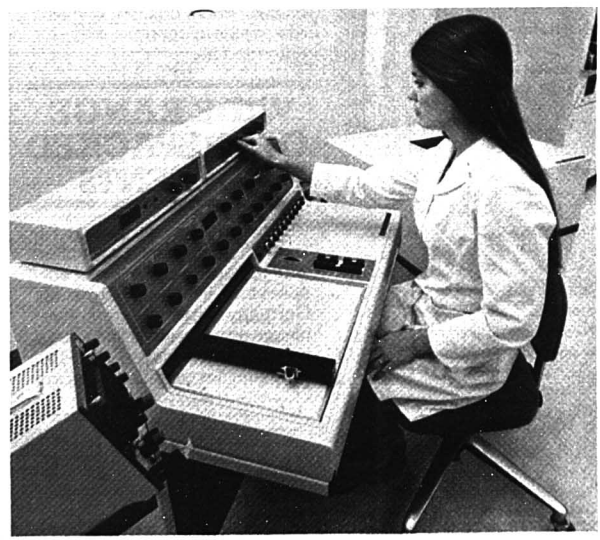

EM-360L 60-MHz NMR spectrometer has many of the operational features found in the high-performance 90-MHz EM-390 and offers proton as well as optional fluorine and phosphorus observation. The 14-kG permanent magnet needs no cooling water, and the top power consumption is 260 W. Other features include a wide range of sweep widths (0.2–100 ppm), digitally selectable offsets (−200 to +200 ppm, plus 1 ppm continuous vernier), six sweep times (0.5–20 min), seven filter time constants (0.05–5 s), and a full continuous RF power control and provision for fast normalization of spectrum amplitude. Varian Instrument Div. **402**

FIRST AID FOR YOUR L.C.

It's about time you gave your LC a little "Tender Loving Care." After all your liquid chromatograph does for you, turning out all those chromatograms day after day, shouldn't you do something nice for it?

Consider changing your column packing and putting in Hamilton's Resins. You'll get better resolution of peaks, you can operate at lower back pressures, have higher peak selectivity, and get better stability.

Hamilton's line of concentrated buffers save preparation time and storage space. You can also eliminate wasted reagents and the growth of mold. Sodium and lithium citrate buffers are available for specific amino acid methodologies and a ready-to-use buffer is available for use in narrow bore columns.

Try our miniature 1X and 2X inert valves. For automatic operation a motorized valve driver and a digital timer let you make buffer or solvent changes at preselected time intervals.

There's a full line of tubing, tube fittings, connectors and adaptors. We'll even provide tube assemblies to your specifications. To help you make leak-tight butt-end connections for our fittings, you can use our new Flanging Tool. And we can fit you out with stainless steel columns, a slurry packer, and column supports.

And don't forget our precision syringes. In particular, the 1800 series designed for LC.

All these aids for your LC are described in our new LC Catalog. For your free copy, write to J.V. Benson, Jr., Hamilton Company, Post Office Box 10030, Reno, Nevada 89510.

HAMILTON

CIRCLE 96 ON READER SERVICE CARD

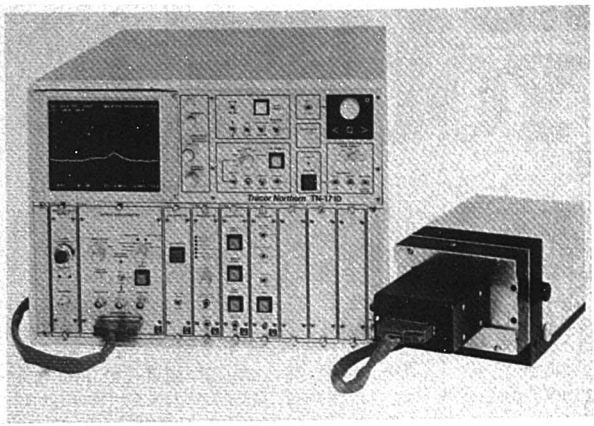

TN-1710-21 diode array rapid scan spectrometer system provides capabilities for simultaneous, parallel, high-resolution spectral measurements spanning the range of 200–1100 nm. The system consists of a lag- and bloom-free silicon photodiode array detector, a newly developed holographic grating spectrograph, and the modular microcomputer-based TN-1710 data analysis system with display. Real-time dynamic range of 4096:1 is achieved by thermoelectric cooling of the detector, which is placed in the focal plane of the flat-field spectrograph. A 512-element detector is scanned in 5.12 ms, with exposure times per scan adjustable from 5.16 ms to 8192 s. Spectral data processing is carried out with full computer capability, and a wide range of accessories is available. Tracor Northern, Inc. **403**

Glucose Analyzer

Glucose Analyzer 2 is based on the oxygen rate method for measuring glucose in foods, wine, and beer. The instrument offers simplified, one-step operation. After calibration, a 10–100-μL sample is injected. The results are digitally displayed in 15 s in mg/dL or mm/L. Three pumps assure fresh reagent in exact measure. A drain pump empties the sample cup of spent reagent, a fill pump refills it with fresh reagent, and a sip pump removes excess fluid until the precise amount remains. Routine output is up to 67 determinations per hour. $3190. Beckman Instruments, Inc. **411**

Hollow Cathode Lamps

These handmade hollow cathode lamps for atomic absorption spectrophotometers feature high spectral response, increased light output, stability of light source, and longer lamp life. Two types of lamps are available: single- and multielement lamps; and single- and multielement Gold-Band pretest, preselected lamps. The Gold-Band lamps are pretested on standard solutions and must meet designated criteria on spectral purity and intensity to attain Gold-Band nomenclature. Sci Tech Corp. **412**

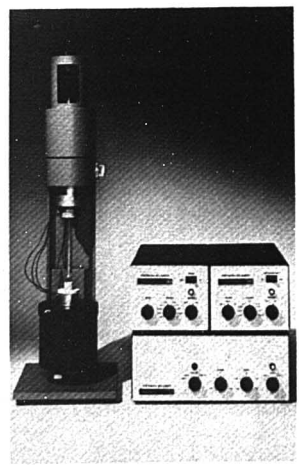

Model TMS-2 thermomechanical analyzer system replaces the TMS-1 and is completely compatible with other thermal analysis modules. Features of the TMS-2 include high sensitivity, wide temperature range, and derivative capability with the first derivative computer accessory. The instrument uses a unique float assembly for precise and reproducible setting of sample loading and a low mass furnace system. Perkin-Elmer Corp. **404**

Digital Multimeter

Model 174 features high sensitivity of 100 nV/digit, high-resolution 30 000-count display, and many other convenience features. Automatic zeroing and standardization occur during each A-D conversion to assure stable, accurate readings. The basic instrument is capable of dc voltage measurements from 100 nV/digit to 1200 V full scale. Choice of automatic or manual ranging is available on most ranges. A rear-panel analog output (fixed gain of 100) for the 3- and 30-mV ranges provides a means of monitoring low-level signals. Other measurement functions (ac volts, dc current, ac current and resistance) are offered as options. $995. Keithley Instruments, Inc. **413**

Graphite Furnaces

HGA-2200 and HGA-76B are compatible with all current P-E atomic absorption spectrophotometers. They feature built-in ballistic heating and relative temperature control. Rapid ballistic heating significantly improves the sensitivity for refractory elements such as titanium and boron, and permits furnace temperatures of 3000 °C to be reached quickly. A special silicon diode temperature sensing device is employed to provide relative temperature control. All of the features typical of the HGA-2100 and HGA-76 are included in the new power supplies. The P-E AS-1 automatic sampler can be coupled directly to these new furnaces. Perkin-Elmer Corp. **414**

Graphite Tubes for Electrothermal AA Spectrophotometry

With the Profile graphite tube and the SP9-01 digital flameless atomizer, sensitivity is improved up to 10 times for electrothermal atomic absorption spectrophotometry. The tube is profiled to the shape of the light beam of the spectrophotometer so that the atoms formed are concentrated in the smaller area of the light beam rather than across the whole diameter of an ordinary tube. The Profile tubes can be used in any Pye Unicam AA spectrophotometer and are directly interchangeable with the standard tubes. Pye Unicam Ltd., York St., Cambridge, England **415**

For more information on listed items, circle the appropriate numbers on one of our Readers' Service Cards

The smartest label around.

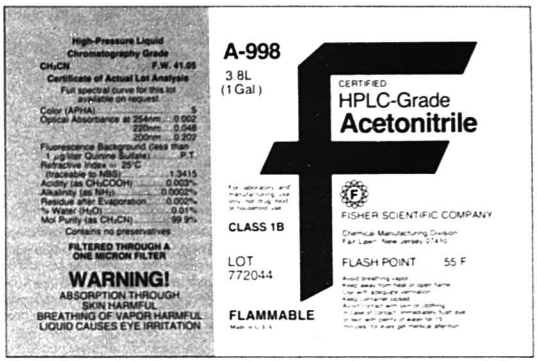

Fisher Certified HPLC Solvents. Only label around that tells you everything you need to know.

Optical absorbance at a variety of wavelengths (full spectral curves on request). Refractive index directly traceable to NBS. Background fluorescence. Assay as mol % determined by GC. Water and preservative/inhibitor content. And much much more.

Fisher HPLC solvents are **distilled in glass.** Painstakingly filtered to eliminate particulates. And shipped by today's fastest distribution system.

After all, high-pressure liquid chromatography columns, detectors and samples are valuable things. They **deserve** the best. Only Fisher defines and certifies **every parameter** for their protection.

Only Fisher provides such tailormade services as Customer Reserve Quantity. Your nearest branch reserves your HPLC solvent needs for you alone, releasing them to your timetable. (Reserve an entire lot if you wish, assuring absolute uniformity month-to-month!)

Also: as today's largest lab supplier, Fisher provides an impressive selection of **auxiliary** HPLC materials -- apparatus, appliances, supplies — to simplify your ordering.

Write for HPLC catalog **today!**

Fisher Scientific Company
711 Forbes Avenue Pittsburgh PA 15219

CIRCLE 75 ON READER SERVICE CARD

THE SYMBOL OF EXCELLENCE SINCE 1959

Distilled in Glass

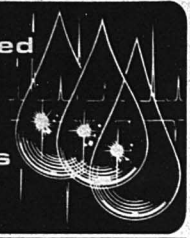

RESIDUE-FREE SOLVENTS FROM BURDICK & JACKSON

Purified to the exacting requirements of gas chromatography, liquid chromatography and spectrophotometric analysis.

Acetone
Acetonitrile
Benzene
Butanol-1
Butanol-2
Butyl Chloride
Butyl Formate
Carbon Tetrachloride
Chloroform
Cyclohexane
Cyclopentane
o-Dichlorobenzene
Dimethyl Acetamide
Dimethyl Formamide
Dimethyl Sulfoxide
Dioxane
2-Ethoxyethanol
Ethyl Acetate
Ethyl Ether
Heptane, 95-99°
Hexadecane
Hexane, 68-69°
Isobutyl Alcohol
Methanol
2-Methoxyethanol
Methylene Chloride
Methyl Ethyl Ketone
Methyl Isobutyl Ketone
N-Methylpyrrolidone
n-Nonane
Pentane
Petroleum Ether, 30-60°
beta-Phenethylamine
Propanol-2
Propylene Carbonate
Pyridine
Tetrahydrofuran
Toluene
2, 2, 4-Trimethylpentane, 99-100°
o-Xylene

Ask for Bulletin BJ-25/U.S. Agencies use F.S.S.

BURDICK & JACKSON LABORATORIES, INC. (616) 726-3171

1953 S. HARVEY ST., MUSKEGON, MICHIGAN 49442

CIRCLE 22 ON READER SERVICE CARD

New Products

Model D-600 automatic fluorescence monitor is a self-contained automatic monitoring system for the fluorescence quantitation of primary amines. Using a microsampling valve, the system transfers a calibrated aliquot of sample into a buffered stream where it is reacted with a fluorogenic reagent. The resultant fluorescence is measured in a fluorometer and plotted on a strip chart recorder. A major application of the system is effluent monitoring of preparative columns where high sensitivity and low sample consumption are important. Durrum Instrument Corp. **405**

Ion Pump Control Units

Three new models are available: a dual-voltage unit which powers large ion pumps in the 220–600 L/s range, a constant-voltage unit for 60–300 L/s ion pumps, and a dual-power model for the 1–80 L/s ion pump range. Standard features on all units include overload protection and safety interlocks, as well as amp/hour indicators for maintaining pump life. Perkin-Elmer Ultek Inc. **418**

Oxygen and Toxic Gas Monitor

The OTOX 80 measures the proportion of oxygen in the atmosphere and, cumulatively, a specific toxic gas content. It incorporates an electrochemical cell with an output directly proportional to the absolute percentage oxygen level in the atmosphere. When the oxygen level falls below 17% concentration in air, a solid-state, self-checking circuit activates a two-tone audible alarm and a flashing yellow light. A prepacked card carrying a chemical reagent is pushed into a slot in the instrument to detect the toxic gas. If it is detected above the accepted level, the alarm and a red flashing light are activated. Cards for detecting hydrogen sulfide are available; cards for carbon monoxide, chlorine, sulfur dioxide, and ammonia are under development. Neotronics Ltd., Building 102, FSTS Site, Stansted Airport, Stansted, Essex, CM24 8QX, England **416**

Nitrogen-Phosphorus GC Detector

Model 702 combines a unique mechanical design with the latest electronic technology to provide burnout protection for the alkali source. An exclusive desensitizing mode allows routine use of chlorinated solvents and derivatizing reagents not possible with previous designs. Tracor Instruments **417**

Chemicals

Standards for Air Pollution Measurements

Methane in air (SRM 1658 and 1659) and methane and propane in air (SRM 1660) are intended for calibrating instruments and techniques used to analyze the hydrocarbon content of the air. The concentration of methane or methane and propane is certified with total uncertainty of 1% relative and is considered to be stable for at least one year. They are supplied in steel cylinders containing 0.85 m^3 at standard temperature and pressure at a cost of $283/cylinder. Office of Standard Reference Materials, Chemistry Building, Room B311, National Bureau of Standards, Washington, D.C. 20234

For more information on listed items, circle the appropriate numbers on one of our Readers' Service Cards

GC upgrading!

SGE

Glass capillary columns:
(S.C.O.T.)(W.C.O.T.)

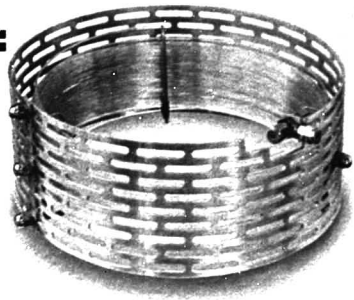

- **Deactivated**
- **Low Cost**
- **High Sample Loading**
- **High Efficiency**

SGE can provide a variety of split or splitless inlet systems for most commercially available chromatographs. Utilizing our glass-lined tubing for connections and graphite ferrules, the system is all glass and has a minimum dead volume for optimum capillary performance.

Scientific Glass Engineering Pty. Ltd.

Head Office
Scientific Glass Engineering Pty. Ltd.
111 Arden Street
North Melbourne, Australia 3051
Tel. 329-6633

U.S. Office
Scientific Glass Engineering, Inc.
2600 Longhorn Blvd., Suite 103
Austin, Texas 78759
Tel 512-837-7190

European Office
Scientific Glass Engineering (U.K.) Ltd.
657 North Circular Road
London NW2 7AY, Great Britain
Tel 01-452-6244

Pittsburgh Conference
booths 242 and 244

CIRCLE 193 ON READER SERVICE CARD

Progress Toward Synthetic Oils

Shale, coal, oil-bearing sands all offer an opportunity to add to our energy reserves. The potential for each is examined in this tape recorded symposium.

4 Speakers
Length: 125 Minutes
47 Figures

The Speakers:

H.W. Sternberg (Lawrence Livermore Lab.)—The Nature of Coal Liquefaction Products

S.K. Kunchal (Paraho Oil Shale Demo.)—Energy and Dollar Requirements in an Oil Shale Industry—Based on the Paraho Process

G.A. Myers (Atlantic-Richfield)—Prerefining of Shale Oil

R.H. Fischer (Mobil)—Non-Hydrogenative Demetalation of Residua Using Manganese Nodules

PRICE: $18.00 (Cassettes Only)

(Postpaid, includes printed copies of slides used)

Order From: American Chemical Society
1155 Sixteenth Street, N.W.
Washington, D.C. 20036
ATTN: Dept. AP

Name _____
Address _____
City _____
State _____ Zip _____

(allow 4 to 6 weeks for delivery)

RAPID REDUCTION - REPRESENTATIVE SAMPLES

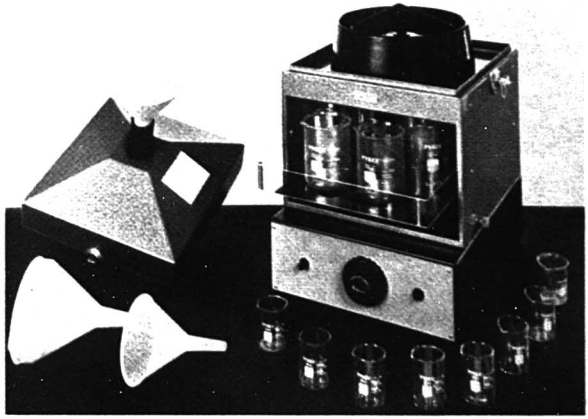

The H/I Swift Rotary Sample Splitter allows unbiased samples to be obtained from bulk material. First pass – – 6 or 12 fold reduction. Accepts most materials – – dry or wet – – to 15 mm diameter.

H/I HACKER INSTRUMENTS INC.

Box 657,
Fairfield, N.J. 07006
(201) 226-8450

CIRCLE 97 ON READER SERVICE CARD

your pipeline to high performance results

the Aminco HPLC System

It starts where others stop

Increased detectability and selectivity due to:
- a superior fluoresence detector - 1000 fold more sensitive than absorbance
- a unique resin
- the ability to perform chemical derivatizations

A detector to fit your needs:
- fluoresence detector standard
- electro-chemical
- UV
- ninhydrin
- colorimetric

Unattended, 24 hours/day operation with automatic sample injection and temperature programming

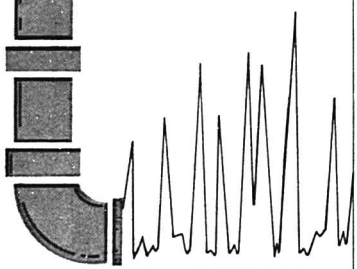

For information on the Aminco HPLC system, contact your local representative or

AMERICAN INSTRUMENT COMPANY
DIVISION OF TRAVENOL LABORATORIES, INC.
Silver Spring, Maryland 20910 Phone: 301-589-1727

AMINCO®

©1977 Travenol Laboratories, Inc.

CIRCLE 2 ON READER SERVICE CARD

LAW ENFORCEMENT

EXPLOSIVES CONTROL SYSTEMS DEVELOPMENT

SCIENTISTS/PHYSICAL CHEMISTS

Challenging and interesting openings exist in our Washington, D.C. office in support programs under contract to the departments of the Treasury and Justice for the development of techniques for the detection and identification of illegally used explosives. For these positions we are seeking individuals with outstanding management and technical skills supported by experience in one or more of the following areas:

—Development of Program Requirements and Implementation Plans.
—Testing and Evaluation of High Energy Materials.
—Non-destructive Inspection (X-Ray, Radiography and Fluorescents, Tomography).
—Analytical Techniques (GC/MS, Infrared, Ultraviolet).
—Experimental Design and Statistical Analysis.

These positions require a Ph.D. and 5 years of experience or the equivalent. Other positions are available for qualified individuals having a masters degree and three years of experience or the equivalent. Qualified individuals are invited to send resume and salary history in confidence to:

THE AEROSPACE CORP.
Personnel Dept.
955 L'Enfant Plaza, S. W.
Suite 4040
Washington, D.C. 20024

An Equal Opportunity Employer

GFS CHEMICALS

WE ARE
MANUFACTURERS
PRODUCING MOST OF THE
ANALYTICAL CHEMICALS
WE SUPPLY
AND YOU CAN STILL BUY
DIRECTLY

GFS

"ANALYTICAL CHEMICALS SINCE 1928"

G. FREDERICK SMITH CHEMICAL COMPANY

867 McKinley Ave.
Columbus. Ohio 43223

FOR PROMPT SHIPMENT
614 224-5343

CIRCLE 192 ON READER SERVICE CARD

Manufacturers' Literature

Ozone Meter. Features the Model 1100, designed to provide specific measurement of ozone without interference from NO_2, SO_2, or other interfering gases. 6 pp. Columbia Scientific Industries Corp. **421**

Strip Chart Recorder. Describes the Model 9176 10-in. laboratory recorder which offers both single- and dual-pen models and a choice of plug-in span and chart speed modules. 4 pp. Varian Instrument Div. **422**

Photon Counting Spectrofluorometer. SLM 8000 features modular design and the latest state-of-the-art electronic and fluorescence technology. 8 pp. SLM Instruments, Inc. **423**

Pharmaceutical Newsletter. Vol. 3, No. 1 contains articles on the use of Technicon automated systems by a poultry breeding farm and small pharmaceutical manufacturers, as well as information on literature and books of interest. 6 pp. Technicon Industrial Systems **424**

Liquid Chromatography. LC at Work Series offers three new application notes, "Quantitative Determination of Caffeine in Beverages", "Separation and Quantitative Analysis of Phenothiazines by Liquid Chromatography", and "Separation and Quantitative Determination of Corticosteroids in Pharmaceutical Preparations". Varian Instrument Div. **425**

Microparticle Standards. Describes the expanded line of standards useful as reference compounds to calibrate particle analyzers, check filters, and compare microscopy specimens. 4 pp. Duke Scientific Corp. **426**

Hydrogen Purifiers. Features full line of palladium alloy hydrogen purifiers ranging from 1 to 500 SCFH. 4 pp. Resource Systems, Inc. **427**

Ultrafiltration Membranes and Systems. Guide includes information on the complete line of laboratory-scale systems for concentrating, desalting, and fractionating macromolecules and viruses. 9 pp. Millipore Corp. **429**

Molecular Weight Standards. Describes narrow molecular weight distribution standards for instrument calibration and polymer characterization by membrane osmometry, vapor-pressure osmometry, liquid chromatography, gel permeation chromatography, and light scattering. Arro Laboratories **443**

Conductivity Instruments. Describes the SM-400 Series Solu Meter Controllers for continuous measurement and control of acid or caustic solutions. 2 pp. Beckman Instruments, Inc. **430**

COD Digestion. Discusses a semiautomatic digestion technique using reagent ready-sealed glass ampuls as combustion tubes and cuvettes. 4 pp. Oceanography International Corp. **431**

Liquid Scintillation Counting Theory and Techniques. Presents an overview covering the aspects of LS counting necessary for valid interpretation of experimental data: physical process, instrumental operation of the LS counter, and chemical and mechanical processes. 56 pp. Beckman Instruments, Inc. **432**

A/D and D/A Conversion Modules. Includes the complete line of data conversion products and a wide variety of new products and improved specifications as well as guidelines to design and selection. 16 pp. Analogic **433**

Quantitative Gas Chromatography. Bulletin 770 is a basic introduction to quantitative GC and points out limitations in the technique and how to overcome them. 4 pp. Supelco, Inc. **435**

Digital Temperature Standards. Discusses line of temperature measurement standards available in complete systems consisting of a calibrated platinum RTD probe and a drift-free precision digital indicator calibrated to match the probe characteristics. 6 pp. Doric Scientific Div., Emerson Electric Co. **434**

Oscilloscopes. Two brochures describe Explorer II and Explorer III, two general-purpose digital oscilloscopes for low-frequency, high-precision waveform measurement. Nicolet Instrument Corp. **436**

Dual-Detector Spectrophotometer. Describes Model D-117 dual-detector stopped-flow spectrophotometer for dual-wavelength and polarization measurements of fast chemical reactions. The modular design is explained, and applications are discussed. 4 pp. Durrum Instrument Corp. **437**

Aminco Laboratory News. Vol. 32, No. 1 features many articles of interest including ones on mutant respiratory proteins, a new creatine phosphokinase screening method, automated blood chemistry analysis, and a radioactive waste gas compressor. 28 pp. American Instrument Co. **438**

OUR SMALL-SPACE METERING PUMP IS BIG ON ACCURACY.

Our Series 20 Chem/Meter hydraulic diaphragm metering pump will give you repetitive accuracy within ± 1% or better.

Measuring only 9¾" x 4⅛" x 3⁷⁄₁₆", it's designed for steady, continuous feeding of clear fluids. How? The programmed cam drive produces a constant velocity discharge—when the full displacement of two plungers working 180° apart are combined in a common manifold, a steady flow is established. And it provides capacities to 4.9 and 16.0 ML/min—with pressures to 1000 psig.

The series 20 Chem/Meter's wetted parts are made of corrosive resistant stainless steel with sapphire balls-seats and teflon diaphragms. With its totally enclosed, no-seal leakproof design and remote capacity control, its features make it ideal for applications such as chromatography columns, laboratory apparatus and industrial wet process analytical equipment.

To get all the details on why our little Chem/Meter is a big performer, write Chempump Division, Crane Co., Warrington, Pa. 18976.

CRANE **CHEMPUMP**

CIRCLE 32 ON READER SERVICE CARD

Gas Chromatographs. Features new generation of Basic gas chromatographs to perform one of 15 different specific applications. 8 pp. Carle Instruments, Inc. **428**

Recorder. Bulletin F614 describes the Miniservo 10 CM recorder and lists specifications of the battery-operated DC Miniservo recorder. 2 pp. Esterline Angus Instrument Corp. **440**

Gas Analyzer Calibration Instruments. Features the Dynacalibrator line of calibration instruments and includes applications information and full specifications for three different models. 6 pp. Metronics Associates, Inc. **441**

Inkless Recorder. Model VP-6232S heat-sensitive inkless recorder with 16 input spans of 1 mV to 100 V and 22 chart speeds is described. Soltec Corp. **442**

Solvents for Liquid Chromatography. Features complete line of ChromAR solvents and includes tables of performance figures and prices. 4 pp. Mallinckrodt, Inc. **444**

High-Purity Metals for Thin Film Evaporation Sputtering. Application note series covers all metals of practical interest including aluminum and its alloys, gold, chromium, silver, titanium/tungsten, and platinum. Materials Research Corp. **439**

Glucose Analyzer. Describes the Model 23A which provides stat glucose analysis under normal operating conditions at an analysis rate of at least 40 samples/h. 4 pp. Yellow Springs Instrument Co., Inc. **445**

Catalogs

Laboratory Products. Science Specialties, summer 77, features new additions to the product line and introduces the Digi-Sense digital thermistor thermometer. 32 pp. Cole-Parmer Instrument Co. **447**

For more information on listed items, circle the appropriate numbers on one of our Readers' Service Cards

Light Measurement Instrumentation. Contains information on high-voltage power supplies, photomultiplier tube housings, photon counting instrumentation, current measuring instrumentation, light systems, and accessories. 35 pp. Pacific Photometric Instruments **448**

Safety Supplies. Includes a wide variety of products including toxic vapor monitoring equipment and an analysis service for air samples. Also describes the hazardous waste disposal service for both spent chemicals and radioactive waste disposal. 72 pp. Interex Corp. **449**

Diagnostic Reagents. Lists reagents available for use in metabolite chemistry, protein chemistry, lipid chemistry, electrolyte chemistry, enzyme chemistry, hormone chemistry, and hemoglobin chemistry. 13 pp. Hycel, Inc. **451**

Gases. Contains sections on pure gases, gas mixtures, cross reference services, gases in disposable containers, and gas handling equipment and accessory products. 128 pp. Scott Specialty Gases **454**

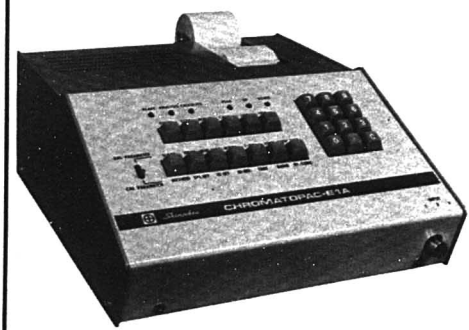

WRONG! The CHROMATOPAC-E1A DATA PROCESSOR will automatically select the most ideal operating parameters for your needs.
The system adjusts the slope sensitivity and drift parameters automatically to analyze your chromatograms no matter what the baseline does.
Its ability to calculate contents in five different ways, not to mention its capability to be used for peak heights, as well as peak areas, make the CHROMATOPAC-E1A suitable for use with other types of instrumentation, not just gas and liquid chromatographs.
One of the most amazing things is that it will do all this without breaking your budget.
Contact us today for all details on this latest addition to an excellent line of gas chromatographs and accessories.

Just Another Computing Integrator?

SHIMADZU SCIENTIFIC INSTRUMENTS, INC.
9147 Red Branch Road, Columbia, Md. 21045, U.S.A.
Phone:(301)596-6978,(301)997-1227 Telex No.:23087959

SHIMADZU (EUROPA) GmbH
4000 Düsseldorf, Georg-Glockstr, 14, F.R. Germany
Phone: (0211) 4570290 Telex No.: 08584119

SHIMADZU SEISAKUSHO LTD.
1, Nishinokyo-Kuwabaracho, Nakagyo-ku, Kyoto 604, Japan
Cable Add.: SHIMADZU KYOTO Overseas Telex No.: 05422-166

CIRCLE 191 ON READER SERVICE CARD

Cancer— The Outlaw Cell

is the theme of the *special series* starting in the **January-February** issue of CHEMISTRY magazine.

If you want to read the latest on cancer research, written in terms the non-cancer researcher can understand, you'll want this distinctive issue that carries seven of the cancer series articles.

All are written by leading scientists in clear, readable prose and are vividly illustrated.

- **Cancer — The Outlaw Cell** Donald S. Fredrickson
- **Cancer — An Overview** Henry C. Pitot
- **Tumor Growth and Spread** I. J. Fidler and M. L. Kripke
- **Control of Cell Growth in Cancer** Arthur B. Pardee and David S. Schneider
- **Cancer as a Problem in Development** Armin C. Braun
- **Puzzling Role of Cell Surfaces** David I. Meyer and Max M. Burger
- **Cancer-Causing Chemicals** Elizabeth K. Weisburger

Fill out the coupon below, mail it back with your $2.00 check and receive this remarkable issue. Add $6.00 to the check and you'll get all TEN issues of this year's CHEMISTRY magazine including all 15 articles in the cancer series.

CHEMISTRY
American Chemical Society
1155 Sixteenth Street, N.W.
Washington, D.C. 20036

January-February issue of CHEMISTRY ☐ $2.00

One Year Subscription (10 issues) *starting with the January-February 1977 issue.* ☐ $8.00

Name

Street Address

City

State Zip code

Make Checks payable to the American Chemical Society 950

From Buchler...keeping pace with the age of discovery:

A programmable controller that automates almost any laboratory.

Buchler's new Program-A-Lab automatically operates up to eight pieces of lab equipment so that you can set up virtually any procedure and leave it to run itself. Use your existing equipment without modification.

Program-A-Lab is tireless and accurate. It's all-solid-state and ultra-reliable, yet extremely simple to use. No programming knowledge is required.

The coupon below will bring you full details. Or, contact any leading laboratory supply house. Program-A-Lab, from Buchler.

SEARLE **Buchler Instruments**
Division of Searle Diagnostics Inc.
1327 Sixteenth Street
Fort Lee, N.J. 07024 U.S.A.
201 - 224-3333

Buchler Instruments: made in the United States, sales and service worldwide.

Buchler Instruments, Division of Searle Diagnostics Inc.
1327 Sixteenth Street, Fort Lee, N.J. 07024, U.S.A.

Gentlemen: Please send me FREE full details on the new Program-A-Lab.

Name _____ Title _____

Organization _____

Address _____

City _____ State _____ Zip _____

Phone ( ) _____

New and Best-Selling Books from Wiley...

MODERN PRACTICE OF GAS CHROMATOGRAPHY
Robert L. Grob

Presents an in-depth treatment of the theory, interpretation of data, selection of system variables, and applications of modern gas chromatograpy. Ideal for readers with varied scientific backgrounds.
654 pp. (0 471 01564-4) **1977** $22.50

THE ANALYTICAL CHEMISTRY OF SYNTHETIC DYES
Edited by K. Venkataraman

A comprehensive survey of synthetic dyes and their analytical chemistry, incorporating the contributions of numerous authorities in this field. Contains a classification of dyes for analytical purposes and describes all the important methods for making this analysis. Offers specific analytical procedures for identifying dyes on textile and nontextile substrates, in food, drug and cosmetic colors, and hair dyes; and special techniques for ecological and toxicological monitoring.
591 pp. (0 471 90575-5) **1977** $42.50

CONTAMINATION CONTROL IN TRACE ELEMENT ANALYSIS
Morris Zief & James W. Mitchell

A state-of-the-art review of contamination control techniques, specifically applicable to trace analysis but also useful in other ultrapurity work.
262 pp. (0 471 61169-7) **1976** $23.75

ORGANIC ELECTRONIC SPECTRAL DATA, Vol. XII—1970
John P. Phillips, Henry Feuer & B.S. Thyagarajan

Part of the largest collection of spectral data of its kind, containing spectral maxima, extinction coefficients, and source references for ultraviolet and visible spectra of organic compounds. Entries are organized according to the molecular formula index system used by Chemical Abstracts. Indexed for easy reference.
1,138 pp. (0 471 02305-1) **1976** $48.50

MICROSCALE MANIPULATIONS IN CHEMISTRY
T.S. Ma & V. Horak

This comprehensive sourcebook lists the techniques needed for separating, purifying, and isolating *less-than-a-gram* and *microgram* substances. In-depth coverage includes fractionalizing, chromatographic, electrophoretic, and multicomponent separation procedures, augmented by numerous high-quality illustrations. Also included are explanations of devices for extraction, filtration, drying, disintegration, homogenization, and agitation. Chemical Analysis Series, Vol. 44.
488 pp. (0 471 55799-4) **1976** $29.25

TRACE ANALYSIS: Spectroscopic Methods for Elements
James Dudley Winefordner

Provides essential knowledge for those involved with trace analysis of elements in real samples. Teachers, researchers, and students will discover all the information they need to perform a specific trace elemental determination as well as an invaluable critical comparison of spectroscopic methods. For each atomic technique, the principles, instrumentation, methodology, and applications are briefly reviewed.
484 pp. (0 471 95401-2) **1976** $26.50

"...a lucid account of modern theory written with a strong analytical bias...a monumental work..." —Nature

TREATISE ON ANALYTICAL CHEMISTRY
Part 3, Volume 4, A Comprehensive Account in Three Parts: Part 1—Theory and Practice; Part 2—Analytical Chemistry of Inorganic and Organic Compounds; Part 3—Analytical Chemistry in Industry.
Edited by I.M. Kolthoff, Philip J. Elving, & Fred H. Stross

688 pp. (0 471 02765-0) **1977** $39.95

AQUAMETRY, 2nd Ed., Part 1 A Treatise on Methods for the Determination of Water
John Mitchell, Jr. & Donald Milton Smith

Evaluates methods of analysis for determining amounts of water (ranging from traces to major concentrations) in gases, liquids, and solids. Provides background information on structure and physical properties followed by chemical, thermal, separation, spectroscopic and other instrumental techniques, and radiochemical and physical methods. This edition has been expanded to describe all methods of value and major breakthroughs for determining water. Chemical Analysis Series.
Approx. 768 pp. (0 471 02264-0) **1977** $29.95

ANALYTICAL APPLICATIONS OF NMR, Vol. 48
D.E. Leyden & R.H. Cox

An introduction to the principles, practices, instrumentation, and applications of nuclear magnetic resonance in analytical chemistry. Discusses the theory of NMR, experimental and instrumental aspects of NMR, analysis of spectra and determination of structure, carbon-13 NMR, methods of quantitative measurements, and examples of analytical applications.
Approx. 448 pp. (0 471 53403-X) **1977** $27.50

THE MINICOMPUTER IN THE LABORATORY With Examples Using the PDP-11
James W. Cooper

Covers in detail the use of the minicomputer for the acquisition and analysis of laboratory data and describes the programming of the DEC PDP-11 minicomputer in language understandable to the beginner. Examples and problems take the student through each phase of the programming language.
365 pp. (0 471 01883-X) **1977** $19.50

WILEY-INTERSCIENCE
a division of John Wiley & Sons, Inc.
605 Third Avenue
New York, N.Y. 10016
In Canada: 22 Worcester Road, Rexdale, Ontario

Please send the books indicated for
15-DAY FREE EXAMINATION.
(Restricted to the continental U.S. and Canada.)

Mail to: WILEY-INTERSCIENCE
P.O. Box 092
Somerset, N.J. 08873

- ☐ Grob (0 471 01564-4)
- ☐ Venkataraman (0 471 90575-5)
- ☐ Zief (0 471 61169-7)
- ☐ Phillips, Vol. XII (0 471 02305-1)
- ☐ Ma (0 471 55799-4)
- ☐ Winefordner (0 471 95401-2)
- ☐ Kolthoff, Part 3, Vol. 4 (0 471 02765-0)
- ☐ Mitchell, 2nd E., Part 1 (0 471 02264-0)
- ☐ Leyden (0 471 53403-X)
- ☐ Cooper (0 471 01883-X)

☐ Payment enclosed, plus sales tax. Wiley pays postage/handling. We normally ship within 10 days. If shipment cannot be made within 90 days, payment will be refunded.
☐ Bill me. ☐ Bill firm or institution.

NAME

AFFILIATION

ADDRESS

CITY STATE/ZIP
092 A 8121-51 Prices subject to change without notice.

CIRCLE 234 ON READER SERVICE CARD

Principles, Apparatus, and Applications of Stripping Analysis

Electrochemical Stripping Analysis. Frantisek Vydra, Karel Štulik, and Eva Juláková. 283 pages. Halsted Press, 605 Third Ave., New York, N.Y. 10016. 1977. $40

Reviewed by K. W. Hanck, Department of Chemistry, North Carolina State University, Raleigh, N.C. 27607

Stripping analysis has been used for many years for trace level determinations; the theoretical principles of the method have also been stated and experimentally verified. The practical procedures and theoretical/experimental investigations of principle have in many instances been published in different sections of the analytical literature. The authors of this monograph have successfully gathered into one book most of what is known about the principles, apparatus, and applications of stripping analysis.

Since the book includes both theoretical principles and practical applications, it should be of value to both practitioners of stripping analysis and fundamental electrochemists. The book uses a review style and cites over 500 references.

The key operations in stripping analysis are examined in a systematic fashion with frequent examples from the literature. These include preconcentration by deposition, the stripping process, and methods for monitoring the stripping step. The systematization and discussion of the methods used to electrolytically strip the deposit from the working electrode should be of particular value to the nonelectrochemist. The principles of each approach are briefly reviewed, and key equations presented by use of a consistent set of symbols. Few derivations are given, but original literature citations are included. Developments which occurred after 1975 are not included, but the coverage prior to 1975 is complete.

The section describing the construction and electrochemical properties of indicator electrodes is an excellent source of ideas and data for both the practitioner and the fundamentalist. Since mercury is the most common component of electrodes used in stripping analysis, the authors give it particular emphasis by discussing the

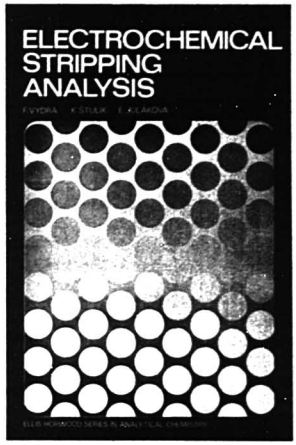

chemistry and properties of amalgams. Data pertaining to metal solubility in mercury, diffusion coefficients of metals in mercury, solubility product values for intermetallic compounds, and kinetic parameters of amalgam electrodes are included and used to rationalize the behavior of mercury electrodes in stripping analysis.

Diagrams of several electrolytic cells and working electrodes are included. A few schematic diagrams of instruments are presented, but no attempt is made to explain their electronic operation.

The purification of solvents and electrolytes for use in stripping analysis is briefly discussed. This is not, however, one of the better sections of the book. For example, purification of water via ion exchange is deemed not suitable for stripping analysis; yet, several studies have shown that water purified by ion exchange and ultrafiltration is superior in trace metal content to that obtained by repeated distillation.

The most valuable chapter in the book, in my view, is the one systematizing applications of stripping analysis by element. The order in which elements appear in the periodic table is followed. Both metals and nonmetals are included. Although many of the references are in journals that may be difficult to obtain, sufficient detail is given to permit the method to be tried without consulting the original literature.

The book is made easy to read by the excellent English used throughout. I found no obvious errors and recommend it to both the practitioner of stripping analysis and the fundamental electrochemist as an excellent review of stripping analysis and its applications.

Polarographic Oxygen Sensors. I. Fatt. 278 pages. CRC Press, Inc., 18901 Cranwood Parkway, Cleveland, Ohio 44128. 1976. $54.95

Reviewed by J. J. Lingane, 94 Adams St., Lexington, Mass. 02173

Oxygen is the most abundant of the terrestrial elements, since in combined form it makes up about one-half of the lithosphere, two-thirds of the human body, and in free form one-fifth of the atmosphere. Only seldom are we concerned with the determination of combined oxygen because we know it is there and evaluate it by difference. In the free state in gas mixtures, the classical methods of gas analysis or, more recently, oxygen's paramagnetic properties serve quite well for its determination. But the determination of the concentration of oxygen dissolved in liquid media was for past generations a difficult problem. It was not until the invention of polarographic analysis with the dropping mercury electrode by Jaroslav Heyrovsky about 50 years ago that it became possible to measure dissolved oxygen relatively easily. In isolated samples under laboratory conditions, this is still the most exact method.

However, the physical characteristics of the dropping mercury electrode are not easily adaptable to determining dissolved oxygen under many "field" conditions of crucial interest, such as deep in the Gulf Stream or in the circulating blood in a living animal body. The first attempted remedy was to replace the dropping mercury electrode with a solid metal cathode (usu-

ally platinum or gold), which was successful in some solutions but generally unsuccessful in biological media. In the latter case, adsorption of organic materials onto the platinum cathode often caused its response to become erratic and unreliable. Furthermore, when solutions contain easily reducible ions, their reduction currents can interfere with that of oxygen. During a few years prior to 1956, Leland C. Clark, Jr., discovered an elegantly simple way to prevent such interferences. He devised a polarographic cell in which the platinum cathode was in an innocuous electrolyte solution (e.g., potassium chloride), but this solution was separated from the test solution by a polymeric membrane (e.g., polyethylene). Oxygen diffuses easily through the membrane to reach the platinum cathode, but the membrane effectively prevents the transfer of organic and ionic substances. Because the membrane is impermeable to ions, it has a very large electrical resistance so that the second (auxiliary or reference) electrode of the cell must be in direct contact with the internal solution, but this is easily accomplished. When a constant voltage is impressed across the cell, the resulting current is a measure of the oxygen concentration in the external test solution, and the cell is calibrated with solutions of known oxygen concentration or solutions which are in equilibrium with a gas phase of known oxygen partial pressure. In its original form the dimensions of this Clark cell were similar to that of an ordinary glass electrode, but miniature designs of it have been constructed tiny enough to fit into a catheter for insertion into an artery of a living animal.

The present book is concerned primarily with the remarkable progress that has been made in determining dissolved oxygen in biological systems, chiefly by means of a Clark-type cell in various modified forms. However, some other designs of oxygen sensors are also described.

The first three chapters comprise a brief but adequate review of pertinent electrochemical theory. The remaining eight chapters describe applications of polarographic oxygen sensors and the results obtained in a wide variety of biological media, including various organs of the animal body in vivo. Quite properly, the emphasis is on the many different physical designs of the sensors that have been described in the literature for specific purposes. It is not feasible in the space available here to even list all these, but some examples may perhaps serve to indicate the scope of the treatment. There are detailed discussions of: the Clark-type sensor for determining the oxygen tension in isolated blood samples and other liquids; tiny catheter sensors inserted directly into the blood circulatory system; sensors for measuring oxygen tension in earlobe blood for possible correlation with that of arterial blood; sensors for oxygen tension in tissues, such as in the fetal scalp at the time of birth to detect possible fetal hypoxia; and tiny "needle" sensors for measurements deep in animal tissue. In every case, the very clearly executed line drawings of the cells and measuring techniques that are presented serve excellently to make the discussions exceptionally lucid.

Quite justifiably, the author takes for granted the commercial availabili-

ULTREX®
Ultrapures

When you simply can't tolerate impurities or uncertainties in your starting materials.

Over 100 of the purest reagents and chemicals available anywhere in the world. Every product is accompanied by a detailed Certificate of Analysis of the actual lot supplied. In terms of spectrochemically detectable impurities, ULTREX products are typically 99.995% to 99.99995% pure. And the extremely low content of all impurities (often at the parts per billion level) satisfies the most rigid use requirements.

Whenever your requirements for purity and product definition are stringent, ULTREX ultrapures can indeed insure against loss of time, effort, and other expenses.

Consider ULTREX when you just can't afford to gamble with impurities or uncertainties.

Write for new ULTREX ultrapure Reagent brochure

J. T. Baker Chemical Co.
Phillipsburg, N.J. 08865
201 859-5411

J.T.Baker
CHEMICALS

CIRCLE 19 ON READER SERVICE CARD

Electrochemical Studies of Biological Systems

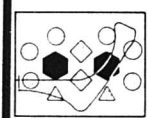

The twelve papers in this significant new collection provide a representative cross section of the kinds of electrochemical methods used to characterize biological systems, as well as the kinds of biological problems that are being studied by such methods

ACS Symposium Series No. 38

Donald T. Sawyer, *Editor*
University of California

A symposium sponsored by the Division of Analytical Chemistry of the American Chemical Society.

CONTENTS

vitamin B_{12} and related cobalamins • bioelectrochemical modelling of cytochrome c • potentials of metal ion couples in complexes • metalloporphyrins in aprotic solvents • N-bridged dimer in nonaqueous media • reduction of nitrogenase substrates • manganese (II) and -(III) 8-quinolinol complexes • interfacial behavior of purines • coulometric titration of biocomponents • rotating ring disk enzyme electrode • left ventricle/aorta simulator • EDTA and NTA in phytoplankton media

216 pages (1977) clothbound $15.50
LC 76-30831 ISBN 0-8412-0361-X

Order from:
SIS/American Chemical Society
1155 16th St., N.W./Wash., D.C. 20036

ANALYTICAL CHEMISTS . . . ORGANIC CHEMISTS . . . BIOCHEMISTS . . . TEACHERS . . . STUDENTS

ADD TO YOUR REPERTORY OF ANALYTICAL TECHNIQUES WITH THE NEW

ACS AUDIO COURSE

C-13 NMR SPECTROSCOPY

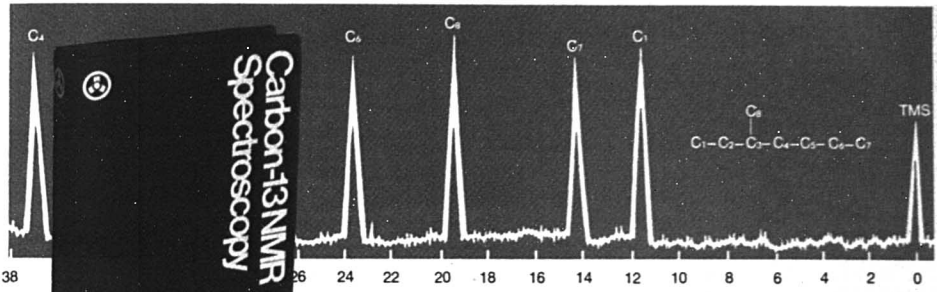

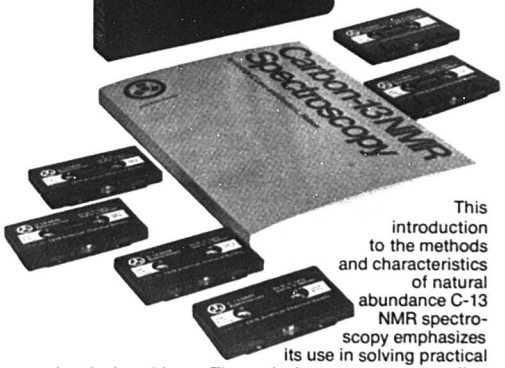

This introduction to the methods and characteristics of natural abundance C-13 NMR spectroscopy emphasizes its use in solving practical chemical problems. Theoretical treatments are qualitative; applications to molecular structure analysis are stressed. It also provides a non-mathematical introduction to Fourier transform NMR and discussions of various classes of compounds including aliphatics, aromatics, ions and other intermediates, organometallics, natural products, and synthetic and biological macromolecules. Spin-relaxation parameters are introduced and their use in C-13 NMR is demonstrated with examples.

Learn from nationally recognized authorities

Dr. George C. Levy, Associate Professor of Chemistry, Florida State University. Dr. Levy is co-author of *Carbon-13 Nuclear Magnetic Resonance for Organic Chemists;* editor, *Topics in Carbon-13 NMR Spectroscopy;* and member of the editorial boards of *The Journal of Magnetic Resonance* and *Organic Magnetic Resonance.*

Dr. Gordon L. Nelson, Manager, Combustibility Technology for General Electric Plastics Division. Dr. Nelson is the author of over 20 publications and co-author, with Dr. Levy, of *Carbon-13 NMR for Organic Chemists.*

The convenient way to learn

This complete Audio Course combines the ease of listening to the tapes with the reinforcement of studying the material in the manual and the challenge of doing the exercises. It also provides charts, data, illustrations—the same materials Dr. Levy and Dr. Nelson would normally use in classrooms or auditoriums.

Individual or group use

Like all ACS Audio Courses, C-13 NMR Spectroscopy is ideal for individual or group use, with extra manuals available for each student.

No-risk guarantee

If you are not completely satisfied with your ACS course, just return it in ten days for full refund or cancellation of invoice.

The unit

Six audiotape cassettes (6.3 hours playing time) and a 240-page manual, $160.00. Additional manuals, 1-9 copies . . . $14.00 each; 10-49 . . . $12.00 each; 50 or more . . . $11.00 each. (Catalog no. C-31)

Department of Educational Activities
American Chemical Society, 1155 Sixteenth Street, N.W.
Washington, D. C. 20036 / (202) 872-4588

☐ Please send ____ *C-13 NMR Spectroscopy* Audio Courses @ $160.00 each.

☐ Please send ____ manuals at a total cost of $ ____.

☐ Purchase order enclosed ☐ Payment enclosed

Note: Payment must accompany orders of $25.00 or less. Please allow up to five weeks for delivery.

☐ Please send information on other ACS Audio Courses.

Name _____

Organization _____

Address ☐ Home ☐ Business _____

City _____ State _____

ZIP _____ Phone _____

Required Reading

from Waters the Liquid Chromatography People

New!

Analysis of Pharmaceutical Products

Describes rapid, economical assay & quantitation methods for many drug products. LC separations of cough preparations, antibiotics, vitamins, and tranquilizers are detailed as well as various specialized LC techniques.

CIRCLE 235 ON READER SERVICE CARD

New!

Paired-Ion Chromatography

The technique of Paired-Ion Chromatography, an alternative to ion exchange is described. PIC™ allows simultaneous analysis of acids, bases, and neutral compounds.

CIRCLE 236 ON READER SERVICE CARD

New!

Detectors Brochure

Discusses choosing a LC detection system for specific applications. The merits of Model 440 UV/Visible Absorbance Detector and 400 Series Differential Refractometers are cited.

CIRCLE 237 ON READER SERVICE CARD

free from

WATERS ASSOCIATES

215 Maple Street, Milford, MA 01757
Telephone (617) 478-2000

ty of the necessary electrical circuitry for performing the measurements. However, there is a 10-page Appendix written by Richard C. LaForce on the application of operational amplifiers for this purpose.

The coverage of the pertinent literature seems to be thorough. There are about 600 references, and most of these are to papers published during the past 10 or 15 years. Professor Fatt not only has a gift for concise, lucid expression, but he also has the ability to critically interpret the significance of experimental data. He was not content merely to describe experimental techniques and catalog the literature, but he also provides interpretations of the significance of the reported results.

As far as I know, this is only the second book devoted specifically to the determination of dissolved oxygen. The first was that of Fritz Tödt (Elektrochemische Sauerstoffmessungen, W. deGruyter & Co., Berlin, 1958) which was concerned with galvanic rather than polarographic sensors. The present book is, I believe, the first to comprehensively describe the applications of electrochemical sensors in medical practice, as well as other biological applications. Anyone concerned with these applications will certainly want to consult this book, but it should also be of interest to investigators in other fields that require measurements of dissolved oxygen.

Analytical Chemistry. 2nd Ed. Gary D. Christian. xvi + 648 pages. John Wiley & Sons, Inc., 605 Third Ave., New York, N.Y. 10016. 1977. $16.95

Reviewed by Donald F. Logdson, USAF Occupational and Environmental Health Laboratory, McClellan AFB, Calif. 95652

Although many different courses teach analytical procedures, there are relatively few courses entitled analytical chemistry. However, there is a definite need for a course of this type where the student can learn careful and quantitative laboratory skills and techniques. This textbook is designed for use in such a course.

The book includes 25 chapters grouped into 11 parts, three appendices, and a subject index. Part one introduces basic principles and methods of analytical chemistry. Parts two and three discuss data handling and sample preparation. Methods of separation are presented in part four, including chapters on gravimetric analysis, solvent extraction, and chromatographic procedures. Parts five–eight discuss different methods of measurement, including volumetric methods, electrical methods, optical methods, and methods based on rate. Gas analysis is presented in part nine, and part ten is a brief review of automation in the laboratory. The last part discusses applications of analytical chemistry to such areas as clinical chemistry, drug analysis, and pollution analysis. The first appendix briefly describes pertinent references useful to those studying analytical chemistry. The second appendix is a short review of some basic mathematical operations. The third appendix includes five tables of useful constants.

A number of additions and updatings have been made in this second edition. Some experiments have been deleted, and others added to bring the total to 51. It is unfortunate that it was necessary to leave out the chapter on laboratory safety, but this is a minor objection to an otherwise excellent textbook. This textbook should definitely be considered for courses in analytical chemistry and also as a supplementary or reference text for other chemistry courses.

Chemisorption: An Experimental Approach. Gerd Wedler (Translated by Derek F. Klemperer). 250 pages. Butterworths Inc., 19 Cummings Park, Woburn, Mass. 01801. 1976. $23.50

Reviewed by W. Henry Weinberg, Division of Chemistry and Chemical Engineering, California Institute of Technology, Pasadena, Calif. 91125

This short book represents an English translation of an extensively revised version of Professor Wedler's text that appeared in 1970 with the title "Adsorption, Eine Einführung in die Physisorption und Chemisorption". The revised text discusses adsorption thermodynamics and kinetics as well as the nature of the adsorbed species from the point of view of experimental measurements. The latter include optical spectroscopies (IR, visible, UV, and ellipsometry), resonance spectroscopies (NMR and ESR), surface electrical and magnetic measurements (contact potential difference, surface conductivity, thermoelectric power, Hall effect and magnetic susceptibility measurements), low-energy electron spectroscopies and diffraction (field emission, Auger, appearance potential and characteristic electron energy loss spectroscopies, electron stimulated desorption, and low-energy electron diffraction), photoelectron spectroscopies (UPS and XPS), and the use of ion beams to

Our gases are rare. Our hardware is not.

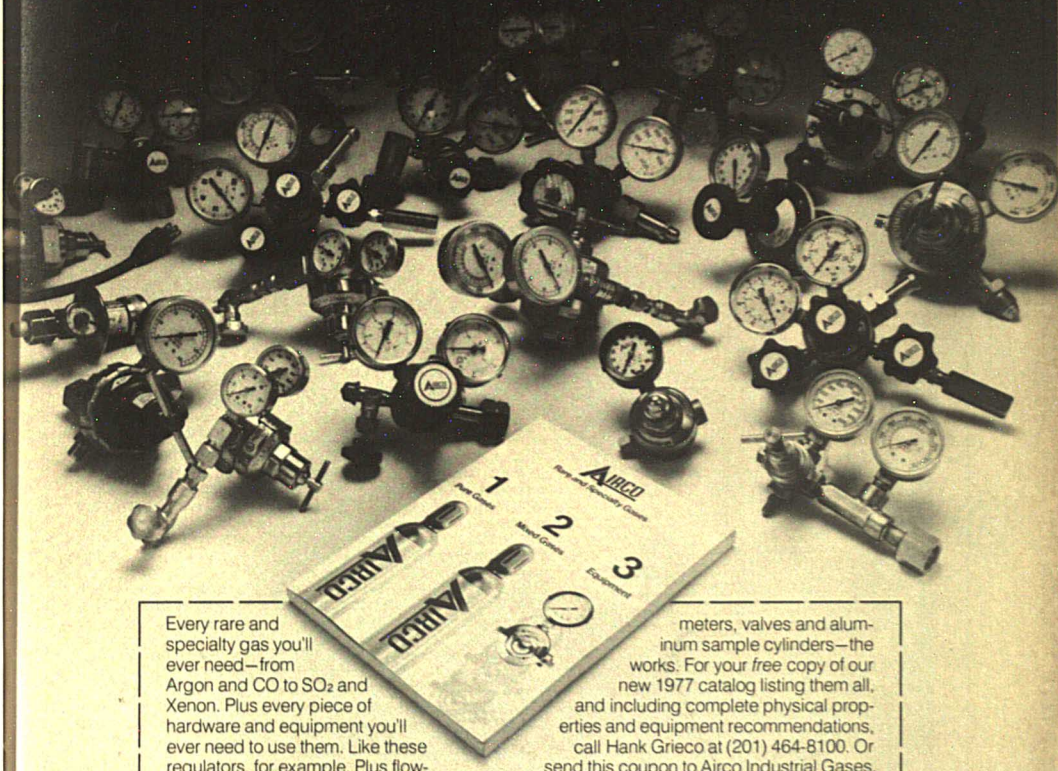

Every rare and specialty gas you'll ever need—from Argon and CO to SO_2 and Xenon. Plus every piece of hardware and equipment you'll ever need to use them. Like these regulators, for example. Plus flowmeters, valves and aluminum sample cylinders—the works. For your *free* copy of our new 1977 catalog listing them all, and including complete physical properties and equipment recommendations, call Hank Grieco at (201) 464-8100. Or send this coupon to Airco Industrial Gases.

Name_____ Title_____

Company_____

Address_____

City_____ State_____ Zip_____

Airco Industrial Gases, Rare & Specialty Gases Dept., 575 Mountain Ave., Murray Hill, NJ 07974.

CIRCLE 4 ON READER SERVICE CARD

probe adsorption (ion backscattering, secondary ion mass spectrometry, and ion neutralization spectroscopy).

Of necessity, when discussing such a large number of topics in such a short book, the treatment is broad and rather superficial. As the title of the book implies, the emphasis is on experimental techniques and results. Indeed, there are very few derivations of equations, and the little theory present in the book is generally naive. Due to the personal interests of the author, there is considerable emphasis in the book on experimental investigations of thin films, and rather less emphasis on studies of well-characterized surfaces of single crystals. This is a matter of taste, but the reader should be forewarned. More unfortunate, perhaps, is the fact that the author chose not to discuss three of the more important current thrusts of research in surface chemistry, namely, the use of inelastic electron scattering to obtain the vibrational structure of admolecules (either the scattering of monochromated electron beams from surfaces or inelastic electron tunneling with either a diode or a field emission configuration), the use of angle-resolved UV–photoelectron spectroscopy to determine the bonding geometry of admolecules, and the use of tunable (synchrotron) photon sources in photoelectron spectroscopy to determine the composition of bonding, nonbonding, and antibonding orbitals of the adsorbate–substrate complex.

It is not easy to decide for whom this book was written. It is far too superficial for an expert in the field; yet, a sufficient number of details are omitted that a novice might well find it difficult to follow. Perhaps the best feature is the extensive number of references to the original literature (a total of 744 citations). Unfortunately, the literature is only surveyed through mid-1974, and a great deal of new results have appeared in the past three years. However, it does represent a good starting point. This book could be used as a supplemental text for a specialized course on surface chemistry, but it would not be suitable as the sole text in such a course. The quality of reproduction is good, and there are very few typographical errors. The price is only moderately unreasonable.

New Books

Characterization of Metal and Polymer Surfaces. Vol. 1, Metal Surfaces.
Lieng-Huang Lee, Ed. xiv + 517 pages. Academic Press, Inc., 111 Fifth Ave., New York, N.Y. 10003. 1977. $26.50

Characterization of Metal and Polymer Surfaces. Vol. 2, Polymer Surfaces.
Lieng-Huang Lee, Ed. xv + 465 pages. Academic Press, Inc., 111 Fifth Ave., New York, N.Y. 10003. 1977. $24

During the Centennial Meeting of the American Chemical Society in New York City in the spring of 1976, the Symposium on Advances in Characterization of Metal and Polymer Surfaces was held to mark the achievements of surface science. The papers presented at the symposium are now collected in these two volumes. The arrangement does not follow the original order of presentation at the symposium. Rather, the volumes are divided as follows: Volume 1 (Metal Surfaces)—atomic probe and Mössbauer spectroscopy, Auger electron spectroscopy and electron microprobe, low-energy electron diffraction,

ANAC SPECIALISTS IN ION OPTICS

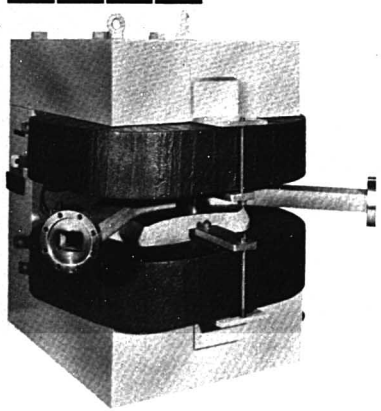

ANAC MODEL 3442E
Mass Spectrometer Electromagnet
Mass Energy Product 3.4 amu.MeV/Z^2
Bending Angle 90°
Bending Radius 229mm
Object Distance 724mm
Image Distance 724mm

ANAC specializes in the design and manufacture of electromagnetic ion optics elements (quadrupoles, switchers, beam steerers, analyzers, mass spectrometer magnets) offering both a complete custom design and manufacturing service and a wide range of "standard" magnets. Our precision ion optics are in use at nuclear research laboratories throughout the world and increasingly by mass spectroscopists and OEM system manufacturers who are demanding a higher level of performance from their ion optics — Why?

We use a sophisticated computer field modelling and precision ray tracing design technique which optimizes source to image resolution within system constraints of acceptance angle, object/image distance, etc. This design technique is superior to analytical techniques which generally limit the aberration correction to only first or second order analysis.

We incorporate design features which insure the predicted performance will be achieved — homogenizing air shims to improve field homogeneity, uniformly saturating pole edge contours to maintain optical constancy at all fields, precision mechanical construction to accurately set and maintain the gap, and special rolled, annealed and tested low carbon steel to improve homogeneity and magnetic circuit efficiency.

We have the manufacturing experience to execute the design practically and economically.

We back up magnet sales with a full range of accessories — bakeable vacuum chambers, stands, power supplies, magnetic field control, etc.

High performance ion optics? — write or call the specialists for more information.

ANAC Inc.
PO Box 7453, Menlo Park, CA 94025
Tel (415) 322-8664

AD-29

CIRCLE 5 ON READER SERVICE CARD

Try our **it-can't-be-a-balance** balance

[There's never been anything quite like it.]

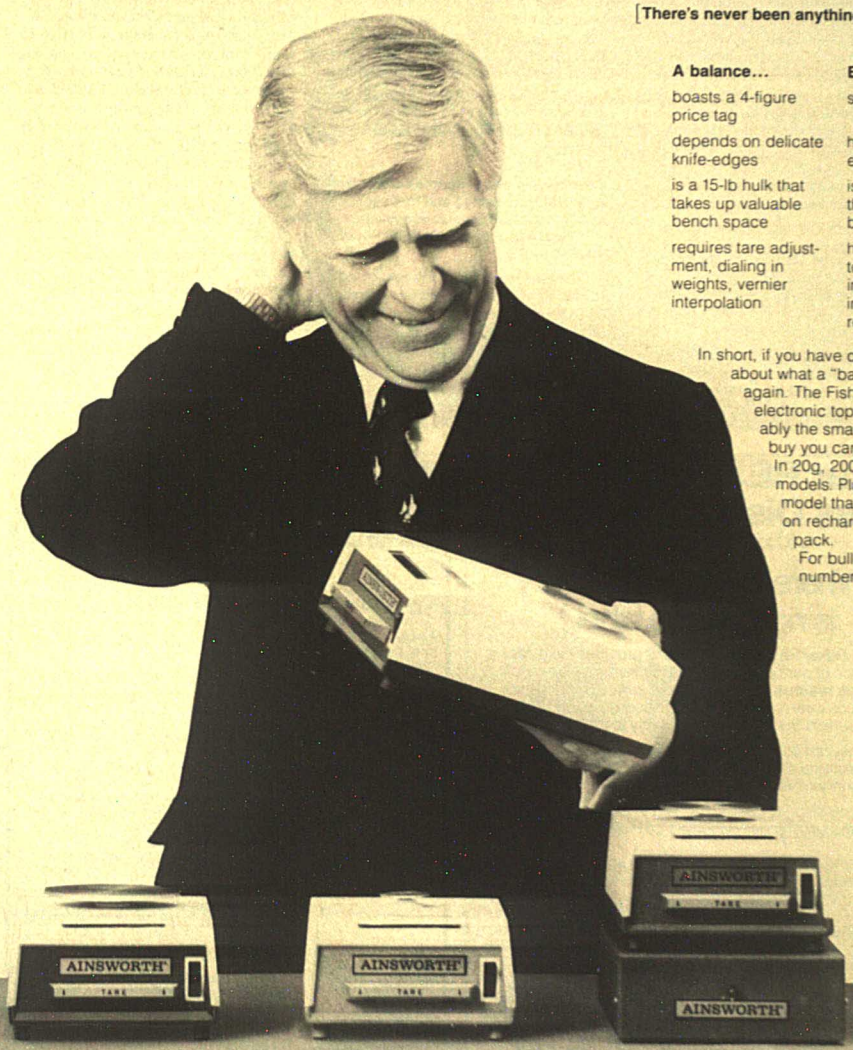

A balance...	But ours...
boasts a 4-figure price tag	starts at $795
depends on delicate knife-edges	has rugged electronics
is a 15-lb hulk that takes up valuable bench space	is a 5-lb wonder that fits into a briefcase
requires tare adjustment, dialing in weights, vernier interpolation	has a single touch-bar for instant tare, instant sample readout

In short, if you have certain thoughts about what a "balance" is, think again. The Fisher/Ainsworth electronic toploader is probably the smartest balance buy you can make.

In 20g, 200g, and 2000g models. Plus a 200g field model that runs 8 hours on rechargeable battery-pack.

For bulletin, circle number below.

Fisher Scientific Company

CIRCLE 74 ON READER SERVICE CARD

secondary ion mass spectroscopy, and photoelectron and electron tunneling spectroscopy; Volume 2 (Polymer Surfaces)—electron spectroscopy for chemical analysis, infrared and laser Raman spectroscopy, microscopy for polymers, and surface-chemical and radiation analyses. For each of these parts, there is at least one plenary lecture paper to provide an authoritative survey of the subject matter. Other contributed papers then present recent research results related to the same theme. Two postconference contributions have been included while several of the original papers have been published elsewhere. A total of 36 papers as well as transcripts of the discussion sessions is presented. The volumes are reproduced from typewritten text.

Hazards in the Chemical Laboratory. 2nd Ed. G. D. Muir, Ed. xvii + 473 pages. The Chemical Society, Burlington House, London, W1V 0BN, England. 1977. $14

The major part of this laboratory manual is devoted to the alphabetical listing of hazardous chemicals. Accompanying each entry are the measures to be taken in the event of accidents. The recommended measures for most of the chemicals listed include information on how to deal with toxic effects, spillage, and fires where appropriate. This chapter consists of approximately 75% of the total space and is printed in yellow tinted paper. The remainder of the book contains chapters on the Health and Safety at Work Etc. Act 1974 (United Kingdom), planning for safety, fire protection, reactive chemical hazards, chemical hazards and toxicology, medical services and first aid, and precautions against radiation.

Colorimetric and Fluorimetric Analysis of Steroids. J. Bartos and M. Pesez. xii + 274 pages. Academic Press Inc., 111 Fifth Ave., New York, N.Y. 10003. 1976. $21.50

The analytical methods presented in this 13-chapter volume are restricted to those based on chemical reactions performed in solution which yield a visible spectrum or a fluorescence spectrum. Qualitative tests are quoted only when quantitative procedures might be derived from them. The first chapter deals with nomenclature, the second with functional group analysis, and the third chapter deals with halochromism and halofluorism. In the remaining 10 chapters, different analytical methods for analysis of various classes of steroids are discussed. These classes include sterols and vitamin D, bile acids, estrogens, gestogens, androgens, corticosteroids, contraceptive progestogens, cardiac glycosides, steroid saponins and sapogenins, and steroid alkaloids. Although most of the procedures described are detailed enough to permit duplication without consulting the original work, extensive lists of the literature references are provided at the end of each chapter, and these include some as recent as 1975.

Molecular Spectroscopy. Alan R. West, Ed. xx + 578 pages. Heyden & Son Inc., Kor-Center East, Bellmawr, N.J. 08030. 1977. $60

The articles assembled in this book were presented at the Sixth Conference on Molecular Spectroscopy organized by the Institute of Petroleum,

'Baker RESI-ANALYZED' Glass Distilled Solvents

(Where the proof of purity is right on the label.)

The J. T. Baker Resi-Analyzed brand provides the greatest assurance of performance for any solvents designed for **pesticide residue analysis.** These solvents exhibit no extraneous peaks, have excellent baseline stability, show a narrow solvent front, and return rapidly to the baseline.

Resi-Analyzed solvents are controlled by 8 or more quality tests, including 4 GC determinations (ECD, FPD for P and S, Hall conductivity detection for N).

The testing also includes water, APHA color, non-volatile matter and substances darkened by H_2SO_4.

Write for technical literature

For Instrumental Analysis
The Professional Chooses J. T. Baker

J. T. Baker Chemical Co.
Phillipsburg, N.J. 08865
201 859-5411

J.T.Baker ® CHEMICALS

CIRCLE 20 ON READER SERVICE CARD

Topics in . . .
Chemical Instrumentation—II

An ACS Reprint Collection

A volume of reprints from the *Journal of Chemical Education*

Galen W. Ewing, *Editor*

310 pages (1977) hardback $12.00
ISBN 0-8412-0367-9
LC 73-153064

This new collection of selected reprint articles from the "Topics in Chemical Instrumentation" column in the JOURNAL OF CHEMICAL EDUCATION provides excellent coverage of the field from January 1970 through November 1975.

In order to furnish the most complete, up-to-date information on the subject many of the authors have added supplemental material to their papers. The 36 reprints are listed according to subject matter rather than by chronological order.

This useful collection will be of particular interest to analytical chemists, college chemistry faculties, research chemists, librarians, and those seeking an introduction to the state of the art.

SIS/American Chemical Society
1155 16th St., N.W./Wash., D.C. 20036

Please send _____ copies of *Chemical Instrumentation—II* at $12.00 per copy.

☐ Check enclosed for $ _____ . ☐ Bill me. Postpaid in U.S. and Canada, plus 40 cents elsewhere.

Name

Address

City State Zip

Students Instructors Researchers Problem-Solvers . . .

keep on top of recent advances in analytical chemistry.

MODERN CLASSICS IN ANALYTICAL CHEMISTRY

Volume II

Edited by Alvin L. Beilby

A selection from the best feature articles that appeared in issues of ANALYTICAL CHEMISTRY from 1970 through 1975.

Particularly suitable as supplementary reading for the advanced student of analytical chemistry and for those who must keep up with the latest developments in analytical chemistry and instrumentation, this convenient collection of source material contains valuable information presented only in outline form in many modern textbooks.

Volume II 314 pages (1976) $8.50 paperbound
Volume I 268 pages (1970) $5.75 paperbound

CONTENTS (Volume II)

- Development of Analytical Chemistry
- Spectroscopy (11 articles)
- Electrochemistry (2 articles)
- Chromatography (3 articles)
- Automation and Instrumentation(6 articles)
- Measurement Techniques (7 articles)
- The Analytical Approach (9 articles)
- Art Conservation (2 articles)

SIS/American Chemical Society
1155 16th St., N.W./Wash., D.C. 20036
Please send the following books:
Modern Classics in Analytical Chemistry
_____ (**Vol. II** $8.50 paperbound)
_____ (**Vol. I** $5.75 paperbound)
☐ My check for $ _____ is enclosed. ☐ Bill me. Postpaid in U.S. and Canada, plus 40 cents elsewhere. (Prices subject to change without notice.)
Name
Address
City State Zip

PHILIPS LC-3

VARIABLE WAVELENGTH UV DETECTOR FOR LIQUID CHROMATOGRAPHY

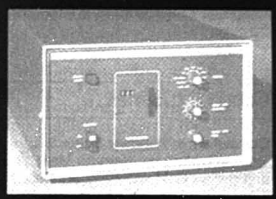

The Philips *Pye Unicam* LC-3 is simply the best variable wavelength UV Detector for the money. The LC-3's reference compensated optics gives the stability of Double Beam with the high energy of Single Beam. High energy means high performance even down to 190 NM.

Write or call today for complete literature
PHILIPS ELECTRONIC INSTRUMENTS, INC.
85 McKee Drive, Mahwah, N.J. 07430
Tel: (201) 529-3800

PHILIPS®

CIRCLE 173 ON READER SERVICE CARD

1 Quality Source

For all your liquid sampling needs.

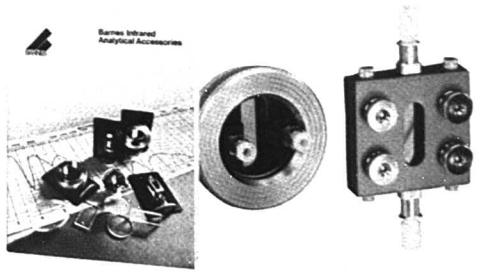

Barnes offers a variety of cells and holders to meet virtually every liquid sampling requirement. Sealed or demountable, the cells have precise pathlengths and are leakproof. And they are available with almost any window material.

Barnes cells fit all types of spectrometers, including Beckman, Perkin-Elmer and Varian, and are significantly lower priced.

For all your liquid sampling needs, check pages 8 through 19 in our new 40 page catalog, "Barnes Infrared Analytical Accessories." Write or phone for your copy. Barnes Engineering Company, 30 Commerce Road, Stamford, Connecticut 06904. Call toll free (800) 243-3498 Ext. 281 or in Conn. (203) 348-5381 Ext. 281. **NOW GSA LISTED.**

BARNES **Your IR Spectroscopy Source.**

CIRCLE 23 ON READER SERVICE CARD

Chromatography-Automatically

From Automatic, Sequential Sample Injection

GC or LC

Our 770 Auto Sampler and 560GC or 6970LC combine to

- make your time available for other activities
- make accurate reports routinely
- make use of your chromatographs even when you aren't there

With more versatility than the rest

To Automatic Report Generation

Ask us

Tracor Instruments

Tracor Inc.
6500 Tracor Lane
Austin, Texas 78721
Telephone 512-926-2800

Books

Hydrocarbon Research Group, and held at the University of Durham, England, March 30–April 2, 1976. The conference was one of a series initiated in 1954 with the aim of presenting essentially review papers on a wide variety of spectroscopic subjects to provide an up-to-date overview and to highlight important new developments. This book contains 29 articles contributed by 41 authors from the international community and arranged under four general headings: nuclear magnetic resonance spectroscopy, infrared and Raman spectroscopy, electron spectroscopy, and applied spectroscopy. The literature is surveyed through 1975.

Continuing Series

Computers in Polymer Sciences. James S. Mattson, Harry B. Mark, Jr., and Hubert C. MacDonald, Jr., Eds. xi + 374 pages. Marcel Dekker, Inc., 270 Madison Ave., New York, N.Y. 10016. 1977. $34.75

Published as Volume 6 of the series on computers in chemistry and instrumentation, this book describes various ways that polymer chemists use the power of computers to solve their research problems. It presents 10 in-depth articles written by 15 experts. The first six chapters are devoted to theoretical considerations of polymerization reactions and to understanding the reaction variables and their influence on polymer products. The final four chapters demonstrate the uses of computers to control experiments and to simulate data obtained from experimentation on polymer material. The book is a good quality photo-offset copy of typewritten text.

Toxicology Annual, Vol. 2. Charles L. Winek and Sydney P. Shanor, Eds. xii + 272 pages. Marcel Dekker, Inc., 270 Madison Ave., New York, N.Y. 10016. 1977. $29.50

The 15 articles dealing with various aspects of toxicology were prepared in manuscript form in 1975 and originally published in "Clinical Toxicology", Volume 10, Numbers 1 and 2. Included are articles on veterinary toxicology, laboratory support of drug abuse control programs, beryllium in the environment, XAD-2 resin drug extraction methods, and safety testing of fragrances. Also included are studies of adverse drug reactions, drugs and children, drug abuse proficiency testing, and some historical aspects of marijuana, as well as a new section of Free Communications. The book is a good quality photo-offset copy of typewritten text.

Selected Annual Reviews of the Analytical Sciences, Vol. 4. L. S. Bark, Ed. v + 73 pages. The Chemical Society, Burlington House, London, W1V 0BN, England. 1976. $19

Two areas of instrumental analytical techniques are reviewed in Volume 4 of the series devoted to the annual review of analytical sciences. The first article on voltammetric techniques reviews the developments in polarographic and related techniques. It covers advances in instrumental and applications areas in separation sections. The second article reviews the developments in high-frequency electrodeless plasma spectrometry. Topics discussed in this review include classification of plasma types, emission spectrometry, nebulizers, inductively coupled radio frequency plasma torch, and microwave plasma. The literature is surveyed through 1975.

U.S. Government Publications

Order printed copies of the following PREPAID at the price shown and by SD Cat. No. from Superintendent of Documents, U.S. Government Printing Office, Washington, D.C. 20402. Foreign remittances must be in U.S. exchange and include an additional 25% of the publication price to cover mailing costs. Order microfiche copies PREPAID by NTIS No. from National Technical Information Center, Springfield, Va. 22151; the price is $2.25 (domestic) or $3.75 (foreign) a copy

Bibliography on Atomic Energy Levels and Spectra, July 1971 through June 1975. Lucy Hagan. 186 pages. 1977. $2.50 (SD Cat. No. C13.10:363 Suppl., NTIS No. NBS-SP-363/1

This is the first supplement to the NBS Special Publication 363, "Bibliography on Atomic Energy Levels and Spectra, July 1968 through June 1971". The supplement covers the most recent literature from July 1971 through June 1975. It contains approximately 2150 references classified by subject for individual atoms and atomic ions. A number index identifies the references. An author index is included. References contain data on energy levels, classified lines, wavelengths, Zeeman effect, Stark effect, hyperfine structure, isotope shift, ionization potentials, or theory which gives results for specific atoms or atomic ions.

CIRCLE 200 ON READER SERVICE CARD

Editors' Column

ANALYTICAL CHEMISTRY's Advisory Board Meeting

Comments from readers on Professor Laitinen's editorials and on any A-page material such as the REPORT, INSTRUMENTATION, THE ANALYTICAL APPROACH, EDITORS' COLUMN, and NEWS are welcomed by ANALYTICAL CHEMISTRY. We plan to start a LETTERS section in a forthcoming issue and to continue this section as we get interesting letters from our readers. Professor Laitinen has established some ground rules for this section which he describes in this month's EDITORIAL, page 1281.

Appropriate topics for LETTERS are opinions on analytical chemistry as a profession and discipline. Of special interest are discussions of the role of the discipline in society, special strengths and problems in the discipline, and education in analytical chemistry. General comments and questions on editorial policies and on peer review and its role in scientific publication are also possibilities as topics.

Do let us hear from you if you have ideas and opinions that you would like to share with other readers of ANALYTICAL CHEMISTRY.

The instigation of a LETTERS section was only one of many topics covered at this year's Advisory Board meeting held in May at our editorial headquarters in Washington, D.C. All 15 members of the Board plus contributing editor Claude Lucchesi joined Professor Laitinen and the editorial staff for lively and critical discussion on the adoption of SI units, the role and status of the journal, and many other subjects. In addition to the formal meetings, visits to the editorial offices by Board members permitted informal chatting with staff. Members also had an opportunity to contribute names of experts to serve as reviewers to update our files.

Advisory Board members were favorably disposed toward the move to adopt the Internationale Système (SI) of units by American Chemical Society publications. This move to SI has been under study by the ACS for some time. The ACS will publish general guidelines to the use of SI in a revised "Handbook for Authors" scheduled for publication late this year. Individual ACS journals can adapt and make exceptions as needed to accommodate their constituencies.

Problems with SI units arise not so much with units where only a name is changed for conformity, but where a new numerical value is required. A list of proposed acceptable and proscribed non-SI units will be circulated to Board members for comment. This process should culminate in a guide for the use of SI in papers published in ANALYTICAL CHEMISTRY. These guidelines will be included in the January 1978 publication of the "Guide for Authors".

The editorial staff reported improved speed of publication data to the Advisory Board. Of the manuscripts published January through May 1977, 65.5% required six months or less from submission date to publication date. Six to eight months were required for 21.1%, and the remaining 13.4% required over eight months. Through April 1977, incoming manuscripts have increased in number about 9% over those received in 1976. The 1976 figure was 6% over 1975. At the current rate, about 950 manuscripts will be submitted to ANALYTICAL CHEMISTRY this year.

Professor Laitinen told the Advisory Board of plans to celebrate the 50th anniversary year of the journal in 1978. A 50th Anniversary Symposium in honor of Lawrence T. Hallett, former editor of ANALYTICAL CHEMISTRY, will take place at the fall 1978 ACS meeting in Miami Beach. Invited speakers will discuss the science and the journal over the decades from the 1930's to the 1970's.

Some discussion was held on the new copyright law that goes into effect in January 1978. Although the details have yet to be worked out, it is clear that scientific publications will need specific, written transfer of copyright by individual authors. Despite this requirement, the relationship on copyright between the American Chemical Society as publisher and the authors will remain essentially unchanged. Further details on these requirements will be given in a future issue of the JOURNAL.

The Advisory Board meeting is an essential activity for the editor to get advice on the operation of the JOURNAL. This year's meeting, like many before, was particularly helpful in that it provided insights and ideas for the future development of ANALYTICAL CHEMISTRY.

Josephine Petruzzi

SPECIAL OFFER

. . . A free $44.50 starter kit with every model 715 general purpose laboratory X-Y recorder.

Free kit features: 5, fifty sheet pads of MFE's exclusive PAD/LOAD® paper plus 2 packages of fiber tip pens (6 pens per package) . . . a $44.50 value.

Model 715 features: 5 ranges; overdrive protection; 0.2% F.S. accuracy; zero check pushbuttons; 17"/second slew speeds; English or Metric models plus much more for only $925.00.

Call (603) 893-1921 for free special offer coupon and information on equivalent offer on model 815 (11" X 17") recorders.

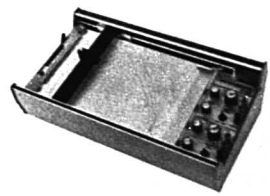

MFE

KEEWAYDIN DRIVE, SALEM, N.H. 03079 U.S.A.

MFE PRODUCTS SA
AV DU GENERAL GUISAN 58
CH-1800 VEVEY SWITZERLAND
TELEPHONE 021 52.80.40
TELEX 26238 MFEPR CH

CIRCLE 143 ON READER SERVICE CARD

HPLC... easier... faster... more precise.

The HP 1084 combines advanced technology with design innovations that benefit every aspect of high performance liquid chromatography—solvent preparation, sample injection, flow control, separation, detection, data processing, recording and reporting.

The HP 1084—the first microprocessor controlled liquid chromatograph—sets a new standard for LC instruments.

Combining a high performance liquid chromatograph, digital processor, control keyboard and printer/plotter in a single integrated instrument, the HP 1084 does the whole job by itself.

The HP 1084 is easy to operate. You enter all operating instructions on a control keyboard simply by pushing buttons which are labeled in familiar chromatographic terms. These instructions are acknowledged immediately on the printer/plotter.

The HP 1084 is fast. You push the start button and the microprocessor takes over full control. It automatically injects the sample at full column pressure. It constantly monitors the operation of the pump and adjusts it to achieve the desired isocratic, gradient or flow-programmed conditions. It calculates the retention time and area of every peak, and computes component concentrations according to any of four methods. It plots the chromatogram and prints a detailed analytical report.

The HP 1084 is precise. Due to its injector, pump and flow control system, detector and time programming capability, it can alter flow rates, mobile phase composition, integration parameters and recorder presentation precisely at the times you specify on the keyboard. It insures the best performance that your columns can produce... without requiring your attention during the run.

Get the full story on the HPLC solution from your nearest HP office.

The HPLC solution

HEWLETT hp PACKARD

Route 41, Avondale, Pennsylvania 19311

Europe: 7, rue du Bois-du-Lan, P.O. Box, CH-1217 Meyrin 2—Geneva, Switzerland

CIRCLE 95 ON READER SERVICE CARD

Near Infrared Reflectance Spectrophotometric Analysis of Agricultural Products

C. A. Watson
ARS—USDA, North Dakota State University, Fargo, N.D. 58102

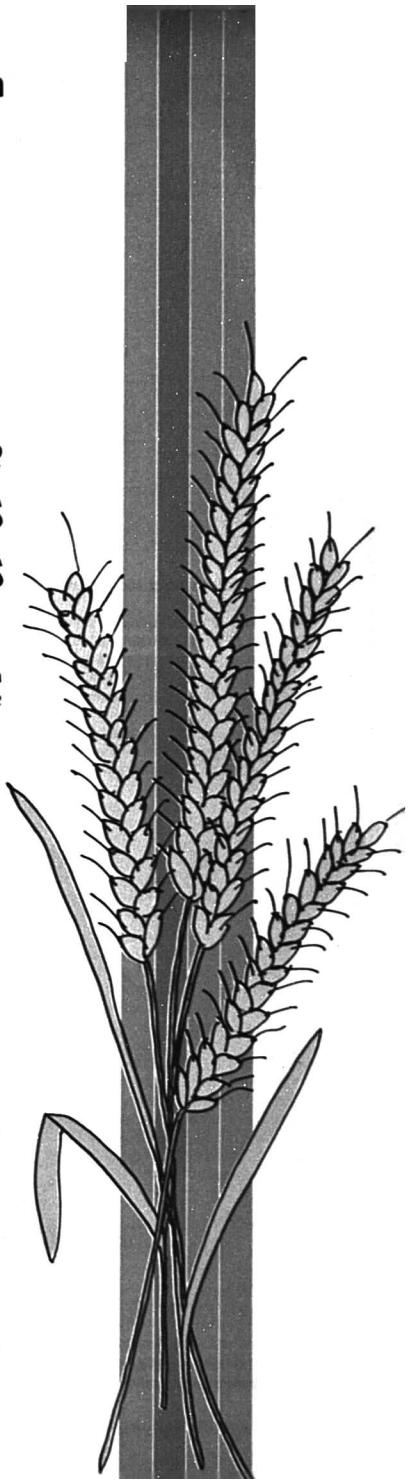

There has long existed in the agricultural industries a need for a rapid and accurate measurement of the chemical composition of the raw and processed products—for example, the measurement of the protein content of grains, oilseeds, and forages and their processed products; the oil content of oilseeds; and the moisture content of nearly every product including grains, oilseeds, and forages. With this information, a more refined marketing and processing system of agricultural products would be realized from a quality and nutritional standpoint. Developments in near infrared spectrophotometry hold many promises of fulfilling these needs.

Until recently the near infrared (NIR) region of the spectrum has been neglected for the analysis of agricultural products. In 1962 Hart et al. (*1*) reported a method for determining moisture content of seeds based on the NIR spectrophotometric analysis of their methanol extracts. Later, Norris and Hart (*2*) and Ben-Gera and Norris (*3*) published additional research on improvements or modifications in the method. In 1963 Hoffman (*4*) pointed out the advantages of NIR diffuse reflectance spectrophotometry for the determination of moisture content in solids. He showed the relation of reflectance at 1930 nm to moisture content of several solids including flour and starch. Massie and Norris (*5*) reported the reflectance properties of several grains in the NIR region of the spectra. This work was primarily related to drying of grain.

Ben-Gera and Norris (*6*) showed the effect of fat concentration in milk on the absorption spectrum in the NIR region and in 1968 (*7*) reported on a method for determining fat and moisture content of meat products by using direct NIR spectrophotometry. The correlation coefficients between the NIR method and standard methods were +0.974 and +0.977 for fat and moisture, respectively.

Karl Norris and associates at the Agricultural Research Service, USDA, Beltsville, Md., have done considerable research since the mid-1960's in developing and perfecting NIR reflectance spectrophotometry for determining the quality constituents of agricultural products. Much of this early developmental work was not published. One of the primary aspects of the technique was the use of measurements at two wavelengths for each constituent analyzed as a way to correct for spectral changes not related to concentration of the constituent. One measurement was taken at a wave-

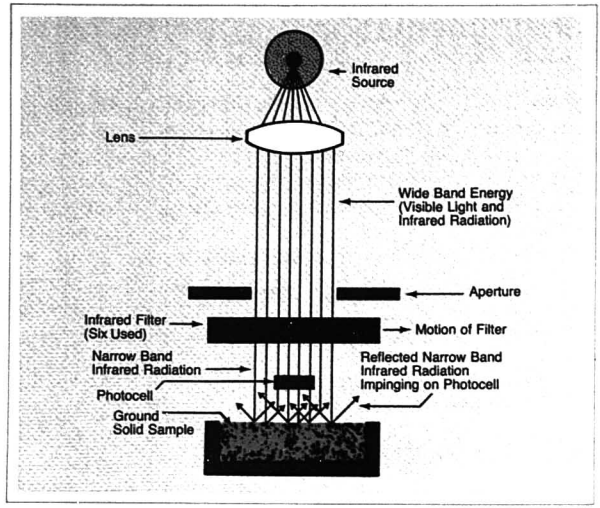

Figure 1. Schematic of source, aperture, interference filters, photocell, and sample for InfraAlyzer

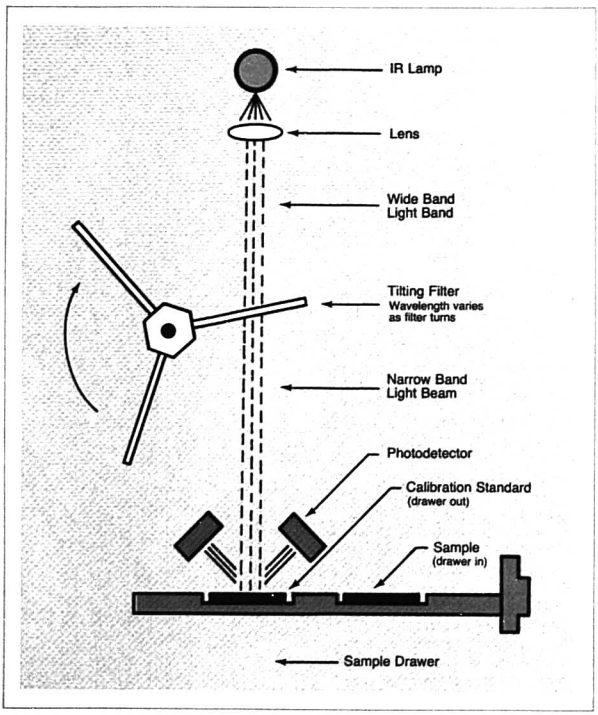

Figure 2. Schematic of source, aperture, interference filters, photocells, and sample for grain quality analyzer

length where absorbance was most affected by changes in the concentration of the constituent being measured. A second measurement was taken at a closely adjacent wavelength that was not absorbed or was little affected by the specific constituent or by other constituents in the sample. The absorbance was measured by reflectance (R) and then converted by a minicomputer to log $1/R$. The difference in absorbance as measured by reflectance $\Delta(\log 1/R)$ between the two wavelengths was more accurately and precisely related to the concentration of the constituent than a measurement at one wavelength (*8*). Other important factors in the technique were development of minicomputers, which could be designed as an integral part of an instrument, for storing and analyzing relatively large amounts of data; developments of techniques to make precise optical filters, which permit high energy illumination in the NIR spectrum, at a reasonable cost; development of electronic circuitry capable of detecting and amplifying minute signals; and development of scanning optical filter arrangements that allow precision multiple wavelength measurements (*9*). Norris and colleagues expanded their early work (*10*) on determination of moisture in grains by NIR reflectance spectrophotometry to include protein and oil.

Based on the research and development of Norris and colleagues, two commercial companies introduced NIR reflectance instruments to the grain industries in 1971 (*11*). These instruments were designed to estimate protein, oil, and moisture contents on a ground sample of grain or oilseed without the use of any solvent.

Instruments for Grains and Oilseeds

Two companies manufacture instruments for the determination of protein, oil, and moisture in grains, oilseeds, and feedstuffs by NIR reflectance spectrophotometry. Technicon Industrial Systems, Tarrytown, N.Y. 10591, markets the InfraAlyzer made by the Dickey-john Co., Auburn, Ill.; and Neotec Instruments, Inc., Rockville, Md. 20852, markets several models of their grain quality analyzer (GQA).

The basic principles of the instruments (InfraAlyzer and GQA) are the same. The difference in the log $1/R$ at two wavelengths (maxima and adjacent minima) is determined for each constituent analyzed. Protein, oil, and moisture exhibit different peaks of major absorbance in the NIR spectrum; however, each substance also absorbs appreciably at other wavelengths (*9*). By making log $1/R$ measurements at all three maxima and at

the adjacent minima on samples having a known range of all three components similar to that in the unknowns, equations can be solved by use of multiple linear regression analyses for constants that relate the $\Delta(\log 1/R)$ to the contents of protein, oil, and moisture. These constants are used to calibrate the instruments for the various constituents. The measuring system includes interference filters to isolate selected wavebands of infrared energy, a photosensor and associated signal-conditioning amplifier, and a minicomputer or microprocessor for analyzing the data; all units are built into a compact instrument. The schematics of the light source, lenses, filters, detectors, etc., for the InfraAlyzer and GQA are shown in Figures 1 and 2, respectively.

The main difference between the two instruments is that the InfraAlyzer has six interference filters to isolate precise wavelengths, whereas the GQA has three filters mounted in a rotating paddle wheel. Each of the three filters passes a variable wavelength depending on the angle between the filter and the light source. An encoder attached to the paddle wheel permits selection of the six precise wavelengths to be used in the analysis. Only two wavelengths are obtainable from any one filter at any one time. The bandpass increases as the filter tilts from the normal to the light beam which decreases the precision of the filter. With both instruments the reflected light is detected, and the data produced are introduced into a built-in computer which reads out percentage protein, oil, or moisture. The wavelengths used by the InfraAlyzer and the GQA-31 are compared below:

InfraAlyzer, nm	GQA-31, nm
1680	1867
1940	1920
2100	2118
2180	2167
2230	2250
2310	2297

The GQA-41 allows for convenient changes in wavelength if necessary by a push-button control system of its tilt-filter wheel. This has certain advantages if the determination of certain constituents require slightly different wavelengths for maximum sensitivity, but there is no published information which shows this arrangement increases the accuracy of the instrument. The GQA-41 does not cover the full range of the near infrared spectrum.

The computation processes for the instruments differ slightly. The log $1/R$ values (referred to as L_1, L_2, etc.) for the six wavelengths of the InfraAlyzer are combined with a set of K_i values (constants) which are determined by a set of three equations as follows:

$$\%\ \text{moisture} = K_{1m}L_1 + K_{2m}L_2 + K_{3m}L_3 + K_{4m}L_4 + K_{5m}L_5 + K_{6m}L_6 + K_{7m}$$

$$\%\ \text{oil} = K_{1o}L_1 + K_{2o}L_2 + K_{3o}L_3 + K_{4o}L_4K_{5o}L_5 + K_{6o}L_6 + K_{7o}$$

$$\%\ \text{protein} = K_{1p}L_1 + K_{2p}L_2 + K_{3p}L_3 + K_{4p}L_4 + K_{5p}L_5 + K_{6p}L_6 + K_{7p}$$

where L_1, L_2, etc. = Log $1/R_1$, Log $1/R_2$, etc.

The values of log $1/R$ measured by the GQA-31 at six wavelengths are combined to give three values of log $1/R$ differences as follows:

$$\Delta(\text{Log } 1/R_m) = \text{Log } 1/R_{1920} - \text{Log } 1/R_{1867}\ \text{(moisture)}$$

$$\Delta(\text{Log } 1/R_o) = \text{Log } 1/R_{2297} - \text{Log } 1/R_{2250}\ \text{(oil)}$$

$$\Delta(\text{Log } 1/R_p) = \text{Log } 1/R_{2167} - \text{Log } 1/R_{2118}\ \text{(protein)}$$

These $\Delta(\text{Log } 1/R)$ values, which are labeled on the GQA-31 as "C" values, are then combined into equations to give the percentage of each constituent as follows:

$$\%\ \text{moisture} = K_0 + K_1\,\Delta(\text{Log } 1/R_m) + K_2\,\Delta(\text{Log } 1/R_o) + K_3\,\Delta(\text{Log } 1/R_p)$$

$$\%\ \text{oil} = K_0' + K_1'\,\Delta(\text{Log } 1/R_m) + K_2'\,\Delta(\text{Log } 1/R_o) + K_3'\,\Delta(\text{Log } 1/R_p)$$

$$\%\ \text{protein} = K_0^* + K_1^*\,\Delta(\text{Log } 1/R_m) + K_2^*\,\Delta(\text{Log } 1/R_o) + K_3^*\,\Delta(\text{Log } 1/R_p)$$

The K_i values determined from the above equations are set in the instruments by 10k potentiometers, seven for each constituent in the InfraAlyzer and four for each constituent in the GQA-31. The "K" values are constants characteristic of the component being measured in the sample.

For determination of constituents, the instruments must be calibrated against other analytical laboratory results, e.g., Kjeldahl nitrogen content for protein. Calibration is based on analyses of about 50 samples covering the range in content of the constituents expected in the samples to be analyzed. Other constituents (i.e., moisture and lipid) that affect the specific constituent being analyzed (protein) must exhibit a range that would be expected in the unknown; otherwise, constants for multiplying certain absorbances may be weighted in error.

The Model GQA-41 analyzes the data differently from the other models of the GQA and the InfraAlyzer. The GQA-41 computes the approximate slope of the reflectance curve by using the first derivative, or dR/R, divided by the reflectance (R). This computation has been termed "normalization" of the slope.

Table I. Coefficients of Correlation Between Constituents in Several Products Determined by NIR Reflectance Spectrophotometry and by Accepted Methods

Constituent	Product	Ref	Correlation coefficient
Protein	Corn	14	0.910
	Soybeans	14	0.943
	Oats	14	0.945
	Wheat	16	0.988
	Soybeans	15	0.971
	Wheat	12	0.982
	Flour	18	0.998
	Forages	22	0.992
	Barley	25	0.986
	Barley malt	25	0.972
Oil	Corn	14	0.913
	Soybeans	14	0.969
	Oats	14	0.978
	Soybeans	15	0.977
	Rice (whole grain)	19	0.783
Moisture	Corn (whole)	17	0.997
	Grain sorghum (whole)	17	0.974
Ash	Flour	18	0.968

Application to Grains and Oilseeds

Several articles (*12–19, 25*) have reported the relation between constituents determined by the NIR instruments and by standard procedures. These results are summarized in Table I. For more detail, the reader should consult the cited references. The data in Table I show excellent

The only thing variable about the SF 770 Spectroflow Monitor for liquid chromatography ...is the wavelength!

- It consistently offers highest sensitivity with low noise and baseline drift.
- It classically follows Beer's law in its measurements.
- It routinely includes an automatic gain control and zero suppression.
- It equally interfaces with all Liquid Chromatography systems.
- It inconspicuously takes up very little room.
- It uniquely incorporates a double-beam design.
- It invariably is an honest instrument, not relying on gimmicks to achieve unrealistic specs.
- It indubitably is preferred by more liquid chromatographers than all other models combined.

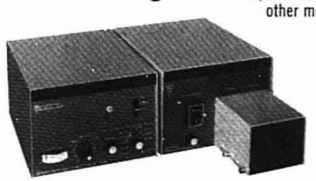

Call or write now!

24 BOOKER STREET, WESTWOOD, NEW JERSEY 07675
(201) 664-7263

SCHOEFFEL
INSTRUMENT CORPORATION

CIRCLE 462 ON READER SERVICE CARD

Send my free copy of your new Single Source Liquid Chromatography Catalog.

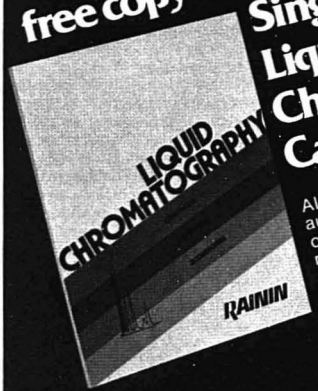

ALSO — you'll receive automatic supplements on new items in the most comprehensive line of liquid chromatography apparatus and supplies.

RAININ
INSTRUMENT CO. INC.

94 Lincoln St., Brighton, MA 02135 • 1-800-225-4590

CIRCLE 179 ON READER SERVICE CARD

relations between the accepted methods and the NIR methods. Note that differences between the two methods can be attributed to errors in both methods and not just the NIR method.

Other Applications

Reports of the determination of constituents in agricultural products other than grains and grain products have been published. Massie (*20*) reported a correlation coefficient of +0.82 between fat content of ground beef determined with a gallium arsenide infrared emitter and by a chemical method. However, there were problems with the life of the emitter and accuracy of the determination.

Neotec Instruments, Inc., markets a ground meat analyzer (GM/A) for the estimation of percentage fat in ground meat. The GM/A uses a low intensity light source to illuminate the meat sample. An optical scanning system measures the amount of light reflected by the sample at the appropriate absorption wavelengths of the fat. The instrument is calibrated to a sample of known fat content.

The author is not aware of any published information regarding the precision and accuracy of the GM/A. However, Weiner Associates, Inc. (*21*), evaluated the GM/A, and their unpublished report shows that the standard deviation band for measurements of fat content of ground beef differs by less than 1 wt % fat content from the standard deviation of measurements made by the official AOAC procedure.

Norris et al. (*22*) showed the potential of NIR reflectance for prediction of the quality of forages. They correlated the second derivative of log $(1/R)$ vs. wavelength with compositional and nutritional data of 87 forage samples. When up to nine wavelength points were used for the prediction equations, correlation coefficients ranged from +0.80 for digestible matter intake to +0.99 for crude protein and +0.98 for neutral detergent fiber.

Norris (personal communication) also found excellent correlations between the contents of certain amino acids in agricultural products and NIR reflectance values.

Problems

The primary problem of NIR analysis of grains and oilseeds for protein, oil, and moisture is preparation of the sample. These problems have been discussed (*23*) and are summarized here. Because the samples in most cases must be ground, uniform grinding is a major problem. Hymowitz et al. (*14*) showed that grinding time affected protein and oil results of soybeans and oats determined by NIR. A

There are many reasons why we have already updated over 3000 DU's.*

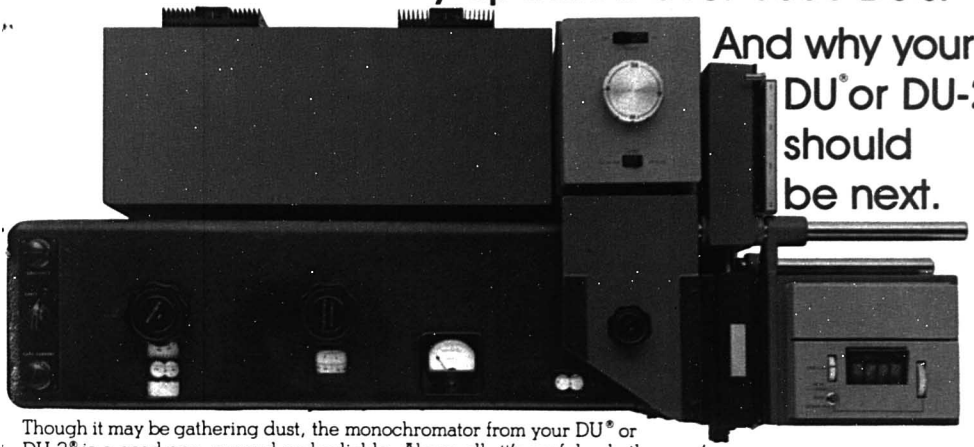

And why your DU® or DU-2® should be next.

Though it may be gathering dust, the monochromator from your DU® or DU-2® is a good one, rugged and reliable. Above all, it's useful, whether you're into industrial or biomedical research, quality control, pollution studies, or similar disciplines. By replacing everything *except* the monochromator with a Gilford Series 252 update, we create for you a complete, modern spectrophotometer.

For less than $4000, here's what you're getting:

Solid-state linear absorbance photometer:

L.E.D. display to 3.0004; readout in absorbance *and* concentration units; recorder calibration controls; BCD output for interface with printers, computers; easy operation, no need for sensitivity or dark current adjustments, no shutters.

NBS-traceable absorbance standards:

Easy absorbance calibration at three points in absorbance range; routine determination of photometric linearity.

Four-place manual cuvette positioner:

Precise cam-operated positioning and sliding aperture mask for routine measurement with standard, micro, or flow-through cuvettes; integral full-flooding thermoplates for circulation of fluids from constant temperature source; economical option for automatic cuvette positioning.

Optical bench adapter/dual light source:

Tungsten and deuterium lamps plus new optical components for enhanced energy throughput; easy interchangeability of standard positioner with optional accessories for enzyme analysis, gel electrophoresis, thermal melts, rapid sampling, and more.

Solid-state power supply:

Stable, transistorized power for entire spectrophotometer; no batteries, reduced maintenance.

You'll find nothing with matching capabilities at anything NEAR the price.

For further information, call or write GILFORD INSTRUMENT LABORATORIES INC., Dept 7-8-12, Oberlin, OH 44074 (216) 774-1041.

* Registered trademark of Beckman Instruments, Inc.

gilford® INSTRUMENT

Oberlin, Ohio 44074
Paris (Malakoff), France
Düsseldorf, W. Germany
Teddington, Middx., England
(216) 774-1041 Telex: 98-0456

CIRCLE 82 ON READER SERVICE CARD

significant grinding X genotype interaction was shown for protein determinations of corn. Williams (*13*) showed that grinding samples on seven different grinders affected NIR determinations. Accuracy of the calibration of the NIR instruments was affected by season and location where wheat was grown. Watson et al. (*12*) reported particle size distribution of five classes of wheat ground on three types of mills. Differences in particle size between classes of wheat were large regardless of the mill used. The type of grinder appeared to affect the NIR determinations, but there was no consistent relation between particle size distribution and NIR results. Pomeranz and Moore (*16*) reported significant differences due to variety and location on the protein content of wheat determined by several methods including NIR. Watson et al. (*24*) reported that protein content determined by NIR was influenced to a large extent by wheat class but could not relate these differences to particle size differences of the ground wheat.

Future

Future use of NIR reflectance spectrophotometry for the determination of various constituents in agricultural products is promising. Scientists and technicians must realize that the instrumentation and methodology have not reached their ultimate levels of refinement. Additional research should be able to overcome the problems now encountered with NIR reflectance spectrophotometry. We need to learn about the commodities and properties that can be measured, the traits that are actually measured at the chemical and molecular levels, the factors that affect the measurements, and the best means to minimize errors. Comprehensive information on these aspects of the technique should be considered before the role of NIR reflectance in agricultural science can be fully established. Despite its problems, the system has already gained considerable acceptance. The rapid acceptance of NIR reflectance methods is attributed to the ease and cleanliness of the operation (i.e., no chemicals are required), the short time and low cost per sample if large numbers are analyzed, and the relative accuracy of the method.

References

(1) J. R. Hart, K. H. Norris, and C. Golumbic, *Cereal Chem.*, **39**, 94 (1962).
(2) K. H. Norris and J. R. Hart, "Humidity Moisture", P. N. Winn, Jr., Ed., Vol IV, p 19, Reinhold, New York, N.Y., 1965.
(3) I. Ben-Gera and K. H. Norris, *Israel J. Agric. Res.*, **18**, 125 (1968).
(4) K. Hoffman, *Feuchtemessung durch Infrarotreflexion, Chem. Ing. Tech.*, **35**, 55 (1963).
(5) D. R. Massie and K. H. Norris, *Trans. ASAE*, **8**, 598 (1965).
(6) I. Ben-Gera and K. H. Norris, *Israel J. Agric. Res.*, **18**, 117 (1968).
(7) I. Ben-Gera and K. H. Norris, *J. Food Sci.*, **33**, 64 (1968).
(8) Technicon Industrial Systems, Technical Publication No. TA5-0340-00, 1975.
(9) R. D. Rosenthal, presented to Milling & Baking Div., American Assoc. of Cereal Chemists 1973 Annual Mtg., Denver, Colo., 1973.
(10) K. H. Norris, *Agric. Eng.*, **45**, 370 (1964).
(11) R. D. Rosenthal, Annual Mtg. Kansas Assoc. Wheat Growers and Kansas Wheat Comm., Hutchinson, Kan., Dec. 10–11, 1971.
(12) C. A. Watson, D. Carville, E. Dikeman, G. Daigger, and G. D. Booth, *Cereal Chem.*, **53**, 214 (1976).
(13) P. C. Williams, *ibid.*, **52**, 561 (1975).
(14) T. Hymowitz, J. W. Dudley, F. I. Collins, and C. M. Brown, *Crop Sci.*, **14**, 713 (1974).
(15) R. W. Rinne, S. Gibbons, J. Bradley, R. Seif, and C. A. Brim, Agric. Res. Ser., USDA, ARS-NC-26, July 1975.
(16) Y. Pomeranz and R. B. Moore, *Bakers Dig.*, **50**, 44 (1975).
(17) R. A. Stermer, Y. Pomeranz, and R. J. McGinty, *Cereal Chem.*, in press (1977).
(18) C. A. Watson, G. Etchevers, and W. C. Shuey, *ibid.*, **53**, 803 (1976).
(19) R. A. Stermer, C. A. Watson, and E. Dikeman, Annual Mtg. ASAE, Paper No. 76-3030, 1976.
(20) D. R. Massie, reprinted from ASAE Pub. 1-76, 1973.
(21) Weiner Assoc. Inc., unpublished report prepared for Alexander Grant & Co., July 29, 1974.
(22) K. H. Norris, R. F. Barnes, J. E. Moore, and J. S. Shenk, *J. Animal Sci.*, **43**, 889 (1976).
(23) Technicon Industrial Systems, Tarrytown, N.Y., TIS News 2, 1976.
(24) C. A. Watson, W. C. Shuey, O. J. Banasik, and J. W. Dick, *Cereal Chem.*, submitted for publication.
(25) Y. Pomeranz, R. B. Moore, and F. S. Lai, *ASBC J.*, **35**, 86 (1977).

Mention of a trademark name or proprietary product does not constitute a guarantee or warranty of the product by the U.S. Department of Agriculture and does not imply its approval to the exclusion of other products that may also be suitable.

C. A. Watson is a research chemist with the North Central Region, Agricultural Research Service, U.S. Department of Agriculture, Department of Cereal Chemistry and Technology, North Dakota State University, Fargo

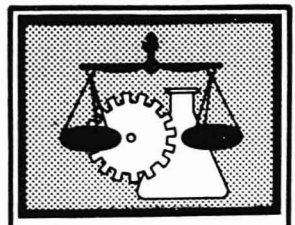

Legal Rights of Chemists and Engineers

Advances in Chemistry Series No. 161

Warren D. Niederhauser, *Editor*
Rohm and Haas Company
E. Gerald Meyer, *Editor*
University of Wyoming

A symposium cosponsored by the Division of Professional Relations and the Council Committee on Professional Relations of the American Chemical Society.

Here is the first volume of its kind to cover an entire spectrum of legal rights of chemists and engineers and the problems they encounter as professionals.

Included in twelve highly instructive papers are well-established legal precedents, legislation currently before Congress, suggested new legislation, and extensive bibliographies which permit the reader to pursue particular areas of interest.

The collection contains a great deal of new information and data useful to university chemistry and engineering departments, law schools, patent attorneys, medical scientists, architects and technicians, chemical process companies, and professional associations.

CONTENTS

Careers Combining Chemistry and The Law • Patent Law Revision • Special Compensation for Salaried Chemists and Rewards for Inventors • Confidentiality, Secrecy Agreements, and Trade Secrets • Employment Contracts • Legalization of Employment Guidelines • Layoffs and Serious Grievances • Union's Effect on Legal Obligations • Societal Responsibilities of Chemists • Equal Opportunity Employment • Tax Effects of Retirement Plans • Federal Tax Law

109 pages (1977) clothbound $16.00
LC 77-9364 ISBN 0-8412-0357-1

SIS/American Chemical Society
1155 16th St., N.W./Wash., D.C. 20036

Please send _____ copies of *Advances 161 Legal Rights of Chemists and Engineers* at $16.00 per copy.

☐ Check enclosed for $ _____ . ☐ Bill me. Postpaid in U.S. and Canada, plus 40 cents elsewhere.

Name

Address

City State Zip

LC/MS NOW

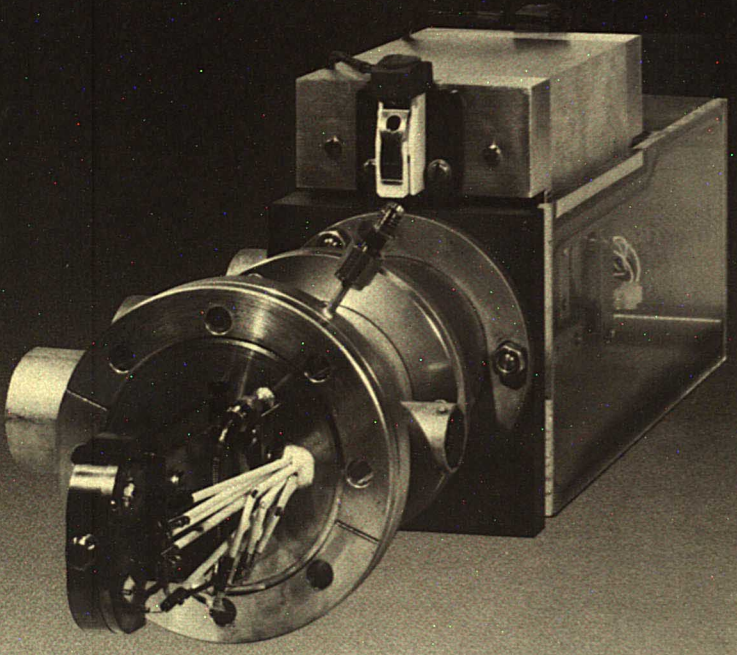

HIGH CHROMATOGRAPHIC INTEGRITY
HIGH SENSITIVITY LC DETECTION
HIGH SAMPLE YIELD
FREE CHOICE EI/CI IONIZATION
NO INTERFERENCE WITH GC/MS OR PROBE OPERATION

ASK THE SPECIALISTS — ASK FINNIGAN

finnigan **INSTRUMENTS**
845 W. MAUDE
SUNNYVALE, CALIFORNIA 94086
CIRCLE 74 ON READER SERVICE CARD

BRUKER

WP 200

LOW-COST SUPERCON

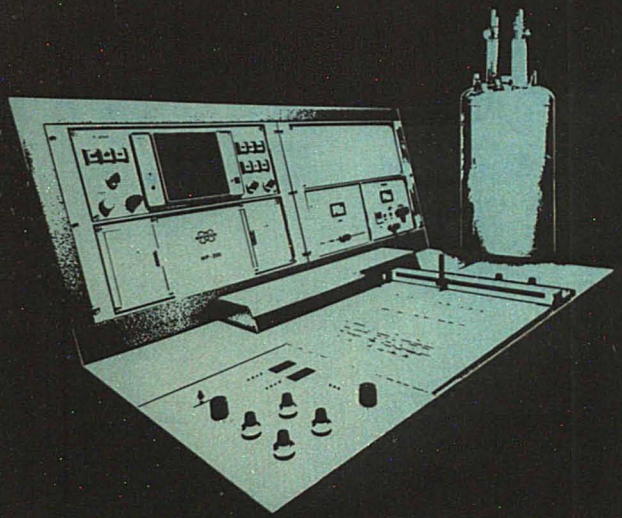

A New Generation in NMR Spectroscopy

- HIGH FIELD PERFORMANCE . . . 200 MHz for Proton
- LOW COST . . . $160,000 for Proton and Carbon FT
- LOW OPERATING COST . . . Approx. 25 l Helium per month

For more information on this exciting new spectrometer, call or write:

BRUKER INSTRUMENTS, INC.
Manning Park
Billerica, Mass. 01821
Tel: 617 272-9250

BRUKER INSTRUMENTS, INC.
539 Beall Avenue
Rockville, Maryland 20850
Tel: 301 762-4440

BRUKER INSTRUMENTS, INC.
1801 Page Mill Road, Suite 212
Palo Alto, California 94304
Tel: 415 493-3173

BRUKER SPECTROSPIN LTD.
2410 Dunwin Drive, Unit 4
Mississauga, Ontario, Canada
L5L 1J9 Tel: 416 625-2374

BRUKER - WORLD LEADER IN MAGNETIC RESONANCE

CIRCLE 18 ON READER SERVICE CARD

Use this card to receive *your own* monthly copy of

1977

ANALYTICAL CHEMISTRY

Start my subscription as follows:

	U. S.	PUAS**	CAN.**	Foreign**
ACS Members*	☐ $ 9.00	☐ $17.00	☐ $18.00	☐ $18.00
Nonmembers	☐ $12.00	☐ $23.00	☐ $21.00	☐ $24.00

☐ Bill me ☐ Bill Company ☐ Payment enclosed

(Make payable: American Chemical Society)

Name _____

Position _____

Your Employer _____

Address ☐ Home ☐ Business _____

City _____ State _____ ZIP _____

Employer's business ☐ Manufacturing ☐ Academic ☐ Government ☐ Other _____

If manufacturer, type of products produced _____

_____

*Subscriptions at ACS member rates are for personal use only.

**Payment must be made in U.S. Currency, by international money order, UNESCO coupons, U.S. bank draft; or through your book dealer.

Allow 60 days for your first copy to be put in the mail.

Mail this postage-free card today

Use this card to receive *your own* monthly copy of

1977

ANALYTICAL CHEMISTRY

Start my subscription as follows:

	U. S.	PUAS**	CAN.**	Foreign**
ACS Members*	☐ $ 9.00	☐ $17.00	☐ $18.00	☐ $18.00
Nonmembers	☐ $12.00	☐ $23.00	☐ $21.00	☐ $24.00

☐ Bill me ☐ Bill Company ☐ Payment enclosed

(Make payable: American Chemical Society)

Name _____

Position _____

Your Employer _____

Address ☐ Home ☐ Business _____

City _____ State _____ ZIP _____

Employer's business ☐ Manufacturing ☐ Academic ☐ Government ☐ Other _____

If manufacturer, type of products produced _____

_____

*Subscriptions at ACS member rates are for personal use only.

**Payment must be made in U.S. Currency, by international money order, UNESCO coupons, U.S. bank draft; or through your book dealer.

Allow 60 days for your first copy to be put in the mail.

Mail this postage-free card today

FIRST CLASS
Permit No. 1411-R
Washington, D.C.

BUSINESS REPLY MAIL
No postage stamp necessary if mailed in the United States

Postage will be paid by

AMERICAN CHEMICAL SOCIETY
1155 Sixteenth Street, N. W.
Washington, D.C. 20036

ATTN: G. HEBRON

FIRST CLASS
Permit No. 1411-R
Washington, D.C.

BUSINESS REPLY MAIL
No postage stamp necessary if mailed in the United States

Postage will be paid by

AMERICAN CHEMICAL SOCIETY
1155 Sixteenth Street, N. W.
Washington, D.C. 20036

ATTN: G. HEBRON

analytical
chemistry

Editor: **Herbert A. Laitinen**

EDITORIAL HEADQUARTERS
1155 Sixteenth St., N.W.
Washington, D.C. 20036
Phone: 202-872-4570 Teletype: 710-8220151

Managing Editor: Josephine M. Petruzzi
Associate Editor: Andrew A. Husovsky
Associate Editor, Easton: Elizabeth R. Rufe
Assistant Editors: Barbara Cassatt, Nancy J. Oddenino, Deborah C. Stewart
Production Manager: Leroy L. Corcoran
Art Director: John V. Sinnett
Designer: Alan Kahan
Artist: Diane Reich

Advisory Board: Donald H. Anderson, Richard P. Buck, Velmer Fassel, David Firestone, Robert A. Hofstader, Marjorie G. Horning, Philip F. Kane, Barry L. Karger, J. Jack Kirkland, Lynn L. Lewis, Harry B. Mark, Jr., Walter C. McCrone, Harry L. Pardue, Eugene A. Sawicki, W. D. Shults

Instrumentation Advisory Panel: Gary D. Christian, Nathan Gochman, Robert W. Hannah, Gary Horlick, Peter J. Kissinger, James N. Little, Sidney L. Phillips, R. K. Skogerboe, Donald E. Smith

Contributing Editor: Claude A. Lucchesi
Department of Chemistry, Northwestern University, Evanston, Ill. 60201

Published by the
AMERICAN CHEMICAL SOCIETY
1155 16th Street, N.W.
Washington, D.C. 20036

Books and Journals Division
Director: D. H. Michael Bowen
Editorial: Charles R. Bertsch
Magazine and Production: Bacil Guiley
Research and Development: Seldon W. Terrant
Circulation Development: Marion Gurfein

Manuscript requirements are published in the April 1977 issue, page 686. Manuscripts for publication (4 copies) should be submitted to ANALYTICAL CHEMISTRY at the ACS Washington address.

The American Chemical Society and its editors assume no responsibility for the statements and opinions advanced by contributors. Views expressed in the editorials are those of the editors and do not necessarily represent the official position of the American Chemical Society.

Letters to the Editor

At the 1977 Advisory Board meeting, it was decided to launch a new feature, *Letters to the Editor.*

It is important to distinguish clearly between this feature, which will appear in the "A" pages, and *Correspondence,* which will continue to appear as a category of articles in the research section. To quote from our Manuscript Requirements [*Anal. Chem.,* **49,** 686 (1977), "*Correspondence* may be brief disclosures of analytical concepts of unusual significance. They may also represent important comments on the work of others, in which case the authors of the work being discussed will, ordinarily, be allowed to reply". This procedure guards against the publication of scientific material which has not undergone the peer review process.

Letters to the Editor will include material not intended to become a part of the permanent scientific literature. It will not be abstracted or indexed, and is not intended for citation. Appropriate topics will be those of professional, educational, or general interest to analytical chemists and other readers of this journal. Letters of broad interest to the chemical profession as a whole will find a more appropriate outlet in *Chemical and Engineering News.*

In the interests of conservation of space, the Editors reserve the right to reject any contribution without specific cause, and to excerpt material from letters considered excessively long. Unsigned letters will not be considered. It is hoped that this new feature will prove to be of interest and service to our readers.

Factors Affecting Quantitative Determinations by X-ray Photoelectron Spectroscopy

C. D. Wagner

Shell Development Company, P.O. Box 1380, Houston, Texas 77001

The technique of dividing photoelectron line areas by elemental sensitivity factors or standard intensities can be applied to single-phase systems but not to multiple-phase systems. Elements other than transition metals can be determined with a standard deviation of 10% if photoelectrons of similar energy are used. Larger errors result from using lines of widely different energies because of variations in mean free path ratios among materials, and, more importantly, surface contamination. Transition metals pose special problems because of the prevalence of multielectron processes.

Many laboratories today are utilizing XPS (X-ray photoelectron spectroscopy), known also as ESCA (electron spectroscopy for chemical analysis) as a means of estimating relative amounts of elements at and near the sample surface. All workers realize the method in its general application is not as quantitative as desired, but there is no agreement on the origins of the errors observed.

In an initial effort to provide data for quantitative use on single-phase systems, the present author in 1971 (*1*) presented empirical data on relative measured intensities per atom of the strongest lines of the elements. A Varian spectrometer with Al x rays was used. Berthou and Jorgensen supplemented those data with further data for Al x rays (*2*) and Mg x rays (*3*). They also used a Varian spectrometer with retarding voltage applied to the sample, and they too adopted the convention of utilizing the F 1s intensity as the unit of comparison, terming the unit w. This parameter, originally designated "elemental sensitivity", I now prefer to call "standard intensity". Numerous other comparisons have also appeared. Typically, "quantitative" analysis is done by dividing peak areas in the spectrum of the sample by the standard intensities to obtain relative numbers of atoms detected.

It was recognized in the earliest article (*1*) that reproducibility is a problem, and that the method is at best semiquantitative. It was felt that the principal problem is the difficulty in attaining sample homogeneity, and that standard intensities vs. Z really should fall on smooth curves, that are relatable to interaction cross sections for the photoelectric process; in fact the standard intensity curve for 1s lines vs. Z seemed to track well with elemental photoelectron cross sections then known. However, Jorgensen and Berthou (*2, 3*) claim good reproducibility for each element among different compounds, but the resulting curves for standard intensity vs. Z are far from monotonic. Tentatively they ascribe the specific strong variations from monotonic curves to different probabilities for multiple electron processes that are characteristic of each element. Swingle (*4*) finds clear experimental evidence that probability of shakeup and other multiple electron processes varies from compound to compound of the same element, and attributes lack of quantitivity to this effect and problems with contamination. Ng and Hercules (*5*), on the other hand, present evidence that the intensity of photoelectron emission by an element strongly varies depending upon the extent of screening of emission by atoms that are nearest neighbors. Other studies have been made by Nefedov et al. (*6*), and Carter et al. (*7*). With this variety of views, it would clearly be advantageous to be able to assess the magnitude of the various factors that adversely affect quantitivity. This is the purpose of this paper.

The counting rate detected in a photoelectron peak from an element in a thick homogeneous sample covered by a contaminating adsorbed layer is given by:

$$I = Anf\sigma\phi yT\lambda C \tag{1}$$

where f is the photon flux in photons/cm^2 s, A is the sample area from which photoelectrons are detected, n is the number of atoms of the element per cm^3, σ is the cross section per atom for photoionization of the particular level, and λ is the mean free path for the photoelectron in the sample medium. The remaining factors are efficiency factors: T is the inherent efficiency of detection by the spectrometer of electrons originating from the sample; y is the fraction of photoelectric transitions from the given level that result in an ion in the ground state and a photoelectron of the appropriate kinetic energy; ϕ is an angular correction factor, relating the intensity of the particular photoelectrons at the spectrometer angle (photon beam–sample–electron acceptance) to that expected if the emission were isotropic; and C is the fractional efficiency of emergence through a contaminating adsorbed layer.

Let us assume in any given accumulation of data from a single homogeneous solid:

$$n = \frac{I}{Af\sigma\phi yT\lambda C} = \frac{I}{S} \tag{2}$$

where S is assumed to be a constant, so that for two elements in a solid,

$$\frac{n_1}{n_2} = \frac{I_1/S_1}{I_2/S_2} \tag{3}$$

While S_1 and S_2 will be different with another solid in the same spectrometer, it is assumed S_1/S_2 will remain the same, with f, σ, y, λ, and C assumed to change identically or by the same factor. A, ϕ, and T of course are invariant. It is on this assumption that many practicing spectroscopists perform quantitative work with XPS.

However, in reality the following may contribute to variability in the derived value of n_1/n_2 from the true value:

(1) There can be inaccuracy in integrating the photoelectron peaks (in essence, uncertainty in choosing the baseline), leading to variability in I_1/I_2.

(2) The flux, f, can vary with time between recording data for peak 1 and peak 2.

(3) If the lines differ significantly in kinetic energy, different degrees of adsorptive contamination result in variability of C_1/C_2.

(4) If the lines differ significantly in kinetic energy, the mean free path ratio, λ_1/λ_2, can vary among chemical states.

(5) The photoelectron cross section can vary slightly with chemical state, so that variations in σ_1/σ_2 can exist.

(6) Probability of multielectron processes, shakeup and shakeoff, can vary for atoms from compound to compound,

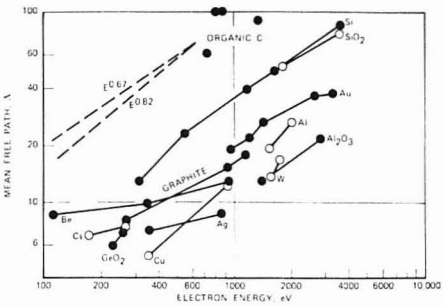

Figure 1. Line pair area ratios from the same atom (error limits not shown). (○) 2s/2p, (□) 3s/3p, (△) 3p/3d, (▽) 4d/4f

and therefore variations in y_1/y_2 can be a major source of error.

EXPERIMENTAL

Data were obtained on a Varian IEE spectrometer, detecting 100 eV electrons, with scanning by varying a retarding voltage applied to the sample. Instrumental contribution to the line width is 1.0 eV FWHM. Both Mg and Al high intensity anodes were used at 10 kV, 100 mA, providing counting rates with a copper sample of a ~450000 counts/s for the Cu $2p_{3/2}$ line. Instrumental vacuum was 1 to 8×10^{-6} Torr. Sufficient scanning was used with the samples to obtain peak heights of at least 5 kilocounts over background, and peak heights of 10–40 kilocounts ordinarily were used. Curves were integrated, using a baseline drawn tangent to the base at both sides of the peak.

Samples used were the best available commercially. They were ground in clean alumina mortars in a nitrogen glove box atmosphere to expose fresh surface. The powder was dusted onto double-sided Scotch tape on cylindrical sample holders and transferred into the instrument without exposure to air.

All compounds applicable to this study that were run in the past four years are included except those with which independent observations indicated nonstoichiometry, hydrolysis, or presence of other impurities. On this basis, spectra from 13 compounds were rejected.

DISCUSSION

Measurement of Peak Areas and Constancy of Flux. Data on line area ratios can be used to determine the inherent reproducibility of line area determinations by examining line area ratios for the same pair of lines for the same atom in the same compound with the same x rays in determinations over the period of four years. For lines of similar kinetic energy (see below), the only factors that can contribute to variations in I_1/I_2 are variations in the actual line area measurement, and variations in x-ray flux between the times of data gathering on the two lines. The average percent standard deviation in a total of 65 repetitive values for 29 compounds was 7.22%. This should not be regarded as the limit of error in the technique; extraordinary care, more time in data gathering, and special precautions to maintain constant x-ray flux would reduce this error.

Elimination of Factors Sensitive to Kinetic Energy. Three factors, λ, T, and C, are sensitive to kinetic energy. Data on mean free paths, λ, plotted on a log–log scale are shown in Figure 1 (*8*). From data for those elements with more than two points, it appears the function is similar to the form

$$\lambda = kE^p \tag{4}$$

Kemeny et al. (*9*) recognized that the relation is instead

$$\lambda = aE/(\ln E - b) \tag{5}$$

and Penn (*10*) actually calculated theoretical values for most of the elements using this equation. (The calculations were stated to be valid for free-electronlike materials, but those for other elements were believed to be not in serious error.) Examination of his data shows there is actually little deviation from the simpler Equation 4, with p between 0.68 and 0.82. Such a range is compatible with most of the experimental data in Figure 1.

Wyatt, Carver, and Hercules (*11*) presented data from a two-phase system which they believed showed that the values for λ can vary widely (as much as a factor of five) among different chemical forms of an element. It is believed the results can be explained as well by assuming different degrees of friability or plasticity upon grinding, so that relative areas of the two phases presented to the spectrometer slits can vary in a regular fashion but characteristic of the particular compound pair (MoO_3:$PbCl_2$ vs. MoO_3:PbI_2). With either or both explanations, it is clear that the use of two phases for quantitative purposes is not a sound procedure.

Of more importance is the question of the variability of λ_1/λ_2 among different compounds, where λ_1 and λ_2 refer to two electrons of different energy emitted from the same phase. With this spectrometer the transmission coefficient operates in opposite fashion, so it is more convenient to consider these effects together.

Instruments that sort electrons by applying a variable retarding potential, such as the Varian (*12*), have a theoretical detection efficiency varying with E^{-1}. Combining these relations,

$$I \sim E^{p-1} \tag{6}$$

where p is between 0.68 and 0.82, or, using the average value,

$$I \sim E^{-0.25} \tag{7}$$

Contamination by a hydrocarbon layer d_c thick, leads to attenuation according to

$$I/I_0 = e^{-d_c/\lambda_c} \tag{8}$$

where λ_c is the mean free path in hydrocarbon of the photoelectron to be detected. Examination of the original data indicate a range of intensities for C 1s from adventitious hydrocarbon to be 10–20% of the value for hydrocarbon in a thick layer. From the easily derivable relation of I and λ for thin layers, d_c/λ_c must be in the range 0.10–0.18.

On the assumption that the thickness of the adventitious hydrocarbon is one-fifth of the mean free path of 1000-V electrons and with the assumption that λ_c has the same exponential energy relationship as that of the average λ, ($\sim E^{0.75}$), it can be shown that the effect of λ, T, and C is given by:

$$\frac{\lambda_1 T_1 C_1}{\lambda_2 T_2 C_2} = \left(\frac{E_1}{E_2}\right)^{-0.25} e^{35.6(E_2^{-0.75} - E_1^{-0.75})} \tag{9}$$

It can further be shown that if E_1/E_2 lies between 0.75 and 1.20, and $E > 400$, the value for $\lambda_1 T_1 C_1/\lambda_2 T_2 C_2$ in Equation 9 lies between 1.03 and 0.98.

For this reason, data for pairs of lines within those kinetic energy limits were examined to trace the magnitude of the remaining factors.

Variations in Photoelectric Cross Sections among Chemical States. Scofield's calculated cross sections (*13*) fall on smooth monotonic curves when plotted against Z. Yet it is an experimental fact that the x-ray absorption cross sections for elements are variable to the extent of several percent, especially when the photoelectron emitted has low kinetic energy, ca. <300 eV (*14*). The origin of this effect is the interaction of surrounding atoms with the emitted electron.

Thus, to be complete, we should consider structural effects on σ. These variations will only be significant, however, in

Table I. Relative Intensities of Lines from the Same Atom

Line 1/line 2	Element	Compound	X rays	I_1/I_2	$\phi_1 y_1/\phi_2 y_2$	Average	Std dev, %
2s/2p	Na	NaCl	Al	2.03	0.92		
		$Na_2Cr_2O_7$	Al	2.74	1.25		
		Na Zeolite[a]	Al	2.63	1.19		
		Na Zeolite[b]	Al	2.54	1.155	1.13	12.4
	Mg	MgO	Al	1.80	1.06[j]		
		MgF_2	Mg	1.62	1.12		
		MgF_2	Al	1.70	0.97[j]		
		Mg acac$_2$	Al	1.74	1.00		
		$MgSO_4 \cdot 7H_2O$	Al	1.67	0.96		
		Mg erucate	Al	1.38	0.79		
		Mg CH butyrate[o]	Al	1.52	0.875	0.97	11.3
	Al	α-Al_2O_3[d]	Al	1.44	1.02		
		α-Al_2O_3[e]	Al	1.45	1.025		
		Na Zeolite[c]	Mg	1.15	0.975		
		Na Zeolite[a]	Al	1.53	1.08		
		Na Zeolite[b]	Al	1.54	1.09	1.04	4.5
	Si	Si[f]	Al	1.25	1.06		
		SiO[g]	Al	0.965	0.82		
		SiO_2[g]	Al	1.06	0.90		
		SiO_2 gel	Al	1.09	0.925		
		Na Zeolite[c]	Mg	0.84	0.855		
		Na Zeolite[a]	Al	0.915	0.775		
		Na Zeolite[b]	Al	1.02	0.865	0.885	10.3
	P	$NaPO_3$	Mg	0.67	0.796		
		$NaPO_3$	Al	0.84	0.84	0.82	3.8
	S	FeS_2	Al	0.555	0.645		
		WS_2	Mg	0.50	0.70		
		WS_2	Al	0.59	0.79		
		Na_2SO_3	Mg	0.52	0.727		
		Na_2SO_4	Al	0.68	0.79		
		K_2SO_4	Mg	0.49	0.685		
		$MgSO_4 \cdot 7H_2O$	Al	0.70	0.815		
		Na thioglycollate	Al	0.73	0.85		
		KNDS[i]	Al	0.695	0.81	0.755	10.0
	Cl	NaCl	Al	0.585	0.785		
		KCl	Mg	0.37	0.60		
		KCl	Al	0.55	0.835		
		CuCl	Al	0.62	0.835		
		$PbCl_2$	Mg	0.34	0.55		
		$PbCl_2$	Al	0.54	0.725		
		$KClO_3$	Mg	0.50	0.81	0.735	15.8
	Ar	Ar in SS[j]	Al	0.43	0.66		
		Ar in SS[j]	Al	0.49	0.75	0.705	9.1
	K	KF	Mg	0.32	0.67		
		KCl	Mg	0.30	0.625		
		KBr	Mg	0.32	0.67		
		KI	Mg	0.31	0.645		
		KNO_3	Mg	0.325	0.68		
		$K_3Mn(CN)_6$	Mg	0.39	0.815		
		$K_3Fe(CN)_6$	Mg	0.37	0.773		
		$K_3Co(CN)_6$	Mg	0.315	0.657		
		$K_2Ni(CN)_4$	Mg	0.355	0.74		
		$K_2Ni(CN)_4$	Al	0.406	0.70		
		K_2PdCl_4	Mg	0.325	0.68		
		K_2WO_4	Mg	0.345	0.72		
		$KReO_4$	Mg	0.275	0.573		
		K_2PtCl_4	Mg	0.308	0.642		
		K_3AlF_6	Al	0.314	0.545	0.675	10.4
	Ca	$CaCO_3$	Al	0.33	0.64		
		CaF_2	Al	0.325	0.63	0.635	1.0
	Ti	K_2TiF_6	Al	0.217	0.525	0.525	
3s/3p							
	Cr	Na_2CrO_4	Al	0.44	0.865		
	Fe	$K_3Fe(CN)_6$	Al	0.46	1.03		
		$K_4Fe(CN)_6$	Al	0.42	0.93[h]	0.98	7.1
	Co	$K_3Co(CN)_6$	Al	0.41	0.96		
	Ni	$K_2Ni(CN)_4$	Al	0.378	0.935		
	Cu	CuF_2	Al	0.42	1.08		
		Cu[m]	Mg	0.356	1.00		
		Cu[n]	Al	0.37	0.95	1.01	6.5
	Zn	Zn[f]	Al	0.358	0.97		
		Zn[m]	Al	0.339	0.92		
		ZnF_2	Al	0.42	1.13		
		$Zn(PT)(BF_4)_2$[k]	Al	0.40	1.08	1.025	9.5
3p/3d	Zn	Zn[f]	Al	3.06	0.87		
		Zn[m]	Al	2.48	0.705		

Table I (*Continued*)

		$Zn(acac)_2$	Al	2.57	0.73	0.77	11.6
	Ga	Ga_2O_3	Al	2.26	0.76		
	Ge	GeO_2	Mg	2.02	0.97		
		GeO_2	Al	1.97	0.76	0.81	13.6
	As	As_2O_3	Al	1.74	0.77		
		As_2O_5	Al	1.78	0.79		
		$NaAsO_2$	Mg	1.73	0.945		
		$NaAsO_2$	Al	1.81	0.80[h]		
		$KAsF_6$	Al	1.73	0.765	0.81	9.3
	Se	Se[f]	Al	1.50	0.75		
		Na_2SeO_3	Mg	1.42	0.88		
		Na_2SeO_3	Al	1.84	0.92		
		$(NH_4)_2SeO_4$	Al	1.83	0.915	0.865	9.2
	Br	NaBr	Mg	1.24	0.87		
		NaBr	Al	1.62	0.93		
		KBr	Mg	1.20	0.84		
		$C_{16}H_{33}Me_3NBr$	Al	1.62	0.93	0.89	5.0
$3p_{3/2}/3d$	Y	YF_3	Mg	0.57	0.875		
		YF_3	Al	0.77	0.96	0.92	6.5
	Zr	Na_2ZrF_6	Mg	0.62	1.03		
		Na_2ZrF_6	Al	0.58	0.785	0.91	18.7
	Nb	K_2NbF_7	Mg	0.366	0.645		
		K_2NbF_7	Al	0.53	0.78	0.71	13.5
	Mo	Mo[i]	Al	0.54	0.855		
		Na_2MoO_4	Mg	0.345	0.672		
		K_2MoO_4	Al	0.466	0.74	0.755	12.3
$3p_{3/2}/3d_{5/2}$	Rh	K_3RhCl_6	Al	0.84	0.97		
		Na_3RhCl_6	Mg	0.50	0.71	0.84	21.4
	Ag	Ag[m]	Al	0.625	0.82[h]		
		Ag[n]	Al	0.74	0.97[h]		
		Ag[f]	Al	0.76	0.995	0.93	10.0
	Cd	Cd	Al	0.665	0.925		
		CdO	Al	0.737	1.025	0.975	7.2
$4d_{5/2}/4f$	Hf	HfF_4	Mg	0.62	0.66		
		HfF_4	Al	0.87	0.73	0.695	7.2
	Ta	K_2TaF_7	Mg	0.47	0.55		
		K_2TaF_7	Al	0.62	0.57	0.63	13.2
	W	WC	Al	0.58	0.58		
		WS_2	Mg	0.53	0.68		
		WS_2	Al	0.715	0.72		
		$K_4W(CN)_8$	Al	0.64	0.64		
		$Na_2WO_4 \cdot 2H_2O$	Mg	0.535	0.68		
		$Na_2WO_4 \cdot 2H_2O$	Al	0.76	0.765		
		K_2WO_4	Mg	0.49	0.625	0.655	10.7
	Re	$NaReO_4$	Al	0.49	0.53		
	Pt	K_2PtCl_4	Mg	0.34	0.59[h]		
		K_2PtCl_4	Al	0.55	0.743	0.655	16.8
	Au	Au[f]	Al	0.56	0.79		
	Hg	HgF_2	Al	0.427	0.66		
	Pb	Pb[f]	Al	0.39	0.67[j]		
		PbO	Mg	0.245	0.545		
		PbO	Al	0.374	0.645		
		PbS	Al	0.38	0.655		
		$PbCl_2$	Mg	0.29	0.645		
		$PbCl_2$	Al	0.39	0.67		
		PbF_2	Mg	0.29	0.645		
		PbF_2	Al	0.40	0.69		
		$PbCO_3$	Al	0.385	0.665		
		PbOHOAc	Al	0.405	0.70	0.655	6.4
5d/4f	Pb	Pb	Mg	0.115	1.20		
		Pb[f]	Al	0.145	1.21		
		PbS	Al	0.15	1.25		
		$PbCl_2$	Al	0.15	1.25		
		PbF_2	Al	0.155	1.29		
		$PbCO_3$	Al	0.148	1.23	1.24	2.6

[a] Sodium zeolite, $Na_{12}Al_{12}Si_{12}O_{48} \cdot 27H_2O$, sample No. 1. [b] Sodium zeolite, $Na_{12}Al_{12}Si_{12}O_{48} \cdot 27H_2O$, sample No. 2. [c] Sodium zeolite, $Na_{12}Al_{12}Si_{12}O_{48} \cdot 27H_2O$, sample No. 3. [d] α-Alumina, abrasive, low surface area. [e] γ-Alumina, high surface area "Catapal". [f] Vapor-deposited. [g] Flamed Vycor tubing. [h] Average of two values on the same material (cf. Experimental section). [i] Potassium salt of 2-naphthol-6,8-disulfonic acid. [j] Argon, ion-implanted in stainless steel. [k] $Zn(Py_3tren)(BF_4)_2$, where Py_3tren is a cage-type ligand, $C_{24}H_{27}N_7$. [l] Molybdenum powder, reduced in H_2, analyzed without air access. [m] Metal abraded in N_2, no air access. [n] Metal, argon-ion sputtered. [o] Magnesium cyclohexanebutyrate.

photoelectric processes giving very low energy electrons. In the Tables, only Na 1s (Table III) might exhibit noticeable effects of this sort, with low kinetic energies of 182 and 415 eV. There should be negligible variations in cross section for processes yielding 1000-V electrons.

Experimental Variability in Cross Section and Photoelectron Yield. Comparison of two lines from the same atom in different compounds can provide information on the

Table II. Intensities of Pairs of Lines from Different Atoms

Line 1	Line 2	Compound	X rays	I_1/I_2 (per atom)	$\phi_1 y_1/\phi_2 y_2$	Average	Std dev, %
B 1s	N 1s	$Zn(PT)(BF_4)_2$[a]	Al	0.35	1.30		
		BN	Al	0.224	0.83	1.06	31.1
N 1s	O 1s	$NaNO_2$	Mg	0.55	0.88		
		$NaNO_3$	Al	0.72	1.17		
		KNO_3	Mg	0.75	1.20		
		KNO_3	Al	0.71	1.155		
		$(NH_4)_2SO_4$	Al	0.635	1.033		
		$N_2H_6SO_4$	Al	0.615	1.00		
		$(NH_4)_2SeO_4$	Al	0.485	0.79		
		$Co(NH_3)_6(NO_3)_3$	Al	0.60	0.975		
		BNBP[b]	Al	0.71	1.155		
		cellulose nitrate[c]	Al	0.585	0.955		
		BPO[d]	Al	0.63	1.025		
		stearamide	Al	0.455	0.74	1.005	14.9
B 1s	Na 2s	$NaBF_4$	Mg	0.885	0.697		
C 1s	Na 2s	NaOAc	Al	1.83	0.775		
Na 2s	Al 2s	Na Zeolite[e]	Mg	1.17	2.04		
		Na Zeolite[f]	Al	0.87	1.55		
		Na Zeolite[g]	Al	0.79	1.41	1.67	19.8
Na 2s	Si 2s	Na Zeolite[e]	Mg	0.98	2.15		
		Na Zeolite[f]	Al	0.68	1.55		
		Na Zeolite[g]	Al	0.72	1.64	1.78	18.0
C 1s	Ca 2p	$CaCO_3$	Al	0.196	0.99[h]		
N 1s	P 2p	$Mn(PT)(PF_6)_2$[i]	Al	1.16	0.76[h]		
		$Fe(PT)(PF_6)_2$[i]	Al	1.09	0.72		
		$Co(PT)(PF_6)_2$[i]	Al	1.17	0.775		
		$Ni(PT)(PF_6)_2$[i]	Al	1.19	0.788		
		$Cu(PT)(PF_6)_2$[i]	Al	1.15	0.76		
		$Fe(MPT)(PF_6)_2$[j]	Al	0.97	0.642		
		$Fe(PMI)(PF_6)_2$[k]	Al	1.06	0.702		
		$Fe(BP)(PF_6)_2$[l]	Al	1.03	0.682	0.729	7.0
	S 2p	$(NH_4)_2SO_4$	Al	0.98	0.91		
		$N_2H_6SO_4$	Al	0.92	0.855		
		cystine	Al	1.09	1.013		
		cysteine HCl	Al	1.01	0.94[h]		
		MNA[m]	Al	1.06	0.985		
		IQS[n]	Al	0.93	0.865		
		thiourea	Al	1.00	0.93	0.928	6.25
	Cl 2p	$Co(NH_3)_6Cl_3$	Al	0.66	0.835		
	K 2p	KNO_3	Mg	0.366	0.83		
		KNO_3	Al	0.368	0.81	.82	1.7
F 1s	Mn $2p_{3/2}$	MnF_2	Al	0.60[o]	1.24		
O 1s	Ca 2p	$CaCO_3$	Al	0.59	1.02[h]		
Na 2s	P 2p	$NaPO_3$	Al	0.382	1.07		
Na 2s	S 2p	Na_2SO_3	Mg	0.26	1.165		
		Na_2SO_3	Al	0.31	1.23		
		Na_2SO_4	Al	0.26	1.03		
		$Na_2S_2O_3$	Al	0.34	1.34		
		Na thioglycollate	Al	0.325	1.285	1.21	10.0
	Cl 2p	NaCl	Al	0.188	1.01		
		Na_2PdCl_4	Al	0.210	1.13	1.07	7.9
Mg 2s	S 2p	$MgSO_4 \cdot 7H_2O$	Al	0.378	1.10		
B 1s	Zn 3p	$Zn(PT)(BF_4)_2$[a]	Al	0.217	1.27		
N 1s	Br 3p	$C_{16}H_{33}Me_3NBr$	Al	0.42	1.18		
Na 2s	Cr 3p	Na_2CrO_4	Mg	0.535	1.53		
		Na_2CrO_4	Al	0.725	2.00		
		$Na_2Cr_2O_7$	Al	0.87	2.42	1.98	22.2
Mg 2s	Se 3p	$MgSeO_4$	Al	0.161	1.27		
N 1s	Pd $3d_{5/2}$	$Pd(CN)_2$	Al	0.185	0.975		
O 1s	Ag $3d_{5/2}$	Ag_2SO_4	Al	0.28	1.02		
	Te $3d_{5/2}$	Na_2TeO_4	Al	0.188	1.16		
	Xe $3d_{5/2}$	Na_4XeO_6	Al	0.118	0.88		
F 1s	Sb $3d_{5/2}$	$KSbF_6$	Mg	0.172	0.647		
	Ba $3d_{5/2}$	BaF_2	Mg	0.172	0.99		
		BaF_2	Al	0.148	0.865	0.93	9.5
Na 2s	Se 3d	Na_2SeO_3	Mg	0.131	0.83		
		Na_2SeO_3	Al	0.205	1.10	.965	19.7
	Zr 3d	Na_2ZrF_6	Mg	0.056	1.035		
		Na_2ZrF_6	Al	0.0655	1.09	1.06	3.7
O 1s	Bi $4d_{5/2}$	$NaBiO_3$	Mg	0.328	1.19		
Na 2s	Te 4d	Na_2TeO_4	Al	0.135	1.16		
		Na_2TeO_4	Al	0.152	1.31	1.24	8.5
C 1s	Pb 4f	$PbCO_3$	Al	0.046	1.045		
Na 2s	W 4f	Na_2WO_4	Al	0.065	1.50[h]		
	Bi 4f	$NaBiO_3$	Al	0.0214	1.25		
P 2p	Cl 2p	$(Phen_3P)_2IrCOCl$	Al	0.48	0.92		

Table II (*Continued*)

Cl 2p	Ca 2p	$CaCl_2$	Mg	0.58	1.26		
	Sc 2p	$ScCl_3$	Al	0.43	1.20		
K 2p	S 2p	K_2SO_4	Mg	2.26	0.98		
		K_2SO_4	Al	2.90	1.225		
		KNDS[p]	Al	2.35	0.99	1.065	13.0
	Cl 2p	KCl	Mg	1.87	1.09		
		KCl	Al	1.74	1.00		
		K_3RhCl_6	Al	1.70	0.975		
		K_2PdCl_4	Mg	2.15	1.26		
		K_2PtCl_4	Mg	1.98	1.16[h]		
		K_2PtCl_4	Al	2.05	1.18		
		$KClO_3$	Mg	1.79	1.04		
		$KClO_3$	Al	1.93	1.11		
		$KClO_4$	Al	1.83	1.05	1.096	8.4
P 2p	Mn 3p	$Mn(PT)(PF_6)_2$[i]	Al	1.25	1.50[h]		
	Fe 3p	$Fe(PT)(PF_6)_2$[i]	Al	1.35	1.90		
		$Fe(BP)_3(PF_6)_2$[l]	Al	0.91	1.28		
		$Fe(MPT)(PF_6)_2$[j]	Al	0.89	1.25		
		$Fe(PMI)_3(PF_6)_2$[k]	Al	0.86	1.21	1.41	23.4
K 2p	Cr 3p	$K_3Cr(CN)_6$	Al	5.8	1.70[h]		
	Mn 3p	$K_4Mn(CN)_6$	Mg	7.1	2.62		
		$K_3Mn(CN)_6$	Al	7.05	2.53		
		$K_4Mn(CN)_6$	Al	5.35	1.92	2.35	16.2
	Fe 3p	$K_4Fe(CN)_6$	Mg	5.0	1.95[h]		
		$K_4Fe(CN)_6$	Al	4.5	1.90[h]		
		$K_4Fe(CN)_6$	Al	4.5	1.90	1.92	1.5
	Co 3p	$K_3Co(CN)_6$	Mg	5.05	2.25		
		$K_3Co(CN)_6$	Al	3.9	1.90	2.075	12.0
	Ni 3p	$K_4Ni(CN)_4$	Mg	3.6	1.82		
		$K_2Ni(CN)_4$	Al	2.9	1.62	1.72	8.1
S 2p	Ag $3d_{5/2}$	Ag_2SO_4	Al	0.188	1.20		
Cl 2p	Rh $3d_{5/2}$	Na_3RhCl_6	Mg	0.34	1.21		
	Pd $3d_{5/2}$	Na_2PdCl_4	Mg	0.27	1.085		
		Na_2PdCl_4	Al	0.256	1.06	1.07	1.6
K 2p	As 3d	$KAsF_6$	Al	2.9	1.325		
	Br 3d	KBr	Mg	1.565	1.19		
	Nb 3d	K_2NbF_7	Mg	0.52	1.08		
		K_2NbF_7	Al	0.575	1.19	1.135	6.9
	Mo 3d	K_2MoO_4	Al	0.545	1.30		
		$K_4Mo(CN)_8$	Al	0.655	1.57		
		$K_4Mo(CO)_3(CN)_3$	Al	0.55	1.315	1.395	10.8
	Rh $3d_{5/2}$	K_3RhCl_6	Al	0.48	1.015		
	Pd $3d_{5/2}$	K_2PdCl_4	Mg	0.70	1.64		
S 2p	Sb 4d	Sb_2S_3	Al	0.36	0.676		
	Ba 4d	$BaSO_4$	Al	0.26	0.91		
Cl 2p	Cs 4d	CsCl	Al	0.33	0.763		
	Ba 4d	Ba chloranilate	Al	0.30	0.772		
K 2p	I 4d	KI	Mg	1.13	1.07		
S 2p	W 4f	WS_2	Mg	0.181	1.05		
		WS_2	Al	0.170	0.995	1.02	3.8
Cl 2p	Ir 4f	$(Phen_3P)_2IrCOCl$	Al	0.12	1.40		
	Pb 4f	$PbCl_2$	Mg	0.104	0.99		
		$PbCl_2$	Al	0.104	1.04	1.015	3.4
K 2p	Ta 4f	K_2TaF_7	Mg	0.46	1.02		
		K_2TaF_7	Al	0.51	1.11	1.065	6.0
	W 4f	K_2WO_4	Mg	0.52	1.30		
		$K_4W(CN)_8$	Al	0.62	1.525	1.41	11.3
	Re 4f	$KReO_4$	Mg	0.395	1.115		
	Pt 4f	K_2PtCl_4	Mg	0.302	1.18[h]		
		K_2PtCl_4	Al	0.345	1.34	1.26	8.7

[a] $Zinc(Py_3tren)(BF_4)_2$, where Py_3tren is a cage-type ligand, $C_{24}H_{27}N_7$. [b] 4,4′-Dinitrobiphenyl. [c] Cellulose nitrate, assuming N/O = 6/22. [d] BPO = α,α′-bipyridyl di-*N*-oxide. [e] Na Zeolite, No. 3. [f] Na Zeolite, No. 1. [g] Na Zeolite, No. 2. [h] Average of two values obtained on same compound (cf. Experimental section). [i] Compounds of other metals like the zinc compound (*a*) but salts of PF_6^-. [j] MPT = 6MePy$_3$tren, with empirical formula $C_{27}H_{33}N_7$. [k] PMI = 3 ligands, $C_6H_4N_2$, per iron. [l] BP = 3 bipyridyl ligands per iron. [m] MNA = α-mercaptyl-*N*-2-naphthylacetamide. [n] IQS = 8-hydroxyl-7-iodo-5-quinolinesulfonic acid. [o] Area of Mn $2p_{3/2}$ measured with sigmoidal baseline, tangent to baseline on both sides. (Low kinetic energy side had high baseline.) [p] Potassium salt of 2-naphthol-6,8-disulfonic acid.

constancy of σ and y for different shells of the same atom among different chemical states. In that instance n_1 and n_2 are identical, ϕ_1/ϕ_2 should be constant, and

$$\frac{I_1 I_2}{(f_1/f_2)(\sigma_1/\sigma_2)} = \frac{\phi_1 y_1}{\phi_2 y_2} \tag{10}$$

Variability in σ_1/σ_2 or y_1/y_2 among different chemical states should be shown by an increase above 7.2% in standard deviation.

In Table I are shown data on compounds of elements for line ratios 2s/2p, 3s/3p, 3p/3d, 4d/4f, and 5d/4f. The areas of the photoelectron lines were measured, and division of the ratio by the ratio of Scofield's cross sections (*13*) yields the data in column 6. Data include separate entries for the same compound under Al and Mg x rays, but otherwise the same

compound is not repeated. Averaged values are used for multiple analysis on the same compound with the same x rays. For 133 compound-photon entries for 30 elements, the average standard deviation in $\phi_1 y_1/\phi_2 y_2$ for multiple entries per element was 9.65%. Thus, the extra variability is less than 2.5%. We can therefore conclude that σ_1/σ_2 and y_1/y_2 for two lines from the same atom are highly constant among different chemical states, and that calculated values for σ for Mg x rays bear the correct relation to calculated σ for Al x rays.

Angular Effects on Intensities. Angular effects will not contribute to variability in intensity among chemical states but considerations of angular effects are necessary for the discussion in the following sections. Photoelectrons are not usually emitted isotropically. The differential cross section, and hence the intensity, is of the form (*15*)

$$d\sigma/d\Omega = (\sigma_{tot/4\pi})[1 - {}^1/_4\beta(3\cos^2\theta - 1)] \qquad (11)$$

where θ here is the angle between the photon beam and the photoejected electron and β is a parameter that has been tabulated for Mg and Al x-ray interactions (*16*). Integration of $d\sigma$ over all solid angles gives the total cross section, σ_{tot}. It is the latter that has been calculated by Scofield. We are interested in the partial cross section for the θ of our spectrometer for all of the photoelectrons cited in the Tables. Lacking that, we need to predict the angular correction factors, ϕ_1/ϕ_2, for the line pairs of interest. Calculation of the most extreme case possible for ϕ_1/ϕ_2, for Na 2s/Na 2p at a spectrometer angle of 90°, leads to the value 1.28. This is modified downward toward unity by the facts that the actual spectrometer angle ranges from 90° to 180°, with the most probable angle somewhere between, and elastic scattering in the solid renders the electron emission more isotropic. For purposes of this discussion, ϕ_1/ϕ_2 can be assumed unity.

Variations in Stoichiometry and Photoelectron Yield. Fadley (*17*), from theoretical considerations, concluded that y should be the same for all core atomic orbitals of an atom, so that the previous conclusion that y_1/y_2 is constant in Table I should be expected. It is then instructive to make the same comparison for different atoms. This was done in Table II.

In this instance we have the similar relation:

$$\frac{I_1/I_2}{(n_1/n_2)(\sigma_1/\sigma_2)} = \frac{\phi_1 y_1}{\phi_2 y_2} \qquad (12)$$

but n_1/n_2 is now assumed to be that of the stoichiometry of the compound, and σ and y refer to photoelectron processes in different atoms in different chemical states. If n_1/n_2 is physically correct in the surface layers examined and σ_1/σ_2 values derived theoretically are correct, the values for $\phi_1 y_1/\phi_2 y_2$ should turn out to be near unity. Deviations from unity are likely to reflect untrue values of n_1/n_2 or significant differences in y_1/y_2.

Certain features are evident in Table II. Line pairs involving transition metals (Cr–Ni, Mo–Pd, W–Pt), which are always presented as line 2, nearly always have values of $\phi_1 y_1/\phi_1 y_2$ significantly larger than unity. In the Table, these average 1.556 for 38 entries, standard deviation 0.44, compared to 1.01 for the remaining 92 entries (omitting Na zeolite, see below), standard deviation 0.18. It is concluded that the most likely explanation is a low and variable value of y for the process involving the transition metal. In accordance with this conclusion it may be noted that the original published values for S for the first series of transition metals exhibited anomalously low values compared to neighboring elements (*1*). Probability of shakeup and shakeoff phenomena in photoelectron processes in noble gas atoms have been determined to be about 20% (*18*), so the maximum value of y under XPS conditions is 0.80. The value for transition metals can be much lower, perhaps 0.5 or even 0.3.

Values for Na 2s/Al 2s and Na 2s/Si 2s for zeolite are also high. This is believed due to excess sodium ion on the surface, a not unlikely state when one considers the method of preparation. The value for K 2p/As 3d in $KAsF_6$ was also unusually high (1.325) and is probably also due to faulty stoichiometry, but was included in the above tabulation.

Data for $AgOOCCF_3$, $K_2Pd(NO_3)_4$, $(NH_4)_3InF_6$, NaI, $NaAsO_2$, $NaReO_4$, cyano complexes (N 1s/K 2p), and cysteine HCl (N 1s/Cl 2p) were the 13 compounds or line pairs omitted from the tabulation because of obvious poor stoichiometry. With the cyano complexes and cysteine HCl, there is evidence the heat generated upon grinding played a role.

Deviations from unity for $\phi_1 y_1$ are not the appropriate test for the use of standard values for S in quantitative analysis, but furnish clues as to what types of line pairs can validly be included in deriving values of S. When line pairs involving transition metals and the zeolite are excluded, the data in Table II show an average percent standard deviation of 9.81% from the average for each multiple line pair (66 compounds of 17 line pairs). Thus, for the bulk of the data, compared to the data from the two lines from the same element (Table I), we conclude n_1/n_2 is accurate and y_1/y_2 is consistent for atoms other than transition elements among different compounds.

Ng and Hercules (*5*) found trends in I_1/I_2 for alkali metal halides that seemed to indicate unusually low photoelectron yields when the emitting atom is small and surrounded by near large atoms. The effect amounted to a diminution by as much as a factor or two to three compared to the reverse situation. This could be considered to be a special type of fractional photoelectron yield, not due to intrinsic atomic processes, but due to the geometry of nearest neighbors in the solid state. We have not included similar data with the compounds they used, because in our experience our samples of cesium and rubidium compounds have never been sufficiently pure; they always exhibited clear evidence for hydration in spite of our best efforts in handling in rigorously dry atmosphere. Iodides are also not included because of their instability under the ionizing radiation. It is clear from our generally consistent data that their reported observation does not invalidate the general applicability of the method.

Swingle (*4*) presented evidence for lack of uniformity of results for an element in its different chemical states that could be ascribed to varying values of y. However, our data in Table II, with the exception of data for transition metals, show remarkable uniformity, and indicate that the method in general is inherently more quantitative than one might surmise from the particular results he cited.

Berthou and Jorgensen (*3*) attribute low values for standard intensities that are peculiar to certain elements to low values of y. Elements that seemed unusually low in standard intensity, besides the transition metals, were Mg, Al, S, Cl, Ge, As, Se, Nb, Mo, Sn, Te, I, Cs, Ba, Pt, Au, and Hg. These elements possessed standard intensities approximately 60–80% of the expected values. The data in this paper do not show evidence for such large deviations for the elements, other than a general conclusion about the transition metals.

Absolute Values of Photoelectron Cross Sections. Fadley (*17*) concluded from theoretical considerations that the probability for two-electron processes should be similar in all core levels. If this is true, substantial deviations of $\phi_1 y_1/\phi_2 y_2$ from unity in Table I may reflect inaccuracy in the calculations of the cross sections. In Table I it is seen that this ratio, derived by dividing I_1/I_2 by σ_1/σ_2, decreases in the 2s/2p series from 1.13 for Na to 0.64 for Ca. The progression is rather regular. The progression in the maximum value for ϕ_1/ϕ_2 for 90° emission, 1.28 to 1.12, does move in the right

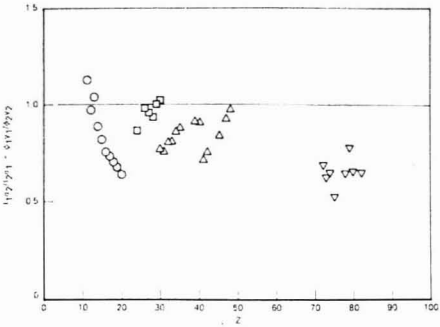

Figure 2. Electron mean free path in solids (from data collected in Ref. 8). Slopes representing $E^{0.67}$ and $E^{0.82}$ are shown; these are the slope limits resulting from the calculations by Penn (*10*)

direction to help explain the trend, but the ratio for the integrated, effective angle with elastic scattering is believed barely to exceed unity. The lines measured were narrow, with baselines easily defined. This consistent trend of experimental results lends concern that there may be a significant error trend in the cross section calculation in this series.

A second set that could lead to concern is the $4d_{5/2}/4f$ set in Table I. Here data for $\phi_1 y_1/\phi_2 y_2$ range from 0.63 to 0.70. That for lead is 0.66. An error in measurement can explain at least part of the discrepancy. The 4d lines are very broad, so that the energy loss background rises strongly within the peak. Drawing the baseline tangent in the usual way could enclose an area considerably too small. The remaining data in Table I (see Figure 2) show no significant obvious inconsistencies; the data range from 0.7 to unity. The lack of systematic differences in data for Mg and Al x rays indicate theory compensates well for the change in photon energy.

Role of Mean Free Path and Contamination. The above treatment shows that the quantitative concept on a homogeneous solid system is valid for quantities not sensitive to the electron kinetic energy. However, the original suggestion whereby sensitivity factors (or as we now prefer to call them, standard intensities) were derived from line intensity ratios from fluorides, sodium salts, and potassium salts, had an extra complicating factor: the photoelectrons used, F 1s, Na 1s, and K $2p_{3/2}$, possess widely different energies, so the factors sensitive to kinetic energy must be considered. Thus the constancy of λ_1/λ_2 and C_1/C_2 among different chemical states for the same photoelectron pair has importance. T is, of course, a spectrometer function and T_1/T_2 is invariant.

An extreme test of these factors is the variation of the ratio $I(\text{Na 2s})/I(\text{Na 1s})$ among different compounds. Data obtained are shown in Table III.

An approximate assessment can be derived as follows: We assume the exponential limits derived from an approximate fit to Penn's calculations of mean free paths, namely

$$\lambda = kE^{0.68} \text{ to } kE^{0.82} \tag{13}$$

and assume validity to the theoretical expression that $T \sim E^{-1.0}$. We further assume hydrocarbon contamination to approximate one-fifth of the mean free path for 1000-V electrons in hydrocarbon. Then from Equation 9 we calculate the expression $\lambda_2 T_2 C_2/\lambda_1 T_1 C_1$ (2 = Na 2s, 1 = Na 1s) to be 0.86–1.01 for Al radiation and 0.96–1.26 for Mg radiation. (The limits are the exponential limits for λ). The effect of λT is to decrease I_2/I_1, that of contamination is to increase it. The contamination factor alone under the above assumptions is 1.26 for Al radiation and 1.76 for Mg radiation. For such wide

Table III. Intensity Ratios, Na 2s/Na 1s (In table 2 = 2s, 1 = 1s)

	$I_2/I_1 \times 1000$	$\sigma_2/\sigma_1 \times 1000$
Mg x rays		
$NaBF_4$	36	
$NaNO_2$	45	
Na Zeolite[a]	69	
Na_2SO_3	72	
Na_2TiF_6	76	
Na_2CrO_4	40	
Na_2GeF_6	50	
$NaAsO_2$	57	
Na_2ZrF_6	81	
$Na_2SnO_3 \cdot 3H_2O$	66	
Av	59.2	48.2
Std dev	15.8	
Std dev, %	26.7	
Al x rays		
$NaBF_4$	50	
NaOAc	44	
NaEDTA[d]	56	
$NaNO_3$	54	
NaF	57	
	58	
	61	
Na Zeolite[b]	66	
Na Zeolite[c]	61	
Na_2SiF_6	60	
$NaPO_3$	52	
Na_2SO_4	51	
Na_2SO_3	56	
$Na_2S_2O_3$	65	
NaSCN	62	
Na thioglycollate	44	
NaCl	46	
Na_2CrO_4	67	
$Na_2Cr_2O_7$	58	
$NaAsO_2$	58	
Na_2SeO_3	51	
Na_2ZrF_6	54	
Na_2PdCl_4	64	
$Na_2SnO_3 \cdot 3H_2O$	65	
Na_2TeO_4	69	
	47	
$Na_2WO_4 \cdot 2H_2O$	48	
Av	56.4	49.5
Std dev	7.2	
Std dev, %	12.8%	

[a] Na Zeolite No. 3 (cf Table II). [b] Na Zeolite No. 2. [c] Na Zeolite No. 1. [d] Na salt of ethylenediamine tetracetic acid.

kinetic energy differences, variations in contamination can be most important. Variation in the mean free path within Penn's limits would permit a range in λ_2/λ_1 of 16% for Al radiation and 26% for Mg radiation. It is therefore not surprising that the standard deviation observed in Table III is 13% for Al radiation and 27% for Mg radiation. For kinetic energy ratios ordinarily encountered, the effect of λTC on variability of S would lead to extra error of only a few percent.

CONCLUSIONS

Use of standard intensity values to obtain relative numbers of atoms in the surface layers of a sample is attended by several sources of error. This work leads to the following conclusions regarding the sources of error.

(1) Error in line measurement and variability of x-ray flux lead to an error of ±7%.

(2) From data in Table III, we conclude the method is inherently quantitative to ±10% with different chemical states if the lines are of similar kinetic energy and transition metals are not involved. This includes variability in σ and y, for the same lines in different chemical states, as well as the variability

in flux and area determination (No. 1 above).

(3) When lines far apart in kinetic energy are compared, validity of the method requires that λ_1/λ_2 in the material analyzed be the same as that in the materials from which standard intensity data were derived. Calculations based on the work of Penn indicate that the ratio of λ_1/λ_2 for two lines can be variable by as much as 10% for $E_1/E_2 = 2$, or 22% for $E_1/E_2 = 6$. For most line pairs the effect is minimal.

(4) When lines of widely different kinetic energies are used, adsorbed contamination layers can present problems. In the Na 2s/Na 1s line pair (Mg x rays) a 10% adsorbed hydrocarbon layer (C 1s signal equaling 10% of the infinitely thick value) should give an enhancement in I(Na 2s)/I(Na 1s) (Mg x rays) of 31%. Most line pairs are much closer in kinetic energy, so that variation in contamination normally contributes a few percent to the error.

(5) The photoelectron yield, y, is greatly diminished in compounds of transition metals because of prevalent multielectron processes. To the extent that these effects are variable among different chemical forms of such an element, quantitative applications in the general sense will be difficult with these elements. There seems to be no evidence here for strongly varying y among nearest neighbors in Z or for serious variability in elements other than the transition elements.

(6) The possible variable screening of photoelectron emission by nearest neighbor atoms is not evident in this study, but further work might establish whether it is a real effect and worthy of concern.

(7) Use of internal standards comprising a second phase has no validity for quantitative analysis, because of variability in absolute values of electron mean free paths in different materials, and probably more importantly, variability in friability and plasticity among different materials.

ACKNOWLEDGMENT

Many of the spectra were obtained by R. H. Raymond of this laboratory, and some by David Zatko of the University of Alabama while he was in residence at this laboratory. The cage-type ligand compounds were kindly furnished by Lon J. Wilson of Rice University.

LITERATURE CITED

(1) C. D. Wagner, *Anal. Chem.*, **44**, 1050 (1972).
(2) C. K. Jørgensen and H. Berthou, *Chem. Soc. Faraday Disc.*, **54**, 269 (1973).
(3) H. Berthou and C. K. Jørgensen, *Anal. Chem.*, **47**, 482 (1975).
(4) R. S. Swingle II, *Anal. Chem.*, **47**, 21 (1975).
(5) K. T. Ng and D. M. Hercules, *J. Electron Spectrosc. Relat. Phenom.*, **7**, 257 (1975).
(6) V. I. Nefedov, N. P. Sergushin, J. M. Band, and M. B. Trzhaskovskaya, *J. Electron Spectrosc. Relat. Phenom.*, **2**, 383 (1973).
(7) W. J. Carter, G. K. Schweitzer, and T. A. Carlson, *J. Electron Spectrosc. Relat. Phenom.*, **5**, 827 (1974).
(8) C. J. Powell, *Surf. Sci.*, **44**, 29 (1974).
(9) P. C. Kemeny, A. D. McLachlan, F. L. Battye, R. T. Poole, R. C. G. Leckey, J. Liesegang, and J. G. Jenkin, *Rev. Sci. Instrum.*, **44**, 1197 (1973).
(10) D. R. Penn, *J. Electron Spectrosc. Relat. Phenom.*, **9**, 29 (1976).
(11) D. M. Wyatt, J. C. Carver, and D. M. Hercules, *Anal. Chem.*, **47** 1297 (1975).
(12) J. C. Helmer and N. H. Weichert, *Appl. Phys. Lett.*, **13**, 266 (1968).
(13) J. H. Scofield, *J. Electron Spectrosc. Relat. Phenom.*, **8**, 129 (1976).
(14) F. W. Lytle, *Appl. Phys. Lett.*, **24**, 45 (1974).
(15) J-T J. Huang, J. W. Rabalais, and F. O. Ellison, *J. Electron Spectrosc. Relat. Phenom.*, **6**, 85 (1975).
(16) R. F. Reilman, A. Msezane, and S. T. Manson, *J. Electron Spectrosc. Relat. Phenom.*, **8**, 389 (1976).
(17) C. S. Fadley, *Chem. Phys. Lett.*, **25**, 225 (1974).
(18) M. O. Krause, *J. Phys. (Paris), Colloque C4, Suppl. 10*, **32** C4–67 (1971).

RECEIVED for review December 9, 1976. Accepted May 4, 1977.

Surface Studies of Mammalian Cells Grown in Culture by X-ray Photoelectron Spectroscopy

Merle M. Millard* and James C. Bartholomew

Western Regional Research Center, U.S. Department of Agriculture, Berkeley, California 94710 and Laboratory of Chemical Biodynamics, Lawrence Berkeley Laboratory, University of California, Berkeley, California 94720

The surface elemental composition of Balb 3T3 A31 HYF mouse fibroblast cells and transformed MSV/MLV Balb 3T3 A31 HYF cells was obtained using x-ray photoelectron spectroscopy (XPS). The surface composition of the cells was sensitive to the nature of the specimen preparation; however, the oxygen to nitrogen (O/N) atom ratio varied between 3 and 1 for washed cells and fixed cells. The oxygen to nitrogen atom ratio was generally lower for transformed cells. Cell coverage on glass substrate was estimated to be 95% by comparing the silicon 2p signal from clean glass and glass substrate overlaid with cells. The change in concentration of phosphorus and sodium to a depth of approximately 40 nm into the surface of the cells was obtained combining XPS surface analysis data and oxygen plasma etching. The change in phosphorus concentration was linear with time and fairly similar for the cells before and after tranformation.

Among the changes that occur in a cell after malignant transformation are alterations in the cell surface. This conclusion has been drawn primarily from three types of observations. First, new antigens appear on the surface of malignant cells that are missing from their normal counterpart (*1–10*). Second, various plant lectins agglutinate malignant cells at much lower concentrations than required to agglutinate normal cells (*11–19*). And third, the carbohydrate content of the cell surface is altered in malignant cells (*20–28*). Despite the large amount of information regarding changes in the macromolecular structure of the cell surface induced by malignant transformation, little is known about the elemental composition of the surface of transformed and nontransformed cells. The major reason this information is lacking has been that techniques for analysis of surface elemental composition have not been applied to such biological samples.

X-ray photoelectron spectroscopy (XPS) is a relatively new technique capable of analyzing the surface of solid materials (*29*). The discrete energies of core electrons photo-ejected from the elements on the surface can yield information on both elemental composition and chemical bonding. Only the region less than 10 nm into the surface is analyzed; therefore, the technique is blind to substances situated more than a few nanometers below the surface. In a relatively brief time, a considerable number of experiments have applied XPS to the structural and analytical characterization of metals, refractory oxides, and polymer surfaces (*30*). The unique surface analysis

Table I. Description of Cell Specimen Preparations

Specimen	Preparation	Substrate	Angle between specimen plane and detector
1. Normal cells	growth medium decanted away	polystyrene	90
2. Normal cells	washed with isotonic saline solution	polystyrene	90
3. Normal cells	washed with distilled water	polystyrene	90
4. Normal cells	not fixed	polystyrene	90
5. Transformed cells	not fixed	polystyrene	90
6. Normal cells	fixed with glutaraldehyde ethanol critically dried with Freon 113	glass mounted on gold holder	90
7. Normal cells	"	glass on metal mount	90
8. Transformed cells	"	glass on metal mount	90
9. Normal cells	"	glass	90
10. Normal cells	"	glass	15
11. Transformed cells	"	glass	90
12. Transformed cells	"	glass	15

capabilities of XPS have, however, been neglected as a method to study the surface of biological materials. The binding of magnesium ions to cell walls of gram positive bacteria, as well as the chemical nature of osmium tetraoxide fixation and staining of membranes (*31*), has been studied using XPS (*32*). Human blood cells (*33*), various bacteria cells (*34*), and bacterial spores (*35*) have been surface-analyzed using XPS.

The combination of a surface analysis technique with a method of removing the outer surface of a specimen allows measurement of the change in concentration of various elements as a function of depth into the specimen. Oxygen plasma has been used to gently etch outer layers of organic material from the surface of biological specimens without altering the surface morphology of inorganic components (*36*).

XPS and oxygen plasma have been combined to surface analyze and depth profile bacterial cells (*34*). Electron microscopy was used to ascertain the uniformity of plasma oxidation of bacterial cells, and changes in dimensions of polystyrene spheres were used to calibrate the oxidation process (*35*). Meisenheimer et al. (*33*) used argon ion etching and XPS to depth profile red blood cells. We have explored the use of XPS and oxygen plasma etching to study the surface of Balb 3T3 A31 HYF cells before and after viral transformation. Tissue culture cells have the desirable property of forming a monolayer of cells on the substrate, and their surface morphology is relatively well known from scanning electron microscope studies (*8, 37, 38,*). It would seem natural to apply XPS to the study of mammalian cell membranes to learn more about what components are on the surface of these cells and how the surface may change with different growth states.

EXPERIMENTAL

Cells. All cells were carried in 100-mm polystyrene dishes (Falcon, Oxnard, Calif.) and incubated at 37 °C in a 5% CO_2 incubator. The medium used to grow the cells was Eagle's minimal medium (*39*) (GIBCO, Grand Island, N.Y.) containing 10% fetal calf serum. Balb 3T3 A31 mouse fibroblasts were obtained from Helene Smith of the Naval Biomedical Research Laboratory (Oakland, Calif.) and cloned prior to use to give Balb 3T3 A31 HYF, the clone used in all these experiments. All viral transformants used in these experiments were derived from Balb 3T3 A31 HYF. The cells were judged free of mycoplasma by incorporation of ^{3}H-thymidine (20.1 Ci/mM; New England Nuclear, Boston, Mass.) into the nucleus of cells and not the cytoplasm (*40*). The Balb 3T3 A31 HYF cells will subsequently be referred to as normal.

Viral Infection. The Moloney strain of murine sarcoma virus (MSV/MLV) used in these experiments was obtained from Adeline Hackett of the Naval Biomedical Laboratory (Oakland, Calif.) and carried in high passage mouse embryo cells. The focus forming units were measured on Balb 3T3 A31 HYF as described by Calvin et al. (*41*). The continuous line of MSV/MLV Balb 3T3 A31 HYF was obtained by infecting 2×10^5 Balb 3T3 A31 HYF cells 24 h after seeding with approximately 6×10^5 focus forming units of MSV/MLV. After the cells reached saturation density they were transferred, for a total of 4 passages, by seeding cells at approximately $^1/_{10}$ their saturation density. At passage number 4, the cells were suspended in medium containing 20% serum and 10% dimethyl sulfoxide (DMSO) and frozen at 203 K in a liquid nitrogen freezer. The cells used in these experiments were one passage beyond the frozen stocks. The MSV/MLV Balb 3T3 A31 HYF cells will subsequently be referred to as transformed.

Specimen Preparation. *Specimen Substrates.* A signal is obtained in the spectrometer from a surface with a circular area 6.35 mm in diameter. Cells were grown as confluent monolayers on polystyrene tissue culture dishes, and 6.35-mm disks cut from the bottom of the dish. To minimize contamination due to handling, cells were later grown on precut 6.35-mm polystyrene disks. A similar procedure was used with glass substrates. Initially, cells were grown on glass microscope cover slips, and 6.35-mm disks cut from the coverslips containing the cells. Later, cells were grown on precut 6.35-mm diameter disks. Glass substrates were cleaned and sterilized for cell growth by treatment with an oxygen plasma.

Unfixed Cells. Cells were grown on polystyrene culture dishes. While in the dish, the culture medium was decanted away, and the cells were given several washes with isotonic saline or distilled water. These liquids were decanted away, and 6.35-mm disks cut from the bottom of the dishes. The disks were introduced into the spectrometer moist and evacuated to 10^{-6} Torr in 3–5 min.

Fixed and Critical-Point Dried Cells. The cells were fixed at pH 7.35 in 2% glutaraldehyde in growth medium without serum and dehydrated by washing in 0.1 M sodium cacodylate buffer, pH 7.4 followed in order by water, 20, 50, 70, 95, and 100% ethanol. To prepare these cells for critical point drying, they were washed in 25, 50, and 75% Freon 113 in ethanol. Table I contains a description of the specimens studied in this paper. These specimens will be referred to by number in subsequent tables and discussion.

X-ray Photoelectron Spectra. Core binding energies were measured with a standard DuPont 650 electron spectrometer with a magnesium anode. The x-ray source was operated at standard maximum voltage and current.

Grazing-angle spectra were obtained using a machined sample mount designed so that the electron take-off angle, between the electron analyzer entrance and the plane of the sample surface was 15° (*42–44*). The 15° mount exposes a bullet shaped area to radiation, and cells were grown on bullet shaped pre-cut glass surfaces for the grazing angle spectra.

Electron lines from the surface of cells were obtained using a routine scan rate of 1 eV/cm. Data were accumulated over the energy region between 550 and 50 eV using a multichannel analyzer. Data were collected using half of the memory address group consisting of 512 channels. The scan rate was fixed at 0.1 s per channel, and data were accumulated for 16 scans. Samples were maintained at ambient temperature in the spectrometer.

Line intensities were determined by manually estimating a baseline and measuring the peak height at half-width. Elemental

line widths were approximately 2.0 eV. Atom ratios were determined by dividing the estimated line intensity by sensitivity factors taken from Wagner's data (*45*).

Surface Etching for Depth Profile Analysis. The surface of cells was oxidized and etched by exposure to oxygen plasma generated at ambient temperature using a "Plasmod" plasma system manufactured by Tegal Corp. (Richmond, Calif.). This system consists of a cylindrical glass chamber approximately 3 inches in diameter and 6 inches in length. A gas may be introduced into the chamber, and the chamber is evacuated by means of a mechanical vacuum pump. Up to 100 W of radio-frequency power at 13.56 MHz can be coupled into the gas flow system through external electrodes surrounding the cylindrical chamber. The gas pressure in the system during routine operation conditions was typically around 1 Torr. In order to assume that sample oxidation occurred under the mildest possible conditions, samples were oxidized at the lowest power setting obtainable for the instrument. This power level was probably below 5 W.

RESULTS AND DISCUSSION

Technical Considerations. *Specimen Preparation.* The specimen was held at a pressure of approximately 10^{-6} Torr in the photoelectron spectrometer. Excluding the possibility of maintaining specimens at low temperature in the instrument, the specimen must be evacuated and dehydrated. The disruptive effects of dehydration and evacuation on biological samples are well documented in the electron microscopy literature (*37, 38, 46–48*). After some preliminary studies on cells introduced directly into the spectrometer and evacuated, we adopted standard procedures used to fix and critical point dry specimens prior to introduction into the spectrometer.

Specimen Substrates. Different substrates were used to overcome the difficulties resulting from interferences of elemental line intensity contribution from the substrate and the specimen covering the substrate. The spectrometer had a variable carbon contamination which always seemed to contribute a signal at 285 eV. Because of the uncertainty involved in assigning line intensities from the carbon line at 285 to the specimen, this line was not used to characterize the specimen surface.

Glass and polystyrene were used as substrates. Polystyrene has the disadvantage of contributing a substrate carbon line, while glass contributes an interfering line due to oxygen. The silicon line from glass is unique to the substrate and was used to estimate the degree of surface coverage by cells. The difference in the silicon intensity from clean glass disks and disks covered with cells was taken as a measure of surface coverage. The contribution of the oxygen signal from the glass substrate was estimated by measuring the oxygen to silicon line intensity ratio for clean glass and assuming that the silicon intensity from the substrate containing cells had associated with it a similar oxygen intensity. Polystyrene has a negligible oxygen signal, and the oxygen intensity characteristic of cells could be obtained using polystyrene as the substrate. The oxygen signal from cells on polystyrene and from cells on glass with the appropriate substrate correction were in reasonable agreement.

Electron Escape Depths. A unique and important feature of XPS is the fact that only the outer surface of the sample is analyzed. Although there is some uncertainty in the escape depth of electrons photoejected from the surface, there is general agreement that electrons escape from a region less than 10 nm from the surface (*49*), and an escape depth of around 5 nm is usally quoted for electrons ejected from organic substrates such as organic polymers (*50*). It is possible to decrease the effective sampling depth into the surface of the sample by decreasing the angle between the plane of the sample and the observation direction of the energy analyzer component of the spectrometer (*42–44, 51*). Normal measurements are made with the sample 90° to a line normal to the entrance region of the energy analyzer. The effective sampling depth can be decreased by a factor of four by making measurements on a wedge shaped sample mount so that the angle between the plane of the sample and the direction of observation is 15°. Data collected with the sample mounted at an angle of less than 90° are usually referred to as grazing angle measurements. When spectra were measured with the sample flat, low intensity electron lines due to silicon were detected if the cells were grown on glass coverslips as a substrate. This signal could arise from areas not covered by cells or the thin outer portions of the cells. A distinction between these two alternatives could not be made. Cells are thickest at the center, and this regular array could lead to shadowing effects; however, little systematic work has been published dealing with these questions (*42, 52*).

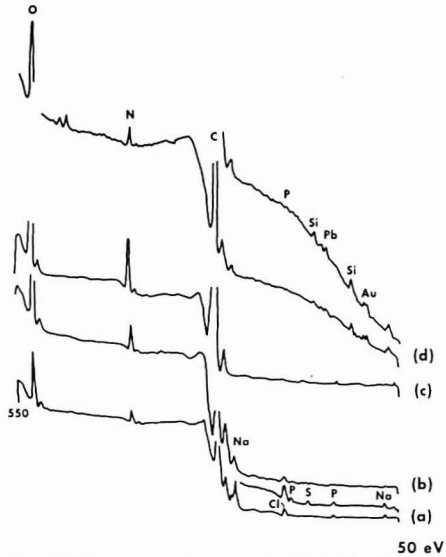

Figure 1. Wide scan spectra from normal cells washed in various ways. Effect of cell surface cleanup on surface composition. Sample numbers refer to Table I (a) sample 1, (b) sample 2, (c) sample 3, (d) sample 6

Radiation Damage. Another possible difficulty in studying biological specimens, such as cells, is the alteration of the sample due to decomposition as a result of exposure to x-rays. In these studies, the intensities of lines arising from the surface did not change appreciably during the time the sample was exposed to radiation, and radiation decomposition did not appear to be a serious problem.

Preliminary Results on Vacuum Dehydrated, Unfixed Normal Cells. In order to ascertain the sensitivity of electron line signals to the external composition of the cell surface, wide scan spectra were obtained over the region 550 eV to 50 eV for normal cells after several cleanup procedures. Wide scan spectra are presented in Figure 1 for cell samples No. 1–3, unwashed, washed with isotonic saline solution, and washed with distilled water. The position, intensity, and the structural interpretation for the photoelectron lines obtained from these samples are given in Table II. The electron line positions are tabulated in order of decreasing binding energy. The intensity of the individual electron lines was obtained from single scan spectra.

In each of these spectra, the most intense lines are the oxygen 1s at 532 eV, the nitrogen 1s at 400 eV and the carbon

Table II. Parameters Derived from the Electron Spectra of Cells[a]

Sample	O 1s	N 1s	C 1s	Cl 2p (Cl^-)	S 2p (SO_4^{2-})	S 2p (S-S)	P 2p (PO_4^{2-})	Na 2s (Na^+)	Oxygen/ nitrogen
1	532.2 (32.0)	400.0 (7.8)	285.0 (82.5)	198.1 (1.2)	168.5 (0.4)	162.5 (0.4)	133.2 (1.2)	63 (0.7)	2.78
2	531.5 (18.2)	400.0 (7.5)	285.0 (102.5)	198.4 (2.0)	trace	163 (0.6)	134 (0.3)		1.95
3	532.2 (26)	400.2 (7.5)	285.0 (75)		trace	trace	133 (0.5)		2.78
4	(22.2)	(9)	(70)						2.01
5	(17.5)	(7.25)	(65)						1.95
6[b]	533 (24)	400.8 (5)	285 (70)		trace				1.08

[a] Electron line positions are in units of electron volts. Intensities are in parentheses in units of 1000 counts/s. [b] Additional lines observed in the spectra were Sn 2p, (496), Sn 3s (488), Pb $4f_{5/2, 7/2}$ (144, 138), Si 2p (103), Au $4f_{7/2, 5/2}$ (86.5, 83.0).

1s at 285 eV. Low intensity lines due to chloride ion 198.1 eV, sulfate ion 168.5 eV, organic disulfide 163 eV, phosphate 133.2 eV, and sodium ion 63 eV (Auger KLL 122 270 eV) are present in the spectra obtained from the unwashed cells. In the spectra from the cells washed with isotonic sodium chloride, the line due to chloride ion increases in intensity while the electron lines due to the sulfate and phosphate decrease in intensity. All lines due to those ions except phosphate are essentially absent in the spectra of the cells washed with distilled water. Presumably, the ions, proteins, and amino acids present in the growth medium adsorbed on the surface of the cells would be removed in varying amounts by washing with isotonic sodium chloride solution or distilled water. It is possible that washing with water could rupture the cells and expose interior components of the cells. There were residual lines due to organic disulfide and phosphate. These lines were assumed to be inherent to the surface structure of the cell.

The intensities of the photoelectron lines can be converted to approximate atom ratios using appropriate elemental sensitivity factor (*45*). The surface atom ratios are usually accurate within 5% with organic substrates (*53*) and the instrument used for these studies.

Due to the uncertainty associated with the carbon line intensity, the oxygen 1s and nitrogen 1s line intensities are believed to be the most reliable parameters to characterize the surface of the cells. These line intensities and the oxygen atom to nitrogen atom ratio are presented in Table II.

The oxygen to nitrogen atom ratio varied between 2.78 and 1.95 for these three specimens. The line intensities from normal and transformed cells (unfixed preparations on polystyrene) are presented in Table II. Wide scan spectra from those specimens contained lines due to oxygen, nitrogen, carbon, sodium, and phosphorus. The oxygen to nitrogen atom ratio was 2 to 1 within experimental error for these two specimens. This atom ratio was not changed due to viral transformation.

Preliminary Results on Fixed Cells. The wide scan spectra of a sample of fixed cells is shown in Figure 1 spectrum d, and the CNO line intensities and line positions are given in Table II. Several lines were present in the spectrum of the fixed cells that were absent in the spectra of the unfixed cells. These new lines were tin (496 eV, 2 p_3; 488 eV, 3s); lead (144 and 139 eV, $4f_7$); silicon (154 and 103 eV, 2s and 2p); and gold (86.5 and 83.0 eV, $4f_{7/2}$, $4f_{5/2}$). The silicon lines resulted from the exposed substrate, and the gold lines originated from the sample mount surface not covered by the glass disk containing the cells. Tin and lead were found in varying amounts in the fixed cell samples and not in the fresh unfixed cells. These elements were apparently introduced from the reagents and solvents used in the fixing procedure.

Results on Fixed Normal and Transformed Cells. A number of normal and transformed cell preparations were surface analyzed to see if reproducible differences could be measured. These cell specimens were all grown on glass substrates and chemically fixed and critical-point dried prior to analysis. Wide scan spectra indicated the presence of varying amounts of tin and lead in these preparations. Figure 2 illustrates the single scan electron lines obtained from normal cells (specimen 7, Table II). Table III contains data from two different preparations of cells. For each preparation, normal and transformed cells were analyzed. The oxygen to nitrogen atom ratio for normal cells grown at different times was fairly reproducible. This ratio was 2.6 for specimen No. 7 and 2.5 for specimen No. 9. The corresponding ratio for the transformed cells was 2.0 for specimen No. 8 and 2.2 for specimen No. 11. These data would suggest that the oxygen to nitrogen ratio on the surface decreases slightly when the cells are

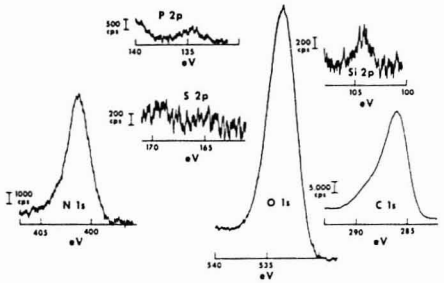

Figure 2. Elemental electron lines from normal cells. Sample 7, Table I

Table III. Electron Line Intensities and Atom Ratios for Chemically Fixed and Critically Point Dried Normal and Transformed Cells

Sample	Core level	Intensity (1000 counts/s)	Corrected intensity	Oxygen/ nitrogen atom ratio
7	C 1s	75		
	O 1s	53.5	85	2.6
	N 1s	14	53.3	
	Si 2p	1.5 (O 1s, 9.52)		
8	C 1s	72.5		
	O 1s	58.5	76	2.0
	N 1s	15.7	37.5	
	Si 2p	3.0		
9	C 1s	61.5		
	O 1s	45	78	2.5
	N 1s	12	28.5	
	Si 2p	0.7 (O 1s, 4.5)		
10	C 1s	31		
	O 1s	16.8	27.8	
	N 1s	4	9.5	
	Si 2p	0.4 (O 1s, 2.56)		
11	C 1s	55		
	O 1s	43.5	59	
	N 1s	11		2.2
	Si 2p	2.0 (O 1s, 12.7)	26.2	
12	C 1s	26		
	O 1s	16.8	32.3	2.72
	N 1s	5	11.9	
	Si 2p			

transformed. In order to reduce the contribution of the glass substrate signals to the signal from the cells, grazing angle measurements were made on these specimens. The relative carbon, oxygen, and nitrogen signal intensities changed, and the silicon signal was virtually absent in the grazing angle spectra. The oxygen to nitrogen atom ratio for sample No. 9 increased from 2.5 to 2.9 for sample No. 10 for grazing angle measurements. This ratio for the transformed cells changed from 2.2 for sample No. 11 to 2.72 for sample No. 12 from grazing angle measurements. This ratio increased in both cases for the grazing angle data; however, the magnitude of the increase was much greater for the transformed cells. This change was in opposition to the trend observed from flat measurements. This difference may reflect differences in the outer few monolayers only.

Depth Profiling and Ash Analysis of Normal and Transformed Cells. *Depth Profile Analysis.* Conventional composition profile studies on metal and refractory surfaces are usally accomplished by combining Auger spectroscopy for analysis and argon ion bombardment to etch away surface layers (*30, 54–56*). XPS was used in this study to accomplish surface analysis and low temperature oxygen plasma etching to gently remove organic material from the surface of the cells.

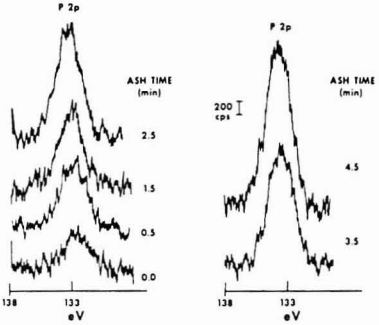

Figure 3. Phosphorus 2p electron line intensity as a function of ash time from normal cells. Sample 12, Table I

Oxygen plasma etching was selected to remove the outer surface of the cells for several reasons. Argon ion etching has been found to alter the surface of oxides causing surface decomposition (*57, 58*). The damaging effect of argon ion bombardment of systems of lower thermal stability, such as biological samples or polymer samples, is much more severe (*59*). Oxygen plasma ashing has been used to oxidize and volatilize organic substances in applications where thermal decomposition and fine structure disruption or damage is to be avoided. The applications of this technique for sample preparation in analytical applications and for sample treatment for fine structure studies have recently been reviewed (*36, 60, 61*).

An important question remains concerning the rate of oxidation and the uniformity of the removal of the outer surface (*36*). Scanning electron micrographs of the surface of cells after exposure to an oxygen plasma for varying periods of time support uniform oxidation at short ash times, but not at long ash times. Nonuniform surface removal usually occurs between 5 and 10 min ashing time (manuscript in preparation).

Under similar conditions, Thomas, Millard, and Scherrer have estimated the rate of oxygen plasma oxidation of an organic substrate to be approximately 9 nm/min by measuring the dimensional changes of polystyrene beads after varying periods of exposure (*35*). This rate was determined only for polystyrene, and some uncertainty exists in estimating a rate of surface removal for the cell system studied here; however, 9 nm/min will be used as an approximate number. In order to obtain a composition profile analysis for various elements as a function of depth into the surface of the cells, the cells were subjected to a low temperature oxygen plasma for varying periods of time, and the electron lines measured on the surface over the region 550 to 50 eV. To minimize the nonuniform oxidation of the outer surface, the cell surface was ashed for half-minute intervals for no longer than 4.5 min total ashing time for composition profile analysis. The phosphorus 2p electron line intensity as a function of ash time for normal cells is given in Figure 3. The electron line intensity data for phosphorus, silicon, and sodium at 1-min ashing intervals up to 4.5 minutes for normal and transformed cells are given in Table IV.

Glass contains sodium, and the contribution of the sodium intensity from the exposed glass substrate has been estimated and substracted from the intensity. The Na/Si intensity ratio is measured from glass and the ratio used to calculate the Na intensity from any given Si intensity. The sodium intensity data presented in Table IV have been adjusted in this way.

A plot of the elemental composition as a function of plasma oxygen ash time yields a composition profile curve. The

Table IV. Phosphorus 2p, Silicon 2p, and Na Auger (KLL 122) Line Intensities from Normal and Transformed Cells as a Function of Oxygen Plasma Oxidation[a]

Plasma exposure time, min	Normal			Transformed		
	P 2p intensity	Si 2p intensity	Na KLL corrected intensity	P 2p intensity	Si 2p intensity	Na KLL corrected intensity
0.0	0.56	1.5	1.85	0.5	3.3	3.05
0.5	1.05	2.5	5.41	0.7	6	9.87
1.5	1.3	4.0	6.55	1.1	8	10.3
2.5	1.74	4.5	8.53	1.3	9.4	10.88
3.5	1.8	6.0	9.67	1.6	10	12.3
4.5	2.6	9.0	11.36	2.0	11.0	13.67

[a] Intensity is in units of 1000 counts/s.

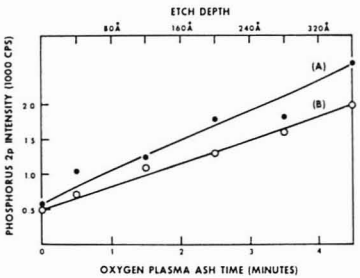

Figure 4. Phosphorus composition profile for normal (A) and transformed (B) cells

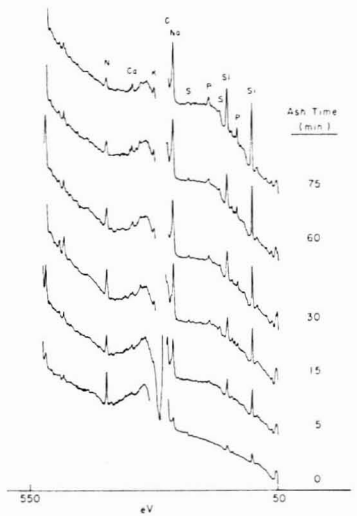

Figure 5. Wide scan spectra as a function of ash time for transformed cells

phosphorus composition profile curve for normal and transformed cells for ash times up to 4.5 min is given in Figure 4. Ash time in minutes can be converted to an approximate etch depth using the conversion factor of 9 nm/min. As can be seen from Figure 4, the composition profile for the two types of cells is fairly similar up to ash times for 4.5 min. The phosphorus concentration increases linearly with time during the first 5 minutes of ashing. This is most reasonably interpreted as a uniform distribution of phosphorus in the region extending from the surface of the cell to well within the interior. A phosphorus rich or depleted region would presumably result in a change in the slope of the curve.

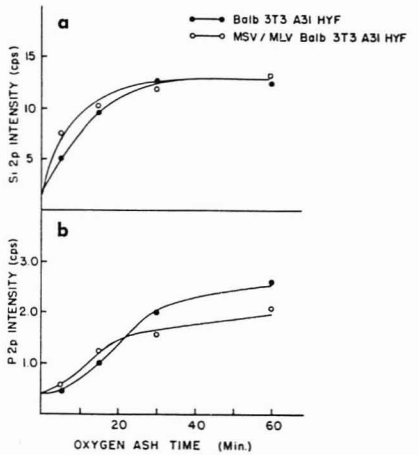

Figure 6. (a) Silicon 2p electron substrate intensity as a function of ash time and (b) phosphorus 2p electron intensity as a function of ash time

Ashing. The results of plasma ashing of biological cells is of interest even under nonuniform conditions when the interpretation of concentration changes in terms of depth profiles is not applicable. Plasma ashing of biological samples is a method of choice for sample preparation when removal of organic components is desired, and retention of elements normally lost during high temperature incineration is of interest. As ashing proceeds and the organic components are lost, the inorganic constituents are concentrated in the form of an ash. The appearance of elements not necessarily on the surface of cells and their buildup in the ash can be followed by analyzing the surface of the ashed sample at varying periods of ashing time. A series of wide scan electron spectra as a function of ash time is presented in Figure 5 for transformed cells. Some lines of interest and the approximate position in units of electron volts for the stronger binding energy lines are as follows: O 1s 531, N 1s 400, Ca 2p 348, K 2p 292, C 1s 285, Na KLL 263, S 2p 168, P 2p 134, and Si 2p 103. The silicon lines are from the substrate. The individual phosphorus 2p line intensity as a function of ash time up to 60 min is given in Figure 6a for normal and transformed cells. As the organic components of the cells are lost, the concentration of the inorganic components, such as phosphorus will increase in

concentration until all of the carbon containing component is lost. It appears that after 60 min the concentration of phosphorus on the surface of the ash is beginning to reach a plateau.

Some estimation of the coverage of the glass substrate by cells and the rate of oxidation of the cells by the oxygen plasma can be obtained from the intensity of the silicon 2p electrons from the glass substrate. The initial silicon 2p intensity is around 2000 counts/s. The silicon 2p electron intensity from a clean 6.35-mm diameter glass disk is around 20 000 counts/s. Assuming that the intensity of the 2p electron signal is inversely proportional to the degree of surface coverage, the culture cells cover about 90% of the glass surface initially. The increase in the silicon 2p signal intensity upon oxygen plasma treatment is related to the rate of oxidation of the cell on the substrate by plasma oxidation. In Figure 6a the silicon 2p electron intensity is plotted as a function of oxygen plasma ash time for the normal and transformed cells. The Si 2p signal increases sharply during the first 10 min of ashing and then increases slowly and steadily. The thin outer portion of the cell near the edge is apparently rapidly oxidized, thereby exposing the substrate. After oxidiation of this thin exterior portion, the substrate is exposed more slowly because of coverage by thicker portion of the cell.

ACKNOWLEDGMENT

We thank Agatha Wang for her assistance in fixing the cells and Hisao Yokota for culturing the cells. M. Millard especially thanks Richard S. Thomas and Rene Scherrer for their helpful discussion and critical review of the manuscript.

LITERATURE CITED

(1) J. Ankerst and H. O. Sjogren, *Int J. Cancer*, **5**, 84 (1970).
(2) J. S. Butel, S. S. Tevethia, and J. L. Melnick, *Adv. Cancer Res.*, **15**, 1 (1972).
(3) C. Cyr de Vaux, A. Herbert, E. Sabczak, R. Wicker, and P. Carabar, *Int. J. Cancer*, **4**, 616, (1969).
(4) K. Habel. *Curr. Top. Microbiol. Immunol.*, **41**, 85 (1967).
(5) G. Haughton and D. R. Nash, *Progr. Med. Virol.*, **11**, 248 (1969).
(6) P. Hayry and V. Defendi, *Virology*, **41**, 22 (1970).
(7) I. S. Irlin, *Virology*, **32**, 725 (1975).
(8) H. T. Robertson and P. H. Black, *Proc. Soc., Exp. Biol. Med.*, **130**, 363 (1969).
(9) R. W. Smith and P. T. Mora, *Virology*, **50**, 233 (1970).
(10) S. S. Tevethio, M. Katz, and F. Rapp, *Proc. Soc. Exp. Biol. Med.*, **119** 896 (1965).
(11) M. M. Burger, and A. R. Goldberg, *Proc. Natl. Acad. Sci.* U.S.A., **57**, 359 (1967).
(12) M. Inbar, H. Ben-Gassat, and L. Sachs, *Nature (London), New Biol.*, **236**, 3 (1972).
(13) M. Inbar, Z. Rabinowtiz, and L. Sachs, *Int. J. Cancer*, **4**, 690 (1969).
(14) G. L. Nicolson, *Int. Rev. Cytol.*, **39**, 89 (1974).
(15) G. L. Nicolson, *Nature (London), New Biol.*, **233**, 244 (1971).
(16) K. D. Noonan and M. M. Burger, *J. Biol. Chem.*, **248**, 4286 (1973).
(17) A. M. C. Rapin and M. M. Burger, *Adv. Cancer Res.*, **20**, 1 (1974) 363.
(18) J. Z. Rosenblith, T. E. Ukena, H. H. Yin, R. D. Berlin, and M. J. Karnovsky, *Proc. Natl. Acad. Sci. U.S.A.*, **70**, 1625 (1973).
(19) J. Shoham and L. Sachs, *Exp. Cell Res.*, **85**, 8 (1974).
(20) C. A. Buck, M. C. Glick, and L. Warren, *Science*, **172**, 169, (1971).
(21) W. J. Grimes, *Biochemistry*, **12**, 990 (1973).
(22) S. I. Hakomori, *Adv. Cancer Res.*, **18**, 265 (1971).
(23) E. Meezan, H. C. Wu, P. H. Black, and P. W. Robbins, *Biochemistry*, **8**, 2518 (1969).
(24) P. T. Mora, F. A. Cumar, and R. O. Brady, *Virology*, **46**, 60 (1971).
(25) N. Ohta, A. B. Pardee, R. R. McAuslan, and M. M. Burger, *Biochim. Biophys. Acta*, **158**, 98 (1968).
(26) R. Sheinin, K. Onodero, G. Yogeeswaren, and R. K. Murray, "Biology of Oncogenic Viruses", L. G. Silvestri, Ed., Elsevier, New York, 1971, p 274.
(27) W. P. Van Beek, L. A. Smets, and P. Emmelot, *Cancer Res.*, **33** 2913 (1973).
(28) H. C. Wu, E. Meezan, P. H. Black and P. W. Robbins, *Biochemistry*, **8**, 2509 (1969).
(29) K. J. Siegbahn, *J. Electron. Spectrosc. Relat. Phenom.*, **5**, 3–97 (1974).
(30) D. M. Hercules and J. C. Carver, *Anal. Chem.*, **46**, 145 R (1974).
(31) D. L. White, S. B. Andrews, J. W. Faller, and R. J. Barrnett, *Biochem. Biophys. Acta*, **436**, 577 (1976).
(32) J. Baddiley, I. C. Hancock, and P. M. A. Sherwood, *Nature (London)*, **243**, 43 (1973).
(33) R. G. Meisenheimer, J. W. Fischer, and S. J. Rehfeld, *Biochem. Biophys. Res. Commun.*, **68**, 994 (1976).
(34) M. Millard, R. Scherrer, and R. S. Thomas, *Biochem. Biophys. Res. Commun.*, **72**, 1209 (1976).
(35) R. S. Thomas M. M. Millard, and R. Scherrer, "34th Annual Proceedings of the Electron Microscopy Society America", Miami Beach, Fla., G. W. Bailey, Ed., 1976 pp 134–135.
(36) R. S. Thomas "Techniques and Applications of Plasma Chemistry", J. R. Hollahan and A. T. Bell, Ed., John Wiley & Sons, New York, 1974, Chap. 8, p 255.
(37) A. Boyde and P. Vesely, "Scanning Electron Microscopy, Part II", "Proceedings of a workshop on biological specimen preparation for scanning electron microscopy", O. Jahari and I. Corvin, Ed., ITT Research Institute, Chicago, Ill., 1972 pp 265–271.
(38) A. Boyde R. A. Weiss, and P. Vesely, *Exp. Cell Res.*, **71** 313–324 (1972).
(39) H. Eagle, *Science*, **130** 432 (1959).
(40) L. A. Culp and P. H. Black, *Biochemistry*, **11**, 2661 (1972).
(41) M. Calvin, U. R. Joss, A. J. Hackett, and R. B. Owens, *Proc. Natl. Acad. Sci. U.S.A.*, **68**, 1441 (1971).
(42) C. S. Fadley, *J. Electron. Spectrosc. Relat. Phenom.*, **5**, 725–754 (1974).
(43) W. A. Fraser J. V. Florio, W. N. Deglass, and W. D. Robertson, *Surf. Sci.*, **36**, 661–674 (1973).
(44) R. S. Swingle, P. P. Groff, and B. M. Monroe, *Phys. Rev. Lett.*, **35**, 452 (1975).
(45) C. D. Wagner, *Anal. Chem.*, **44**, 1050 (1972).
(46) Alan Boyde, Ref. 37, 257–264.
(47) T. Hall, P. Echlin, and R. Kaufmann, Ed., "Microprobe Analysis as Applied to Cells and Tissues", Academic Press, New York, 1974.
(48) "Scanning Electron Microscopy Symposium Proceedings", O. Johari and I. Corvin, Ed., ITT Research Institute, Chicago, Ill. 60616 and preceding volumes (1975).
(49) C. R. Brundle, *J. Vac. Sci. Technol.*, **11**, 212 (1974).
(50) W. M. Riggs, Physical Electrons Industries, Inc., 6509 Flying Cloud Dr., Eden Prairie, Minn. 55343, personal communication.
(51) H. K. Herglotz and H. L. Suchan, *Adv. Colloid Interface. Sci.*, **5**, 84–85 (1975).
(52) R. W. Phillips, *J. Colloid Interfac. Sci.* **47**, 687 (1974).
(53) M. Millard and M. S. Masri, *Anal. Chem.*, **46**, 1820 (1974).
(54) S. Danyluk and G. E. McGuire, *J. Appl. Phys.*, **45**, 5141 (1973).
(55) C. A. Evans, Jr. *Anal. Chem.*, **47**, 819A–829A (1975).
(56) P. W. Palmberg, in "Electron Spectroscopy", D. A. Shirley, Ed., North-Holland Publ. Co., Amsterdam, 1972 p 835.
(57) R. J. Colton and W. J. Rabalais, *Inorg. Chem.*, **15**, 236–238 (1976).
(58) K. S. Kim, W. E. Baltinger, J. W. Amy, and N. J. Winograd, *J. Electron. Spectrosc. Relat. Phenom.*, **5**, 351 (1974).
(59) D. T. Clark and W. J. Feast, *J. Macromol Sci., Rev. Macromol Chem.*, **C12**, 248 (1975).
(60) J. R. Hollahan, "Techniques and Applications of Plasma Chemistry", J. R. Hollahan and A. T. Bell, Ed., John Wiley & Sons, Inc., New York, 1974, Chap. 7 p 246.
(61) R. S. Thomas and J. R. Hollahan, Scanning Electron Microscopy, Proceedings 7th Annual Scanning Electron Microscopy Symposium, Part I, ITT Research Institute, Chicago, Ill., 1974, p 83.

RECEIVED for review February 11, 1977. Accepted May 13, 1977. This research was supported in part by NIH Grant No. NCI-1-RO-1-CA 14828 and the U.S. Energy Resources and Development Administration. Reference to a company or product name does not imply approval or recommendation of that product by the U.S. Department of Agriculture to the exclusion of others that may be suitable.

Simultaneous Analysis of Light Elements Using Prompt Nuclear Reaction Gamma Rays

Robert B. Boulton[1] and George T. Ewan*

Department of Physics, Stirling Hall, Queen's University, Kingston, Ontario, Canada K7L 3N6

A method is described for the simultaneous quantitative analysis of the light elements lithium, boron, fluorine, sodium, magnesium, and aluminum, using prompt nuclear-reaction γ rays emitted when a sample is bombarded with low energy protons. Relative peak areas in a γ-ray spectrum are measured, and elemental concentrations determined using γ-ray data obtained from standards. Factors affecting the accuracy of analysis are considered; the effect of stopping-power is discussed; on-line checks for systematic errors caused by target instability or target nonuniformity are described. A range of different materials has been analyzed with a minimum of sample preparation and selected analytical results are presented.

In recent years, prompt nuclear-reaction γ rays have been used for elemental analysis in a variety of materials. Examples include nitrogen (*1*) and carbon (*2*) in biological materials, carbon in steel (*3*), oxygen in uranium dioxide (*4*), fluorine in dental enamel (*5*), aluminum in stainless steel (*6*), chlorine in aluminum (*7*), oxygen and nitrogen in gases (*8*), fluorine, sodium, and aluminum in archaeological samples (*9*) and carbon, nitrogen, oxygen, aluminum, silicon, sulfur, calcium, and iron in dust samples (*10*). These applications of nuclear-reaction γ-ray analysis have generally been to particular problems, and direct application to other types of sample containing different bulk elements is often not possible. In many cases, a single element was of interest, and no attempt was made to determine several elements simultaneously.

In this paper we describe a method for the simultaneous analysis of several light elements in a wide range of materials using charged particles from a small Van de Graaff accelerator and a high-resolution lithium-drifted germanium detector. Protons of 1.8 MeV were selected to allow the simultaneous analysis of lithium, boron, fluorine, sodium, magnesium, and aluminum. Several types of geological material, lithium–magnesium alloys, blood serum, and leaf material have been analyzed by the same experimental procedure, and selected results are presented in this paper. The emphasis of this work has been on the accuracy of the method. Checks for systematic error caused by target instability or target inhomogeneity are described, and the effect of stopping power on the accuracy of results is discussed.

Fluorescence x rays produced by the proton beam were detected simultaneously in many cases by a lithium-drifted silicon detector. These fluorescence x rays are useful for the analysis of heavier elements. In this paper we describe the nuclear-reaction γ-ray method, and the use of proton-induced fluorescence x rays will not be discussed further.

DESCRIPTION OF NUCLEAR-REACTION γ-RAY METHOD

1. Experimental Method. Samples were bombarded with 1.8-MeV protons from a Van de Graaff accelerator. Gamma rays produced by nuclear reactions in the different elements of the target were detected in a high-resolution lithium-drifted germanium detector. Data were collected and analyzed using a PDP-9 computer. Relative peak areas in a γ-ray spectrum were measured and the relative concentration of different elements calculated by using data from standards, and the simple relation

$$\left(\frac{N_i}{N_j}\right)^{\text{Unknown}} = \left(\frac{Y_i}{Y_j}\right)^{\text{Unknown}} \Bigg/ \left(\frac{Y_i/N_i}{Y_j/N_j}\right)^{\text{Standards}} \quad (1)$$

where Y_i is the detected yield (peak area) of γ ray i and N_i is the atomic density of the element producing that γ ray. This equation and the stopping-power approximation involved are discussed in the following sections. Tests were made on the stability of each target under proton bombardment. The γ-ray data were used to test for systematic errors caused by nonuniformities in the target, and these tests are described in later sections.

The 60 cm^3 Ge(Li) detector had a resolution of 2.6 keV (at 1332 keV) and an efficiency of 14%. Low energy (<1 MeV) γ rays were of interest, and the high resolution of the detector allowed these γ rays to be clearly resolved.

Targets were thick enough to stop the proton beam (at 1.8 MeV, the range of the protons was approximately 45 μm, depending on the target material) and were typically 1 to 3 mm thick. Target currents ranged from 5 to 120 nA depending on target composition, and run times were typically 25 min. The front surface of the target was at 45° to the beam direction and the detector was at 90°. Targets were mounted on a two-dimensional translation stage. This allowed six targets to be mounted and the surface of each to be scanned without breaking the vacuum. The target chamber, which includes a port for a Si(Li) x-ray detector, is shown schematically in Figure 1.

A typical γ-ray spectrum, from a potassium feldspar sample, is shown in Figure 2. The peaks are labeled with the energy of the γ ray and the element. The 431-keV and 478-keV peaks are broader than the other peaks due to Doppler effects from recoiling nuclei.

2. Simple Relation Used for Analysis. The detected thick-target yield $Y_i(E_0)$ of a γ ray i for beam energy E_0 from a homogeneous target containing N_i atoms cm^{-3} of the element producing that γ ray is given by

$$Y_i(E_0) = \frac{Q}{e}\eta_i \cdot N_i \int_0^{E_0} \frac{\sigma_i(E)\mathrm{d}E}{(\mathrm{d}E/\mathrm{d}x)} \quad (2)$$

where $\sigma_i(E)$ is the cross-section of the nuclear reaction in which γ ray i is emitted, η_i is the efficiency of detection, $(\mathrm{d}E/\mathrm{d}x)$ is the stopping-power of the target (in eV-cm^{-1}), Q is the integrated target current and e is the electronic charge.

The stopping-power of any material can be expressed as a sum of the stopping-powers of its component elements, k, so that Equation 2 becomes

$$Y_i(E_0) = \frac{Q}{e}\eta_i \cdot N_i \int_0^{E_0} \frac{\sigma_i(E)\mathrm{d}E}{\sum_k N_k \epsilon_k(E)} \quad (3)$$

with stopping-power $\epsilon_k(E)$ in units of eV·cm^2 $atom^{-1}$.

Since the stopping-power of each of the elements in the target has a different energy dependence, the integral for unknown and standard targets will contain a different sum of energy-dependent terms, and a direct comparison cannot readily be made. This energy dependence is, however, similar for all elements, and the

[1] Present address, Atomic Energy of Canada Ltd., Commercial Products Division, P.O. Box 6300, Station "J", Ottawa, Ontario, Canada K2A 3W3.

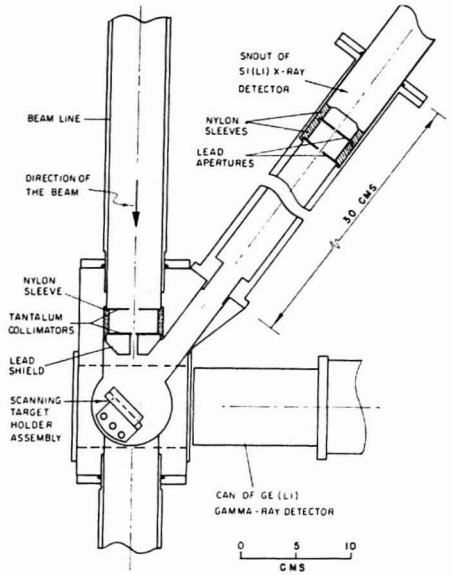

Figure 1. Target chamber used for simultaneous γ-ray and x-ray detection. The target holder assembly allows target scanning in two directions

stopping-power can be expressed in the range of interest as

$$\epsilon_k(E) = a_k \epsilon_0(E)(1 + b_k(E)) \tag{4}$$

where the coefficient a_k represents the magnitude of the stopping-power and is a constant for element k; $\epsilon_0(E)$ is a function describing the energy dependence of some reference material and differences in the energy dependence for element k from $\epsilon_0(E)$ are included in the function $b_k(E)$. Figure 3 shows the magnitude of the function $b_k(E)$ for several elements from 1 to 4 MeV protons.

Equation 3 then becomes

$$Y_i(E_0) = \frac{Q}{e}\eta_i \cdot N_i \cdot \int_0^{E_0} \frac{\sigma_i(E)\mathrm{d}E}{\epsilon_0(E)\cdot\sum_k N_k a_k (1 + b_k(E))} \tag{5}$$

If an approximation is made that the stopping-powers of all elements have the same energy dependence, so that $b_k(E)$ is set to zero, then Equation 5 becomes

$$Y_i(E_0) = \frac{Q}{e}\eta_i \cdot \frac{N_i}{\sum_k N_k a_k} \cdot \int \frac{\sigma_i(E)\mathrm{d}E}{\epsilon_0(E)} \tag{6}$$

where the integral is independent of the composition of the target. The ratio of detected yields for γ rays i and j in the same target is then

$$\frac{Y_i(E_0)}{Y_j(E_0)} = \frac{N_i}{N_j} \cdot \frac{\eta_i \int \frac{\sigma_i(E)\mathrm{d}E}{\epsilon_0(E)}}{\eta_j \int \frac{\sigma_j(E)\mathrm{d}E}{\epsilon_0(E)}} \tag{7}$$

The ratio of integrals can be obtained from a measurement of the "relative yields per target atom" from a standard for which N_i and N_j are known. This then gives the simple relation

$$\left(\frac{N_i}{N_j}\right)^{\text{Unknown}} = \left(\frac{Y_i(E_0)}{Y_j(E_0)}\right)^{\text{Unknown}} \Bigg/ \left(\frac{Y_i(E_0)/N_i}{Y_j(E_0)/N_j}\right)^{\text{Standards}} \tag{8}$$

where E_0 is the bombarding energy, which is the same for sample and standards.

The analysis of a sample therefore requires the measurement of peak areas in the γ-ray spectrum of a sample, and similar measurements on spectra from standard samples. Accurate knowledge of the target current, detector geometry, or target matrix is not required. This analysis gives the relative elemental concentrations of several elements in an unknown sample. Independent knowledge of one of these elements allows a complete analysis of these elements.

3. Effect of the Stopping-Power Approximation. The stopping-power approximation produces a systematic error in results which have been calculated using the simple relation, Equation 8. Although the values of $b_k(E)$ shown in Figure 3 suggest that these effects may be large for some materials, the effect on γ-ray yield ratios is smaller because the thick target yields are an integral over a range of proton energies. The magnitude of the systematic error was calculated for several representative targets and standards.

The sum in Equation 5 was expanded as

$$\sum_m N_m a_m \left(1 + \frac{\sum_k N_k a_k b_k(E)}{\sum_m N_m a_m}\right) \tag{9}$$

where the dummy suffices m,k are summed over the component elements of the target.

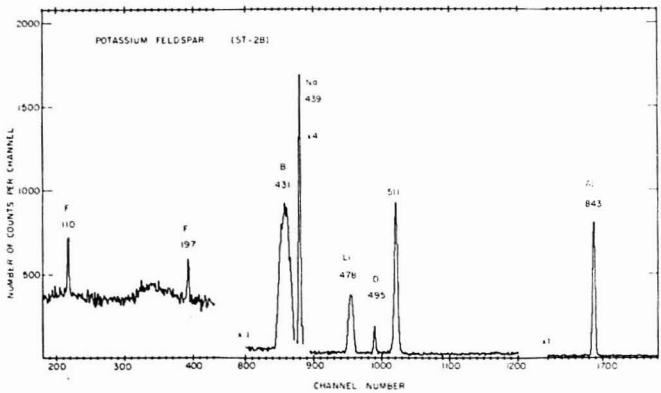

Figure 2. Gamma-ray spectrum of a potassium feldspar sample (number ST-2B) observed in bombardment of sample by 1.8-MeV protons. Energies marked on peaks are in keV. Dispersion is 0.50 keV per channel

Table I. Proton Reactions Which May Be Useful for Elemental Analysis Using Beam Energies of a Few MeV*

Element	Nuclear reaction	Energy of γ ray, keV	Relative yield per atom 1.80 MeV	3.60 MeV
Li	$^{7}Li(p,n\gamma)^{7}Be$	431	0	29[d]
	$^{7}Li(p,p'\gamma)^{7}Li$	478	230	110
B	$^{10}B(p,\alpha\gamma)^{7}Be$	431	78	[d]
O	$^{16}O(p,\gamma)^{17}F$	495	0.018[a]	
F	$^{19}F(p,p'\gamma)^{19}F$	110	130	370
	$^{19}F(p,p'\gamma)^{19}F$	197	75	450
	$^{19}F(p,p'\gamma)^{19}F$	1349–1357	0	18
Na	$^{23}Na(p,p'\gamma)^{23}Na$	439	100	100
	$^{23}Na(p,\gamma)^{24}Mg$	1369		0.17[e]
	$^{23}Na(p,\alpha\gamma)^{20}Ne$	1635	8.1	19
Mg	$^{25}Mg(p,p'\gamma)^{25}Mg$	585	0.55	2.6
	$^{24}Mg(p,p'\gamma)^{24}Mg$	1369	0	4.8[e]
	$^{24}Mg(p,\gamma)^{25}Al$	493	0.0038[a]	
	$^{26}Mg(p,\gamma)^{27}Al$	843	0.011[b]	[b]
	$^{26}Mg(p,\gamma)^{27}Al$	1013	0.017[c]	[c]
Al	$^{27}Al(p,p'\gamma)^{27}Al$	843	1.3[b]	12[b]
	$^{27}Al(p,p'\gamma)^{27}Al$	1013	0.34[c]	18[c]
	$^{27}Al(p,\alpha\gamma)^{24}Mg$	1369	0.026	2.2[e]
	$^{27}Al(p,\gamma)^{28}Si$	1779	0.019	0.8[f]
Si	$^{30}Si(p,\alpha\gamma)^{27}Al$	843	0	0.34[b]
	$^{30}Si(p,\alpha\gamma)^{27}Al$	1013	0	0.42[c]
	$^{29}Si(p,p'\gamma)^{29}Si$	1273	0	0.8[g]
	$^{28}Si(p,p'\gamma)^{28}Si$	1779	0	6.5[f]
P	$^{31}P(p,p'\gamma)^{31}P$	1266	0	8.6[g]
	$^{31}P(p,\alpha\gamma)^{28}Si$	1779	0	0.92[f]
K	$^{41}K(p,\gamma)^{42}Ca$	1525	0.040	
Fe	$^{56}Fe(p,p'\gamma)^{56}Fe$	847	0.007[b]	
	$^{56}Fe(p,\gamma)^{57}Co$	1377	0.055	

* Reactions which produce interfering γ rays are included. Relative yields of detected γ rays per target atom for proton energies 1.80 and 3.60 MeV are also shown. *a*, *b*, *c*, *d*, *e*, *f*, *g* indicate γ-ray interferences.

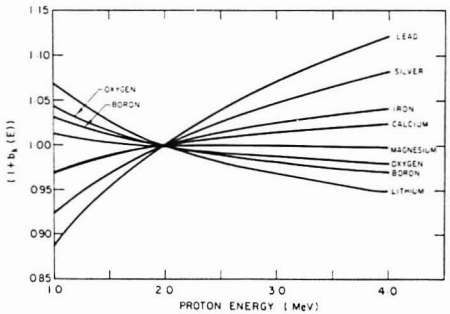

Figure 3. Plot of the function $(1 + b_k(E))$ for several elements for proton energies 1 to 4 MeV. For a beam energy of 1.8 MeV, contributions to γ-ray yields from protons below 1 MeV are small. Aluminum is used as the reference material to define $\epsilon_0(E)$. Stopping-power data are taken from Janni's compilation (*11*)

A binomial expansion of the term

$$\left(1 + \frac{\sum_k N_k a_k b_k(E)}{\sum_m N_m a_m}\right)^{-1} \tag{10}$$

allows a first-order correction factor to be included in Equation 8. This contains terms of the form

$$\frac{\sum_k N_k a_k \int_0^{E_0} \frac{b_k(E)\sigma_i(E)dE}{\epsilon_0(E)}}{\sum_m N_m a_m \int_0^{E_0} \frac{\sigma_i(E)dE}{\epsilon_0(E)}} \tag{11}$$

The individual integrals are independent of target composition and were evaluated from stopping-powers given in Janni's compilation (*11*) and nuclear excitation functions from the literature. The nuclear reactions which were used are discussed in the next section, and are shown in Table I. Some of these reactions have cross-sections which vary smoothly with energy while others have resonant structures.

The correction factors were evaluated for targets of different composition. The systematic error in the analysis of boron relative to sodium in the mineral potassium feldspar (bulk formula $KAlSi_3O_8$), with sodium tetraborate ($Na_2B_4O_7$) being used as a standard, was calculated as 0.06%. For the reactions used in this work, the analysis of lithium contained the greatest error, presumably due to the relatively high threshold for the lithium reaction. A systematic error of 0.12% was calculated for lithium relative to boron in potassium feldspar, with lithium borate ($Li_2B_4O_7$) being used as a standard. Since all samples analyzed in this work were composed of mixtures of light and intermediate elements, these results are thought to be typical of such materials.

As an extreme example of stopping-power effects, calculations were made for boron and lead as stopping materials (see Figure 3 for values of $b_k(E)$). Results indicated that the maximum effect between these two materials was 1.2% for the reactions used in this work.

These results indicate that correction factors are not generally required, and stopping-power effects introduce negligible error into analytical results. The effects can, however, be calculated if desired, and examples are given elsewhere (*12*).

4. Selection of Bombarding Conditions. The elements and nuclear reactions which give a high yield of γ rays for protons of a few MeV are shown in Table I. Choice of beam energy allows optimization for one or more elements or discrimination against an unwanted element by operating at a beam energy below the threshold of that reaction. The relative detected thick target yields of these γ rays for two beam energies are included in Table I. For a beam energy of 1.8 MeV, the highest yields per target atom are obtained from nuclear reactions in lithium, boron, fluorine, and sodium, with useful yields also obtained from magnesium and aluminum. Oxygen is observed, but the yield per target atom is relatively small. Weak interferences are produced by unwanted reactions in iron and magnesium, but these are generally un-

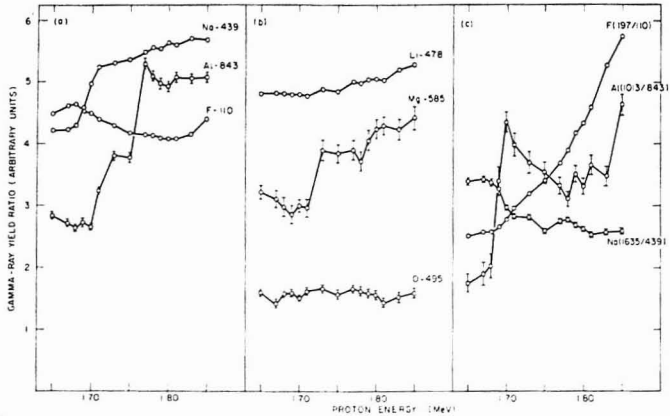

Figure 4. Relative yields of γ rays for proton bombardment of 1.65 to 1.85 MeV. The lines are drawn to guide the eye. (a) and (b) show the ratios of γ rays Na-439, Al-843, F-110, Li-478, Mg-585, and O-495 relative to B-431. (γ rays are labeled by the element producing the γ ray and its energy in keV.) (c) shows yield ratios of γ rays from the same element, F(197/110), Al(1013/843), and Na(1635/439). The nuclear reactions producing these γ rays are shown in Table I

important, and may easily be corrected for if necessary. 1.8 MeV is below the threshold of the $^7Li(p,n)^7Be$ reaction, so that the possibility of neutron damage to the detector is avoided.

At 3.6 MeV, phosphorus and silicon may be analyzed, but several interferences caused by γ rays of the same or similar energy produced by reactions in different elements make an analysis more complicated.

The light elements beryllium, carbon, and nitrogen do not produce usable thick target yields of low-energy γ rays under few MeV proton bombardment, but may be analyzed by deuterons or alpha particles. Reactions in heavier elements are weak due to Coulomb barrier effects, and the technique therefore provides a selective method of analysis for light elements without interference from heavier elements.

Table I shows that protons of approximately 1.8 MeV are well suited to the simultaneous quantitative analysis of lithium, boron, fluorine, sodium, magnesium, and aluminum. In selecting the exact beam energy, it is important that the relative γ-ray yields are insensitive to small changes in the effective beam energy, as may be caused by small variations in accelerator conditions or a thin layer of oxide or carbon on the surface of a target. Figure 4 (parts a and b) shows the γ-ray yields of interest measured relative to the 431-keV γ ray from boron, for beam energies between 1.65 and 1.85 MeV. At 1.80 MeV, these yield ratios are insensitive to the exact beam energy, and this energy was used for analytical measurements.

Charge accumulation on an insulating target can reduce the effective energy of the beam, causing a change in the relative γ-ray yields per target atom and a possible systematic error in an analysis. At 1.80 MeV, these relative yields are insensitive to the exact beam energy, and charge accumulation is therefore unimportant. Carbon coating of insulating targets was not generally used; it was considered necessary only for the standard sodium fluoride, where an accuracy of $\pm 0.5\%$ was desirable.

5. Standards. In this method, it is not necessary to have standards of similar physical form or chemical composition to the unknown samples because target matrix effects are unimportant (Section 3). Thus, the same standards were used for the analysis of all types of material.

The standards used in this work were a set of simple stoichiometric compounds, each containing two of the elements of interest. Each compound selected was anhydrous, had a high melting point, and was stable under beam conditions; each target was tested for the accuracy and reliability of its γ-ray data.

The targets were bombarded in turn, and a set of "relative γ-ray yields per target atom" was obtained linking all the elements of interest. Normalization data for lithium, boron, fluorine, and sodium were obtained from targets of lithium fluoride (LiF), lithium tetraborate ($Li_2B_4O_7$), and sodium tetraborate ($Na_2B_4O_7$). Sodium fluoride (NaF) was used to check the data from the other three targets, and agreement was generally within 1%. A spectrum of lithium fluoride is shown in Figure 5a. Normalization data for magnesium were obtained from a target of magnesium diboride (MgB_2). The estimated accuracy was $\pm 3\%$. A suitable stoichiometric compound containing aluminum could not be found, and data linking aluminum to sodium were obtained from the spectra for four standard rocks, granite G-2, albite AB-1, adularia OR-1, and syenite SY-3. Published analytical data for these rocks (see Ref. 12 or 13) were used, and the mean of these values gave an aluminum calibration to $\pm 3\%$. Data for oxygen were obtained from the spectrum for aluminum oxide (Al_2O_3).

6. Checks for Target Uniformity. Previous authors have agreed that a homogeneous thick target is essential for accurate analysis, but none has considered methods of testing for nonuniformities during the analysis of unknown targets. In this work, two methods of checking for systematic errors caused by nonuniformities in a target have been developed and routinely applied.

For the first method two γ rays produced by different reactions in the same element were selected. For each run their thick-target yields (peak areas) were determined and the ratio calculated. For a homogeneous target and a fixed bombarding energy, this ratio is independent of the concentration of that element or any other element in the target, and is therefore constant, within the limits discussed in Section 3. This can be seen from Equation 7 when N_i and N_j are equal. In general, nonuniformities in a target affect the two thick-target yields differently, and the ratio of the γ-ray yields will change. This method was used very successfully to detect and characterize surface layers on lithium–magnesium alloy samples (at 3.1-MeV proton energy), and is discussed in detail elsewhere (*12, 14*). At a beam energy of 1.8 MeV, fluorine, sodium, and aluminum all produce two intense γ rays. Their yield ratios were monitored whenever statistics permitted, and some cases of target inhomogeneity were detected.

For the second method, the ratio of thick-target yields for any two γ rays was determined in two successive runs at different beam energies. For a homogeneous target the ratio of the values obtained from these two runs should be a constant independent of target composition, within the limits discussed in Section 3. For this method, the same beam spot on a target was bombarded at 1.8 MeV and 1.7 MeV.

Figure 4 (part c) shows the variation with beam energy of the γ-ray yield ratios from fluorine, sodium, and aluminum. By careful interpretation of these ratios, surface effects can often be identified, in particular from the F(197/110) ratio at 1.80 MeV

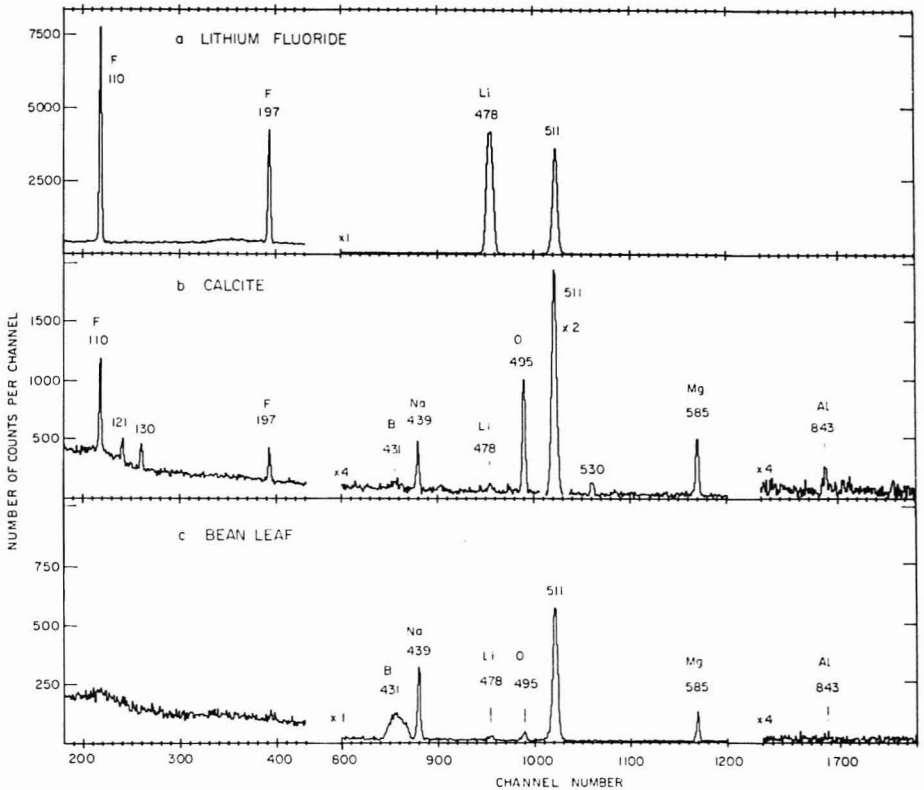

Figure 5. Gamma-ray spectra from standard lithium fluoride, the mineral calcite, and a sample of bean leaf. The beam energy was 1.7 MeV for calcite and 1.8 MeV for the other two. Energies marked on peaks are in keV. Dispersion is 0.50 keV per channel

or the Al(1013/843) ratio at 1.70 MeV. The important function of these checks, however, was to indicate systematic errors caused by nonuniformities. They indicated that data that did not satisfy these checks should not be used for analysis of a sample, and that the analysis should be repeated on another part of the target. For accurate analysis uniform regions were used.

7. Checks for Stability of Targets. The stability of each sample under beam conditions was checked by comparing the γ-ray data from two consecutive runs on the same beam spot of the target. Fluorescence x rays detected during these runs also proved valuable for this purpose.

Samples were generally stable under proton bombardment, although some silicate minerals were found to lose sodium. (It is assumed that this effect is similar to that first reported by Ribbe and Smith (*15*) using electron bombardment of samples in the electron microprobe.) Fluorine was lost from two rocks at high beam current, but was stable at lower beam currents. Freeze-dried leaf material provided the only other example of target instability.

8. Target Preparation. Targets had to be thick enough to stop the proton beam (approximately 45-μm range) and homogeneous within the depth of penetration of the protons (which corresponds to the depth of the analysis), but the nature of the target was otherwise unimportant. Several different types of target were used, but sample preparation was generally kept to a minimum. Some geological samples were analyzed as rough chips; 30-μm thick (the beam entered at 45°, so the effective thickness was 45 μm) polished sections of rock, previously prepared for optical microscope examination, were analyzed directly; powdered samples of rocks (and all standard samples) were compressed into pellets. Blood serum samples and biological materials were freeze-dried and were then compressed.

ANALYTICAL RESULTS

A variety of different samples have been analyzed by this method. Geological materials include standard rocks and glasses, a series of boron-rich potassium feldspars, chondrodite, calcite, kornerupine, quartz, garnet, alkali feldspars, and some mica samples. Results of these analyses are presented in detail elsewhere (*12*, *13*) and only two examples are discussed here. A series of lithium–magnesium alloys was analyzed (at 3.1-MeV proton energy) and is discussed elsewhere (*12*, *14*). The feasibility of analyzing biological and medical materials was investigated by analyzing some blood serum samples and some leaf material, and results are presented in this paper.

1. Potassium Feldspar. A series of boron-rich potassium feldspars has been used in a study of the effect of boron on the cell dimensions of potassium feldspars (*16*). These samples have been analyzed by a curcumin method, but this chemical technique is lengthy and tedious and a search for an alternative method is continuing (*17*).

Figure 2 shows a γ-ray spectrum obtained with 1.8-MeV proton bombardment, for sample number ST-2B. The spectrum was collected in 19 min with a beam current of 130 nA on a compressed powder target. Other measurements were

Table II. Results of Elemental Analysis of Three Selected Samples, Given as the Relative Number of Atoms of Different Elements in Each Sample[a]

Sample	Relative number of atoms						
	Li	B	F	Na	Mg	Al	O
Potassium feldspar (ST-2B)	0.00338 19	0.050[b] 3	0.0023 2	0.063 3	<0.04	0.95[b] 4	7.9 7
Calcite	0.00063 20	0.0041 10	0.038 3	0.0078 8	2.6 2	0.22 5	100[b] 7
Bean leaf	0.002	0.19	<0.02	0.10	7.3	0.21	100[b]

[a] The standard deviation of each value is shown below the value; the figure shown represents the uncertainty in the final digit of the value. [b] Elements used for normalization.

Table III. Results of the Elemental Analysis of Blood Serum Samples Using Prompt Nuclear Reaction γ Rays from 1.8 MeV and 1.2 MeV Proton Bombardment[a]

Serum sample		Lithium, mequiv/L			
No.	Description	Flame photometry[b]	1.8 MeV protons	1.2 MeV protons	Boron, mequiv/L, 1.2 MeV protons
1	Low lithium	0.45	0.476 20		
2	High lithium	1.1	1.15 3		
3	Normal		<0.06	0.045 3	0.9 3

[a] The standard deviation of each value is shown below the value; the figure shown represents the uncertainty in the final digit of the value. [b] Flame photometry values (*18*) have an estimated accuracy of ±5% during routine analysis.

made on rough chips of the feldspar mineral with no sample preparation, and similar spectra were obtained. The spectrum shows that the method is well-suited to the analysis of boron in these samples, where concentrations are in the range of parts per thousand. Gamma-ray peaks from fluorine, sodium, lithium, oxygen, and aluminum were also observed. Boron replaces aluminum in the chemical formula $KAlSi_3O_8$, and results shown in Table II are therefore normalized so that the number of boron plus aluminum atoms equals unity.

2. Calcite. This sample is discussed here because it demonstrates the small concentrations of light elements which can be detected in favorable cases. The sample contained a crystal of the mineral chrondrodite in bulk calcite. A thick section had been polished and analyzed for heavier elements using an electron microprobe.

A γ-ray spectrum from the calcite ($CaCO_3$) is shown in Figure 5b. The count rate was low, and a run of 33 min at 150-nA beam current was used. Some peaks are close to the limit of detection above background. A large oxygen peak can be seen, despite the poor yield per target atom of 495-keV γ rays (Table I).

The results of the analysis are shown in Table II, normalized to oxygen (100 atoms). Very small quantities of lithium, boron, fluorine, and sodium, and small quantities of magnesium and aluminum are determined. The value reported for lithium is equivalent to (6.3 ± 2.0) ppm by weight of Li_2O. The precision of these data could be improved by the use of longer counting times, but this concentration is close to the limit of detection in calcite. In other samples containing large concentrations of fluorine or sodium (which produce a Compton background from high energy γ rays), the limit of detection may be a factor of ten higher.

3. Bean Leaf. The major interest in the analysis of bean leaf (*Phaseolus vulgaris*) was the feasibility of determining the concentration of boron, which is an essential nutrient to plants in trace quantities, but is poisonous in large quantities.

The target for this study was prepared by dipping the leaf sample into liquid nitrogen and crushing it while frozen to facilitate sublimation in the freeze-dryer. After freeze-drying, the sample consisted of a mixture of powder and leaf particles up to 1 mm in diameter. The target formed by compressing this mixture was expected to be heterogeneous, but was considered suitable for this study.

The γ-ray spectrum obtained is shown in Figure 5c. The boron peak is clearly seen, and peaks from other light elements are present. The spectrum was obtained in 23 min with a beam current of 70 nA. Some target instability and non-uniformity effects were observed, and these limit the accuracy of the results. The values shown in Table II are expected to be accurate to within a factor of 2.

Although these results are of a somewhat preliminary nature, it is clear that light elements, and boron in particular, can be analyzed in biological samples, and useful results obtained. The boron concentration in this sample was high (600 ppm) but much smaller quantities could clearly be detected.

4. Blood Serum. The feasibility of analyzing blood serum was demonstrated by using three samples; one was from a normal healthy individual and two were from patients undergoing lithium therapy treatment for mental disorders at Kingston General Hospital. The samples were freeze-dried and the resulting powders compressed into pellets.

The 439-keV peak from sodium and Compton background from higher energy sodium γ rays dominated the spectrum for each sample. The part of each spectrum including the sodium and lithium peaks is shown in Figure 6. Run times were approximately 25 min at 60- to 80-nA beam current.

Results for the two "lithium therapy" samples gave lithium analyses with good precision. Our results are expressed as mequiv/L using a value of 140 ± 2 mequiv/L as the normal sodium concentration. These results show good agreement with values obtained in a routine analysis using a flame photometer (*18*), and are shown in Table III.

The high background from sodium γ rays made it difficult to observe the small quantity of lithium normally present in blood serum (Figure 6C), or any other light elements which may be present.

To reduce the sensitivity to sodium, the beam energy was reduced to 1.2 MeV. At this energy the Li-478/Na-439 ratio was a factor of 18 greater than at 1.8 MeV, and the Li-478

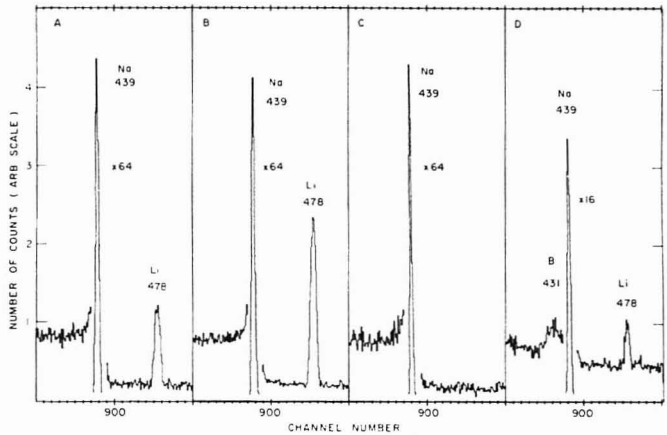

Figure 6. Gamma-ray spectra in the region of the sodium and lithium peaks for blood serum samples. (A) Sample 1, 0.45 mequiv/L lithium, 1.8 MeV protons. (B) Sample 2, 1.1 mequiv/L lithium, 1.8 MeV protons. (C) Sample 3, "Normal" blood serum, 1.8 MeV protons. (D) Sample 3, "Normal" blood serum, 1.2 MeV protons. Channels 800 to 1000 are shown for the four spectra. Energies marked on peaks are in keV. Dispersion is 0.50 keV per channel

peak-to-background ratio was a factor of 2.5 greater. The count rates were very much reduced and a 2-h bombardment at a target current of 100 nA was required to obtain the spectrum shown in Figure 6D. With reduced sensitivity to sodium, a lithium peak is now visible. There is also a small peak from boron and a trace of fluorine. A rock sample, previously analyzed at 1.8 MeV, was used as a secondary standard and the results of an approximate quantitative analysis of the blood sample are shown in Table III. The lithium content corresponds to 0.32 ppm by weight of lithium in normal blood serum.

For the routine analysis of enhanced lithium content, a flame photometer is adequate, but for the determination of very small concentrations of lithium and other light elements nuclear reaction γ rays may be useful.

DISCUSSION

The nuclear reaction γ-ray method for the simultaneous quantitative analysis of a number of light elements has been discussed in detail. Precautions necessary to ensure the accuracy of results have been described. Matrix effects and interferences between different elements have been shown to be unimportant at 1.8 MeV. An analysis of relative concentrations of elements can be obtained from the peak areas in a γ-ray spectrum by use of a simple relation.

Checks on the self-consistency of data and comparison with results of other methods suggest that an accuracy of $\pm 5\%$ can be expected, and this may be improved in some cases. In some materials, minor fluctuations in composition, charge accumulation, and surface effects combine to produce systematic errors of a few percent.

The bombarding particle and beam energy have been chosen so that the light elements lithium, boron, fluorine, sodium, magnesium, and aluminum can be analyzed simultaneously. Quantitative analysis of these elements has been demonstrated on a range of different materials, and selected results have been presented in this paper. Other results are discussed elsewhere (*12–14*).

In many analytical problems, concentrations at the parts-per-thousand level are of interest. This method is well-suited to these concentrations, and an analysis with good precision can be obtained in about 20 min. This was demonstrated by the analysis of light elements in potassium feldspar.

The limit of detection depends on the composition of the sample. If small quantities of elements of interest are present, the low γ-ray (Compton) background allows concentrations at the parts-per-million level to be determined for lithium, boron, fluorine, and sodium. This was demonstrated by the analysis of calcite, and also with the bean leaf sample. For magnesium and aluminum, about 100 ppm is a reasonable estimate of the limit of detection.

The sensitivity to different elements is determined by the choice of beam energy. The usefulness of this was demonstrated in the analysis of blood serum: the traces of lithium and boron were not observed when 1.8-MeV protons were used, because of the high sensitivity to sodium at that energy, but were observed when the beam energy was reduced to 1.2 MeV.

The application to different types of material was demonstrated by the analysis of geological samples, leaf material, and blood serum with no change in the experimental procedure. Target preparation was a minimum: rough chips of some minerals were analyzed, while polished and compressed powder targets were also used.

This work has shown that the prompt nuclear reaction γ-ray method, with low energy protons and a high resolution Ge(Li) detector, is well-suited to the analysis of light elements in a variety of types of material. When fluorescence x rays are detected in the same run, heavier elements may be determined, and the simultaneous use of the two techniques provides a powerful analytical combination.

ACKNOWLEDGMENT

We thank R. F. Martin, J. Bourne, R. G. S. Bidwell, and A. F. Clark for the loan or donation of samples.

LITERATURE CITED

(1) J. J. Malanify and D. A. Close, *Nucl. Instrum. Methods*, **118**, 293 (1974).
(2) E. Ricci, *Anal. Chem.*, **43**, 1866 (1971).
(3) J. Lorenzen, *Nucl. Instrum. Methods*, **121**, 467 (1974).
(4) Z. Hadari, M. Kroupp, and Y. Wolfson, *J. Appl. Phys.*, **42**, 534 (1971).
(5) G. Deconninck, *J. Radioanal. Chem.*, **17**, 29 (1973).
(6) G. Deconninck and G. Demortier, *J. Radioanal. Chem.*, **12**, 189 (1972).
(7) A. R. Knudson and K. L. Dunning, *Anal. Chem.*, **44**, 1053 (1972).

(8) D. J. Macey and W. B. Gilboy, *Nucl. Instrum. Methods*, **92**, 501 (1971).
(9) G. E. Coote, N. E. Whitehead, and G. J. McCallum, *J. Radioanal. Chem.*, **12**, 491 (1972).
(10) L. Shabason and B. L. Cohen, *Anal. Chem.*, **45**, 284 (1973).
(11) J. F. Janni, Tech. Report AFWL-TR-65-150, Air Force Weapons Lab., New Mexico, U.S.A.F. (1966).
(12) R. B. Boulton, Ph.D. Thesis, Department of Physics, Queen's University, Kingston, Ontario, Canada, 1975.
(13) R. B. Boulton and G. T. Ewan, unpublished work.
(14) R. B. Boulton and G. T. Ewan, unpublished work.
(15) P. H. Ribbe and J. V. Smith, *J. Geol.*, **74**, 217 (1966).
(16) R. F. Martin, *Am. Mineral.*, **56**, 281 (1971).
(17) S. J. Horska, Department of Geology, McGill University, Montreal, Canada, private communication, 1975.
(18) A. F. Clarke, Department of Biochemistry, Queen's University, Kingston, Ontario, Canada, private communication, 1974.

RECEIVED for review November 29, 1976. Accepted May 2, 1977. Financial assistance is acknowledged from N.R.C. and A.E.C.B.

Analysis of Thyroid Hormones as Their Heptafluorobutyryl Methyl Ester Derivatives by Gas Chromatography–Mass Spectrometry

B. A. Petersen[1] and Paul Vouros*

Institute of Chemical Analysis, Applications and Forensic Science, Northeastern University, Boston, Massachusetts 02115

The mass spectra of the heptafluorobutyryl methyl ester derivatives of several thyroid hormones and their analogues have been examined, and their fragmentation patterns are discussed. Ions of significant relative intensity dominate the high mass ($m/e > 700$ amu) region of the spectra of these derivatives. In view of the decreased interference of background peaks at that high mass region, this feature has been effectively utilized in the GC-MS analysis of these compounds by selective ion monitoring. Detection limits of 0.5 pg have been attained.

The two thyroid hormones which are found in significant quantities in human serum are thyroxine (T_4) and 3,5,3′-triiodothyronine (T_3). Although their total concentrations are approximately 72 ng/mL and 2 ng/mL, respectively, only about 0.03% of T_4 and 0.03% of T_3 are free, that is, not protein bound, in normal serum. Nevertheless, these forms are of considerable interest because it is only the free hormone (i.e., FT_3 and FT_4) which is believed to penetrate cells, stimulate metabolism and exert feedback control to the pituitary (*1*). In addition, reverse T_3 (3,3′,5′-triiodothyronine; RT_3), although it is generally regarded as physiologically inactive, has recently become of interest partly because it occurs at different levels in the serum of euthyroid and pathological states (*2, 3*). For example, RT_3 is markedly elevated in the serum of the newborn and in amniotic fluid at 15 weeks pregnancy (*4, 5*).

Many difficulties are associated with the quantitation of the thyroid hormones both due to their presence in trace levels and the inexact methods of analysis currently employed. A variety of methods based on radiochemical techniques have been selected for estimating and monitoring FT_3 and FT_4 (*6–9*). Although currently utilized, these methods suffer from certain disadvantages such as the need for accompanying assays of the total amounts of T_3 and T_4 and the necessity to work with short half-lived radioisotopes and their degradation products.

A number of investigators have used gas chromatographic analysis with electron capture detection (GC-ECD) of volatile derivatives of the thyroid hormones as a direct means of quantitation (*10–13*). These methods required a minimum quantity of 1 mL of serum for the analysis, because of their relatively high detection limits and the low concentrations of thyroid hormones involved. Recently, however, it was shown that direct analysis of the free levels of these hormones can be achieved by formation of their *N,O*-diheptafluorobutyryl (HFB) methyl ester (ME) derivatives using GC-ECD (*14*).

In a logical extension of this earlier study we have now looked into the mass spectrometric properties of these derivatives and, in the process, examined the general utility of combined gas chromatography–mass spectrometry for their analysis by selective ion monitoring (SIM). For the purposes of structure elucidation from the mass spectral fragmentation patterns, several related compounds containing different halogen substituents on the phenyl system were synthesized and subsequently derivatized. In the following section we report on the fragmentation patterns of T_3 and RT_3 with particular emphasis on the sample requirements for quantitation of the latter compounds using selective ion monitoring.

EXPERIMENTAL

A. Reagents and Chemicals. Diiodothyronine (T_2), triiodothyronine (T_3), and tetraiodothyronine (T_4) were obtained as the free acids from Sigma (St. Louis, Mo.). Reverse T_3 (RT_3) and tetrachlorothyronine (Cl_4To) were kindly provided by R. I. Meltzer of Warner-Lambert Research Laboratories. The esterifying reagent was 25% (w/w) gaseous HCl (Matheson, Gloucester, Mass.) in methanol (Burdick and Jackson, Muskeegon, Mich.). The methanol was redistilled and dried over molecular sieve Type 5A. The acetylating reagent was heptafluorobutyric anhydride (K & K, Plainview, N.Y.) in acetonitrile (Burdick and Jackson). A deuteriomethyl ester derivative of several of the thyroid hormones was prepared by reacting the free acid with CD_3OD (99.999% isotopic purity; Stohler Isotopes, Billerica, Mass.).

B. Synthesis of 3′,5′-Dibromo-3,5-diiodothyronine (Br_2T_2) and 3′,5′-Dichloro-3,5-diiodothyronine (Cl_2T_2). (*1*) Br_2T_2. Five hundred mg of T_2 was placed in a 50-mL round bottom flask and dissolved in 10 mL of glacial acetic acid. Three hundred mg of Br_2 were then added and the solution was allowed to stand at room temperature for 72 h. The solution was then removed under vacuum with a rotary evaporator at 60 °C. The product (Br_2T_2) was recrystallized from ethanol/2N HCl (95:5,V/V) in 90% yield. (mp 136–138) (*15*).

(*2*) Cl_2T_2. Five hundred mg of T_2 was placed in a 50-mL round bottom flask and dissolved in 10 mL of glacial acetic acid. Cl_2 was allowed to bubble through the solution for 15 min at room

[1] Present address, Battelle Columbus Laboratories, 505 King Avenue, Columbus, Ohio 43201.

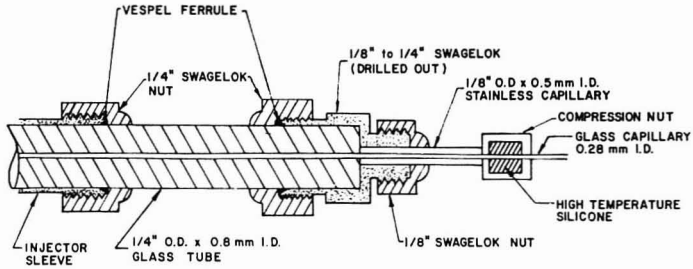

Figure 1. Schematic of capillary column connection to injection port of GC-MS system

Table I. Relative Intensity Values of Significant Ions of the N,O-diHFB-Me Derivatives of the Thyroid Hormones

	1 (X = H)	2 (X = I)	3 (X = I)	4 (X = I)
$(M)^{+\cdot}$	62[a] (931)[b]	67 (1057)	63 (1057)	60 (1183)
$(M - 213)^{+\cdot}$	100 (718)	100 (844)	70 (844)	100 (970)
$(M - 284)^{+}$	22 (647)	67 (773)	100 (773)	48 (899)
$(M - 410)^{+}$	36 (521)	25 (647)	15 (647)	28 (773)
$(M - 213 - I, X)^{+\cdot}$	14 (590)	22 (590)	14 (590)	36 (716)
$(M - 284 - I, X)^{+\cdot}$	32 (519)	35 (519)	38 (519)	30 (645)
$(M - 410 - I, X)^{+}$	17 (393)	6 (393)	5 (393)	8 (519)
$(M - 284 - I, X - 197)^{+\cdot}$	33 (322)	21 (322)	32 (322)	21 (448)

[a] % relative intensity. [b] *m/e* value.

temperature. The excess chlorine was then removed by bubbling N_2 through the solution. The solvent was again removed by use of the rotary evaporator, and the product recrystallized as before in 80% yield (mp 123–126) °C (*15*).

C. Derivative Formation. Esterification of the thyroid hormone standards and related compounds was accomplished separately by placing 1.0 mg of each into a 3-mL microreaction vial (Pierce, Rockford, Ill.) adding 1.0 mL of the 25% HCl–alcohol solution, sealing with a Teflon coated septum and heating to 60 °C for 1 h. The solution was subsequently evaporated to dryness under a stream of dry N_2. A freshly prepared solution of 400 μL of heptafluorobutyric anhydride in 500 μL of acetonitrile was then added to acetylate the amino nitrogen and phenolic oxygen of the thronines. The tube was kept at 60 °C for 1 h, cooled to room temperature, and the solution blown to dryness with dry N_2.

D. Preparation of the Physiological RT_3 Sample. Twenty mL of euthyroid sera were placed in a clean dialysis membrane (Visking Nojax, Union Carbide, Chicago, Ill.). This membrane was then inserted into a clean, silanized 100-mL Erlenmeyer flask and 30 mL of 0.15 M phosphate buffer (19.70 g K_2HPO_4–4.92 KH_2PO_4/L H_2O, pH 7.40) added. Dialysis was allowed to continue for 16 h at 37.0 ± 0.5 °C with gentle stirring. The dialysate was purified using cation-exchange chromatography (AG 50W-X2, 100-200 mesh, Bio-Rad, Richmond, Calif.) by placing on a 10 cm × 1 cm i.d. column, washing with 50 mL of 0.15 M ammonium acetate (pH 8.5), and 6 mL of methanol. The free thyroid hormone fraction was collected with 10 mL of methanol–12 N NH_4OH (97:3,v/v). After evaporation of this solution, the derivatization was conducted in the identical fashion as above. A detailed description of all procedures used in the preparation of the physiological sample has appeared in a recent publication (*14*).

E. Mass Spectra of the Thyroid Hormone Derivatives. Low resolution mass spectra were obtained with a Nuclide 12-90-G mass spectrometer by direct insertion probe. The accelerating potential was 4 kV, electron energy was 70 eV, the ionization current 50 μA, and the temperature of the ion source maintained at 300 °C.

High resolution mass spectra of the thyroid hormone derivatives were kindly provided by Catherine Costello of the Massachusetts Institute of Technology, Cambridge, Mass.

F. Combined Gas Chromatographic–Mass Spectrometric (GC-MS) Analysis. A Varian 2700 gas chromatograph was coupled to the mass spectrometer via a direct transfer line. Since the instrument was equipped with high capacity diffusion pumps and the ion source was differentially pumped, no molecular separator was used. A high temperature valve system (Valco, Chicago, Ill.) was used in the GC detector cavity to direct the effluent from the GC to the MS or to the atmosphere. The direct transfer line was a stainless steel capillary 12 inches long with an inside diameter of 0.010 inch. This transfer line could be resistance heated to 350 °C.

The GC column used to separate the derivatives was a high resolution wall-coated glass capillary (20 m × 0.15 mm i.d.) coated with 1% OV-101. (Gas Chromatographic Supplies, Tokyo, Japan). The injector system of the GC was modified for direct capillary injection without splitting by inserting a glass sleeve ($^1/_4$-inch o.d. × 0.80 mm i.d.) into the injection port and maintained at 350 °C. A $^1/_4$-inch to $^1/_8$-inch reducing union was drilled out so that the capillary column connector could be attached to the glass sleeve without excessive dead volume. The glass capillary was connected to the system with high temperature silicone septums. A schematic diagram of this capillary column connection is shown in Figure 1. The carrier gas was ultra high purity helium (99.999%; Matheson) and the flow rate was 2 mL/min. The column was operated at 290 °C to separate all the thyroid hormone derivatives and at 275 °C during SIM of the T_3 and RT_3 derivatives. The effluent from the GC was monitored using the total ion current detector while the output from the electron multiplier was monitored using both a strip chart and the oscillographic recorder. The valve system, transfer line and ion source were maintained at 300 °C during GC-MS. Ionization conditions were identical to those in Section E.

RESULTS AND DISCUSSION

A. Interpretation of the Mass Spectra of the Thyroid Hormone Derivatives. The compounds examined in this study were the *N,O*-di-HFB-ME derivatives of 3,5-diiodothyronine (T_2; **1**), 3,3′,5-triiodothyronine (T_3; **2**) 3,3′,5′-triiodothyronine (RT_3; **3**), 3,3′,5,5′-tetraiodothyronine (T_4; **4**), 3′,5′-dibromo-3,5-diiodothyronine (Br_2T_2; **5**), 3′,5′-dichloro-3,5-diiodothyronine (Cl_2T_2; **6**), and 3,3′,5,5′-tetrachlorothyronine (Cl_4T_0; **7**). The spectra of these derivatives are summarized in Table I (Compounds 1–4) and Table II (Compounds 5–7). Complete mass spectra are shown in Figures 2–8. To assist in the interpretation of the spectra, the fragmentation of the d_3-methyl ester of the thyroxine derivative T_4 (**4**) was also examined. The mass shifts of the

Table II. Relative Intensity Values of Significant Ions of the N,O-diHFB-Me Derivatives of Compounds Related to the Thyroid Hormones

	Compound		
	5 (X_1 = I, X_3 = Br)[a]	6 (X_1 = I, X_3 = Cl)[b]	7 (X_1 = Cl, X_3 = Cl)[b]
$(M)^{+\cdot}$	24[c] (1087)[d]	75 (999)	7 (815)
$(M - 213)^{+\cdot}$	100 (874)	100 (786)	82 (602)
$(M - 284)^{+}$	47 (803)	42 (715)	69 (531)
$(M - 410)^{+}$	23 (677)	20 (589)	100 (405)
$(M - 213 - X_1, X_3)^{+\cdot}$	29 (668)	8 (624)	8 (532)[e]
$(M - 284 - X_1, X_3)^{+}$	26 (597)	9 (553)	6 (461)
$(M - 410 - X_1, X_3)^{+}$	6 (471)	5 (427)	7 (335)
$(M - 284 - X_1, X_3 - 197)^{+\cdot}$	12 (400)	7 (356)	9 (264)

[a] *m/e* values based on ^{79}Br in ion peak cluster. [b] *m/e* values based on ^{35}Cl in ion peak cluster. [c] % relative intensity. [d] *m/e* value. [e] % relative intensity corrected for isotopic composition from *m/e* 531 (i.e. $[M - 284]^{+}$).

Table III. Mass Shifts of the Principal Ions in the Mass Spectrum of the *N,O*-Diheptafluorobutyryl-d_3-methyl Ester Derivative of T_4

	HFB-ME-T_4	HFB-d_3-ME-T_4	ΔM
$(M)^{+\cdot}$	1183	1186	3
$(M - 213)^{+\cdot}$	970	973	3
$(M - 284)^{+}$	899	899	0
$(M - 410)^{+}$	773	776	3
$(M - 213 - 2I)^{+\cdot}$	716	719	3
$(M - 254\ 2I)^{+}$	645	645	0
$(M - 410 - 2I)^{+}$	519	522	3
$(M - 254 - 2I - 197)^{+\cdot}$	448	448	0

principal fragment ions are indicated in Table III.

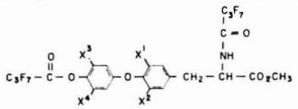

1 (T_2) · X^1 = X^2 = I ; X^3 = X^4 = H

2 (T_3) · X^1 = X^2 = X^3 = I ; X^4 = H

3 (RT_3) · X^1 = X^3 = X^4 = I ; X^2 = H

4 (T_4) · X^1 = X^2 = X^3 = X^4 = I

5 (Br_2T_2) · X^1 = X^2 = I ; X^3 = X^4 = Br

6 (Cl_2T_2) · X^1 = X^2 = I ; X^3 = X^4 = Cl

7 (Cl_4T_0) · X^1 = X^2 = X^3 = X^4 = Cl

The following noteworthy features are common to the mass spectra of compounds 1–7:

(a) The molecular ion peaks of the *N,O*-di-HFB methyl ester derivatives of the thyroid hormones and related compounds investigated were of generally high relative intensity. This intensity seemed to vary with halogen substitution on the phenyl system in the order Cl < Br < I.

(b) Noteworthy is the high intensity of the ion peaks appearing at the high mass region ($m/e > 700$) of the spectra.

(c) A major fragment ion corresponding to $[M - 213]^{+\cdot}$ was observed in all of the spectra. It is conceivably formed via a McLafferty rearrangement as indicated in Scheme I. The three mass unit shift of the $[M - 213]^{+\cdot}$ ion in the spectrum of the d_3-methyl ester of T_4 (Table III) and high resolution data support the structure *a* given in Scheme I.

(d) The abundant ion corresponding to $[M - 284]^{+}$ is formed by cleavage β to the aromatic ring in a manner analogous to the fragmentation of related compounds such as tyrosine (*15, 16*), *N*-trifluoroacetyl-*O*-butyl aromatic amino acids (*17*), and trimethylsilyl (TMS) derivatives of thyroxine (*18*). Scheme II.

(e) An ion corresponding to $[M - 410]^{+}$ is formed by elimination of C_3F_7–CO· from $[M - 213]^{+\cdot}$, as supported by metastable transitions (Scheme III). This ion can be stabilized by resonance through the π-system as indicated by

SCHEME I

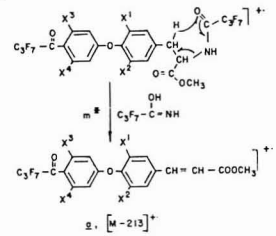

SCHEME II

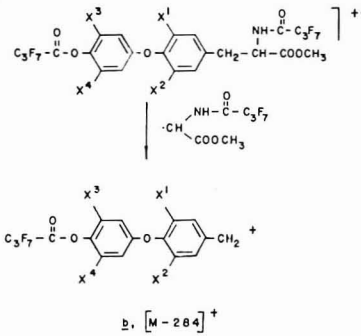

SCHEME III

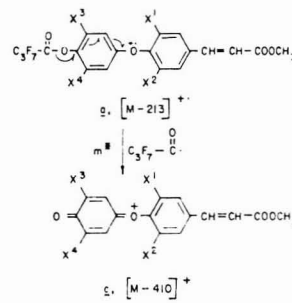

structure *c* (Scheme III). Noteworthy is the increased abundance of this ion in the spectrum of the tetrachloro derivative (7) where it constitutes the base peak. This may

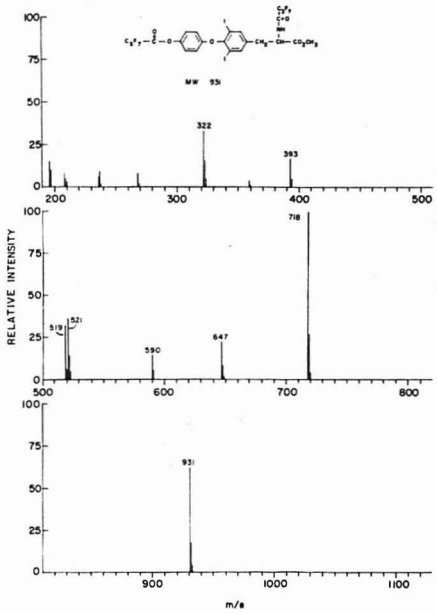

Figure 2. Mass spectrum of the HFB-ME derivative of 3,5-diiodothyronine (T_2; 1)

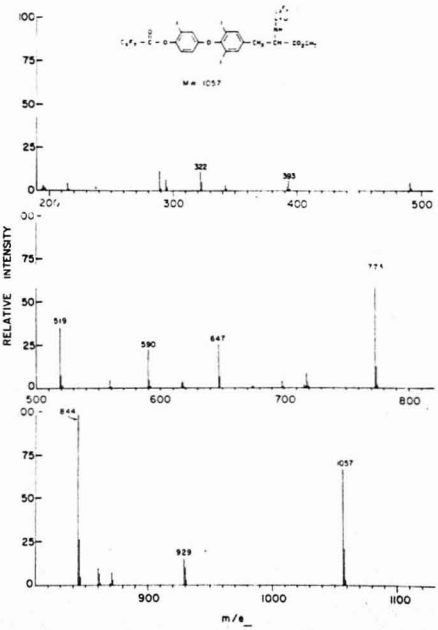

Figure 3. Mass spectrum of the HFB-ME derivative of 3,3′,5-triiodothyronine (T_3; 2)

SCHEME IV

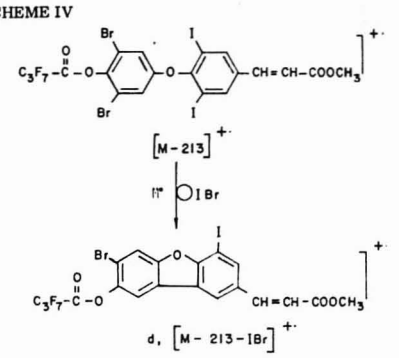

SCHEME V

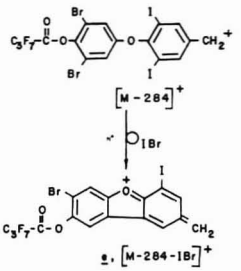

be attributed to the decreased steric inhibition to resonance of the smaller chlorine atoms in 7 compared to the larger bromine and iodine atoms in 1–6. This is consistent with earlier studies by Bursey and co-workers on the effect of ortho substituents on the resonance stabilization of fragment ions (*19*, *20*).

(f) In all of the spectra, appear ions of significant intensity corresponding to the loss of two halogens from the various fragment ions. To ascertain from which phenyl ring the halogens were eliminated, the mass spectra of the related derivatives Br_2T_2 (5) and Cl_2T_2 (6), which contain different halogens on the two phenyl rings, were examined. In the spectrum of Br_2T_2 there is no evidence for the simultaneous loss of either two iodines or bromines from the molecular ion or the major fragment ions. Instead an apparently concerted loss of BrI occurs from $[M - 213]^{+\cdot}$ (m/e 874) and $[M - 284]^+$ (m/e 803) as shown in Schemes IV and V, respectively. It is speculated that these eliminations are accompanied by an intramolecular hydrogen shift to yield the resonance stabilized cyclic structures *d* and *e*. Fragment ions corresponding to the above, and originating from $[M - 213]^+$ (m/e 786) and $[M - 284]^+$ (m/e 715), also appear in the spectrum of Cl_2T_2 (6). They occur at m/e 624 and m/e 553 (i.e. loss of ClI from each). These mechanisms and structures are also supported by metastable transitions and high resolution data.

An additional fragment ion in the spectra of these derivatives, corresponding to the loss of two halogens and presumably ring condensation, also appears after cleavage of the heptafluoro-butyryl group attached to the phenolic oxygen of $[M - 284 - 2X]^+$. The general structure for this fragment ion (*f*) is shown in Scheme VI.

It is interesting that ions representing cleavage of the ethereal bond and retention of the charge with either part of the molecule were not observed. This is unfortunate with

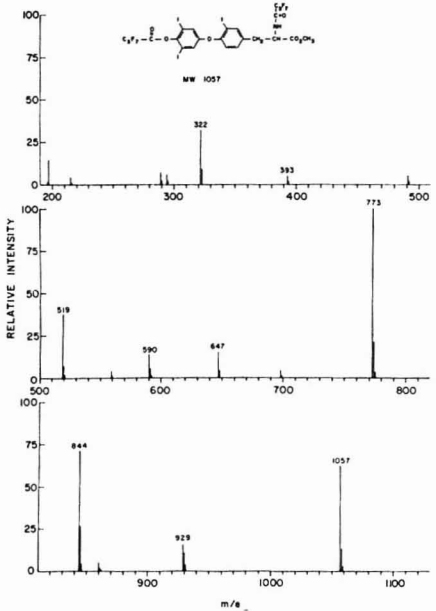

Figure 4. Mass spectrum of the HFB-ME derivative of 3,3′,5′-triiodothyronine (RT_3; **3**)

SCHEME VI

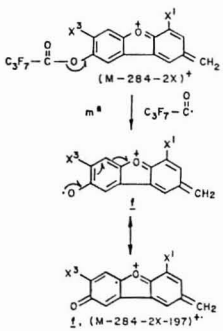

regard to mass spectral identification based on discriminating between the positional isomers T_3 and RT_3. The fragmentation patterns of these isomers are identical, differing only on relative peak intensities. However, in view of the significant difference in chromatographic retention time of these two compounds, a study of their GC-MS properties was conducted using SIM for their detection and quantitation.

GC-MS Studies. As stated earlier, analysis of the free thyroid hormones in serum presents a major challenge due to their occurrence in trace levels. This is further compounded by the fact that the serum sample itself is often in short supply and of such complexity that it requires considerable cleanup and pretreatment to achieve isolation of the hormones in a medium and form suitable for final analysis. Previous investigations (*14*) have shown that, Dialysis–GC–ECD can be

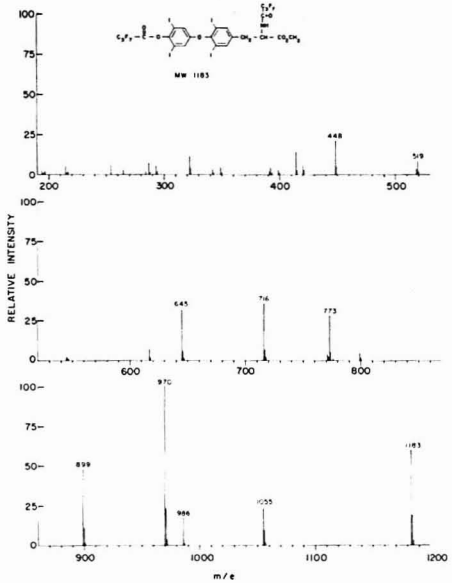

Figure 5. Mass spectrum of the HFB-ME derivative of 3,3′,5,5′-tetraiodothyronine (T_4; **4**)

effectively used for the concurrent analysis of FT_3 and FT_4 in both normal and pathological sera as their di-HFB-ME derivatives. However, due to the fact that free RT_3 (FRT_3) occurs in extremely low concentrations in normal serum (i.e., 0.5–2.0 pg/mL) severe demands are placed on its detection by GC-ECD. Furthermore, confirmation of the identity of the eluted components is also extremely difficult when present in such low concentrations. Because of the fact that formation of the HFB-ME derivatives of these hormones had been shown to be quantitative at physiological concentrations, their excellent mass spectrometric properties, and the high selectivity and specificity of GC-MS, we examined the utility of this technique for the analysis of FRT_3 in normal serum using selective ion monitoring (SIM) techniques.

Some of the requirements for effective utilization of SIM techniques in GC-MC include: (a) the presence of an ion(s) indicative of and specific to the compound(s) in question, (b) occurrence of this ion(s) at an m/e value(s) free of interferences from column bleed or background, (c) possession of a substantial fraction of the total ion current with the ion(s) used for SIM, and (d) the ready availability of an isotopically labeled analogue for use as an internal standard and carrier. Co-injection of this analogue can also minimize the losses arising from adsorption in the chromatographic system and interface, thereby improving the detection limits of the analysis.

The ion in the spectrum of the HFB-ME derivative of RT_3, which satisfied all of these requirements, was $[M - 213]^+$ (m/e 844). The high m/e value of this ion virtually eliminates the possibility of any interference due to column bleed, as such ion peaks usually occur at much lower mass numbers. Furthermore, this ion is common to the spectra of both RT_3 and T_3 comprising over 20% of the total ion current, thus permitting the concurrent analysis of these compounds in view of their significantly different elution times. This is illustrated in Figure 9 which shows the total ion current and selective

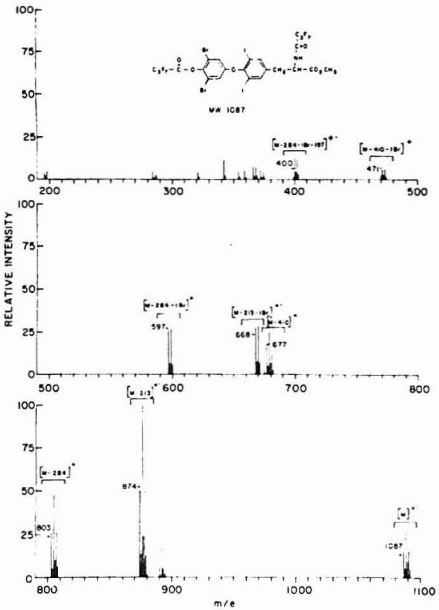

Figure 6. Mass spectrum of the HFB-ME derivative of 3′,5′-dibromo-3,5-diiodothyronine (Br_2T_2; **5**)

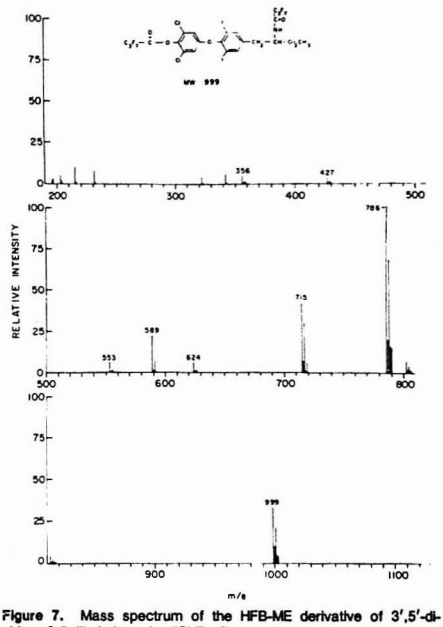

Figure 7. Mass spectrum of the HFB-ME derivative of 3′,5′-dichloro-3,5-diiodothyronine (Cl_2T_2; **6**)

ion chromatograms of a standard mixture containing 100 ng each of T_3 and RT_3. Finally, a deuteriomethyl ester derivative of RT_3 can be easily synthesized and the $[M - 213]^+$ ion contains the CD_3 group (Scheme I), thus shifting its value from m/e 844 to m/e 847. This feature should permit the deuteriated compound to act as an internal carrier to minimize loss of the physiological compound in the chromatographic system.

To establish the conditions for GC-MS analysis and quantitation of T_3 and RT_3, the mass spectrometric sensitivity of their HFB-ME derivatives was determined by SIM of the m/e 844 ion. As the particular instrument employed in this study (Nuclide 12-90-G) was equipped with a retractable Faraday cup in the collector housing, absolute ion current measurements under SIM conditions could be obtained. Therefore, by eliminating the variable of electron multiplier gain, quantitative analysis could be performed in terms of coulombs/microgram (C/μg) of sample introduced into the system. Details of this technique have appeared in an earlier publication (*21*). Standard sensitivity values were obtained by introducing known quantities of the respective derivatives into the ion source via the direct inlet probe and monitoring the ion current over the lifetime of the sample. Values of 9.6×10^{-10} C/μg and 6.5×10^{-10} C/μg for T_3 and RT_3, respectively, were obtained. Based on these measurements the transfer efficiency of the GC-MS system for these derivatives was found to be 97% at sample levels of 0.1 μg. A calibration curve of RT_3 (Figure 10) for quantitative analysis was obtained by injection of standard sample aliquots into the GC-MS system.

The sensitivity values for T_3 and RT_3 were used to evaluate quantitatively the extent to which the isotopically labeled internal carrier can improve the trace level analysis of a compound during GC-MS. To a solution containing known amounts of HFB-ME derivatives of T_3 and RT_3, a 1000-fold

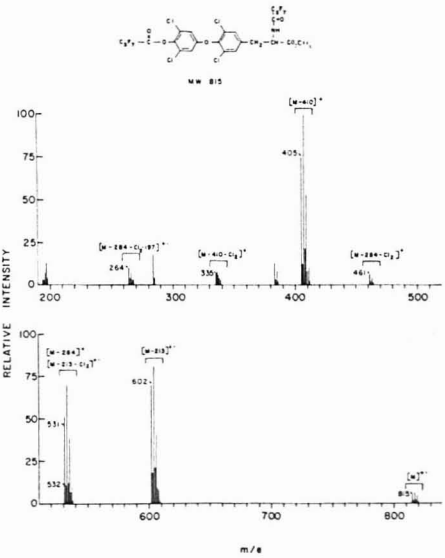

Figure 8. Mass spectrum of the HFB-ME derivative of 3,3′,5,5′-tetrachlorothyronine (Cl_4T_0)

excess of the HFB-d_3-ME derivative of RT_3 was added, and varying amounts of sample over a range exceeding 10^5 (100 ng–0.5 pg) were injected into the GC-MS. The value of using a deuteriated internal carrier is demonstrated from the graph

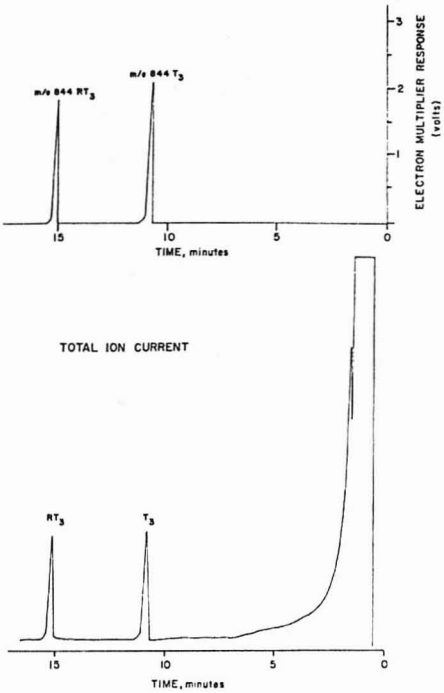

Figure 9. Gas chromatographic separation of 100 ng each of the HFB-ME derivatives of T_3 and RT_3. Simultaneous recording of the total ion current (bottom) and electron multiplier response (SIM of m/e 844; top). GC conditions: 20 m × 0.28 mm i.d. glass capillary coated with 1% OV-101, Gas flow 2 mL/min, temperature: 275 °C, isothermal

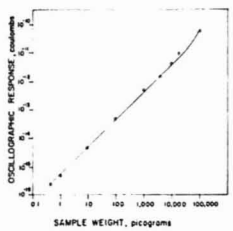

Figure 10. Calibration plot of the HFB-ME derivative of RT_3 as oscillographic peak area (coulombs) vs. weight of RT_3 injected (SIM of m/e 844)

in Figure 11. Under ideal conditions, the sensitivity vs. sample weight curve should have a straight line with a slope of zero, since the sensitivity is normalized with respect to the electron multiplier gain. In fact, the slope for the sensitivity curve of RT_3, which was co-eluted with the deuterium labeled carrier, closely approaches that ideal value while, on the other hand, the sensitivity curve for T_3 drops sharply at levels below 10 ng. Furthermore, the lowest detection limit for RT_3 which was co-eluted with its d_3-labeled counterpart was approximately 0.5 pg as compared to 100 pg for the T_3 derivative. It should be noted that a 0.1-μg sample of the HFB-d_3-ME derivative of RT_3 exhibited no detectable contribution to m/e

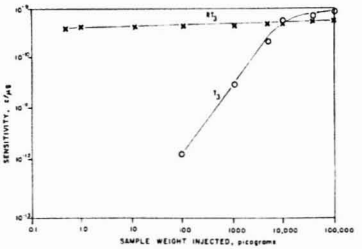

Figure 11. Normalized plot of mass spectrometric sensitivity vs. sample weight of RT_3 and T_3. Effect of labeled internal carrier on sensitivity and detection limits. Component ratio in mixture injected into GC-MS: HFB-ME-T_3:HFB-ME-RT_3:HFB-d_3-ME-RT_3 = 1:1:1000

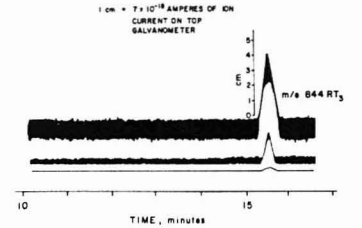

Figure 12. Oscillographic response to m/e 844 during GC-MS-SIM of a physiological sample containing RT_3 and T_3 as their HFB-ME derivatives. Galvanometer sensitivity 30 (top), 10 (middle), 1 (bottom). Electron multiplier gain, $G = 10^6$. Chromatographic conditions as in Figure 9

844 due to any d_0 impurity under SIM conditions.

To assess the general applicability of our results, we examined a physiological sample of known concentration of RT_3 (2 pg/mL). The ratio of free T_3 to free RT_3 in this sample had previously been established at 4:1 by Dialysis–GC–ECD (*22*). After dialysis, ion exchange chromatography, derivatization, and concentration of a 20-mL euthyroid serum sample, an aliquot was analyzed by GC-MS and monitoring of the m/e 844 ion. The oscillographic recording of this analysis is shown in Figure 12. Note that although the physiological concentration of T_3 is 4–5 times higher than that of RT_3, no signal was detected at its expected retention time, (i.e. ~11 min) whereas the response for the RT_3 derivative is clearly evident. Based on our calibration data (Figure 10), the signal obtained corresponds to approximately 1 pg injected, or a free concentration of 2 pg/mL of serum, i.e., well within the expected value. It should be noted that several blanks containing solvent and reagents exhibited no signal under the same conditions at m/e 844. In view of the extremely low concentrations involved, it is not entirely clear at this point whether the RT_3 detected represents the physiologically free forms or may result from mono de-iodination of T_4 during dialysis. However, our data clearly indicate its presence.

CONCLUSIONS

The data presented above point out the usefulness of combined gas chromatography–mass spectrometry and, in particular, the use of selective ion monitoring techniques for the analysis of the thyroid hormones. To perform quantitative analysis at the trace level, the use of an isotopically labeled internal carrier has been evaluated, and was shown to be essential for this purpose.

It should be emphasized that for quantitative analysis, the calibration data of Figure 12 cannot be used on a day-to-day

basis because of the possibility of variations in instrumental conditions as shown in an earlier study (*21*). For this purpose, multiple ion detection using an accelerating voltage alternator (AVA) (*23*) and simultaneous monitoring of several ions, including one or more of the isotopically labeled internal standard, is necessary. Ideally, the internal standard should be subjected to the identical sample preparation and derivatization conditions as the compound in question. This was not possible in this specific case, as the labeled analogue of RT_3 had to be prepared separately during esterification. This problem can be alleviated by using a compound containing deuterium atoms on the thyronine phenyl rings, which, of course, would be a major project in itself. Nevertheless, the methodology developed for the analysis of free RT_3 by Dialysis–GC–MS–SIM can be applied to the analysis of all the thyroid hormones and their precursors as their HFB-ME derivatives.

ACKNOWLEDGMENT

The authors thank B. L. Karger and R. W. Giese for helpful suggestions and T. Hanai for the capillary GC column.

LITERATURE CITED

(1) P. R. Larsen, *Med. Clin. North Am.*, **59**, 1063 (1975).
(2) P. Nicod, A. Burger, V. Stacheli, and M. V. Vallotton, *J. Clin. Endocrinol. Metab.*, **42**, 823 (1976).
(3) H. Meinhold, K. W. Wenzel, and P. Schürnbrand, *Z. Klin. Chem. Klin. Biochem.*, **13**, 571 (1975).
(4) I. J. Chropra and B. F. Crandell, *N. Engl. J. Med.*, **293**, 740 (1975).
(5) D. A. Fisher, *N. Engl. J. Med.*, **293**, 770 (1975).
(6) K. A. Sterling and A. Hegedus, *J. Clin. Invest.*, **41**, 1031 (1962).
(7) S. S. Levinson and S. U. Reider, *Clin. Chem. (Winston-Salem, N.C.)*, **20**, 1568 (1974).
(8) J. S. Annino and R. W. Giese, "Clinical Chemistry", Little, Brown & Co., Boston, Mass., 1976, p 306.
(9) K. A. Sterling and M. A. Brenner, *J. Clin. Invest.*, **45**, 153 (1966).
(10) M. Tajuddin and S. G. Elfbaum, *Clin. Chem., (Winston-Salem, N.C.)*, **19**, 109 (1972).
(11) N. N. Nihei, M. C. Gershengorn, T. Mitsuma, L. R. Stringham, A. Cordy, B. Kuchmy, and C. S. Hollander, *Anal. Biochem.*, **43**, 433 (1971).
(12) P. I. Jaakonmäki and J. E. Stouffer, *J. Gas Chromatogr.*, **5**, 303 (1967).
(13) J. E. Stouffer, P. I. Jaakonmäki, and T. J. Wenger, *Biochim. Biophys. Acta*, **127**, 261 (1966).
(14) B. A. Petersen, R. N. Hanson, R. W. Giese, and B. L. Karger, *J. Chromatogr.*, **126**, 503 (1976).
(15) A. Dibbo, J. C. P. Sly, L. Stephenson, T. Walker, W. K. Warburton, and K. D. E. Whiting, *J. Am. Chem. Soc.*, **90**, 2890 (1968).
(16) K. M. Baker, M. S. Shaw, and D. H. Williams, *Chem. Commun.*, 1108 (1969).
(17) E. Gelpi, W. A. Koenig, J. Bilbert, and J. Oro, *J. Chromatogr. Sci.*, **7**, 604 (1969).
(18) A. M. Lawson, D. B. Ramsden, P. J. Raw, and R. Hoffenberg, *Biomed. Mass Spectrom.*, **1**, 374 (1974).
(19) M. M. Bursey, *J. Am. Chem. Soc.*, **91**, 1861 (1969).
(20) M. M. Bursey and M. K. Hoffman, *J. Am. Chem. Soc.*, **91**, 5023 (1969).
(21) D. J. Marshall, B. A. Petersen and P. Vouros, submitted for publication.
(22) B. A. Petersen, R. W. Giese, B. L. Karger, and P. R. Larsen submitted for publication.
(23) J. F. Holland, C. C. Sweely, R. E. Thrush, R. E. Teets, and M. A. Bieber, *Anal. Chem.*, **45**, 308 (1973).

RECEIVED for January 31, 1977. Accepted May 9, 1977. This work was supported by a grant from the National Institutes of Health, (GM 22787).

Determination of Mefruside and Its Metabolites in Urine by High Performance Liquid Chromatography

C. J. Little,* A. D. Dale, D. A. Ord,[1] and T. R. Marten

Roche Products Ltd., P.O. Box 8, Welwyn Garden City, Hertfordshire, United Kingdom

A method is described for packing high performance liquid chromatography (HPLC) columns using isopropanol as the slurry medium. Highly reproducible columns can be made by this technique which applies equally well to reversed phase columns. Chromatographic conditions are described suitable for the analysis of a urine extract of the sulfonamide "Mefruside" and its metabolites. Prior to extraction with ethyl acetate, the urine should be acidified, to convert all of the major metabolite (5-oxo-Mefruside) into its lactone form. The extract is then quantitatively analyzed by an external standardization technique which gives essentially the same result as a radiochemical check method.

Sulfonamide drugs have been important for many years as antibacterial agents. Recently they have been used as antidiabetic and diuretic agents. Of the many and varied methods described for their analysis, chromatography is one of the more specific. Paper and thin-layer chromatography have been used extensively (*1*), as have chromatography on polyamide (*2*), zinc ferrocyanide (*3*), and paper impregnated with strong cation-exchange resins (*4*). Recently, high pressure anion exchange (*5*), reverse phase (*6*), and ion pair partition (*7*) methods have been published for specific sulfonamides.

This paper describes the application of high performance liquid chromatography (HPLC) on silica columns to the analysis of the sulfonamide Mefruside "I" (Ro-8-3725) and its metabolites "II" and "III" (Figure 1).

EXPERIMENTAL

Apparatus. Modular chromatographic equipment was used comprising the following items: (a) Constametric II pump, (b) Rheodyne 7010 injection valve, (c) Cecil CE 212 UV monitor (set at 248 nm). Column packing was performed with a high pressure pump (maximum ~15 000 psig) from Stansted Fluid Power, Stansted, Essex. "Apollo" stainless steel tubing, with a $^1/_2$-μm internal surface finish was used throughout (Accles and Pollock, Oldbury, Warley, Worcestershire, U.K.).

Reagents. All solvents were of analytical reagent (AR) grade and were used without further purification.

Microparticulate silica used in the course of this work was Partisil-5, and was used straight from the bottle.

TLC investigations were carried out on precoated plates (E.M. Merck, Darmstadt—BDH) which were used without activation.

Samples of Mefruside "I" and its metabolites "II" and "III" were obtained from Bayer.

Column Preparation. The balanced density slurry method of packing columns (*8–10*) and several variants of the method (*11, 12*) are now common practice. For several years we have slurried silica and bonded silicas in alcohol mixtures which rapidly wet the silica surface. Initially we used methanol but now use iso-

[1] Present address, Spectra-Physics Ltd., 17 Brick Knoll Park, St. Albans, Hertfordshire, U.K.

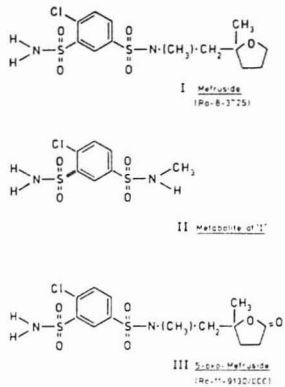

Figure 1. Chemical structures of Mefruside and two of its metabolites

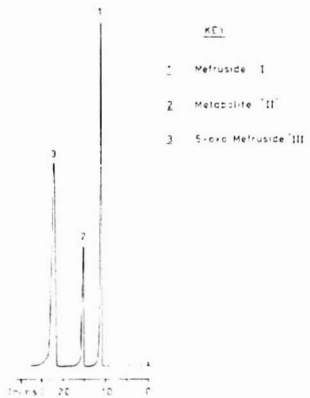

Figure 2. Chromatogram of sulfonamides. Column, Lichrosorb SI 60—5 μm (50 cm), eluent, hexane + ethyl acetate (1:1); flow rate, 1.5 mL/min

propanol which produces a more stable slurry. The slurry was introduced into a column precolumn assembly via a long hypodermic needle. Methanol was then pumped through the column. All columns reported in this paper were packed by this method at 7.5000 psig for 30 min. For convenience and economy the slurry composition was adjusted such that a minimum of support was left in the precolumn after the column has been packed.

The reliability of this method can be judged from the fact that during 1976, some 70 columns (some of which were reversed phase columns) were packed in this manner, all of which were of a similar standard. We feel that this reliability of packing is in no small way attributable to the mirror finished "Apollo" tubing that was used.

Further modification of the slurry can be achieved by the addition of a few percent of glycerol. Using this technique, even 40-μm particles can be slurry packed with ease.

Procedure. Examination of the sulfonamides I–III by TLC suggested the use of ethyl acetate + hexane (1:1) as eluent. Transference of this procedure to the column was relatively easy, a typical chromatogram being illustrated in Figure 2. Optimization of flow rate was readily deduced from the flow dependence of the Height Equivalent to a Theoretical Plate (HETP) as shown in Figure 3.

Obviously, maximum efficiency for all solutes in the mixture occurs at a flow rate of about 0.4 mL/min. In practice one has

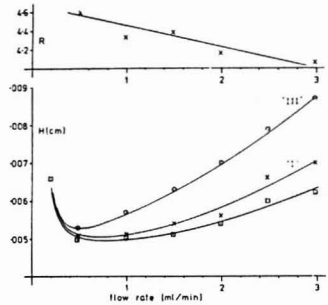

Figure 3. Flow dependence of column efficiency "H" (lower) and resolution "R" (upper). In the upper figure "R" is between the sulfonamide I and III and was calculated from $R = 2\Delta t/(W_1 + W_3)$. Conditions as for Figure 2

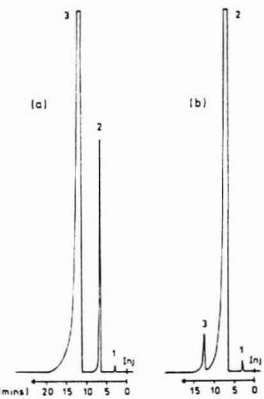

Figure 4. Chromatogram of sulfonamides (trace levels). Column, as in Figure 2, eluent, hexane + ethyl acetate (1:1); flow rate, 2 mL/min. Compounds separated are (*a*) 0.1% I (peak 2) in III (peak 3) and (*b*) 0.1% III (peak 3) in I (peak 2)

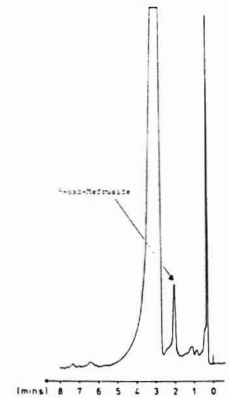

Figure 5. Chromatogram of urine extract. Column, Partisil 5 (25 cm); eluent, hexane + ethyl acetate (1:1); flow rate, 2 mL/min

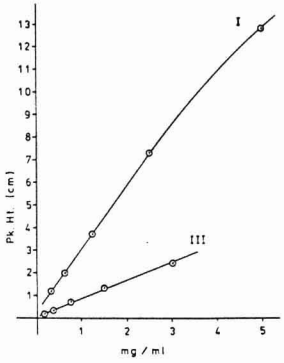

Figure 6. Calibration curves for Mefruside I and 5-oxo-Mefruside III

to compromise between loss of efficiency and decrease in analysis time. It can be seen from the superimposed plot of Resolution "(R)" between I and III vs. flow rate (Figure 3a) that very little resolution is lost if the flow rate is increased beyond the optimum value, resulting in a desirable decrease in analysis time while still preserving adequate resolution.

In biological systems there is often the need to detect traces of unchanged drug in the presence of large quantities of its metabolite and vice versa. The chromatographic system described is compatible with these requirements (Figure 4).

To evaluate this methodology for real samples, a human volunteer was given an oral therapeutic dose of ^{14}C-labeled Mefruside (18.9 μCi per 26 mg). Urine was collected from the volunteer and extracted in the following way.

Urine (10 mL) was adjusted to pH 2 with dilute hydrochloric acid. This was necessary to convert any ring opened metabolite back to the lactone as in Figure 1. The acidified sample was left for at least 30 min to allow for complete lactone formation. The urine was then extracted with ethyl acetate (3 × 10 mL) and the organic phase was blown to dryness under a stream of nitrogen. The residue was redissolved in ethyl acetate (3.0 mL) and analyzed by the method previously described. The chromatography of the biological extract is shown in Figure 5. The analysis was also performed radiochemically as a check procedure.

RESULTS

Quantitation of the chromatography was achieved by an external calibration method. Linear calibration curves (Figure 6) were achieved over the concentration range investigated (0–3 mg/mL).

The results achieved by the chromatographic method showed the presence of 27 μg 5-oxo-Mefruside per 10 mL urine whereas the radiochemical method indicated 30 μg 5-oxo-Mefruside per 10 mL urine. This is very good agreement, particularly when it is realized that the radiochemical method is known to include about 10% of minor radioactive metabolites other than 5-oxo-Mefruside. No interference was observed from paracetamol, an increasingly common analgesic which often interferes with the analysis of biological extracts.

LITERATURE CITED

(1) J. P. Comer and I. Comer, *J. Pharm. Sci.*, **56**, 413 (1967).
(2) Y-T. Lin, K-T. Wang, and T-I. Yang, *J. Chromatogr.*, **20**, 610 (1965).
(3) A. G. Fogg and R. Wood, *J. Chromatogr.*, **20**, 613 (1965).
(4) D. J. Pietrzyk and E. Chan-Santos, *J. Chromatogr.*, **87**, 543 (1973).
(5) T. C. Kram, *J. Pharm. Sci.*, **61**, 254 (1972).
(6) L. D. Bighley and J. P. McDonnell, *J. Pharm. Sci.*, **64**, 1549 (1975).
(7) S. C. Su, A. V. Hartkopf, and B. L. Karger, *J. Chromatogr.*, **119**, 523 (1976).
(8) R. E. Majors, *Anal. Chem.*, **44**, 1722 (1972).
(9) B. Coq, C. Gonnet, and J. L. Rocca, *J. Chromatogr.*, **106**, 249 (1975).
(10) P. J. N. Webber and E. H. McKerrell, *J. Chromatogr.*, **122**, 243 (1976).
(11) J. J. Kirkland, *J. Chromatogr.*, **125**, 231 (1976).
(12) H. R. Linder, H. P. Keller, and R. W. Frei, *J. Chromatogr. Sci.*, **17**, 234 (1976).

RECEIVED for review September 27, 1976. Accepted April 20, 1977.

Determination of Selenium in Blood Serum by Proton-Induced X-ray Emission

Marina Berti, Giampaolo Buso, Paolo Colautti, Giuliano Moschini,* Bianca Maria Stievano, and Cristina Tregnaghi

Laboratori Nazionali dell' Istituto Nazionale di Fisica Nucleare, Via Romea n. 4, 35020 Legnaro (Padova), Italy

Selenium determination in blood serum has been tested for thick (dry-ashed) samples using x-ray emission spectra induced by 1.8- to 4-MeV proton beams. For quantitative analysis the internal standard method has been used. This paper presents the procedure and evaluations of the sample preparation and analysis. The statistical counting error is as low as 6% and the sensitivity ≤10 ppb for 100-min counts with 1.8-MeV protons and for 30-min counts with 4-MeV protons.

A detailed review about the biological role of selenium has recently been carried out by R. F. Burk, O. A. Levander, H. E. Ganther et al. (*1–3*). In particular, some authors (*4–7*) pointed out the importance of measuring the levels of this element in whole blood and blood serum.

In this paper, a method for the analysis of selenium in blood serum samples by proton-induced x-ray emission is described. The advantage of proton excitation has been widely discussed (*8, 9*). This technique permits realization of the required sensitivity (≤10 ppb) without chemical preconcentration (*10*).

EXPERIMENTAL

Apparatus. The x-ray spectra were induced by 1.8- to 4-MeV proton beams ~2 mm in diameter from the AN-2000 and CN Van de Graaff accelerators (High Voltage Engineering Corporation) installed at National Laboratories of Legnaro. Figure 1 shows the bombardment chamber and irradiation and detection geometry.

A Si(Li) detector with an effective area of 30 mm^2 and with a detection solid angle of 0.007·4π steradians was used to detect the x-rays. The overall resolution of the standard electronic chain,

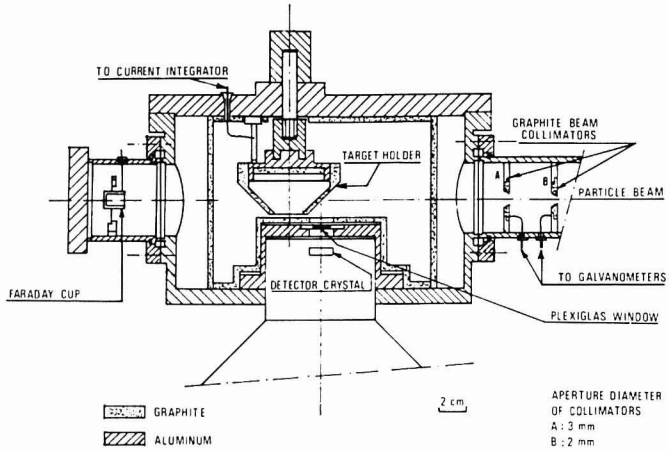

Figure 1. Bombardment chamber

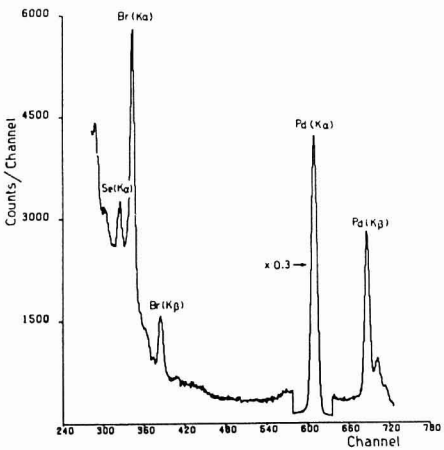

Figure 2. Portion of spectrum from a typical doped (100 ppm palladium) serum specimen: 1.8-MeV, 250-nA proton beam for 100 min

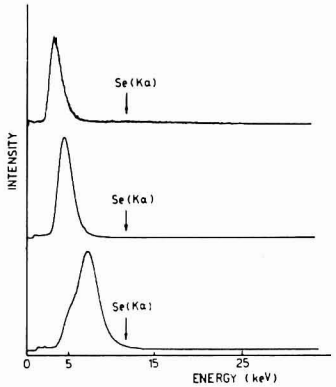

Figure 3. Bremsstrahlung spectra of graphite blanks at proton-beam energy 1.8 MeV (top), 3 MeV (middle), 4 MeV (bottom). At 4 MeV, there is a considerable increase of the bremsstrahlung background under the Se Ka peak

including a pile-up rejector, was 165 eV (FWHM at 5.9 KeV). Data were collected in a 1024-channel pulse height analyzer and processed by computer.

Target Preparation. Palladium was chosen as internal standard (*11*) for the determination of selenium. The targets were prepared in the following way: 1.2 cm^3 of blood serum were doped with 100 ppm Pd as $PdCl_2$. Serum and internal standard were ultrasonically mixed, dry-ashed in borosilicate glass beakers for about 1 h at 60 °C, ground into a fine powder using an agate mortar and then thoroughly mixed with 20% of nuclear graphite powder.

A self-supporting pellet was prepared from this mixture by pressing at 4×10^3 kg/cm^2 into a suitable die. The resulting pellets are 12 mm in diameter and have area density 55–60 mg/cm^2, which constitutes infinite thickness for protons in our energy range. By varying the graphite concentration in the mixture, it was found that about 20% allows the pellets to withstand the beam heating for the time necessary to reach the required sensitivity (see Discussion).

The pellets were inserted into a four-position target holder (Figure 1) and then irradiated.

RESULTS AND DISCUSSION

In Figures 2 and 3 are shown a portion of a typical serum spectrum involving selenium and palladium peaks, and bremsstrahlung spectra obtained at 1.8, 3, and 4 MeV from graphite blanks. The preparation and analysis stages were carefully checked. It has been tested and found that neither selenium nor palladium losses take place during storage (Figure 4b), dry-ashing (Figure 4c), and proton irradiation (Figure 4d, e). The target reproducibility was tested by measuring the Se/Pd yield both in different points of the same target (Figure 4a) and in a lot of targets. The standard deviation of Se/Pd yield in 14 pellets from the same serum, with 50.0 ppb mean selenium concentration, was 5.9%. Each experimental point in Figure 4 is the average of at least two measurements; the reported errors, due to counting statistics, are less than 10%.

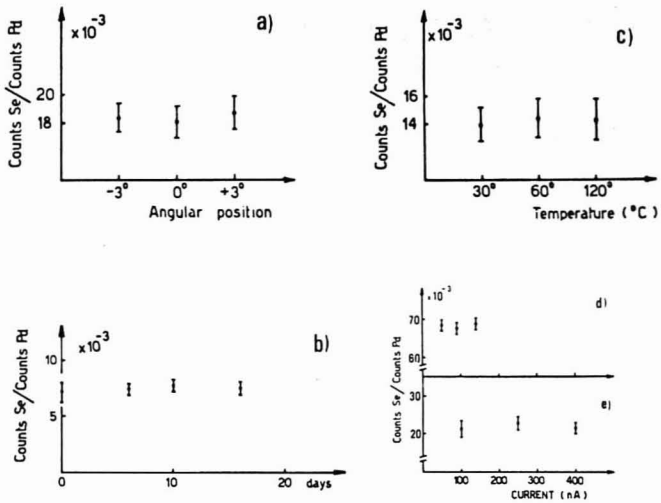

Figure 4. Se/Pd counts vs.: (a) angular position of the target holder; (b) storage time in polyethylene vials at −20 °C. The same results were obtained in Teflon vials; (c) dry-ashing temperature; (d,e) beam current at 4 and 1.8 MeV, respectively

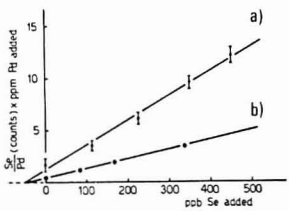

Figure 5. Se/Pd detection efficiency determination at 1.8 MeV (a) and 4 MeV (b). At 4 MeV, the errors are within the dot dimensions. Weighted least squares analysis of the data ($y = bx + a$): at 4 MeV, $b = 0.008$; $a = 0.44$; correlation coefficient = 0.999; at 1.8 MeV, $b = 0.023$; $a = 1.20$; correlation coefficient = 0.989

The working conditions chosen were 60 °C ashing temperature and proton beams at 1.8 MeV, 250 nA, and 3–4 MeV, 80–100 nA. Above these beam currents, the targets were quickly damaged.

The detection efficiency of Se relative to Pd, used to convert observed x-ray intensities to Se concentrations, was obtained from serum samples doped with 100 ppm Pd and increasing concentration of Se. Figure 5 shows the results at 1.8 and 4 MeV; the Plexiglas window thickness was 70 μm and 300 μm, respectively (Figure 1). The errors on the relative detection efficiency, i.e., on the slope of the straight lines (a) and (b) of Figure 5, were 8.6% and 2.5%. It is easy to reduce this error to an insignificant portion of the total error, with longer irradiation time. The original selenium concentration in the sample can be deduced also from the weighted least-squares fit of the data in Figure 5; this is a more precise but time-consuming method. At 4 MeV, for example, we obtained (55.0 ± 3.6) ppb Se.

Good measurement precision requires a compromise among good counting statistics, limitation of the beam current, and reasonable data collection time. Typically in a serum sample with 50 ppb Se, 2500–3000 counts in the selenium peak with a statistical error of ~6% were obtained at 1.8 MeV with 250 nA in 100 min, at 4 MeV with 90 nA in 30 min. The sensitivity for selenium was ≤10 ppb, using the conventional criterion that the minimum peak area is twice the standard deviation of the background under the peak. This sensitivity is adequate to measure selenium whose typical concentrations in blood serum range from 20 to 100 ppb.

LITERATURE CITED

(1) R. F. Burk, "Trace Elements in Human Health and Disease", Vol. II, Academic Press, New York, 1976, p 105.
(2) O. A. Levander, Ref. 1, p 135.
(3) H. E. Ganther, D. G. Hafeman, R. A. Lawrence, R. E. Serfass, and W. G. Hoekstra, Ref. 1, p 165.
(4) R. Cellerino, G. C. Guidi, G. Moschini, G. Perona, B. M. Stievano, and C. Tregnaghi, *Scand. J. Haematol.*, in press.
(5) I. Lombeck, K. Kasperek, L. E. Feinendegen, and H. J. Bremer, *Clin. Chim. Acta*, **64**, 57 (1975).
(6) W. L. Broghamer, K. P. McConnell, and A. L. Blotcky, *Cancer*, **37**, 1384 (1976).
(7) K. P. McConnell, W. L. Broghamer, A. J. Blotcky, and O. J. Hurt, *J. Nutr.*, **105**, 1026 (1975).
(8) F. Folkmann, C. Gaarde, T. Huus, and K. Kemp, *Nucl. Instrum. Methods*, **116**, 487 (1974).
(9) J. A. Cooper, *Nucl. Instrum. Methods*, **106**, 525 (1973).
(10) K. I. Strausz, J. T. Purdham, and O. P. Strausz, *Anal. Chem.*, **47**, 2032 (1975).
(11) V. Valković, R. B. Liebert, T. Zabel, H. T. Larson, D. Milјanič, R. M. Wheeler, and G. C. Phillips, *Nucl. Instrum. Methods*, **114**, 573 (1974).

RECEIVED for review March 8, 1977. Accepted May 3, 1977. Work supported by Istituto Nazionale di Fisica Nucleare (I.N.F.N.).

Optical Multichannel Analyzer for Characterization of Fluorescent Liquid Chromatographic Petroleum Fractions

J. R. Jadamec and W. A. Saner*

U.S. Coast Guard Research and Development Center, Avery Point, Groton, Connecticut 06340

Y. Talmi

Princeton Applied Research Corporation, P.O. Box 2565, Princeton, New Jersey 08540

The continuous, real time, acquisition of fluorescence emission spectra of eluting petroleum oil fractions, separated by high pressure liquid chromatography, was accomplished using an Optical Multichannel Analyzer (OMA) TV-type detector coupled to a spectrofluorometer. A complete readout (frame scan) of the detector target is achieved every 32 ms. The spectral region simultaneously monitored by the detector ("spectral window") may be varied depending on the spectral characteristics of the eluting fraction. The spectral response of the Optical Multichannel Analyzer detector covers the entire 190–900 nm region. However, in this study the spectral window covered the 290–400 nm range only.

The widespread use of fluorescence spectrometric techniques for the identification of polynuclear aromatics derived from petroleum oils has been summarized by Popl (*1*). McKay and Latham (*2*) and Lloyd (*3, 4*) used fluorescence spectrometry (emission and excitation) to characterize hand-collected fractions of petroleum oils separated by gel-permeation and straight phase liquid-chromatography. All collected chromatographic bands were analyzed by conventional fluorescence spectrometric techniques.

The use of rapid scanning spectrometers (RSS) equipped with flow cells in place of stop-flow solution drive mechanisms are potentially very useful not only as detectors for liquid chromatography, but primarily as spectral scanners of eluting peaks during an actual chromatographic analysis. Applications of the RSS for scanning absorption in the ultraviolet and visible regions have been primarily limited to recording spectral changes resulting from biochemical and electrochemical reactions or chemical reaction kinetics. Wightman's work (*5*) provides a noteworthy example of a computer-controlled RSS application in anion protonation studies. Only recently has the RSS (silicon vidicon) been applied as an absorption detector for ion-exchange chromatography (*6*).

This paper reports the preliminary evaluation of a silicon-intensified target (SIT), electronic imager (*7*), as a multichannel spectrofluorometer detector for liquid chromatography. The SIT, controlled by the Optical Multichannel Analyzer (OMA), was specifically tested for its capability to simultaneously monitor the fluorescence emission spectra of petroleum derived polyaromatics during their elution from a liquid chromatographic column. Petroleum samples were studied in an attempt to augment fingerprinting techniques for oil spill identification. The optical-fiber faceplate of the SIT was coated with a very efficient UV-to-visible scintillator (*8*) that extended the spectral response of the detector far into the vacuum UV region. The development of an efficient UV scintillator was necessary since many aromatic compounds, present in petroleum oils, have major fluorescence emissions in the 280–400 nm spectral range.

EXPERIMENTAL

Liquid Chromatograph. Waters Associates Model 660 Solvent Programmer, two Model 6000A pumps, and a Model U6K injector were interfaced with a Waters Associates 440 Absorbance Detector, equipped with dual channel UV detection. Column effluent was first monitored at 254 nm (both channels, but at different sensitivities) prior to passage through a 10-μL flow cell mounted in a Farrand Spectrofluorometer. All chromatographic separations were performed on a 0.64 × 30 cm column packed with Waters μBondapack C_{18}. Teflon tubing (0.012-inch i.d. × 4-inch) connected the spectrofluorometric flow cell to the end of the stainless steel tubing (0.009-inch i.d.). Two Perkin-Elmer Model 56 recorders were used, one on each detector channel. The column was maintained isothermally by means of a column heater block connected to a Haake Water Bath, Model FE. Samples were injected using side-port Auto Sampler Syringes (Precision Sampling Corp.)

Spectrofluorometer–OMA. A Princeton Applied Research Corporation (PARC) Optical Multichannel Analyzer (Model 1205A) controlling a SIT detector (PARC Model 1205D) was interfaced with a Farrand Optical Mark I Spectrofluorometer. The standard 28 000 grooves per inch grating in the emission monochromator was replaced with a 14 000 grooves per inch grating in order to double the simultaneous spectral coverage of the detector, to 110 nm. The emission monochromator was converted into a polychromator via the use of a folding mirror that diverts the diffracted light from the exit slit toward the SIT faceplate (vertically mounted exactly at the focal plane of that polychromator). The emission spectra are detected on the target of the SIT (12.5 mm long and 5 mm wide, which is electronically divided into 500 detection channels) and can be stored (for 32 ms) much like a photographic emulsion, but in a ready-to-process digitized form. The OMA console allows the use of the SIT in either the real time or the accumulation mode. Signal averaging is performed by accumulating many scans (32 ms each) in memory. Fluctuations due to random noise, average towards zero. Weak signals accumulate in each scan and are thus pulled from the background (multiplex advantage).

A Tektronix 604 CRT display was used as a real-time output device. Fluorescence spectra were either photographed from the CRT screen or recorded (from the memory) on a strip chart.

Reagents. De-ionized, glass distilled water and spectroquality methanol (MCBMX 475) were used as the mobile phase in the liquid chromatograph. The solvents were not degassed, but were filtered using 0.22-μm pore diameter Millipore filters (GSWPO 4700) for water and 0.22-μm pore diameter Fluoropore filters (FHOPO 4700) for methanol. The aromatic standards were obtained from Duke Standards Co., Palo Alto, Calif.; solutions of the standards were prepared in spectroquality methanol (MCBMX 475). Glacial acetic acid (reagent grade) was used to acidify methanol to prepare the oil extracting solution (0.4% acid in methanol).

Sample Preparation. Petroleum oils were extracted with acidified methanol after drying, according to a procedure previously described (*9*). The extracts were not concentrated prior to introduction to the column; injection volumes were varied (from

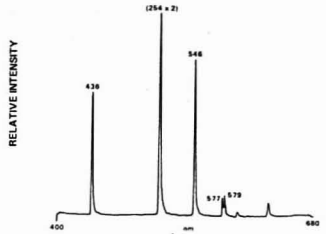

Figure 1. OMA spectral resolution. Hg–arc pen-ray light source, 1-s signal accumulation time

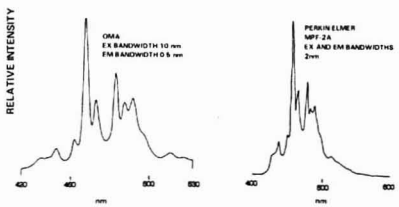

Figure 2. Fluorescence emission spectra of Ovalene (plastic std) Ex λ 350 nm

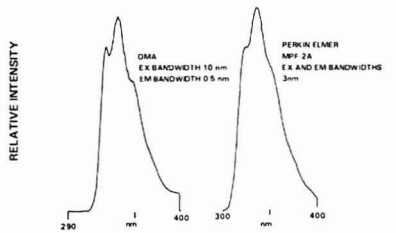

Figure 3. Fluorescence emission spectra of *p*-terphenyl (plastic std) Ex λ 300 nm

2.5 to 75 μL) in order to counter the effects of weathering (loss of the polyaromatic fraction by oxidation and solution, i.e. natural environmental weathering processes).

Separation Procedure. Samples were chromatographed using a gradient from 50/50 methanol in water to 100% methanol (linear increase) in 50 min, at a flow rate of 1 mL/min (≃700 psig). Column temperature was held constant at 60 °C. The chromatograph was allowed to pump 100% methanol for 20 min after completion of the gradient to ensure that all oil components were eluted. The column was regenerated by using a reverse gradient (100% to 50% methanol in water) for 3 min and equilibrated by pumping the initial gradient composition for an additional 23 min before the next injection.

RESULTS AND DISCUSSION

Spectral Resolution of the OMA and Comparison of Flow Cells to Standard Cuvettes. Figure 1 shows a typical OMA response (400–680 nm) to a mercury pen-ray light source. The OMA was coupled to a JACO 0.3-m Ebert mounting polychrometer, PARC Model 1208 with a 150 grooves per mm grating blazed at 500 nm. With a simultaneous spectral coverage of 280 nm, the system has sufficient spectral resolution to clearly distinguish the 577–579 nm Hg doublet (Each OMA channel, approximately, spans 0.56 nm). The OMA was allowed to accumulate signal for 1 s (32 scans) before the spectrum was recorded.

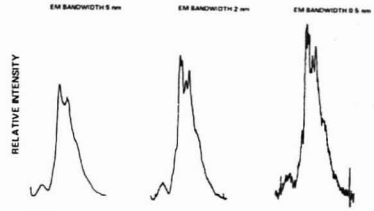

Figure 4. Fluorescence emission spectra of 320 ppb naphthalene in methanol: 1-cm cuvette, Ex λ 270 nm, Em λ 290–400 nm, 100 (A – B) OMA accumulations

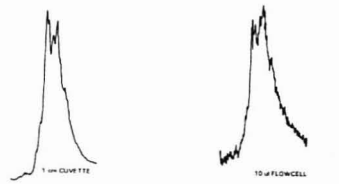

Figure 5. Comparison of fluorescence spectra from a standard cuvette and a flow cell of 2 ppm naphthalene in methanol: 100 (A – B) OMA accumulations, Em bandwidth 0.5 nm

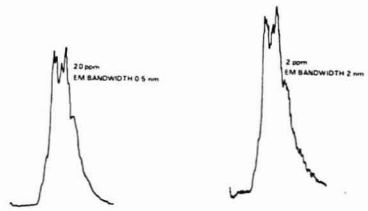

Figure 6. Fluorescence emission spectra of naphthalene at different concentrations in the flow cell: 100 (A – B) OMA accumulations

Figures 2 and 3 compare emission spectra of plastic fluorescence standards (Starna Ltd., London) that were detected by the OMA and a Perkin-Elmer MPF-2A Spectrofluorometer (photomultiplier tube detector). Both OMA spectra represent an integrated signal of 10 consecutive scans (0.32 s). The spectra were recorded in the (OMA) A – B mode where the digitized background accumulated in memory B is subtracted from the digitized raw spectra accumulated in memory A.

The emission spectrum of naphthalene (320 ppb) in methanol in a standard 1-cm cuvette at varying emission bandwidths is shown in Figure 4. An upper time limit of 3 s (100 scans) was imposed on the OMA signal accumulation time. Since liquid chromatographic bands with minimal resolution allowed only 15–20 s between peak maxima, 3 s was nominally set as an upper time limit for scanning so that fluorescence emission spectra could be obtained sufficiently fast to preclude the need to stop-flow. Loss of spectral resolution is evidenced at the 5-nm emission bandwidth setting.

Figure 5 compares the 3-s accumulated spectra of a 2-ppm naphthalene solution in a 10-μL flow-cell and in a standard 1-cm cuvette. The reversal of the two major peak ratios in the flow-cell spectrum is a result of optical distortion, while the decrease in signal-to-noise is a result of decreased flow-cell optical efficiency (increased light dispersion) and also lower fluorescence intensity due to a decrease in pathlength.

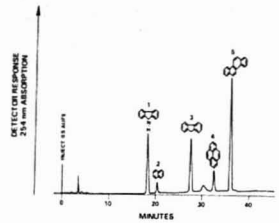

Figure 7. Liquid chromatogram of aromatic standards

Figure 6 illustrates the effect of emission bandwidth on signal-to-noise ratio and spectral resolution. It is clear that a very small loss of resolution, if any, occurred as a result of widening the bandwidth from 0.5 to 2 nm. Nevertheless, to avoid any potential slit limitation on spectral resolution, the narrowest possible slit (0.5 nm) was used.

Aromatic Standards—Chromatographic Separation, OMA Identification. The gradient-elution chromatogram of a mixture of five aromatic hydrocarbon standards is shown in Figure 7. Each numbered peak represents 440 ng of standard introduced onto the column. The band eluting between peaks 3 and 4 is due to contamination of the distilled water. This unintended extraction (trace enrichment) occurred primarily during column equilibration of 50% methanol in water, but also during the actual chromatographic separation over the gradient range from 50 to 80% methanol in water. For methanol concentrations greater than 80%, the impurities from water were not retained on the column. Since the contamination did not fluoresce, it caused no interference with the OMA response, and no attempt was made to remove it.

Figure 8 shows the five fluorescence emission spectra (ex. λ 270 nm, excitation bandwidth 10 nm, emission bandwidth 2 nm) corresponding to the five peaks in Figure 7. Each spectrum represents an OMA accumulation of 92 scans. The spectra were recorded by photographing the CRT display.

Spectral response time dependency is shown in Figure 9, where consecutive fluorescence spectra of fluorene were recorded every 5 s, during its elution from the column into a 10-μL flow-cell (flow rate of 1 mL/min).

Since the OMA was operating in the real time mode (30 scans/s) and the shutter speed of the scope camera, used for recording the CRT display, was only $^1/_{15}$ s (and unsynchronized with the OMA scan) each spectrum shown in Figure 9 actually comprises two separate (and consecutive) real time spectra superimposed on one another. Because the spectral response changed with time (elution), this double-frame superimposition meant a slight deterioration in image fidelity.

[A much more powerful and accurate data acquisition, of time dependent spectral information, can be accomplished by interfacing the OMA to a digital magnetic tape formatter (such as Kennedy Model 9232). Such a system is capable of a real-time recording of about 20 000 OMA spectra (500 channels every 32 ms) within 10–12 min.]

Liquid Chromatographic Separation of a Petroleum Extract and OMA Response to Eluting Fractions. Figure 10 is the chromatogram of the methanol extract of a #2 fuel oil supplied in an interlaboratory collaborative study of oil spill identification methods. The fluorescence emission spectra of the numbered peaks are shown in Figure 11. Reproducibility of the fluorescence spectra is shown by duplicate spectra taken from a second chromatographic separation of the sample. All spectra were obtained by accumulation of 92 consecutive scans. The spectra were recorded on a Farrand Model 100 stripchart recorder using the fastest OMA plot time (16 s). Intermediate fractions were avoided in order to increase purity of outside fractions with marginal chromatographic resolution. Although only a few compounds as yet have been positively identified by means of their OMA spectra, a substantial number of *p*-terphenyls are suspected of being present (fractions 14, 19, and 20), on the basis of spectral similarities to a *p*-terphenyl standard and published data.

In fact, the identification of eluting compounds from petroleum oils was not our primary concern. Rather, any peak identifications were incidental to comparisons of corresponding OMA spectra of liquid chromatographic fractions from oil spill and source samples. Although it was realized that fluorescence does not always distinguish between members of homologous series, or parent aromatics from alkylated derivatives, it was felt that chromatographic retention time differences should spacially separate any nondiscriminatory fluorescence spectra sufficiently to eliminate confusion. Similarly, when chromatographic retention time differences were negligible for two compounds, it was felt that comparisons of their fluorescence spectra would allow their differentiation. An example of this latter case is discussed below.

Fractions 17 and 18 show very dissimilar, yet reproducible spectra for compounds with very minimal chromatographic

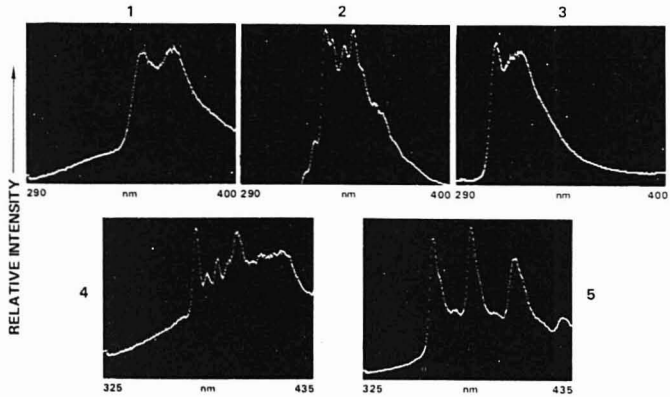

Figure 8. CRT screen photographs of spectra (92 OMA scans) of aromatic standards taken during elution (Ex bandwidth 10 nm, Em bandwidth 2 nm, Ex λ 270 nm)

Table I. Retention Time Reproducibility of Major Peaks from an Oil-Methanol Extract

Peak	Run 89	Run 81	Run 90	Run 75	Run 61	Run 86	$\bar{x}$	Var.	Std dev
a	15.4	15.6	15.8	15.8	16.2	15.4	15.7	0.077	0.277
b	17.3	18.0	17.7	17.8	18.1	17.4	17.72	0.085	0.291
1	19.4	20.4	19.8	19.8	20.4	19.6	19.9	0.143	0.379
3	21.0	22.0	21.3	21.4	22.0	21.1	21.47	0.159	0.399
4	22.1	23.0	22.4	22.4	23.2	22.2	22.55	0.166	0.407
c	23.4	25.3	23.7	23.9	24.5	23.4	24.03	0.459	0.677
9	27.0	28.4	27.1	27.2	27.8	——	27.5	0.28	0.529
13	30.1	30.9	30.0	29.8	——	——	30.2	0.175	0.418
19	33.8	34.4	33.6	33.4	34.1	——	33.86	0.126	0.356
21	36.6	36.9	36.2	36.2	36.7	——	36.52	0.076	0.279
28	39.4	39.6	39.1	39.0	39.4	——	39.3	0.048	0.219
29	39.8	40.0	39.4	39.4	39.7	——	39.66	0.054	0.233
32	42.0	42.1	41.8	41.6	41.9	——	41.88	0.030	0.172

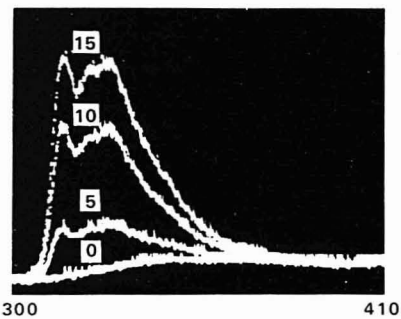

Figure 9. Multiple exposure photograph of the CRT screen, at indicated elution time intervals, of the fluorene peak (real time monitoring). Each exposure represents two separate OMA scans and displays

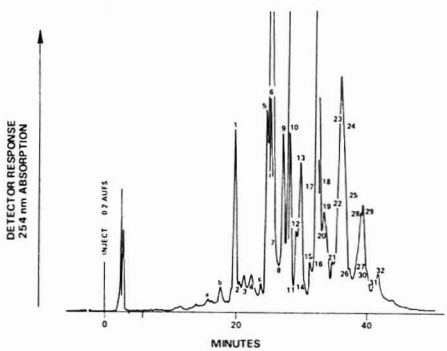

Figure 10. Liquid chromatogram of #2 fuel oil (sample 1)

separation. Fractions 15 and 16 and 19 and 20 are also examples of distinct and reproducible spectra for compounds with minimal chromatographic separation.

Fraction 6, taken on a peak maximum, shows a fluorescence spectrum different from fractions 6a and 7. Fraction 6a, taken between fractions 6 and 7, was sampled in order to observe a transition spectrum. Although no discernible slope changes are evident from the UV absorption chromatogram, the OMA spectra indicate the presence of other compounds "buried" in the downslope of fraction 6.

The capability of the OMA to distinguish a compound present in the unresolved envelope is evident in fraction 8.

Table II. Retention Time Reproducibility of Major Peaks from a Five-Component Aromatic Standard Mixture

Run No.	Peak 1	Peak 2	Peak 3	Peak 4	Peak 5
69	17.40	19.60	27.30	32.28	35.60
51	18.20	20.30	27.70	32.60	36.50
70	17.80	20.20	27.60	32.80	36.20
53	18.00	20.20	27.60	32.70	36.30
54	17.80	20.10	27.48	32.40	35.90
87	18.24	20.30	27.46	32.40	35.80
74	17.20	19.60	26.90	31.90	35.20
73	17.58	19.68	26.96	32.00	35.28
Mean	17.78	20.00	27.38	32.39	35.85
Var.	0.120	0.087	0.079	0.089	0.195
Std dev	0.346	0.294	0.280	0.298	0.442

The OMA spectrum taken in a chromatographic "valley" has the spectral characteristics of acenaphthene (*10*).

Since the triggering of the OMA (start of accumulation) was done manually (based on recorder pen slope changes on the UV absorption detector), duplication of the various data acquisition points for the OMA was not absolutely reproducible (especially for rapid slope changes and minimally distinguishable absorption variations).

This timing problem is clearly evidenced in the duplication of the spectrum corresponding to fraction 8. The fact that some spectral characteristics of fraction 7 are evident in that duplicate (8) suggests that it was acquired too early.

Fractions 22 through 25 comprised a single, large compound peak on the UV chromatogram which was indicated by multiple slope changes. Intermediate fractions 22a and 23a were intentionally recorded from the OMA at non-optimal times in order to observe spectral composites of more than one compound and transition spectra midway between spectra of much higher purity. Spectrum 22a, taken during a slope change, shows spectral characteristics similar to fraction 23; fluorescing bands located at the same wavelengths are indicated by letter. Spectrum 23a was taken just prior to spectrum 24; overall spectral characteristics between 23a and 24 are very similar, although 23a shows less resolution than 24. (This situation is similar to the decreased resolution in the duplication of fraction 8.)

Retention Time Reproducibility. Different extracts of the #2 fuel oil whose chromatogram is shown in Figure 10 were chromatographed by two different individuals over a 16-day time frame. Retention time data for major peaks indicated in Figure 10 are summarized in Table I. Table II lists retention time data for the five aromatic standards (Figure 7). While retention time variability decreases for aromatic standards eluting from 17 to 27 min, variations increase for standards eluting from 22 to 36 min. On the other hand, variability in retention time for oil components increases over

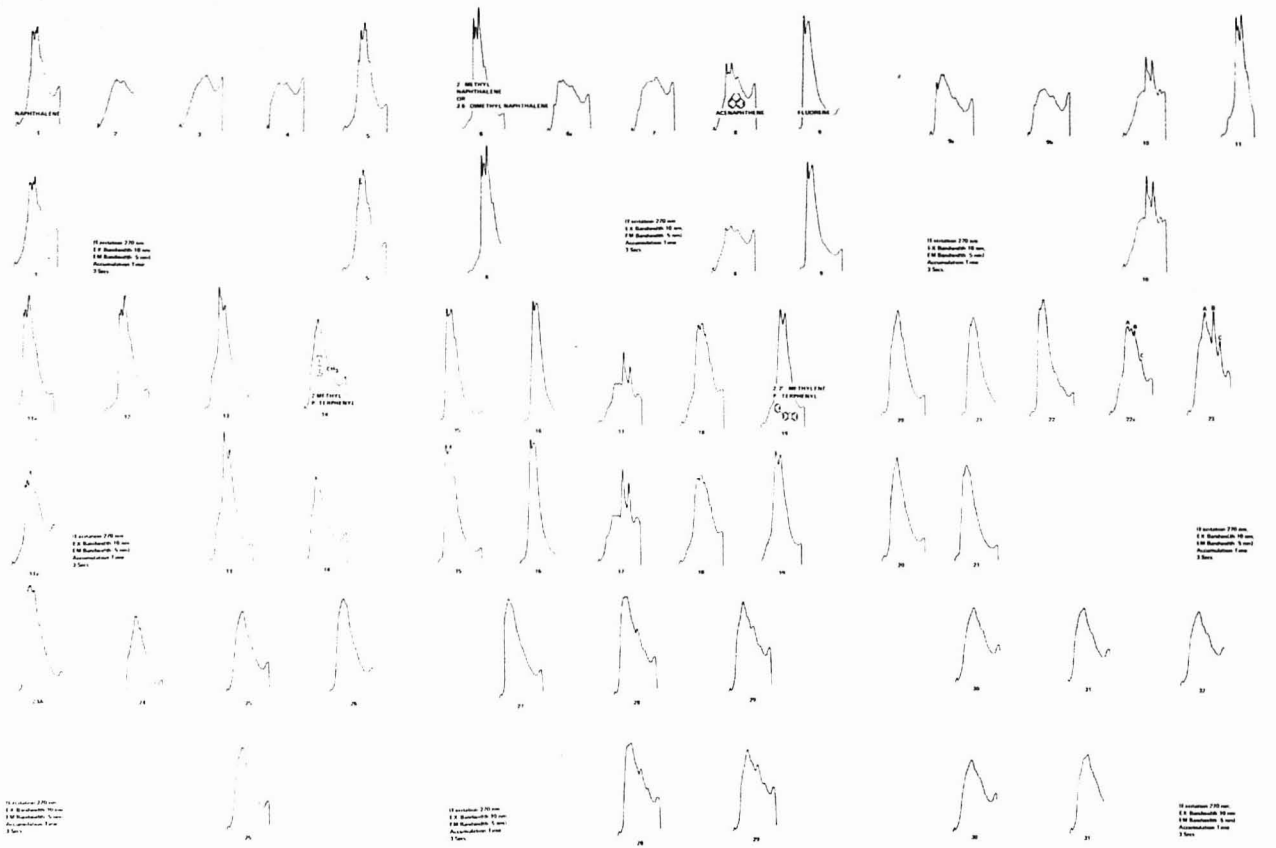

Figure 11. Fluorescence emission spectra (290–400 nm, 92 OMA scans each) of liquid chromatographic oil fractions taken during elution

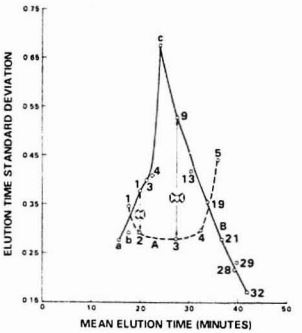

Figure 12. Retention time reproducibility for aromatic standards (A) and oil components (B)

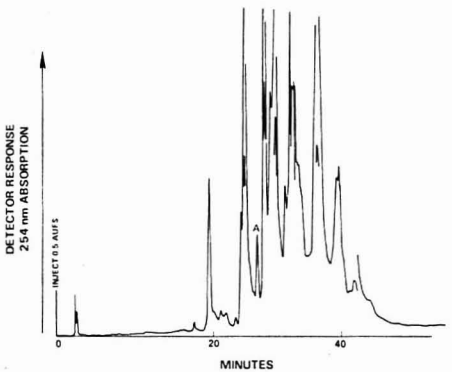

Figure 13. Liquid chromatogram of #2 fuel oil (sample 2)

the elution range of 16 to 24 min and decreases after 25 min.

Figure 12 plots standard deviations vs. mean retention time for the five aromatic standards and for indicated oil peaks. Naphthalene and fluorene (peaks 1 and 9 from the oil; peaks 2 and 3 from the standards, respectively) are common to both mixtures. Both compounds were identified in the oil sample on the basis of their spectral (fluorescence) similarity to the standard compounds as well as by comparison of their spectra to that of published data (*10*). Although the mean retention times of these two compounds in both mixtures is comparable (within 0.1 min), the retention time variances were substantially higher with the complex oil mixture.

It is primarily this enhanced retention time variability that renders the identification of chromatographic bands, on the basis of retention time values alone, somewhat tenuous. This fact is illustrated in the following example. Figure 13 shows the chromatogram of a second #2 fuel oil supplied in an interlaboratory oil spill testing program. The labeled component in Figure 13 is eluted within 0.2 min of peak #9 (fluorene) in Figure 10. Since the standard deviation of the retention time for fluorene in fuel oil samples was 0.53 min, previously calculated, it is obvious that based on retention time values alone, the unknown labeled component in Figure 13 could be identified falsely as fluorene.

Figure 14 shows CRT screen photographs of fluorene (A) and of the unknown spectrum (B), labeled peak A in Figure 13, as very similar but not identical to that of fluorene. The

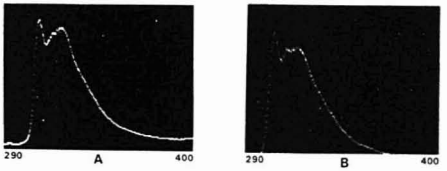

Figure 14. CRT screen photographs of spectra (92 OMA scans) of fluorene (A) and 1-methyl fluorene (B) taken during elution

unknown spectrum, did however match very well with the published spectrum of 1-methyl fluorene (*11*). The presence of this fluorene homologue, intrinsic to only one of these #2 fuel oils, is indicative of two distinct oils, even though this may be the only fraction out of 30 or more which is, in fact, different.

FUTURE OUTLOOK

Although this report has clearly demonstrated the practical use of the OMA as a molecular fluorescence multichannel detector for liquid chromatography, it is in our opinion merely a scratching of the surface. When interfaced to a computer, the system could generate, very rapidly, essential information concerning both the excitation and emission spectra of each eluted component.

Retaining (in the computer's memory) the ratio values of various peaks in the emission spectrum of a *pure* compound will later allow the user to determine the degree of purity of that compound as it is being eluted from the column. Consequently it will be possible to determine the optimal time for data acquisition, i.e., minimal overlap with other eluting compounds. A computer program could be written that will allow automatic (delayed) triggering of the OMA, whenever a new spectral feature, i.e., an absorption transition point, is monitored by the "in-tandem" single channel UV-absorption detector. Finally, a pattern recognition program could be written, which will provide a positive identification of a particular oil spill by comparing its digitized spectral and temporal (retention time values) characteristics to those of known (and stored) oil samples.

ACKNOWLEDGMENT

We acknowledge the contribution of S. Buchanan of the Coast Guard Research and Development Center who carried out chromatographic separations. We also credit E. Callet, S. Cravitt, W. Sombathy, and H. Madlin of Farrand Optical Company and lastly D. Baker of Princeton Applied Research Corporation for the design and formulation of the OMA/spectrofluorometer system.

LITERATURE CITED

(1) M. Popl, M. Stejskal, and J. Mostecky, *Anal. Chem.*, **46**, 1581 (1974).
(2) J. F. McKay and D. R. Latham, *Anal. Chem.*, **44**, 2132 (1972).
(3) J. B. F. Lloyd, *J. Forensic Sci. Soc.*, **11**, 235 (1971).
(4) J. B. F. Lloyd, *Analyst (London)*, **100**, 529 (1975).
(5) R. M. Wightman, R. L. Scott, C. N. Reilley, R. W. Murray, and J. N. Burnett, *Anal. Chem.*, **46**, 1492 (1974).
(6) A. McDowell and H. Pardue, *Anal. Chem.*, **48**, 1815 (1976).
(7) Y. Talmi, *Anal. Chem.*, **47**, 697A (1975).
(8) Y. Talmi and D. C. Baker, Internal publication, Princeton Applied Research Corp., 1976.
(9) W. A. Saner, G. E. Fitzgerald, and J. P. Welsh, *Anal. Chem.*, **48**, 1747 (1976).
(10) I. B. Berlman, "Handbook of Fluorescence Spectra of Aromatic Molecules", Academic Press, New York, 1971, p 345.
(11) Ref. 10, p 202.

RECEIVED for review March 21, 1977. Accepted May 23, 1977. This paper was presented in part at the 1977 Pittsburgh Conference on Analytical Chemistry and Applied Spectroscopy, Cleveland, Ohio, March 1977.

Determination of Trace Concentrations of Cobalt(II) and Other Metals by the Chemiluminescent Oxidation of Gallic Acid

Scott Stieg and Timothy A. Nieman*

School of Chemical Sciences, University of Illinois, Urbana, Illinois 61801

The enhancement of light emission from the chemiluminescent (CL) oxidation of gallic acid by alkaline H_2O_2 has been shown to be applicable to the determination of concentrations of a select group of metals at trace levels. The detection limits found are: Co(II), 0.4 ppb; Mn(II), 0.4 ppm; Ag(I), 0.5 ppm; Cd(II), 0.8 ppm; and Pb(II), 1.0 ppm. The working range for Co(II) determinations is about 5 orders of magnitude, with the other metals being measurable over a much more restricted range. The relative standard deviations are less than 5%. Species which suppress the Co(II)–gallic acid CL have been studied and the results support the idea that the free metal ion is necessary for enhancement. Comparisons of three CL systems were made with respect to detection limits and selectivity of enhancing species.

The modification of the rates of reactions involving the chemiluminescent (CL) oxidation of organic compounds by alkaline H_2O_2, particularly luminol (*1*, *2*) and lucigenin (*3*), has been a highly sensitive method for the determination of trace metals, and other species in trace amounts. Chemiluminescent methods, such as these two, offer potential advantages of simplicity and low cost of instrumentation. However, the lack of selectivity of these systems limits their direct application to analysis of complex, real samples.

In recent work by Slawinska and Slawinski (*4*), the CL oxidation of gallic acid (3,4,5-trihydroxybenzoic acid), a modification of the Trautz–Schorigen reaction (*5*), has been used to determine trace amounts of formaldehyde and other organics. This reaction emits light in two regions, an intense band at 643 nm and a weaker band at 478 nm. In our work with several chemiluminescent systems, we have found that the rate of the CL oxidation of gallic acid, which can be measured by observation of the light emitted, is affected by trace concentrations of metal ions and other inorganic species. Furthermore, the CL obtained is enhanced by only a few species out of some 40 species tested, showing selectivity uncharacteristic of previous CL reaction rate methods.

EXPERIMENTAL

Flow System. The mixing and observation of the CL reactions was necessarily performed in unreactive apparatus not only because of high concentrations of NaOH and H_2O_2, but also because of the fact that metals and soluble organics show enhancement of such CL reactions, and thus increased background emission. Our flow system is shown in Figure 1. It consists of three 2-mL Hamilton gastight syringes, with TFE luers and plungers; check valves consisting of Kel/F bodies and sapphire check balls (The Lee Company); and TFE flow lines. Commercially available fittings and tee-joint mixers were used.

The stopped-flow type system operates as follows: when the syringe plunger bank is raised, solutions flow through the supply check valves into the three syringes: gallic acid (aq), alkaline H_2O_2, and the solution containing the metal analyte. When the plungers are lowered, the supply check valves close, and the solutions flow to the mixer. The mixed reacting solution then travels through the open outlet check valve to the flow cell for observation, flushing the previous reacted solution out through the waste line. Since the reactions observed are not extremely fast, this simple system provided a satisfactory way of performing and observing the CL reactions. Use of check valves eliminates the need for external control of valving functions needed. This also eliminates sample carryover problems due to incomplete rinsing of rotary or slide valves–all flow surfaces are rinsed during each cycle.

Flow Cell. The flow cell consists of several TFE plates pressed together by outer brass plates (Figure 2). A Pyrex glass window is pressed into the front plate of the flow cell. The reacting solution enters the flow cell, flows in a thin, uniform layer across the face of the window, and exits at right angles. This avoids dead volume and subsequent irreproducibility of the reactant concentrations due to incomplete flushing. A cell depth of 4 mm (cell volume = 1.8 mL) was selected for these studies (*6*).

Reagents. Gallic acid, monohydrate (Aldrich Chemical Company), commercially available standardized NaOH solutions, unstabilized 30% H_2O_2 (Mallinckrodt), AR or A.C.S. certified metal chlorides and nitrates, and deionized water were used in all solutions without further purification.

Data Acquisition Procedure. The reacting solution resident in the flow cell after two or three rinsings with reactants X, Y, and Z (Figure 1) and *no* specific enhancing species (M = water, Figure 1), is referred to as the "unenhanced reaction". The emission from this reaction was observed directly by an RCA 4840 PMT (high red sensitivity), with no wavelength discrimination. The current obtained was amplified and processed by a GCA/McPherson model 721 controller, whose output was recorded both by a chart recorder and a peak maximum/integrator circuit. The observation period lasted 1–2 min, and was a constant for a particular experiment. At the end of this period, the maximum intensity of the unenhanced reaction, p_0, and the area integrated over this time, a_0, were obtained, as shown in Figure 3, by the peak maximum/integrator circuit. The timing for this was provided by microswitches on the syringe drive (Figure 1). The metal analyte solution was then substituted for the water blank, the cell flushed, and the emission from a new resident reacting solution observed in the same way, obtaining the enhanced reaction maximum intensity, p, and area, a. The quantitation of the enhancement, then, is expressed by two quantities, $\Delta p = p - p_0$, and $\Delta a = a - a_0$. Δp is referred to as "peak height" and Δa as "peak area". The time from mixing until the maximum emission intensity is reached increases from a few seconds at high concentrations of enhancing species to a minute at low concentrations. The speed of the reaction at all, except very high concentrations of enhancing species, is slow enough that very little reaction occurs during the time the solution flows from the mixer to the flow cell (less than 10 ms). This is shown schematically in Figure 3 in that, during flushing, the CL intensity was observed to drop below that of the unenhanced, or "background" reaction.

RESULTS AND DISCUSSION

Selectivity of Enhancement. Table I gives the relative enhancement for the species tested, all species being at 10^{-4} M. (This high concentration was used to detect even minimal enhancement.) Zero enhancement corresponds to the same response as the unenhanced reaction (within twice the relative standard deviation (RSD) of repetitive trials). Out of some 40 species tested, only six showed appreciable effect on the observed emission. This is in marked contrast to CL systems heretofore studied whose emission is enhanced by a large number of metal and nonmetal species. No organic species were tested in this study. It has previously been reported (*4*) that several aldehydes also enhance response.

We see that the metals Co(II), MnO_4^-, Mn(II), Ag(I), Cd(II), and Pb(II) show significant enhancement of this reaction,

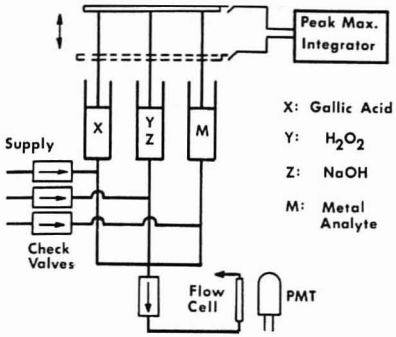

Figure 1. Diagram of CL flow system

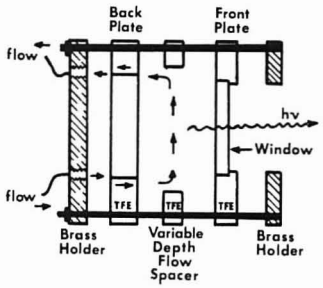

Figure 2. Diagram of CL flow cell

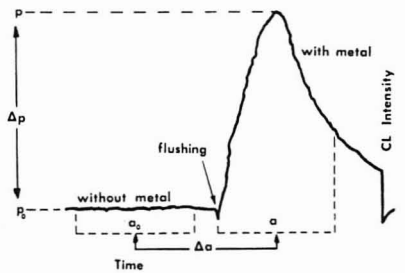

Figure 3. Typical data collection scheme showing parameters obtained

while other related transition elements show no enhancement. In view of previous work on the mechanism of luminol enhancement (*7, 8*), one might suspect that these metal species either form a complex with the H_2O_2 in solution or form a complex directly with the gallic acid. However, it has been shown by Elinany et al. (*9*) that the latter cannot be the case. From polarographic studies involving examination of shifts in $E_{1/2}$ values of 15 metals when gallic acid was added to their solutions, they determined that there was no evidence for complexes of gallic acid with Co(II), Mn(II), Pb(II), or Cd(II)–the enhancing species seen for the gallic acid oxidation (Ag(I) was not tried). Furthermore, definite evidence of gallic acid complexes with As(III), Cr(III), Cu(II), Fe(III), and Mo(VI)–all species which do not enhance gallic acid CL–was found. These results, along with the suppression study results discussed later, suggest that at some point in this reaction the free metal is needed for enhancement, and that the selectivity

Table I. Gallic Acid CL, Relative Response to Various Aqueous Ions at 10^{-4} M

Ion	Relative intensity	Ion	Relative intensity	Ion	Relative intensity
Co(II)	1000	Al(III)	0	Ni(II)	0
MnO_4^-	69	As(V)	0	Pt(IV)	0
Mn(II)	41	Ba(II)	0	Rh(III)	0
Ag(I)	15	Cr(III)	0	Sb(III)	0
Cd(II)	14	Cu(II)	0	Se(VI)	0
Pb(II)	12	Fe(II)	0	Sn(II)	0
Ga(III)	5	Fe(III)	0	Sn(IV)	0
Au(III)	2	$Fe(CN)_6^{3-}$	0	Ti(IV)	0
CrO_4^{2-}	2	I_2	0	Tl(III)	0
Sr(II)	2	I_3^-	0		
V(IV)	2	In(III)	0		
Hg(II)	1	Ir(III)	0		
Pr(III)	1	Mg(II)	0		
Zn(II)	1	Mo(VI)	0		

Table II. Detection Limits, Gallic Acid CL

Metal	Δp	Δa
Co(II)	0.4 ppb	0.4 ppb
Mn(II)	0.7 ppm	0.4 ppm
Ag(I)	1.0 ppm	0.5 ppm
Cd(II)	1.0 ppm	0.8 ppm
Pb(II)	2.0 ppm	1.0 ppm

Table III. Species Tested for Suppression in the Gallic Acid–Co(II) System ([Co(II)] = 10^{-6} M)

Species[a]	$\Delta p_s/\Delta p_u$[b]	Species	$\Delta p_s/\Delta p_u$
EDTA	0.07	CrO_4^{-2}	1.00
CN^-	0.00	Fe(III)	1.00
Pt(IV)	0.07	Hg(II)	1.00
Sn(II)	0.29	I^-	1.00
$Fe(CN)_6^{3-}$	0.41	I_2	1.00
CO_3^{2-}	0.43	I_3^-	1.00
NH_3	0.53	In(III)	1.00
Rh(III)	0.63	Ir(III)	1.00
OCl^-	0.66	Mg(II)	1.00
Pr(IV)	0.75	Mo(VI)	1.00
Ba(II)	0.77	Ni(II)	1.00
Al(III)	0.80	Sb(III)	1.00
Sn(IV)	0.92	Se(VI)	1.00
As(V)	1.00	Sr(II)	1.00
Au(III)	1.00	Zn(II)	1.00
Cr(III)	1.00	Deionized water	1.00
Cu(II)	1.00		

[a] All suppressors are 10^{-4} M, except EDTA which is 10^{-6} M. [b] Δp_s = signal in presence of suppressor; Δp_u signal in absence of suppressor (i.e., due to Co(II) alone).

of this reaction is, by default as it were, dependent on the complexing characteristics of gallic acid. It may be, as in the luminol reaction (*7*), that a metal–H_2O_2 complex forms; however, it is then difficult to explain why different sets of metal–H_2O_2 complexes would react with luminol and gallic acid. Further work in this area is needed.

The oxidizing species MnO_4^- does not cause light emission from gallic acid unless H_2O_2 is also present, as opposed to the case with luminol and lucigenin. The oxidizing species OCl^- gives light emission with gallic acid in a very fast reaction which is obviously different in nature than H_2O_2 oxidation. Finally, Co(II), the chief enhancer, shows a double peak at high concentrations (>10^{-4} M); a very fast initial spike, and the slower peak observed at lower concentrations. This is the same behavior noted in enhancement of luminol with Co(II) (*8*) and Cu(II) (*10*).

Table IV. Working Curves for Co(II) in Various Matrices

Matrix	$\Delta p_s/\Delta p_u$[a]	Slope	σ_{slope}	Intercept	$\sigma_{intercept}$
CN^-	0.6	−0.66	0.03	6.0	0.2
NH	0.6	−0.66	0.02	6.0	0.1
Pt(IV)	0.3	−0.65	0.06	5.8	0.3
Deionized water	1.0	−0.64	0.04	5.9	0.2
Boneyard		−0.67	0.06	6.1	0.3
Boneyard filtered		−0.52	0.03	5.5	0.2

[a] From Figure 6.

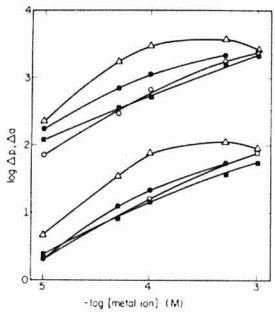

Figure 4. Working curves for Mn(II) (■), Ag(I) (Δ), Cd(II) (O), and Pb(II) (●)

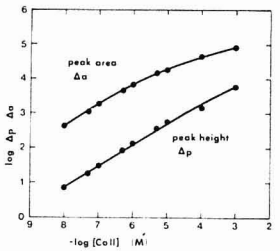

Figure 5. Working curve for Co(II)

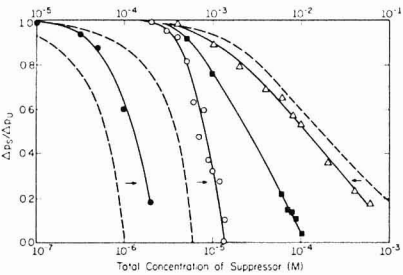

Figure 6. Suppression of CL in the Co(II)–gallic acid system; (---) from calculations based on complexation equilibria; EDTA (●), CN^- (O), Pt(IV) (■), NH_3 (Δ). The calculated curve for NH_3 uses the concentration scale at the top; all other curves use the scale at the bottom

Determination of Optimum Reactant Concentration. Optimization was performed on three reaction variables, [gallic acid], $[OH^-]$, and $[H_2O_2]$, using Co(II) at 10^{-6} M as the enhancer. The optimization was done in two steps. First, a simplex optimization (*11*) was performed in three dimensions, leading to a region in which Δp was maximized. From this point, the response surface of the reaction at constant [gallic acid], was obtained by continuous variation. Optimum concentrations (giving the highest sensitivity, or largest Δp) of stock solutions for our flow system were found to be [gallic acid] = 20 mM, $[OH^-]$ = 50 mM, and $[H_2O_2]$ = 310 mM. These concentrations were used in all subsequent work.

Working Curves for Co(II), Mn(II), Ag(I), Cd(II), and Pb(II). The detection limits (signal-to-noise ratio = 2) (Table II) and working curves (Figures 4 and 5) were determined for standard solutions (in deionized water) of the five chief enhancing metals. It is noteworthy that the four curves in Figure 4 are similar. The detection limit is generally a bit lower using the peak area (Δa) method. This is explained by noting that at low concentrations of enhancer, the reactions are very slow and it is difficult to distinguish between the enhanced and unenhanced reactions. Because the peak area method integrates over time, the precision is improved for measurements at low concentrations. At high concentrations of enhancers, however, the speed of the reaction reduces the accuracy of peak area measurements, and the peak height (Δp) criterion is more useful.

Determination of Co(II). The limit of detection and range for the Co(II) working curve compares favorably with existing conventional methods. The RSD for this CL method is less than 5% over the range 10^{-3} to 10^{-7} M, increasing to the detection limit at 7×10^{-9} M or 0.4 ppb. The limit of detection for cobalt by flame atomic absorption is 10 ppb (*12*). A recent colorimetric method for cobalt (*13*) is limited to the range of 20 ppb to 600 ppb and requires 3 h at elevated temperature for color development.

Because the gallic acid CL detection limit for Co(II) is three orders of magnitude better than for the other four metals, we have investigated the influence of other species on the CL determination of Co(II). The first experiment was to make solutions of equal concentration using different cobalt salts. Within the 5% RSD of the method, solutions from $Co(NO_3)_2$, $CoCl_2$, $CoBr_2$, $CoSO_4$, and $Co(CH_3COO)_2$ produce the same signal and suggest that the method is not sensitive to the choice of the associated anion.

We then undertook to determine the effect and nature of interferences with the CL method. Various species (at 10^{-4} M) were added to the cobalt analyte solution (10^{-6} M) to determine enhancement or suppression of the light emission from that due to Co(II) alone. The species Mn(II), Cd(II), and Pb(II) enhance the emission intensity in the presence of

Table V. Comparison of Detection Limits of Selected Metals by Three CL Systems

Metal	Gallic acid	Luminol	Lucigenin
Co(II)	0.4 ppb	0.0007 ppb (*2*)	0.6 ppb (*15*)
Mn(II)	0.4 ppm	0.5 ppb (*2*)	2.0 ppm (*3*)
Ag(I)	0.5 ppm	30 ppm (*1*)	0.3 ppm (*3*)
Cd(II)	0.8 ppm	suppresses (*1*)	n.a.
Pb(II)	1.0 ppm	1.0 ppm (*1*)	0.2 ppm (*3*)
Cr(III)	>5 ppm	0.05 ppb (*2*)	1.0 ppm (*3*)
Cu(II)	>6 ppm	0.06 ppb (*2*)	3.0 ppm (*3*)
Fe(II)	>6 ppm	0.6 ppb (*2*)	6.0 ppb (*16*)

Co(II); this is expected behavior because each of these species alone results in enhancement of light emission. No species were found which caused enhanced emission from the Co(II)–gallic acid system which did not also enhance emission from gallic acid in the absence of Co(II) (Table I). Table III shows the results for all species tested which either acted as suppressors or showed no effect. All species were allowed to stand for 1 day in the Co(II) solutions; equilibrium of the suppressor reaction, if any, was assumed. The suppression by NH_3 and CO_3^{2-} precludes the use of these species as pH buffers. Interestingly, some species which have no effect on the emission of the unenhanced gallic acid reaction (Table I) cause marked suppression. Notable among these is Pt(IV), which causes suppression of a degree comparable to that from the complexing agent CN^-, and is the only noble metal to show such an effect on the reaction, enhanced or unenhanced. Finally, Rh(III), a Co family metal, causes significant suppression, as opposed to Co itself.

Working curves were then prepared for Co(II) solutions in six matrices: CN^- at 7×10^{-6} M, NH_3 at 1.0×10^{-4} M, Pt(IV) at 5.0×10^{-5}, unfiltered water from the Boneyard Creek (a local stream), Boneyard Creek water filtered through Whatman No. 1 filter paper, and deionized water. (The concentrations of CN^-, NH_3, and Pt(IV) were chosen to suppress 40% to 70% of the signal from a 10^{-6} M solution of Co(II).) The slopes and intercepts, and their standard deviations for these six working curves are given in Table IV. (All values were determined from least squares calculations.) These results show that, except for the Boneyard filtered matrix, the working curve for Co(II) is the same when done in the presence of significant concentrations of suppressors as it is in deionized water; variations in slope and intercept are within the indeterminate error of the method. Of course, at higher concentrations of the first three suppressor species, the curves would show significant suppression at the lowest Co(II) concentrations. The working curves in deionized water and the Boneyard filtered water were also determined on a flame atomic absorption spectrometer (Jarrell-Ash with an air/acetylene flame) and found to be identical. Because these curves are identical by AA but differ by CL, there may exist an uncharacterized suppression mechanism which is counteracted by the presence of the particles in the unfiltered samples.

Some of the best suppressors in Table III are known to form complexes with Co(II) in solution. To test the hypothesis that the free metal is required for enhancement of the gallic acid CL, we compared observed suppression as a function of suppressor concentration to the amount of suppression predicted from complexation equilibrium calculations which give the fraction of free metal.

The working curves have the general form:

$$\log \Delta p = k' + (-n)p\mathrm{Co(II)} \tag{1}$$

or

$$\Delta p = k[\mathrm{Co(II)}]^n \tag{2}$$

where n is the negative of the slope of the log–log working curve, and was found to be 0.65 for this study (see Table IV). If Δp_s is the response in a "suppressed" solution whose total concentration of Co(II) is C_{Co}, and if this response is due only to uncomplexed Co^{2+}, then

$$\Delta p_s = k[\mathrm{Co}^{2+}]^{0.65} \tag{3}$$

Likewise, in a solution containing no suppressing species (i.e., pure water), Δp_u is the unsuppressed response. Since in such a solution, $C_{Co} = [Co^{2+}]$, then

$$\Delta p_u = k(C_{Co})^{0.65} \tag{4}$$

Combining Equations 3 and 4 yields

$$\frac{\Delta p_s}{\Delta p_u} = \left(\frac{[\mathrm{Co}^{2+}]}{C_{Co}}\right)^{0.65} \tag{5}$$

For solutions of Co(II) containing varying amounts of EDTA, CN^-, or NH_3, the quantity $\Delta p_s/\Delta p_u$ was measured experimentally and compared with the value calculated using Equation 5 and literature values for formation constants (*14*). Because Pt(IV) was such a good suppressor, we also measured suppression of Co(II) CL as a function of the concentration of Pt(IV) but could not calculate an expected response because of the lack of a documented complexing mechanism between Co(II) and Pt(IV). (In this case, suppression may well occur for some reason other than complexation.) The results are shown in Figure 6. Because the calculated curves so closely agree with the experimental results, the action of suppressors such as EDTA is probably largely if not completely due to reducing the free metal ion concentration. The calculated curve for NH_3 is identical in shape to the experimental but shifted to concentrations two orders of magnitude higher. This indicates that for NH_3, although complexation to reduce the free metal ion concentration is of significant importance, it is modified by some other consideration. This may be due to an auxiliary reaction which occurs in the time between mixing and observation of maximum CL intensity (p), perhaps an interaction with H_2O_2. Such a consideration is important because the calculations were done for equilibrium concentrations, which are valid only at the initiation of the reaction, while the observations are made some time after.

CONCLUSION

We have seen, then, that the chemiluminescence of gallic acid oxidation is sensitive to a select group of metals, particularly Co(II), and in addition is species selective for the free metal ion and not the complexed forms. It is instructive to compare the detection limits of this system to these and other metals with those detection limits reported for luminol and lucigenin, two comparable alkaline H_2O_2 CL systems. Table V shows such a comparison. These systems differ widely in their relative sensitivity to these eight metals. From this perspective, the gallic acid system becomes a contributor in an array of CL reactions, so arranged that a potential tool for multicomponent trace metal determinations emerges.

ACKNOWLEDGMENT

We are indebted to the Illinois Environmental Protection Agency Lab (Urbana, Ill.) for the use of their atomic absorption apparatus.

LITERATURE CITED

(1) A. Hartkopf and R. Delumyea, *Anal. Lett.*, **7**, 79 (1974).
(2) W. R. Seitz and D. M. Hercules, "Chemiluminescence and Bioluminescence", M. J. Cormier, D. M. Hercules, and J. Lee, Ed., Plenum, New York, 1973, pp 427–449.
(3) A. K. Babko, L. I. Dubovenko, and A. V. Terletskaya, *Ukr. Khim. Zh.*, **32**, 1326 (1966).
(4) D. Slawinska and J. Slawinski, *Anal. Chem.*, **47**, 2101 (1975).
(5) M. Trautz and P. Schorigin, *Z. Wiss. Photog. Photochem.*, **3**, 121 (1905).
(6) S. Stieg and T. A. Nieman, *Anal. Chem.*, submitted for publication.
(7) T. G. Burdo and W. R. Seitz, *Anal. Chem.*, **47**, 1639 (1975).
(8) R. Delumyea, Ph.D. thesis, Wayne State University, Detroit, Mich., 1974.
(9) G. A. Elinany, F. M. Ebeid, A. M. Zahra, and F. I. Ziedan, *J. Electroanal. Chem.*, **72**, 363 (1976).
(10) R. E. Santini and H. L. Pardue, *Anal. Chem.*, **42**, 706 (1970).
(11) S. L. Morgan and S. N. Deming, *Anal. Chem.*, **46**, 1170 (1974).
(12) E. Berman, *Appl. Spectrosc.*, **29**, 1 (1975).
(13) R. M. Pearson and H. J. Selm *Anal. Chem.*, **49**, 580 (1977).
(14) L. Meites, "Handbook of Analytical Chemistry", McGraw-Hill, New York, 1963, pp 1–39.
(15) L. I. Dubovenko and N. V. Beloshitskii, *Zh. Anal. Khim.*, **29**, 111 (1974).
(16) L. I. Dubovenko and A. Yu. Nazarenko, *Ukr. Khim. Zh.*, **41**, 1205 (1975).

RECEIVED for review December 27, 1976. Accepted May 9, 1977. Presented in part at the 3rd meeting of the Federation of Analytical Chemistry and Spectroscopy Societies, Philadelphia, Pa., November 1976. This work was supported, in part, by a grant from Research Corporation.

Chelex-100 Ion-Exchange Filter Membranes for Preconcentration in X-ray Fluorescence Analysis of Water

René E. Van Grieken,* Catharina M. Bresseleers, and Bruno M. Vanderborght

Department of Chemistry, University of Antwerp (U.I.A.), B-2610 Wilrijk, Belgium

Filtering a 200-mL water sample through a pair of Chelex-100 ion-exchange membranes, under a 2–3 bar pressure, at pH 7 to 8 in not less than 20 min, leads to an efficient collection of many trace metals in a form that is ideal for subsequent x-ray fluorescence analysis. Since enrichment factors around 1250 are obtained, the detection limits are at the 1-ppb level. The precision is estimated to be in the 10–15% range. A perfectly linear relationship between concentration and measured x-ray yield is obtained up to the total membrane pair capacity of 0.07 mequiv. The significant affinity of Chelex-100 membranes for the—usually abundant—alkali and alkaline earth ions, together with their limited capacity, restricts the applicability of the described technique to samples with a very low alkali and alkaline earth content.

X-ray fluorescence is essentially a multielement, simple, rapid, and cheap analytical technique. Yet it is rarely applied to aqueous samples. Direct irradiation of aqueous samples in a measuring vial with a thin Mylar bottom leads to typical sensitivities for transition metals in the order of 0.3–5 ppm (*1*). When sensitivities in the ppb region are required, the trace metals must first be preconcentrated and the difficulty lies obviously in preparing targets containing all elements sufficiently enriched and distributed with sufficient uniformity to permit sensitive and reliable analysis.

X-ray fluorescence has been employed in combination with precipitation and coprecipitation, evaporation, solvent extraction, chelation, and adsorption on activated carbon, use of ion-exchange resin or of silica gel with immobilized functional groups.

One drawback of all these methods is that after the preconcentration they require a subsequent step to present the sample in a suitable form to the x-ray instrument. Ion-exchange resin loaded filter papers, however, which incorporate a finely divided ion-exchange resin in a polymer structure, are very thin (5 mg cm^{-2}) and provide a matrix of low atomic number elements. Hence they can be presented directly to the x-ray analysis unit after the trace metal collection is accomplished by a simple filtration, producing intimate contact between the solution to be analyzed and the resin fraction of the filter.

Although several authors (*2, 3*) had already mentioned the use of ion-exchange membranes, Campbell et al. (*4*) first devoted a comprehensive and excellent study to the characteristics of cation- and anion-exchange resin loaded papers. Several applications have since then been published (*5–14*) and reviewed (*15*).

For cation collection all the previous authors, however, used acid ion-exchange filter papers which show a high affinity for the alkaline earth ions that are abundant in many water types. The limited capacity of the filter papers might therefore hamper their application considerably. Moreover, acid filters are optimally used in the lower pH range, requiring pH adjustment of usually almost neutral natural water samples with a risk of contamination. Filtration through commercially available chelating ion-exchange resin loaded filter papers as a means of preconcentration for multielement x-ray analysis has not thoroughly been evaluated in the literature. Yet Chelex-100 papers such as the Acropor type CH membranes contain chelating iminodiacetate functional groups, and columns of this resin (Dowex A-1) show large distribution coefficients in the neutral pH range and have been used advantageously in preconcentrations from seawater (*16, 17*).

Since these membranes might thus have promising properties with respect to environmental water analysis, their important chemical and physical characteristics have been studied. One particularly attractive perspective was the eventual application of Chelex filters for continuous and in-line collections of ions from drinking water supplies and other rather neutral aqueous solutions. Our investigations have generally been directed towards this goal.

EXPERIMENTAL

Apparatus. The x-ray apparatus was a Kevex-0810 system. It includes a Röntgen tube (usually operating at 40 kV–40 mA) and a Mo secondary target. The characteristic x-rays from the sample are counted by a Si(Li) detector with a 170-eV resolution at 5.9 keV. The electronic pulses are led through an amplifier, stored in a 4096 channel analyzer and recorded on magnetic tape for computer evaluation. The data reduction routine (*18*) was based on a subdivision of the spectra in energy regions of particular interest, on a background subtraction relying on the coherently and incoherently scattered peaks in the spectra and on experimentally determined coefficients to evaluate interelement interferences.

Atomic absorption spectrometry was performed on a Perkin-Elmer 503 unit with a graphite furnace Perkin-Elmer HGA-74.

Radioactivity counting was done using a 3 inch × 3 inch NaI(Tl) detector or a liquid scintillation setup connected to a single channel analyzer.

Reagents. All test solutions were prepared by dissolving weighed quantities of metals or metal salts in minimal amounts of HCl and diluting with doubly distilled water. In some cases, Titrisol standards were used. The solutions were prepared and stored in polyethylene containers only.

Chelating ion-exchange filters of the type Acropor CH were obtained from Gelman Company, Ann Arbor, Mich. They contain a resin with iminodiacetate functional groups, as an integral part of a microporous plastic matrix. The 47-mm diameter filters weigh 91.6 ± 0.3 mg, i.e., 5.3 mg cm^{-2}. Chemical analyses of the untreated Chelex-100 filter gave the following results (in weight percent): hydrogen, 8.9; carbon, 59.3; nitrogen, 9.3; oxygen, 11.2; chlorine, 7.1. About 4.2% of the material is not accounted for by these elements.

Procedure. In order to achieve reasonable flow rates through the Chelex-100 membranes, all filtrations were performed in a pressure resistant Gelman No. 4280 stainless steel filter holder with a 200-mL capacity. Filtrations were usually carried out under a 2–3 bar pressure, provided by an air tank. Teflon rings assured the water tightness of the setup.

Preconcentrations were carried out by passing a 200-mL water sample through a pair of Chelex-100 membranes, in not less than

Table I. Percent Collection Efficiency as a Function of pH[a]

Cation	Collection efficiency						
	pH = 4	5	6	7	8	9	10
K^+	58	40	74	71	68	67	28
Mn^{2+}	60	57	78	90	92	66	25
Co^{2+}	55	59	73	83	87	60	27
Ni^{2+}	57	64	76	88	92	64	29
Cu^{2+}	52	59	66	76	74	57	26
Zn^{2+}	49	61	69	74	80	54	25
Rb^+	46	63	66	77	80	68	43
Sr^{2+}	67	68	72	84	85	73	41
Pb^{2+}	67	68	72	84	80	52	19

[a] Standard deviations amount on the average to 6%.

10 min, at a pH of 7–8. This procedure was selected in view of the results of the optimization study, described below. If necessary, precipitates were removed with a prefilter using 0.4-μm Nuclepore membranes.

After loading, the Chelex-membrane pairs were put in glassless slide frames and dried in a $CaCl_2$-NaOH desiccator for more than 12 h. The filters were then suspended tightly on the frame, and offered a reproducible geometry for x-ray fluorescence analysis.

RESULTS AND DISCUSSION

Numbers of Filters Required. One might obtain a more advantageous collection efficiency and capacity by using a stack of several ion-exchange membranes resulting, however, in a higher analysis cost. James (*19*) used three cation-exchange filters simultaneously to obtain complete recoveries.

Experiments were conducted in which 100 mL of a 5 ppm Zn^{2+} solution, at pH 8, were passed through either one, two, or five Chelex-100 filters. The average collection yields determined by both atomic absorption spectrometry of the solution and by x-ray fluorescence of the loaded membranes, amounted to 70 ± 3%; 92 ± 1%, and 99 ± 1%, respectively.

All following experiments were carried out with two Chelex-100 filters, being considered as a suitable compromise between reasonable analysis sensitivity and analysis cost.

Number of Filtrations Required. Campbell et al. (*4*) recommended passing the solution to be analyzed seven times successively through cation exchange papers to achieve high collection efficiencies. James (*19*), however, found satisfactory yields after one pass. When 100 mL of a 5-ppm Zn^{2+} solution was filtered through a pair of Chelex-100 membranes up to five times consecutively, the collection yield amounted to 90 ± 1% after the first pass and did not increase significantly afterwards. This was found from atomic absorption measurements on 2 mL of the eluate after each percolation. All following experiments therefore involved only one single filtration process, leading to satisfactory collection efficiencies for many elements, as will be seen below.

Effect of pH. Two hundred-mL aliquots of solutions of various pH levels containing 0.5 or 0.25 ppm of K^+, Ca^{2+}, Mn^{2+}, Co^{2+}, Ni^{2+}, Cu^{2+}, Zn^{2+}, Rb^+, Sr^{2+}, and Pb^{2+} as chlorides or nitrates, were passed through a pair of Chelex-100 filters. The measured x-ray spectra were corrected for blank and absorption effects (see below). On the basis of the results given in Table I, one can conclude that the collection yields are usually optimal and satisfactorily high at pH 7 to 8, with no critical variations occurring in that region.

In a series of previous experiments involving radioactive tracers (^{54}Mn, ^{60}Co, ^{65}Zn, ^{59}Fe) added separately to 5-ppm solutions and using other batches of Chelex-100 filters, significantly different collection efficiencies were noted in some cases. Also, the yields for Zn differed from those obtained in both previous paragraphs. Variations in pH dependence between different Chelex resin batches, however, have been suspected earlier (*20*). If confirmed, such an effect would imply frequent and painstaking checking of collection yields in routing applications.

The pH dependence of ion collections by larger amounts of Chelex-100 resin has been studied before. Riley and Taylor (*16*) found columns of Chelex-100 to adsorb quantitatively Co^{2+}, Ni^{2+}, Cu^{2+}, Zn^{2+}, Pb^{2+}, and Mn^{2+} at pH 7.6 from seawater. In batch experiments, Holynska (*17*) observed a constant and high recovery of Fe^{3+}, Zn^{2+}, and Pb^{2+} between pH 3 and 8, while the collection efficiency for Cu^{2+} appeared to decrease above pH 6. Leyden and Underwood (*21*) reported lower pH limits for Ca^{2+}, Mn^{2+}, Co^{2+}, Ni^{2+}, Cu^{2+}, and Zn^{2+} around pH 3 and optimal and rather constant efficiencies between 5 and 7.5 for batch experiments on Dowex A-1. The low efficiency of Chelex-100 below pH 3 may be attributed to the protonation of the functional sites (the pK values for Chelex are around 2.8 and 8.3 (*21*, *22*)). Hydrolysis might explain the decrease of efficiency at high pH levels.

Effect of Solution Volume. A preconcentration step involving larger sample volumes obviously leads to higher enrichment factors, an advantage which can, in practice, be offset by lower collection yields, as Campbell et al. (*4*) demonstrated, and by the longer filtration time. In this work, a 200-mL sample volume was chosen, corresponding to the full capacity of the high-pressure filter holder. Experiments with 100- to 400-mL samples proved that the collection yields varied with the solution volume as can be predicted from simple theoretical considerations (*4*).

Effect of Filtration Rate. Campbell et al. (*4*) found the filtration rate did not affect the recovery of metal ions by cation-exchange papers between 120 and 4 mL min^{-1}. Leyden et al. (*23*) and Holynska (*17*) found quantitative uptake of Cr^{3+}, Zn^{2+}, and Fe^{3+} by Chelex-100 resin columns is realized within about 30 min. Since the coordination process is usually slow, an initial electrostatic interaction with the resin followed by chelation was proposed as a mechanism.

For Chelex-100 filters, we found that variations in the flow rate up to 10 mL min^{-1} did not affect the collection yields from a pH 7–8 solution. For higher filtration rates, however, a collection yield above 80% of the optimum was achieved only if the total final filter load amounted to less than $^1/_5$ of the maximum capacity.

Load Homogeneity and Effective Filtration Area. A 200-mL sample of a neutral Zn^{2+} solution containing ^{65}Zn was passed through a pair of Chelex-100 filters. The filters were then cut into 0.25-cm^2 pieces, and the radioactivity of each was counted by NaI(Tl) spectrometry. The filter load appeared to be homogeneous within 3%. The effective filtration area was 15.2 cm^2, i.e., the area of the total filter (17.3 cm^2) minus the Teflon sealing ring. This area is much larger than the 9.6-cm^2 flow-through region of the disk that supports the filters in the filter holder.

Proportionality between X-ray Response and Ion Concentration. Of a standard solution of pH 7.8 containing K^+, Ca^{2+}, Mn^{2+}, Co^{2+}, Ni^{2+}, Zn^{2+}, Rb^+, Sr^{2+}, and Pb^{2+} simultaneously, ten dilutions were prepared with concentrations ranging between 10 ppm and 10 ppb. Each of these solutions was run through a pair of Chelex-100 filters, the measured x-ray signal was corrected for blank and x-ray absorption effects, and the metal ion amounts collected on the filters were calculated. Some results are plotted in Figure 1.

The data for K^+ and Ca^{2+} were erratic due to low affinity for the ion exchanger and contamination effects, respectively. These dilution curves deviate from linearity at the higher concentration end where the limited capacity of the Chelex filters is approached or exceeded, and at the lower end because of contamination effects. For all elements, a perfectly linear relation is found in the intermediate concentration range, implying the collection efficiency to be independent of the

Table II. Average Collection Yield, and Standard Deviation, at pH 7.8

Ion	Mn^{2+}	Co^{2+}	Ni^{2+}	Cu^{2+}	Zn^{2+}	Rb^{+}	Sr^{2+}	Pb^{2+}
Collection yield, %	85.8	86.3	90.5	75.2	77.2	83.7	90.4	86.1
Stand. dev., %	2.5	2.9	3.3	2.9	1.8	0.6	5.4	8.0

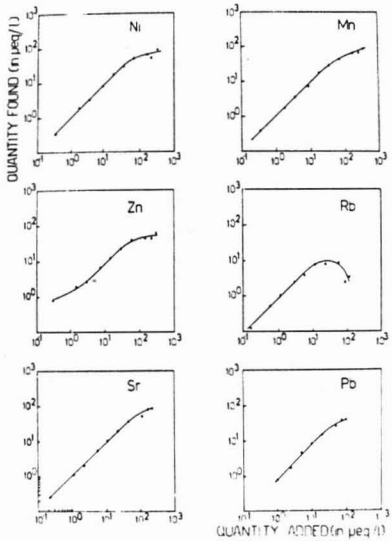

Figure 1. Relationship between determined and added concentrations for Ni^{2+}, Mn^{2+}, Zn^{2+}, Rb^{+}, Sr^{2+}, and Pb^{2+}

ion concentration in the solution to be analyzed. Indeed, assuming a linear relationship with a zero intercept, the following correlation coefficients were calculated: Mn, 0.9975; Co, 0.9988; Ni, 0.9985; Cu, 0.9983; Zn, 0.9985; Rb, 0.9998; Sr, 0.9997; and Pb 0.9981.

Ion Collection Yields. The slope of the straight curves in the intermediate regions of Figure 1 corresponds to the collection efficiency of the enrichment procedure. Assuming that the errors on the given concentrations of the solutions are negligible in comparison with the concentrations on the measured results, and assuming the standard deviations on the latter values to be identical, one can calculate the collection efficiencies given in Table II. These values correspond within 5% with the data in Table I for pH 8.

Qualitative conclusions about relative collection yields can be extracted by examining, in the right sides of the curves in Figure 1, for which ions a deviation from linearity occurs at the lowest concentration. From these and other graphs it was found that K^{+} and Rb^{+} seem to have the lowest affinity for Chelex-100 membranes. The affinity of the other ions can be arranged in the following order:
$Sr^{2+} > Ni^{2+} > Mn^{2+} \geq Pb^{2+} \geq Co^{2+} \geq Ca^{2+} \geq Zn^{2+} \geq Cu^{2+}$
Differences in the group Ni–Mn–Pb–Co–Ca–Zn–Cu are, however, of little or no significance.

This order is not in contradiction with the data in Table I, if one considers the given uncertainties. Of course at pH values differing from 7.8, other selectivity orders might exist.

Some relative selectivity orders have been determined previously for the Chelex-100 resins in batch experiments. Van Willigen and Schonebaum (*22*) found stability constants with Chelex-100 in decreasing order for $Cu^{2+} \simeq Pb^{2+} > Zn^{2+} > Ca^{2+}$, after 120 h of equilibration. They mentioned a strong pH dependence for alkaline earth ions. Holynska (*17*) gives the order $Cu^{2+} > Zn^{2+} > Pb^{2+}$ at pH 5. Another source (*24*) lists $Cu^{2+} >> Pb^{2+} > Ni^{2+} > Zn^{2+} > Co^{2+} > Mn^{2+} > Ca^{2+}$ for nitrate or chloride media. In these experiments, the long equilibration time might enhance chelation relative to the ion-exchange mechanism for some ions, and distinct relative selectivity differences as a function of pH are to be expected (*25–27*).

If one assumes the ion-exchanger weight to be half of the filter weight, and defines the distribution coefficients, D, as:

$$D = \frac{\text{amt. of metal ion/g resin}}{\text{amt. of metal ion/mL solution}} \quad (1)$$

collection efficiencies between 75% (for Cu^{2+}) and 90% (for Ni^{2+} and Mn^{2+}) correspond to log D values of 3.9 and 4.4, respectively. Leyden and Underwood (*21*) quoted log D data near 5 for Cu^{2+} and Ni^{2+}, 4 for Mn^{2+}, and 3.4 for Co^{2+} and Zn^{2+}, for 48-h equilibration times. These results agree well on the average, but, again it appears that the affinity of the Chelex-100 membranes for Cu^{2+} is unexpectedly low.

Filter Capacity. The total ion concentrations for which the curves in Figure 1 start to deviate from linearity illustrate that the total ion load of a pair of Chelex filters is limited to 0.064 mequiv. In another test, a 50-ppm Zn^{2+} solution of pH 7.8 containing some carrier free ^{65}Zn was filtered through a pair of Chelex-100 filters. The eluate was collected in 20-mL fractions. Comparing the radioactivity of each fraction with that of the original sample allowed to determine the Zn^{2+} quantity retained on the filters. A maximum load of 0.066 mequiv was found in this way. This corresponds to 0.8-g exchange capacity per g filter. Campbell et al. (*4*) mentioned a 0.20-mequiv capacity for a 3.5-cm diameter cation-exchange filter, i.e., 1.7 g exchange capacity per g filter weight.

Distribution over the Two Chelex-100 Filters. The distribution of the various ions between the two Chelex-100 filters was studied through the experiments from which the curves in Figure 1 were derived, involving solutions at pH 7.8 of ten ions simultaneously, with a total metal ion concentration ranging from 100 to 2.5 ppm. Of each pair of Chelex-100 filters, the first one (uppermost during filtration) and second one were counted separately. Both filters were measured twice, namely with the front side (upper side during filtration) and with the back side facing the x-ray analysis system. The average of front- and back-side measurements were considered as representative for the filter load. Table III lists the ratios of the ion quantities on the first filter vs. those on the second.

For high ion concentrations, exceeding the filter capacities to a large extent, both filters carry a similar load, except for the most strongly bound ions (Pb^{2+}, Sr^{2+}). At dilution, the first filter collects a larger fraction, and the ratios in Table III increase from ca. 2 for 10 ppm to ca. 4 when the total cation content is lower. Only the cations with the lowest affinity (K^{+}, Rb^{+}) are distributed about equally over both filters in these conditions.

It was found that the distribution was more homogeneous when the solution to be analyzed was passed twice or more times through the Chelex filter pair.

Measurements of the x-ray intensity from the front and back sides of the individual filters could yield information of the distribution of each ion in each filter, as in the procedure, proposed by Adams and Van Grieken (*28*), for deposition

Table III. Distribution of Ions over the Pair of Chelex-100 Filters as a Function of the Concentration Level for Ten Ions Simultaneously present in Equal Concentrations

	Ratio of the quantities on the first and second filter						
	Total cation concentration						
Ion	100 ppm	75 ppm	50 ppm	20 ppm	10 ppm	5 ppm	2.5 ppm
K^+			0.36	0.68	1.20	0.95	1.17
Ca^{2+}	0.99	1.50	0.79	1.96	2.17	1.79	5.55
Mn^{2+}	0.94	1.12	1.03	1.73	1.64	3.95	1.98
Co^{2+}	0.92	1.22	0.93	1.79	1.89	3.87	4.95
Ni^{2+}	0.92	1.14	0.99	1.84	1.85	3.93	3.99
Cu^{2+}	1.11	1.20	0.97	1.19	1.86	3.59	3.35
Zn^{2+}	0.89	1.01	0.89	1.71	1.98	3.64	3.54
Rb^+	1.00	1.30	0.41	0.75	1.08	1.02	1.17
Sr^{2+}	1.40	1.55	1.39	2.48	1.84	4.58	3.40
Pb^{2+}	1.84	2.64	1.84	1.48	2.07	3.72	3.68

Table IV. X-ray Absorption Factors for Different Values of α[a]

	Absorption correction			
Element	$\alpha = 1$	$\alpha = 2$	$\alpha = 4$	$\alpha = \infty$
K	2.26	1.96	1.78	1.56
Ca	1.83	1.65	1.53	1.38
Mn	1.22	1.17	1.14	1.10
Co	1.17	1.11	1.00	1.07
Ni	1.14	1.09	1.07	1.05
Cu	1.07	1.05	1.04	1.03
Zn	1.07	1.03	1.03	1.03
Pb	1.02	1.02	1.02	1.01
Sr	1.02	1.01	1.01	1.01

[a] α = (ratio of ion loads on first and second filter of a pair; see text).

depth evaluation in aerosol loaded filters. However since Chelex-100 filters are quite thin, the relative difference in x-ray yield from both sides is too small even with a nonhomogeneous load, to allow significant conclusions.

X-ray Absorption Effects. The x-ray absorption by the material collected on the filters is always negligible, since the maximum capacity of 0.06 mequiv per filter pair corresponds only to typically 50 $\mu g\ cm^{-2}$ of metal ions.

The absorption by the filters themselves depends on the distribution of the material being measured as a function of the depth ρx within the filter pair. Assuming a homogeneous distribution within each filter of a pair, the total measured intensity for element A is given by:

$$I = I_1 \frac{\int_0^{\rho D} \exp(-\chi \rho x)\,d\rho x}{\int_0^{\rho D} d\rho x} + I_2 \frac{\int_{\rho D}^{2\rho D} \exp(-\chi \rho x)\,d\rho x}{\int_{\rho D}^{2\rho D} d\rho x} \quad (2)$$

where I_1 and I_2 = intensities from first and second filter respectively, in the absence of absorption effects; ρD = filter thickness, in g cm^{-2}; $\chi = \mu_1 \operatorname{cosec} \theta_1 + \mu_2 \operatorname{cosec} \theta_2$ with μ_1 and μ_2 mass absorption coefficients, in $cm^2\ g^{-1}$, of the exciting and characteristic x-rays, respectively; θ_1 and θ_2 = angle between the sample plane and the exciting and characteristic radiation, respectively.

For $\alpha = I_1/I_2$, the absorption correction factor is given by:

$$\frac{I_1 + I_2}{I} = \frac{\alpha + 1}{\alpha + \exp(-\chi \rho D)} \cdot \frac{\chi \rho D}{1 - \exp(-\chi \rho D)} \quad (3)$$

In the previous section, it was shown that α depends on the ion type and concentration in the solution, and varies typically between 1 and 4 (Table III). Table IV represents some typical x-ray absorption corrections. The μ values were determined by transmission measurements through Chelex filters.

The corrections appear to be significant for low Z elements, particularly.

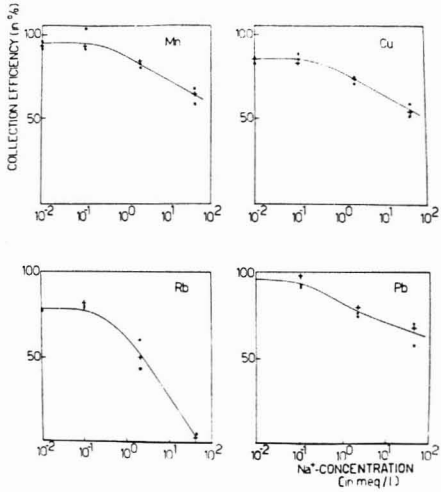

Figure 2. Collection efficiency of Mn^{2+}, Cu^{2+}, Rb^+, and Pb^{2+} in the presence of increasing concentrations of NaCl (·) and $NaNO_3$ (+)

Taking into account the conclusions from the previous section, a realistic value for α can be estimated and a suitable correction can be carried out. Uncertainties on the α values and on the distributions within each filter are expected to yield maximum uncertainties on the absorption correction factor of, e.g., approximately 30% for K, 10% for Mn, 4% for Cu, 1% for Pb.

Influence of Alkali and Alkaline Earth Ions. The capacity of a Chelex-100 filter pair, limited to only 0.065 mequiv, together with the significant affinity for the—usually abundant—alkaline earth ions, might constitute a most serious drawback for the use of Chelex-100 filters. To investigate quantitatively the influence of alkali and alkaline earth ions, solutions with 0.5 ppm of K^+, Ca^{2+}, Mn^{2+}, Co^{2+}, Ni^{2+}, Cu^{2+}, Zn^{2+}, Pb^{2+}, Rb^+, and Sr^{2+} were analyzed after the addition of increasing concentrations of NaCl, KCl, $CaCl_2$ and $MgCl_2$. Most experiments were run in duplicate. Figures 2 and 3 illustrate some typical results. The presence of 1000 ppm or 43 mequiv/L of Na^+ as NaCl lowers the collection efficiency for the transition metals and for Pb^{2+} and Sr^{2+} to 60–70%, to 55% for Cu^{2+}. The collection of Rb^+ and K^+ is then down to about 5%. In comparison with Na^+-free solutions, the average collection efficiency for all the ions studied (without consideration of K^+, Rb^+, and Ca^{2+}) decreases by 10% rel-

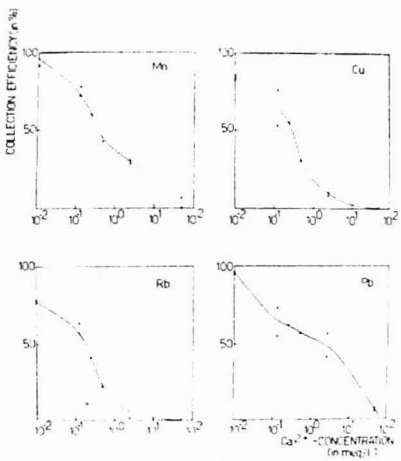

Figure 3. Collection efficiency of Mn^{2+}, Cu^{2+}, Rb^{+}, and Pb^{2+} in the presence of increasing concentrations of $CaCl_2$

atively in the presence of 1 mequiv Na/L or 23 ppm, by 20% for 6 mequiv/L or 138 ppm and by 30% for 35 mequiv/L or 800 ppm Na. No significant differences were observed between the influence of NaCl and $NaNO_3$. Also both for KCl and for KNO_3 exactly the same results were found as for NaCl.

The influence of Ca^{2+} appears to be much more dramatic. Some results are illustrated in Figure 3. For 1000 ppm Ca^{2+} or 50 mequiv/L, the average collection efficiencies amount only to 3%. A 10%, 20%, and 30% decrease is effectuated by the presence of 1.2, 2.6, and 4.2 ppm Ca^{2+}, respectively. The effect on K^{+}, Rb^{+}, and maybe Cu^{2+} is more pronounced than average while Pb^{2+} and Sr^{2+} appear least affected.

The overall effect of Mg^{2+} appeared to be less severe: its concentration can be almost a factor of two higher than for Ca^{2+} to induce the same effect.

The above results clearly point out that the applicability of Chelex-100 ion-exchange filters might be limited for solutions with high or variable alkali and alkaline earth content. Many applications of the resin have been reported involving the removal of di- and trivalent cations from solutions of alkalies and alkaline earths based upon a claimed selectivity of the resin towards ions of greater complexing ability. In these cases, however, the more selective chelation is probably more favored over the ion-exchange process because of long contact times, or the available resin capacity is not critically low.

Blank Filter Impurities and Detection Limits. Typical impurity levels, in $\mu g\ cm^{-2}$, measured on a pair of Chelex filters and typical variations within one batch, were as follows: Cl, 190 ± 50; K, 1 ± 0.6; Ca, 7 ± 1; Ti, 7 ± 0.1; Cr, 0.07 ± 0.01; Mn, 0.07 ± 0.01; Fe, 0.4 ± 0.05; Ni, 0.05 ± 0.01; Cu, 0.06 ± 0.01; Zn, 0.16 ± 0.02. It was observed, however, that different batches contained significantly different blank levels, particularly for Ti, and for W, that was abundant in some lots.

In x-ray fluorescence, detection limits are usually defined as the amount corresponding to three times the standard deviation on the background. Assuming typical filter blank levels, the following interference-free detection limits are calculated, in ppb for a 200-mL solution and a 2000-s counting time in the experimental conditions: K, 14.4; Ca, 17.5; Ti, 10.2; V, Cr, and Mn, 0.8; Fe, 1.5; Co, Ni, and Cu, 0.4; Zn, 0.6. It should be noted that, with the experimental procedure used, the detection limits for Cr, Fe, Co, Ni, Cu, and Zn were all between 2 and 3 ppb, assumingly because of varying contamination by the filter holder.

Precision. From all experiments carried out in multiplicity on the same solutions, it appears that 10–15% is a reasonable estimate of the precision of the proposed procedure.

Applicability. Chelex-100 ion-exchange filter papers can advantageously be used in combination with x-ray fluorescence for solutions with a low alkali and alkaline earth content, e.g., in cooling water systems, distilled water, rain water, etc. The enrichment factors, defined as the original water sample weight to the final specimen weight amount to 1250 in the proposed procedure. This allows analyses at the ppb level for many trace metals.

Drinking water, however, contains typically some 20 ppm Na, 5 ppm K, 5 ppm Mg, and 60 ppm Ca in the dissolved form. Because of the effect of these ions, the heavy metal collection efficiencies from a 200-mL sample would, on the average, be reduced to only 16% of the normal value, mainly because of Ca^{2+}. Small variations on the alkaline earth content will thus induce intolerable errors. If one would allow only a 20% collection efficiency decrease, relative to distilled water, a 8-mL water sample should be diluted to 200 mL and analyzed; the enrichment factor for typical drinking water would then only be 50, resulting in unfavorable detection limits. A similar reasoning holds for ground and surface waters, with similar Ca content.

For seawater, with typically 13 000 ppm Na, 400 ppm K, 1300 ppm Mg, 500 ppm Ca, the applicability of Chelex-100 filters seems even less promising at this stage.

The problem of alkali and alkaline earth ion interferences might, however, be overcome by strongly increasing the equilibration time to favor the more selective chelation process over ion exchange, by adapting the pH or by adding a suitable complexant or precipitant prior to the collection step. This would, of course, exclude simple on-line collections, e.g. for drinking water, by means of Chelex-100 membranes.

ACKNOWLEDGMENT

Grateful acknowledgment is made to L. Van'tdack, H. Nullens, and H. Bosmans who contributed to some of the experimental work. We thank D. E. Leyden, University of Denver, Denver, Colo., and C. Gelman, Gelman Instrument Company, Ann Arbor, Mich., for stimulating discussions and correspondance and A. Sturesson, Lund Institute of Technology, Lund, Sweden, for the elemental analysis of a Chelex-100 filter.

LITERATURE CITED

(1) R. Van Grieken, K. Bresseleers, J. Smits, B. Vanderborght, and M. Vanderstappen, *Adv. X-ray Anal.*, **19**, 435 (1976).
(2) W. T. Grubb and P. D. Zemany, *Nature (London)*, **176**, 221 (1955).
(3) C. L. Luke, *Anal. Chem.*, **36**, 318 (1965).
(4) W. J. Campbell, E. F. Spano and T. E. Green, *Anal. Chem.*, **38**, 987 (1966).
(5) E. F. Spano and T. E. Green, *Anal. Chem.*, **38**, 1351 (1966).
(6) E. F. Spano, T. E. Green, and W. J. Campbell, "Evaluation of a Combined Ion Exchange X-Ray Spectrographic Method for Determining Trace Metals in Tungsten", U.S. Department of the Interior, Bureau of Mines, Washington, D.C., 1964.
(7) G. L. Hubbard and T. E. Green, *Anal. Chem.*, **38**, 428 (1966).
(8) S. N. Ndam and V. C. Rose, *Engineering*, **44**, (7), 2 (1968).
(9) R. D. Walton, *Dev. Appl. Spectrosc.*, **9**, 287 (1971).
(10) S. L. Tackett, G. H. Bender, T. R. Brunner, D. J. Duncan, M. G. Fedak, R. F. Gentile, J. F. Hiller, K. A. Hooker, A. J. McAuley, K. L. Rollick, J. F. Sandolfini, J. C. Smith, J. D. Vojtko, P. H. Pekala and S. A. Williams, *Anal. Lett.*, **6**, 355 (1973).
(11) P. G. Burkhalter, "Trace metal water pollutants determined by X-ray fluorescence", Report NRL-7637, Naval Research Laboratory, Washington, D.C., 1973.
(12) B. Holynska, M. Leszko and E. Nahlik, *J. Radioanal. Chem.*, **13**, 401 (1973).
(13) A. Robert and R. Valles, *Radiochem. Radioanal. Lett.*, **15**, 179 (1973).
(14) C. H. Lochmüller, J. W. Galbraith, and R. L. Walter, *Anal. Chem.*, **46**, 440 (1974).
(15) S. L. Law and W. J. Campbell, *Adv. X-Ray Anal.*, **17**, 279 (1973).
(16) J. P. Riley and H. J. Taylor, *Anal. Chim. Acta*, **40**, 479 (1968).
(17) B. Holynska, *Radiochem. Radioanal. Lett.*, **17**, 313 (1974).

(18) P. Van Espen and F. Adams, *Anal. Chim. Acta*, **75**, 61 (1974).
(19) H. James, *Analyst (London)*, **98**, 274 (1973).
(20) C. W. Blount, D. E. Leyden, T. L. Thomas, and S. M. Guill, *Anal. Chem.*, **45**, 1045 (1973).
(21) D. E. Leyden and A. L. Underwood, *J. Phys. Chem.*, **68**, 2095 (1964).
(22) J. H. H. G. Van Willigen and R. C. Schonebaum, *Recueil*, **85**, 35 (1966).
(23) D. E. Leyden, R. E. Channel, and C. W. Blunt, *Anal. Chem.*, **44**, 607 (1972).
(24) Bio-Rad Laboratories Chemical Division, Technical Bulletin, 114, May 1972.
(25) C. Hertner-Wirguin and G. Markevils, *J. Phys. Chem.*, **67**, 2263 (1963).
(26) H. Luttrell, Jr., C. More, and C. T. Kenner, *Anal. Chem.*, **43**, 1370 (1971).
(27) S. L. Law, *Am. Lab.*, July 1973, p 91.
(28) F. C. Adams and R. E. Van Grieken, *Anal. Chem.*, **47**, 1767 (1975).

RECEIVED for review February 1, 1977. Accepted April 28, 1977.

Determination of Ammonia in Aqueous Solutions by Infrared Spectrometry Following Preconcentration on Zeolite

O. Yavuz Ataman[1] and Harry B. Mark, Jr.*

Department of Chemistry, University of Cincinnati, Cincinnati, Ohio 45221

A new method for the determination of ammonia in aqueous solutions has been developed. In this method, NH_4^+ species is preconcentrated on zeolite AAA matrix in a batch process, and then a portion of the zeolite is sampled by using a KBr pelleting technique. The infrared spectrum of the pellet is taken and the intensity of the NH_4^+ bending vibration band at 1402 cm^{-1} is used to calculate the NH_3–N concentration in the sample solution. The results of analyses had recoveries better than 95.0% and the precision of the method was varying from 5 to 12% mean deviation for NH_3–N concentrations between 14.0 to 0.50 ppm. This infrared method using preconcentration is useful for field studies as it has the advantages of simplifying the transportation and eliminating the necessity of preservation of the samples.

It is often desirable to determine the concentration of ammonia in aqueous systems because of the biological and environmental importance of this compound. Ammonia is a pollutant in the aquatic environment as well as in the air. For natural waters, ammonia exerts a stress in several ways. Among these ways we can mention its contribution to blue-green algae growth (*1*) causing eutrophication, toxicity to fish and aquatic life, causing corrosion of certain metals of construction, reducing the amount of dissolved oxygen in receiving waters due to nitrification process, and inhibiting the water and food intake for both mammals (*2*) and plants (*3*) affecting their appetites. Excess amounts of ammonia and ammonium salts decrease the pH in human blood, causing acidosis which can be monitored by the increase of ammonia in urine (*4*).

The well-known and most popular colorimetric method for ammonia determination was first proposed by Julius Nessler in 1856 (*5*). The Nessler method is not truly a colorimetric method because of the colloidal character of the colored species formed by Nessler reagent, K_2HgI_4. Temperature, alkalinity, time, purity of the chemicals used for the reagent, and the condition of the reagent are the factors affecting the color intensity (*4*). Usually, in order to eliminate several chemical interferences (*4*), a distillation step is necessary. The Nessler method is sensitive down to 20 ppb NH_3–N. Among the other well-established techniques for ammonia determination are the Berthelot method which is based on the blue color formed by the reaction of phenol and sodium hypochlorite with ammonia (*4*), and the pyridine–pyrazolone method which was proposed by Kruse and Mellon (*6*). Several chemical and methodic interferences exist for the Berthelot (*4*, *7*) and the pyridine–pyrazolone methods (*4*, *8*), whose sensitivities are comparable to that of the Nessler method. The most significant one among the novel techniques for the determination of ammonia is the use of ammonia selective electrodes (*9–12*) which also has a claimed sensitivity limit of 20 ppb NH_3–N. Some of the other interesting methods in this field are, the one which uses the rate of change of absorbance with time in the Berthelot method (*13*), Permutit method (*14*), the use of a nuclear backscatter analyzer (*15*), monitoring with differential pulse polarography of the reaction product of ammonia with formaldehyde in an acetate buffer (*16*), and a thermometric titration technique in which BrO^- is used as titrant (*17*).

Infrared spectrometry, on the other hand, despite the belief of some that it is becoming obsolete, is still one of the most important elements of industrial (*18*) and research laboratories. Although infrared spectrometry is commonly used for qualitative purposes, with the advent of on-line computers (*19*, *20*), its quantitative power has gained new dimensions, along with new qualitative conveniences. Quantitative applications with infrared spectrometry are possible providing that the resolution associated with qualitative analysis is sacrificed for a better signal to noise ratio by using large slit values (*21*, *22*). This rule is very important, especially when samples less transparent than solutions such as alkali halide pellets and polymer films are to be analyzed. A critical review of the alkali halide pelletting technique for solid samples will be given in another paper (*23*).

A very common way of improving the sensitivity of detection in a chemical analysis is preconcentration of the species to be determined on a matrix which will not interfere during analysis, so that the species could be determined on the matrix itself (*24*, *25*).

In this study, a new technique for the quantitative determination of ammonia, in ammonium ion form, is based on a preconcentration step on a zeolite ion exchanger followed by quantitative infrared analysis of the sample and the zeolite matrix in a KBr pellet.

EXPERIMENTAL

Apparatus. For the batch processes, wide mouthed and heavy walled Bel-Art polyethylene bottles with 120-mL capacity were used. The bottles containing the sample were agitated in a

[1] Present address, Department of Chemistry, Middle East Technical University, Ankara, Turkey.

constant temperature water bath shaker from LabLine Instruments, Inc.

All the filtrations were made through Millipore GSWP 0.22 μm filters in a Millipore Pyrex 47-mm filter holder.

A shatterbox from Spex Industries, Inc., was used for grinding coarse zeolite materials. The zeolite particles were sized using a 150-mesh, 16-inch U.S. Standard Sieve.

For grinding the sample and KBr mixtures, stainless steel vials from Spex Industries, Inc., 0.5 inch in outer diameter and 1 inch in height, with a capacity of 2 mL, with stainless steel balls ($^1/_8$ and $^1/_4$ inch in diameter) were used with a Wig-L-Bug amalgamator from Crescent Dental Manufacturing Co.

The KBr pellets were made in a Barnes Model 129 KBr die for pressing 13-mm disks. A Carver Laboratory Press Model B with 24 000-lb maximum capacity was used for pressing the pellets.

A Beckman IR-12 infrared spectrophotometer was used for the infrared measurements. This spectrophotometer was continuously flushed with dry air from a double column Beckman Automatic Air Dryer. For the colorimetric determinations, a Cary-14 double beam UV-VIS spectrophotometer was used with a matched pair of 10-mm path length Suprasil round cells from Precision Cells, Inc.

Zeolites. Molecular Sieves 3A, 4A, 5A, and 13X were manufactured by Union Carbide Corp. Hector Clinoptilolite was furnished by R. A. Taft Laboratories, Environmental Protection Agency, Cincinnati, Ohio. The Permutit used in the experiments had the brand name of Ionac C-101, and was purchased from Matheson, Coleman and Bell. Zeolite AAA was kindly provided by Amco (Arizona Minerals).

Reagents. The Nessler reagent was prepared as described in Ref. 26; the HgI_2 and KI used were Analytical Reagent Grade, Mallinckrodt. This reagent was kept in a dark colored bottle and stored in the dark. For the Nessler method working curve, a solution of NH_4Cl (Fisher, ACS certified), 1.0 mg/mL in NH_3–N was prepared and diluted 100 times. Infrared quality KBr from the Harshaw Chemical Co. was used as pellet supporting material. All other reagents were ACS grade or equivalent.

Procedures. Nesslerization Technique (27). Five mL of the sample is diluted with distilled water in a 50-mL volumetric flask to the line; 1 mL of Nessler reagent is added and the flask is shaken up and down several times. Colorimetric measurements are made at 400-nm wavelength, 10 ± 1 min after the addition of the reagent. Ordinary distilled water was stored in batches of 5 L to be used for one set of measurements, a blank of this water was run with Nesslerization. The absorbance obtained was adopted as the new intercept for the working line, since this line has a positive intercept on the absorbance axis. This procedure was preferred to compensate for the small amounts of ammonia in the water, rather than extensive purification procedures.

Treatment of Zeolite AAA. Zeolite AAA, in original form, had a mesh size of 10–15. After separating the foreign objects with a pair of tweezers, zeolite was crushed in a shatterbox for 2 min; fine powder was sifted through a 150-mesh size sieve. Ten-gram parts of 150-mesh size or finer powder of zeolite was then washed with 4 parts of 2 L distilled water each time by stirring for 30 s and then decanting 5 min after the stirring was stopped, in order to eliminate very small particle sizes. Finally, zeolite was dried in the oven at 105 °C for 1 h and then equilibrated with room humidity for 30 min prior to storage.

Measurement of the Kinetics of Ion Exchange in the Zeolite. One hundred mg of Zeolite AAA was added to 100 mL of a 14-ppm solution of NH_4Cl in NH_3–N, the combination was continuously agitated in a polyethylene bottle, and aliquots were filtered through Millipore apparatus into a 125-mL filter flask. The time elapsed between the addition of the zeolite and the end of the filtration for each aliquot was recorded with a stopwatch. NH_3–N concentration in the filtrate was determined by the Nessler method.

Isothermic Study. Zeolite AAA in varying amounts between 1000 and 10 mg was added to 100 mL NH_4Cl solution of 17 ppm in NH_3–N, in a polyethylene bottle, and the mixture was agitated 20 min with a shaker at 20 °C. At the end of the agitation period, the contents of the bottle was filtered through Millipore apparatus into a 125-mL filter flask, and the filtrate was used to determine the NH_3–N concentration remaining with the Nessler method. The amount of NH_3–N on the zeolite matrix was calculated from the difference in the initial concentration and the value found remaining in the filtrate.

Batch Process for the Separation of Ammonium Ion from the Sample. The samples were taken in 100-mL portions and put into polyethylene bottles. Approximately 1000 mg of Zeolite AAA which was carefully weighed was added into the sample bottle. The tightly closed bottle was agitated for 30 min in the shaker. After the agitation process, the mixture was filtered through the Millipore apparatus, and zeolite was placed on a watch glass 7.5 cm in diameter, with the Millipore filter removed. Zeolite sample containing the NH_4^+ was dried in an oven for 30 min at 105 °C. At the end of the drying period, the zeolite was stored in a 2-dram sample vial with a plastic screw cap until analysis.

Preparation of the KBr Pellets. The following procedure was found to give the greatest precision in measurement. The KBr was kept in a tightly closed bottle, stored in a desiccator over $CaSO_4$. Zeolite samples were equilibrated with the room humidity for 20–30 min prior to the start for the procedure of making KBr pellets. Approximately 200 mg of KBr was placed on a piece of weighing paper or the balance pan, and the weight was recorded. The KBr was distributed evenly with a spatula to an area of 1–2 cm on the weighing paper, and about 5 mg of zeolite was placed on KBr powder, taking care not to place any zeolite on the weighing paper directly. After recording the weight, the mixture was transferred into a stainless steel grinding vial and the weighing paper was weighed again.

w_1 = weighing paper + KBr
w_2 = weighing paper + KBr + Zeolite
w_3 = (weighing paper + KBr + Zeolite) − (total amount transferred to steel vial)
w_4 = amount of Zeolite in the steel vial = $w_2 - w_1$
w_5 = total amount in the steel vial = $w_2 - w_3$

As the zeolite is placed carefully on top of the KBr, it is assumed that none of the zeolite particles stay on the weighing paper after transfer to the steel vial, and the above can be used with confidence.

The two stainless steel balls were placed in the steel vial with the zeolite–KBr mixture, and the vial was agitated for 3 min, unless specified otherwise, using the Wig-L-Bug amalgamator. At the end of each 1-min grinding period, the contents of the steel vial were mixed with a spatula to prevent packing at both ends of the vial.

After grinding, the contents were transferred into the sample cavity of the KBr die, and the steel balls were removed. As a satisfactory mixing as well as the grinding of the contents is achieved, quantitative transfer from the vial to the die is not necessary, as the resulting pellet is weighed. The powder in the die was distributed evenly with a glass rod flattened in the end; the plunger was then replaced into the die and rotated gently on the powder in both directions.

After the die was placed in the hydraulic press, the pressure on the die was increased at a rate of approximately 400 lb/s, until a total pressure of 12 000 lb was reached. This value corresponds to approximately 50 000 psi for the 13-mm diameter disks. No evacuation was used.

Contents in the die were pressed for 2 min, the pressure was released, and the extracted pellet was weighed.

W_6 = Weight of the pellet
W_7 = Weight of the zeolite in the pellet = $(W_6 \times W_4)/W_5$

The pellets were stored in a desiccator over $CaSO_4$ until the spectra were measured.

Infrared Spectra of KBr Pellets. In order to minimize the variations due to the inhomogeneities in the pellet, the sample holder was positioned somewhere near the middle of the sample compartment, so that almost the whole pellet was illuminated. An empty pellet holder of the same type was used on the reference beam.

For the quantitative measurements, the region between 1300 and 1500 cm^{-1} was scanned in the double beam absorbance mode, twice or more as desired. A baseline was drawn between the points of the spectrum at 1370 and 1440 cm^{-1} values. The tip of the 1402 cm^{-1} infrared band for NH_4^+ was connected to the baseline with a perpendicular line. The length of this line between the tip of

Table I. Values for the Working Curve of the Infrared Method

NH_3-N in the pellet, μg	(Absorbance units) × 100
0.65	1.1
1.13	1.5
1.65	2.3
2.30	2.8
3.27	4.3
4.10	5.2
4.85	6.2
5.66	7.1
6.41	8.4
7.50	9.6
8.31	10.8

Slope = 1.27. Intercept = 0.10.

the band and the intersection point with the baseline was recorded in absorbance units × 100.

Calculation of NH_3-N Concentration. A calibration curve for the method developed in this study was constructed by using NH_4Cl solutions with varying concentrations in NH_3-N, and about 1000 mg of zeolite AAA. Following the batch process, recovery was checked with Nesslerization in the solution from which NH_4^+ ions are removed. Thus, the pellets with known NH_3-N concentrations were made (Table I).

NH_3-N concentrations in the unknown samples were found from the experiments performed in a similar manner to those of the working curve.

The NH_3-N concentration was calculated as follows:

y = Absorbance units × 100
W_0 = Weight of initial zeolite used in batch process, in mg
W_7 = Weight of the zeolite in the pellet, in mg
a = Slope of the working curve of the infrared method, in absorbance units × 100/μg NH_3-N in the pellet
b = Intercept of the working curve in absorbance units × 100
W_8 = Weight of NH_3-N in the sample used in the bath process, in mg = $[(y - b)/a] \times [(W_0/W_7)] \times 10^{-3}$

RESULTS AND DISCUSSION

Recently, we found that zeolite 13x in contact with dilute NH_4Cl solution showed, as a result of ion exchange on zeolite, a sharp infrared band for the zeolite matrix at 1402 cm^{-1} (see Figure 1) which had sufficient intensity for quantitative measurement (*28*). This 1402 cm^{-1} band arises from tetrahedral bending vibration of NH_4^+ species and has been designated as ν_4, with T_4 symmetry (*29*). Several kinds of zeolites were also tested for selectivity and sensitivity for NH_4^+ exchange with their native cations and IR activity in the 1400 cm^{-1} region. Zeolite AAA had significantly better characteristics than the others, as shown in Table II. Zeolite AAA

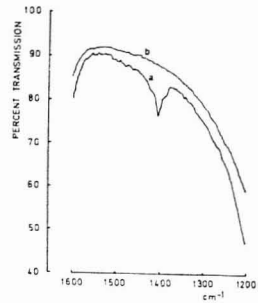

Figure 1. Infrared spectra showing NH_4^+ exchange on Zeolite-13X. (a) NH_4^+ on Zeolite-13X. (b) Zeolite-13X

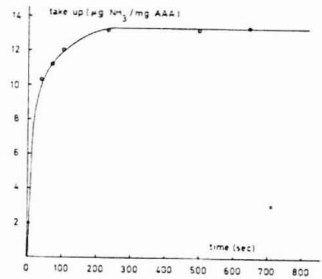

Figure 2. Kinetics of NH_4^+ exchange on Zeolite-AAA. The data were taken with 100 mg AAA and 100 mL of an NH_4Cl solution with a 14 ppm NH_3-N concentration

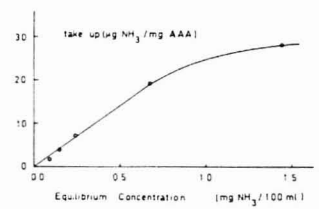

Figure 3. Isotherm for NH_4^+ exchange on Zeolite-AAA at 25 °C

Table II. Comparative Characteristics of Various Zeolites

Designation	Chemical formula	NH_3-N relative[a] recovery (From 14.0 ppm NH_4Cl solution)	NH_3-N relative[b] recovery (From 14.0 ppm NH_4Cl simulated secondary effluent[f])	IR background
3A	$K_{12}[(AlO_2)_{12}(SiO_2)_{12}]\cdot XH_2O$[c]	0.78	0.65	Peak, 1375 cm^{-1} (small)
4A	$Na_{12}[(AlO_2)_{12}(SiO_2)_{12}]\cdot XH_2O$[c]	0.88	0.77	Intermediate
5A	$Ca_{4.5}Na_3[(AlO_2)(SiO_2)]\cdot XH_2O$[c]	0.69	0.53	Peaks, 1420 and 1485 cm^{-1} (large)
13X	$Na_{86}[(AlO_2)_{86}(SiO_2)_{106}]\cdot XH_2O$[c]	0.94	0.77	Low
HC	$Na_x[(AlO_2)_x(SiO_2)_{3.0}]\cdot 24H_2O$[d]	0.71	0.73	Peaks, 1405 and 1450 cm^{-1} (large)
P	Not known	0.28		
AAA	$Na\cdot(AlO_2)(SiO_2)_{3.0}\cdot 3\cdot 9H_2O$[e]	1.00	1.00	Low

[a] Recovery values are normalized with respect to AAA's recovery which was 88.9% with 100 mg AAA and 100 mL of 14.0 ppm NH_3-N solution of NH_4Cl. [b] Recovery values are normalized with respect to AAA's recovery which was 62.9% with 100 mg AAA and 100 mL of simulated secondary effluent solution. [c] Linde Molecular Sieve Data Sheets, Union Carbide Corp., New York, N.Y. [d] D. W. Breck, "Zeolite Molecular Sieves", J. Wiley and Sons, New York, N.Y., 1974. [e] This study. [f] The simulated secondary effluent contained 130.0 ppm NaCl, 15.0 ppm KCl, 120.0 ppm $CaCl_2$, and 50.0 ppm $MgCl_2$.

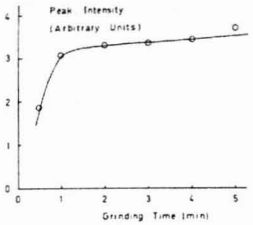

Figure 4. Effect of grinding time on the peak intensity (1402 cm^{-1})

Table III. Analysis Results for Simulated Secondary Effluent with Various NH_3-N Concentrations

Taken, ppm NH_3-N	Found,[a] ppm NH_3-N	Mean dev, %	Recovery, %
14.01	13.31 ± 0.67	5.03	95.0
11.91	11.45 ± 0.63	5.50	96.1
7.71	7.44 ± 0.45	6.05	96.5
5.60	5.39 ± 0.36	6.68	96.3
4.90	4.76 ± 0.33	6.93	97.1
4.20	4.12 ± 0.29	7.04	98.1
2.80	2.71 ± 0.23	8.49	96.8
1.40	1.38 ± 0.15	10.87	98.6
0.50	0.49 ± 0.06	12.24	98.0

[a] Found value ± mean deviation, of 5 replicate KBr pellets for each sample solution.

is a synthetic amorphous material; its formula was determined as $Na{\cdot}(AlO_2)(SiO_2){\cdot}3.9\ H_2O$ (*28*).

The rate of NH_4^+ exchange on zeolite AAA is shown on Figure 2. The curve shows that at least a 4-min agitation period for batch process is necessary to reach equilibration of the phases. Figure 3 shows the isotherm of NH_4^+ exchange on AAA.

There are a number of precautions that must be taken to obtain quantitative results. First, it is important to note that the peak at 1402 cm^{-1} is actually that of NH_4Br which is a product of a slow solid-state ion-exchange process. Similar cases have been reported (*30–34*) and details of this process has been discussed elsewhere (*35*). Reproducible results are attained, however, if the true period between preparation of the sample pellet and the IR measurement are kept constant. For best results and greatest sensitivity, it is best to heat the KBr pellets at 135 °C for 60 h, which drives the ion-exchange reaction to completion (the thermal stability of the KBr pellets is discussed below).

Figure 4 shows the effect of grinding time on the peak intensities. Although the slope of the curve decreases markedly after 1 min, it never reaches a plateau. Thus, a fixed grinding time is necessary for accurate results. Although the sensitivity increases with increasing grinding, it is obvious that little is gained after 2 min.

The zeolite samples containing preconcentrated NH_4^+ species must be heated to drive off the H_2O after the batch process, and studies have shown that some NH_4 is lost, probably volatized, if the drying time exceeded 50 min. The dried zeolite containing the sample can be stored indefinitely in screw capped vials without change in peak intensity. Once the KBr pellets are prepared, they are very stable. Volatilization of NH_4^+ species in KBr pellets could be expected, as NH_4Br is known to sublime. However, pellets which were kept in a vacuum oven at 135 °C for 60 h showed no decrease in the intensity of 1402 cm^{-1} band.

Typical results for the analysis of simulated secondary effluent samples containing known amounts of NH_3-N are shown in Table III.

Table IV. Analysis Results for Secondary Effluent Sewage Water

Days after sample collection	NH_3-N ppm ± mean dev[a]	Mean dev, %
0	14.25 ± 0.76	5.53
8	12.11 ± 0.78	6.44
20	10.23 ± 0.51	4.99
25	8.79 ± 0.62	7.05
42	7.28 ± 0.48	6.46
75	2.12 ± 0.23	10.85

[a] Results of 5 replicate pellets for each sample solution.

Table V. Results of a Duplicate Batch Analysis

	ppm NH_3-N	
Pellet No.	Batch 1	Batch 2
1	15.11	15.21
2	14.23	15.08
3	14.01	13.93
4	13.78	15.49
5	15.12	15.81
6	15.69	14.10
	Mean ± mean dev	Mean dev, %
Among pellets:		
Batch 1	14.66 ± 0.65	4.43
Batch 2	14.94 ± 0.61	4.08
Among batches:	14.80 ± 0.14	0.93

Table VI. Results of Standard Addition to Aged Secondary Effluent Solution

Spike added, ppm NH_3-N	True value,[a] ppm NH_3-N	Found, ppm NH_3-N	Mean dev, %	Recovery, %
0.00		2.12 ± 0.23	10.85	
1.20	3.32	3.18 ± 0.25	7.86	95.8
2.40	4.52	4.61 ± 0.34	7.38	102.0
3.60	5.72	5.43 ± 0.33	6.08	94.9
4.80	6.92	6.81 ± 0.48	7.05	98.4
6.00	8.12	7.96 ± 0.46	5.78	98.0
			Mean =	97.0

[a] Assuming that the analysis with no spike was 100% recovery.

A series of analyses were also carried out on actual effluent samples taken from a waste water treatment plant and typical results are shown in Table IV. These results illustrate an important point. In the sewage samples left in closed polyethylene bottles, natural nitrification reduces the amount of ammonia in the system, converting it into NO_3^- species, which shows that time dependent degradation of the sample is a real problem.

Evaluation of the Infrared Method. *Accuracy and Precision.* The precision of the method varies between approximately 5 to 12% mean deviation for NH_3-N concentrations of 14.0 to 0.5 ppm. Theoretically smaller concentrations than 0.5 ppm, down to about 0.10 ppm, can be determined. However, the precision is very poor with such low NH_3-N concentrations.

Precision between the batches and the pellets has been compared in a duplicate batch analysis with 5 KBr pellets contributing more to the errors than the difference between the batches. The results are shown in Table V.

The accuracy of the method was tested by standard additions to an aged sewage sample. The results are shown in Table VI.

The Advantages and Disadvantages of the Infrared Method. Providing that the sample contains a NH_3-N concentration larger than 0.5 ppm, the infrared method has several advantages.

As the equilibration time can be as short as 4 min (Figure 2), the infrared method offers an attractive solution for the traditional problems of transportation and preservation of the samples in the field studies. The batch process part of the analysis can be carried out at the field. As 1 g of zeolite is used for 100 mL of the sample, the amount of sample to be transported to the lab will be 100-fold lighter. Furthermore, immediate separation of NH_4^+ from the sample provides a procedure free of the necessary precautions to be taken for preservation of solution, as the problem of biological activity is especially important for ammonia due to the nitrification process, as discussed previously.

Another distinct advantage of the infrared method is that none of the other cations present in large concentration are infrared active. Therefore, they do not interfere with the infrared spectroscopic determination step. So far, no spectroscopic interference has been observed. It is important to keep in mind that other cations can lower the ammonia recovery if their concentration is high enough.

The infrared method for the analysis of ammonia also has several disadvantages. First of all, like any analytical technique involving a recovery step in a batch process, this method will always have inherently less than 100% recoveries. To have very large recovery percentages, a very large amount of zeolite must be used in a batch process. However, when the concentration of the NH_4^+ is very low on zeolite, the analyst will have to use larger amounts of zeolite in a KBr pellet. This affects the precision of the analysis because of a low transmission of infrared light through the pellets and poor S/N values. A compromise, such as employed in this paper, is necessary.

Another disadvantage of the method is its sensitivity limit. At this stage of the development, this method cannot be used for low pollution level environments.

A Comparison between the Infrared Method and the Other Methods Available. The infrared method has a poorer sensitivity than the other methods in the field of ammonia determination. However, for heavily polluted waters, this method is advantageous for the reasons discussed in the preceding section.

For the colorimetric methods, many ions interfere with color formation (*4*). In the Nessler method, the use of EDTA is suggested (*26*) to prevent the precipitation due to the hydrolysis of Mg^{2+} and Ca^{2+}. Although it is suggested that excess Nessler reagent should be used in this case (*26*), this is not a safe procedure as the EDTA destroys the color formation by complexing with mercury in the Nessler reagent. Therefore, a separation step by distillation is almost always inevitable for the Nessler method.

Probably one of the best methods available for ammonia determination is the use of Ammonia Selective Electrode. However, although a sensitivity limit of 20 ppb NH_3–N is given for this method, accuracy for such a low concentration is poor, with a % of difference of +23.0 from the true value (*10*). Also, equilibration time for the electrode is as long as 7 min for 20 ppb NH_3–N (*9*). Long equilibration times require the use of air tight apparatus with ammonia electrode; otherwise ammonia gas may be lost to the air as the electrode operates at a pH 10–11.

Among the most wisely used methods for ammonia analysis, only the pyridine–pyraxolone method is performed at low pH, like 2.7 (*4*). All the other methods have the disadvantage of high pH conditions which is a possible cause for the loss of ammonia to the air. The infrared method developed in this work responds to NH_4^+, not NH_3. Therefore, it is used at pH 5–7, which eliminates any concern about the loss of ammonia gas.

CONCLUSION

For future studies, the idea of using self-supporting pellets seems to be very attractive. The self-supporting pellets made in this laboratory have a higher sensitivity, as much as 30-fold, than the KBr pellets, although these pellets were not quantitative. This problem may be solved by using a special die. In the case that such a study is carried out, the infrared method may reach the sensitivity level of other commonly used methods.

LITERATURE CITED

(1) G. E. Fogg, W. D. P. Stewart, P. Fay, and A. E. Walsby, "The Blue-Green Algae", Academic Press, New York, N.Y., 1973.
(2) P. C. Simson and D. A. Booth, *Physiol. Behav.*, **11**, 329 (1973).
(3) B. Quebedeaux, Jr., and J. L. Ozbun, *Plant Physiol.*, **52**, 677 (1973).
(4) M. J. Taras, "Colorimetric Determination of Nonmetals", D. F. Boltz, Ed., Interscience Publishers, New York, N.Y., 1958, Chap. 4.
(5) J. Nessler, *Chem. Zentralbl. (N.F.I.)*, **27**, 529 (1856).
(6) J. M. Kruse and M. J. Mellon, *Anal. Chem.*, **25**, 1188, (1953).
(7) E. D. Noble, *Anal. Chem.*, **27**, 1413, (1955).
(8) "Handbook of Analytical Chemistry", M. Meites, Ed., 1st ed., McGraw-Hill, New York, N.Y., 1963.
(9) T. R. Gilbert and A. M. Clay, *Anal. Chem.*, **45**, 1757 (1973).
(10) R. F. Thomas, and R. L. Booth, *Environ. Sci. Technol.*, **7**, 523 (1973).
(11) H. F. Proelss and B. W. Wright, *Clin. Chem. (Winston-Salem, N.C.)*, **19**, 1162 (1973).
(12) G. T. B. Sanders and W. Thornton, *Clin. Chim. Acta*, **46**, 465 (1973).
(13) T. E. Weichselbaum, J. C. Hagerty, and H. B. Mark, Jr., *Anal. Chem.*, **41**, 848 (1969).
(14) O. Folin and R. D. Bell, *J. Biol. Chem.*, **29**, 329 (1917).
(15) J. O. Rasmussen, Jr., US Patent, 3,761,225 (Cl. 23-230R: G 01n), 25 Sep., 1973, Appl. 94,456, 02 Dec., 1970.
(16) Application Brief A-3, Princeton Applied Research Corp., Princeton, N.J., 1974.
(17) A. Halasz, J. Rusz-Szorad, and M. Ifcsics, *Acta Chim. (Budapest)*, **78**, 135 (1973).
(18) P. R. Griffiths, *Anal. Chem.*, **46**, 1207A (1974).
(19) M. J. D. Low, *Anal. Chem.*, **41**, 97A, (1969).
(20) J. S. Mattson, H. B. Mark, Jr., and H. C. MacDonald, Jr., ed., "Computers in Chemistry and Instrumentation", Vol. 7, M. Dekker, New York, N.Y., 1977.
(21) J. A. Perry, *Appl. Spectrosc. Rev.*, **3** (2), 229 (1970).
(22) R. G. J. Miller and B. C. Stace, Ed., "Laboratory Methods in Infrared Spectroscopy", Heyden and Son Ltd., New York, N.Y., 1972.
(23) O. Y. Ataman and H. B. Mark, Jr., "Alkali Halide Pelleting Technique for Solid Sampling in Infrared Spectroscopy". *App. Spectrosc. Rev.*, **13** (in press).
(24) H. B. Mark, Jr., *J. Pharm. Belg.*, **5**, 367 (1970).
(25) D. E. Leyden and R. E. Channel, *Anal. Chem.*, **44**, 607 (1972).
(26) "Standard Methods for the Examination of Water and Wastewater", 13th ed., American Public Health Association, Washington, D.C., 1971.
(27) A. I. Vogel, "A Textbook of Quantitative Inorganic Analysis", 3rd ed., Longmans, Green and Co., Ltd., London, 1962.
(28) O. Y. Ataman, Ph.D. dissertation, 1975.
(29) G. Herzberg, "Molecular Spectra and Molecular Structure", Part 2, D. Van Nostrand, New York, N.Y., 1962.
(30) L. F. Power and A. M. Tait, *Anal. Chem.*, **47**, 1721 (1975).
(31) F. Vrâtný, *J. Inorg. Nucl. Chem.*, **10**, 328 (1959).
(32) R. O. French, M. E. Wadsworth, M. A. Cook, and I. B. Cuttler, *J. Phys. Chem.*, **58**, 805 (1954).
(33) W. A. Pliskin and R. P. Eischens, *J. Phys. Chem.*, **59**, 1156 (1955).
(34) V. W. Meloche and G. E. Kalbus, *J. Inorg. Nucl. Chem.*, **6**, 104 (1958).
(35) O. Y. Ataman and H. B. Mark, Jr., "Ion Exchange Between Ammonium Zeolite and the Supporting Matrix in KBr Pellets", *Anal. Lett.*, **9**, 1135 (1976).

RECEIVED for review March 11, 1977. Accepted May 16, 1977. This research was supported in part by the National Science Foundation, Grant No. MPS72-05014. One of us, O.Y.A., gratefully acknowledges financial support for graduate study from the Middle East Technical University and the U.S. Agency for International Development.

Use of Internal Standards for Atomic Absorption Spectrometric Analyses of Samples Atomized by Sputtering

D. C. McDonald

Division of Chemical Physics, CSIRO, P. O. Box 160, Clayton, Victoria, Australia 3168

Concentrations of iron, chromium, nickel, and copper in a number of different alloys and in powdered metallic and nonmetallic samples were determined by atomic absorption measurements of atomic vapors produced by cathodic sputtering in a low-pressure, rare-gas discharge. The ratio of the analyte absorbance to the absorbance of an internal standard element in the sample was compared with the corresponding ratio in a reference sample. This allowed accurate determinations to be made even when the sputtering rate of the sample was quite different from that of the reference sample.

Up to the present, work on the analysis of metals and alloys by atomic absorption and atomic fluorescence measurements of vapors produced by cathodic sputtering has been restricted to samples which have similar sputtering rates (*1–5*). Changes in sputtering rate may occur when different matrices are sputtered or when there is a change in the energy or flux of the bombarding ions (*6*). The energy and flux of the bombarding ions depend upon the discharge current, discharge voltage, and the pressure in the sputtering cell.

This paper extends the work of Gough (*5*) to series of metallic and nonmetallic samples which sputter at different rates. It describes a simple and effective method of correcting for changes in sputtering rates. The method involves the use of an internal standard, which may be either a constituent element of known concentration in the sample or another element with which the sample is mixed in a known proportion. A single reference sample is used to determine concentrations of the analyte in the samples.

When alloys are to be analyzed, the approximate concentration of the major constituent element is often known. With low-alloy steels, for example, only a small error is introduced by simply assuming that the concentration of iron in the sample is 94% and using iron as an internal standard. Accurate analyses may also be made using a minor constituent element of known concentration as the internal standard.

A different approach (*7*) is to mix a powdered sample in known proportion with, for example, copper powder, press the mixed powders into a disk, and sputter the disk using copper as the internal standard. Copper is a particularly useful internal standard because it has many resonance lines with absorbance sensitivities spanning a very wide range (1.00 to 0.00017, see Table I). Copper is readily pressed into disks, and it also sputters very efficiently.

THEORETICAL

The absorbance, A, of an atomic vapor, for values in the linear absorbance region, can be expressed (*8*), as

$$A \propto (k_0 l)\,\Phi \tag{1}$$

where k_0 is the peak absorption coefficient for a single, Doppler-broadened line, l is the absorption path length, and Φ is a line-profile factor (*8*) expressing the departure of the actual absorbance from that of the ideal case of a monochromatic line source and a single, unshifted, Doppler-broadened absorption line. The absorption coefficient, k_0, is proportional to the steady-state concentration of absorbing atoms in the sputtered vapor, and hence to the concentration of those atoms in the sample (*9*).

Table I. Absorbance Sensitivities, Line Profile Factors (Φ) and Oscillator Strengths (f) for Copper (*8*)

Resonance line, nm	Relative absorbance Sensitivity[a] ($\Phi\lambda f$)	Φ	f[b], absolute
324.7	1.00	0.32	0.43
327.4	0.44	0.28	0.215 ± 0.009
217.9	0.123	0.20	0.127 ± 0.010
216.5	0.092	0.25	0.077 ± 0.004
218.2	0.088	0.25	0.071 ± 0.004
222.6	0.048	0.30	0.033 ± 0.002
202.4	0.018	0.22	0.018 ± 0.002
249.2	0.0077	0.27	0.0052 ± 0.0004
224.4	0.0045	0.29	0.0031 ± 0.0002
244.2	0.0018	0.19	0.0018 ± 0.0001
236.3	0.00017	0.30	0.00011 ± 0.00004

[a] For a hollow-cathode lamp source (low current) and a sputtering-type absorption cell. [b] Normalized relative to $f_{324.7} = 0.43$.

The absorbances of two resonance lines of the same element, measured under the same conditions, are related (*8*) by

$$A_2 = A_1 \frac{\Phi_2}{\Phi_1}\frac{\lambda_2}{\lambda_1}\frac{f_2}{f_1} \tag{2}$$

where f_j is the oscillator strength of the resonance line of wavelength λ_j, and the product $\Phi\lambda f$ can be referred to as the absorbance sensitivity. Thus the measured absorbance of one resonance line can accurately be converted to the absorbance of another resonance line if the Φ-factors and the oscillator strengths are known.

Determinations of the absorbance sensitivities ($\Phi\lambda f$) have recently been made for 11 resonance lines of copper using a hollow-cathode source and a sputtering absorption cell (*8*), and these results are included in Table I, together with the measured f-values and the calculated Φ-values.

When an internal standard is used together with a reference sample of known analyte concentration, the w/w concentration, C_a^S, of the analyte element in the analytical sample can be determined using

$$C_a^S = \left[C_i^S \frac{A_a^S}{A_i^S}\right]\left[\frac{C_a^R}{C_i^R}\frac{A_i^R}{A_a^R}\right] \tag{3}$$

where the superscripts S and R denote the unknown and reference samples, respectively, and the subscripts a and i denote the analyte element and internal standard element, respectively. This is the equation used to calculate the concentrations reported in this paper; it is based upon the assumption that the ratio of the absorbance of an element in the vapor phase to its concentration in the solid remains constant from sample to sample for a given element. The validity of this assumption is discussed later.

EXPERIMENTAL

Apparatus. The absorption measurements were made using a Varian-Techtron Model AA-6 atomic absorption spectrophotometer, in which a Pyrex sputtering cell was substituted for the

burner. The sputtering cell and associated gas-control system were the same as those described by Gough (*5*). The flow-rate of argon was 0.25 L/min and the pressure was typically 4 Torr. The sputtering-discharge power supply was a regulated dc supply capable of delivering 100 mA at 800 V. Current-regulation was used to maintain a constant current-density on the restricted, sputtered surface area of the specimen. A four-digit meter was used to display the value of the discharge voltage. The changes of voltage during the establishment of steady-state sputtering conditions gave some indication of the state of the sputtering surface.

Samples. *Alloys.* The following certified materials were used. Low-alloy steels SS404, SS406, SS409, SS410 (e.g., SS410, Fe 92.96, Ni 2.04, Cr 1.72, Si 1.00, Cu 0.47, V 0.46, Mn 0.43, Mo 0.41, C 0.39, P 0.066, S 0.053%) from Bureau of Analysed Samples Ltd., U.K.; H 1168 (Fe 96.7, Ni 1.03, Cr 0.54, Mn 0.47, C 0.26, Cu 0.26, Mo 0.20, V 0.17, Co 0.16, W 0.077, Si 0.075%) from NBS, Washington. High-speed steel SS486 (Fe 80.66, W 6.48, Mo 5.23, Cr 4.53, V 1.92, C 0.74, Si 0.14, Co 0.13, Mn 0.12, S 0.029, P 0.021%) from Bureau of Analysed Samples Ltd. Cartridge Brass C1110 (Cu 67.4, Zn 32.2, Pb 0.106, Fe 0.072, Sn 0.055, Ni 0.052, Ag 0.019, As 0.019, Sb 0.018, Cd 0.013, P 0.010%) and Commercial Bronze C1115 (Cu 87.9, Zn 11.7, Fe 0.13, Sn 0.10, Ni 0.074, Pb 0.013, P 0.005%) from NBS.

Analyzed alloys used were Product Steel No. 5 (Fe 88.61, Ni 4.28, C 3.51, Cr 1.28, Mn 0.99, Si 0.93, Mo 0.26, P 0.098, S 0.046%) from Broken Hill Proprietary Ltd., Australia. Aluminum SAC 1576 (Al 93.3, Si 5.13, Fe 1.13, Cu 0.16, Mn 0.11, Ni 0.10, Mo 0.025, Cr 0.008%) from Alcoa, Australia.

The alloys were required to have a flat surface (*5*) of 3.5 cm minimum diameter to seal against an O-ring. The sputtered area was only 0.4 cm^2 in the center of the flat surface, i.e., 4% of the minimum prepared surface area.

The alloys were supplied in the form of short (≈3 cm length) cylinders. They are not guaranteed to be homogeneous, and the part most likely to differ from specification is the central, most conveniently sputtered, region.

Nonmetallic Materials. A number of copper smelting and refining slags that had been obtained using submerged combustion (*10*) and which had been analyzed chemically, were studied, as also were seven nickel salts of laboratory or reagent grade purity. They were ground to −200 mesh (<75-μm diameter), mixed with copper, silver, nickel, or iron powder of this particle size or smaller, and pressed at about 1000 MPa (10 tonne cm^{-2}) into disks of 2.5-cm diameter and about 0.2 cm thick. A more detailed description of the preparation of disks incorporating powdered samples will be given in a separate paper devoted to the analysis of powdered samples.

Procedure. The hollow-cathode lamp currents were sufficiently low that self-absorption did not occur for the selected resonance lines (≈2–4 mA for strong lines and up to 8 mA for resonance lines of low oscillator strength).

The sputtering-discharge currents were limited to values for which the ratio A_a/A_i remained constant. This required that the absorbances of the selected resonance lines never exceeded 0.15.

Nonatomic absorbance, due to the presence of agglomerates (*5*, *11*, *12*), was measured using a hydrogen or deuterium lamp and subtracted from the measured absorbance of the resonance line. Typical values measured at 324.7 nm, for a sputtering current of 40 mA and a discharge voltage of 470 V, were 0.004–0.006 for silver disks, and 0.001–0.002 for copper disks. For the samples with major constituents other than silver and copper, the nonatomic absorbance was found to be smaller still.

The monochromator slits were set sufficiently narrow to eliminate spectral interference; for Fe (248.3 nm) and Ni (232.0 nm), this required a spectral bandpass of only 0.07 nm.

In some cases (Tables III, V and VIII), absorbances were measured at one copper wavelength and corrected to absorbances at another wavelength using the absorbance sensitivities given in Table I.

RESULTS

Solid Alloys. The time taken to reach equilibrium sputtering conditions for these samples was 5–6 min.

Chromium in Steel. For this analysis the discharge voltage varied only between 425 and 460 V. Table II shows that the measured concentrations of chromium are in good agreement with the certificate values, except for sample SS486. Some metal was scraped from the sputtered area of this sample, dissolved in hydrochloric acid, and analyzed by flame atomic absorption spectrometry, which gave a result in very close agreement with that determined by sputtering. This appears to be an example of the central region of a standard sample differing from the specification for the bulk.

Table II. Analysis of Solid Alloy Samples[a]

Sample	Element	λ, nm	Analyte, % Certificate	Measured
SS404	Fe	386.0	95.83	
	Cr	357.9	0.68	0.66
SS409	Fe	386.0	92.91	
	Cr	357.9	1.22	1.24
SS486	Fe	386.0	80.66	
	Cr	357.9	4.53	4.22[b]
B.H.P. No. 5	Fe	386.0	88.61	
	Cr	357.9	1.28	1.30
SS406	Fe	386.0	93.66	
	Ni	352.5	1.69	1.65
SS408	Fe	386.0	93.16	
	Ni	352.5	4.58	4.54
SS410	Fe	386.0	92.96	
	Ni	352.5	2.04	2.06
B.H.P. No. 5	Fe	386.0	88.61	
	Ni	352.5	4.28	4.37

[a] Internal standard: iron. Reference samples: SS407 (3.00% Cr); SS409 (3.14% Ni). Sputtering discharge conditions: Cr: 12 mA, 425–460 V, 3.7 Torr Ar; Ni: 16 mA, 400–500 V, 3.7 Torr Ar. [b] Chromium was determined as 4.23 percent by flame atomic absorption analysis of scrapings taken from the sputtered area.

Table III. Analysis of Solid Alloy Samples[a]

Sample	Element	λ, nm	Analyte, % Certificate	Measured
SS406	Cu	324.7	0.32	
(low alloy steel)	Ni	352.5	1.69	1.75
1168	Cu	324.7	0.26	
(low alloy steel)	Ni	352.5	1.03	0.94
SAC 1576	Cu	324.7	0.16	
(aluminum)	Ni	352.5	0.10	0.097
C1100	Cu	224.4[b]	67.43	
(cartridge brass)	Ni	352.5	0.052	0.050
C1115	Cu	224.4[b]	87.96	
(commercial bronze)	Ni	352.5	0.074	0.076

[a] Internal standard: copper. Reference sample: SS407 (0.43% Cu, 0.61% Ni). Sputtering discharge conditions: 60 mA, 480 V, 4–6 Torr Ar. [b] A_{Cu} is measured at 224.4 nm and corrected to 324.7 nm.

Nickel in Steel. The discharge voltages for these samples varied between 400 and 500 V. The measured nickel concentrations are also shown in Table II.

Nickel in Different Alloys Containing Copper. For these very different matrices, the argon pressure in the sputtering cell was varied (4–6 Torr) from sample to sample to maintain a constant discharge voltage (480 V) at a constant sputtering current (60 mA). This was necessary to obtain an adequate sputtering rate under suitable discharge conditions for all samples. The measured concentrations of nickel are shown in Table III.

Powdered Samples Incorporated into Disks. Equilibrium sputtering conditions for the disk specimens were achieved in a maximum of 10 min for newly-pressed disks.

Nickel and Iron in Low-Alloy Steel Incorporated into a Copper Disk. A needle file was used to obtain 100 mg of fine filings from a piece of SS408. These filings were thoroughly mixed with 1 g copper powder, and the resulting mixture was

Table IV. Samples Incorporated in Copper Disks[a]

Sample	Element	λ, nm	Analyte, % Certificate	Analyte, % Measured
SS408	Cu	249.2		
	Fe	248.3	93.16	93.9
	Ni	232.0	4.58	4.58
			By solution AAS	
Nickel compounds:	Cu	249.2	98-99[b]	
hydroxide	Ni	232.0	60.2	57.6
oxide (green)	Ni	232.0	68.6	67.2
carbonate	Ni	232.0	45.5	44.2
sulfate (heated to 180 °C)	Ni	232.0	33.4	32.3
fluoride	Ni	232.0	36.9	37.2
chloride (hydrated)	Ni	232.0	24.3	24.4
sulfide (precipitated)	Ni	232.0	47.8	46.4

[a] Internal standard: copper. Reference specimens: For SS408, a Cu disk containing 0.481% Ni, 1.29% Fe. For Ni compounds, a Cu disk containing 0.309% Ni. Sputtering discharge conditions: SS408: 50 mA, 470 V, 4.5 Torr Ar; Ni compounds: 30 mA, 450-480 V, 4.5 Torr Ar. [b] From composition of disk as prepared.

made up to 5 g by mixing with more copper powder. The discharge voltage was 470 V for the specimen containing SS408 and 490 V for the reference specimen (known amounts of nickel and iron powders pressed into a disk with copper powder). The measured concentrations of nickel and iron in SS408 are shown in Table IV.

Nickel in Nickel Compounds Incorporated into Copper Disks. The disks were made up to contain 1% by weight of nickel, irrespective of the nature of the salt. The discharge voltages for these specimens varied only between 450 and 480 V although the sputtering rate of the nickel carbonate specimen was found to be 11% higher than that of the nickel oxide specimen. Copper was used as the internal standard. Measured concentrations for nickel in the different compounds are also shown in Table IV.

Copper in Copper Slags Incorporated into Silver Disks. Silver has only two usable resonance lines (328.1 and 338.3 nm), each of which is almost totally absorbed when high concentrations of silver are sputtered, and so it is unsuitable as an internal standard. Nickel was chosen instead for this purpose, and disk specimens of 1% nickel, 30% copper slag, and 69% silver were pressed. One slag sample was known to contain 0.1% Ni but the others contained no significant nickel concentrations. The discharge voltages varied over a wide range from 320 to 500 V, but the measured copper concentrations are in good agreement with the values determined chemically (Table V).

DISCUSSION

The advantages of the method outlined in this paper are best illustrated by the results obtained for the copper slags in the silver disk specimens. Although a very wide range of sputtering rates was evident (Table VI), the measured concentrations do not reflect the substantial errors (as much as 500%) which would have arisen without the use of internal standards. In addition, the time taken to weigh, mix, press, clean-up by sputtering, and measure the absorbances for each of these slag samples was only 15 min. This time is to be compared with the 3-4 h taken to determine the concentrations by conventional chemical methods.

Further, Table III shows that, when the absorbance sensitivities are known for several resonance lines of an element, accurate analyses may be made over a wide range of concentrations without adjustment of the sputtering conditions.

Table V. Slag Samples Incorporated in Silver Disks[a]

Sample	Element	λ, nm	Analyte, % Chemical analysis	Analyte, % Measured
CR8	Ni	232.0		
	Cu	249.2[c]	73.2	72.1
CR7/Dip 1	Ni	232.0		
	Cu	327.4[c]	14.9	14.9
E.R. & S.	Ni	232.0		
	Cu	327.4[c]	5.3	5.2[b]
CC 12	Ni	232.0		
	Cu	324.7	1.19	1.24
CC 14	Ni	232.0		
	Cu	324.7	0.44	0.42

[a] Internal standard: nickel, 1.00% incorporated in disk. Reference specimen: Ag disk containing 5.00% Cu, 5.00% Ni. Sputtering discharge conditions: 40 mA, 320-500 V, 4.5 Torr Ar. [b] Corrected for 0.1% nickel in the slag sample. [c] A_{Cu} is measured at this wavelength and corrected to 324.7 nm.

Table VI. Relative Sputtering Rates for Copper Slag Samples Incorporated in Silver Disks[a]

Sample	Relative sputtering rate	Discharge voltage, V
E.R. & S.	1.00	490
CR8	0.87	500
CC 12	0.37	500
CR7/Dip 1	0.24	320
CC 14	0.22	470

[a] Measured by the absorbance for 1.00% nickel incorporated in each disk. Sputtering discharge conditions: 40 mA, 4.5 Torr Ar.

Table VII. Variation of Ratio of Absorbances of Analytes and Internal Standard in Copper Disks[a]

	Discharge conditions, mA	$A_{Cu\ 244.2}$	$A_{Ni\ 232.0}/A_{Cu\ 244.2}$	$A_{Fe\ 248.3}/A_{Cu\ 244.2}$
Voltage, 470 V. Pressure, 6.5-4.0 Torr Ar	50	0.040	2.15	1.73
	45	0.043	2.19	1.79
	40	0.045	2.11	1.78
	35	0.042	2.14	1.76
	30	0.038	2.13	1.76
	25	0.032	2.25	1.78
Voltage, 510-425 V. Pressure, 6 Torr Ar	55	0.048	2.19	1.77
	50	0.047	2.11	1.70
	45	0.040	2.13	1.73
	40	0.032	2.13	1.78

[a] Specimen: Cu 98.82%, Ni 0.309%, Fe 0.874%.

The interesting possibility of analysis without the use of a reference sample, first proposed by Walsh (*13*) in 1955, can again be raised. For small absorbances, the absorbance ratio for two elements in any sample is given by

$$\frac{A_a}{A_i} = \frac{(\Phi_a \lambda_a f_a \sqrt{M_a} F_a)}{(\Phi_i \lambda_i f_i \sqrt{M_i} F_i)} \frac{N_a}{N_i} \tag{4}$$

where M is the atomic weight, N the steady-state number density of sputtered atoms, and F the fraction of those sputtered atoms in the ground state. In the absence of preferential effects, such as preferential sputtering, preferential ionization, or the preferential agglomeration of one element, then

$$\frac{N_a}{N_i} = \left[\frac{D_i}{D_a}\right] \frac{C_a}{C_i} \tag{5}$$

where D is the diffusion coefficient of the sputtered atoms

Table VIII. Proportionality of Concentration Ratios to Absorbance Ratios for Solid Alloy Samples[a]

Sample	$R_c = C_{Ni}/C_{Cu}$	$R_A = A_{Ni}/A_{Cu}$	R_c/R_A
SS406	5.28	0.851	6.2
H 1168	3.96	0.572	6.9
SAC 1576	0.625	0.0952	6.6
C 1100	0.000771	0.000116[b]	6.6
C 1115	0.000841	0.000136[b]	6.2

[a] Copper measured at 324.7 nm and nickel measured at 352.5 nm. [b] A_{Cu} is measured at 224.4 nm and corrected to 324.7 nm.

in the sputtering cell. If the constants in Equations 4 and 5 are known, it is possible to determine the concentration of any element relative to any other in the sample. The results in Table VII show that the absorbance ratios A_{Ni}/A_{Cu} and A_{Fe}/A_{Cu} for a copper disk specimen are not affected by changes in discharge current, voltage, or pressure over the ranges investigated. Furthermore, Table VIII shows that for several very different alloys the ratio A_{Ni}/A_{Cu} for the sputtered vapor is directly proportional to the ratio of the concentrations, C_{Ni}/C_{Cu}, in the solid. The results shown in both these Tables indicate that preferential sputtering, ionization, and agglomeration, if present, remain constant over a wide range of conditions. This suggests that preferential effects do not occur at all in the type of discharge used in this investigation, and hence that Equation 5 is valid. Thus it may be possible, knowing the concentration of one constituent of a sample, to determine that of any other constituent without the need for a reference sample.

ACKNOWLEDGMENT

The author thanks A. Walsh for suggesting this study and for his continued encouragement and interest, J. M. Floyd for supplying the analyzed copper slag samples, J. B. Willis for analyzing the nickel compounds and incorporating them into copper disks, and P. Hannaford for many valuable suggestions.

LITERATURE CITED

(1) B. J. Russell and A. Walsh, *Spectrochim. Acta*, **15**, 883 (1959).
(2) B. M. Gatehouse and A. Walsh, *Spectrochim. Acta*, **16**, 602 (1960).
(3) A. Walsh, Proceedings of the Xth Colloquium Spectroscopicum Internationale, Washington, 1962, p. 127
(4) D. S. Gough, P. Hannaford, and A. Walsh, *Spectrochim. Acta, Part B*, **28**, 197 (1973).
(5) D. S. Gough, *Anal. Chem.*, **48**, 1926 (1976).
(6) G. M. McCracken, *Rep. Prog. Phys.*, **38**, 241 (1975).
(7) M. Dogan, K. Laqua, and H. Massman, *Spectrochim. Acta, Part B*, **26**, 631 (1971).
(8) P. Hannaford and D. C. McDonald, unpublished work.
(9) H. Jäger and F. Blum, *Spectrochim. Acta, Part B*, **29**, 73 (1974).
(10) J. M. Floyd, Institute of Fuels Conference, Adelaide, Australia, 1974.
(11) K. Kimoto, Y. Kamiya, M. Nonoyama, and R. Uyeda, *Jpn. J. Appl. Phys.*, **2**, 702 (1963).
(12) Yu. I. Petrov, *Opt. Spectrosc. (USSR)*, **27**, 359 (1969).
(13) A. Walsh, *Spectrochim. Acta*, **7**, 108 (1955).

RECEIVED for review February 22, 1977. Accepted May 10, 1977.

Laser-Vaporized Atomic Absorption Spectrometry of Solid Samples

Toshio Ishizuka,* Yoshinori Uwamino, and Hiroshi Sunahara[1]

Government Industrial Research Institute, Nagoya 1-1, Hirate-machi, Kita-ku, Nagoya, 462 Japan

A Q-switched ruby laser was used to produce the atomic vapor from the solid samples, such as brass, steel or aluminum alloy. The atomic vapor produced with the laser beam was introduced into the absorption path by the flow of Ar gas. The absorption signals of Al, Cr, Cu, Fe, Mn, Mo, Ni, and V were traced with an oscilloscope, and those elements were determined with the peak-height or integration method. Precision (relative standard deviation) was 2.1 to 10% for the peak-height method, and 1.0 to 12% for the integration method. The analytical curves prepared with both methods were linear for all the elements studied. The detection limits obtained with the peak-height method were lower than those obtained with the integration method.

Flames or graphite furnaces are normally used as an atomizer for solution samples in atomic absorption spectrometry (AAS). In the case of solid samples, they are converted into solution samples, and the analyses are performed. In order to analyze directly various elements in solid samples, some methods for the atomization of solid samples have been investigated (*1*).

Laser beam has been used as the atomizer for the atomic absorption of solid samples by several investigators (*2–6*). In these studies, the plumes produced on the sample surfaces by the laser beam were used as an absorption path. A xenon flash lamp (*2*), the continuum at the base of the laser plume (*3*), pulse-radiated hollow-cathode lamps (*4*, *5*), and dc-operated hollow-cathode lamps (*6*) were used as the primary light source for AAS.

The instantaneous emission from the laser plume is significantly intense compared with the light from the hollow-cathode lamps of conventional light source for AAS. In the laser plume, the line spectra from excited atoms or ions and the continuous spectrum from bremsstrahlung of electrons are observed. When the laser plume is used as the absorption path in AAS, those emission spectra may interfere with atomic absorption measurement. Then compensation for background emission must be performed.

The authors designed and constructed an atomization-absorption cell in which the chamber for atomizing solid sample was separated from the absorption path. An atomic absorption spectrophotometer with conventional hollow-cathode lamps and monochromator was used. Laser-vaporized

[1] Present address, The Faculty of Engineering, Hiroshima University, Hiroshima, Japan.

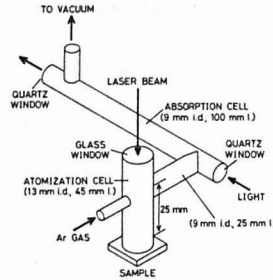

Figure 1. Schematic diagram of atomization-absorption cell. The cell is made up of stainless steel walls and quartz or glass windows. The scheme is represented in inside dimensions

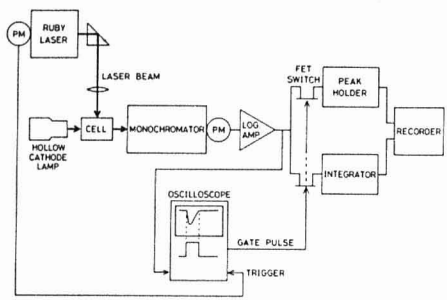

Figure 2. Block diagram of measuring system

atomic absorption spectrometry (LVAAS) of solid samples was studied with the atomization-absorption cell system. The oscillograms of absorption signals for several elements in metal samples, optimum operating conditions, precision, analytical curves, and detection limits are discussed.

EXPERIMENTAL

Apparatus. A model JLR-02A Giant Pulse Laser with a ruby rod 10 cm long and 10 mm in diameter (Japan Electron Optics Lab. Co., Ltd., Japan) was used as the atomizer for solid samples. The maximum peak power is about 70 MW; the maximum output energy, about 1.5 J; the pulse-width, less than 20 ns; and the reproducibility of laser energy, ±5%. The laser energy increases with an increase of the capacitor voltage (CV) for the power supply to the xenon flash lamp used to pump the laser rod. According to the test record offered by the maker, the laser energies at various CVs were approximately as follows: 0.4 J at 3800 V, 1.0 J at 4000 V, 1.2 J at 4200 V, and 1.3 J at 4400 V. The optical system of a model AA-1 Atomic Absorption Spectrophotometer (Nippon Jarrell-Ash Inc., Japan) was used in this study.

The atomization-absorption cell made up of stainless steel walls and quartz or glass windows was designed and constructed. Figure 1 shows the schematic diagram represented in inside dimensions. The cell attached to the atomic absorption apparatus was connected to a vacuum line with a rotary oil vacuum pump (Hitachi Ltd., Japan, Model 4VP-C). The pressure inside the vacuum line was measured with a Pirani gauge (Daia Vacuum Engineering Co., Ltd., Japan, Model PT-S200). A needle valve (Edwards Vacuum Components, England, Model LB1B) was used for the controlled introduction of argon gas into the cell. The flow rate of argon gas (FRAG) was measured with rotameters (Ueshima Brooks, Japan). When a sample was mounted to the atomization cell, an O-ring was used to seal the sample.

The atomic vapor produced from a sample by the laser beam stayed in the absorption cell for the time of millisecond order. The profile of the very rapid absorption signal by the atomic vapor could not be directly recorded by a conventional strip chart recorder. Therefore, absorption signals were measured by means of the measuring system shown in Figure 2. The absorption signal (percent absorption) from a photomultiplier (Hamamatsu TV, Japan, Model R-106) was transformed into the logarithm (absorbance) by a logarithmic amplifier (Teledyne Philbrick, U.S.A., Model 4363). The output signal from the logarithmic amplifier followed into a peak holder or a integrator through FET switches (Teledyne, U.S.A., Model 2110BE). The FET switches were turned ON by the gate pulse generated from an oscilloscope (Matsushita Communication Industrial Co., Ltd., Model VP-5410A). The oscilloscope was triggered by the pulse-radiation from the xenon flash lamp used to pump the laser rod. The peak holder and integrator using 0.01-μF polystyrene capacitors were arranged with operational amplifiers (Teledyne Philbrick, U.S.A., Model 1026). The peak holder was used for measuring the peak value of the absorption signal profile (peak absorbance). The integrator was used for measuring the area of the profile (integrated absorbance). The value of integrated absorbance is expressed in the product of absorbance and time (ms). The signals stored in the peak holder or integrator were recorded by a two-pen strip chart recorder (Matsushita Communication Industrial Co., Ltd., Japan, Model VP-654A).

Table I. Hollow-Cathode Lamp Settings

Element	Analytical line, nm	Lamp current, mA
Al	396.2	10
Cr	429.0	10
Cu	324.7	8
Fe	372.0	10
Mn	279.5 or 403.1	10
Mo	313.3	12
Ni	352.5	10
V	318.4	12

Samples. Metal samples were used as solid samples in this study. The metals were as follows: brasses (the National Bureau of Standards, U.S.A., C1103–C1105); carbon steels (the Bureau of Analysed Samples, Ltd., England, SS431–SS435); alloy steels (the Iron and Steel Institute of Japan, Japan, 152–154); and aluminum alloys (Alcoa Research Laboratories, U.S.A., KA-213-B, KA-356-E, KB-356-B, KC-356-E, and SS-138-R).

Procedure. The flat and smooth surfaces of samples were obtained by polishing with a 400-mesh silicon carbide paper. The samples with the polished surfaces were washed with distilled water and ethyl alcohol, and dried with hot air. A sample was mounted on the atomization cell. A laser beam was directed downward by a 45° quartz prism and focused on the sample surface by using a 10-cm focal length lens. The diameter of the laser beam was about 1 mm on the sample surface. A plume was produced from the sample by the laser beam. The atomic vapor in the laser plume was introduced into the absorption cell by the flow of argon gas. The absorption signal from the atomic vapor was traced by the oscilloscope and measured by means of the measuring system shown in Figure 2. The laser beam was shot on the sample at 30-s intervals.

The following elements in each sample were determined: iron and nickel in brass; aluminum, chromium, copper, manganese, molybdenum, and nickel in carbon steel; vanadium in alloy steel; and copper, iron, and manganese in aluminum alloy. The concentrations of most of the above elements were too high to use the most sensitive analytical lines. Less sensitive lines were used for most of the elements. Table I shows the wavelengths of analytical lines and the lamp currents for each element used in this study.

RESULTS AND DISCUSSION

Oscillograms of Absorption Signals. The signals from the photomultiplier followed directly into the oscilloscope. The absorption signals for each element were traced with the oscilloscope. The profiles of absorption signals were affected by FRAG (i.e., pressure in cell) and CV (i.e., laser energy). In the oscillograms for several elements, emission signals were

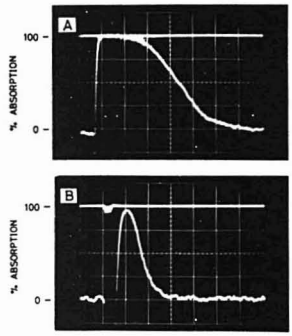

Figure 3. Oscillograms of the absorption signals for copper in brass and aluminum in aluminum alloy. (A) Cu (61.3%) in brass; analytical line, 324.7 nm; time scale, 2 ms/div. (B) Al (92.3%) in Al alloy; analytical line, 396.2 nm; time scale, 1 ms/div. FRAG, 200 mL/min. CV, 4100 V

observed first, followed by absorption signals under conditions of FRAG up to 100 mL/min (2.5 Torr). The emission intensities decreased with an increase of FRAG, and increased with an increase of CV. The oscillograms of absorption signals were taken under conditions of FRAG from 20 to 1000 mL/min (0.9 to 40 Torr) and of CV from 3800 to 4400 V (0.4 to 1.3 J). The effects of FRAG and CV on the absorptions for several elements are quantitatively discussed in successive sections. In this section, the oscillograms obtained under the optimum conditions of FRAG of 200 mL/min (5 Torr) and of CV of 4100 V (1.1 J) are presented.

The absorption signals for copper in brass, iron in steel, and aluminum in aluminum alloy were traced with the oscilloscope. Figure 3 shows the oscillograms of absorption signals for copper and aluminum. In the oscillograms, emission signals were observed prior to absorption signals. In the oscillogram for copper, the light of 324.7 nm from the copper hollow-cathode lamp was fully absorbed by copper vapor introduced into the absorption cell. The oscillogram for iron was similar to that for copper in Figure 3. The emission signal in the oscillogram for aluminum was significantly intense compared with those for copper or iron. The lifetime of atomic vapor of aluminum was appreciably shorter than those of copper or iron. The shorter lifetime of aluminum atoms is concluded to be due to the immediate combination of aluminum atoms with oxygen as an impurity in argon gas.

A check for scattered radiation was made using the non-absorbing line at 352.1 nm from neon of filler gas in a hollow-cathode lamp and with a deuterium hollow-cathode lamp. Neither of the oscillograms obtained with the samples of brass, steel, and aluminum alloy represented absorption signals.

The absorption signals for each element of minor concentrations in brass, steel, and aluminum alloy were traced with the oscilloscope. Figure 4 shows the oscillograms of absorption signals for iron (0.26%) in brass, manganese (0.37%) in steel, and copper (0.055%) in aluminum alloy under conditions of FRAG of 200 mL/min and of CV of 4100 V. The absorption profiles for manganese in steel and copper in aluminum alloy were simple. That for iron in brass showed a shoulder after peak absorption occurred. The shoulder was observed also in the oscillogram for nickel in brass. However, the shoulder was not observed in the oscillograms for iron in aluminum alloy and nickel in steel. The shoulder may be related to the fact that brass is composed of the two matrix elements of copper and zinc. In the atomic vapor produced from brass by the laser beam, the lifetime of zinc atoms was

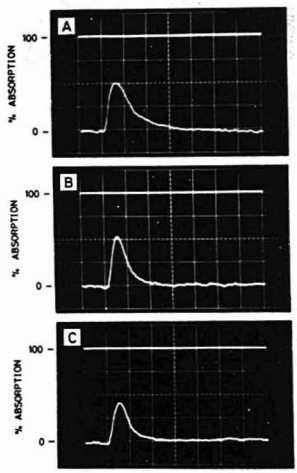

Figure 4. Oscillograms of the absorption signals for several elements. (A) Fe (0.26%) in brass; analytical line, 372.0 nm. (B) Mn (0.37%) in steel; analytical line, 403.1 nm. (C) Cu (0.055%) in Al alloy; analytical line, 324.7 nm. FRAG, 200 mL/min. CV, 4100 V. Time scale, 1 ms/div

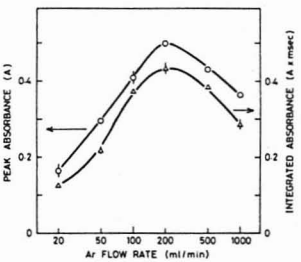

Figure 5. Effect of flow rate of argon gas on the peak and integrated absorbance for copper in steel. Cu concn, 0.046%. Analytical line, 324.7 nm. CV, 4100 V

longer than that of copper atoms. It is expected that a part of the atomic vapor of iron or nickel reacts with the zinc vapor. The absorption profiles for other elements in steel or aluminum alloy were similar to those for manganese and copper shown in Figure 4. The memory effect in the cell was not observed for all the elements studied.

The absorption profiles for various elements obtained with the oscilloscope were discussed in this section. In successive sections, the results obtained by means of the measuring system shown in Figure 2 are discussed.

Effect of Flow Rate of Argon Gas. The peak and integrated absorbance for several elements were measured by varying FRAG from 20 to 1000 mL/min under conditions of CV of 4100 V. The elements measured were chromium in steel, copper in steel or aluminum alloy, and iron in brass or aluminum alloy. The same point on a sample surface was shot five times by the laser beam. The average value of five data obtained with each laser shot was taken as the value at the point. Figure 5 shows the effect of FRAG on the peak and integrated absorbance for copper in steel. Each plot is the average of values obtained at two points on the sample. The two ends of the vertical line on each plot represent the values obtained at the two points. The peak and integrated ab-

Table II. Precision Data[a]

Sample	Element	Relative standard deviation, % Peak-height	Integration
Brass	Fe (0.088%)	9.1	1.0
	Fe (0.26%)	4.3	2.3
	Ni (0.07%)	2.7	3.5
	Ni (0.16%)	8.0	1.4
Steel	Al (0.026%)	2.6	7.6
	Al (0.070%)	10	5.0
	Cr (0.13%)	2.2	2.1
	Cr (0.21%)	2.5	2.3
	Mo (0.039%)	2.1	3.4
	Mo (0.085%)	5.1	6.6
	V (0.11%)	6.1	7.1
	V (0.22%)	2.8	4.5
Al alloy	Cu (0.055%)	6.1	2.9
	Cu (0.20%)	4.5	4.1
	Mn (0.22%)	3.8	12
	Mn (0.30%)	4.6	4.2

[a] The precision was evaluated from the data obtained at the five points which were shot every five times with the laser beam.

Table III. Concentration Ranges of Elements Studied for the Preparation of Analytical Curves

Element	Sample	Analytical line, nm	Concentration range, %
Al	Steel	396.2	0.012-0.070
Cr	Steel	429.0	0.13 -0.21
Cu	Steel	324.7	0.017-0.062
Cu	Al alloy	324.7	0.055-0.20
Fe	Brass	372.0	0.044-0.26
Fe	Al alloy	372.0	0.075-0.48
Mn	Steel	403.1	0.37 -0.95
Mn	Al alloy	279.5	0.13 -0.30
Mo	Steel	313.3	0.015-0.085
Ni	Brass	352.5	0.043-0.16
Ni	Steel	352.5	0.069-0.24
V	Steel	318.4	0.11 -0.33

sorbance increased with an increase of FRAG up to 200 mL/min. Those decreased with an increase of FRAG over 200 mL/min. The effect of FRAG on both absorbances for chromium in steel was similar to that for copper in steel. For iron in brass, both absorbances increased with an increase of FRAG in the range from 20 to 1000 mL/min. For copper and iron in aluminum alloy, both absorbances increased with an increase of FRAG up to 200 mL/min. Those slightly increased with an increase of FRAG over 200 mL/min.

Judging from the results obtained above and the functions of the rotary oil vacuum pump used, FRAG of 200 mL/min was selected as optimum conditions.

Effect of Capacitor Voltage. The effect of CV on the peak and integrated absorbance for the same elements as described in the preceding section was studied by varying CV from 3800 to 4400 V under conditions of FRAG of 200 mL/min. The peak and integrated absorbance were measured in the same way as mentioned in the preceding section. Both absorbances for the elements studied were low at CV of 3800 V near the threshold voltage for the Q-switched ruby laser used in this study. Both absorbances highly increased with an increase of CV from 3800 to 4000 V. Those increased little by little with an increase of CV from 4000 to 4400 V. From the results obtained above, 4100 or 4200 V was selected as the suitable CV for all elements studied.

Precision. A method for data treatment to get as high precision as possible was studied, and the following method was employed as most suitable in this study. The same point on a sample surface was shot several times (five times in this study) with the laser beam. The average or sum of five values obtained with each laser shot was treated as the value at the point. This method was particularly effective for the measurements of copper, iron, and manganese in aluminum alloy. Because the surface of aluminum alloy was unevenly sputtered with each laser shot, the values obtained varied widely with each laser shot. However, with the method for the treatment of data mentioned above, the values obtained at each point did not mutually vary widely.

Table II shows the precision data for the peak and integrated values obtained for various elements in brass, steel, and aluminum alloy. The precision (relative standard deviation) in Table II was evaluated from the data obtained at

Table IV. Detection Limits for Various Elements in Brass, Steel, and Aluminum Alloy

Element	Sample	Analytical line, nm[a]	Detection limit: Peak-height method Concn (ppm)	Peak-height method Weight, g	Integration method Concn, ppm	Integration method Weight, g
Al	Steel	396.2	11	1.0×10^{-11}	39	3.5×10^{-11}
		(309.3)	(7.3)	(6.7×10^{-12})	(26)	(2.3×10^{-11})
Cr	Steel	429.0	20	1.8×10^{-11}	98	8.8×10^{-11}
		(357.9)	(2.7)	(2.4×10^{-12})	(13)	(1.2×10^{-11})
Cu	Steel	324.7	7.2	6.5×10^{-12}	33	3.0×10^{-11}
	Al alloy	324.7	32	2.6×10^{-11}	120	9.6×10^{-11}
Fe	Brass	372.0	17	1.7×10^{-11}	29	2.9×10^{-11}
		(248.3)	(1.9)	(1.9×10^{-12})	(6.4)	(6.4×10^{-12})
	Al alloy	372.0	100	8.0×10^{-11}	330	2.6×10^{-10}
		(248.3)	(11)	(8.9×10^{-12})	(37)	(3.0×10^{-11})
Mn	Steel	403.1	37	3.3×10^{-11}	93	8.4×10^{-11}
		(279.5)	(2.1)	(1.9×10^{-12})	(7.4)	(6.7×10^{-12})
	Al alloy	279.5	20	1.6×10^{-11}	42	3.4×10^{-11}
Mo	Steel	313.3	10	9.0×10^{-12}	24	2.2×10^{-11}
Ni	Brass	352.5	24	2.4×10^{-11}	38	3.8×10^{-11}
		(232.0)	(4.7)	(4.7×10^{-12})	(7.5)	(7.5×10^{-12})
	Steel	352.5	29	2.6×10^{-11}	62	5.6×10^{-11}
		(232.0)	(5.7)	(5.1×10^{-12})	(12)	(1.1×10^{-11})
V	Steel	318.4	22	2.0×10^{-11}	30	2.7×10^{-11}
		(318.5)	(16)	(1.4×10^{-11})	(21)	(1.9×10^{-11})

[a] The values calculated for the most sensitive lines are shown in parentheses.

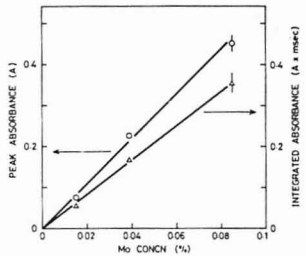

Figure 6. Analytical curves for molybdenum in steel. Analytical line, 313.3 nm. FRAG, 200 mL/min. CV, 4200 V

the five points on a sample. The precision was 2.1 to 10% for the peak-height method, and 1.0 to 12% for the integration method. No differences in precision for the peak-height and integration methods were found from the results shown in Table II.

Analytical Curves. The analytical curves for various elements were prepared with the peak-height and integration methods. Table III shows the concentration ranges of elements studied for the preparation of analytical curves. Figure 6 shows the analytical curves for molybdenum in steel. Each plot in Figure 6 represents the average of the values obtained at the five points. The vertical lines on each plot represent the standard deviations. The analytical curves for molybdenum in steel were linear for both the peak-height and integration methods. The analytical curves for other elements also were linear for both methods.

Detection Limits. Detection limits were determined by use of the samples containing the lowest concentrations of each element. The detection limit was defined as the concentration or weight of element which gives a signal equal to twice the standard deviation of the background level. The weight of the detection limit was calculated from the concentration of the detection limit and the weight of the sample sputtered with the laser shot. The weights of brass, steel, and aluminum alloy sputtered with one laser shot were about 1.0, 0.9 and 0.8 μg, respectively. In this study, the most sensitive analytical lines for most elements were not used for the determination of the detection limits. By multiplying the detection limits obtained with less sensitive lines by the relative sensitive factors for each analytical line, the detection limits for the most sensitive lines were obtained for most elements.

Table IV shows the detection limits obtained with the less sensitive lines and those calculated for the most sensitive lines. The detection limits for the most sensitive lines ranged from 1.9 ppm (1.9×10^{-12} g) of iron in brass to 32 ppm (2.6×10^{-11} g) of copper in aluminum alloy with the peak-height method. Those ranged from 6.4 ppm (6.4×10^{-12} g) of iron in brass to 120 ppm (9.6×10^{-11} g) of copper in aluminum alloy with the integration method. As the time for measuring the integrated value was about one order of magnitude over that for measuring the peak value, the fluctuation of light from the hollow-cathode lamps affected the integrated value more than the peak value. Therefore, the detection limits obtained with the peak-height method were lower than those obtained with the integration method. Because the copper hollow-cathode lamp used picked up a ripple of 60 Hz derived from the power supply, the background level fluctuated. The detection limit for copper was poorer than that predicted. The detection limits for copper, iron, and manganese in aluminum alloy were poorer than those in brass or steel. As mentioned previously, the atomic vapor of aluminum disappeared most rapidly in the atomic vapors of copper, iron, and aluminum of the matrix elements. The aluminum of the matrix element is assumed to affect the behavior of elements coexisting in the aluminum alloy. Therefore, the detection limits for the elements in the aluminum alloy were poorer than those in brass or steel.

The atomization-absorption cell used in this study does not always have the optimum geometry. If the diameter of the absorption cell is reduced, higher sensitivity might be brought about by the improved geometry, and the detection limits can be lowered considerably.

LITERATURE CITED

(1) H. Massmann, "Flame Emission and Atomic Absorption Spectrometry", J. A. Dean and T. C. Rains, Ed., Marcel Dekker, New York, 1971, Vol. 2, Chapter 4.
(2) V. G. Mossotti, K. Laqua, and W. D. Hagenah, *Spectrochim. Acta, Part B*, **23**, 197 (1967).
(3) A. V. Karyakin and V. A. Kaigorodov, *Zh. Anal. Khim.*, **23**, 930 (1968).
(4) E. K. Vul'fson, A. V. Karyakin, and A. I. Shidlovskii, *Zavod. Lab.*, **40**, 945 (1974).
(5) D. E. Osten and E. H. Piepmeier, *Appl. Spectrosc.*, **27**, 165 (1973).
(6) J. P. Matousek and B. J. Orr, *Spectrochim. Acta, Part B*, **31**, 475 (1976).

RECEIVED for review January 17, 1977. Accepted May 12, 1977.

Spectrophotometric Determination of Vitamin K Compounds

J-C Viré and G. J. Patriarche

Institut de Pharmacie, Université Libre de Bruxelles, Campus Plaine, 205/1 Bruxelles, Belgium

Robert J. Nowak and Harry B. Mark, Jr.*

Department of Chemistry, University of Cincinnati, Cincinnati, Ohio 45221

A spectrophotometric method for the determination of Vitamin K (naphthoquinones) compounds has been developed. Titanium (III) is employed to reduce naphthoquinone to its corresponding naphthohydroquinone which subsequently forms a highly colored complex with Ti(IV). Complex formation as a function of time, sulfuric acid concentration, and Ti(III) and Ti(IV) concentration is reported. The method yields highly linear calibration data in the region of 10^{-5} M.

Menadione (vitamin K_3) and analogues (naphthoquinones) are of considerable importance because of their role in blood coagulation processes. Thus, trace analytical techniques for these compounds are necessary for the study of their biological actions as well as in pharmacological and toxicological studies. Previously, these compounds were determined spectrophotometrically (*1–3*) and spot titanium(IV) tests for the identification of naphthoquinones as characteristic complexes had been reported (*4*). Also, similar phenolic type compounds such as chromotropic acid (*5*), sodium 1,3-dihydroxybenzene-3,5-disulfonate (*6*) and thymol (*7*) had been employed as spectrophotometric reagents for the determination of titanium.

Thus, the purpose of this spectrophotometric study of the complexes found on the reaction of titanium(IV) and the naphthoquinones of the vitamin K series was to develop trace analytical techniques for the differentiation and quantitative analyses of these compounds, as reported below.

The method is based on the formation of a colored complex which is obtained on the reaction of a solution containing an excess of a mixture of titanium(III) and titanium(IV) in 14 M sulfuric acid. The presence of titanium(III) in the reaction media is essential to reduce the naphthoquinones to the corresponding naphthohydroquinones which are the actual complexing agents which coordinate with excess titanium(IV). For example:

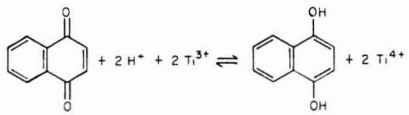

Naphthoquinone, NQ — Naphthohydroquinone, NHQ

Ti(IV) (NHQ) (*1*) (colored)

Although Ti(IV) is a product of the reduction reaction of NQ to NHQ, the reaction goes to completion only when there is a large excess of titanium(IV) present. It is important to note that only the phenolic forms yield a colored complex with Ti(IV); quinonic forms are unreactive.

The compounds examined in this study were:

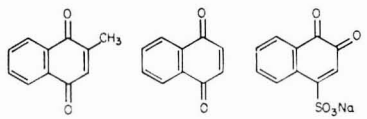

Menadione (Vitamin K_3) — 1,4-Naphthoquinone — Sodium 1,2-naphthoquinone-4-sulfonate

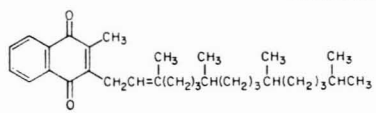

2-Methyl-3-phytyl-1,4-naphthoquinone (Vitamin K_1)

EXPERIMENTAL

Apparatus and Reagents. All of the sulfuric acid solvent solutions were made by dilution of Merck P.A. concentrated sulfuric acid. The titanium(III) stock solutions were 15% $Ti_2(SO_4)_3$ in 23% H_2SO_4 by weight and the stock titanium(IV) was prepared by dissolving $TiCl_4$ in water according to the method of Arthur and Donahue (*8*). Because of solubility problems, the stock 2-methyl-1,4-naphthoquinone solutions were prepared by dissolving 100 mg of the naphthoquinone in 100 mL of methanol as other compounds except sodium 1,2-naphthoquinone-4-sulfonate, which was dissolved in water. It was necessary to prepare these solutions daily and maintain them in the dark because of decomposition problems.

All spectra were taken with a Beckman Acta V spectrophotometer (chart speed 0.5 nm s^{-1}) at room temperature, and blanks of identical solvent composition were employed in the reference beam.

RESULTS AND DISCUSSION

For convenience, the spectral properties and optimization of the reaction variables are discussed for each naphthoquinone separately below.

Menadione (Vitamin K_3). A specific aliquot of the menadione stock solution is placed into a 25-mL volumetric flask and 0.5 mL of the $Ti_2(SO_4)_3$ stock solution and 0.3 mL

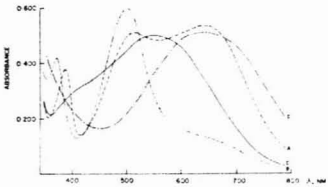

Figure 1. The spectra of the different naphthoquinones complexed with titanium. Medium: H_2SO_4: 14 M; Ti^{3+}: 1.6×10^{-2} M; Ti^{4+}: 2×10^{-2} M. (A) 2-Methyl-1,4-naphthoquinone: 1.1×10^{-4} M. (B) 1,4-Naphthoquinone: 9.5×10^{-5} M. (C) Sodium 1,2-naphthoquinone-4-sulfonate: 1.2×10^{-4} M. (D) 2-Methyl-3-phytyl-1,4-naphthoquinone: 8.9×10^{-5} M

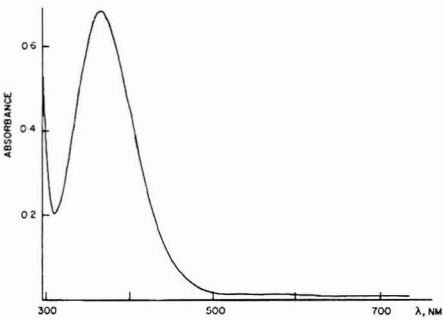

Figure 2. The spectrum of menadione (2-methyl-1,4-naphthoquinone) in 14 M H_2SO_4 solution

of the $TiCl_4$ stock solution (diluted twice with methanol to minimize the violence of the HCl evolution when mixed with 14 M H_2SO_4) are then added. After cooling, the volume of the solution is brought to 25 mL with 14 M H_2SO_4 and it is left in the dark for 30 min prior to use.

Figure 1A shows a typical spectrum for menadione, using the above conditions, which exhibits a broad maximum at 645 nm, a peak at 510 nm, and an acute peak at 391 nm. It is evident that there are actually two distinct complexes formed under these conditions, as the initial color of the reaction solution is blue which slowly changes to a deep blue-violet after standing 30 min in the dark. It is thought the peak at 510 nm would correspond to a red complex and the peak at 645 nm would represent some blue type complex. The ratio of the concentrations of these two complexes was found to be dependent on both the concentration of the Ti(IV) and the concentration of the H_2SO_4. It was also found that the structural nature of the various naphthoquinones also has a strong influence on the color of the final solution. These points will be discussed later. Note that the spectrum of menadione in 14 M H_2SO_4 as shown in Figure 2 is significantly different and exhibits no peaks at 510 and 640 nm which indicates that there is a strong coordination interaction of Ti(IV) in the complex.

A kinetic study of the evolution of the spectrum of the complex showed that the peak at 645 nm shows a steady decrease while concomitantly, the peak at 510 nm increases and reaches a constant value after about 30 min.

Effects of H_2SO_4 Concentration. It has been shown that the concentration of H_2SO_4 has a drastic effect on the nature of the formation of the Ti(IV) complex. Below 8 M H_2SO_4, although it is possible to obtain a colored complex with Ti(IV) for sodium 1,2-dihydroxybenzene-3,5-disulfonate or chro-

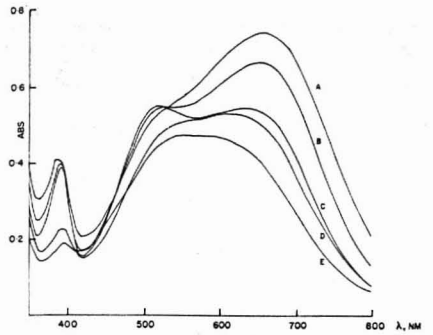

Figure 3. Menadione (2-methyl-1,4-naphthoquinone): study of spectra as a function of acidity. (A) H_2SO_4, 15 M (B) 14 M, (C) 13 M, (D) 12 M, (E) 11 M

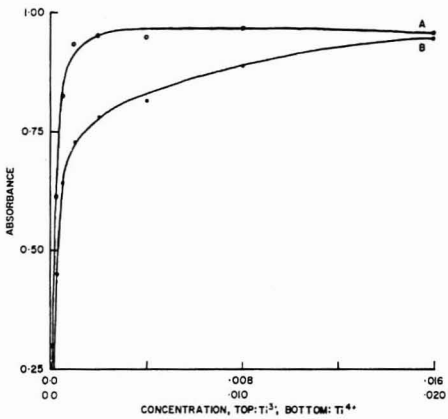

Figure 4. Menadione: absorbance as a function of the concentration of titanium. Concentration of menadione: 2.3×10^{-4} M. (A) at the 510 nm peak. (B) at the 530 nm isosbestic point

motropic acid, no spectral evidence for the formation of a Ti(IV) complex with the naphthoquinone is observed. Figure 3 shows that the peak at 510 nm is observed only at high H_2SO_4 concentrations; 15 M to 13 M in H_2SO_4 (curves A, B, and C, respectively) and that the magnitude of the 645 nm peak decreases markedly with decreasing acid concentration. The isosbestic point at 530 nm is of particular importance because at that wavelength the absorbance of the solution is essentially independent of the concentration of the H_2SO_4 (there is a change of only 0.002 absorbance unit for a change of acid concentration of 13 M to 15 M). It was observed that for H_2SO_4 below 10 M, hydrolysis of Ti(IV) occurs which results in turbidity of the solution making optical measurements impossible.

Effects of Concentration of Titanium Ions. It was found that the concentration of the complexing ion, Ti(IV), has a large influence on the degree of completion of the formation of the complexes as can be seen in Figure 4. The peak at 510 nm reaches a maximum value for Ti(IV)/Ti(III) concentration of 2.5×10^{-3} M/2×10^{-3} M, respectively, as shown in Figure 4. The peak at 645 nm, however, continues to increase with increasing concentrations of Ti(IV) and Ti(III). The isosbestic point at 530 nm also increases in

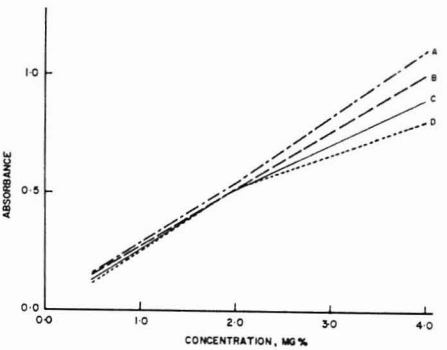

Figure 5. Absorbance as a function of the concentration of menadione at 530 nm. Concentration of titanium: (A) $Ti^{3+} = 2.4 \times 10^{-2}$ M; $Ti^{4+} = 3 \times 10^{-2}$ M. (B) $Ti^{3+} = 1.6 \times 10^{-2}$ M; $Ti^{4+} = 2 \times 10^{-2}$ M. (C) $Ti^{3+} = 8 \times 10^{-3}$ M; $Ti^{4+} = 1 \times 10^{-2}$ M. (D) $Ti^{3+} = 4 \times 10^{-3}$ M; $Ti^{4+} = 5 \times 10^{-3}$ M

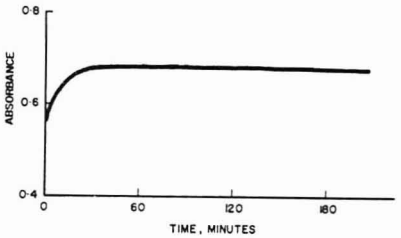

Figure 6. Absorbance of menadione complex (1.2×10^{-4} M) as a function of time at 530 nm

absorbance as the Ti(IV) and Ti(III) concentrations increase, as shown in Figure 4.

Figure 5 shows the variation of absorbance at 530 nm (isosbestic point) as a function of menadione concentration for five different values of Ti(IV)/Ti(III) concentrations. It is evident from this study that the Ti(IV) concentration must be about 2.0×10^{-2} M and Ti(III) must be about 1.6×10^{-2} M in order to obtain a linear calibration curve.

Effect of Development Time. Figure 6 shows that the time required to reach a constant absorbance value at the isosbestic point at 530 nm is approximately 30 min (the optical density increases by 0.001 absorbance unit between 30 and 60 min). A calibration curve for menadione concentrations between 0 and 5.8×10^{-5} M yields a straight line with a correlation coefficient of 0.9998, with $\epsilon = \pm 5150$ when the absorbance was measured at 530 nm after 30 min.

1,4-Naphthoquinone. The complex formed by reaction with 1,4-naphthoquinone, which differs from menadione only in the absence of a two position methyl group, shows a significantly different spectrum, as shown in Figure 1, curve B. The peak in the 645 nm region appears as only a small shoulder and there is a principal peak at 505 nm and smaller sharp peak at 375 nm. The optimum reaction parameters, [Ti(IV)], [Ti(III)], [H_2SO_4], and time were identical to those for menadione. The calibration curve for concentrations between 1.25×10^{-5} and 7.6×10^{-5} M 1,4-naphthoquinone as measured at the 505 nm peak was linear with a correlation coefficient of 0.99991 ($\epsilon = \pm 5590$).

Sodium 1,2-Naphthoquinone-4-sulfonate. With the carbonyl groups in the 1,2-position, the spectra of the resulting Ti(IV) complex are drastically different. An extremely broad

single band with a maximum at 545 nm is observed with no evidence for a 645 nm peak. There is, in addition, an ill-defined shoulder in the 385 to 430 nm region. As sodium 1,2-naphthoquinone-4-sulfonate in 14 M H_2SO_4 in the absence of titanium shows a peak at 390, this shoulder could possibly indicate that the complexation reaction is not quite complete under these conditions. This complex is violet-blue in color. In contrast to the previous two compounds, the peak maximum at 545 nm does not change drastically at high acid strengths (13 to 15 M). Decomposition sets in above 15 M H_2SO_4.

As the effect of Ti(IV) and Ti(III) concentrations was the same as that found for the previous two compounds, except that the absorbance was measured at 545 nm, the experimental conditions for the analysis of sodium 1,2-naphthoquinone-4-sulfonate were identical as described above. A calibration curve for this compound from 7.7×10^{-6} to 4.6×10^{-5} was linear with a correlation coefficient of 0.999987 ($\epsilon = \pm 4350$) and, for the range 1.9×10^{-5} to 2.3×10^{-4} M, the correlation coefficient was 0.99994 ($\epsilon = \pm 4350$).

2-Methyl-3-phytyl-1,4-naphthoquinone (Vitamin K_1). This molecule is different from the others because of the long side chain in the 3-position which perturbs complex formation. The spectrum (Figure 1, curve D) shows a single absorbance band with a rounded maximum between 640 and 655 mn. The two peaks at 510 and 390 nm have disappeared and the color of the complex is different. It is blue and corresponds to a single type of complex. The time needed to form the complex, 45 min, is longer, presumably because of steric hindrance. A calibration curve for this compound from 8.9×10^{-6} to 8.9×10^{-5} M was linear with a correlation coefficient of 0.99999 ($\epsilon = \pm 5730$).

Nature of the Complexes Formed. The structural nature of the complexes formed between titanium(IV) and these naphthoquinones is unknown although there is some indirect evidence that the less sterically hindered species, i.e., 1,4-naphthoquinone, forms dimeric while the more sterically hindered 2-methyl-3-phytyl-1,4-naphthoquinone forms monomeric complexes. Menadione forms a complex which appears to be in equilibrium with its dimeric form. Evidence for these speculations is as follows: (i) All complexes were found to have 1:1 stoichiometry (determined by Job curves). (ii) The absorption spectrum of the menadione complex as a function of acidity indicates the presence of two species in equilibrium (monomer/dimer) as is evidenced by the isosbestic point at 530 nm. Further, lower H_2SO_4 concentrations favor the species absorbing at 510 nm (dimer). (iii) The menadione complex shows a shift in the absorption spectrum as a function of time; the 510 peak increases (dimer) while the 645 nm peak decreases (monomer). (iv) The complex formed with the sterically hindered 2-methyl-3-phytyl-1,4-naphthoquinone exhibits a single peak at 645 nm (monomer favored) while (v) the complex formed with 1,4-naphthoquinone exhibits one peak at 510 nm (dimer favored).

It has been assumed that the presence of an aliphatic side chain (i.e., methyl, phytyl) alters the absorption spectra of these complexes through steric effects exclusively.

Presumably all of these complexes are bound through Ti–O–C bonds which are well documented. The concentration of H_2SO_4 determines the form of the Ti(IV) species which in turn affects the absorption spectrum of the complex (cf. Figure 3). If the concentration of H_2SO_4 is too low, Ti(IV) hydrolyzes and complex formation with most naphthoquinones does not occur.

The spectrum of the complex formed with sodium 1,2-naphthoquinone-4-sulfonate is difficult to explain on the basis of these arguments because this ligand is quite different from the others studied.

LITERATURE CITED

(1) E. E. Van Koetsveld, *Recl. Trav. Chim. Pays-Bas*, **69**, 1217 (1950).
(2) H. Wachsmuth and R. Denissen, *J. Pharm. Belg.*, **42**, 173 (1960).
(3) S. S. M. Hassan, M. M. Abd El Fattah, and M. T. M. Zaki, *Fresenius' Z. Anal. Chem.*, **275**, 115 (1975).
(4) I. M. Kolthoff and P. J. Elving, "Treatise on Analytical Chemistry", Part II, Vol. 5, Interscience, New York, N.Y., 1961 p 1.
(5) T. C. J. Ovenston, C. A. Parker, and C. G. Hatchard, *Anal. Chim. Acta*, **6**, 7 (1952).
(6) J. H. Yoe and A. R. Armstrong, *Anal. Chem.*, **19**, 100 (1947).
(7) J. V. Griel and R. J. Robinson, *Anal. Chem.*, **23**, 1871 (1951).
(8) P. Arthur and J. F. Donahue, *Anal. Chem.*, **24**, 1612 (1952).

RECEIVED for review March 10, 1977. Accepted May 12, 1977. Thanks are expressed to the Fonds National de la Recherche Scientifique (F.N.R.S. Belgium) and the National Science Foundation (Grant No. CHE76-04321) for support of this research.

Fourier Transform Infrared Spectrometric Determination of Gaseous Performic Acid

P. D. Maker, Hiromi Niki,* C. M. Savage, and L. P. Breitenbach

Research Staff, Ford Motor Company, Dearborn, Michigan 48121

Gaseous performic acid in the concentration range 0.01 to 1.0 Torr was analyzed using a Fourier infrared spectrometer system. Sample stability problems were overcome by the fast data acquisition speed and high sensitivity of the system. Sample purity problems were circumvented by taking full advantage of the system's high resolution and spectral subtraction capabilities.

Definitive identification of performic acid (HC(=O)OOH) as a reaction product in the photo-oxidation of hydrocarbons is crucial for the understanding of atmospheric chemistry (*1*). However, because of gas handling problems, no reliable analytical technique has been available. According to Giguere and Almos (*2*), gaseous performic acid decomposes spontaneously to formic acid even at 0 °C and is highly explosive in concentrated form. Nevertheless, they succeeded in recording its IR spectrum but with unknown sample pressure. Unfortunately, its major absorption bands are not readily distinguishable under low resolution from those of formic acid.

The work reported here demonstrates that the IR Fourier spectroscopic method can overcome these difficulties. By combining the following essential capabilities, it becomes a

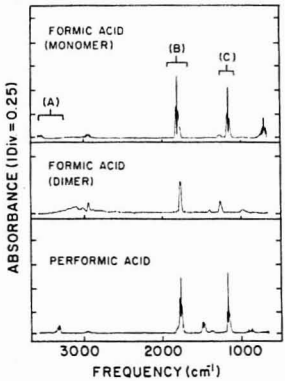

Figure 1. IR spectra of formic acid monomer (0.2 Torr) and dimer (0.05 Torr) and performic acid (0.6 Torr) in the frequency region of 600 to 3600 cm^{-1}. Absorption path length, 1 m. $\Delta\nu = {}^{1}/_{16}$ cm^{-1}. Samples were pressurized with 700 Torr air

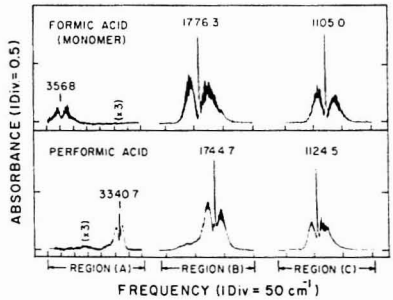

Figure 2. Comparison of three major bands of formic acid (monomer) and performic acid in expanded frequency scales. Frequency regions (*A*), (*B*), and (*C*) correspond to those indicated in Figure 1. Experimental conditions are the same as in Figure 1

uniquely suited analytical tool. Fast data acquisition speed minimizes sample degradation. High detection sensitivity enables trace analysis of hazardous samples and ensures gas handling safety. High spectral resolution and frequency calibration facilitate compound identification. Computer-aided spectral analysis used to remove spectra of known compounds from a composite spectrum enables the use of samples containing known impurities. The technique has been applied successfully to the determination of unstable compounds of atmospheric importance, such as pernitric acid and organic ozonides (*3*, *4*).

EXPERIMENTAL

The Fourier-transform IR facility consisted of a rapid scan, high resolution EOCOM Model 7001 interferometer, a PDP 11/40 on-line computer and in-house software (*5*). The interferometer was equipped with a liquid N_2 cooled HgCdTl detector and was capable of monitoring IR signals in the 600~4000 cm^{-1} range with $\Delta\nu \pm {}^{1}/_{32}$ cm^{-1} and scanning speed <10 s. Spectra were derived from interferograms, ratioed against background, converted to absorbance, and analyzed by expressing them as a linear combination of reference spectra. Typical spectra, recorded in 1.5 min (16 scans) at $\Delta\nu = {}^{1}/_{16}$ cm^{-1} and transformed from the interferogram in 3 min, displayed signal to peak-to-peak noise in excess of 200:1 at 1000 cm^{-1}.

Three KCl-window equipped absorption cells with 0.5, 1, and 40 m (40 pass) path lengths were used to obtain IR spectra and also to examine the stability of performic acid over a wide range of sample pressures (10 mTorr to 1 Torr) diluted in 700 Torr purified air. Formic acid monomer and dimer were present as impurities in the performic acid samples. Reference spectra of these compounds, shown in Figure 1, were obtained by analyzing a series of formic acid spectra recorded at 0.1 to 5 Torr. This series exhibited varying ratios of monomer to dimer as given by an equilibrium constant $K = 5.5 \pm 0.3$ Torr.

Gaseous performic acid samples (<0.100 μmol) were prepared in the condensed phase following the method of Kuhlmann (*6*). Hydrogen peroxide (90% pure, 0.5 cm^3) and sulfuric acid (concd, 0.1 cm^3) were added dropwise to metaboric acid (HBO_2, 1 g) at 0 °C in a 50-cm^3 Pyrex flask. Formic acid (pure, 0.8 cm^3) was then added to the mixture. The flask was kept at 15~18 °C for 1 h and was subsequently evacuated at −78 °C. The condensed material was transferred to the cold finger of a 1-L bulb and to the IR cells using a glass and Teflon gas-handling system.

RESULTS AND DISCUSSION

IR spectra of the gaseous performic acid samples were recorded at pressures ranging from 1 mTorr to 1 Torr as a function of sample storage time (1~30 min) in the IR cells. The results showed that formic acid was the only detectable impurity (<25%) in these samples, and that the decay rate of performic acid was less than 15% in 30 min under these conditions. Thus, it can be stated that performic acid is reasonably stable at low pressures under high dilution in a glass and Teflon gas-handling system. Shown in Figure 1 is a typical absorbance spectrum of performic acid which was obtained from a sample spectrum by subtracting the contribution of formic acid monomer and dimer.

The spectral features shown in Figure 1 are in good agreement with those determined by Giguere and Almos (*2*). However, the present high resolution spectrum exhibits much more pronounced Q-branches for nearly all the bands. In Figure 2, the spectral regions (*A*), (*B*), and (*C*) of Figure 1 are expanded for a closer comparison of formic acid and performic acid. Frequency assignments are given for the most conspicuous peaks in each band, and not necessarily for the band centers. The major absorption bands in these three regions correspond roughly to the stretching modes of the O–H, C=O, and C–O bonds, respectively. The large downward shift (~200 cm^{-1}) in the OH stretching frequency for performic acid is caused by internal hydrogen-bonding (*2*). It should be emphasized that despite the pressure broadening induced by the diluent air at 700 Torr, these spectra have sufficiently fine structures to permit unique identification and quantitative analysis of performic acid in the presence of formic acid.

In the present work, the lower detection limit of performic acid was about 2.5 ppb for the 1124.5 absorption line for 1.5 min of signal averaging (16 scans) and 40-m path length. This analytical capability is sufficient for laboratory studies of atmospheric chemistry. However, in view of the reasonable stability of performic acid, an order of magnitude improvement in the detection sensitivity could be realized by employing longer signal averaging time and increasing the absorption path length.

LITERATURE CITED

(1) K. L. Demerjian, A. J. Kerr, and J. G. Calvert, *Adv. Environ. Sci. Technol.*, **4**, 1 (1974).
(2) P. A. Giguere and A. W. Almos, *Can. J. Chem.*, **30**, 521 (1952).
(3) H. Niki, P Maker, C. M. Savage, and L. P. Breitenbach, *Chem. Phys. Lett.*, **45**, 564 (1977).
(4) H. Niki, P. Maker, C. M. Savage, and L. P. Breitenbach, *Chem. Phys. Lett.*, **46**, 327 (1977).
(5) P. Maker, H. Niki, C. M. Savage, and L. P. Breitenbach, 30th Symposium on Molecular Structure and Spectroscopy, Paper FA-10, Ohio State University, Columbus, Ohio, June 16–20, 1975.
(6) U. Kuhlmann, British Patent No. 10703 (1967).

RECEIVED for review March 7, 1977. Accepted May 31, 1977.

Double Wavelength Spectrophotometry with a Rapid Scanning Instrument

Robert Szentrimay and Theodore Kuwana*

Department of Chemistry, Ohio State University, Columbus, Ohio 43210

A laboratory rapid scanning spectophotometer employing an oscillating mirror for wavelength scanning was adapted to a rapid wavelength selection technique. Rapid wavelength selection (20 to 100 Hz) in the wavelength range 200 to 700 nm enables the application of this system for the analysis of turbid solutions using double-wavelength spectrophotometry. This system is applied to acquiring spectra of intact mitochondria.

The basic principles, instrumentation, and fundamental applications of double-wavelength spectroscopy, including derivative spectroscopy, have recently been reviewed by T. J. Porro (*1*). In essence, the technique offers considerable enhancement in selectivity and sensitivity for the analysis of turbid samples in the UV–vis region. These may include for example solutions of high molecular-weight polymers, colloidal suspensions, powders, smoke, and biological samples, which scatter a large portion of the sampling light beam. Britton Chance, in his ingenious work on the study of the mechanism of cell respiration by mitochondria over the past three decades has developed a number of instruments and techniques utilizing the double-wavelength approach for spectral and kinetic studies (*2–5*) in highly turbid suspensions. In addition, a number of special techniques and quality instruments have been developed as a result of Chance's original work (*1, 6*).

The potential value of an oscillating-mirror rapid-scanning spectrometer as a highly versatile instrument for analytical applications has been recently emphasized in a number of reports. These applications include spectroelectrochemical studies (*7*), stopped-flow measurements (*8*), rapid spectral signal averaging techniques (*9*), and as a multiwavelength detector system for liquid chromotography (*10*) and microwave plasma emission spectrometry (*11*). The simplicity, compactness of design, large dynamic range (PMT detection), and flexibility of design make the system readily adaptable to numerous experimental applications. The oscillating mirror (galvanometer suspension) system can be readily adapted to computer control and data acquisition.

Our current interest in the analysis of turbid solutions of mitochondrial respiratory particles has encouraged us to investigate the feasibility of utilizing this galvanometer based spectrometer as a tool for wavelength modulation techniques. Strojek et al. (*12, 13*) previously had shown the feasibility of using a more sophisticated version of the rapid scanning instrument for SO_2 analysis (18 ppb for 10-m cell) by a combination of correlation and derivative spectroscopy. In this present application, we investigated some of the advantages and limitations of the galvanometer based spectrometer as a double-wavelength instrument for turbid solutions. We also investigated the possible uses in cases where rapid and versatile wavelength selection would be desirable.

EXPERIMENTAL

Optics and Operations. The optical configuration for the laboratory built spectrometer was analogous to that described in a previous report (*13*) (RSS available from Harrick Scientific Corp., Ossining N.Y.) and modification to those published previously (*12*). The light sources used were a 75-W Xenon Arc Lamp, Illumination Industries, Sunnyvale, Calif., and a Philips 13.2-V–100-W Rallye Tungsten Iodide Lamp (sports car headlamp, 5-mm filament). The source focusing mirror (32-cm radius) (see Scheme 1 of ref. 13) focused the source image approximately $^5/_6$ the distance between the source and the galvanometer mirror. A cylindrical mirror galvanometer (8.9-cm radius) focused the slit image approximately $^4/_{10}$ the distance between the galvanometer and spherical mirror, M_2 (radius 30.5 cm). M_2 focused the galvanometer image on the grating and also on the exit slit. Four Bausch and Lomb "Certified Precision" gratings (300 l/mm blazed at 500 nm, 600 l/mm blazed at 300 nm, 600 l/mm blazed at 750 nm, 1200 l/mm blazed at 300 nm) were mounted on a rotating stand so they could be used interchangeably. The configuration resulted in a 3:1 magnification of the entrance slit image at the exit slit. The galvanometer used was a self-contained 7-380 Galvanometer (Bell and Howell, Pasadena, Calif.) with an aluminized surface (0.15 inch wide × 0.20 inch high). The fluid damped galvanometer was specified to operate at 3.5 mA/degree beam rotation, terminal resistance of 75 ohms ± 10%, and at an undamped natural frequency of 575 ± 10% Hz. Two RCA type 7151Z head-on 3.8-cm diameter multi-alkali PMTs were used.

The resolution of the instrument (1.2-nm width at half-height) had been previously determined by the use of a HeNe laser (633 nm) by replacing the light source with the laser. For this study the resolution was approximated by replacing the Xenon Arc Source with a Hg-Arc source (Illumination Industries, Inc.) and determining the width half-height of the 546-nm line. The Hg-Arc spectrum was taken utilizing the current output of only one of the two PMTs and measuring the voltage drop across a 100-kΩ resistor to ground. Spectrometer slits were set for a resolution of 1.6 nm for all spectra reported in this paper unless specified otherwise.

Mitochondrial solutions were contained in a Lucite cell specially constructed for use in indirect coulometric titrations (1.25-cm path length and 10-mL volume). Scattered light from the sample cell was focused onto the PMT with a double convex lens. The necessity of a conventional size stirrer prevented moving the cell closer to the PMT. A reference cell also containing a mitochondrial suspension which was not stirred during the course of the experiment, was placed near to the reference PMT (~2 cm) and positioned to balance the baseline. The flatness of the baseline was thus limited by the mismatch between the sample and reference cells and their placement. With two matched 1-cm cuvettes a flat baseline within ±0.01 absorbance unit could be achieved between 500–650 nm for the absorbance difference between fully reduced suspensions of mitochondria.

Electronics. The circuit used for driving the galvanometer mirror is presented in Figure 1. OA1 and OA2 are voltage followers (Fairchild μA 741) which track the input linear ramp (OA1) for wavelength. The relay (Teledyne 712-12) switches between these two voltages at a frequency imposed by an external square wave source (+12 V). OA3 (μA 741) serves as a unity gain amplifier in the dual wavelength mode and is used as a summing amplifier in the derivative or modulation mode. In the derivative mode the relay is closed to OA1 (not switching) and a sine wave of the desired modulation amplitude is added to the linear ramp. Trim capacitor, C, is adjusted to give the optimal RC constant for galvanometer operation (damping). OA4 (Teledyne Philbrick 1009) and booster amp OA5 (Teledyne Philbrick 2001) serve as a current pump for the galvanometer coil (G). In this configuration the load current through the coil is proportional to the input voltage at OA4 and R. The computer operations were similar to

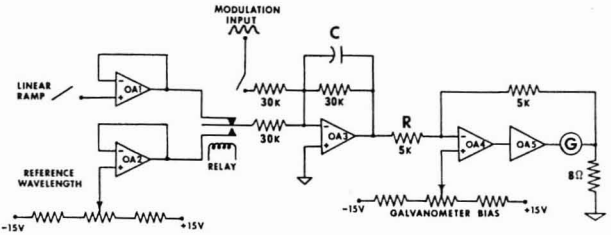

Figure 1. Circuit diagram of the electronics utilized for driving the rapid scanning galvanometer mirror

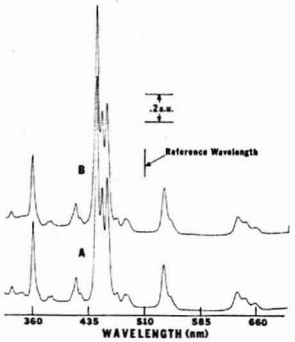

Figure 2. Absorbance spectra of a holmium oxide filter obtained using a 300 l/mm grating blazed at 300 nm: (*A*) Spectrum obtained in the normal simple sweep mode; (*B*) spectrum obtained in the double-wavelength mode at 40 Hz modulation; scan time = 200 s and reference λ at 510 nm

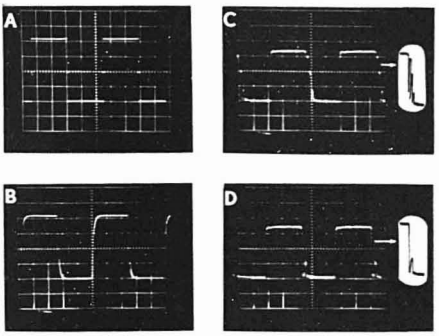

Figure 3. Driving and response waveforms for dual-wavelength operation between 578 nm and the 536 nm peak of a holmium oxide filter: (*A*) Driving waveform for the galvanometer (output of OA3 in Figure 1) at 40 Hz with no galvanometer damping; (*B*) Driving waveform with damping (RC ≈ 0.5 ms); (*C*) and (*D*) are the absorbance response signals for (*A*) and (*B*), respectively. Full scale time axis for all traces is 50 ms. For Figures *A* and *B* full scale y-axis = 1.60 V. For Figures *C* and *D* full scale y-axis = 0.80 V (or 0.80 absorbance unit). The insets on the right of the figures are retraces for clarity of the transients for traces *C* and *D*

those described previously (*14*). The output of a 12-bit Datal DAC-VR-12B Digital-to-Analog converter was applied directly to the input of OA1 when the spectrometer was computer driven.

The outputs of the two PMTs were balanced by adjusting the high voltage power applied to each. The PMT outputs were converted to log ratio output (absorbance) through a bipolar current log amp (Philbrick-Teledyne Model 4361) and processed directly by the Lock-in-Amplifier (PAR Model 126 with a Model 116 preamplifier. A lock-in time constant of 300 ms was used unless stated otherwise at the output stage. For transmitting data not processed by the lock-in to the computer, the signals were band pass filtered (RC = 0.1 ms) and amplified (gain of 5). The information from the lock-in was then directly plotted on a x-y recorder (Houston Model 2000) and sent in parallel to the computer when desired. A Tektronix Model 7613 storage oscilloscope with Polaroid Camera attachment was utilized to monitor modulation frequencies and responses.

RESULTS AND DISCUSSION

Figure 2*A* illustrates the absorbance spectrum of a holmium oxide optical filter obtained by the spectrometer described in the simple sweep mode. Figure 2*B* shows the same spectrum obtained in the dual-wavelength mode where a 40-Hz modulation was used. The signal was demodulated and rectified by the lock-in. A reference wavelength of 510 nm was used for the spectrum. This spectrum provided a serious test for the performance of the modulation technique because of the sharp absorbance peaks and the large wavelength excursions required by the galvanometer during the spectral scan. A careful analysis of the spectrum obtained in the dual-wavelength mode shows a slight loss in resolution (10–20%) probably due to harmonic vibrations of the galvanometer mirror and to the method of signal rectification by the lock-in. Slight spectral distortions are also evident at large excursions of the mirror (i.e., see spectrum at 350 nm). The resolution of this spectrum may be maximized and the spectral clarity optimized by adjusting the RC time constant (C) for the galvanometer drive waveform. This is most easily accomplished by monitoring one of the holmium oxide peaks in the dual-wavelength mode and adjusting the RC constant until a maximum peak height is observed. The reasons for these variations and approaches to possible improvements to the system will become evident during the discussion.

Figures 3*A* and 3*B* show the oscilloscope traces of the galvanometer driving waveforms monitored as the input voltage to OA4. A similar type of voltage response can be monitored in parallel with the galvo coil. The corresponding spectral response for dual-wavelength operation as the mirror oscillates between 578 nm and the 536 nm peak of holmium oxide is shown in Figures 3*C* and 3*D*. If the driving waveform is undamped (3*A* and 3*C*) three to four vibrations of the mirror are observed about the peak in the spectral response. Damping the driving waveform (RC ≈0.5 ms) reduces the vibrations to a single oscillation and considerably improves the spectral characteristics and resolution (10–20%) obtained by the rectification procedure. In either mode of operation, the mirror usually requires approximately 2 ms to reach a constant position as determined from the PMT response. This response time should be a function of the galvanometers "natural frequency" (500 Hz) and might be improved by

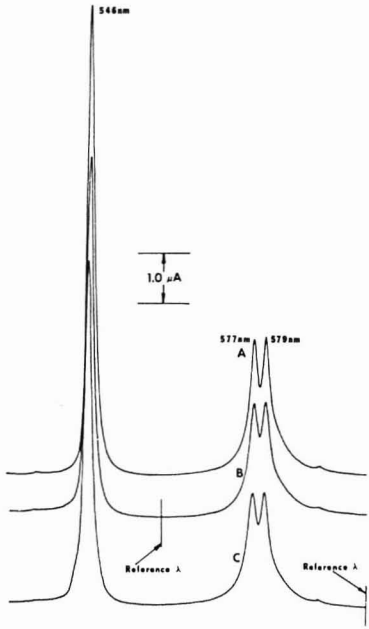

Figure 4. Transmission spectrum obtained of a Hg-Arc source utilizing a 1200 l/mm grating blazed at 300 nm; (*A*) Spectrum obtained in simple sweep mode; (*B*) spectrum taken with respect to 560 nm; (*C*) spectrum taken with respect to 598 nm; 40-Hz modulation; lock-in time constant = 100 ms; 200-s scan time

selecting higher frequency galvanometers and by utilizing more sophisticated damping procedures. Since the lock-in is sampling the entire waveform during rectification, this error contributes to an apparent loss in resolution and represents the most serious limitation to the spectroscopic procedure at present.

Perhaps a clearer representation of the capabilities and limitations of the procedure employed is shown in Figure 4. The normal spectrum and double-wavelength spectrum are shown for the 579–577 nm doublet of a Hg-Arc used as a source for the spectrometer. Figure 4*A* shows the spectrum taken in the simple sweep-mode. Figures 4*B* and *C* depict the spectra obtained in the double wavelength mode taken at a 40-Hz modulation frequency. *B* and *C* were taken with respect to two different reference wavelengths for comparison. An approximate 20% loss in resolution between the two bands is observed. This can be decreased to ≈10% by optimizing the RC time constant in the driving circuit (Figure 1). Further improvement of the system might be made using a type of demodulation enploying a sample and hold or boxcar type integration procedure to discriminate between the desired signal and the galvanometer response time. This type of cross-channel interference (Crosstalk) is a common problem for signal modulation and demodulation techniques (*3–5*).

Two advantages for using the double-wavelength mode are in the enhanced sensitivity and selectivity afforded by the signal rectification and also in data representation. These have been summarized by T. J. Porro (*1*). In turbid solutions or in solutions where background solution fluctuations (density, refractivity) occur, the double-wavelength approach introduces an added dimension of baseline stability. By the inherent

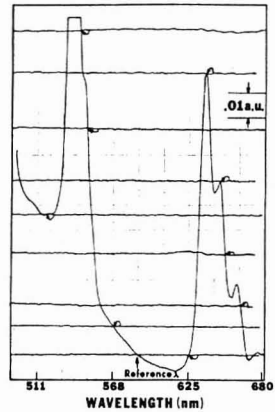

Figure 5. Absorbance spectrum taken at 20-Hz modulation of an expanded portion of the holmium oxide filter shown in Figure 2. Arrows show which points (wavelengths) in the spectrum are monitored for a duration equivalent to the scan time (180 s). A 600 l/mm grating blazed at 750 nm was used

nature of the technique, the background fluctuations that are common to both wavelengths are eliminated in the demodulation procedure. However, care must be taken to account for the changes in the background (i.e., scattering) which are wavelength dependent. In addition, extreme caution and care must be taken in the interpretation of data obtained in the dual-wavelength approach.

When the RSS spectrometer is operated in its usual split beam mode utilizing two PMTs, the low frequency noise and drift are caused primarily by the flicker and arc wander of the xenon source and by the fluctuations of the PMTs. The drift has been found to vary from 1×10^{-3} to 1×10^{-2} absorbance unit per hour. When using the double-wavelength approach, baseline drift was found to be within the limits of measurement imposed by the signal to noise ($<5 \times 10^{-4}$ abs. unit/2-h period). Baseline drift when analyzing turbid samples for small absorbance changes (<0.01) varies with the sample and chemical conditions and becomes prohibitive using normal spectroscopic techniques on samples containing inhomogeneities. Thus, the major advantage of utilizing this technique for clear solutions in our RSS system is to eliminate low frequency noise such as that resulting from a magnetic stirrer (effect of magnetic field on PMT) or from signal drift. Further, it enables the system to handle turbid solutions without any modification necessary in the optical system.

The approximate noise level at various wavelengths in double-wavelength operation is shown in Figure 5 for an expanded segment of the holmium oxide absorption spectrum. The wavelengths designated by the arrows in the Figure were monitored for approximately 180 s. The results are shown superimposed on the spectrum. Peak to peak noise varies from $\sim 5 \times 10^{-4}$ abs. unit for wavelengths near the reference wavelength (0–25 nm) to $1\text{–}2 \times 10^{-3}$ abs. unit for large excursions of the galvanometer mirror. However, noise appears to be more a function of spectral features. Drift and noise appear to be degraded worst for steep portions of the spectrum where mirror instabilities or higher order vibrations are more apparent by the spectral characteristics. Using a xenon arc source, the minimum noise level typically varies from 5×10^{-4} to 1×10^{-3} absorbance unit. This is the value of noise typically expected as a limit of spectrometers employing an arc source without utilizing special source stabilization and compensation

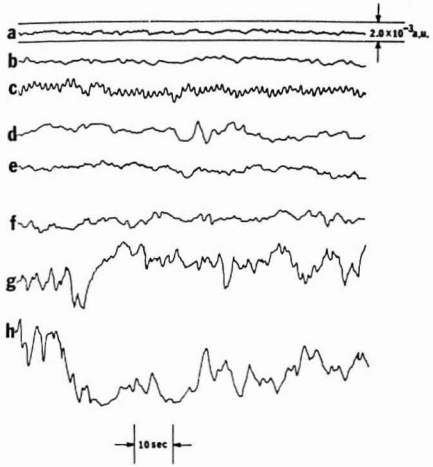

Figure 6. Illustration of the dependence of noise on the modulation frequency of the galvanometer mirror for operation between 587 and 637 nm in the holmium oxide spectrum (*a* through *h* taken at 20-Hz intervals from 20 to 160 Hz)

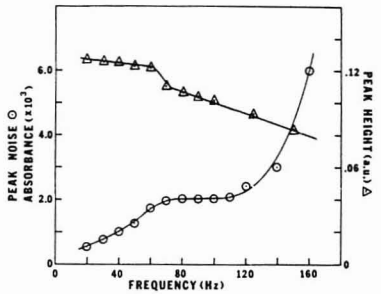

Figure 7. Plot of the dependence of peak to peak noise and peak height of the 637-nm band of holmium oxide on dual-wavelength modulation frequency. Experimental parameters were the same as those described in Figures 5 and 6

techniques (*15*). The dependence of S/N on the modulation frequency is shown in Figures 6 and 7 for operation between 587 nm and 637 nm (the holmium oxide peak). Clearly, the galvanometer operation is limited to low frequencies for optimal results. Higher frequencies probably result in higher order vibrations of the galvanometer and corresponding loss in sensitivity and resolution. The phase lag for the signal response between 20 to 160 Hz varies linearly from 25° to 190° as determined by the lock-in phase adjustment. This phase lag results from mechanical inertia of the mirror which is determined by the specifications of the particular galvanometer used.

Perhaps a more unique and useful capability of the RSS is for rapid sampling of several predetermined wavelengths for desired intervals of time. Such can be easily achieved by digital logic or computer control of the galvanometer mirror positions. In trace *A* of Figure 8, wavelength selection spectroscopy is illustrated by the monitoring of the absorbance at 10 arbitrary wavelengths of the holmium oxide spectrum. The time interval of sampling is 10 ms for each wavelength.

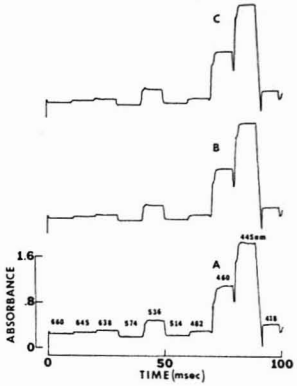

Figure 8. Computer acquired absorbance response for the rapid selection of 10 consecutive wavelengths in the holmium oxide spectrum shown in Figure 2. The numbers above the response curve represents the wavelengths selected. (*A*) One sweep through the procedure; (*B*) the average of 10 runs; (*C*) the average of 100 runs

It should be noted that the wavelengths chosen correspond to the maxima or minima of absorbance of the holmium oxide spectrum shown in Figure 2. The choice and resulting resolution to wavelength were limited by the resolution of the D/A which determined the position of the galvanometer mirror (ca. 1800 bits at 2.5 mV/bit). The reproducibility of the absorbance at each 10 wavelengths is illustrated by traces *B* and *C* in Figure 8 which are the results for 10 and 100 averaged scans. The absorbance during the initial 2 ms at each wavelength corresponds to a composite of the absorbance over that part of the spectrum being scanned during the excursion of the galvanometer from the initial to final position (wavelength). Thus, the absorbance during only the latter 8 ms at each wavelength is the one of interest. This multiwavelength selection spectroscopy is well suited for computer controlled operation and can lend itself for rapid monitoring of desired wavelengths for HPLC, multielement flame emission or atomic absorption spectroscopy, and other methods where spectral detection is desirable.

The spectrophotometric analysis of the cytochrome components of intact mitochondria offered a good test for our double-wavelength procedures. The spectroscopic and chemical properties of these enzymes have been well documented. In addition, we were interested in investigating the feasibility of applying indirect coulometric techniques for the redox titration and turnover of the respiratory system. The turbid solution absorbance at 2 mg/mL of particles typically varied from 0.5 a.u. to 1.5 a.u. (500–700 nm) depending on the wavelength and on the collection efficiency of scattered light from the sample. Turbidity changes also occur (1 to 4 h) due to the mixing and settling of the particles and due to chemical changes which are imposed during the course of the experimentation. In addition, the instrumental zero drift should be small to permit the achievement of the sensitivity required for the analysis of the low concentration of membrane bound enzymes that are present (1 to 2 μM).

The type of spectra obtained using the double-wavelength mode with intact beef heart mitochondria (2.25 mg/mL) is shown in Figure 9*A* for cytochrome oxidase and cytochrome $c + c_1$ in the α region of their spectrum (500–630 nm) obtained during the course of a potentiometric titration (*16*, *17*). The reference wavelength used for these spectra is the isosbestic point at 542 nm for cytochrome $c + c_1$. Mitochondria (2.25

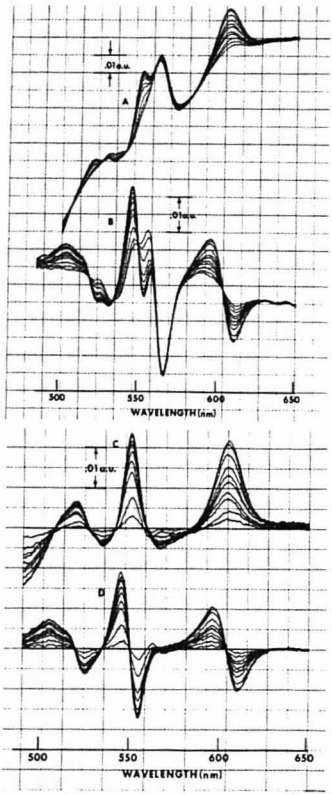

Figure 9. Series of spectra of intact mitochondria obtained during the course of an indirect coulometric titration under potentiometric conditions (see text): (*A*) Double-wavelength spectra using 542 nm as the reference λ; (*B*) derivative spectra taken alternately with the spectra in *A*; (*C*) spectra from *A* after computer subtraction of the "baseline" spectrum; (*D*) spectra from *B* after computer subtraction of derivative "baseline"

mg/mL) were suspended in 100 mM sucrose solution in pH 7.0 phosphate buffer and rendered anaerobic. Potentiometric mediators added were hydroquinone (50 μM), duroquinone (40 μM), $Fe(CN)_6^{3-}$ (45 μM), CoQ_0 (40 μM), and CoQ_1 (40 μM). Indirect coulometric titrants (*18*) utilized were methyl viologen (1.0 mM) for reduction and oxygen generated at a platinum wire microelectrode for oxidation. The solution absorbance under these conditions typically varied from 0.6 a.u. to 1.4 a.u. depending on the wavelength and on the collection efficiency of scattered light from the sample. The corresponding "derivative" spectra obtained alternately using a 10-nm peak to peak sine wave modulation is shown in Figure 9*B*. The spectra obtained in Figures 9*A* and 9*B* were stored by the computer on disk as 1000 points per spectrum. The baseline spectra in Figures 9*A* and 9*B* were then subtracted from the rest of the spectra in each series using the computer for calculations. The baseline corrected series of spectra are presented in Figures 9*C* and 9*D*, respectively.

Under the conditions employed in Figure 9, a linear correlation was observed for the cytochrome oxidase derivative absorbance at 615 nm and concentration (correlation coefficient of 0.9966 for 11 points) as determined by the 620 nm – 605 nm absorbance difference value (*17*). The magnitude of the "derivative" signal depends on the amplitude of the peak to peak sine wave modulation. Clearly, the modulation parameters used for "derivative" spectroscopy must be carefully defined and the correlation between signal amplitude and concentration verified for the chemical system of interest. For cytochromes $c + c_1$, a linear correlation (0.9930 for 11 points) was observed between the "derivative" amplitude at 544 nm and the concentration of $c + c_1$ as determined by the 550 nm – 540 nm absorbance difference. For the cytochrome $b_K + b_T$ region (spectral changes not shown in Figure 9), a correlation coefficient of 0.9987 (9 points) was found for the derivative amplitude at 565 nm and the concentration of $b_K + b_T$ as determined by the absorbance difference at 560 nm – 540 nm. The implications of these preliminary results suggest that the proper selection of the amplitude of the derivative modulation and the proper wavelength selection in the analysis of "derivative" spectroscopic data may result in the same information in one derivative spectrum as is obtained in a series of dual-wavelength spectra referenced to different wavelengths for different species. The derivative spectral approach also has the definite advantage of achieving a flatter baseline where the baseline may be the limiting feature for data amplification or signal averaging. Computer acquisition or computer modeling techniques should greatly aid in defining the proper parameters for optimizing dual-wavelength and the derivative spectral approach in the analysis of complex systems such as mitochondria. We anticipate that the dual-wavelength approach as described herein will be equally applicable using vidicon or array type detectors.

ACKNOWLEDGMENT

We appreciate the sample of mitochondrial particles received from J. S. Rieske.

LITERATURE CITED

(1) T. J. Porro, *Anal. Chem.*, **43** (4), 93A (1972).
(2) B. Chance, *Science*, **120**, 767 (1954).
(3) B. Chance and N. Graham, *Rev. Sci. Instrum.*, **42**, 941 (1971).
(4) B. Chance, *Rev. Sci. Instrum.*, **22**, 638 (1951).
(5) B. Chance, N. Graham, J. Sorge, and V. Legallais, *Rev. Sci. Instrum.*, **43**, 62 (1971).
(6) J. A. Peterson, *Anal. Biochem.*, **67**, 468 (1975).
(7) E. E. Wells, Jr., *Anal. Chem.*, **45**, 2022 (1973).
(8) R. M. Wightman, R. L. Scott, C. N. Reilley, R. W. Murray, and J. N. Burnett, *Anal. Chem.*, **46**, 1492 (1974).
(9) E. Steckhan, D. Yates, and T. Kuwana, *Ber. Bunsenges, Phys. Chem.*, submitted, 1976.
(10) M. S. Denton, T. P. DeAngelis, A. M. Yacynych, W. R. Heineman, and T. W. Gilbert, *Anal. Chem.*, **48**, 20 (1976).
(11) O. Rose, Jr., D. W. Mincey, A. M. Yacynych, W. R. Heineman, and J. A. Caruso, *Analyst (London)*, **101**, 753 (1976).
(12) J. W. Strojek, G. A. Gruver, and T. Kuwana, *Anal. Chem.*, **41**, 487 (1969).
(13) J. W. Strojek, D. Yates, and T. Kuwana, *Anal. Chem.*, **47**, 1050 (1975).
(14) D. Yates and T. Kuwana, *Anal. Chem.*, **48**, 510 (1976).
(15) B. Chance, D. Mayer, N. Graham, and V. Legallais, *Rev. Sci. Instrum.*, **41**, 111 (1970).
(16) D. F. Wilson, P. L. Dutton, M. Erecinska, J. G. Lindsay, and N. Sato, *Acc. Chem. Res.*, **5**, 234 (1972a).
(17) B. Chance, R. Oshino, T. Sugano, and N. Oshino, *Biochem. Biophys. Acta*, **368**, 298 (1974).
(18) W. R. Heineman, T. Kuwana, and C. R. Hartzell, *Biochem. Biophys. Res. Commun.*, **49**, 1 (1972).

RECEIVED for review March 14, 1977. Accepted May 31, 1977. Financial support provided by USPHS Grant No. 19181 and NSF Grant No. CHE73-04882.

Effect of Cavity Loading on Analytical Electron Spin Resonance Spectrometry

Ira B. Goldberg* and Harry R. Crowe

Science Center, Rockwell International, Thousand Oaks, California 91360

The effect of cavity loading during magnetic resonance absorption on the accuray of analysis by electron spin resonance is calculated. Large samples which degrade the cavity *Q*-factor because of absorption of a large fraction of the incident radiation cause a nonlinearity of the absorption as a function of the quantity of material. This is reflected by a broadening of the first derivative spectrum and reductions of the peak-to-peak amplitude and double integal of the ESR signal from that predicted on the basis of a dilute sample. The consequence of this effect is to underestimate the quantity of sample. Calculations of this effect were verified with samples of $MnSO_4 \cdot H_2O$. Nonlinearities in the order of 1% may be obtained with samples of 0.4 to 1.0 mg of $MnSO_4 \cdot H_2O$ or 0.1 to 0.25 mg of diphenylpicrylhydrazyl which are commonly used standards for ESR.

Electron spin resonance (ESR) derives much of its value from its high sensitivity and resolution. Hence, it is often used in the identification and quantification of trace impurities (*1*). However, there are many situations in which ESR can be used to quantitatively measure materials which exhibit intense paramagnetic absorption. Examples of this case include the calibration of ESR spectrometers, the analysis of fine grained iron in Lunar return samples (*2*), the determination of initial atom concentrations in studies of gas kinetics (*3*), the analysis of concentrated solutions of radical ions or transition metal ions, and the separation and quantification of solid materials in mixtures by virtue of their unique temperature dependencies such as antiferromagnetic–paramagnetic transitions (*4*). While much attention has been devoted to the high sensitivity feature of ESR (*5*), the effect of the variation of the cavity *Q*-factor across the magnetic resonance has been studied only in terms of its effects on increasing the apparent linewidth of spectra (*6*).

We report here the effect of intense paramagnetic resonance absorption on the various parameters used in analysis. These include the peak-to-peak amplitude of the derivative of the absorption, the double integral of the first derivative, and the peak-to-peak amplitude multiplied by the square of the peak-to-peak linewidth. Both Lorentzian and Gaussian lineshapes are treated, and experimental data are presented.

EXPERIMENTAL

The ESR–computer system has been described in detail (*7*). It consists of a modified V-4502 (Varian) ESR spectrometer with a Magnion 38-cm magnet and a PDP 8/m computer with 32K words of core storage. Data were collected from the ESR spectrometer using a BASIC program with assembly language functions for control of the multiplex, analog to digital converter (ADC), clock, and other peripheral equipment. Two output registers control the upfield or downfield sweep direction, and the starting or stopping of the magnetic field sweep. A power meter was used to monitor the incident power to the cavity.

$MnSO_4 \cdot H_2O$ (Mallinckrodt reagent grade) was recrystallized from water at 80 °C and dried under N_2 for 48 h. Heating two samples at 325 °C for 16 h showed a 10.62% weight loss as compared to 10.66% theoretical. The ESR linewidth of this sample is 200 G, peak-to-peak. Each spectrum contained 1536 points, with 44 points between derivative extrema. Samples were weighed to ±0.05 mg.

Integration of the spectra was carried out subsequent to the data acquisition. The intensity of each spectrum was between 70–100% of the full scale output of the ADC. Since the ADC is 12 bits, it is necessary to minimize numerical round-off errors.

Theoretical calculations of the effect of loading of the ESR cavity were also carried out using the PDP 8/m computer. Integrals of the absorption were computed to within ±0.0002% by Simpson's rule. Derivatives were calculated from the computed absorption by finite differences. Due to the finite word size, accuracy was limited to ±0.001 in the relative peak-to-peak width and ±0.0002 in the relative peak-to-peak amplitudes.

THEORY

Cavity *Q* Variation during Resonance. The *Q*-factor of the microwave cavity during resonance, Q, is related to its *Q*-factor off resonance, Q_o, and to the *Q*-factor of the sample Q_s, according to Equation 1.

$$\frac{1}{Q} = \frac{1}{Q_o} + \frac{1}{Q_s} \tag{1}$$

Q_o is the *Q*-factor of the microwave cavity containing the paramagnetic sample and sample holder, but in which the magnetic field is such that there is no significant interaction of the magnetization of the sample with the incident radiation. The microwave loss caused by the sample magnetization in the ESR cavity is due entirely to its susceptibility, χ'', and to the filling factor, η, of the sample within the cavity (*8*). In cgs units,

$$\frac{1}{Q_s} = 4\pi\eta\chi'' \tag{2}$$

The filling factor is defined as the integral of the square of the microwave magnetic field, H_1^2 over the sample to that in the entire cavity

$$\eta = (\int_{\text{sample}} H_1^2 d\upsilon)/(\int_{\text{cavity}} H_1^2 d\upsilon) \tag{3}$$

Filling factors of rectangular and cylindrical cavities containing a variety of sample geometries have been calculated by Poole (*8*). These and several other cases are presented in Table I. The filling factor can be treated as being proportional to a constant, κ, times the ratio of the sample volume V_s to the cavity volume V_c,

$$\eta = \kappa \frac{V_s}{V_c} \tag{4}$$

The microwave susceptibility for the case in which the field is held constant and the frequency is swept is given by Eqution 5 (*9*),

$$\chi'' = \frac{1}{2}\omega_o \chi_o \frac{T_2}{1 + (\omega - \omega_o)^2 T_2^2} \tag{5}$$

where ω and ω_o are the incident and resonant frequencies, T_2 is the relaxation time and χ_o is the static magnetic suscep-

Table I. Typical Filling Factors[a]

	η	η if $2a = d$
TE_{011} (Cylindrical)		
Small sample at cavity center	$\frac{12.33}{1+\left(\frac{0.82a}{d}\right)^2}\cdot\frac{V_s}{V_c}$	$10.56\frac{V_s}{V_c}$
Tube of radius r, R along cavity axis	$\frac{6.16}{1+\left(\frac{0.82a}{d}\right)^2}\cdot\frac{V_s}{V_c}$	$5.27\frac{r^2}{R^2}$
TE_{102} (rectangular)		
Small sample of cavity center	$\frac{4}{1+\left(\frac{d}{2a}\right)^2}\cdot\frac{V_s}{V_c}$	$2.00\frac{V_s}{V_c}$
Tube of radius r along sample axis	$\frac{2}{1+\left(\frac{d}{2a}\right)^2}\cdot\frac{V_s}{V_c}$ (if $r < a$)	$1.00\frac{\pi r^2}{bd}$
Flat cell of thickness d' and width b'	$\frac{2}{1+\left(\frac{d}{2a}\right)^2}\cdot\frac{V_s}{V_c}$	$1.00\frac{b'd'}{bd}$
Special case Varian TE_{01n} with 2.17-cm i.d. quartz tube		0.331

[a] V_c = cavity volume; V_s = sample volume. Cylindrical cavity: a = radius; d = length. Rectangular cavity: a = thickness; b = width (parallel to static field); d = length.

tibility. We assume that the line is not saturated by the level of incident radiation. For a paramagnetic material,

$$\chi_o = \frac{g^2\beta^2\,(S)(S+1)N}{3k(T-\theta)V_s} \tag{6}$$

where N is the number of paramagnetic centers, S is the electron spin, g is the spectroscopic splitting factor, β is the Bohr magneton, k is the Boltzmann constant, T is the absolute temperature, and θ is the paramagnetic Curie temperature. The term $\eta\chi''$ is therefore proportional to the number of paramagnetic sites in the sample.

Equations 1 and 2 can now be rearranged to give

$$\frac{Q_o - Q}{Q_o} = \frac{\Delta Q}{Q_o} = \frac{4\pi\chi'' Q_o\eta}{1 + 4\pi\chi'' Q_o\eta} \tag{7}$$

Since the ratio of the absorbed power to the incident power is dependent on $\Delta Q/Q_o$, nonlinearities in the response to the microwave susceptibility can result if $4\pi\chi''\eta Q_o$ is not negligible compared to unity. There are two consequences of this condition. The first is simply a saturation of $\Delta Q/Q_o$ due to an increase in the denominator of Equation 7. This is of primary interest here. The second effect is caused by the nonlinear response of the microwave detector to large changes in microwave power. Both of these effects can lead to distortions of the lineshape.

RESULTS AND DISCUSSION

Lorentzian Lineshape. Since Equation 6 is not useful for typical analytical purposes, it can be converted to the conventional case of a fixed frequency of incident microwave radiation and a variable magnetic field, Equation 8,

$$\chi'' = \frac{1}{\sqrt{3}}\chi_o H_o \frac{1}{\Delta_o}\frac{\Gamma^2}{[\Gamma^2 + (H - H_o)^2]} \tag{8}$$

where the halfwidth at one half of the maximum height of the absorption, Γ, is given by $\hbar/(T_2 g\beta)$, and the magnetic field H is given by $\hbar\omega/(g\beta)$. The peak-to-peak width, Δ_o, is equal to $2/\sqrt{3}\,\Gamma$. The maximum value of χ'' occurs when $H = H_o$. Thus the term $\eta Q_o\chi''_{max}$ where

$$\chi''_{max} = \frac{1}{\sqrt{3}}\chi_o H_o \frac{1}{\Delta_o} \tag{9}$$

is dependent on the nature and number of spins in the sample and on the parameters of the ESR cavity, and can be used to characterize the performance of the loaded cavity. The parameter $\eta Q_o\chi''_{max}$ is given by Equation 10.

$$\eta Q_o\chi''_{max} = \kappa Q_o \frac{H_o}{\sqrt{3}\,\Delta_o}\cdot\frac{g^2\beta^2 S(S+1)N}{3V_c k(T-\theta)} \tag{10}$$

In order to compute the relative analytical parameters, $\Delta Q/Q_o$ was calculated from Equations 7 and 8 as a function of $4\pi\eta Q_o\chi''_{max}$. The relative analytical parameter is the value of the computed parameter, e.g., peak-to-peak amplitude (A) or double integral of the derivative spectrum, divided by the value of the parameter if $4\pi\eta\chi''_{max}Q_o \ll 1$. The values of those parameters which could be used for routine analysis are given as a function of the cavity loading parameter in Table II. A more detailed comparison is shown in Figure 1.

Table II. Relative Peak-to-Peak Linewidths, Amplitudes, and Double Integrals for Various Cavity Loading Parameters to That in the Absence of Loading for a Lorentzian Line

Parameter ($4\pi\eta\chi''_{max}Q_o$)	Peak-to-peak width (Δ/Δ_o)	Amplitude (A/A_o)	Double integral limit
0.000	1.000	1.0000	1.0000
0.001	1.000	0.9988	0.9995
0.002	1.000	0.9972	0.9990
0.005	1.001	0.9928	0.9975
0.010	1.003	0.9854	0.9950
0.020	1.009	0.9709	0.9901
0.050	1.026	0.9296	0.9759
0.080	1.032	0.8912	0.9622
0.100	1.046	0.8669	0.9534
0.150	1.064	0.8111	0.9325
0.200	1.087	0.7609	0.9129
0.350	1.153	0.6377	0.8606
0.500	1.210	0.5444	0.8165
0.800	1.347	0.4142	0.7454
1.000	1.416	0.3537	0.7071
1.500	1.565	0.2530	0.6324
2.000	1.722	0.1925	0.5774
3.500	2.094	0.1048	0.4713
5.000	2.430	0.0681	0.4082
8.000	2.981	0.0371	0.3333
10.000	3.277	0.0275	0.3015

The parameters that are least affected by cavity loading are $\Delta^2 A$ and the doubly integrated first derivative spectrum where the limits of integration are between magnetic fields greater than about 10 times the peak-to-peak linewidth on either side of the absorption maximum. Coincidentally, relative double integrals of the spectrum recorded over a large span, such as greater than about $200\Delta_o$ on either side of the resonance field are approximately equal to relative values of $\Delta^2 A$. Apparently the increased linewidth compensates for the reduction in the peak-to-peak amplitude. Also, by computing the double integral of the first derivative spectrum far out into the wings of the line, a greater fraction of the area under the absorption that is negligibly affected by cavity loading is contributed to the analytical parameters. On the other hand, the peak-to-peak amplitude shows the greatest effect toward cavity loading. While the amplitude of the absorption would be reduced only by a factor equal to approximately $1/(4\pi\eta Q_o\chi''_{max})$, Figure 1 shows that the peak-to-peak amplitude

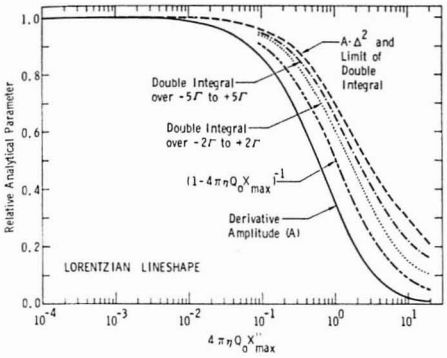

Figure 1. Plot of the relative peak-to-peak amplitude, peak-to-peak amplitude multiplied by the square of the linewidth, and double integrals over different magnetic field regions vs. the cavity loading parameter $4\pi\eta Q_o\chi''_{max}$ for a Lorentzian lineshape. The parameter $(1 + 4\pi\eta Q_o\chi''_{max})^{-1}$ is included for reference. Values of the relative parameter less than unity reflect deviations from linearity in the particular ESR signal vs. concentration or quantity of material

is reduced by a greater amount. One would initially suspect that this should not be the case, since the points of the derivative extrema occur at absorptions in which $\chi'' < \chi''_{max}$. To illustrate this point, Equation 7 can be rewritten as $F(H) = ag(H)/[1 + ag(H)]$, where $g(H)$ is the lineshape function and a is a parameter proportional to $\eta Q_o\chi''_{max}$. The derivative of this function is then $dF(H)/dH = |a/[1 + ag(H)]^2| \cdot dg(H)/dH$. Thus, where the amplitude is reduced by the factor $[1 + ag(H)]^{-1}$, the derivative is reduced by $[1 + ag(H)]^{-2}$. This accounts for a greater reduction for the derivative amplitude than the absorption maximum.

To decide upon the appropriate parameter to be used in analysis by ESR methods, the precision with which each term can be measured must be considered. For small quantities of paramagnetic material, in which intrinsic broadening due to the chemical exchange processes does not occur, the peak-to-peak amplitude is often the most convenient. At higher concentrations, however, this parameter is most greatly affected by cavity loading. Measurements of the peak-to-peak width are not precise, precluding $A\cdot\Delta^2$ as a suitable analytical parameter. Also, if the line is doubly integrated far into the wings, baseline drift and offset errors become a problem (*10*). Thus a good compromise appears to be the integration of Lorentzian lines over the magnetic field range of $H_o - 10\Delta_o$ to $H_o + 10\Delta_o$. At these extremes, the derivative curve does not change rapidly as a function of magnetic field, so that small errors in the magnetic field limits will not affect the double integral. In order to determine the entire double integral, only a 13% correction needs to be made. This correction factor allows the instrument to be calculated by a different material than is to be analyzed as suggested in Ref. 11, for example.

The significance of the term $\eta Q_o\chi''_{max}$ is given by several examples using the TE_{011} cavity ($V_c = 56$ cm^3, $Q_o = 15000$) and TE_{102} cavity ($V_c = 12.1$ cm^3, $Q_o = 6500$) at 9.5 GHz with a sample temperature of 25 °C. Using the filling factors given in Table I, values of $4\pi\eta Q_o\chi''_{max}$ can be calculated. For example, consider a small sample of $MnSO_4{\cdot}H_2O$ (*12*), where $g = 2.00$, $\Delta_o = 200$, and $\theta = -26°$ placed at the center of the ESR cavity. If $4\pi\eta Q_o\chi''_{max}$ (Equation 10) is to be smaller than 0.01, the sample must contain less than 3.4×10^{18} paramagnetic ions in a TE_{102} cavity, or less than 1.2×10^{18} ions in a TE_{011} cavity. Thus, a sample of $MnSO_4{\cdot}H_2O$ used as a standard should be smaller than 0.4 to 1.0 mg, depending on the cavity used. At lower temperatures, the maximum sample size will be smaller since the susceptibility will increase. At higher frequencies, $\chi_o H_o$ becomes considerably greater while the cavity volume is also made smaller. This also results in a smaller sample size which can be used, although this is partially compensated by lower values of Q_o.

Often the stable radical diphenylpicrylhydrazyl (DPPH) is used to calibrate ESR spectrometers. Although its lineshape is neither purely Lorentzian nor Gaussian, with a peak-to-peak linewidth of about 2 G, the maximum amount of sample that should be used can be estimated. For $4\pi\eta Q_o\chi'' < 0.01$, for a TE_{102} cavity the number of spins should be smaller than 3.6×10^{17}, while for a TE_{011} cavity, it should be smaller than 1.4×10^{17}. These correspond to samples of 0.1 to 0.25 mg, respectively.

A final example, which pertains to the analysis of aqueous media serves to illustrate the effect of cavity loading. Typically, a flat cell of 0.05 cm^3 volume within the ESR cavity is used in a TE_{102} cavity. This arrangement reduces the Q-factor to about 2250 (*13*). For a sample of Mn^{2+} which exhibits a six-line spectrum with linewidth of 15 G, the concentration required to yield a value of $4\pi\eta Q_o\chi''_{max} = 0.01$ is about 0.25 M. Thus, a significant deviation of the peak-to-peak amplitude from linearity should be observed at concentrations of this order. This deviation has been observed (*14*). Unfortunately, because the hyperfine splitting is in the order of 85 G, there is significant overlap between adjacent lines which causes a greater value χ'' than we predict, and also because at these concentrations electron exchange can also cause line broadening, the actual cause of the nonlinearity cannot be unequivocally assigned to cavity loading effects.

Gaussian Lineshapes. A Gaussian lineshape, Equation 11, reflects inhomogeneous broadening of Lorentzian lines

$$g(H) = \exp[-T_2^2(\omega - \omega_o)^2 \ln 2] \tag{11}$$

Since the integral of this line should equal that of the Lorentzian line for a material of the same transition probability, Equation 11 must be normalized by a factor of $(\pi \ln 2)^{1/2}$. Substituting relations for H and Γ, and by making use of the fact that Δ_o for a Gaussian line is equal to $(2/\ln 2)^{1/2}\Gamma$, the microwave susceptibility is given by Equation 12.

$$\chi'' = \left(\frac{\pi}{2}\right)^{1/2} \chi_o H_o \frac{1}{\Delta_o} \cdot \exp\left[-1.1768\left(\frac{H - H_o}{\Delta_o}\right)^2\right] \tag{12}$$

The value of χ''_{max} is therefore

$$\chi''_{max} = \left(\frac{\pi}{2}\right)^{1/2} \chi_o H_o \frac{1}{\Delta_o} \tag{13}$$

which is a factor of about 2.17 times greater than that of a Lorentzian line of the same peak-to-peak width. The Gaussian line is subject to less tailing than a Lorentzian line, and thus virtually all of the integral of the Gaussian absorption is contained within a span of about $-4\Delta_o$ to $+4\Delta_o$ from the absorption maximum. Various analytical parameters are shown as a function of $4\pi\eta Q_o\chi''_{max}$ in Figure 2. Here, as for a Lorentzian lineshape (Figure 1), $\Delta^2 A$ is much less affected by cavity loading than is the value of A itself. However, $\Delta^2 A$ is much less affected than the double integral because the extent of broadening is considerably greater for the Gaussian line than for the Lorentzian line.

Ferromagnetic Materials. If one assumes that a is saturated, then the susceptibility χ'' is given by Equation 14

$$\chi'' = \mu_{eff}\beta N g(H) \tag{14}$$

where μ_{eff} is the effective number of Bohr magnetons per ferromagnetic atom or molecule. The function $g(H)$ may be

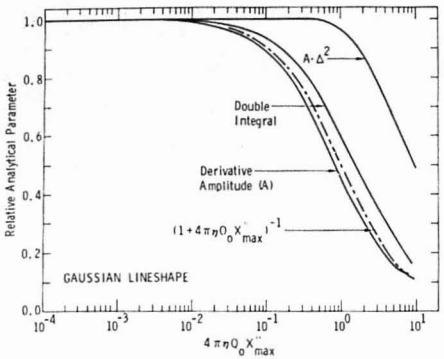

Figure 2. Plot of the relative peak-to-peak amplitude, double integral, and peak-to-peak amplitude multiplied by the square of the linewidth for a Gaussian lineshape. Deviations from unity in the relative values reflect a nonlinearity of the ESR signal vs. concentration or quantity of material

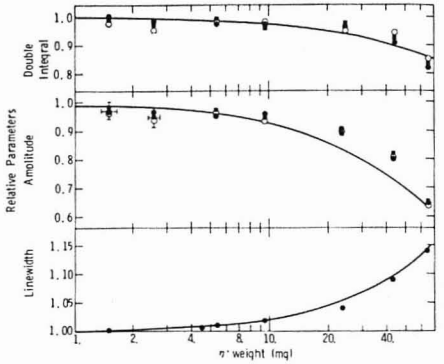

Figure 3. Double integral recorded over the field range H_o – 20 to H_o + 20, peak-to-peak amplitude, and peak-to-peak linewidth of the derivative ESR signal for $MnSO_4 \cdot H_2O$ *vs.* the filling factor times the weight of the sample in a TE_{104} cavity. Curves show the theoretical values based on the parameters: Q = 7500; ν = 9.50 GHz; θ = –26 K; T = 300 K, g = 2.00; Δ_o = 200 G; S = 5/2. Samples are weighed to ±0.05 mg. Incident microwave power: ● 0.82 mW; ■, 2.46 mW; O, 25.0 mW

Lorentzian. Lunar return samples, however, exhibit neither Guassian nor Lorentzian lineshapes, but rather are convolutions of the Lorentzian shape onto the envelope of the density of states as a function of magnetic field predicted for cubic crystalline Fe spheres (*2*). It is probably best to use a Gaussian shape to estimate the loading factor for this case because the spectrum of a particle is dependent on its shape, crystalline orientation and anistropy energy and is thus analogous to an inhomogeneously broadened line.

Integration of ESR signals. We have suggested that ESR signals can be doubly integrated with precisions within ±2% or better (*4*). The method that we used here is the following: In order to determine the baseline, the data points symmetrically disposed about the mid-point of the derivative curve are averaged. The data file is then doubly integrated after subtracting the calculated baseline from each data point. Usually the spectrum between a magnetic field range of 10 and 15 times Δ_o is used in the integration process.

Since this value is significantly smaller than the value of the area under the entire absorption, a correction factor is applied to the system. This factor is determined by the limits of magnetic field over which the derivative curve is integrated (*1*), and is given by Equation 15

$$f = \left\{ \frac{2}{\pi} \tan^{-1}\left(\frac{H - H_o}{\Gamma}\right) - \frac{((H - H_o)^2/\Gamma)^2}{1 + [(H - H_o)^2/\Gamma]^2} \right\}^{-1} \quad (15)$$

where the spectrum over the magnetic field range $H_o - H$ to $H_o + H$ is integrated. The value of Γ is assumed to be equal to $\sqrt{3}/2\ \Delta$.

Signals which exhibit appreciable baseline drift, are usually those recorded at high amplification. Since integration processes reduce the noise, reproducible double integral values can be obtained even with noisy derivative spectra. Although this is not the main topic of interest here, it is worth mentioning that we have found that the baseline drift is reproducible since it is most likely caused by magnetostriction of the ESR cavity. Thus, signal averaging a number of spectra of the baseline, with the cavity containing the sample holder, provides a useful signal which can be subtracted from the ESR signal of the sample. From this point, the same procedure discussed above can be used to doubly integrate the ESR signal.

A representative example of the reproducibility of the double integration process is in the six repetitions of a 1.5-mg sample of $MnSO_4 \cdot H_2O$. The sample was left at the same instrumental parameters so that other uncertainties, e.g., positioning, setting the power level, and changing the field sweep rate do not affect the result. The peak-to-peak amplitude agreed to within ±1 bit of the A to D converter (0.02%) and the standard deviation of the double integral processing where the field between H_o – 20Γ and H_o + 20Γ was utilized was 0.9%. A smaller standard deviation was obtained when the integration limits were reduced to H_o – 10Γ to H_o + 10Γ.

Experimental Verification. In order to confirm the calculations presented here, samples of $MnSO_4 \cdot H_2O$ weighing between 1.5 and 105 mg were recorded. The filling factors of each sample were calculated from Equation 16, which is derived in Ref. 4

$$\kappa = \frac{1}{2}\left[1 + \frac{L}{\pi l_s} \sin\left(\frac{\pi l_s}{L}\right)\right] \quad (16)$$

where L is the length of the cavity (2.24 cm) and l_s is the length of the sample in the 3-mm i.d. quartz tube. Since a TE_{104} cavity was used here rather than the TE_{102} cavity described earlier, the factor of $^1/_2$ corrects for the cavity volume so that V_c remains 12.1 cm^3. The longest sample used here was 1.8 cm which has a value of κ equal to 0.62. Note that in a TE_{104} cavity twice as much material is required to degrade the Q-factor by the same amount as a TE_{102} cavity.

Double integrals, peak-to-peak amplitudes, and peak-to-peak linewidths are shown in Figure 3. The bold curves are derived from the calculated values for $MnSO_4 \cdot H_2O$ in the previous sections, and from the data in Table I. The experiments show remarkable agreement with the theory considering that there are no adjustable parameters, and the perturbation of the microwave field due to the sample dielectric or absorption is not taken into account.

Significant degradation of the cavity Q-factor for samples of 25 mg or more can be seen from the oscilloscope trace of the cavity mode as the magnetic field is passed through resonance. This permits a crude approximation of the change in cavity Q on and off resonance. For example, cavity Q-factors with the sample containing 47 mg and κ = 0.90, were measured. Assuming that the maximum of the klystron mode corresponded to the total reflected power, the half width of

the cavity mode was measured at zero field, and at the resonance maximum, and the microwave frequency was calibrated with a wavemeter. The value of Q_0 was estimated to be 6700 ± 300, while Q at resonance was 5400 ± 250. The value of $\Delta Q/Q_0$ is therefore 0.19 ± 0.08. From the previous calculation, a sample of 1.88 mg at $\eta = 1$ should cause a value of $\Delta Q/Q$ of 0.01. Thus for the 47-mg sample, $\Delta Q/Q$ is predicted to be about 0.23, in agreement with the estimated value.

ACKNOWLEDGMENT

Helpful discussions with Robert M. Housley and William Ho are gratefully acknowledged.

LITERATURE CITED

(1) I. B. Goldberg and A. J. Bard, "Analytical Applications of Electron Spin Resonance" in "Treatise on Analytical Chemistry", 2nd ed., Pt. 1, Vol. 6, I. M. Kolthoff, P. J. Elving, and M. M. Bursey, Ed., in press: Science Center Manuscript SCM-76-125.
(2) R. M. Housley, E. H. Cirlin, I. B. Goldberg, and H. R. Crowe, *Proc. Lunar Sci. Conf., 7th*, **1**, 23 (1976).
(3) A. A. Westenberg, *Prog. React. Kinet.*, **7** (1), 23 (1973).
(4) I. B. Goldberg, H. R. Crowe, and W. M. Robertson, *Anal. Chem.*, in press.
(5) G. Feher, *Bell Syst. Tech. J.*, **36**, 449 (1957).
(6) B. Vigouroux, J. C. Gourdon, P. Lopez, and J. Pescia, *J. Phys. E*, **6**, 557 (1973).
(7) I. B. Goldberg, H. R. Crowe, and R. S. Carpenter, *J. Magn. Reson.*, **18**, 84 (1975).
(8) C. P.Poole, "Electron Spin Resonance", Interscience, New York, 1967, Chapters 8 and 14.
(9) G. E. Pake, "Paramagnetic Resonance", W. A. Benjamin, New York, 1962, pp 21–30.
(10) M. L. Randolph, "Quantitative Considerations in Electron Spin Resonance of Biological Materials", in "Biological Applications of Electron Spin Resonance", H. M. Swartz, J. R. Bolton, and D. C. Borg, Ed., John Wiley, New York, 1972, Chapter 3.
(11) J. R. Bolton, D. C. Borg, and H. M. Swartz, "Experimental Aspects of Biological Electron Spin Resonance Studies", in "Biological Applications of Electron Spin Resonance", H. M. Swartz, J. R. Bolton, and D. C. Borg, Ed., John Wiley, New York, 1972, Chaper 2.
(12) Y. Allain, J. P. Krebs, and J. de Gunzbourg, *J. Appl. Phys.*, **39**, 1124 (1968).
(13) Varian Aqueous Sample Cell Instruction Manual.
(14) G. G. Guilbault and G. J. Lubrano, *Anal. Lett.*, **1**, 725 (1968).

RECEIVED for review February 22, 1977. Accepted May 2, 1977. This work was supported by the Office of Naval Research.

Representation-Space Transformation for the Display of Multivariate Chemical Information

Chi-Hsiung Lin* and Hwa-Fu Chen

Department of Chemistry, National Cheng Kung University, Tainan, Taiwan, Republic of China

A new algorithm for displaying multivariate chemical information on a three-dimensional coordinate system is presented. The transformation is basically the extraction of three characteristics from the information and assures the preservation of data structure to a satisfactory degree if the information is normalized. Since the transformation is independent of other existing information, the display coordinates are unique and representative on the given information. This promises utility in treating a huge amount of chemical information with pattern recognition and other modern techniques. The display coordinates also serve as the index codes in the computer retrieval of such information. Other applications such as the signal shape analysis in spectroscopy with this method are suggested.

The application of pattern recognition technique in chemistry (*1–4*) has aroused wide interest in recent years. This technique is the central part of the "learning machine" (*5*) utilized for the analysis of mass spectra (*6*), infrared spectra (*7*), NMR spectra (*8*), polarograms (*9*), etc. Besides this conventional classification method, some chemical problems are also solved by the unsupervised learning method which utilizes the technique of cluster analysis (*10, 11*). This is a method developed in the past several years and widely utilized in the fields of taxonomy, psychology, social sciences, and medical diagnosis. It is a powerful tool in detecting some obscure properties of a collection of objects through the recognition of a natural classification among them (*1*). In the field of chemistry, the application is still in the beginning stages. But, since chemistry at the present stage already abounds in scientific information, its future development can be easily anticipated.

To find an intrinsic property hidden in a huge set of information, it is necessary to perceive the mutual relationships among this set of information. At the present stage of development, the most reliable detecting device is still the human perception whose working principles are bases for the development of theories of cluster analysis (*12*). But to be perceptible, it is necessary to present that information in some strictly limited forms. Some chemical information such as spectra of compounds are already in such forms, and chemists are taught to differentiate and identify them properly. As the number and complexity of information for such study increases, however, the human capability quickly becomes inapt unless some new presentation scheme which is simple for perception and efficient for numerical treatment can be devised. The present study offers such a new scheme of presentation which transforms multivariate chemical information into their corresponding points on a three-dimensional display space for visual perception and numerical analysis.

The Display Method. Multivariate chemical information can be thought of as a set of N measurements. A set of chemical information can then be represented as a set of points on an N-dimensional measurement space where each axis corresponds to one of those N measurements. The distribution of these points, or the data structure, is the object of study in the cluster analysis. To study this by human visual perception, however, it is necessary to transform it into a display space of dimensionality no higher than three while keeping the data structure practically intact. In most cases, the N-dimensional measurement space is thought of as an orthogonal coordinate system, but it is not always necessarily so. A ^{1}H NMR spectrum with a singlet at δ 1.0, for instance, resembles one with a singlet at δ 1.5 rather than one with a singlet at δ 7.5. To demonstrate this on the measurement space, the relation between the axis for δ 1.0 and that for δ

1.5 has to be different from the relation between the former and the axis for δ 7.5. Though even if so, it is the usual practice to adopt an orthogonal coordinate system for the measurement space for mathematical convenience. A display space is also an orthogonal coordinate system with a low dimensionality. A display method is, therefore, a proper scheme of dimensionality reduction which keeps the data structure as intact as possible (*13*).

The Karhunen–Loeve transformation (*14*) is one of the dimensionality reduction treatments, general difficulty of which is thoroughly discussed by Olsen (*15*). Another is the method of nonlinear mapping (NLM) developed by Sammon. In this method, the data structure is thought to be kept by an iterative adjustment of inter-point distances so as to make the sum of deviations minimal. The benefit and limitation of this method are also discussed in detail (*16*). Besides those difficulties on their practical applications, a serious shortcoming of these methods, seldom noticed, is that they treat all information as a set and, consequently, a revised computation is necessary whenever new information is added to the set. And what is more, the revised computation gives different coordinate values for each information.

In the study of quickly accumulating chemical information, we hope to have a method which will assign for a given information its unique display coordinates, Fukunaga and Olsen (*17*) present a two-dimensional display which partly satisfies this goal. The uniqueness of the display coordinates will make it possible to utilize them as index codes of that information for later retrieval and comparison. Futhermore, we hope that the display coordinates are themselves related to some conceivable characteristics of the information in the ordinary chemical sense. A spectrum for instance, should give a higher y-value if it is more intense, and a larger x-value if its bands are bathochromically shifted. Chemical information as such is often a continuous function which is sampled every (N – 1)-interval to give the N measurements. If the display coordinates are truly representative of the information, then the number of samplings should not be dominant. We hope, in this connection, that the display will not shift too far by reducing the number of samplings as long as the very nature of the information is not lost.

Obviously, a display which satisfies the above desiderata is more than an ordinary display. The display space where data structure is preserved by the dimensionality reduction from a high dimensional measurement space is here also a space on which the data points are representative of the characteristics of original information. We call this display space the "representation space" of the chemical information, and the method of dimensionality reduction the "representation-space transformation".

THE REPRESENTATION-SPACE TRANSFORMATION

Multivariate chemical information comprises several measured values either from a single measuring instrument or from several independent sources. These values do or do not possess a natural sequence of arrangement. When they do not, then an arrangement is assigned in accord with some chemical consideration or just arbitrarily in the stage of preprocessing. This stage also includes any transformation specifically taken for some purpose and a normalization process to give a new set of values each of which is in the range of 0.0 to 1.0. The ith information is now

$$\mathbf{P}_i = \{P_{i1}, P_{i2}, \ldots P_{iN}\} \tag{1}$$

and occupies a point on the N-dimensional information space inside a hypercube, the edges of which are all of the same unit length. The representation-space transformation, T_R, is to give three values, x_i, y_i, and z_i, as the coordinates of its "representation point" on the display space, i.e.,

$$T_R\,\mathbf{P}_i = ((x_i, y_i, z_i)) = ((P_i)) \tag{2}$$

Let us consider three pairs of reference information, $\mathbf{X}_-$ and $\mathbf{X}_+$, $\mathbf{Y}_-$, and $\mathbf{Y}_+$, and $\mathbf{Z}_-$ and $\mathbf{Z}_+$, of the same dimensionality. These reference points are so assigned as to represent three special characteristics of the chemical information of interest. For their display, coordinates are given the following values regardless of the dimensionality of the information space.

$$((X_-)) = ((-k, 0, 0)), \qquad ((X_+)) = ((k, 0, 0))$$
$$((Y_-)) = ((0, -k, 0)), \qquad ((Y_+)) = ((0, k, 0))$$
$$((Z_-)) = ((0, 0, -k)), \qquad ((Z_+)) = ((0, 0, k)) \tag{3}$$

Here, k is the limiting value for the representation space, to which 10 000 is commonly assigned for the convenience of computer handling of the coordinates in one-word integers.

The representation-space transformation is to transfer information points to the display space by holding their proximity relationships to each pair of the reference information intact. Thus, for instance, the ratio of distances from $\mathbf{P}_i$ to $\mathbf{X}_-$ and to $\mathbf{X}_+$ on the information space is used to assign the x-value of the representation point so as to give the same ratio of distances from $((P_i))$ to $((X_-))$ and to $((X_+))$ on the display space. Thus, in general,

$$\frac{\text{dist}\,[((P_i)), ((R_-))]}{\text{dist}\,[((P_i)), ((R_+))]} = \frac{\text{dist}\,[\mathbf{P}_i, \mathbf{R}_-]}{\text{dist}\,[\mathbf{P}_i, \mathbf{R}_+]} \equiv \frac{d_{i\mathrm{R}_-}}{d_{i\mathrm{R}_+}} \tag{4}$$

where $\mathbf{R}$ stands for $\mathbf{X}$, $\mathbf{Y}$, or $\mathbf{Z}$. There is no limitation on which distance measure should be used. Generally, the Mahalanobis expression

$$\text{dist}[\mathbf{P}_i, \mathbf{R}_-] = \left(\sum_{j=1}^{N} |P_{ij} - R_{-j}|^{\mu}\right)^{1/\mu} \tag{5}$$

with three independently assigned exponents, μ_x, μ_y, and μ_z, for each pair of distances is quite proper. The representation coordinates, $((P_i))$ become

$$((P_i)) = k\left(\left(\frac{d_{i\mathrm{X}^-} - d_{i\mathrm{X}^+}}{d_{i\mathrm{X}^-} + d_{i\mathrm{X}^+}}, \frac{d_{i\mathrm{Y}^-} - d_{i\mathrm{Y}^+}}{d_{i\mathrm{Y}^-} + d_{i\mathrm{Y}^+}}, \frac{d_{i\mathrm{Z}^-} - d_{i\mathrm{Z}^+}}{d_{i\mathrm{Z}^-} + d_{i\mathrm{Z}^+}}\right)\right) \tag{6}$$

The three pairs of reference information can be assigned rather arbitrarily. Information of two special compounds, for instance, could be assigned as a pair of reference information in some cases. Utilization of typical factors (*18*) as reference information is specially suitable. Another recommendation is the assignment of both extremes of a characteristic for each pair. For information such as chemical spectra, they could be such as to illustrate the left–right inclination, the low–high intensity, and the diverse–centralized distribution. In this sense, the following set is most serviceable through its simplicity in form and generality in nature:

$$\mathbf{X}_- = \{1 - \beta_m\}, \quad \mathbf{X}_+ = \{\beta_m\};$$
$$\mathbf{Y}_- = \{0\}, \quad \mathbf{Y}_+ = \{1\};$$
$$\mathbf{Z}_- = \{(1 - 2\beta_m)^2\}, \quad \mathbf{Z}_+ = \{(1 - |1 - 2\beta_m|)^2\} \tag{7}$$

where β_m represents $(m - 1)/(N - 1)$ for the mth component of the N-dimensional vector point. An illustration on such reference information with eleven components is shown in Figure 1.

The simplest case is when the information space is three-dimensional. This space is itself perceivable. Information of the six references on this space and their representation points on the display space are compared in Figure 2. This information space has three axes [1], [2], and [3].

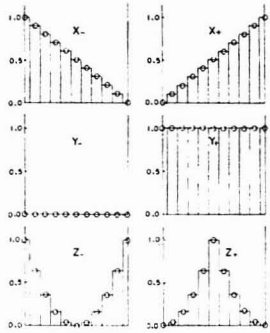

Figure 1. 11-dimensional reference information

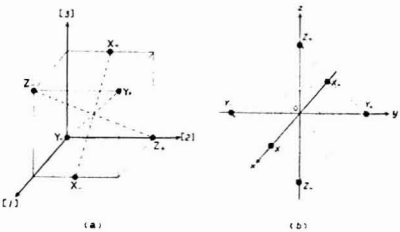

Figure 2. Reference information on the three-dimensional information space (a) and their representation points on the display space (b)

If they are mutually orthogonal, then the line $\overline{X_- X_+}$ becomes shorter than either $\overline{Y_- Y_+}$ or $\overline{Z_- Z_+}$. Here we see the distortion on the representation-space transformation. But, on the other hand, we can also say that the transformation does not distort the data structure at all if we admit a nonorthogonal information space where the angle between axis [1] and axis [3] is a little larger and, consequently, those three lines somehow become mutually orthogonal and of the same length. By extension, this consideration to high-dimensional information space vindicates the capability of the present algorithm in preserving the data structure.

The normalization process taken in the preprocessing of the measurement values assures that all information points are in a hypercube of unit edge lengths. Owing to the nature of the present algorithm, the data structure outside the hypercube is not preserved on the transformation. Such hypercubes with dimensionality larger than three are very difficult to conceive. They can be, however, transformed into the display space for visual examination. Examples are shown in Figure 3. All information will give representation points in the region enclosed.

COMPUTATION

All plotting and most calculations required for this study were carried out on a Hewlett-Packard 9810A Desk Calculator equipped with a 9861A Output Typewriter, a 9862A Calculator Plotter, and a 9865A Cassette Memory. Other calculations which require a high capacity memory core were carried out on the UNIVAC 90/30 in the Engineering Research Center of the National Cheng Kung University.

RESULTS AND DISCUSSION

The ability of the representation space to be the classification medium for high dimensional data was thoroughly studied with several artificial data sets. The comparison with the results of NLM treatment showed higher excellence with the present algorithm. The present transformation on a set of sixty 12-dimensional data took less than 10 ms of CPU time while the iterative NLM took more than 10 min on a UNIVAC 90/30. The preservation of the data structure is also found better with our algorithm. This is a natural consequence of the limitation of pattern space inside the hypercube of unit edge lengths; the NLM treatment does not impose any limitation of similar nature. A pair of exact same patterns, for instance, appears as a single point on the representation space, but it always gives two points on the two-dimensional map obtained by the NLM method. Another decisive factor of practical importance in computation is the memory size required. Even the largest computer now available cannot handle a collection of 1000 infrared spectra with 400 features each on its core memory with the nonlinear dimensionality reduction of NLM, which requires a core memory larger than 5400 kB. With our algorithm, on the other hand, even a desk calculator with a cassette memory can efficiently handle such a job since the representation transformation is made on each information independently and the resultant representation point is displayed one by one.

In this transformation, the sequence of arrangement of those features in the pattern matrix is a decisive factor for its computed coordinate value. Thus, when the information is measurements from various sources, the arrangement can be used as a means for finding different modes of clustering. This is caused by the fact that the hypercube on the representation space is not exactly symmetrical as illustrated in Figure 3. When a certain property is to be extracted from a set of information, there must exist an optimum arrangement which gives the most definite classification in regard to that property. In this arrangement, it is generally observed that components which are intrinsically similar in contribution to the given property are arranged in proximity in the series of information. In a supervised learning, it is possible to compare those $N!/2$ arrangements and pick up the arrangement which gives the best separation of classes. From this, in turn, we can deduce the relationships of intrinsic contribution among those components to the given property under classification.

It is suggested by Kowalski that the most important valence (V), melting point (MP), covalent radius (R_C), ionic radius (R_I), electronegativity (El), and heat of fusion (H) of elements

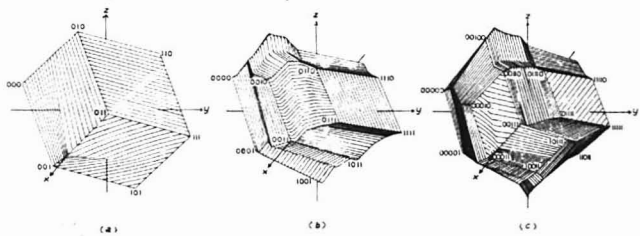

Figure 3. (a) Three-dimensional, (b) four-dimensional, and (c) five-dimensional hypercubes on the representation space. $\mu_x = \mu_y = \mu_z = 1$

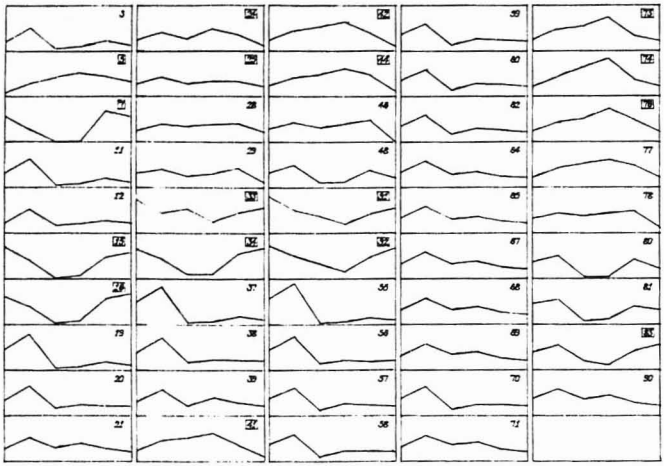

Figure 4. Property spectra of elements with known acid–base criterion. Properties from left to right in the series R_C–R_I–H–MP–El–N_V. Element with acidic oxide is illustrated with a frame around its atomic number

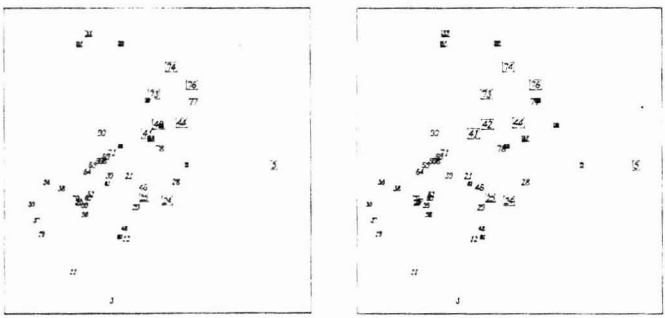

Figure 5. Data structure of Figure 4 spectra on the representation space. A stereoscopic view of the three-dimensional display from the direction of the x-axis. $\mu_x = \mu_y = \mu_z = 1$

can be used for classifying whether their oxides are acidic or basic (2). This series of measurements can be arranged in 6!/2 or 360 ways, and consequently we may obtain 360 displays with slightly different clusterings. That is to say that we have 360 ways to look into the 6-component information set to obtain insight into some hidden characteristics of elements; the acidity of oxides is merely one of them. For a chemist, the pattern recognition is rather easier to understand if the information is presented in the form of a spectrum. Those six properties of an element arranged in the order R_C–R_I–H–MP–El–N_V, with N_V as the number of valence shell s,p electrons instead of V, gives a set of spectra easily classified under the acid–base criterion (Figure 4). The representation-space transformation gives a three-dimensional data distribution which is to be recognized only by the proximity relationship. Figure 5 shows the stereoscopic display of those representation points. The discrimination under this property is obvious. There are only three elements, namely Ni^{28}, Ir^{77}, and Pt^{78}, in the wrong category. A similar clustering is shown in the NLM treatment (2) on a smaller group of elements, in which those three elements as well as Cu^{29}, Pd^{46}, Ho^{67}, and Y^{70} are missing.

The above example is a clear demonstration of our finding that any set of information which is well classified by human perception in the form of a spectrum will give clusters in the same category on the representation space recognizable by the proximity relationship. The latter can be handled by the computer.

The representation-space transformation is unique. That is to say that the information always gives the same values of representation coordinates regardless of how much other information is there. This feature has no comparison in other display methods. Thus, once the reference information and the set of Mahalanobis distance exponents in Equation 5 are specified, information can be uniquely appointed with the representation coordinates of its own.

When the information deviates from time to time owing to the fluctuation of observation conditions, special precaution is necessary in data handling utilizing the computed representation coordinates as the index codes. Especially in case the information is a continuous function such as an electronic spectrum, the effect on the coordinate values due to the number of samplings, the random noise, and the resolution of the spectrum needs consideration.

Table I. Effect of Sampling Numbers on the Computed Representation Coordinates (x, y, z) of the Electronic Spectrum of Chlorophyll a in the Range 4.0 ~ 9.0 × 10^{15} cm^{-1}

Sampling number	Distance exponent, $\mu_x = \mu_y = \mu_z$														
	1			2			3			4			5		
631	2230	−2803	268	1685	−2177	735	1348	−1647	927	1132	−1249	991	997	−977	1003
316	2234	−2811	287	1688	−2183	751	1353	−1653	942	1140	−1264	1004	1010	−981	1015
211	2229	−2809	293	1683	−2181	759	1350	−1651	950	1141	−1263	1013	1016	−981	1025
127	2234	−2822	323	1689	−2191	786	1358	−1659	976	1153	−1270	1038	1033	−987	1049
106	2242	−2825	345	1690	−2191	808	1362	−1660	996	1161	−1271	1056	1045	−988	1066
91	2233	−2843	348	1687	−2207	804	1360	−1674	991	1162	−1285	1052	1048	−1001	1062
71	2231	−2839	382	1693	−2202	842	1369	−1668	1026	1173	−1276	1082	1062	−992	1088
64	2256	−2864	410	1700	−2225	862	1378	−1692	1048	1188	−1303	1108	1084	−1020	1118
46	2268	−2888	451	1707	−2243	909	1399	−1713	1103	1224	−1324	1170	1135	−1042	1184
36	2229	−2999	530	1702	−2234	964	1387	−1699	1136	1208	−1310	1188	1120	−1031	1195
22	2199	−2856	741	1660	−2184	1095	1401	−1662	1279	1283	−1290	1352	1247	−1025	1378

With a sampling number not too small to lose its main features, the deviation of computed representation coordinates from those on infinite sampling seldom exceeds 150 on the display scale, or 0.8% of the length of an axis. An example of the computation is given with the electronic spectrum of chlorophyll a (Figure 6a). The representation coordinates of this spectrum with different sampling numbers are compared in Table I. The main features of the spectrum are not seriously lost if the sampling number is not smaller than 60 in the given range (Figure 6b,c). Generally speaking, the deviation is very small in the y-value, probably owing to the averaging effect of such bar spectra on the overall intensity which is the characteristic represented by the y-value. Most serious is the z-value which is the measure of peak centralization. An effect of the distance exponent is also seen in Table I. In general, a smaller distance exponent offers better separability for patterns located in the central part of the representation space.

In the on-line generation of representation coordinates, the effect of white noise appears as the predominant cause of deviation. This effect was studied on several spectra with the addition of random noises generated numerically. An example of such a study on the same spectrum is shown in Table II. The original information is the 127-feature bar spectrum of chlorophyll a. A series of 127 random numbers in the range 0.1~−0.1 is added to the original information resulting in a noisy spectrum. Twenty such noisy spectra are studied for the scattering of their representation points with different values for the distance exponent. The representation coordinates of the noise-free bar spectrum is available in Table I. An example of those noisy spectra is shown in Figure 6d. A general conclusion obtained from our study is that, when the noise level is less than 10% of the highest intensity, the representation point of a noisy spectrum is seldom located outside the sphere of radius 150 around the point of the noise-free spectrum.

The effect of spectral resolution owing to the change of slit width is another problem. A sharper spectrum from an instrument of higher resolution has a smaller overall intensity after normalization. The representation point of this spectrum gives a smaller y-value than that of lower resolution. Besides the intensity, two other characteristics also lose their weights. In general, a steady improvement in resolution shifts the representation point toward the bottom of the y-axis, namely ((0,−10000, 0)). The locus is a slightly bent line. This tendency can be taken into account in due retrieval.

In chemical practice, the representation space gives various applications. This is a space where the characteristics of the complicated chemical information can be studied with high efficiency. No existing display method offers such additional utility values. Any chemical information of graphical nature can be, as a rule, studied on the representation space. A most

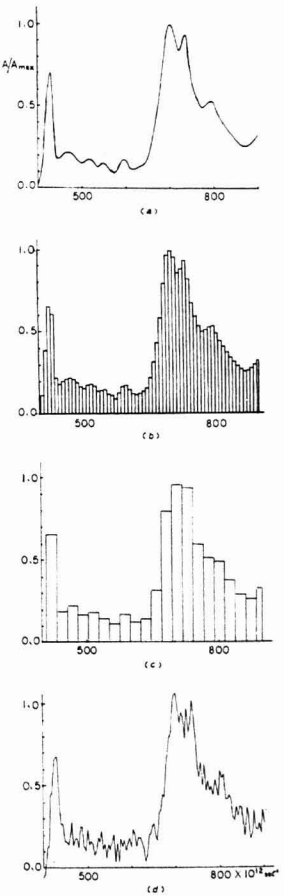

Figure 6. Electronic spectrum of chlorophyll a. (a) Original spectrum, (b) 64-feature bar spectrum, (c) 22-feature bar spectrum, and (c) spectrum added with ±10% noise

comprehensible example of such application is the line-shape analysis in spectroscopy. This capability of this algorithm

Table II. Effect of Random Noise on the Computed Representation Coordinates of the Same Spectrum with Sampling Number 127

	Distance exponent, $\mu_x = \mu_y = \mu_z$				
	1	2	3	4	5
Range[a]					
x	2339 ~ 2085	1761 ~ 1517	1494 ~ 1066	1294 ~ 977	1217 ~ 887
y	−2695 ~ −3013	−2000 ~ −2347	−1527 ~ −1781	−1139 ~ −1372	−964 ~ −1255
z	490 ~ 95	944 ~ 614	1117 ~ 831	1187 ~ 842	1260 ~ 796
Center (deviation)					
x	2212(−22)	1639(−50)	1280(−78)	1135(−18)	1052(+19)
y	−2854(−32)	−2174(+17)	−1654(+5)	−1255(+15)	−1110(−122)
z	292(−31)	779(−7)	974(−2)	1015(−23)	1028(−21)

[a] After 20 runs each. Noise level: ±10% of the maximum intensity.

derives from the fact that a certain line-shape corresponds to a definite diagram on the representation space.

To any finite portion of a single-valued function $f(x)$, we can assign a representation point. If we fix one end of the portion (x: $a \sim b$) and change the other end, we obtain each time a new portion of that function giving a representation point; the successive connection of these points forms a line on the representation space. We call this the "representation line" for the portion of function $f(x)$ left or right of the fixed point a. Obviously, the representation line is only related to the characteristics of that function. A half portion of a Gaussian function, for instance, gives the same representation line regardless of whether it is tall or short and is broad or narrow. This representation line of the Gaussian "halfwave" is naturally different from that of a Lorentzian halfwave. Thus, when a waveform is observed in a spectrum, we can easily decide whether it is Gaussian or Lorentzian by simply comparing its representation line with those two standard lines obtained beforehand. This prevents the ordinary practice of complicated curve-fitting in which the knowledge of the parameters of the line-shapes is a prerequisite. The comparison of representation lines can be even simplified by taking two or three representation points for different portions of the unknown curve and observing their relative locations. In most cases, the comparison is quite satisfactory without one of those three coordinate values.

The above process is easily extended to the analysis of some parameters which alter the characteristics of the shape of the curve. An example is the detection of the shifted baseline of a spectral peak. As above, the theoretical representation lines for the given waveform with different heights, h, of baseline are obtained (Figure 7). The same method of line fitting is used to find out this parameter for an unknown spectral peak. The value of the baseline height in Figure 7 is in percentage to the maximum intensity. The value r on the diagrams is used to calculate the halfwidth, H, of the spectral peak using the relationship $H = w/r$, where w is the width of the portion of curve taken for the calculation of the representation coordinates.

Figure 8 is another standard chart of this kind with which a ^{1}H NMR signal of two exchanging protons can be analyzed with satisfactory accuracy. The protons are assumed to be with the same halflife. The center of the symmetrical signal is taken as the fixed point, and the portion right of this point is considered. The diagram for the left portion is quite similar with a reversed x-axis. The r-value on the diagram is used to calculate the difference of chemical shifts with the relationship $|\nu A - \nu B| = w/r$. Definition of w is the same as above. The time factor, τ, is then computed with this value and the t-value on the diagram using the relationship $\tau = t/2\pi\,|\nu A - \nu B|$.

The application of the representation space in this fashion will be immense in such a science as chemistry. The general application of the display in connection to the pattern rec-

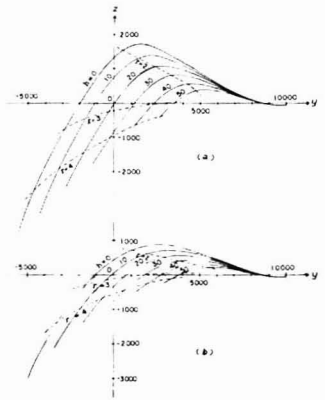

Figure 7. Standard charts for the analysis of a Gaussian waveform (a) and a Lorentzian waveform in regard to the halfwidth and the height of baseline. Fixed point a at the peak position. $\mu_y = 1.0$ and $\mu_z = 0.5$

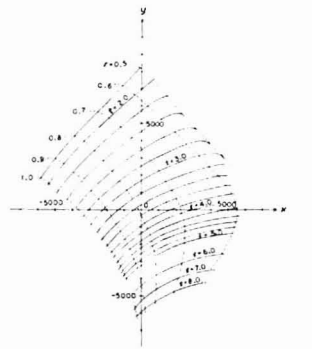

Figure 8. Standard chart for the analysis of the exchange phenomenon of two protons of equal population on PMR spectrum. The fixed point a at the midpoint of the symmetric signal. $\mu_x = 2.0$ and $\mu_y = 1.0$

ognition technique finds its superiority over conventional display methods especially in its incomparable quickness and simplicity in treatment of complicated information. Our colleagues have tried this algorithm in various branches of science including medical diagnosis through electrocardiogram, identification of spoken words and speaker, classification of seismograms, and recognition of Chinese characters. Their

success implies the applicability of this algorithm in the field of chemistry where scientific information not yet fully analyzed abounds. The analysis and classification of industrial products will be greatly benefited by the pattern recognition technique (*19, 20*). The present algorithm makes it possible to apply this technique routinely in the chemical laboratory with a small calculator.

ACKNOWLEDGMENT

We are grateful to Min-Hon Rei of the National Science Council of the Republic of China for his interest and encouragement in this work.

LITERATURE CITED

(1) T. L. Isenhour and P. C. Jurs, *Anal. Chem.*, **43** (10), 20A (1971).
(2) B. R. Kowalski and C. F. Bender, *J. Am. Chem. Soc.*, **94**, 5632 (1972).
(3) P. C. Jurs and T. L. Isenhour, "Chemical Application of Pattern Recognition", Wiley-Interscience, New York, N.Y., 1975.
(4) B. R.Kowalski, *Anal. Chem.*, **47**, 1152 (1975).
(5) P. C. Jurs, B. R. Kowalski, and T. L. Isenhour, *Anal. Chem.*, **41**, 1949 (1969).
(6) T. J. Stonham, I. Aleksander, M. Camp, W. T. Pike, and M. A. Shaw, *Anal. Chem.*, **47**, 1817 (1975).
(7) B. R. Kowalski, P. C. Jurs, and T. L. Isenhour, *Anal. Chem.*, **41**, 1945 (1969).
(8) T. R. Brunner, C. L. Wilkins, T. F. Lam, L. J. Soltzberg, and S. L. Kaberline, *Anal. Chem.*, **48**, 1146 (1976).
(9) L. B. Sybrandt and S. P. Perone, *Anal. Chem.*, **43**, 382 (1971).
(10) S. R. Heller, C. L. Chang, and K. C. Chu, *Anal. Chem.*, **46**, 951 (1974).
(11) W. S. Meisel, "Computer-Oriented Approaches to Pattern Recognition", Academic Press, New York, N.Y., 1972.
(12) C. T. Zahn, *IEEE Trans. Comput.*, **C-20**, 68 (1971).
(13) B. R. Kowalski and C. F. Bender, *J. Am. Chem. Soc.*, **95**, 686 (1973).
(14) K. Fukunaga and W. L. G. Koontz, *IEEE Trans. Comput.*, **C-19**, 311 (1970).
(15) D. R. Olsen and K. Fukunaga, *IEEE Trans. Comput.*, **C-22**, 915 (1973).
(16) J. W. Sammon, Jr., *IEEE Trans. Comput.*, **C-18**, 401 (1969).
(17) K. Fukunaga and D. R. Olsen, *IEEE Trans. Comput.*, **C-20**, 917 (1971).
(18) R. W. Rozzett and E. M. Peterson, *Anal. Chem.*, **47**, 2377 (1975).
(19) D. L. Duewer and B. R. Kowalski, *Anal. Chem.*, **47**, 526 (1975).
(20) H. A. Clark and P. C. Jurs, *Anal. Chem.*, **47**, 374 (1975).

RECEIVED for review January 31, 1977. Accepted May 2, 1977. Financial support of the National Science Council of the Republic of China is gratefully acknowledged.

Buffer Solutions for Testing Glass Electrode Performance in Aqueous Solutions over the pH Range 0–14 at 25 °C

Arthur K. Covington* and M. Isabel A. Ferra

Department of Physical Chemistry, University of Newcastle upon Tyne, NE1 7RU, England

The new method of testing glass electrodes has been extended to cover the whole pH range. It is based on indirect comparison of potentials with those of hydrogen gas electrodes but using silver–silver chloride electrodes in cells without liquid junction. Using specially developed chloride-containing test buffers, it is now possible to determine the errors of glass electrodes with an accuracy of ±0.6 mV (±0.01 pH) over the pH range 0–14 and to measure sodium errors at up to 1 M Na^+ at constant pH for pH > 6.5. The method is illustrated by results from testing commercial electrodes.

In this laboratory a new method of testing the performance of glass electrodes has been developed using buffer solutions containing no sodium ion in the pH range 6 to 12 (*1*). Sodium ion was then added to each of these solutions at three different Na^+ concentrations to test the pH-response of glass electrodes in the presence of this cation. The method is based on indirect comparison of glass electrodes with the hydrogen gas electrode, using silver–silver chloride electrodes in cells without liquid-junction, and it was designed to be simple, accurate, and rapid so that it can be easily employed by manufacturers and users with the resources available in most analytical laboratories. The method has now been extended at both ends of the pH scale by devising suitable buffer solutions containing chloride ion. Results obtained with some commercial glass electrodes are given.

METHOD

The criterion of perfect behavior of a hydrogen-ion responsive glass electrode is that the emf of the cell

$$\text{Pt, } H_2|\text{solution}|\text{glass electrode} \qquad \text{(I)}$$

should be constant independent of solution composition. Departure from this behavior, or error, is indicated by the difference between emf values obtained with two different solutions.

The following glass (G) and hydrogen (H) cells, which correspond to the invariant cell (I) if the solution used is identical, can be set up:

$$\text{glass electrode}|\text{solution}|\text{AgCl}|\text{Ag} \qquad \text{(G)}$$

$$\text{Pt, } H_2|\text{solution}|\text{AgCl}|\text{Ag} \qquad \text{(H)}$$

Denoting the emf of cell I when a reference solution R is employed by E_I^R, then

$$E_I^R = E_H^R - E_G^R \qquad (1)$$

where E_H^R, E_G^R are the emfs of cells H and G, respectively, containing also a reference solution R. Replacing solution R in which the glass electrode is assumed to be error-free by another solution (T) of different pH, will give, in general new values E_I^T, E_H^T, E_G^T so that

$$E_I^T = E_H^T - E_G^T \qquad (2)$$

The error of the glass electrode ΔE is defined by (2)

$$\begin{aligned}\Delta E &= E_I^T - E_I^R \\ &= (E_H^T - E_G^T) - (E_H^R - E_G^R) \\ &= (E_H^T - E_H^R) - (E_G^T - E_G^R) \qquad (3)\end{aligned}$$

Thus the error of a glass electrode, relative to a solution where it is assumed to be error-free, can be obtained by subtracting the difference between the two values obtained for cell G from the corresponding two values for cell H, which have been determined for specially devised buffer solutions in this work. The reference solution is chosen to be a neutral pH buffer (pH 6.58) for tests over the range 0–14. For direct measurement of the sodium ion error in the alkaline region the chosen reference solution has the same pH as the test solution but

Table I. Substances Used in the Preparation of Buffer Solutions

Substance	Supplier	Formula	Mol wt	mp/bp, °C	Stated purity	Drying temp (°C)/detected water content
Tetramethylammonium hydroxide (TMAH) (25% aq. soln)	BDH	$(CH_3)_4NOH$	91.15	...	≥24.5% Halide (as bromide) <0.05%	...
Glycine (G)	BDH (AnalaR)	NH_2CH_2COOH	75.07	...	≥99.0%	75/0.016%
Succinic acid (H_2Suc)	BDH (AnalaR)	CH_2COOH | CH_2COOH	118.09	186.5-188.5 (solid)	≥99.5%	110/0.014%
2,2-Bis(hydroxyethyl) imino-tris(hydroxymethyl) methane. "Bis-Tris" (BT)	Aldrich-U.S.A.	$NC(CH_2OH)_3$ | $(CH_2CH_2OH)_2$	209.24	102-103 (solid)	≥98%	75/0.21%
Tris(hydroxymethyl) methylamine. "Tris" (T)	BDH (AnalaR)	$NH_2C(CH_2OH)_3$	121.14	170-171 (solid)	≥99.8%	110/0.019%
Ethanolamine (E)	BDH	$CH_2(OH)CH_2NH_2$	61.08	169-173 (liquid)	≥99%	...
Piperidine (P)	BDH	$C_5H_{10}NH$	85.15	105-108 (liquid)	≥98%	...
Sodium chloride	BDH (AnalaR)	NaCl	58.44	801 (solid)	≥99.9%	110
Sodium perchlorate	BDH (AnalaR)	$NaClO_4.H_2O$	140.46	130 (solid)	≥99.0%	do not dry

Table II. Composition and Preparation of Buffer Solutions[a]

Soln no.	Soln composition	Acid component	Base component	Additive
A0	1 M HCl	1000 mL 1 M HCl		
A1	0.1 M HCl	100 mL 1 M HCl		
A2	0.05 M GHCl + 0.05 M G	50 mL 1 M HCl	7.507 g glycine	
A4	0.02 M H_2 Succ + 0.02 M NaHSucc	4.724 g H_2Succ	20 mL 1 M NaOH	5.844 g NaCl
A5	0.02 M NaHSucc + 0.02 M Na_2Succ	4.724 g H_2Succ	60 mL 1 M NaOH	5.844 g NaCl
A6	0.05 M BTHCl + 0.05 M BT	50 mL 1 M HCl	20.924 g BT	
A7	0.10 M THCl + 0.05 M T	100 mL 1 M HCl	18.171 g T	
A9	0.03 M EHCl + 0.02 M E	30 mL 1 M HCl	3.054 g E	
A11	0.05 M PHCl + 0.075 M P	50 mL 1 M HCl	10.644 g P	
A12	0.05 M TMAH + 0.1 M TMACl		54.69 g TMAH (25% soln[b])	100 mL 1 M HCl
A14	0.80 M TMAH + 0.1 M TMACl		328.14 g TMAH (25% soln[b])	100 mL 1 M HCl

[a] The amounts given are those required to prepare 1 L of solution at 20 °C by addition of distilled water (except in case of A0). [b] If the concentration of the TMAH stock solution is x mol/kg solution, the required amount to prepare A12 is $(0.15/x) \times 10^3$ g and to prepare A14 is $(0.9/x) \times 10^3$ g.

Table III. Preparation of Buffer Solutions Containing Sodium Ion

Solution	Components	Final volume/mL
A*i*Na2	0.3511 g $NaClO_4.H_2O$ + A*i* (*i* = 6, 7, 9, 11) to	250
A*i*Na1	3.511 g $NaClO_4.H_2O$ + A*i* (*i* = 6, 7, 9, 11) to	250
A*i*Na0	35.115 g $NaClO_4.H_2O$ + A*i* (*i* = 6, 7, 9, 11) to	250
A12Na2	25 mL 1 M HCl + 13.67 g TMAH (25% soln) + 0.146 g NaCl + H_2O to	250
A12Na1	4.56 g TMAH (25% soln) + 1.461 g NaCl + H_2O to	250
A12Na0	20 mL 1 M HCl + 30 mL 1 M NaOH + 23.877 g $NaClO_4.H_2O$ to	200
A14Na2	25 mL 1 M HCl + 82.03 g TMAH (25% soln) + 0.146 g NaCl + H_2O to	250
A14Na1	72.92 g TMAH (25% soln) + 1.461 g NaCl + H_2O to	250
A14Na0	50 mL 1 M HCl + 125 mL 4 N NaOH + H_2O to	500

the latter contains sodium ions at 0.01, 0.1 or 1M.

In the previous work, attention was concentrated on the alkaline region and the choice of amine buffer substances was made to avoid the complications of response of the glass electrode to small cations, that due to sodium ion being the most important. Initially this principle was extended to solutions in the range 3-5, but tests showed that no sodium ion errors were discernible in this pH range so the presence of sodium ions was permitted in these buffers making the solutions simpler and less costly to prepare.

Two changes have been made in the composition of the buffers devised earlier (*1*). To avoid confusion, a new code for the buffer solutions has been introduced. Solutions are designated by A*i*, indicating that the pH of a particular buffer solution lies between i and $i + 1$. The composition of A12 differs from B6 used previously in order to keep the chloride concentration close to 0.1 M. The concentration of A6 (formerly B1) has been increased so that its buffer capacity is higher, and it is therefore less likely to contamination. This solution is particularly important since it is chosen as reference solution in which glass electrodes are assumed error-free and electrodes will be used more frequently in this solution than in others. Apart from these two differences, the following present and previous solutions are the same: A7 = B2, A9

Table IV. Observed emf Differences (mV) for a Perfect Glass Electrode Transferred between Buffer Solutions A6 → A*i*

From	To A0	A1	A2	A4	A5	A6	A7	A9	A11	A12	A14
A0	0	120.2	219.9	294.7	374.5	461.8	523.3	640.0	743.2	802.6	896.3
A1	−120.0	0	99.7	174.5	254.3	341.6	403.1	519.8	623.0	682.4	776.1
A2	−219.9	−99.7	0	74.8	154.6	241.9	303.4	420.1	523.3	582.7	676.4
A4	−294.7	−174.5	−74.8	0	79.8	167.1	228.6	345.3	448.5	507.9	601.6
A5	−374.5	−254.3	−154.6	−79.8	0	87.3	148.8	265.5	368.7	428.1	521.8
A6	−461.8	−341.6	−241.9	−167.1	−87.3	0	61.5	178.2	281.4	340.8	434.5
A7	−523.3	−403.1	−303.4	−228.6	−148.8	−61.5	0	116.7	219.9	279.3	373.0
A9	−640.0	−519.8	−420.1	−345.3	−265.5	−178.2	−116.7	0	103.2	162.6	256.3
A11	−743.2	−623.0	−523.3	−448.5	−368.7	−281.4	−219.9	−103.2	0	59.4	153.1
A12	−802.6	−682.4	−582.7	−507.9	−428.1	−340.8	−279.3	−162.6	−59.4	0	93.7
A14	−896.3	−776.1	−676.4	−601.6	−521.8	−434.5	−373.0	−256.3	−153.1	−93.7	0

= B3, A11 = B4. The substances used for, and compositions of the buffers are given in Tables I, II and III.

Buffer solutions containing sodium ion are coded A*i*Na*j* (*j* = 0, 1, 2) where *j* indicates pNa = −log [Na^+]. Thus A6Na2 means the pH of this solution lies between 6 and 7 and its sodium ion concentration is 10^{-2} M. Solutions A*i*Na*j* for *i* = 6, 7, 9, 11 and *j* = 0, 1, 2; also for *i* = 12, *j* = 0 are obtained by adding sodium perchlorate monohydrate. In solutions containing tetramethylammonium ions, perchlorate precipitates and it is replaced by sodium chloride. Solutions A12Na1 and A12Na2 are identical with B6Na1 and B6Na2, respectively, but the higher sodium concentration A12Na0 can now be prepared using sodium hydroxide which is less costly than tetramethylammonium hydroxide. A new A14 series of solutions has been devised thus extending the range to pH 14.

In devising the testing procedure, the philosophy of keeping the solution preparation and testing procedure as simple as possible was adopted. Accordingly it is not intended that rigorous precautions to exclude carbon dioxide should be taken.

EXPERIMENTAL

Solution Preparation. The substances used in the preparation of the buffer solutions are detailed in Table I and details of the solutions and their preparation in Tables II and III.

Solutions should be prepared with laboratory grade distilled water using Grade B volumetric glassware (20 °C). No special precautions to exclude carbon dioxide should be taken apart from keeping solutions stoppered.

Hydrochloric Acid was provided in ampoules for the preparation of 1 M HCl. They contain 0.001% w/v mercury(II) chloride but no difference could be detected in the results for cell H between solutions prepared from this material and from constant boiling hydrochloric acid.

Sodium Hydroxide was provided as carbonate-free 0.1, 1, and 4 M solution in polythene bottles. Preferably, solutions were prepared from freshly opened bottles which then were restoppered immediately.

Tetramethylammonium Hydroxide (*TMAH*) was available in 100-mL quantities as approximately 25% w/w aqueous solution. Several samples were titrated and the concentration was found to vary by 1.5%; hence it is necessary to titrate the solution before the preparation of the buffer solutions. This may be done with 0.25 M HCl to a pH of 4 electrometrically or with a suitable indicator. The low pH is chosen because of the presence of carbonate detected by differential potentiometric titration and confirmed using a carbon dioxide electrode (Radiometer Type E5037) as 5×10^{-2} M in a freshly opened bottle. Analysis also showed typically 10^{-2} M Na^+, 4×10^{-5} M K^+, 2×10^{-3} M Cl^-, 10^{-4} M Br^-, 10^{-3} M I^-, and 10^{-4} M SO_4^{2-} in the solution as supplied.

Ethanolamine should be used from a freshly opened bottle or for preference distilled (bp 171 °C) and a middle fraction collected.

Piperidine should be used from a freshly opened bottle or for preference distilled (bp 106 °C) and a middle fraction collected. Yellowish colored samples should be rejected.

Experimental details of how the tests should be carried out have been given previously (*1*). Tests should be made in a draft-free atmosphere, all solutions being at the same temperature 25 ± 2 °C.

Table V. Observed emf Differences (mV) for a Perfect Glass Electrode Transferred between Solutions of Increasing Na^+ Concentration at Approximately Constant pH

From	To	A*i*Na2	A*i*Na1	A*i*Na0
A*i*				
A6		1.1	6.2	23.7
A7		0.3	3.1	9.7
A9		1.2	6.7	20.8
A11		0.7	5.0	20.9
A12		−2.5	−0.5	−3.0
A14		−3.7	−3.2	−17.5

Assessment of Probable Errors Arising in Solution Preparation. All solutions were prepared by volume, in order to maintain the preparation process as simple as possible.

The variation of emf due to changes in the concentration of buffer solutions can be evaluated as follows. The electromotive force, *E*, of cell H is given by

$$E = E^\circ - k \log m_H m_{Cl} \gamma_H \gamma_{Cl} \quad (4)$$

where $k = (RT \ln 10)/F$, E° is the standard potential of silver–silver chloride electrode (E° = 222.5 mV). The uncertainty δE in *E*, due to errors of the concentration is

$$\delta E = \frac{RT}{F}\left(\frac{\delta m_H}{m_H} + \frac{\delta m_{Cl}}{m_{Cl}}\right) \quad (5)$$

obtained by differentiation of Equation 4 assuming γ_H and γ_{Cl} are constant over small variations of the ionic strength. The difference between the molal or molar scales will be ignored.

In preparing a solution by volume, three main sources of error arise: (1) Calibration of pipets and flasks, (2) Temperature variation, (3) Experimental technique.

In the preparation of 1 L of A1 from dilution of 100 mL of A0 with water, the probable error produced can be calculated as follows: The concentration of A1, (0.1 M), is given by

$$c_1 = \frac{c_0 v_0}{v_1} \quad (6)$$

where v_1 is the final volume of A1 (1000 mL), and c_0 and v_0 are the concentration (1 M) and volume (100 mL) of A0, respectively. Differentiation of Equation 6 gives

$$\frac{\delta c_1}{c_1} = \frac{\delta c_0}{c_0} + \frac{\delta v_0}{v_0} + \frac{\delta v_1}{v_1} \quad (7)$$

where δc_0 = 0.001 M, as stated on the ampoules supplied. The volume v_0 was dispensed by using a 50-mL pipet twice, and the tolerance on its capacity (*3*) is ±0.08 mL (therefore, $\delta v_0 = 2 \times 0.08$ mL). The tolerance on the capacity of a 1-L flask (δv_1) is ±0.80 mL (*4*). Substituting these values in Equation 7 gives δc_1 = 0.00034 M. For this solution, $m_H = m_{Cl}$ and $\delta m_H = \delta m_{Cl}$, therefore, from Equation 5 δE_1 = ±0.17 mV, which is the error in the emf, assuming the solutions are prepared at 20 °C, since pipets and flasks are calibrated at 20 °C.

If the solutions are prepared at 25 °C, the corresponding difference in the density of water is 0.00116 g cm^{-3}. Assuming

Table VI. Manufacturers' Information on Glass Electrodes Tested

Glass electrode	pH range	Temperature range, °C	Additional information
A	0-12	0-70	Combination electrode
E	0-14	0-70	...
F	0-14	0-130	...
G	0-12	-20-70	...
K	0-14	10-100	Negligible sodium error
M	0-14	10-120	Negligible sodium error
N	0-12	10-70	...
O	0-14	20-70	High alkaline
P	0-11	-10-70	Low temperature
S	0-12	0-60	...
T	0-14	10-140	No appreciable acid error down to 0 pH. Alkaline error very small
X	0-11	0-50	Very low electrical resistance
GG	0-10	-	Corning 015 composition

Table VII. Errors (mV) for Glass Electrodes Transferred between Buffer Solutions, at pH < 6

Glass electrodes	A5	A4	A3	A1	A0
A_1	-0.2	-0.1	-0.1	-0.3	+0.2
A_2	-0.3	-0.1	-0.2	-0.3	+0.1
E_1	-0.3	-0.2	-0.2	-0.5	+0.3
E_2	-0.2	0.0	-0.1	-0.1	+0.2
F_1	-0.4	-0.2	-0.3	-0.4	-0.1
F_2	-0.4	-0.1	-0.2	-0.3	+0.1
G_1	-0.2	-0.3	-0.2	-0.5	-0.9
K_1	0.0	+0.2	+0.3	+0.1	+0.2
K_2	+0.1	+0.3	+0.3	0.0	+0.1
M_1	-0.1	-0.2	+0.1	-0.2	0.0
M_2	-0.3	-0.1	-0.2	-0.2	+0.1
N_1	-0.1	0.0	-0.4	-0.5	-0.3
N_2	-0.2	-0.2	-0.3	-0.3	-0.2
O_1	-0.3	-0.1	-0.3	-0.5	-0.2
O_2	-0.2	-0.1	-0.2	-0.4	-0.1
P_1	-0.5	-0.2	-0.1	-0.2	-1.8
P_2	-0.4	-0.1	0.0	-0.4	-5.5
S	0.0	-0.3	-0.3	-0.6	+0.1
T_1	-0.7	+0.1	-0.2	-0.6	-0.1
T_2	+0.4	+0.8	+0.3	-0.3	+0.5
X_1	-0.3	-0.3	-0.4	-0.6	-0.5
X_2	-0.4	-0.3	-0.4	-0.6	-0.4
GG_1	-1.1	-0.2	+0.1	+0.3	+0.4
GG_2	-0.4	+0.3	+0.6	+0.2	-25.4
pa_H	5.36	4.02	2.49	1.09	0.07

the density of the solution is the same as that of water, and neglecting the expansion of the glass, $\delta c_0 = 0.00116$ M. $\delta v_0 = 0.1163$ mL and $\delta v_1 = 1.163$ mL. Substituting these values in Equation 7, $\delta c_1 = 0.000349$ M and where $\delta E_2 = \pm 0.18$ mV is the error due to a change in temperature, from 20 to 25 °C.

To estimate the possible error in the volumetric technique, it was assumed that one drop corresponds to 0.05 mL, and the effect was calculated of a difference of two drops of water when preparing the two solutions (1M and 0.1 M HCl), and one drop in each use of the 50-mL pipet; these assumptions yield the results that $\delta c_0 = 0.000099$ M, $\delta v_0 = 0.10$ mL and $\delta v_1 = 0.10$ mL. Using Equation 7, as before, $\delta c_1 = 0.00012$ M and $\delta E_3 = \pm 0.06$ mV.

The likely error produced by these three sources will be given by

$$\delta E = \sqrt{\delta E_1^2 + \delta E_2^2 + \delta E_3^2} = \pm 0.25 \text{ mV} \quad (8)$$

A similar error is likely to result in the preparation of the other buffers.

It can be seen that the temperature variation is quite important as a source of error. In practice, if the ambient temperature does not change very much during the course of the experiments, the error would be smaller. In fact, the error found for A0 and A1 was ±0.1 mV, from four measurements for A0 and 6 measurements for A1.

The variation of pH of the buffers with dilution is very small as can be seen from the results of the following experiment: equimolar bis-tris buffer solutions (0.02 M) were prepared in 250-mL flasks, previously calibrated with water, in order to vary the final volume by ±1 mL; the emf readings of cell H were 713.3, 713.5, and 713.7 mV. Thus, the addition of 1 mL of water to 250 mL solution altered the electromotive force only by 0.2 mV. However, solutions of strong acids and bases, although having higher buffer capacities than dilute weak acid systems, have much higher dilution values (e.g., for 0.1 M HCl, $\Delta pH_{1/2} = 0.28$) (5).

Calculation of pH Values of Buffers. From Equation 4 it follows that

$$p(a_H \gamma_{Cl}) = -\log a_H \gamma_{Cl} = \frac{E - E^\circ}{k} + \log m_{Cl} \quad (9)$$

which is an experimental quantity. Using the Bates-Guggenheim convention (6) for γ_{Cl}, $pa_H = pH$ was calculated. Values can be found in Tables VII, VIII and IX. These values are intended only as a guide to the pH of the solutions, because the Bates-Guggenheim convention has been applied above its intended limit of I, 0.1. An alternative procedure was used for buffers A0 and A1 where γ_{Cl} was equated to γ_{HCl} and calculated directly using the equation and constants given by Pitzer (7) which relate to the molality scale. Correcting for concentration scale using density data indicates a difference in pH of no more than 0.01 at 1 M.

RESULTS

Results for Hydrogen Gas Electrode Transfers. The emf differences for a perfect glass electrode (that is for a hydrogen gas electrode) when transferred between solution A6 and any other are given in Table IV. Assuming the glass electrode is error free in A6, the error in any other solution is obtained by subtracting the observed emf difference, $E_{A(i \neq 6)} - E_{A6}$, from the corresponding difference for the hydrogen gas electrode, given in Table IV.

Table VIII. Errors (mV) for Glass Electrodes Transferred between Na^+-free Buffer Solutions at pH > 6

Glass electrode	A7	A9	A11	A12	A14	C12	C12Na0
A_1	-0.1	+0.5	+0.3	+1.5	+11.6	-0.1	+23.8
E_1	+0.3	+0.3	+0.3	+1.2	+3.7	-0.3	+2.4
F_1	-0.2	+0.1	+0.3	+1.1	+4.9	-0.1	+2.2
G_1	-0.2	+0.5	+0.3	+2.4	+20.8	0.0	+59.6
K_1	+0.3	+0.1	+0.2	+1.1	+5.2	-0.3	+5.8
M_1	+0.3	+0.3	+0.4	+0.5	+3.5	-0.3	+1.9
O_1	+0.4	+0.2	+0.4	+0.9	+3.2	-0.3	+0.4
P_2	+0.3	+0.2	+0.4	+8.3	+55.1	-0.2	+98.2
S	+1.5	+0.5	+0.9	+2.8	+19.6	-0.2	+40.5
X_1	+0.3	+1.9	+3.0	+18.1	+59.7	+1.0	+120.2
GG_1	+0.6	+2.0	+3.6	+10.8	+58.4	+0.3	+115.0
GG_2	+0.3	+2.1	+2.6	+7.4	+42.4	+1.3	+92.4
pa_H	7.90	9.38	11.34	12.60	14.1	12.7	12.6

To determine the sodium error, it is necessary to measure the difference between the electromotive forces of cells

Glass electrode | Ai | AgCl | Ag (G′)

Glass electrode | AiNaj | AgCl | Ag (G″)

with i = 6, 7, 9, 11, 12, or 14 and j = 0, 1, 2; each value of i and j corresponds to a particular value of pH and pNa, respectively, as described previously. Since the solution in the first cell above contains no sodium, the error is obtained by subtracting the emf difference, between the two cells, $E_{AiNaj} - E_{Ai}$, from the corresponding difference, when the hydrogen gas electrode replaces the glass electrode. These emf differences are given in Table V.

Results for Commercial Glass Electrodes. *Acid Region* ($pH < 6$). Some commercial glass electrodes (Table VI) were tested, following the procedure described. The glass electrodes are represented by code letters and duplicates are indicated by subscripts. Some were new electrodes and some had been used in the previous work (*1*) (the same code letters have been retained for the same electrodes).

Example: An emf difference of 339.7 mV was obtained for a glass electrode when transferred between A6 and A12. Subtracting this from the corresponding emf difference for the hydrogen gas electrode, 340.8 mV (Table IV), 6th row, 10th column), the error is 1.1 mV.

The errors determined are given in Table VII. These were obtained using values for hydrogen electrodes determined at the same time. Use of the average values leads to values which may differ by up to ±0.6 mV (0.01 pH) because of difficulties in reproducing solution preparation and solution contamination by carbon dioxide and solution carry over by the electrode transfer.

Alkaline Region ($pH > 6$). Twelve glass electrodes were also tested in the alkaline region (pH > 6), and the results obtained using hydrogen electrode values determined at the same time are given in Table VIII.

Sodium Errors. Since the sodium error becomes important in the alkaline region, the glass electrodes were transferred from solutions without sodium to solutions containing sodium at three different concentrations, at each pH value, from 6 to 14. The errors, given in Table IX, were calculated using the emf differences shown in Table V.

Example: An emf difference of 4.9 mV was obtained for a glass electrode when transferred from A12 to A12Na0. Subtracting this value from −3.0 mV (Table V, 5th row, 3rd column), the error is +1.9 mV.

Although addition of sodium ions alters the pH, it is constant within ±0.2 pH, for each group of buffer solutions (Table IX). Thus the sodium error for each glass electrode has been determined at approximately constant pH.

Figure 1 shows the variation of the sodium error for glass electrode X_1 at various pH values.

DISCUSSION

The performance of glass electrodes over the whole pH range at 25 °C can now be tested simply, by preparing the appropriate buffer solutions and measuring the corresponding emfs, using the silver–silver chloride reference electrode. The method is more accurate than any involving the use of the calomel electrode, because of the irreproducibility of liquid junction potentials.

Although electrode potentials vary with temperature, the testing temperature is not critical, since the method is based on comparison of *differences* between two emf readings; but it is important that the two readings are taken at the same temperature. The measurements described were taken with temperature variation of no more than ±0.50 °C; this could be responsible for some scatter found in the results, but better temperature control is not necessary, since a reproducibility

Table IX. Errors (mV) for Glass Electrodes Transferred between Solutions of Increasing Na^+ Concentration at Approximately Constant pH

Glass electrode	A6Na2	A6Na1	A6Na0	A7Na2	A7Na1	A7Na0	A9Na2	A9Na1	A9Na0	A11Na2	A11Na1	A11Na0	A12Na2	A12Na1	A12Na0	A14Na2	A14Na1	A14Na0
A_1	−0.4	−0.2	−0.5	−0.2	−0.9	−0.5	+0.2	+0.2	+0.7	+1.1	+2.2	+9.9	+2.3	+7.9	+19.2	+5.7	+21.0	+38.9
E_1	−0.3	−0.1	−0.3	−0.1	−0.9	−0.5	+0.1	+0.1	+0.3	+0.6	+0.4	+2.2	+0.1	+0.7	+1.9	−0.4	+2.3	+4.8
F_1	−0.3	−0.2	−0.3	−0.1	−0.9	−0.5	0.0	0.0	+0.2	+0.8	+0.4	+2.4	0.0	+0.6	+1.7	−0.4	+1.8	+4.1
G_1	−0.3	−0.1	−0.4	−0.1	−0.8	−0.2	+0.2	+0.5	+2.7	+2.6	+7.2	+24.7	+7.1	+21.9	+45.4	+12.5	+38.4	+67.2
K_1	−0.4	−0.3	−0.6	−0.2	−0.8	0.0	+0.1	+0.2	+0.5	+0.9	+1.0	+4.2	+0.9	+2.2	+4.5	+0.4	+4.5	+8.6
M_1	−0.4	−0.2	−0.5	−0.2	−0.9	−0.5	0.0	+0.1	+0.1	+0.7	+0.2	+2.5	−0.1	+0.5	+1.5	−0.6	+1.5	+4.6
O_1	−0.2	−0.2	−0.4	−0.1	−0.8	−0.5	+0.9	+0.1	+1.2	+0.2	−0.4	+1.3	−0.1	−1.2	+1.5	−1.8	−1.5	−0.7
P_1	−0.2	−0.2	−0.0	0.0	−0.5	+1.2	+2.1	+3.5	+11.0	+8.4	+22.3	+57.6	+19.4	+48.2	+86.6	+21.5	+62.3	+102.7
S_1	−0.2	−0.2	−1.1	−0.6	−1.5	−1.0	+1.9	+1.2	+3.1	+3.2	+6.8	+21.1	+3.2	+16.7	+33.3	+8.0	+27.2	+48.4
X_1	−0.1	+0.3	+1.6	+0.5	+1.1	+5.7	+4.5	+9.6	+23.0	+17.9	+36.7	+74.5	+26.6	+55.3	+93.0	+22.4	+61.3	+97.3
GG_1	−0.4	+0.5	+0.7	+0.4	−0.2	+1.5	+1.3	+3.1	+11.5	+9.0	+25.8	+66.0	+22.4	+56.6	+98.4	+25.3	+69.6	+111.5
GG_2	0.0	+0.3	+0.1	0.0	−0.8	0.0	+1.4	+1.6	+8.1	+5.6	+19.6	+56.3	+18.7	+50.4	+89.3	+24.2	+67.5	+108.3
pa_H	6.6	6.6	6.8	7.9	7.9	8.0	9.4	9.4	9.6	11.3	11.4	11.6	12.6	12.6	12.5	14.1	13.9	13.8

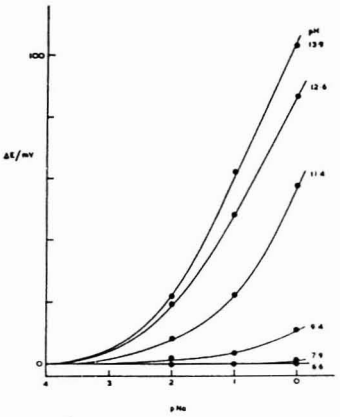

Figure 1. Sodium errors of glass electrode X_1

better than ±0.6 mV is not achievable (by inspection of Tables VII–IX). The probable error in preparing a buffer solution was shown to be about ±0.25mV; since the calibration of glass electrodes, at a particular pH, involves the preparation of four buffer solutions, the expected error would be $\pm 4 \times 0.25/\sqrt{4} = \pm 0.5$ mV. Since the accuracy of most pH meters is ±0.01 pH, which corresponds to ±0.6 mV, solution preparation by volume is of adequate accuracy.

Examining the results shown in Table VII it can be seen that, with the exception of electrodes G_1, P_1, P_2, and GG_2 in A0, all glass electrodes show no error in the acid region. The apparent errors observed are mainly caused by temperature variation, solution contamination, and uncertainties in the concentration of the solutions. In the alkaline region (Table VIII), for most glass electrodes the errors, up to pH 11, are very small and in good agreement with results for the same electrodes determined previously (*1*). Electrode S in A7 (Table VIII) and electrode GG_1 in A5 (Table VII) show errors which are out of line (+1.5 mV and −1.1 mV, respectively) with the results obtained in neighboring solutions for these same electrodes; this could be explained by a poor electrical connection on those occasions. It indicates that the performance of a glass electrode should not be judged on a single determination.

In Table IX the errors observed in A7Na1 are higher and of the opposite sign than expected, and of the same magnitude for all electrodes; this suggests that the solution has been contaminated. Electrode O_1 seems to be the best electrode of the series; it shows no sodium error, even at pH 14, but the scatter in the results obtained with it is greater than for any other electrode.

Generally, the errors observed at pH > 12 may be due either to the sodium ion impurity in tetramethylammonium hydroxide or to some response to tetramethylammonium ions themselves (*8*). No other explanation has ever been advanced of errors in alkaline solution except partial response to small cations. Light and Fletcher (*9*) have described a method for evaluating glass errors using silver–silver chloride electrodes. They employed three solutions: an acid solution (0.1 M HCl), an alkaline solution (0.05 M barium hydroxide), and an alkaline solution with added sodium ion (0.05 M barium hydroxide + 0.5 M $NaNO_3$). The ionic strength was kept high (2 M) by the addition of barium chloride to all solutions, thus providing chloride ions and permitting use of Ag|AgCl reference electrodes. It was thus possible to determine the electrode response between pH 1 and 12 approximately and the sodium ion error at pH 12.

To test the hypothesis of response to tetramethylammonium ions, two barium-containing solutions C12 (0.1 M $Ba(OH)_2$ + 0.1 M HCl) and C12Na0 (+1 M $NaClO_4$) were prepared. The results of testing the same range of glass electrodes has been incorporated in Table VIII. All electrodes showed errors less than 1 mV in C12. In C12Na0 the errors are comparable to those in A12Na0 shown in Table IX. Preparation of C12Na3 and C12Na4 gave errors for electrode P_2 of 2.3 mV and 0.8 mV, respectively, and for G_1 of 1.9 mV and 0.4 mV, respectively. This suggests that if the errors found in A12 were due to sodium ions their concentration would have to be higher than 10^{-3} M, which is not so according to flame photometric analysis (4.3×10^{-4} M). Solutions with the same composition as A12 were prepared from tetraethyl- and tetrabutylammonium hydroxides. Electrode P_2 gave errors of 4.7, 13.3, and 10.5 mV and electrode G_1, 0.8, 4.9, and 12.4 mV in TMAH, TEAH, and TBAH. The Na^+ analysis were 5.4×10^{-3} M (TMAH, new batch), 7.4×10^{-4} M (TEAH), and 7.7×10^{-5} M(TBAH). The new lower error in TMAH is consistent with the lower Na^+ concentration but, on the other hand, it is known from previous work that the alkaline error depends on the immediate previous usage of the glass electrode. Although the matter is not resolved, response to low level Na^+ concentration seems a more likely explanation than response to tetraalkylammonium ions. An attempt to remove Na^+ ions from A12 by complexation with added benzo-15-crown-5, 18-crown-6 (*10*) or phenacyl kojate (*11*) gave no significant difference in the determined errors for the two crowns but an increased error in the presence of kojate.

These findings are of considerable interest to the understanding of the origin of the errors of the glass electrode. It is hoped that the improved methods of testing glass electrodes described in this paper will lead to results which will stimulate manufacturers to make improvements in some of the glass electrodes now available, but will also lead to a better understanding of its mechanism of response.

ACKNOWLEDGMENT

We thank various manufacturers for donating samples of their electrodes and members of British Standards Institution Technical Committee LBC/16 for their advice and encouragement.

LITERATURE CITED

(1) M. F. G. F. C. Camoes and A. K. Covington, *Anal. Chem.*, **46**, 1547 (1974).
(2) M. Dole, *J. Am. Chem. Soc.*, **53**, 4260 (1931).
(3) British Standard BS 1583 (1961).
(4) British Standard BS 1792 (1960).
(5) R. G. Bates, "Determination of pH—Theory and Practice", 2nd. ed., Wiley, New York, 1973, p 111.
(6) R. G. Bates and E. A. Guggenheim, *Pure Appl. Chem.*, **1**, 163 (1960).
(7) K. S. Pitzer and G. Mayorga, *J. Phys. Chem.*, **77**, 2300 (1973).
(8) G. Eisenman, in "The Glass Electrode", Wiley, New York, 1965, p 289.
(9) T. S. Light and K. S. Fletcher, *Anal. Chem.*, **39**, 70 (1967).
(10) C. J. Pedersen and H. K. Frensdorff, *Angew. Chem., Int. Ed. Engl.*, **11**, 16 (1972).
(11) Cambrian Chemicals Ltd. (Croydon, Surrey), *News Bull.*, **1** (2), 1 (1975).

RECEIVED for review March 15, 1977. Accepted May 2, 1977. Thanks are due to the Portugese Government for partial financial support of M.I.A.F.

Application of Pattern Recognition Techniques to the Interpretation of Severely Overlapped Voltammetric Data: Theoretical Studies

Q. V. Thomas[1] and S. P. Perone*

Purdue University, Department of Chemistry, West Lafayette, Indiana 47907

Pattern recognition methods were used here to determine the multiplicity of Stationary Electrode Polarographic (SEP) curves. While earlier work in this area considered only reversible SEP data, here an extended data base was used which included the irreversible and quasi-reversible cases in addition to the reversible case. Using this more general data base, evaluations were made for several feature definition, selection, and pattern classification methods, each of which was based on either the linear learning machine (LLM) or the k-Nearest-Neighbor (kNN) classification rule. These evaluations led to the selection of a method which could be used to classify synthetic, noise-free singlet and severely-overlapped doublet SEP data with an accuracy of 94%. This method was then extended to the classification of alternate data bases consisting of noisy synthetic SEP data, and of reversible synthetic SEP data outside the limits of the training set. Conclusions derived from these studies can be applied directly to classification of real SEP data.

There are many examples of analytical measurements which can yield multiple component information under the guise of a single response peak. In these cases the single peak is actually a summation of two or more components which are so closely overlapped that visual or mathematical detection of the multiplicity is virtually impossible. When the response peak results from a known number of components, various deconvolution (*1–3*) methods may be applied to determine the relative contribution of each. If, however, the number is not known *a priori*, it becomes desirable to use an independent method to determine the peak multiplicity before deconvolution is attempted.

In this work we have evaluated the use of pattern recognition techniques for the detection of singlets and doublets in stationary electrode polarography (SEP). Previous work in this laboratory (*4, 5*) has demonstrated that either the linear learning machine (LLM) (*6–8*) or k-Nearest Neighbor (kNN) (*9, 10*) approach may be used to classify synthetic doublet and singlet reversible SEP data with about 90% to 95% accuracy. In those studies the SEP waveforms were not complicated by electron transfer kinetics, so any shape differences between singlets and doublets arose primarily from the actual peak multiplicity.

In the more general case of real voltammetric data, electron transfer kinetics and other factors affect the shape of waveforms, and these complications must be considered when generating a data base for the classification of real patterns. In this paper we report the preparation of an extensive set of synthetic SEP data (QUIRDS data set) which includes QUasi-reversible, Irreversible and Reversible Doublet/Singlet patterns. This data base provided a convenient means of exploring questions crucial to the classification of real doublet/singlet SEP data—such as what are the most meaningful data features and most appropriate classification technique. The results of these studies are reported here, while applications to real voltammetric data are reported elsewhere (*11*).

General Considerations for Pattern Classification. When selecting a pattern recognition method to solve a particular problem in chemical analysis, the analyst must be aware of the unique characteristics of available methods. The LLM, for example, assumes that the patterns under study are linearly separable. This results in the training of weight vectors which converge to a decision surface that classifies the data 100% correctly. Lack of linear separability prohibits convergence and lowers the prediction percentage. Training weight vectors is an iterative process and therefore time consuming for large data sets. Prediction by weight vectors on the other hand is a very quick process requiring only one calculation for each pattern classified.

The kNN algorithm makes no assumption of linear class separability and can be applied to multiclass problems. There is no training process as such with kNN, but prediction requires distance calculations for the entire training set, a process requiring substantially more time than LLM predictions.

The most crucial aspect of pattern recognition is the intelligent definition of pattern descriptors or features (*feature definition*). Features must be defined so as to effect class separation on the basis of real class differences and not on the basis of trivial information. This is often a highly intuitive step but it must be based on the analyst's best understanding of his data.

The general procedure for evaluating these various factors is described below. This procedure was followed for each of two independent feature sets in order to determine which classification method and features were best applied to our SEP data base. The first step, data base generation, involves the process of collecting the raw analog or digital data which represent patterns of each of the classes to be considered. These data may result from actual physical measurements or may be derived from theoretical considerations. Subsets of this data base may be selected for use as training or prediction sets during the later processes of feature evaluation and selection. Training sets should include as wide a representation as possible of those patterns which may be found in a prediction set. In a case where only small numbers of real patterns are available, this may become a limiting factor in classification accuracy.

The *feature extraction* process simply involves the calculation of values for each feature from the raw data. This is also the point at which various signal and feature preprocessing methods may easily be applied. These may include digital smoothing techniques (*12–14*), numerical transformations (*15, 16*), and autoscaling (*17*).

[1] Current address, Finnigan, 845 West Maude Avenue, Sunnyvale, Calif. 94086.

Feature selection (sometimes referred to as *feature elimination*) is a process used to eliminate those features which actually supply little or no useful information to the classification routine. The resulting decrease in dimensionality usually provides for higher classification accuracy while requiring less computation time. If feature elimination causes only a decrease in classification results, methods used for feature definition and extraction should be reexamined as well as the classification method itself.

Computer Hardware/Software. All calculations were programmed in FORTRAN IV on a Hewlett-Packard 2100S computer, with 32K words of core memory and floating point hardware, operating under the H-P DOS-M executive. Peripherals include a HP-7900 disk drive with 5 Mbytes of storage, a Centronics 306 printer, a Calcomp 565 digital plotter, Teletype, paper tape reader and punch, and a Tektronix 603 storage monitor.

Generation of the Data Base. There are several factors which influence the shape of a multipie-component SEP curve. If the effects of coupled chemical reactions and surface complications like adsorption or precipitation are avoided, then the primary shape factors include the degree of reversibility, the number of electrons involved in the reduction step, concentration, and peak potential for each component. Considering only the doublet case, the size of a representative data base which included various combinations of all of these becomes quite large. Experimental generation of this type of all-inclusive data base would be impractical. For this reason, we chose to generate our data base synthetically from SEP theory (*18, 19*). Hopefully, the synthetic data base could then be used as a training set for classifying real experimental doublet/singlet data, or at least for identifying useful features for the classification of real data.

There are several advantages to this approach beside the practicality of synthesis. Because each of the above shape factors can be varied at random, a data base can be prepared which would be thoroughly representative of the range of possible waveforms that might be expected in real data.

A second advantage is that a synthetic data base would be free from instrumental artifacts, noise, and bias. The presence of these distortions in real data might mask intrinsic relationships important for classification. Such relationships may become clear only in the absence of these distortions.

A synthetic data base also provides a convenient source of information for the feature selection process. Because all of the synthesis parameters are available, correlations between features and parameters are easily studied. This can be useful to eliminate trivial features, a process far more difficult with real data.

Finally, pattern recognition studies with a synthetic data base determine, at least, whether or not the proposed classification objective is feasible. That is, if the idealized synthetic patterns are not classifiable, it is unlikely that classification of real patterns can be achieved.

THEORY

Equations 1 and 2 describe SEP current for the reversible and irreversible (*18*) cases, respectively, where values of $\chi(at)$ and $\chi(bt)$ are available as tabulated functions of $n(E - E_{1/2})$ or $\alpha n(E - E_{1/2})$, respectively. (n = number of electrons, E = electrode potential, $E_{1/2}$ = halfwave potential, α = transfer coefficient)

$$i_{rev} = nFAC_0^*(D\pi a)^{1/2}\chi(at) \quad (1)$$

where $a = nFV/RT$.

$$i_{irr} = nFAC_0^*(D\pi b)^{1/2}\chi(bt) \quad (2)$$

where $b = \alpha nFV/RT$, V = voltage scan rate, F = faraday, A = electrode area, C_0^* = bulk concentration, D = diffusion coefficient, and other symbols have their usual significance. A more general expression which includes these two limiting cases as well as the quasi-reversible case can be expressed by Equation 2 where $\chi(bt)$ is replaced by an expression, derived by Nicholson (*19*), which may be tabulated as a function of $n(E - E_{1/2})$ for various values of ψ, a reversibility factor, and α. For values of ψ greater than 7.0, the function describes totally reversible behavior and is independent of α. For ψ less than 0.01, the function represents totally irreversible behavior with intermediate values pertaining to quasi-reversible cases.

To generate the synthetic data base used in this work, $\chi(\psi,\alpha)$ functions were calculated using 10 values of ψ, ranging from totally irreversible to reversible, and 5 values of α. Using Equation 3, 1200 singlets and 2400 doublets were synthesized

$$i = C_1^*\chi_1([E - E_{p_1}]n_1]) + C_2^*\chi_2([E - E_{p_1}]n_2]) \quad (3)$$

by randomly selecting values for ψ, α, n, and $E_{p_2} - E_{p_1}$ from the values listed in Table I. Concentration ratios were assigned by selecting a random number between 1.0 and 10.0 for each component of the curve. For singlet curves, C_2^* was set equal to zero. Each synthetic curve is composed of 250 points calculated at a resolution of 2 mV per point with the peak falling between data points 150 and 154.

The data base of 3600 patterns (QUIRDS) was then scrambled to obtain a random mixture of singlets and doublets throughout. This step was taken to prevent pattern order from exerting a strong influence on weight vectors calculated by the LLM. From this scrambled data base, a training set of 1000 patterns was selected as well as several prediction sets of 200–300 patterns. In each case the ratio of singlets to doublets was very close to the 1:2 ratio expected, indicating that thorough mixing was obtained.

Feature Definition. We have defined two feature sets of 62 each, one set based on theoretical considerations of SEP shape factors and the other based upon the discrete Fourier Transform (*20, 21*) of the raw SEP curve. A list of typical

Table I. Parameter Ranges for Synthetic SEP Doublet/Singlet Data Base (QUIRDS)

ψ	0.01, 0.02, 0.05, 0.10, 0.20, 0.50, 1.0, 2.0, 5.0, 10.0
α	0.3, 0.4, 0.5, 0.6, 0.7
n[a]	0.9, 1.0, 1.1; 1.8, . . ., 2.2; 2.7, . . ., 3.3
$E_{p_2} - E_{p_1}$	4, 6, 8, 10 mV
C_1^*/C_2^*[b]	10:1 to 1:10

[a] . . . represents increments of 0.1. [b] $C_2^* = 0$ for singlets, all other values chosen at random.

Table II. Typical SEP Features[a]

$(\Delta E$ at 75% $i_p)/(\Delta E$ at 80% $i_p)$
$(\Delta E$ at 75% $i_p)/(\Delta E$ at 80% $i'_p)$
(Area above 75% $i_p)/(\Delta E$ at 75% $i_p)$
(Area above 75% $i_p)/($Area above 80% $i_p)$
Efunction at 70% i_p
Efunction at 80% i'_p
Ifunction at ΔE_{i_p} = 16 mV
i''_{p_1}/i''_{p_2}
$(i''_{p_1})^2/(i''_{p_1}i_{p_1})$
Δi at $E_p \pm 10\%$

[a] See Ref 4 and 22 for complete definition of all features and terms. Efunction $= (E_2 - E_p)(E_p - E_1)/((E_2 - E_p) - (E_p - E_1))^2$. Ifunction $= i_2^* i_1/(i_2 - i_1)^2$, i_p = peak current, i'_p = 1st derivative peak current, i''_p = 2nd derivative peak current.

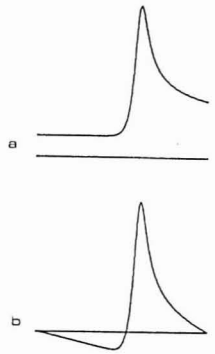

Figure 1. Translation–rotation of SEP curves for Fourier transformation. (a) Original curve. (b) After translation–rotation

SEP-based features is found in Table II. A complete list may be found in Ref. 22. Thirty-four features were defined as ratios which would eliminate any dependence on shape factors such as α or n. This type of ratio was shown to be an important feature in earlier studies (*4*, *5*). Another 28 features were selected from the list of arbitrarily-defined features which Sybrandt (*4*) found to be the most useful for classification of reversible SEP data by the LLM. Note that in both cases there are several features which are derived from the first and second derivatives of the SEP curve. Significant noise on the zero derivative curve could result in distortion of these features.

An alternative method for describing the shape of a waveform is by a series expansion of orthogonal functions. The Fast Fourier Transform (FFT) provides a convenient method of obtaining such an expansion in terms of sine and cosine functions. The low frequency components of the transform will contain most of the fundamental shape information while the high frequency components may be regarded as noise information. Using the low frequency components as features allows the retention of shape details while discriminating against background noise. For this work, 31 real and 30 imaginary coefficients corresponding to the lowest frequency components of the discrete Fourier transformation were retained as features. (The first imaginary coefficient was not used because it is always zero.)

Feature Extraction. A minimum amount of signal preprocessing was performed on the raw SEP data in order to maintain curve fidelity as much as possible. All curves were normalized to a peak current of 1.0 prior to extraction of both the SEP and FFT features. During extraction of the SEP features, derivatives were calculated using an 11-point cubic convolution function (*12*). All SEP features were calculated directly from the raw curve and these derivatives.

Before extraction of the FFT features each curve was shifted to place E_p at data point number 96 and then truncated to 128 points. These two operations were carried out to ensure that all Fourier transformations were performed on the same potential window. Failure to do this would invalidate any comparisons made between FFT features of different patterns. Several E_p positions were tried, (e.g. 32, 64, 96, 128) but the best overall classification results were obtained when E_p was located at point 96.

Finally, each peak-adjusted curve was translated and "rotated" about the origin to bring the initial and final data points to a value of zero (Figure 1). (This is not a true rotation, but rather involves a point-by-point subtraction of the line connecting the initial and final data points (*23*).) This has been shown to be a most effective means of maintaining the fidelity of electrochemical data during Fourier transformations (*23*). After the translation-rotation step, each curve was converted to real values and Fourier transformed. The FFT routine returned 128 imaginary and 128 real coefficients from which 61 features were selected as described earlier. Both feature sets were autoscaled to give each feature a unit variance and zero mean. No weighting of features was performed.

Generation of Noisy Synthetic Data. In order to study the effects of noise on our two feature sets, a set of noisy patterns was prepared by summing a real noise signal with the raw curves of the QUIRDS prediction set. This noise signal was obtained from a computer automated electroanalytical instrument which has been described elsewhere (*24*). The noise was scaled to achieve a S/N ratio of about 100. In addition, the noise data array was rotated a random number of points before being added to each raw synthetic curve. This was done to prevent an artificial bias from being added to the data which might result if all synthetic data had exactly the same noise pattern. Both feature sets were extracted from these noisy data and auto-scaled as before.

Two signal preprocessing methods were used to smooth the noisy QUIRDS data prior to feature extraction, a Savitzky-Golay 15-point cubic convolution (*12*) and a rectangular Fourier filter function (*23*). The Fourier filter function was applied to the noisy QUIRDS prediction set as follows. Each raw curve of 250 points was translated and rotated about the origin as in Figure 1. The data were expanded to 256 points by adding zeros and then Fourier transformed. The Fourier coefficients corresponding to the 208 highest real and imaginary frequency components were then set to zero. This cut-off was found to maintain smooth data fidelity better than any other cut-off tried. Finally, all 256 Fourier coefficients were inverse transformed, rotated, and translated to obtain a smoothed curve. The features were then extracted following peak adjustment and truncation as described earlier.

FFT features should show good noise immunity since most noise transforms to the high end of the frequency spectrum. However, noise can create difficulties in locating true peak potentials. Noise can cause slight shifts (1 to 2 data points) of the apparent peak location and thus change the potential window viewed by the FFT. This can then result in erroneous FFT feature values. Fourier filter smoothing prior to peak adjustment helps to minimize the errors associated with locating E_p by making the apparent peak location and the true peak location coincide more exactly.

The Savitzky–Golay smooth is a weighted moving average method which utilizes information on both sides of a data point to calculate its smoothed value. A 15-point smooth was required to achieve a S/N level comparable to that obtained with the Fourier filter function. This is a rather severe processing step which can result in peak distortions.

Feature Selection. The goal of feature selection is to find an optimum set of features which will accurately classify a set of test patterns (prediction set). We have evaluated the ability of three feature selection methods to achieve this goal; two are based on the LLM and one on the kNN approach. Each method was applied to both feature sets (SEP and FFT) to determine which combination would yield the best results. Prior to these studies a correlation coefficient matrix was generated for both feature sets obtained from the QUIRDS data. Eigenanalysis (*25*) of these matrices provides the number of independent factors inherent in the data and this gives an indication of the information content of each feature set. For the SEP features, the first 5 eigenvectors account for 87% of the total variance, where the respective eigenvalues are: 11.7, 7.06, 3.41, 2.50, 1.37. For the FFT features the first

Table III. Feature Selection and Classification Results for QUIRDS Data Base

	SEP features			FFT features		
		% ACC			% ACC	
Selection method	No. retained	Singlets	Doublets	No. retained	Singlets	Doublets
kNN (IFS)	3[a]	98.6	93.0	9[b]	97.4	91.8
LLM (Variance)	54	73.6	68.7	30	11.5	94.3
LLM (Sign-magnitude)	23	54.4	75.3	27	32.0	79.5

[a] Features No. 1, 20, 25, Ref. 22. [b] Features No. 1, 3, 8, 11, 17, 27, 28, 29, 30, Ref. 22.

4 eigenvectors account for 97% of the total variance, where the respective eigenvalues are: 18.9, 5.56, 3.61, 1.08.

During feature selection, a prediction set should be used which is as representative as possible of the final set of unknown data to be classified. This will ensure that those features selected are most likely to correctly classify the unknown patterns. Failure to do so will cause the selection of a set of features which may optimize the classification of a given prediction set but fail to classify the patterns of real interest.

Sign-Magnitude Method. This approach is based on the LLM and has been described elsewhere (*4*). Briefly, features are removed from the feature set as a result of two conditions. If, after convergence (or interruption of training if convergence does not occur) of two simultaneously-trained, oppositely-initialized weight vectors, the weights corresponding to a given feature differ in sign, that feature is removed from the feature set. The remaining weight vectors are then reinitialized and the cycle is repeated. When no further features are removed by this criterion, those features whose weights have the smallest values are eliminated. The entire process continues until linear separability is lost, or, in the case of nonseparable data, prediction falls below some arbitrary limit.

Variance Selection Method. The variance selection method (*26*) is based on the LLM and begins by training a series of weight vectors, each of which has been initialized differently. Features are then ranked in importance by the magnitude of the relative standard deviations for their corresponding weights. A set of suitable features is then selected corresponding to those weights which have the smallest standard deviations. This set is then broken down into smaller sets until separability is lost, with the last successful set being retained as the important features. Variance selection theory assumes the data are linearly separable and cannot necessarily be applied otherwise.

The One-Dimensional kNN Method. With this method (*5*), prediction set patterns are classified by the kNN rule, one feature at a time, rather than starting with all 62 at once as in the previous two methods. The m features scoring the highest accuracy are then retained for multidimensional analysis. The value of m is chosen somewhat arbitrarily and typically includes 10% to 20% of the original features. Single feature histograms and feature correlations are then used to aid rejection of overlapping or redundant features from the set chosen above. The remaining features are then combined in groups of two or more for multidimensional analysis.

Following initial feature elimination with the one-dimensional method, an Iterative Feature Selection (IFS) approach, in which one feature at a time is removed from the feature set, was applied to the remaining features. If its removal results in a loss of classification accuracy, that feature is retained. If its removal results in an increase in the classification accuracy, it is eliminated from the feature set. This process is repeated until each feature has been tested, completing one iteration. Additional iterations are performed, using those features retained during the previous iteration, until no further features are eliminated.

The order in which features are tested is arbitrary. In this work it was decided that those features which are most likely to be affected by noise distortions should be tested first. While they should be eliminated whenever tested, removal of suspect features at the beginning of the first iteration will speed-up the overall feature selection process.

Condensed kNN Algorithm. One of the primary disadvantages of the kNN algorithm is the amount of time required to classify data when the training set is composed of a large number of patterns. Classification time can be significantly decreased if the training set can be reduced to a smaller number of patterns which lie on or near the decision surface between pattern classes. Generally, information contained in patterns far beyond the decision surface can be found to exist in the decision surface, and since they represent essentially redundant information, these patterns could be eliminated from the training set without a loss in classification ability.

The condensed kNN algorithm (*9*) is a method utilizing the kNN decision rule which can be used to reduce pattern redundancy in the training set. The method proceeds as follows: The first training set pattern is placed in an empty set of condensed patterns. Each of the remaining training set patterns is then classified using the condensed set patterns by the kNN rule. If the pattern is classified incorrectly, it is placed in the condensed data set; if it is classified correctly, the pattern remains in the original training set.

Once all training set patterns have been classified, the process is then repeated using the new condensed set and the patterns remaining in the original training set. When no further transfers to the condensed set occur, the process is complete. This usually occurs within four cycles.

RESULTS

The results of a feature selection study for the QUIRDS data base are summarized in Table III. These results suggest that a kNN approach is the most appropriate selection and classification method for both features sets. Not only is the classification accuracy for both classes the highest of the three methods, but the number of features retained is also the smallest.

In the case of variance selection with SEP features, virtually no feature selection occurred.

While fewer FFT features were selected by the variance method, the final weight vector essentially classisfied all the patterns as doublets. The sign-magnitude approach likewise did not select a useful set of features for linearly separating the two pattern classes in either feature space. The fact that neither learning machine method converged to 100% classification accuracy is proof that these data are nonlinearly separable in both FFT and SEP feature spaces and prevents their use as effective pattern classifiers for the QUIRDS data set.

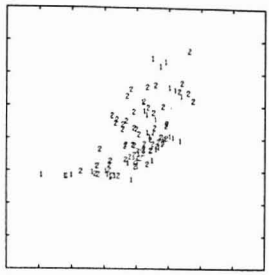

Figure 2. Nonlinear map, QUIRDS prediction set; kNN-selected FFT features. (1) = singlet; (2) = doublet

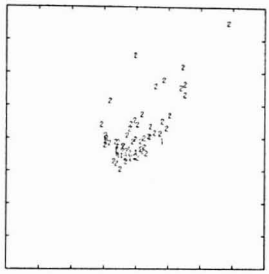

Figure 3. Nonlinear map, QUIRDS prediction set; kNN-selected SEP features, (1) = singlet; (2) = doublet

Visual inspection of the QUIRDS prediction set allows further interpretation of these results. Figures 2 and 3 present information in the form of nonlinear mappings (27) (NLM) of both feature sets. NLM allows d-dimensional data to be plotted in two dimensions while retaining as nearly as possible the d-dimensional pattern distances. These plots were obtained by mapping the kNN features selected in Table III for 100 patterns selected at random from the prediction sets. Plots were restricted to 100 patterns because of core memory limitations. In the mapping of the kNN-selected SEP features (Figure 3), singlets are found as two tightly clustered groups, the centers of which are reversible and irreversible patterns. Quasi-reversible singlets are found between and surrounding these two clusters. It is this high local density which allows the singlets to be classified correctly by kNN even in the presence of overlapping doublets. Any factor, such as noise, which tended to reduce singlet density could be expected to cause a significant reduction in kNN classification accuracy.

The mapping of kNN-selected FFT features (Figure 2) shows an entirely different spatial distribution where singlets tend to lie on a curve surrounded by doublets. As in the case of the SEP features, reduction of the singlet density along this curve by noise or other distortions could be expected to reduce significantly classification accuracy.

Classification of Noisy Data. It was suggested above that noise on raw data curves could cause serious problems in feature extraction and pattern classification, especially where features are derived from derivatives of the curves. If a smooth synthetic training set is to be used for classification of real data, there must be a method of dealing with patterns which have a finite signal-to-noise (S/N) ratio, that is, to select features which have an inherent immunity to noise distortions. Thus, a set of noisy synthetic patterns (noisy QUIRDS, NQUIRDS) was generated as described in the Theory section above.

Table IV. Effect of Noise on kNN Classification of QUIRDS Data[a]

	Classification accuracy, %			
	3 SEP Features		9 FFT Features	
Prediction set	Singlet	Doublet	Singlet	Doublet
Smooth QUIRDS (From Table III)	98.6	93.0	97.4	91.8
Noisy QUIRDS (NQUIRDS)	22.2	88.9	34.6	64.8
Savitzky-Golay-smoothed NQUIRDS	33.3	78.7	35.9	80.3
Fourier-Filter-smoothed NQUIRDS	40.2	90.6	44.9	75.4

[a] Smooth QUIRDS used as training set.

Table V. Classification of QUIRDS Prediction Sets by Noise-Optimized Features

	Classification accuracy, %			
	4 SEP features[a]		12 FFT features[b]	
Prediction set	Singlet	Doublet	Singlet	Doublet
Smooth QUIRDS	99.1	86.0	85.9	84.4
Noisy QUIRDS (NQUIRDS)	57.1	89.9	64.1	85.3
Savitzky-Golay smoothed NQUIRDS	7.4	93.2	57.7	68.0
Fourier Filter smoothed NQUIRDS	80.8	89.4	82.1	90.9

[a] Features No. 2, 35, 37, 43, Ref. 22. [b] Features No. 1, 6, 7, 9, 10, 12, 13, 16, 20, 21, 22, 23, Ref. 22.

The kNN classification results using smooth QUIRDS training set and both smooth and noisy QUIRDS prediction sets are shown in Table IV. The features used were the same as those used to compile Table III. The data show that the presence of noise causes a significant loss of classification accuracy for both the SEP and FFT features used. Table IV also lists the results obtained for the classification of the smoothed NQUIRDS prediction set, using both Savitzky-Golay and Fourier filter smoothing. Both smoothed data sets show slight improvements in classification accuracies for the SEP and FFT features over the unsmoothed noisy data. However, none of the results begin to approach those obtained for the smooth QUIRDS data.

Recalling the importance of choosing the correct prediction set for feature selection, the results described above were not unexpected. For this reason, kNN (IFS) feature selection was performed again using the Fourier-filtered noisy QUIRDS data as the prediction set. The new "noise-optimized" sets of SEP and FFT features were then applied to each QUIRDS prediction set to obtain the results shown in Table V. There was a significant improvement in the classification of both the noisy and Fourier-filtered data sets using these noise-selected features. This underscores the importance of selecting features to optimize prediction set classification. In addition, the higher results of row 4 compared to row 2 can be attributed to more reliable location of peak potentials prior to peak adjustment made possible by Fourier filtering. The smooth QUIRDS prediction set was classified about as well as the Fourier-smoothed noisy data. However, the Savitzky-Golay smoothed data showed essentially no improvement in classification with the noise-selected features. This is an indication that poor classification is due to factors other than noise alone (e.g., smoothing distortions).

Because the data show no clear advantage to using either the SEP or FFT features, a mixed feature set was created which included the best noise-optimized features of each type.

Table VI. Identification of Noise-Optimized Features

SEP feature No.	Definition[a]
2	$(E_2$ at 70% $i_p - E_p)/(E_p - E_1$ at 70% $i_p)$
35	Efunction at 70% i_p
37	Efunction at 80% i_p
43	$(E_{3/4} - E_p)/(E_{1/4} - E_p)$
FFT feature No.	1, 6, 7, 9, 10, 12, 13, 16, 20, 21, 22, 23

[a] See Reference 22 for complete description of all terms.

The purpose of this was to determine if combinations of SEP and FFT features would be more effective than each individually. (Note that these are not linear or algebraic combinations of features, but new groupings of the feature sets.) An optimum set of nine mixed features was found, but they provided no enhancement beyond the results of Table V.

Summarizing the results of Tables III through V, we see that kNN classification, using appropriately selected SEP or FFT features, is the method of choice for classification of synthetic singlet/doublet SEP data. Not only does this approach yield the best classification results for both smooth and noisy data, but it also requires fewer features than either LLM approach.

Noise Optimized Feature Lists. Table VI identifies those features which were found to be the most important for the classification of noisy QUIRDS data. Each of the four noise-optimized SEP features listed in Table VI is a function concerned with ratios of potential differences. This general class of feature has previously been shown to be most useful for classification of smooth SEP data (*4*, *5*). Their selection here demonstrates the additional ability to discriminate against distortions caused by noise.

There is no simple way to describe the physical significance of the optimized FFT features. Each feature is the magnitude of a sinusoid whose frequency is proportional to the feature number with units of volts^{-1} (this corresponds to Hz for the time domain transformation). Those feature numbers listed in Table VI represent fairly low frequency information as might be expected considering the shape of SEP data (Figure 1). These features were selected because of their particular ability to faithfully represent singlet/doublet shape information while discriminating against noise distortions.

Classification of Independent Data Sets. While the previous results demonstrate that it is possible to accurately classify singlet/doublet SEP data which fall within the QUIRDS data base, it is also important to know how classification is affected by the presence of patterns which fall outside the limits of the training set. To evaluate this, an additional prediction set was generated, based solely on reversible synthetic SEP data which contained patterns inside and outside the QUIRDS limits. Equation 3 was again used to synthesize the SEP data. In this case, the chi function corresponding to totally reversible behavior was used for all curves. Doublet concentration ratios were allowed to vary between 20:1 and 1:20, limits twice those of the training set. Curves synthesized near those limits could be expected to show more singlet character than doublets of the training set. Values for n were chosen randomly between 0.9 and 3.3 with no minimum increments. Peak separations for doublets varied between 6 and 12 mV.

A subset of reversible synthetic SEP curves was selected from the QUIRDS data set to act as a reference prediction set for comparison of classification results. Classification was performed by the kNN method using the best multidimensional feature sets (Table V) determined by the IFS feature selection process, and results are given in Table VII.

There are two major observations which can be made concerning the results found in Table VII. The first of these is concerned with the classification of singlets and doublets

Table VII. Classification of Test SEP Data Lying Outside the QUIRDS Training Set Limits[a]

Parameters		Classification accuracy, % FFT features[b]		SEP features[b]	
n	C_1/C_2	Ref[c]	Test	Ref	Test
Singlets					
WL[d]		99	100	100	79
OL[d]			41		75
Doublets					
WL	WL	80	78	87	78
OL	WL		77		80
WL	OL		45		78
OL	OL		65		74

[a] See Table I for limits. [b] Features used were the "noise optimized" set from Table V. [c] Reference data composed of a reversible subset of the QUIRDS data base not found in the training set. [d] WL = within limits, OL = outside limits.

exceeding any of the training set limits and a second which relates to classification of test set patterns falling within the training set limits.

Of the two feature sets used, the SEP features appear to have the advantage in classification of patterns outside the QUIRDS limits. The average accuracy obtained for all singlets and doublets outside the limits was 76% for the SEP features and only 61% for the FFT features. From these results it can be concluded that FFT features are more sensitive than SEP features to those shape factors which make patterns fall within certain regions of feature space (e.g., the concentration ratio for doublets and n for singlets). Apparently, singlet patterns are affected the greatest by these factors as the FFT features show a strong bias towards their classification as doublets. Reference to Figure 2 suggests why this may occur. Singlet patterns tend to be distributed curvilinearly in FFT feature space, with doublets scattered around them. Any singlets which are forced slightly away from the singlet region by various shape factors are likely to be misclassified. On the other hand, doublets, because of their wide distribution in feature space, should be less affected by these slight changes in position. This conclusion is consistent with the results obtained here and is supported further by the results obtained in noise studies (Table IV).

The second major fact observed in Table VII is the difference in the classification results for the test and reference sets for WL (within limit) singlet/doublet patterns using SEP features. One would expect the results to be similar for all WL data sets, as observed for FFT features. Inconsistent results like these for SEP features were obtained for several different subsets of the test data, indicating some unreliability associated with their use. FFT features, on the other hand, maintained consistently good results for WL patterns. While these results don't specifically indicate that one type of feature is more useful than the other for classification of SEP data, factors such as consistency and overall higher classification results for QUIRDS prediction sets tend to support the use of FFT features over SEP features for most classification problems.

Of even more importance is the fact that the FFT feature extraction approach is more generally applicable to analytical wave forms than the SEP approach. The SEP approach would require a complete redefinition of features to take advantage of particular theoretical relationships governing a given analytical response while the FFT method could be used directly.

Condensation of the Training Set. The condensed kNN algorithm described in the Theory section was applied to the QUIRDS training set. Figures 4 and 5 show the results of

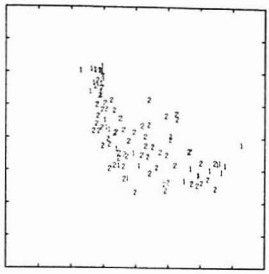

Figure 4. Nonlinear map, QUIRDS training set; noise-optimized FFT features. (1) = singlet; (2) = doublet

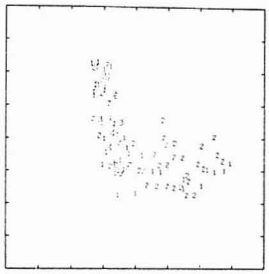

Figure 5. Nonlinear map, condensed QUIRDS training set; noise-optimized FFT features. (1) = singlet; (2) = doublet

Table VIII. kNN Classification of QUIRDS Prediction Sets by a Condensed Training Set[a]

Prediction set	Classification accuracy, %	
	Singlet	Doublet
Smooth QUIRDS	87.2	86.1
Noisy QUIRDS (NQUIRDS)	58.9	79.5
Savitzky-Golay-Smoothed NQUIRDS	52.6	70.5
Fourier-Filter-Smoothed NQUIRDS	83.3	87.7

[a] Feature set used is noise-optimized FFT set (see Table V).

condensation on the QUIRDS training set using the best noise-optimized FFT features (from Table V). Figure 4 is a NLM of 100 representative QUIRDS training patterns. Note the relative similarity between the two class distributions compared to those of Figure 5, a map containing 100 of the 334 patterns retained by the condensation procedure. The main effect of condensation has been to lower pattern density while retaining those patterns necessary for good classification.

Table VIII lists the results obtained by applying the condensed training set to classification of various prediction sets. Comparison of these results with those of Table V shows little change in the overall classification accuracies. However, by using one-third the number of training patterns these results were obtained approximately 3 to 4 times faster than with the complete training set.

CONCLUSIONS

There are several observations, based on the work with synthetic voltammetric data, which affect significantly the approach to be taken for applying pattern recognition to the classification of real voltammetric data. The first of these is that the classification of singlets and severely overlapped doublets appears, at least, to be feasible. Secondly, it appears that the kNN classification algorithm should be the most appropriate. Finally, FFT features seem to allow the most reliable and consistent classification of voltammetric doublets and singlets. The conclusions from these studies have been applied in the classification of real voltammetric data reported elsewhere (*11*).

ACKNOWLEDGMENT

The authors thank Lilly Lai for her help in computing theoretical SEP data and Phil Gaarenstroom for development of the nonlinear-mapping subroutine.

LITERATURE CITED

(1) R. W. Dwyer, Jr., *Anal. Chem.*, **45**, 1380 (1973).
(2) D. W. Kirmse and A. W. Westerberg, *Anal. Chem.*, **43**, 1035 (1971).
(3) K. Yamaoka and T. Nakagawa, *Anal. Chem.*, **47**, 2050 (1975).
(4) L. B. Sybrandt and S. P. Perone, *Anal. Chem.*, **44**, 2331 (1972).
(5) M. A. Pichler and S. P. Perone, *Anal. Chem.*, **46**, 1790 (1974).
(6) N. J. Nilsson, "Learning Machines", McGraw Hill, New York, N.Y., 1965.
(7) P. C. Jurs and T. L. Isenhour, "Chemical Applications of Pattern Recognition", Wiley-Interscience, New York, N.Y., 1975.
(8) K. S. Fu, "Sequential Methods in Pattern Recognition and Machine Learning", Academic Press, New York, N.Y., 1968.
(9) K. Fukanaga, "Introduction to Statistical Pattern Recognition", Academic Press, New York, N.Y., 1972.
(10) B. R. Kowalski and C. F. Bender, *Anal. Chem.*, **44**, 1405 (1972).
(11) Q. V. Thomas, R. A. DePalma, and S. P. Perone, *Anal. Chem.*, following paper in this issue.
(12) A. Savitzky and M. J. E. Golay, *Anal. Chem.*, **36**, 1627 (1964).
(13) D. E. Aspenes, *Anal. Chem.*, **47**, 1181 (1975).
(14) Gary Horlick, *Anal. Chem.*, **44**, 943 (1972).
(15) K. G. Beauchamp, "Signal Processing", George Allen and Unwin LTD, London, 1973.
(16) B. R. Kowalski and C. F. Bender, *Anal. Chem.*, **45**, 2234 (1973).
(17) B. R. Kowalski and C. F. Bender, *J. Am. Chem. Soc.*, **94**, 5632 (1972).
(18) R. S. Nicholson and I. Shain, *Anal. Chem.*, **36**, 706 (1964).
(19) R. S. Nicholson, *Anal. Chem.*, **37**, 1351 (1965).
(20) J. W. Cooley and J. W. Tukey, *Math. Comput.*, **19**, 297 (1965).
(21) G. D. Bergland, *IEEE Spectrum*, **6**, 41 (1969).
(22) Q. V. Thomas, Ph.D. Thesis, Purdue University, 1976.
(23) J. W. Hayes, D. E. Clover, and D. E. Smith, *Anal. Chem.*, **45**, 277 (1973).
(24) Q. V. Thomas, L. Kryger, and S. P. Perone, *Anal. Chem.*, **48**, 761 (1976).
(25) R. J. Rummel, "Applied Factor Analysis", Northwestern University Press, Evanston, Ill., 1970.
(26) G. S. Zander, A. J. Stuper, and P. C. Jurs, *Anal. Chem.*, **47**, 1085 (1975).
(27) B. R. Kowalski and C. F. Bender, *J. Am. Chem. Soc.*, **95**, 686 (1973).

RECEIVED for review November 29, 1976. Accepted May 23, 1977. This work has been supported by the Office of Naval Research and by the National Science Foundation Grant No. MPS74-12762

Application of Pattern Recognition Techniques to the Interpretation of Severely Overlapped Voltammetric Data: Studies with Experimental Data

Q. V. Thomas,[1] R. A. DePalma, and S. P. Perone*

Department of Chemistry, Purdue University, West Lafayette, Indiana 47907

Pattern recognition methods have been used to determine the multiplicity of real Stationary Electrode Polarographic (SEP) data. Evaluation of several pattern classification and feature selection procedures led to the identification of real SEP singlets with an accuracy of 78% and severly overlapped doublets ($\Delta E_p < 30$ mV) with accuracies between 73% and 83%. These results were obtained using the k-Nearest-Neighbor (kNN) decision rule and features based on the discrete Fast Fourier Transform (FFT). The identification of useful features was aided by previous studies with synthetically generated doublet/singlet SEP data, although classification of real data with the synthetic training set was shown to be limited by differences in feature space pattern distributions.

Quantitative analysis of multiple component solutions with voltammetric methods has been limited by the inability to resolve closely overlapped electrochemical peaks (*1*, *2*). Peaks separated by more than 150 mV have been sucessfully analyzed using computer optimized derivative techniques for concentration ratios up to 1000:1 (*1*). An on-line curve-fitting technique has been described which allows quantitative analysis of equimolar metal ions whose peak potentials are separated by only 35 to 40 mV (*2*). However, for peaks separated by less than 35 mV, it was not possible to distinguish between doublet and singlet peaks (*2*).

Previous work in this laboratory has demonstrated the application of pattern recognition techniques to the detection of severly overlapped (4–12 mV) Stationary Electrode Polarographic (SEP) data (*3*–*5*). In each of these studies, the training and prediction sets used for pattern classification and feature selection were derived from SEP theory (*6*) and were prepared to include a wide variety of both singlet and doublet curve shapes. Sybrandt (*3*) and Pichler (*4*) dealt with totally reversible SEP data sets and demonstrated that either the Linear Learning Machine (LLM) or the k-Nearest-Neighbor (kNN) algorithm could be used to achieve classification accuracies greater than 90%. Thomas (*5*) extended this work to include the irreversible and quasi-reversible cases as well, and obtained classification accuracies greater than 90% for the kNN approach, with significantly lower results for the LLM. Synthetically generated noisy SEP curves were also found to be classifiable with the kNN algorithm using features based either on the Fast Fourier Transform (FFT) or SEP theory, if the noisy curves were first smoothed by a Fourier filter function. These smoothed data were classified 87% correctly compared to an accuracy of 72% for unsmoothed noisy data. The overall results suggested that a FFT–kNN approach would be the most promising for classification of real experimental SEP data.

[1] Current address, Finnigan, 845 West Maude Avenue, Sunnyvale, Calif. 94086.

Table I. Experimental Conditions for Collection of SEP Data Base (PRED1)

Metal ion[a]	Electrolyte[b]	E_p, mV[c]
Cd^{2+}	SO_4^{2-}, NO_3^-	−540, −600
Ni^{2+}	SCN^-, NO_3^-	−950, −600
Co^{2+}	Cl^-	−1180
Pb^{2+}	NO_3^-	−410
Sb^{3+}	Tartrate	−385
Tl^+	Ammonium citrate, NO_3^-	−510, −505
Cu^{2+}	ammonium citrate	−155

[a] Metal concentrations ranged between 1×10^{-3} M and 1×10^{-4} M. [b] 0.1 M electrolyte concentration. [c] Potential vs SCE.

In this work, we have investigated the application of both the LLM and kNN classification methods to the identification of real singlet/doublet SEP data. These methods were evaluated using both the FFT and SEP features. In addition, we have compared feature-space distribution plots for real and synthetic SEP data. The results of these studies indicate that real SEP data may be classified with good accuracy when appropriate training and features sets are used.

EXPERIMENTAL

Stationary electrode polarograms of seven metal ions were obtained under a variety of experimental conditions (Table I). The metal ions selected for use in this study were chosen on the basis of their known polarographic behavior in order to obtain data for various degrees of reversibility as well as several values of n (the number of electrons transferred) and α (the electron transfer coefficient). All solutions were prepared using reagent grade chemicals and distilled, de-ionized water. Each was thoroughly deoxygenated prior to analysis by purging with purified, solvent-saturated nitrogen (*7*) for 20 min.

The SEP data were obtained using a general purpose electrochemical instrument with computerized data acquisition and control (*8*, *9*). The instrument contained an analog signal generator capable of supplying potential ramps of 0 to 5000 mV/s, a general purpose potentiostat, and a three-electrode electrochemical cell. The working electrode was a digitally controlled DME which could supply mercury drops with computer-selected lifetimes from 1 to 10 s. Using this system, voltammograms were ensemble averaged by performing potential scans at the end of precisely reproducible drop lifetimes. For this work, each SEP curve was the composite of eight ensembles performed on a 5-s mercury drop. The 250-point data curves were obtained for each of the metal–electrolyte combinations listed in Table I using scan rates of 750, 1000, 1500, 2000, and 3000 mV/s and data resolutions of 2, 3, 4, and 5 mV/point. Metal concentrations and scan rates were selected so as to minimize signal distortions which can result from uncompensated IR drop across the cell.

SEP curves which contained obvious instrumental distortions (e.g., discontinuities, ADC overflow, or excessively high noise) were rejected for use in this study. A total of 77 singlet curves were retained, representing each of the metal ion–electrolyte combinations listed in Table I.

The instrumentation computer used was a Hewlett-Packard 2115A with 8K words of core memory. Peripherals included a

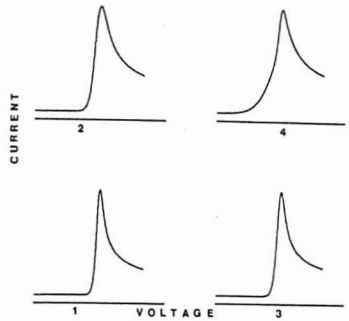

Figure 1. Typical singlet and doublet voltammograms from PRED1. (1) = singlet, (2) = singlet, (3) = doublet, (4) = doublet. The line at the bottom of each curve is a reference line, not baseline current

paper tape reader and punch, a Tektronix 601 storage display monitor and a Teletype. Data acquisition and hardware control subroutines were written in Hewlett-Packard assembly language and called by main programs written in BASIC. In order to provide a data link to the pattern recognition processing computer, the raw SEP data were punched on paper tape. Each raw data curve was corrected for background contributions by subtraction of a blank electrolyte curve obtained under an identical set of experimental conditions. These corrected curves were stored in individual disk files for easy retrieval and pattern recognition processing.

The pattern recognition processor was a Hewlett-Packard 2100S computer with 32K words of core memory. Peripherals included a 5-Mbyte moving head disk drive (HP-7900), paper tape reader and punch, a Tektronics 603 storage display monitor, a Centronics 306 serial printer, a Calcomp 565 digital plotter, and a Teletype. All preprocessing, feature extraction, and pattern recognition programs were written in FORTRAN IV and operated under the Hewlett-Packard DOS-M executive.

The Training Set. The QUIRDS training set used in this work is composed of 1000 singlet and doublet synthetic SEP curves. The QUIRDS data set contains reversible, irreversible, and quasi-reversible waveforms and has been described in detail in Ref. 5. This training set has been used to classify synthetic SEP data sets with accuracies exceeding 94%. While that work suggested that FFT features might be most useful for classification of real data, both SEP and FFT feature sets were used here in order to prevent arbitrary exclusion of information which could be critical for successful pattern classification. Feature extraction methodology was described previously (*5*). A complete list of feature definitions may be found in Ref. 8.

The Prediction Set. The 77 real singlet polarograms described above were included in the real prediction set. Because these curves were obtained at various voltage resolutions, each singlet was recalculated for a resolution of 2 mV by linear interpolation between points. This procedure was necessary to ensure that the Fourier transformation would obtain the same frequency scale for both the real data and the training set data which were synthesized with a resolution of 2 mV. Each singlet peak height was also normalized to a value of 1.0. Typical singlet voltammograms are shown in Figure 1 (curves 1 and 2).

Due to the difficulty of obtaining a large number of experimental doublets with known peak overlaps less than 10 mV, most prediction set doublets were prepared by the linear combination of two previously processed singlets. Peak separations and concentration ratios for these doublets were adjusted to fall within those limits established for the synthetic training set doublets (*5*). Each doublet peak current was also normalized to a value of 1.0. The 120 doublets prepared by this procedure were combined with the 77 singlets described earlier to form a real prediction set (PRED1). Each curve in this set was smoothed by the Fourier filter function described elsewhere (*5*). Each peak location was then determined and shifted in the data array so that all curves had the same peak location prior to feature extraction (*5*). Typical PRED1 doublet voltammograms are shown also in Figure 1 (curves 3 and 4).

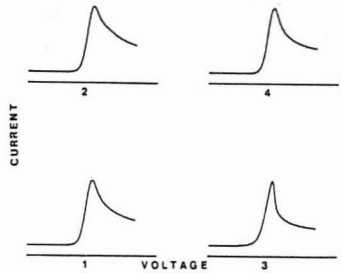

Figure 2. Typical doublet voltammograms from PRED2

Curve	Ratio C^*_{Pb}/C^*_{Tl}	pH
1	4:1	2.5
2	2:1	2.15
3	1:1	4.5
4	10:1	2.5

All curves are background corrected. The line at the bottom of each curve is a reference line, not baseline current

Table II. Initial Classification Results for Real SEP Data Set, PRED1[a]

Classification method	Classification accuracy, %			
	SEP features		FFT features	
	Singlet	Doublet	Singlet	Doublet
kNN[b]	7.8	90.8	32.5	73.7
LLM[c]	19.5	85.8	42.9	51.7
LLM[d]	37.4	98.3	55.8	45.0
LOO[b] (kNN)	48.1	71.7	51.9	83.3

[a] Training set was QUIRDS synthetic data (*5*). [b] Features used were "noise-optimized" with synthetic noisy QUIRDS prediction set (*5*). [c] Features used were variance-selected by QUIRDS training set (*5*). [d] Features used were sign-magnitude selected by QUIRDS training set (*5*).

An alternative prediction set of real doublets (PRED2) was prepared from polarograms obtained for a series of Pb/Tl citrate solutions. The peak potentials of Pb and Tl in 0.1 M citrate exhibit slightly different dependencies on pH and are severely overlapped within the pH range of 2.0 to 6.0. A total of 33 doublet curves was obtained at several pH values for solutions with Pb/Tl concentration ratios ranging between 10:1 and 1:5. Exact peak overlap values for these conditions are unavailable, but are estimated to be between 0 and 30 mV based on the pH behavior of the individual metals. Concentration ratios of Tl to Pb greater than 5:1 were excluded from this prediction set due to obvious doublet distortions (e.g., dual peaks and shoulders) which make them a trivial classification problem. Background corrections were made using 0.1 M potassium citrate blanks run at appropriate values of pH. Typical PRED2 doublet voltammograms are shown in Figure 2.

RESULTS AND DISCUSSION

The primary goal of this work was to apply pattern recognition methods to the classification of experimental doublet/singlet SEP data. To this end, it was desired to evaluate the use of synthetically generated data as a training set and to evaluate the effectiveness of those features identified as useful for classifying synthetic prediction sets (*5*). The difficulty of the classification problem addressed here is obvious from a visual examination of the singlet/doublet voltammograms in Figures 1 and 2.

Table II lists the results obtained by applying the kNN and LLM classification algorithms to the real data set (PRED1) using the best SEP and FFT feature sets selected with

Table III. kNN-IFS Selection of Optimum Features for Real SEP Data Set[a]

Training set	Feature type	No. retained	Classification accuracy % Singlet	Doublet
PRED1[b]	FFT	3[c]	77.9	83.3
PRED1[b]	SEP	4[d]	59.7	75.0
QUIRDS	FFT	19	48.0	75.0
QUIRDS	SEP	7	19.5	94.2
Reversible only QUIRDS	FFT	11	38.9	83.3

[a] The prediction set for all classifications was PRED1. [b] Leave-One-Out method used. [c] Features No. 4, 5, 9, Ref. 8. [d] Features No. 2, 20, 36, 44, Ref. 8.

synthetic data (5). As can be seen, none of the method/feature combinations provide statistically significant classification results. As a point of reference, a Leave-One-Out (LOO) (10) analysis of the real data set was performed. The LOO method is performed by removing one pattern at a time from the data set and then applying a kNN classification to that pattern using the remaining patterns as a training set. Once classified, the pattern is returned to the data set and the next one removed and classified, etc. In this case, where the LOO training set is actually the real data under study (PRED1), the results obtained represent the best possible classification accuracies obtainable for the real data with these particular features. However, as shown in Table II, even the LOO results are quite low for the feature set used.

Several possible explanations for the behavior observed in Table II may be considered: (1) The QUIRDS training set is not representative of the patterns found in the real data set and thus cannot be used as a training set for their classification. This might be due to any of several reasons, including instrumental artifacts and distortions, the presence of surface interactions or coupled chemical reactions, or other aberrations in the real data not accounted for in the synthetic training set. (2) The noisy synthetic prediction set used for feature selection in Ref. 5 is not representative of the real data set obtained here and thus a non-optimum set of features was applied to real data. (3) Neither the SEP nor the FFT features actually exploit intrinsic class differences of real data and a new set of features should be defined.

In order to determine which of these explanations was most correct, kNN-IFS (Iterative Feature Selection) was performed for several combinations of training and prediction sets. This procedure was shown in Ref. 5 to be the most effective approach to feature selection for this type of data.

Feature Selection Studies. Studies with synthetic data showed that features selected using a smooth prediction set could not be used to classify noisy data. Successful classification resulted only when a noisy prediction set was used during feature selection. Similarly, Table II shows that features selected by noisy synthetic data cannot be used to classify real SEP patterns; thus, feature selection should be performed again using a prediction set composed of real data.

The results of feature selection are shown in Table III. The results in row 3 and 4 indicate that the implications of explanation 2 above are not entirely correct. That is, there appears to be no optimal multidimensional SEP or FFT feature combination which can be used to classify this real data set with the QUIRDS training patterns. The results in rows 1 and 2 suggest that explanation 1 above is correct and that explanation 3 is not. That is, because both the SEP and FFT features give statistically significant classification results, the poor results found in Table II are most likely not the results of poorly defined features. On the contrary, the FFT features provide acceptable results while requiring 75% fewer features than for the synthetic data set, a clear indication that FFT features do discriminate between real singlet/doublet SEP data.

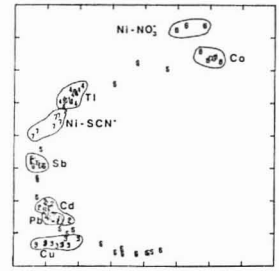

Figure 3. Nonlinear map, singlets only, QUIRDS training set and PRED1 prediction set; real-optimized FFT features. S = QUIRDS training set. 1–8 = PRED1 prediction set. 1 = Pb(II), 2 = Cd(II), 3 = Cu(II), 4 = Tl(I), 5 = Sb(III), 6 = Ni(II)–NO_3^-, 7 = Ni(II)–SCN^-, and 8 = Co(II)

If explanation 1 is correct, then the QUIRDS data set is not representative of real polarograms, and it would be very worthwhile to consider the possible reasons. Table I shows that the real data set is primarily composed of reversible reductions (e.g., Cd, Pb, Tl, Sb). The QUIRDS training set, having been designed to include patterns of all degrees of reversibility, could have a built-in bias as the result of a possible localized low density of reversible singlets surrounded by a higher density of doublets in feature space. If this were the case, real reversible singlets might have a good chance to be misclassified as doublets. To check this explanation, a set of totally reversible singlets and doublets was selected from the QUIRDS data base to act as a training set for feature selection on real data. Row 5 of Table III lists the results obtained for IFS selection of FFT features. Comparison of these results with rows 3 and 4 suggests that a low density of reversible training set patterns is not the primary limitation in applying the QUIRDS training set to classification of real data.

Thus, all evidence points to a significant difference between the feature space distributions of the QUIRDS data base and the PRED1 patterns. To help clarify this point, nonlinear mappings (11) were obtained for representative singlets selected from both the QUIRDS and PRED1 data sets, using the set of 3 FFT features which provided the best classification results for real doublet/singlet SEP data (Table III). Examination of this mapping in Figure 3 reveals several things. First of all, in most cases the real singlets fall on essentially the same distribution line as the synthetic singlets. The exceptions are Ni(II) in 0.1 M KNO_3, Co(II) in 0.1 M KCl, and Cu(II) in 0.1 M ammonium citrate. The Co singlets appear to lie on the extension of the distribution line. The absence of synthetic singlets in this region may be due to the restricted range of α-values (0.3 to 0.7) allowed in the generation of the QUIRDS data set. Other studies have indicated that α-values for Co(II) in 0.1 M KCl might be lower than 0.3 (12), thus putting these singlets outside the range of the QUIRDS distribution.

Ni(II)–NO_3^- singlets appear to lie outside of the projected singlet distribution. This may be because of distortions related to metallic Ni formation on the mercury surface.

The copper cluster in Figure 3 is spread out and extends outward from the singlet distribution line. A recent publication by Anderson and Shain (13), indicating that the Cu(II) reduction wave involves a chemical reaction coupled between each electron transfer step (ECE mechanism), provides the explanation for our observed behavior. Detailed examination

Table IV. kNN Classification of Pb-Tl Doublets (PRED2)

Training set	Features	Classification accuracy, %
QUIRDS	1, 6, 7, 9, 10, 12, 13, 16, 20, 21, 22, 23[a]	78.8
PRED1	4, 5, 9[b]	72.7
PRED1	1, 6, 7, 9, 10, 12, 13, 16, 20, 21, 22, 23[a]	39.4

[a] These are the "noise-optimized" FFT features (5). [b] These are the "real-optimized" FFT features from Row 1, Table III.

of the spread in the Cu cluster shows that the deviation from the pure singlet distribution increases with increased scan rate. This would be expected for an ECE electrode process, and is consistent with the observations of Anderson and Shain (13).

Another observation on Figure 3 is that singlet waves for each of the several elements cluster in separate areas. With the exception of Cu, the tightness of these clusters is remarkable, considering the wide range of experimental conditions applied in their collection. This provides a vote of confidence for the instrumental methodology employed.

Finally, when each of the individual clusters of real singlets is mapped separately, a slight trend is observed with respect to scan rate. This may be due to experimental distortions at higher sweep rates. Alternatively, it may be due to the fact that the noise contribution to data collected at higher sweep rates appears as "low frequency" information to the FFT procedure; thus, more of this information is retained after truncation than for the data obtained at lower sweep rates. In either case, this is a subtle aberration in the data which may account for some of the diminishment in classification accuracy obtained with real data.

On the basis of the above observations it can be seen why the QUIRDS data set was not appropriate for classification of the PRED1 data set. One of the electrode systems (Co) provided singlets outside the range of the QUIRDS distribution; one system (Cu) had an unsuspected complication which caused a sweep rate dependence not accounted for in the QUIRDS set; and one system (Ni–NO_3^-) provides singlets which are apparently outside the projected distribution. Moreover, Figure 3 shows that even for those real singlets which fall on the same distribution line as synthetic singlets, locally dense regions of real singlets may not coincide with a heavy population of synthetic singlets. This is probably the primary reason for misclassification of real singlets by the QUIRDS training set, and future studies of pattern classification of voltammetric data with synthetic training sets must address this problem.

It is worthwhile noting, however, that Figure 3 also illustrates why the real data are classifiable when the LOO procedure is used with PRED1 as its own training set (Table III, column 1). Because the real singlets are reasonably tightly clustered in this feature space, the kNN algorithm classifies singlets and doublets with about 80% accuracy. Moreover, if the slight dispersion in these clusters due to scan rate variation were avoided by using uniform scan rates in data collection, it is likely that classification accuracy could be significantly improved.

Classification of Real Doublets. As a final test of the kNN-FFT approach for classification of real doublet/singlet SEP data the small set of real Pb–Tl doublets (PRED2) was classified. Table IV lists the classification results obtained using the kNN decision rule and several optimized FFT feature sets. While the QUIRDS training set results appear to be good, it should be remembered that this set of noise-optimized features was biased toward classification of all

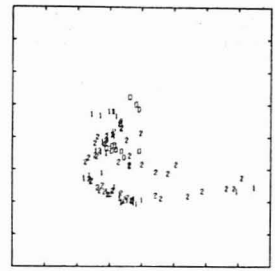

Figure 4. Nonlinear map. PRED1 and PRED2 prediction sets; real-optimized FFT features. (1) = singlet, (2) = mixed doublet, (D) = real doublet (Pb/Tl)

patterns as doublets (Table II, row 1), and therefore these results may not be significant.

The optimum feature set for real data ("real-optimized" features), obtained from row 1, Table III, provides significant classification accuracy for the real doublets, although not as high as for the doublets in PRED1. Figure 4 shows the feature space distributions for PRED1 (1 = singlets, 2 = doublets) and PRED2 (D = doublets) together in the same nonlinear map. Most PRED2 doublets appear to fall within the PRED1 doublet distribution. However, a small group tends to be located closer to a group of PRED1 singlets and thus are classified incorrectly. This may be related to the fact that it is impossible to select exact peak overlaps for real doublets, and therefore some of them may lie outside the limits of the doublets contained in the real training set (PRED1).

CONCLUSIONS

The primary goal of classification of real SEP data has been met. It was achieved by means of a Leave-One-Out analysis using a feature set optimized for the classification of real data. All doublets used in this study were known to have peak separations of less than 30 mV and have been identified at accuracy levels previously unattainable. The results obtained here for real SEP data are encouraging and suggest that other types of doublet/singlet identification problems may be successfully solved using a pattern recognition approach (e.g., GC, NMR, ESCA, etc.).

The application of synthetic training sets to the classification of real data appears to be limited by differences in the feature space distributions of real and synthetic SEP data. Some possible causes for these distribution differences have been examined here and suggest ways to improve the utility of synthetic data for future studies.

The kNN decision rule has been shown to be the most effective approach to this particular classification problem. Associated feature selection methods have demonstrated an ability to significantly reduce the dimensionality of feature space while at the same time increasing pattern classification accuracy. Furthermore, the resulting reduction of feature dimensionality reduces the time required for pattern classification, an important consideration for on-line processing.

Finally, features derived from the discrete Fast Fourier Transform have been shown to be useful for the enhancement of intrinsic class differences in real SEP data. These features are easily extracted from analytical response curves by the use of the axis translation–rotation procedure (5). Because of this, these features are an attractive method for the representation of analytical waveforms for pattern recognition, when intrinsic waveshape information is sought.

LITERATURE CITED

(1) S. P. Perone, D. O. Jones, and W. F. Gutknecht, *Anal. Chem.*, 41, 1154 (1969).

(2) W. F. Gutknecht and S. P. Perone, *Anal. Chem.*, **42**, 906 (1970).
(3) L. B. Sybrandt and S. P. Perone, *Anal. Chem.*, **44**, 2331 (1972).
(4) M. A. Pichler and S. P. Perone, *Anal. Chem.*, **46**, 1790 (1974).
(5) Q. V. Thomas and S. P. Perone, *Anal. Chem.*, preceding paper in this issue.
(6) R. S. Nicholson and I. Shain, *Anal. Chem.*, **36**, 706 (1964).
(7) L. Meites, *Anal. Chim. Acta*, **18**, 364 (1958).
(8) Q. V. Thomas, Ph.D. Thesis, Purdue University, 1976.
(9) Q. V. Thomas, L. Kryger, and S. P. Perone, *Anal. Chem.*, **48**, 761 (1976).
(10) K. Fukanaga, "Introduction to Statistical Pattern Recognition", Academic Press, New York, N.Y., 1972.
(11) J. W. Sammon, Jr., *IEEE Trans. Comput.*, **C-18**, 401 (1969).
(12) S. P. Perone and C. V. Evins, *Anal. Chem.*, **37**, 1643 (1965).
(13) J. L. Anderson and I. Shain, *Anal. Chem.*, **48**, 1274 (1976).

RECEIVED for review November 29, 1976. Accepted May 23, 1977. This work has been supported by the Office of Naval Research and by the National Science Foundation Grant No. MPS74-12762.

Determination of Sulfide and Thiols in the Presence of Vitamin B_{12a} by Pulse Polarography

Manoutchehr Youssefi and Ronald L. Birke*

City University of New York, Department of Chemistry, The City College, New York, New York 10031

The differential pulse polarographic (DPP) method is applied to the analysis of sulfide ion, cysteine, and glutathione by utilizing a cathodic pulse which strips the dropping mercury electrode of an adsorbed film of mercury compound. In the presence of vitamin B_{12a} DPP peaks for both the sulfur-containing compound and vitamin B_{12a} can be seen in the same scan. A comparison is made of normal pulse polarography and differential pulse polarography and the latter method is found to be more convenient for sulfide and thiol analysis. The differential pulse peaks of glutathione and cysteine each split into two peaks as the concentration is increased beyond a certain point with the new peak being shifted in a positive potential direction. Calculation supports the contention that the peaks are due to monolayer and multilayer dissolution. Application of the DPP method is made in the study of the reaction of vitamin B_{12a} with cysteine and an amperometric titration shows a 1:1 stoichiometry for the reactants. The nature of the reaction products is also discussed.

The analysis of sulfides and thiols in the presence of biologically active compounds is important since many enzyme systems require sulfur-containing compounds for catalytic activity. One such system is methionine–synthetase which requires a vitamin B_{12} compound and a thiol, e.g., dithiothreitol, for activation (*1*). In the course of studying the reaction of vitamin B_{12a} with sulfide or thiols, we investigated the normal (integral) and differential pulse polarographic method as a means of determining both the sulfur-containing compound and vitamin B_{12a}.

The polarographic method which has been widely applied for the investigation of sulfides and thiols is predominately based on the anodic wave which originates from the oxidation of mercury resulting in the formation of insoluble mercury compounds. The dc and ac polarographic behavior (*2*) of cysteine and glutathiene, for example, shows multiple waves and peaks due to films formed by these mercury compounds. The film formation on the electrode leads to a nonlinear relationship between current and concentration. Recently the rapid direct current method (*3*) and the normal pulse polarographic method (*4*) have been used to cope with these problems.

We have found, however, that although differential pulse polarography (DPP) is subject to many of the problems inherent with film formation, the convenience and resolution it offers make it preferable especially when several species are present in the solution. In the specific case of a mixture of vitamin B_{12a} and a sulfide or thiol, the normal pulse method sometimes proved difficult to use because the plateau and/or baseline of the normal pulse wave was quite sloped and because the vitamin B_{12a} reduction wave was not completely separated from the thiol oxidation wave. For the differential pulse polarographic determination of sulfide and thiols, we investigated a method which is not based on determining the anodic current but rather on the cathodic current which results in the reduction of the film of mercury salt built up over the drop life. Earlier DPP studies of such a process (*2*) showed that the method was quite sensitive with a detection limit around 10^{-6} M; however, the behavior of these peaks as a function of concentration was not investigated. The DPP peaks for the reduction process would be expected to be sharply resolved. Thus the possibility of using these highly resolved and sensitive peaks for the analytical determination of sulfide or thiol in a mixture containing vitamin B_{12} compounds was the motivation for their further investigation. Such a technique allows a determination of both the thiol and vitamin V_{12a} in one scan at physiological pH. We have applied this analysis to study the reaction between thiols and vitamin B_{12a}.

EXPERIMENTAL

The glutathione and L(+)-cysteine hydrochloride were Fisher Scientific Co. reagent grade. The L-cystine was Sigma Chemical Co., sigma grade. Stock solutions of glutathione and cysteine were freshly made up by dissolving the weighed reagent in a nitrogen deaerated buffer solution. The buffer was 0.2 M in Na_2HPO_4 and in KH_2PO_4 leading to a pH = 6.80. This value was the pH of the phosphate buffer unless mentioned otherwise. Some solutions were adjusted with NaOH to pH 7.2 which is closer to physiological pH. The stock solutions of Na_2S (Fisher Reagent grade) were made up with nitrogen-deaerated distilled water in 10^{-3} M NaOH and stored in polyethylene bottles over nitrogen. These solutions were standardized by reaction with excess primary reagent grade KIO_3 and KI in acid. The liberated iodine was titrated with sodium thiosulfate to the disappearance of the starch indicator which was added near the end point. The thiosulfate was also standardized by the KIO_3/I^- and starch indicator method.

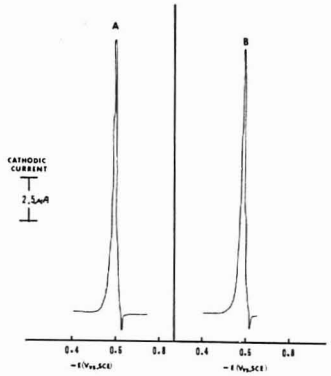

Figure 1. DPP current-potential curves for 4.4×10^{-4} M Na_2S in 0.2 M phosphate buffer (pH 7.2). Polarographic conditions are $\Delta E = 50$ mV, $\tau = 1.00$ s, $A = 0.00123$ cm^2, scan rate = 4.00 mV/s. (A) scan taken immediately, (B) scan taken 15 min later

Calculation of Na_2S concentration was based on the loss of I_2 caused by its reaction with H_2S. Precision was 0.5%. Aliquots of the Na_2S stock solution were dissolved in the buffer solution in an air-tight polarographic cell which was blanketed with Ar.

The vitamin B_{12a} was purchased from Sigma Chemical Co. as hydroxycobalamin hydrochloride and stock solutions were made up determinately. The percentage purity of the B_{12a} was calculated spectrophotometrically by conversion to dicyanocobalamin and by using the well-known extinction coefficient of the γ peak (*5*). All other reagents used were reagent grade.

The polarographic measurements were made with a Tacussel Type PRG-5 pulse polarograph and an MFE 815 plotamatic x-y recorder. A Keithley model 160B digital multimeter was used to monitor the initial potential. Either prepurified Ar or N_2 was used and flowed through a gas train consisting of acidic chromous chloride solution over amalgamated zinc (*6*) followed by a NaOH solution. The polarographic cell was a Metrohm EA 874-876 cell, and the dropping mercury, platinum counter, and saturated calomel electrodes were placed into the cell by thermometer adapters which make a glass to plastic seal in the cell top. The glass joints of the adapters were wrapped with Teflon tap. A special fitting with a rubber septum which allowed additions to be made with a syringe was placed in one of the inlets in the cell top. This fitting served as a gas outlet when a bare syringe needle was inserted. The observation of a constant sulfide peak over a 15-min period was used to confirm air-tightness. Ar flow was maintained over the cell solution for all sulfide measurements. The thiols were not volatile in the buffer medium and air-tight precautions were not necessary.

For controlled potential coulometry which was used to produce vitamin B_{12r} the platinum counter electrode was placed inside a tube which contacted the electrolysis solution by a porous Vycor plug. A heavy platinum gauze working electrode was used with a Wenking 68 FR 0.5 potentiostat to control the potential. Integration of the current-time curve was accomplished using a Linear-Instruments recorder with a built in integrator.

Our aim in this work was not ultimate sensitivity but accurate analysis in a concentration range of ca. 5×10^{-5} M to 8×10^{-4} M which is the range of interest for the reaction of vitamin B_{12} compounds with thiols. Thus pulse polarographic parameters were chosen for convenience and not for high sensitivity; this was especially true for the drop time which was short. In all experiments, unless otherwise mentioned, the pulse height, ΔE, was 50 mV; the drop time, τ, was 1 s; the time of the pulse duration before the current sampling was 40 ms; the sampling time over which the current is averaged was 8 ms; and the scan rate was 4 mV/s. The height of the mercury column was kept at 84 cm, and the mass flow rate m was 1.74 mg/s giving an area of 1.23 $\times 10^{-2}$ cm^2. All potentials quoted are with reference to the saturated calomel electrode.

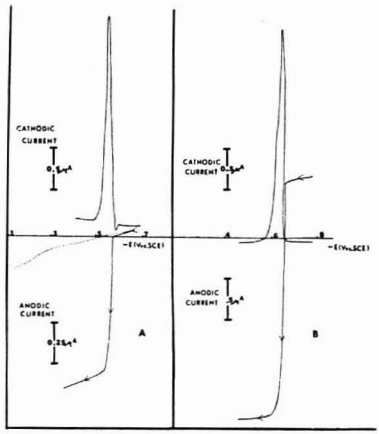

Figure 2. DPP and NPP current-potential curves. Polarographic conditions given in Figure 1. Arrows indicate scan direction. (A) 3×10^{-4} M Na_2S in phosphate buffer (pH 7.2). Dashed line is the background current of buffer. (B) 1×10^{-4} M Na_2S in borate buffer (pH 9.0)

The UV-vis spectral characteristics were obtained with a Cary model 15 recording spectrophotometer.

RESULTS AND DISCUSSION

Normal and Differential Pulse Characteristics for Na_2S Solutions. Figure 1 shows the cathodic differential pulse peak which results from applying a waveform which has pulses of constant amplitude superimposed on a negative going ramp when using a solution of Na_2S in 0.2 M phosphate buffer(pH 7.2). Thus the potential, when the pulse is applied, is greater in absolute magnitude than the value of the potential before the pulse and such a waveform can be symbolized as (⤡). We found that the same curve was traced out no matter whether the potential scan was started at a potential positive to the peak potential and scanned in the negative direction or started at a potential negative to the peak potential and scanned in the positive direction.

The electrode reaction giving rise to the current is

$$HgS + H^+ + 2e \rightarrow Hg + HS^-$$

since the reduction process taking place can only be the dissolution of the HgS layer which is built up on the drop. Also, since the same curve was traced by scanning in either direction, the amount of surface film formed during the drop life before the pulse is applied is constant and does not depend on the scan direction.

Curve B in Figure 1 shows that there is no significant loss of peak height after a 15-min wait which indicated that H_2S does not escape from the polarographic cell. If the gas stream is flowed through the solution, all of the sulfide can be swept out of the cell.

In additon to a cathodic current peak, it is also possible to use DP polarography to obtain an anodic current peak by sweeping the potential in either direction. If the waveform applied to the cell is a negative going ramp with superimposed constant potential pulses such that the potential before the pulse is greater in absolute magnitude than after (⤢), then an anodic current peak develops. The peak for this mode was found to vary with concentration but was not investigated further since we were interested mainly in the waveform (⤡) in order to study a system which had several cathodic processes, i.e., those of vitamin B_{12a}.

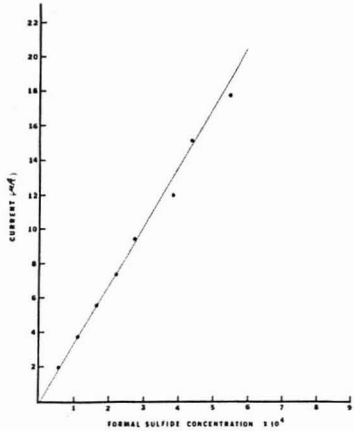

Figure 3. Calibration curve. Current in μA vs. formal concentration of Na_2S in 0.2 M phosphate buffer (pH 7.2). E_p = −0.58 V vs. SCE

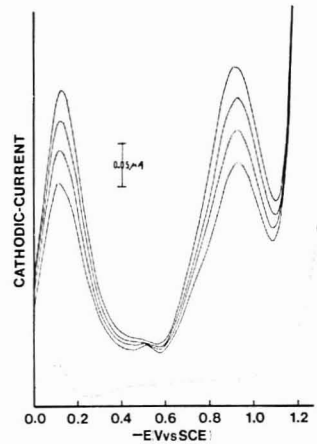

Figure 4. DPP current–potential curve for increasing concentrations of Vitamin B_{12a} in 0.2 M phosphate buffer (pH 6.80). Dashed line is background current. Polarographic conditions are given in Figure 1 except that ΔE = 100 mV

Comparison of the DPP current–potential curve (wave) with the normal pulse polarographic (NPP) wave is shown in Figure 2. The comparison in part A of the figure, which is for a phosphate buffer, shows that the normal pulse wave is somewhat affected by the sloping baseline because of the phosphate supporting electrolyte whereas the DP wave is less affected by the background current. In part B of Figure 2, which is for a sodium borate buffer (pH 9.0), the normal and the pulse waves are both ideally behaved. In both media, the cathodic DP peak is highly resolved with a peak potential of −0.58V (pH 7.20) and −0.66V (pH 9.0).

Figure 3 is a calibration plot of the DP cathodic peak current showing fair linearity up to ca. 2.8×10^{-4} M with some scattering at higher concentrations. On the basis of these results, it was concluded that the cathodic pulse polarographic wave could be used for the determination of the formal concentration of sulfide ion at pH 7.2.

Differential Pulse Characteristics of Vitamin B_{12a}. The central cobalt atom of vitamin B_{12a} can exist in three oxidation states: III, II, and I. The Co(II) species is called vitamin B_{12r} and differs at pH 7 from B_{12a}, the Co(III) species, by the loss of a coordinated H_2O molecule making it a 5-coordinate species. The Co(I) species is called vitamin B_{12s} and is 4-coordinate since the nucleotide side chain of the cobalamin corrin ring which is bound to cobalt in B_{12r} through a benzimidazole in an axial position decoordinates in B_{12a} (7). Two peaks of nearly equal heights are found in the differential pulse polarogram of B_{12a} in 0.2 M phosphate buffer (Figure 4) with a small third peak at ca −0.5V which is probably an impurity. The current rise at −1.1 V is not due to supporting-electrolyte reduction but is most likely due to a catalytic hydrogen wave (8). The first peak at −0.12 V represents the vitamin B_{12a} to B_{12r} reduction and the second peak at −0.92 V represents the B_{12r} to B_{12a} reduction. The two peaks are somewhat irreversible since they are shifted by ca. 0.1 V negative to the $E_{1/2}$ potentials of −0.01 V and −0.85 V (9–11) found by dc polarography and linear sweep voltammetry.

A plot of peak current vs. concentration is linear over the concentration range of interest 8×10^{-5} M to 1×10^{-3} M (Figure 5) and the calibration curve for the first peak is slightly skewed and separated from the second (by 0.12 μA). The difference in slopes may arise from a difference in reversibility which affects the shape of the peaks (see Figure 4). As can be seen, the calibration line does not extrapolate to zero

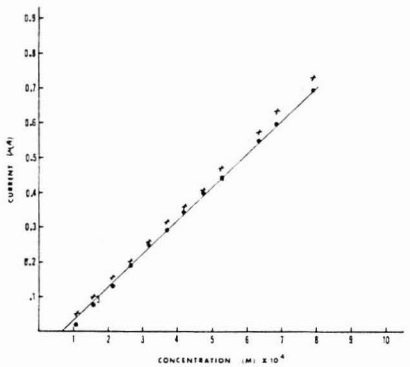

Figure 5. Calibration curves. Current in μA vs. concentration of vitamin B_{12a}. (-----) E_p = −0.12 V vs. SCE, (——) E_p = −0.92 V vs. SCE. Conditions are those for Figure 4

current for zero concentration but shows a negative intercept. This behavior is most likely due to two causes, one being adsorption and the other the background current. The background current in the 0.2 M phosphate buffer has a differential pulse peak at −0.09 V which is probably caused by mercuric phosphate reduction and which in any event obscures the vitamin B_{12a} peak at low concentrations. The background current was subtracted in two ways, first by using the actual phosphate buffer curve and second by drawing a baseline under the peaks; however, in neither case did the calibration curve go through zero. With another electrolyte buffer medium, a more ideal behavior might be found, but we have not investigated this effect further since we were specifically interested in the phosphate buffer medium.

Controlled potential reduction of vitamin B_{12a} at −0.4 V vs. SCE on a Pt gauze electrode gives vitamin B_{12r}. The fact that the product of the controlled potential reduction is B_{12r} was shown by controlled potential coulometry and UV–vis spectrophotometry. Integration of the current time curve for

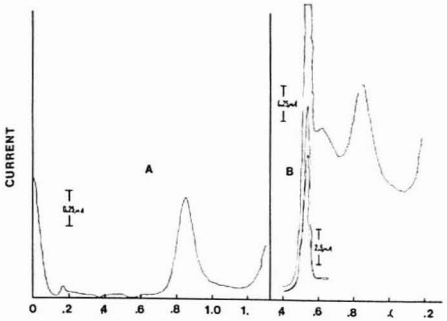

Figure 6. DPP current–potential curves. (A) 2.37 × 10^{-4} M vitamin B_{12r} in 0.2 M phosphate buffer (pH 6.80). (b) Reaction mixture of Na_2S and vitamin B_{12a} with excess sulfide. The curves at ca. E_p = −0.54 V vs. SCE were measured after various reaction times. All polarographic conditions are those in Figure 1

two separate reductions on Pt gave n values of 1.06 and 0.93. In addition the UV–vis spectrum of the product was identical to authentic B_{12r}. The spectrum was obtained by withdrawing the solution from the electrolysis cell with a degassed air-tight syringe and transferring the solution to a degassed spectrophotometry cell which had a rubber septum as a top.

The differential pulse polarogram of B_{12r}, shown in Figure 6, part A, has a small peak at −0.17 V which may be a trace of B_{12a} and a well defined symmetrical peak at −0.85 V. The latter is the B_{12r} to B_{12a} peak shifted from −0.92 V in the B_{12a} DP polarogram to the reversible peak potential. The peak at zero volts must be due to some interfacial phenomenon associated with the electrolyte or possibly a chloride impurity and not a B_{12} compound.

When Na_2S is added to B_{12a} it is seen from the DP polarogram that a reaction takes place. A DP polarogram of a reaction mixture with a slight excess of sulfide is shown in Figure 6B, where a sharp HgS reduction peak and the second peak of B_{12a} are seen. The HgS reduction peak decays with time, which it does not do in the absence of B_{12a}, suggesting a chemical reaction between HS^- and B_{12a}.

The second B_{12a} reduction peak was found to shift towards positive potentials and it becomes more symmetrical during the course of the reaction. After an excess of Na_2S is added, this peak has moved to −0.85 V, another peak at −0.62 V has appeared (see Figure 6B) and the B_{12a} peak in the −0.1-V region has disappeared. These phenomena suggest that B_{12a} is converted to B_{12r} and another species which may be a complex of HS^- and B_{12r}. If the sulfur donor replaced the nitrogen donor of the benzimidazole in forming a complex, it might cause a positive shift in the reduction potential which is consistent with the finding of a peak at −0.62 V.

A UV–vis spectrophotometric investigation of the reaction shows that when a Na_2S solution is added under anaerobic conditions to a phosphate buffer solution containing B_{12a} in a sealed spectrophotometry cell, the very intense peak of vitamin B_{12a} at 350 nm decays and a peak characteristic of B_{12r} develops at 312 nm. The spectrum of the reaction mixture after excess Na_2S is added has similar, but not identical, features to the spectrum of pure B_{12r}. Thus the B_{12r} peaks at 312 nm and 475 nm can be observed but a shoulder in the 370–390 nm region and a hump in the 500–560 nm region appear which are not present in the spectrum of pure B_{12r}. These results are consistent with the polarographic results and suggest a reaction product which is a mixture of B_{12r} and another species. However, other spectroscopic methods would

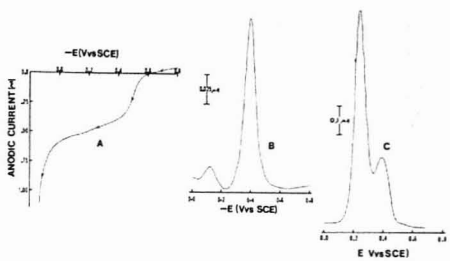

Figure 7. NPP and DPP current–potential curves for glutathione solutions. Polarographic conditions given in Figure 1. Arrows indicate direction of scan. (A) NPP wave of 6.6 × 10^{-5} M glutathione in 0.2 M phosphate buffer (pH 6.80). (B) DPP wave of 4.1 × 10^{-5} M glutathione in 0.2 M phosphate buffer (pH 6.80). (C) 3.3 × 10^{-4} M glutathione in 0.2 M phosphate buffer (pH 6.80)

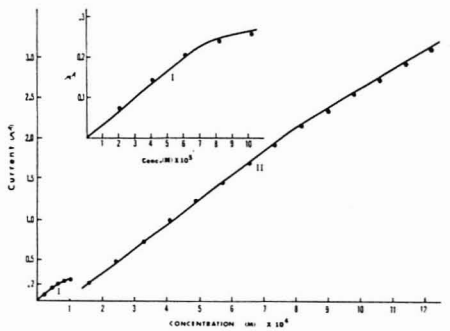

Figure 8. Calibration curves. Current in μA vs. concentration of glutathione in 0.2 M phosphate buffer (pH 6.80). (I) E_p = −0.39 V vs. SCE. (II) E_p = −0.25 V vs. SCE. Other polarographic conditions given in Figure 1

be necessary to elucidate the nature of this species.

Normal and Differential Pulse Characteristics for Glutathione and Cysteine. The characteristics of the DP polarography of the thiols are more complex than those of sodium sulfide. A comparison of the normal pulse wave (A) and the differential pulse peak (B) of glutathione is shown in Figure 7. The normal pulse wave is about two times more sensitive; however, the slanting nature of the prewave baseline and of the plateau compared to the symmetrical peaks of the DP wave makes the latter more appealing, especially when resolution and not sensitivity is a major concern. A study of the DP peak as a function of concentration shows that the peak at −0.39 V vs. SCE splits into two peaks above about 1 × 10^{-4} M with a new peak developing at −0.25 V vs. SCE (Figure 7C). Two calibration plots were made–one for concentrations below 1 × 10^{-4} M and the other for concentrations in the range of 2 × 10^{-4} to 10^{-3} M. Both plots show curvature as they approach their extremities (Figure 8); however, they are reproducible and could be used for analysis.

With cysteine, we investigated only the DPP characteristics. Again as the concentration is increased, a concentration is reached where the single peak splits into two peaks. Here the peak potential for the low concentrations comes at −0.38 V and splits at 4 × 10^{-4} M into two peaks, the new one coming at −0.33 V and the other remaining at −0.38 V vs SCE. Figure 9 shows the calibration curve over the range 2 × 10^{-5} to 4 × 10^{-4} M for the −0.38-V peak. This plot was repeated on at least three occasions and found to be very reproducible. It

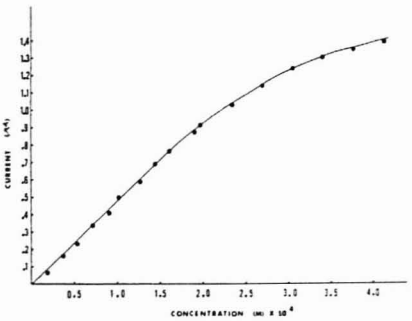

Figure 9. Calibration curve. Current in μA vs. concentration of cysteine in 0.2 M phosphate buffer (pH 6.80). E_p = −0.38 V vs. SCE. Other polarographic conditions given in Figure 1 except ΔE = 100 mV

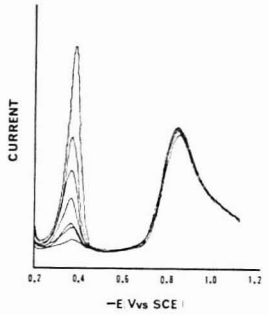

Figure 10. Current–potential curves recorded after the end point in an amperometric titration of vitamin B_{12a} with cysteine in phosphate buffer (pH 6.80)

is seen from Figure 9 that the plot is curved; however, because of its reproducibility we consider that it is quite useable for analysis.

The question arises as to the nature of the process that gives rise to the current–potential curve characteristics for thiols. The dc polarography of the anodic wave of glutathione (*12*) and cysteine (*13*) has been investigated by Kolthoff and co-workers. They found diffusion controlled phenomena described by the electrode reaction

$$HgSR + e + H^+ \rightleftarrows RSH + Hg$$

where for anodization the product of the electrode reaction is a Hg(I) thiol compound. The thiol is protonated if the pH is less than 9 since both glutathione and cysteine have pK values greater than 9 for the sulfhydryl hydrogen. Evidence for the adsorption of the mercury thiol compounds was found from drop-time vs. potential data (*12*).

The fact that the cathodic DPP peaks of glutathione and cysteine split into two at given concentrations (the new peak being shifted in the positive potential direction) can be explained by postulating that above a certain concentration, a multilayer is formed on the electrode. The mercurous thiolate in contact with the mercury electrode would be more difficult to reduce than the compound in the bulk of the multilayer if the forces of attraction at the mercury surface are greater than those in the bulk of the solid. Thus two waves appear, once the multilayer is formed.

The presence of a compact film formed on anodization of a convection-type mercury electrode in a cysteine solution was shown by Kolthoff, Stricks, and Tanaka (*14*). These investigators found a cathodic dissolution wave for the film on scanning from positive to negative potential. The dissolution pattern disappeared at 80 °C indicating the desorption of the mercurous cysteinate film. Calculation showed that a monomolecular layer of mercurous cysteinate formed on the convection mercury electrode which was independent of cysteine concentration in the 2×10^{-4} to 1×10^{-2} M range. A prewave at the dropping mercury electrode was attributed to a Brdicka adsorption prewave and a value of the maximum surface concentration, Γ_m, calculated as 7.4×10^{-10} mol/cm^2 from Brdicka's equation (*15*). Using this value of Γ_m and a diffusion coefficient of 8.2×10^{-6} cm^2 s^{-1} for cysteine (*14*), we can calculate the concentration necessary for a monolayer to form from the relationship $\Gamma_m = 7.36 \times 10^{-4} C_m D^{1/2} \tau^{1/2}$. For τ = 1 s, which was our experimental condition, C_m is found to be 3.5×10^{-4} M which corresponds to the value of 4×10^{-4} M found experimentally for the concentration at which the DPP peak starts to split for cysteine. Thus the explanation of multilayer formation for the cause of peak splitting is

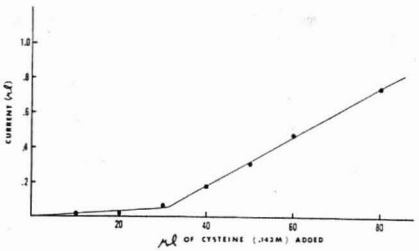

Figure 11. Amperometric titration curve of vitamin B_{12a} and cysteine in phosphate buffer (pH 6.80). E_p = −0.38 V vs. SCE

consistent with this calculation. Another recent explanation (*18*) of this surface phenomenon is that there is a "tight" packing or a compact surface film formed at a concentration of cysteine above 4×10^{-4} M. The fact that the cathodic DP current at −0.33 V continues to increase as the concentration is increased above 1×10^{-3} M indicates that a multilayer may be formed.

Pulse Polarographic Study of the Reaction of Vitamin B_{12a} with Cysteine. As an application of cathodic DP polarographic analysis for thiols, we studied the reaction of vitamin B_{12a} with cysteine in 0.2 M phosphate buffer (pH 6.80). A solution of 1.32×10^{-4} M vitamin B_{12a} containing 0.00488 mmol was placed in a polarographic cell, deaerated, and microliter aliquots of 0.143 M cysteine were added. The DP polarogram was run after each addition with several minutes allowed for equilibrium to be reached. These polarograms were rerun until the cysteine peak appeared not to change; however, the reaction was slow and complete equilibrium may not have been reached. A small but rather broad peak at ca. −0.2 V was seen to decrease with each addition of cysteine while the peak at −0.88 V started to grow and shifted slightly positive to −0.86 V. This peak reached a maximum which was 2.4 times the initial current when the peak at −0.2 V disappeared. With further addition of cysteine after the end point, the very characteristic cysteine peak began to grow at −0.38 V (Figure 10) with practically no change in the peak at −0.86 V vs. SCE. A plot of the current vs. the microliters of cysteine added to B_{12a} for one such titration is given in Figure 11. Extrapolation of both arms of this amperometric titration plot allows one to interpret the stoichiometry for the reactants in the reaction. The end point comes at 31.4 μL of 0.00448 mmol of cysteine added which gives a mole ratio of cysteine to B_{12a} of 0.920 to 1 or just about

1:1 ratio of reactants. The fact that the peak at −0.86 V grows during the reaction but remains constant after the end point leads one to think that it is due to products of the reaction. A one-electron homogeneous reduction would give B_{12r} and a cysteine radical and the radicals could couple to produce the disulfide-cystine. Thus the overall reaction stoichiometry would be

$$2B_{12a} + 2HSCH_2CH(NH_2)COOH \rightarrow 2B_{12r} + (HO_2C(NH_2)CHCH_2S)_2 + 2H^+$$

The UV–vis spectrum of the reaction mixture past the end point shows absorption maximums at 312, 405, and 475 nm with shoulders in the 370–380 nm and 570–580 nm region, whereas, authentic B_{12r} has maxima at 312, 405, and 473 nm but there are no shoulders. Addition of cystine to B_{12r} did not affect its spectrum. With an excess of cysteine, the lower wavelength shoulder in the spectrum of the reaction product becomes a peak at 370 nm which we attribute to a weak cysteine–B_{12r} complex.

In order to test the hypothesis that the growth of the pulse peak at −0.86 V is due to the disulfide, L-cystine, we ran its dc and DP polarograms. The dc polarogram exhibits two waves with the $E_{1/2}$ of the first wave coming about −0.41 V. The first wave does not reach a well defined plateau and the second wave rises irreversibly from the top of the first wave to a plateau at ca. −0.9 V. The pulse polarogram of L-cystine shows a sharp peak at −0.40 V and a broad one at −0.8 V. In the presence of vitamin B_{12r}, which is very surface active on Hg, the cystine wave is shifted to the −0.85-V region in the dc curve with a pure capacity current (inversion at −0.4 V) coming before the rise of the wave. Only one peak is seen in the DP polarogram at −0.86 V. From the dc polarogram, the diffusion coefficient for cysteine is found to be about twice that of vitamin B_{12r}. The increase of the peak current at −0.86 V by a factor of 2.4 during the titration is consistent with the production of 1 mol of cystine for every 2 mol of B_{12r} formed where B_{12r} electroreduction is a one-electron process and cystine is a two-electron process. Thus we conclude that the current increase at −0.86 V in the titration is most likely due to L-cystine which is a product of the reaction.

If the reaction product of the amperometric titration, after a large excess of cysteine is added, is allowed to sit open to the atmosphere, a very large magnitude wave develops after about an hour at −0.85 V which implies that all of the cysteine has been converted to cystine. The auto-oxidation of thiols catalyzed by vitamin B_{12} derivatives in the presence of oxygen is a well-known reaction (*16*), the mechanism of which is unsettled (*17*). It would appear from our results that this mechanism is the reduction of vitamin B_{12a} by the thiol to form B_{12r} (or a B_{12r}–thiol complex) and the disulfide and then reoxidation of B_{12r} by oxygen so that the process can cycle with a net conversion of thiol to disulfide.

CONCLUSION

The present investigation demonstrates the utility of the cathodic DP polarographic technique for the determination of sulfide ion (or HS^-) and thiols in the presence of vitamin B_{12a} at physiological pH. Although calibration plots are limited in range because of wave splitting at higher concentrations and also show curvature, they can nevertheless be used to obtain important chemical information where an accuracy of greater than a few percent is not necessary.

Application of the analysis methods shows that vitamin B_{12a} reacts with cysteine in a 1:1 ratio of reactants and that the products are most likely cystine, vitamin B_{12r}, and a B_{12r} species which appears to be weakly complexed by cysteine at neutral pH. Similar studies with glutathione now being investigated suggest that the reaction

$$2RSH + 2B_{12a}^+ \rightarrow 2B_{12r} + RSSR + 2H^+$$

is a general one.

ACKNOWLEDGMENT

The authors thank Paul Fuchs for making some of the spectrophotometric measurements.

LITERATURE CITED

(1) H. Rudiger, *Eur. J. Biochem.*, **21**, 264 (1971).
(2) C. A. Mairesse-Ducarmois, G. J. Patriarche, and J. L. Vanderbalck, *Anal. Chim. Acta*, **71**, 165 (1974); **76**, 299 (1975).
(3) D. R. Canterford, A. S. Buchanan, and A. M. Bond, *Anal. Chem.*, **45**, 1327 (1973).
(4) J. A. Turner, R. H. Abel, and R. A. Osteryoung, *Anal. Chem.*, **47**, 1343 (1975).
(5) J. M. Pratt, "Inorganic Chemistry of Vitamin B_{12}", Academic Press, New York, N.Y., 1972, p 46.
(6) L. Meites, "Polarographic Techniques", 2nd ed., Interscience, New York, N.Y., 1965, p 89.
(7) J. M. Pratt, "Inorganic Chemistry of Vitamin B_{12}", Academic Press, New York, N.Y., 1972, p 109.
(8) J. C. Abbot, Ph.D. Dissertation, The Ohio State University, 1964, University Microfilms, Inc., Ann Arbor, Mich.
(9) R. L. Birke, G. A. Brydon, and M. F. Boyle, *J. Electroanal. Chem.*, **52**, 237 (1974).
(10) D. Lexa and J. M. Saveant, *J. Am. Chem. Soc.*, **98**, 2652 (1976).
(11) T. M. Kenyhercz, T. P. De Angelis, B. J. Norris, W. R. Heineman, and H. B. Mark, Jr., *J. Am. Chem. Soc.*, **98**, 2469 (1976).
(12) W. Stricks and I. M. Kolthoff, *J. Am. Chem. Soc.*, **74**, 4646 (1952).
(13) I. M. Kolthoff and C. Barnum, *J. Am. Chem. Soc.*, **62**, 3061 (1940).
(14) I. M. Kolthoff, W. Stricks, and N. Tanaka, *J. Am. Chem. Soc.*, **77**, 5211 (1955).
(15) R. Brdicka, *Z. Electrochem.*, **48**, 278 (1942).
(16) J. L. Peel, *Biochem. J.*, **88**, 296 (1963).
(17) J. M. Pratt, "Inorganic Chemistry of Vitamin V_{12}", Academic Press, New York, N.Y., 1972, p 209.
(18) M. T. Stankovich and A. J. Bard, *J. Electroanal. Chem.*, **75**, 487 (1977).

RECEIVED for review December 2, 1976. Accepted May 12, 1977. Acknowledgement is made to the National Institutes of Health for support under HEW-PHS Grant 5 RO1 AM18440 and to the City University of New York for a Faculty Research Award Grant.

Phase-Selective Cathodic Stripping Voltammetry for Determination of Water-Soluble Mercaptans

W. Michael Moore* and V. Frances Gaylor

The Standard Oil Company (Ohio), 4440 Warrensville Center Road, Cleveland, Ohio 44128

The application of phase-selective cathodic stripping (PSCS) voltammetry to analyses of water-soluble mercaptans has been demonstrated using a micrometer hanging mercury drop electrode. The sensitivity limit was near 1 ppb for sodium mercaptoacetate (SMA) analysis when a 2-min deposition interval was employed. The average deviation for six independent experiments with 25 ppb SMA was 3.62%. The dependence of PSCS peak currents upon mercaptan concentration, applied ac voltage magnitude, signal frequency, and dc potential scan rate was investigated. Because ac voltammetry discriminates against irreversible electrode processes, mercaptan PSCS experiments could be performed in air-saturated electrolytes. As a result, the method appears to be suitable for analyses of volatile mercaptans when inert gas purging to remove oxygen is not practical.

The search for more sensitive electroanalytical techniques led to the development of stripping voltammetry (SV) (*1*). The extraordinary sensitivity of SV arises from preconcentration of trace material into or onto a microelectrode by an electrochemical deposition before reversing the process and "stripping" the substance from the electrode. Anodic stripping voltammetry has been frequently utilized for the determination of trace metals (*2, 3*). Cathodic stripping voltammetry has been employed for analyses of halide ions (*4*), other inorganic anions which form insoluble mercury compounds (*5*), and several mercaptans (*6, 7*).

The resolution and sensitivity of SV can be improved when the stripping process is performed using ac-modulated or pulsed potential waveforms. Differential pulse cathodic stripping voltammetry at a hanging mercury drop electrode (HMDE) has been employed to determine 2-mercaptopyridine-*N*-oxide ion with a sensitivity limit of 8×10^{-10} M (*8*). Several studies have been devoted to phase-selective anodic stripping (PSAS) (*9–11*); however, little attention has been given to the cathodic counterpart.

Several polarographic studies involving mercaptan compounds have been reported (*12–14*). The generally accepted electrode mechanism for the reaction of mercaptans at a mercury electrode involves the formation of a mercurous mercaptide species in a reversible one-electron process

$$RSH + Hg \rightleftarrows RSHg + H^+ + e \qquad (1)$$

which is represented by Equation 1.

Unfortunately, oxygen cannot be removed by inert gas purging during analyses of volatile mercaptans. Sodium sulfite (*15*) and ascorbic acid (*16*) have been employed to destroy oxygen in situ prior to electrochemical analysis. Since ac voltammetry discriminates against irreversible electrode processes (*17*), it can occasionally be employed for analyses performed in the presence of oxygen if caution is exercised (*18, 19*).

At present, there is no exact theoretical treatment to describe ac stripping currents obtained at the HMDE. Some features of the phase-selective cathodic stripping (PSCS) peak current are, however, suggested by theoretical treatments of the direct voltammetric process. Underkofler and Shain (*20*) derived an equation which describes the ac current obtained for a reversible process using the planar diffusion model; this equation was modified by Delmastro and Smith (*21*) to account for the geometry and spherical diffusion effects of a metal ion–amalgam system and found applicable to ac amalgam stripping by Moorhead and Davis (*9*).

In the present study, use of PSCS for analyses of water-soluble mercaptans was investigated using a micrometer HMDE and the experimental variables affecting in-phase peak current were examined. Based upon results obtained, PSCS is a sensitive and reliable technique for mercaptan analyses.

EXPERIMENTAL

Apparatus. PSCS experiments were performed using a Princeton Applied Research (PAR) Model 170 Electrochemistry System with PAR 9301 polargraphic cells. A calibrated Kemula-type Metrohm E-410 micrometer hanging mercury drop electrode [HMDE(K)] was employed as the working electrode for all cathodic stripping experiments. The reference electrode was a saturated calomel (SCE) which was separated from the cell solution by a salt bridge tube with porous cracked-glass tip (*22*) containing pH 5.5 sodium acetate solution. A PAR 9350 water-jacketed cell was used with a Haake Model S-84833 external-circulating constant-temperature bath for some thermostated (25 ± 0.1 °C) experiments.

The cell solution was stirred by a 3-mm × 12-mm Teflon-coated spin bar driven at 600 rpm by a larger (7-mm × 35-mm) spin bar mounted on the shaft of an inverted Sargent S76485 Synchronous Rotator. A stainless-steel cylinder with a 2-cm diameter hole cut in the top was mounted over the rotator shaft. The tapered PAR 9301 polargraphic cells fit nicely into the positioning device which ensured that the cell spin bar position remained invariant from run to run. Figure 1 illustrates the electrochemical cell and stirring assembly employed for PSCS experiments.

Mercaptan solutions were standardized by a coulometric titration procedure. A Brinkmann Model E524 Coulostat, Brinkmann E436 Potentiograph, E436D Multititration Stand, standard Metrohm cells, silver wire generating and auxiliary electrodes, and a dual-silver detecting electrode were employed in the coulometric titration procedure.

Reagents. Electrolyte used for the electrochemical cell and SCE salt bridge compartment was sodium acetate solution which was prepared by adjusting 0.5 M acetic acid to pH 5.5 with 50% sodium hydroxide solution. Water of sufficient purity for these experiments was prepared by simple distillation, passage through a demineralizer (Bantam Model BD-1 Demineralizer), and a final distillation from a Corning AG-3 Still.

High purity argon (Airco, Inc.) was used for experiments which required a purge gas. Argon was deoxygenated by passage through an acidic vanadous chloride solution (*23*) and humidified with a distilled water scrubber.

Mercury for the HMDE and DME was triple-distilled product from Bethlehem Instrument Company. Sodium mercaptoacetate (SMA) and *tert*-butylmercaptan (TBM) were reagent-grade chemicals used without further purification.

Standardization and Monitoring Procedures for Mercaptan Solutions. Mercaptan solutions used for calibration purposes were standardized coulometrically by titration with electrogenerated silver ion in acetate solution. Excess silver at the end point was detected amperometrically by a dual-silver electrode.

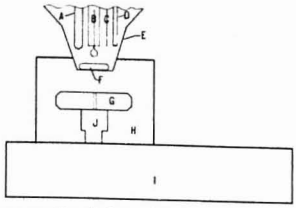

Figure 1. Lower portion of electrochemical cell and stirring assembly. (A) Salt bridge tube containing SCE, (B) hanging mercury drop electrode, (C) platinum wire auxiliary electrode, (D) nitrogen inlet, (E) polarographic cell bottom, (F) cell spin bar, (G) driven spin bar, (H) stainless steel cell positioner, (I) synchronous rotator, (J) rotator shaft

A 10^{-2} M (1150 ppm) SMA solution was prepared in 0.1 M acetic acid and standardized by the coulometric titration procedure; a 20-fold dilution of this solution using *degassed* 0.1 M acetic acid as diluent yielded 58 ppm SMA. A portion of this solution was sealed under argon in a Hypo-Vial (Pierce Chemical) for syringe sampling.

The 58-ppm SMA standard solution was not entirely stable and decreased about 5% per week. Since the coulometric titration procedure was rather time-consuming, differential pulse polarography (DPP) at a DME was employed as a quick method for monitoring SMA concentration. Aliquots from a freshly prepared 58-ppm SMA solution were added to 10.0 mL pH 5.5 sodium acetate solution and DPP performed (100-mV pulse amplitude, 2-s mercury drop time, and potential scan rate of 5 mV/s). Peak currents obtained at −0.25 V vs. SCE for several concentrations were used to create a calibration curve which was subsequently used to monitor SMA concentration in standard solutions.

Procedure for PSCS Experiments. To perform PSCS experiments, 10.0 mL of electrolyte solution was added to a cell and (for some experiments) deoxygenated for 5 min with humidified argon. Low-level mercaptan concentrations were generated by syringing aliquots from standard solutions into the electrolyte. Following addition of sample or standard, degassing was continued for 30 s before the argon was switched to blanket the solution. A mercury drop of area 0.035 cm^2 was obtained by dialing eight divisions of the E-410 HMDE assembly. Stirring was commenced 15 s before the applied potential was switched from −0.6 to +0.1 V vs. SCE to initiate the anodic plating process. After precisely 1.5 min, the stirrer was switched off to allow the solution to become quiescent for 30 s before the applied dc potential was scanned from +0.1 to −0.6 V vs. SCE to record either a blank or mercaptan stripping peak. In all cases, the rms ac current component *in-phase* with the superimposed ac voltage signal was recorded. For most experiments, the frequency and amplitude of the modulating ac voltage were 90 Hz and 10 mV peak-to-peak, respectively, and the potential scan rate was 100 mV/s.

RESULTS AND DISCUSSION

Selection of pH. Selection of electrolyte pH for mercaptan stripping experiments was a compromise between peak resolution and mercaptan stability. The first oxygen reduction step resulted in a broad ac current response near −0.06 V vs. SCE in air-saturated sodium acetate solution. In order to resolve mercaptan stripping peaks sufficiently from the oxygen wave, pH 5.5 or greater was required. However, since the rate of mercaptan to disulfide oxidation is faster at high pH values (*19*), pH 5.5 was selected for the present study.

All mercaptans examined by PSCS exhibited in-phase peak currents (i_p) near −0.36 V vs. SCE in pH 5.5 sodium acetate solution. Peak potentials were shifted negatively by 58 mV per unit increase in pH; this result is predictable from the Nernst expression of the mercaptan electrode reaction (Equation 1).

Selection of Deposition Potential. The value of deposition potential (E_i) for mercaptan PSCS experiments

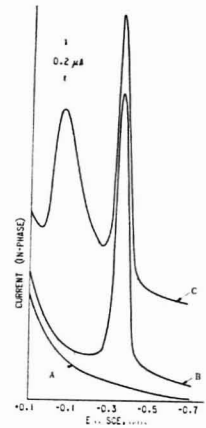

Figure 2. PSCS voltammograms for a blank and 25 ppb SMA in both deaerated and air-saturated sodium acetate solution. Experimental conditions for the blank (A), and PSCS performed in deaerated (B) and air-saturated (C) solution were: ν = 100 mV/s, ω = 90 Hz, ΔE = 10 mV, A = 0.035 cm^2, τ = 2.0 min, pH = 5.5, and E_i = +0.1 V vs. SCE

performed in air-saturated solution was critical. Initially, E_i = −0.1 V vs. SCE was employed, but stripping peak currents were erratic and sensitivity was poor. Although a relatively small ac response was obtained for oxygen reduction in air-saturated electrolyte, the dc reduction flux of oxygen to hydrogen peroxide was quite large at −0.1 V vs. SCE. It appears that hydrogen peroxide reacted with mercaptans in the vicinity of the HMDE which resulted in the observed decrease in experimental sensitivity and precision.

A background dc polarogram was obtained in air-saturated electrolyte solution. A narrow potential region centered about +0.1 V vs. SCE was revealed in which neither mercury oxidation nor oxygen reduction took place. PSCS results for mercaptans were greatly improved when the deposition step was performed at +0.1 V vs. SCE, a potential at which no extraneous electrode reactions occur.

Results for Sodium Mercatoacetate (SMA). Figure 2 shows PSCS voltammograms for a blank and 25 ppb SMA (2.2×10^{-7} M) obtained in deaerated and air-saturated sodium acetate solution. Figure 2 is a graphic illustration of mercaptan sensitivity enhancement and oxygen discrimination by PSCS; although the molar concentration of oxygen was more than 10^4 times larger than SMA, the mercaptan stripping peak at −0.36 V in Figure 2C is larger than the oxygen peak at −0.06 V. The sensitivity limit for SMA was near 1 ppb when a 2-min stirred deposition interval was utilized.

Figure 3 illustrates calibration curve data obtained for PSCS experiments in both deaerated and air-saturated solutions using 0–100 ppb SMA. From Figure 3, it is clear that the presence of oxygen has only a small effect on the magnitude of i_p obtained for a given SMA concentration. A linear response was obtained only for SMA concentrations below about 50 ppb when a 2-min stirred deposition interval was employed. Evidently, at higher sample concentrations, the HMDE was partially blocked by insoluble mercurous mercaptide deposit. The "electrode blockage" supposition is supported by the experimental observation that dc deposition currents were not constant, but declined with time when sufficiently large SMA concentrations were employed.

In order to extend the concentration range over which a linear peak current response was obtained, a 60-s nonstirred

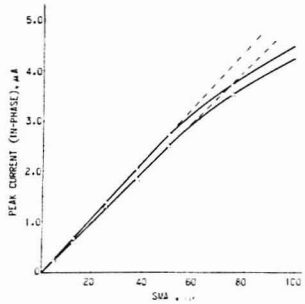

Figure 3. PSCS calibration plots for 0–100 ppb SMA in deaerated and air-saturated electrolyte using a 2.0-min stirred deposition interval. Experimental conditions for data obtained in deaerated electrolyte solution (upper curve) and air-saturated solution (lower curve) were the same as in Figure 2

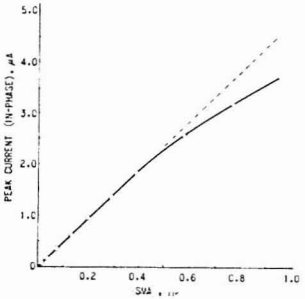

Figure 4. PSCS calibration plot for 0–1 ppm SMA using a 1.0-min quiescent deposition interval. Except for the 1.0-min quiescent deposition interval, experimental conditions were the same as in Figure 2. Air-saturated electrolyte solutions were employed

deposition interval was employed. Figure 4 is a calibration plot obtained for experiments employing the 60-s quiescent plating interval; with this experimental modification, a linear current response was obtained for SMA concentrations up to 500 ppb, although the sensitivity limit increased to 20 ppb.

Comparison of PSCS and DPCS Using SMA. PSCS was compared to differential pulse cathodic stripping (DPCS) using 20 ppb SMA and a 2-min deposition interval in both deaerated and air-saturated solutions. For each technique, electrical parameters (scan rate, etc.) were adjusted in order to optimize current response for the sake of comparison.

In air-free electrolyte, PSCS and DPCS yielded peak currents of 0.87 and 2.51 μA, respectively. In air-saturated solution, however, PSCS yielded 0.91 μA, while accurate measurement of DPCS peak current was prevented by a severely sloped baseline due to superimposed oxygen reduction. Figure 5 illustrates the DPCS trace obtained for 20 ppb SMA in air-saturated solution; SMA peak current is located at −0.25 V and appears as a shoulder on the much larger oxygen peak.

The above results indicate that DPCS is inherently more sensitive than PSCS for trace mercaptan determinations. PSCS is the superior technique for mercaptan analyses performed in the presence of oxygen, however, because of the ability to discriminate against oxygen reduction.

Results for *tert*-Butylmercaptan (TBM). PSCS would appear to be a promising technique for determinations of

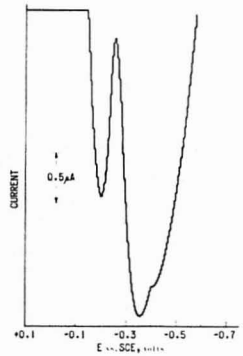

Figure 5. Differential pulse cathodic stripping voltammogram for 20 ppb SMA in air-saturated sodium acetate solution. Experimental conditions were: 100-mV pulse amplitude, pulse repetition time of 1 s, ν = 5 mV/s, A = 0.035 cm^2, τ = 2.0 min, pH = 5.5, and E_i = +0.1 V vs. SCE

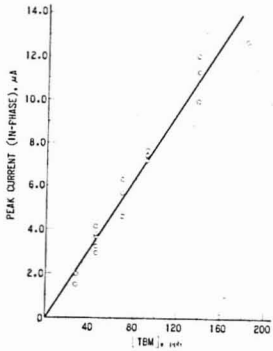

Figure 6. PSCS calibration plot for *tert*-butylmercaptan. Experimental conditions were the same as in Figure 2. Air-saturated electrolyte solutions were employed

volatile mercaptans because it is not necessary to remove oxygen prior to performing the experiment. Therefore, the PSCS behavior of TBM (bp = 64 °C) was investigated.

The procedure for TBM experiments was essentially the same as described for SMA. Stock solutions were more stable when prepared in ethanol because of increased TBM solubility in this solvent; these solutions were used immediately following standardization by coulometric titration. When not being sampled, TBM stock solutions were stored at 0° C.

Figure 6 is a calibration plot obtained for TBM in air-saturated electrolyte; each data point was obtained by an independent experiment. Although a considerable degree of scatter was present in experimental i_p data, the calibration curve shown for TBM is linear over the 0–200 ppb concentration range examined. A linear regression correlation coefficient of 0.979 was obtained for the data illustrated in Figure 6.

Precision of PSCS Data. In order to evaluate the precision of stripping peak currents, six *independent* PSCS experiments were performed with 25 ppb SMA. Results of these experiments are shown in Table I. The average deviation, which generally decreased as mercaptan concentration increased, was 3.62% with 25 ppb SMA. Experimental

Table I. Reproducibility of PSCS Peak Currents Obtained with 25-ppb SMA in Deaerated Electrolyte[a]

Run No.	i_p, μA
1	1.42
2	1.24
3	1.44
4	1.41
5	1.38
6	1.42
Mean	1.39
% Av dev	3.62

[a] Experimental parameter values: $\nu = 100$ mV/s, $\omega = 90$ Hz, $\Delta E = 10$ mV, $A = 0.035$ cm^2, $\tau = 2.0$ min, pH = 5.5, $E_i = +0.1$ V vs. SCE.

precision was definitely improved through use of the cylindrical cell positioning device which ensured reproducible convection during the deposition interval, although this apparatus required working at ambient temperature (25 ± 0.5 °C). Reproducibility of experiments performed using the cell positioner was better than for temperature-thermostated experiments in which the cell and rotator shaft were aligned by sight only.

The greatest obstacle to achieving reproducible results with SMA and TBM was the reactive nature of the mercaptans. Although not particularly volatile, SMA appeared to react slowly during PSCS experiments as evidenced by a steady decline of stripping peak currents for several stripping scans employing the same test solution. Therefore, to achieve best results, determinations were performed without delay after SMA was syringed into the cell.

The extreme volatility of TBM rendered reproducible results difficult to achieve. The average per cent deviation of the 17 data points in Figure 6 from the linear regression straight line was determined to be 10.1%, an acceptable figure considering the nature of the analysis.

Effect of Frequency upon Peak Current. It was deemed desirable to determine the effects of various electrical parameters upon i_p for PSCS experiments to compare with functional dependencies observed in phase-selective *anodic* stripping (PSAS) and predicted by ac polarographic theory. Therefore, the effects of signal frequency (ω), peak-to-peak ac voltage magnitude (ΔE), and dc potential scan rate (ν) upon i_p were determined using 25–30 ppb SMA with a 2-min stirred deposition interval.

The effect of changes in signal frequency was examined over the interval 25–500 Hz. In-phase stripping peak currents were proportional to $\omega^{1/2}$ in this frequency range (linear regression correlation coefficient = 0.9996) which is predicted by basic ac polarographic theory (*23*). Moorhead and Davis also found that in-phase stripping peak currents for PSAS experiments using Cd(II) (*9*) and Ga(III) (*10*) were proportional to $\omega^{1/2}$.

A frequency of 90 Hz was employed for most experiments. Although stripping peak currents increased linearly as a function of $\omega^{1/2}$, extremely high signal frequencies were avoided because of the presence of large background currents.

Effect of ΔE upon Peak Currents. Figure 7 illustrates the linear dependence of i_p upon peak-to-peak ac voltage magnitude (ΔE) obtained for sufficiently small ΔE values; the linear relationship is in agreement with theory for ac polarography (*24*) and is similar to results obtained by PSAS for Cd(II) reduction (*9*). A 10-mV ac modulating voltage was employed for most of this work because of the sensitivity enhancement achieved.

Effect of Scan Rate upon Peak Current. The effect of potential scan rate (ν) upon stripping peak currents was investigated using a 25-ppb SMA solution. Figure 8 shows that a linear plot was obtained when i_p was plotted vs. $\nu^{1/2}$. A linear regression correlation coefficient of 0.9980 was ob-

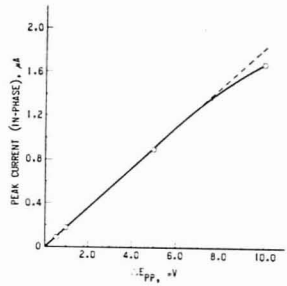

Figure 7. PSCS peak current (in-phase) vs. peak-to-peak ac signal magnitude (ΔE). Except for 30 ppb SMA and variable ΔE, experimental conditions were the same as in Figure 2

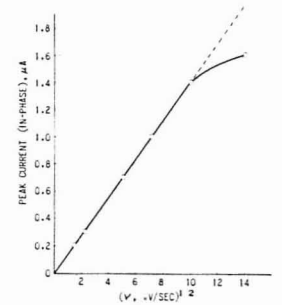

Figure 8. PSCS peak current (in-phase) vs. square root of potential scan rate (ν). Except for variable ν, experimental conditions were the same as in Figure 2

tained for the linear portion of the graph ($\nu \leq 100$ mV/s).

Peak width at half height was near 80 mV for SMA stripping peaks at moderate scan rates. PSCS current response became increasingly broadened for potential scan rates greater than 100 mV/s and i_p steadily declined. Deteriorating ac response is expected when conditions of the "slow scan limit" ($\omega \Delta E \gg \nu$) are not met (*20*). In addition, there may be insufficient time for complete reduction of deposited mercurous mercaptide at extremely rapid scan rates. From Figure 8, 100 mV/s was the fastest scan rate employed which yielded a current response on the linear portion of the plot and was, therefore, employed for most experiments in this study.

PSAS results for Cd(II) reduction (*9*) exhibited a monotonic decline of in-phase peak currents for increasing values of scan rate between 10 and 90 mV/s. As a result, we were surprised by the linear relationship obtained between i_p and $\nu^{1/2}$ in this study.

The fate of plated material may explain the differences observed in scan rate behavior between PSAS results for Cd(II) and mercaptans by PSCS. Deposited cadmium is soluble in mercury and diffuses into the HMDE while the mercurous mercaptide species is insoluble in mercury and simply coats the electrode surface (*25*). As a result, *all* deposited mercurous mercaptide should remain at the electrode surface during PSCS experiments and be available for stripping during the potential scan; as a consequence of amalgam formation, the same is not true for deposited cadmium.

The effect of potential scan rate upon *dc* cathodic stripping peak currents was investigated using 30 ppb SMA and a 2-min

stirred deposition interval. A linear dependence of peak current upon scan rate was obtained (linear regression correlation coefficient = 0.9997) so long as the quantity of coulombs involved in the stripping process remained constant.

The dependence of first and second harmonic responses in ac voltammetry on experimental parameters was recently outlined by Smith et al. (*26*). The effect of dc scan rate was not described explicitly in this study, although the basic equations involved in ac voltammetry were presented which show that the alternating current response is proportional to surface concentrations of oxidized and reduced forms. Since deposited mercurous mercaptide is insoluble in the solution and electrode phases, its activity should be near unity throughout the stripping scan (*27*) and the resulting PSCS current response proportional to mercaptan concentration at the electrode surface. Thus, the square root relationship of PSCS peak currents and scan rate results primarily from the dependence of generated mercaptan surface concentrations upon dc scan rate.

ACKNOWLEDGMENT

The authors are grateful to Donald E. Smith for aid in understanding the scan rate dependence of PSCS peak currents.

LITERATURE CITED

(1) E. Barendrecht in "Electroanalytical Chemistry—A Series of Advances", Vol. 2, A. J. Bard, Ed., Marcel Dekker, New York, N.Y., 1967, pp 53–109.
(2) W. Kemula and Z. Kublik in "Advances in Analytical Chemistry and Instrumentation", Vol. 2, C. N. Reilley, Ed., Interscience, New York, N.Y., 1963, Chap. 3.
(3) I. Shain in "Treatise on Analytical Chemistry", Part I, Vol. 4, I. M. Koltoff and P. J. Elving, Ed., Interscience, New York, N.Y., 1963, Chap. 50.
(4) G. Colovos, G. S. Wilson, and J. L. Moyers, *Anal. Chem.*, **46**, 1051 (1974).
(5) Kh. Z. Brainina, *Talanta*, **18**, 513 (1971).
(6) H. Berge and P. Jeroschewski, *Fresenius' Z. Anal. Chem.*, **212**, 278 (1965).
(7) M. J. D. Brand and B. Fleet, *Analyst (London)*, **93**, 498 (1968).
(8) D. A. Csejka, S. T. Nakos, and E. W. DuBord, *Anal. Chem.*, **47**, 322 (1975).
(9) E. D. Moorhead and P. H. Davis, *Anal. Chem.*, **45**, 2178 (1973).
(10) E. D. Moorhead and P. H. Davis, *Anal. Chem.*, **47**, 622 (1975).
(11) E. D. Moorhead and G. A. Forsberg, *Anal. Chem.*, **48**, 751 (1976).
(12) M. L. Mittal and A. V. Pandey, *J. Electroanal. Chem.*, **36**, 249 (1972).
(13) R. S. Saxena and U. S. Chaturvedi, *J. Electroanal. Chem.*, **36**, 515 (1972).
(14) W. Stricks, J. K. Frischman, and R. G. Mueller, *J. Electrochem. Soc.*, **109**, 518 (1962).
(15) S. Kukuchi, *Bull. Chem. Soc. Jpn.*, **27**, 65 (1954).
(16) T. M. Florence and Y. J. Farrar, *J. Electroanal. Chem.*, **41**, 127 (1973).
(17) A. M. Bond, *Anal. Chem.*, **44**, 315 (1972).
(18) A. M. Bond and J. H. Canterford, *Anal. Chem.*, **43**, 228 (1971).
(19) A. M. Bond, *Talanta*, **20**, 1139 (1973).
(20) W. L. Underkofler and I. Shain, *Anal. Chem.*, **37**, 218 (1965).
(21) J. R. Delmastro and D. E. Smith, *Anal. Chem.*, **38**, 169 (1966).
(22) J. J. Lingane, *J. Electroanal. Chem.*, **1**, 379 (1960).
(23) Princeton Applied Research Corporation, Princeton, N.J., Application Note 108.
(24) D. E. Smith in "Electroanalytical Chemistry—A Series of Advances", A. J. Bard, Ed., Marcel Dekker, New York, N.Y., 1966, Chap. 1.
(25) M. Brezina and P. Zuman, "Polarography in Medicine, Biochemistry, and Pharmacy", Interscience, New York, N.Y., 1958, pp 470–478.
(26) A. M. Bond, R. J. O'Halloran, I. Ruzic, and D. E. Smith, *Anal. Chem.*, **48**, 872 (1976).
(27) T. Berzins and P. Delahay, *J. Am. Chem. Soc.*, **75**, 555 (1953).

RECEIVED for review February 22, 1977. Accepted April 27, 1977. This material was presented in part at the 3rd Annual Meeting of the Federation of Analytical Chemistry and Spectroscopy Societies in Philadelphia, Pa., November 1976.

Peak Shapes in Semidifferential Electroanalysis

Penny Dalrymple-Alford

Trent University, Peterborough, Canada

Masashi Goto

Nagoya University, Japan

Keith B. Oldham*[1]

Bristol University, United Kingdom

A derivative neopolarogram is the peaked curve that is generated by semidifferentiation of the current that flows in response to an imposed ramp signal on a stationary electrode. The predicted dependences of peak height, peak potential, and peak width on concentration, electron number, scan rate, etc., are confirmed experimentally using one established and two new circuits to monitor the electroreduction of several metal ions in aqueous solution. Features of the technique that make it attractive for qualitative and quantitative chemical analysis are cited, and comparison is made with pulse polarography.

Semidifferential electroanalysis was first described by Goto and Ishii (*1*). More recently, the present authors (*2*) have discussed some theoretical aspects of this voltammetric technique. The purpose of the current article is to compare the theoretical predictions with experimental data, to demonstrate that semidifferentiation may be effected digitally or by simpler circuitry than that used hitherto, and to discuss the analytical potentialities of the method.

In semidifferential electroanalysis, a cathodic-going ramp signal is applied to a working electrode immersed in a solution containing, in addition to excess supporting electrolyte, one or more species that are electroreducible. The semiderivative e of the cathodic current that flows in consequence of the electroreduction is displayed as a function of the applied potential E. Figures 1 and 2 show examples of the resulting curves, which are termed "derivative neopolarograms" (*2*). A derivative neopolarogram consists of one or more peaks, each of which corresponds to a single reduction process. In Figure 1, for example, the two peaks correspond to the reductions of the In^{3+} and Zn^{2+} ions. Each peak is independent of the others; thus when In^{3+} was omitted from the solution used

[1] Permanent address, Trent University, Peterborough, Canada.

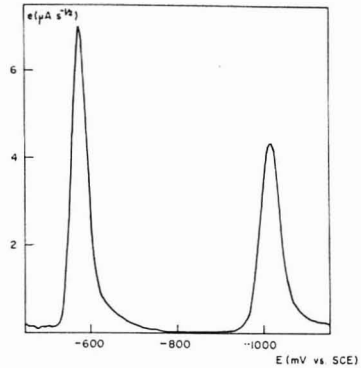

Figure 1. A derivative neopolarogram of 100 μM In(III) and 100 μM Zn^{2+} in 100 mM KCl. Scan rate: 100 mV s^{-1}; electrode area: approximately 4.5 mm^2; instrumentation: Circuit C

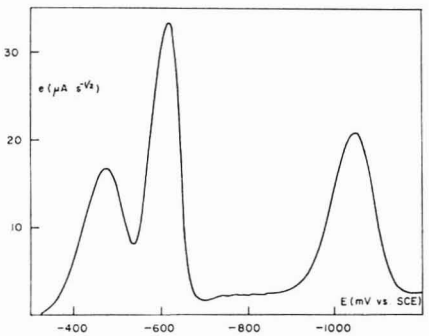

Figure 2. A derivative neopolarogram of 1.0 mM each of Tl^+, Cd^{2+}, and Ni^{2+} in 100 mM KNO_3. Scan rate and electrode area: as Figure 1; instrumentation: Circuit B

to generate Figure 1, the Zn^{2+} peak remained unchanged.

A derivative neopolarographic peak may be characterized by three features: e_p, the peak height (the maximum value attained by the semiderivative); E_p, the peak potential (the potential corresponding to the maximum); and W_p, the peak width (the potential range spanned by the peak at a height equal to one-half the maximum height). The values predicted (*2*) for these features are listed in Table I for both reversible and irreversible electroreductions. The symbols used in this tabulation have the following significances: n is the number of faradays needed to reduce 1 mol of the reducible species; F and R are Faraday's and the gas constants (96 487 C mol^{-1} and 8.3143 J K^{-1} mol^{-1}); T is the temperature (K); c and D are the concentration of the reducible species and its diffusion coefficient (mol m^{-3} and m^2 s^{-1}); α is the transfer coefficient of the electron exchange process; A is the area of the electrode (m^2) and v is the rate (V s^{-1}) at which it is made more negative; $E_{1/2}$ is the halfwave potential (V) in classical polarography with a dropping mercury electrode, τ being the corresponding droptime (s).

Notice in Table I that the peak height, for both reversible and irreversible processes, is predicted to be proportional to the concentration of the reducible species, to the electrode area, and to the scan rate v. The peak potential for reversible process is a constant equal to the polarographic halfwave

Table I. Features of Derivative Neopolarographic Peaks

	Reversible	Irreversible
Peak height, e_p	$\dfrac{n^2F^2AvcD^{1/2}}{4RT}$	$\dfrac{\alpha n^2F^2AvcD^{1/2}}{3.367\,RT}$
Peak potential, E_p	$E_{1/2}$	$E_{1/2} + \dfrac{RT}{2\alpha nF} \ln\left[\dfrac{0.613\,RT}{\alpha nFv\tau}\right]$
Peak width, W_p	$3.53\dfrac{RT}{nF}$	$2.94\dfrac{RT}{\alpha nF}$

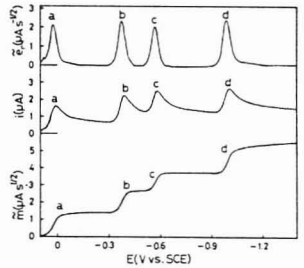

Figure 3. Comparison of resolutions of a derivative neopolarogram, a voltammogram, and a neopolarogram of the same four-component solution: 50 μM each of (a) Cu^{2+}, (b) Pb^{2+}, (c) Cd^{2+}, and (d) Zn^{2+} in 100 mM KNO_3. Scan rate: 100 mV s^{-1}; electrode area: 4.69 mm^2; instrumentation: Circuit A

potential, but for irreversible reductions E_p should typically be about 45 mV negative of $E_{1/2}$ (based on $\alpha n = 1$ and v = 100 mV s^{-1}) and will shift cathodically as the scan rate is increased (by 30 mV for a tenfold v increase). The peak shape is very dependent on n, the number of transferred electrons: as n increases, the peak is predicted to become narrower and much higher.

The formulas given in Table I are predicated on a planar electrode, whereas in the Experimental section of this article the electrodes used are hanging mercury spheres. However, it has been demonstrated (*2*) that the mild sphericity encountered in our experiments is adequately corrected for by subtracting the quantity $iD^{1/2}/r$ from measured values of e. Here i denotes the cathodic current and r is the radius of the mercury drop. We shall use a tilde to indicate quantities corrected in this way; thus $\tilde{e} = e - (iD^{1/2}/r)$ and $\tilde{e}_p$ represents the peak of an $\tilde{e}$ vs. E curve.

Semidifferential electroanalysis is closely related to the techniques of linear scan voltammetry (*3*) and semiintegral electroanalysis (*4*); in fact, it is simply the derivative of the latter. That linear scan voltammetry is a method intermediate between semiintegral electroanalysis and semidifferential electroanalysis is brought out in Figure 3. Whereas linear scan voltammetry is the easiest of the three techniques to implement, it is the most difficult to interpret. Implementation with linear scan voltammetry is easy because the displayed quantity is simply the current i. To obtain e, the quantity displayed in semidifferential electroanalysis, however, requires the processing of i data. We now take up the topic of how i is semidifferentiated to obtain e.

IMPLEMENTATION

As with semiintegration, two techniques are available for semidifferentiation: digital and analog. Digital methods will be preferred whenever computer-augmented experimentation

Scheme I

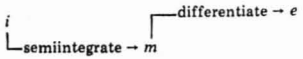

Scheme II

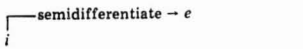

Scheme III

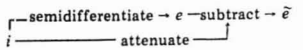

Scheme IV

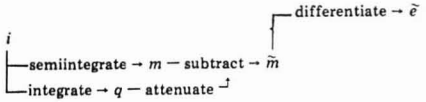

is employed, or when data of the highest accuracy are sought. Under other circumstances, the tedium of numerical semidifferentiation may be avoided by analog instrumentation. Sphericity correction is a simple matter with either technique.

Digital Techniques Several algorithms for numerical semidifferentiation have been described (*5*). The simplest, the so-called G1 algorithm, uses N equally spaced current data to compute e by the concatenation scheme

$$\frac{t^{1/2}}{N^{1/2}}e = \left[\left[\left[\cdots\left[\left[i_1\left(\frac{2N-5}{2N-2}\right)+i_2\right]\left(\frac{2N-7}{2N-4}\right)+i_3\right]\cdots\right]\left(\frac{1}{4}\right)+i_{N-1}\right]\left[\left(\frac{-1}{2}\right)+i_N\right]\right]$$

which is very easily implemented by a multiplication–addition–multiplication–...multiplication–addition procedure. In this algorithm, i_1, i_2, i_3,... i_{N-1}, and i_N denote the instantaneous currents at times t/N, $2t/N$, $3t/N$,... $(N-1)t/N$, and t. As with all algorithms, there is a discretization error implicit in this G1 formula; its magnitude diminishes as N increases.

Analog Techniques. A number of analog schemes are possible whereby the cell current may be electronically processed to give a signal proportional to e. The instrument previously described (*1*) is based on Scheme I. whereas a more direct scheme, Scheme II, is also possible. When correction for the sphericity is introduced, the direct scheme, Scheme III, becomes significantly simpler than Scheme IV (*1*). In the Experimental section of this article, we describe results obtained with instrumentation based on Schemes II and IV. The latter, which will be referred to as Circuit A, differs from that previously described (*1*) only in having a gain-adjustment potentiometer inserted between the subtractor and differentiator stages. The instrumentation based on the direct Scheme II will be described in some detail below. In use, it has been incorporated into the output stage of a Princeton Applied Research Corporation Model 170 Electrochemical System.

The output of the PAR 170 is a dc voltage in the range −10 V to +10 V, proportional to the electrochemical current. This output is normally fed (via an optional 10:1 attenuator) directly to the Y-drive of the instrument's X-Y recorder. Our modification is to insert a battery-powered operational amplifier circuit into the output lead. A rotary switch enables a variety of circuit elements to be inserted into the input of the operational amplifier, and into its feedback loop. However, the only circuits relevant to the present experimentation are those shown in Figure 4, both of which semidifferentiate.

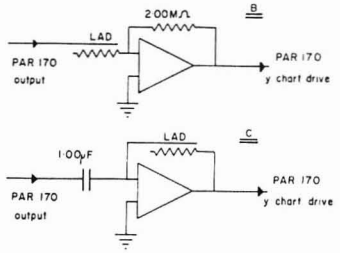

Figure 4. Circuits B and C, the two direct semidifferentiators. In both circuits LAD represents the ladder network shown as Figure 10 in Ref. *6* except that an 8300-kΩ resistor replaces the one mislabeled 830 kΩ in the publication

By arguments that closely parallel those governing the behavior of semiintegrating circuits (*6*) it can be shown that the output of a circuit resembling Figure 4B is

$$V_{out} = -R_f\sqrt{\frac{C_1}{R_1}}\frac{d^{1/2}}{dt^{1/2}}V_{in}$$

where V_{in} is the input voltage, R_f is the feedback resistance and the $\sqrt{R_1/C_1}$ ratio is a characteristic impedance term for the ladder network. In our circuit, R_f equals 2.00 megohms, R_1/C_1 equals 1.00 megohm per microfarad, and therefore

$$V_{out} = -(2.00\ s^{1/2})\frac{d^{1/2}}{dt^{1/2}}V_{in}$$

When incorporated into the PAR 170 system as described above, the effect of the Figure 4B modification is to multiply the PAR 170 sensitivity setting by the factor 0.5 $s^{-1/2}$, and to change the sign; thus with the current range set to "100 microampere full scale", the actual full scale signal is 50 μA $s^{-1/2}$.

Similarly the circuit in Figure 4C processes a voltage signal according to the

$$V_{out} = -C_1\sqrt{\frac{R_1}{C_1}}\frac{d^{1/2}}{dt^{1/2}}V_{in} = -(1.00\ s^{1/2})\frac{d^{1/2}}{dt^{1/2}}V_{in}$$

rule. Apart from the sign inversion, the effect of this modification is simply to change the units of the sensitivity setting. Thus if the unmodified instrument has a full scale deflection when the electrochemical current is 20 μA, full scale deflection is achieved after modification when the semiderivative of the electrochemical current is 20 μA $s^{-1/2}$.

EXPERIMENTAL

Hydrates of the salts $Zn(NO_3)_2$, $Cd(NO_3)_2$, $TlNO_3$, $InCl_3$, $Ni(NO_3)_2$, $ZnSO_4$, $Pb(NO_3)_2$, and $CuSO_4$ were used as solutes in either 100 mM KNO_3 or 100 mM KCl. Solutions were prepared by direct weighing of the appropriate quantities of "laboratory grade", "analytical grade", or "special grade" reagents, without further purification. Prior to the electrochemical experiments, solutions were deoxygenated by passage of Ar or N_2 gas.

A hanging mercury drop (Beckman Model 39016) working electrode and a saturated calomel reference electrode were used. Drop areas and radii were calculated from the metered volume of extruded mercury by assuming the electrode to be a perfect sphere. Measurements were made at room temperature, 293–296 K.

The instrumentation was either Circuit A: that described in the prior publication (*1*); or the PAR 170 instrument augmented as described above: Circuit B or Circuit C. Sphericity correction was incorporated into the results obtained using Circuit A, but

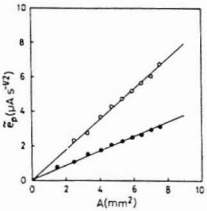

Figure 5. Relationship between peak heights of derivative neopolarograms and electrode area. O: 100 μM Cd^{2+} in 100 mM KNO_3; ●: 100 μM Ni^{2+} in 100 mM KNO_3; scan rate: 100 mV s^{-1}

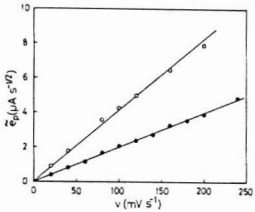

Figure 6. Relationship between peak heights of derivative neopolarograms and scan rate. Solutions: as Figure 5; electrode area: 4.69 mm^2

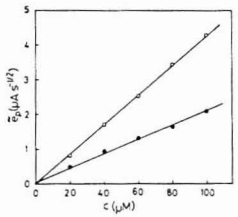

Figure 7. Relationship between peak heights of derivative neopolarograms and concentration of electroactive solutes Cd^{2+} (O) and Ni^{2+} (●). Scan rate: 100 mV s^{-1}; electrode area: 4.69 mm^2; supporting electrolyte 100 mM KNO_3

not into those using Circuits B or C, which were of a more qualitative nature.

RESULTS

Figures 1, 2, and 3 show derivative neopolarograms for an assortment of reversibly and irreversibly reduced cations, using Circuits C, B, and A, respectively. Figure 3 also shows the corresponding linear scan voltammogram and neopolarogram.

Table I predicts a linear dependence of peak height on each of three experimental variables: the electrode area A, the potential scan rate v, and the concentration c of the electroactive species. These proportionalities are tested in Figures 5, 6, and 7 for Cd^{2+} (reversible) and Ni^{2+} (irreversible) reductions. In all cases linearity is satisfactory and the lines pass through the origins.

The slope $d\tilde{e}_p/dc$ for Cd^{2+} in Figure 7 has an experimental value of 43 μA $s^{-1/2}$ m^3 mol^{-1}, compared with a theoretical value, $n^2AF^2vD^{1/2}/4RT$ of 46 μA $s^{-1/2}$ m^3 mol^{-1}, calculated on the basis of a diffusion coefficient (7) of 6.9×10^{-10} m^2 s^{-1}. Similarly for the Ni^{2+} line, the experimental slope $d\tilde{e}_p/dc$ = 21 μA $s^{-1/2}$ m^3 mol^{-1} compares well with the theoretical value $\alpha n^2AF^2vD^{1/2}/3.367RT$ = 20 μA $s^{-1/2}$ m^3 mol^{-1}, based on D = 6.9×10^{-10} m^2 s^{-1} (8) and α = 0.36 [from a plot (9) of ln (m_d − m/i) vs. E]. The slopes of the lines in Figures 5 and 6 are likewise within a few percent of the predicted values.

Table II. Peak Potentials for Cd^{2+} and Ni^{2+} Derivative Neopolarograms

c/μM	$\tilde{E}_p$ for Cd^{2+}/ mV vs. SCE	$\tilde{E}_p$ for Ni^{2+}/ mV vs. SCE
20	−571	−1015
40	−570	−1022
60	−571	−1028
80	−575	−1025
100	−573	−1026
Theoretical (see text)	−578	−1034

Supporting electrolyte: 100 mM KNO_3; scan rate: 100 mV s^{-1}; electrode area: 4.69 mm^2; instrumentation: Circuit A.

Table III. Scan Rate Dependence of the Peak Potential of Cd^{2+} and Ni^{2+} Derivative Neopolarograms

	$\tilde{E}_p$/mV vs. SCE		
v/mV s^{-1}	Cd^{2+} (exptl)	Ni^{2+} (exptl)	Ni^{2+} (theor)
20	−574	−1007	−1001
40	−573	−1015	−1012
60		−1020	−1019
80	−575	−1022	−1024
100	−573	−1026	−1027
120	−576	−1028	−1030
140		−1030	−1033
160	−576	−1035	−1035
180		−1035	−1038
200	−579	−1041	−1039

Supporting electrolyte: 100 mM KNO_3; electroactive concentration: 100 μM; electrode area: 4.69 mm^2; instrumentation: Circuit A.

Table IV. Peak Width Values for Cd^{2+} and Ni^{2+} Derivative Neopolarograms

c/μM	v/mV s^{-1}	A/mm^2	$\tilde{W}_p$ for Cd^{2+}/mV	$\tilde{W}_p$ for Ni^{2+}/mV
20	100	4.69	45	109
40	100	4.69	46	105
60	100	4.69	47	98
80	100	4.69	46	105
100	20	4.69	46	
100	40	4.69	47	98
100	120	4.69	47	103
100	160	4.69	50	101
100	200	4.69		105
100	100	2.48	46	104
100	100	4.02	46	102
100	100	4.69	46	100
100	100	5.31	46	102
100	100	6.47	46	104
100	100	7.53	48	103
		Theoretical:	45	103

Conditions: as Table II.

The derivative neopolarographic peak potentials $\tilde{E}_p$ for the reduction of Cd^{2+} and Ni^{2+} ions were found to be independent of concentration, as shown in Table II, and to average respectively −572 and −1023 mV vs. SCE (the latter value refers to v = 100 mV s^{-1}). The experimental Cd^{2+} peak potential of −572 mV vs. SCE is to be compared with the literature polarographic $E_{1/2}$ value (7) of −578 mV vs. SCE. The $\tilde{E}_p$ for Ni^{2+} of −1023 mV vs. SCE may likewise be compared with the −1034 mV vs. SCE value calculated from the halfwave potential (−980 mV vs. SCE at τ = 4.48 s) in classical polarography (8) by application of the relation in Table I.

For Ni^{2+}, the peak potential should vary with scan rate in accordance with the relationship contained in Table I, while

$\tilde{E}_p$ should be v-independent for Cd^{2+} reduction. Table III reports the experimental data and, in the nickel case, lists the theoretical $\tilde{E}_p$ on the assumption that α equals 0.39. Agreement is within a few millivolts in all cases.

Table IV assesses how well the observed peak widths in semidifferential electroanalysis agree with theoretical predictions. The data refer to the reductions of Cd^{2+} (reversible) and Ni^{2+} (irreversible) in 100 mM KNO_3 supporting electrolyte. The theoretical predictions are again based on Table I.

In addition to the experimental correlations with theory that have just been described, numerous comparisons were also carried out of derivative neopolarographic features with neopolarographic features (*9*). As might be expected, the agreement is even closer than those we have reported above.

DISCUSSION

All theoretical predictions concerning semidifferential electroanalysis have been adequately confirmed.

It is evident from Figures 1 through 3 that semidifferential electroanalysis provides an attractive and efficient method for the identification and assay of electroactive solute species. Features of the method that should be noted include: ease of correction for electrode sphericity; the independence of the measured response on any prior electrode process that may have occurred; the good resolution (see Figure 2) between adjacent peaks; the marked dependence of peak shape on electron number; the fact that the "gain" of the method is adjustable by changing the scan rate; the distinguishability of irreversible from reversible peaks because of the independence of peak potential on scan rate for reversible electroreductions; and the possibility of exploiting v-dependence in irreversible cases to separate two peaks that would otherwise overlap. Though this entire article is couched in terms of cathodic processes, it is evident that the conclusions are easily widened to embrace electrooxidations.

The readout in semidifferential electroanalysis resembles a differential pulse polarogram. In fact, the two techniques have much in common. Thus, for reversible processes, the peak shape is exactly the same in the two techniques (*10*), so that the peak potentials and peak widths coincide (for small enough pulse amplitudes ΔE). Moreover, very similar factors enter into the determination of the peak height, as will be apparent on comparison of the first entry in Table I with the corresponding expression,

$$\frac{n^2F^2AcD^{1/2}}{4RT}\frac{\Delta E}{\sqrt{\pi t}}$$

for the peak height in differential pulse polarography. One feature in which semidifferential electroanalysis excels is the speed with which a determination can be made: one second may suffice for the complete run.

The method suffers from the disadvantages inherent in the use of hanging mercury drop electrodes and, in this connection, one thinks particularly of surface contamination of the mercury by adsorbable impurities. Though we have not attempted to implement it, one solution to this difficulty would be to adapt semidifferential electroanalysis to the later stages in the life of a dropping mercury electrode. In fact, as long ago as 1959, Barker (*11*) made essentially the same suggestion as a means of improving the readout in linear scan voltammetry at a dropping electrode.

Experiments with Cd^{2+} at dilutions much greater than those reported above suggest a detection limit in semidifferential electroanalysis of about 100 nM: this is comparable to the limit cited by Bond (*12*) for differential pulse polarography, though detection limits as low as 10 nM have been claimed (*13*) for this pulse technique. A less empirical method of assessing the lowest detectable concentration is to compare the faradaic signal e_p with the background signal arising from interfering effects. If we take the latter to be predominantly the nonfaradaic contribution from charging the capacitance C_d of the double layer, then the magnitude of the interference can be found by semidifferentiating the expression

$$i_{nf} = -AC_d(dE/dt) = AC_d v$$

for the nonfaradaic current, to give

$$e_{nf} = AC_d v/(\pi t)^{1/2} = AC_d v^{3/2}/\pi^{1/2}(E_o - E_p)^{1/2}$$

as the capacitative contribution to the semiderivative at the peak potential. The detection limit may now be compared with the concentration at which the faradaic contribution to the signal equals 10% of the total signal. Using Table I we find this concentration to be

$$\frac{0.44\,RTC_d v^{1/2}}{\pi^{1/2}n^2F^2D^{1/2}(E_o - E_p)^{1/2}}$$

for a reversible peak. Notice the squareroot dependence on the scan rate, and the inverse squareroot dependence on the length E_0–E_p of the potential range available prior to the peak. Taking $n = 2$, $C_d = 0.2$ F m^{-2}, $D = 1 \times 10^{-9}$ m^2 s^{-1}, E_0–E_p = 0.5 V, and $v = 0.1$ V s^{-1}, this formula gives 50 nM, close to the detection limit found empirically. Decreasing the scan rate should permit even lower concentrations to be detected.

ACKNOWLEDGMENT

We are grateful to Daido Ishii for his helpful advice, and to Ian Williams for computational assistance.

LITERATURE CITED

(1) M. Goto and D. Ishii, *J. Electroanal. Chem.*, **61**, 361 (1975).
(2) P. Dalrymple-Alford, M. Goto, and K. B. Oldham, *J. Electroanal. Chem.*, in press.
(3) R. S. Nicholson and I. Shain, *Anal. Chem.*, **36**, 706 (1964).
(4) M. Grenness and K. B. Oldham, *Anal. Chem.*, **44**, 1120 (1972).
(5) K. B. Oldham and J. Spanier, "The Fractional Calculus", Academic Press, New York, 1974.
(6) K. B. Oldham, *Anal. Chem.*, **45**, 39 (1973).
(7) J. Heyrovsky and J. Kuta, "Principles of Polarography", Academic Press, New York, 1965.
(8) P. Kivalo, K. B. Oldham, and H. A. Laitinen, *J. Am. Chem. Soc.*, **75**, 4148 (1953).
(9) M. Goto and K. B. Oldham, *Anal. Chem.*, **45**, 2043 (1973).
(10) E. P. Parry and R. A. Osteryoung, *Anal. Chem.*, **37**, 1634 (1965).
(11) G. C. Barker, "Proceedings of the Second International Congress on Polarography, Cambridge 1959", Pergamon Press, London, 1960, p 140.
(12) A. M. Bond, *Anal. Chim. Acta*, **74**, 163 (1975).
(13) G. C. Barker and A. W. Gardner, *Fresenius' Z. Anal. Chem.*, **79**, 173 (1960).

RECEIVED for review July 9, 1976. Resubmitted January 26, 1977. Accepted May 2, 1977. The authors thank the National Research Council of Canada for continuing support, and the United Kingdom Science Research Council for the award of a Senior Visiting Fellowship.

Carbon and Mercury–Carbon Optically Transparent Electrodes

Thomas P. DeAngelis,[1] Roger W. Hurst, Alexander M. Yacynych,[2] Harry B. Mark, Jr., and William R. Heineman*

Department of Chemistry, University of Cincinnati, Cincinnati, Ohio 45221

James S. Mattson

Center for Experiment Design and Data Analysis, Environmental Data Service, National Oceanic and Atmospheric Administration, Washington, D.C. 20235

A carbon optically transparent electrode (C OTE) has been prepared by vapor-depositing a thin carbon film (150–310 Å thick) on glass and quartz. The electrode properties are similar to those of a conventional graphite electrode with a higher resistance (1000–1700 Ω/□). Optical transparency is good throughout the ultraviolet–visible region. Electrochemical and spectroelectrochemical measurements were made with ferricyanide and *o*-tolidine respectively. The C OTE serves as a good substrate for deposition of a thin mercury film (15–25 Å) to form a mercury film transparent electrode (Hg-C OTE). The Hg-C OTE exhibits electrochemical properties of conventional mercury film electrodes as evidenced by Pb^{2+} cyclic voltammograms. The Hg-C OTE enabled the spectroelectrochemical characterization of cysteine oxidation, which was shown to involve the oxidation of mercury to form mercurous cysteinate.

Optically transparent electrodes (OTEs) have proved useful in spectroelectrochemical studies of a variety of redox systems (*1–3*). Various types of OTEs have been prepared and characterized in the past several years (*1*). OTEs consisting of very thin conductive films of Pt, Au, SnO_2, and InO_2 which are deposited on glass or quartz substrates have been used extensively; gold minigrids have proved to be especially adaptable to the thin-layer cell configuration; germanium plates have been used for infrared studies. OTEs with mercury characteristics have been formed by electrodepositing thin films of mercury onto Pt OTEs and Au and Ni minigrids.

One of the most useful electrode materials is carbon or graphite, which exhibits good positive and negative potential ranges (*4, 5*). Past attempts to prepare carbon/graphite OTEs have been thwarted by poor adhesion between the vapor-deposited carbon film and the substrate (*6*). Recently, an OTE consisting of a thin carbon film deposited on a germanium substrate was prepared and used successfully for infrared spectroelectrochemical measurements in aqueous solutions (*7, 8*). We report here the characterization of an OTE formed by depositing a thin layer of carbon onto a glass or quartz substrate (C OTE). This electrode enables ultraviolet–visible spectroelectrochemical measurements to be made on an electrode surface which is similar to that of the conventional graphite electrode.

Graphite and glassy carbon electrodes have been used extensively as substrates for mercury film electrodes, especially in anodic stripping voltammetry (*9–11*). The usefulness of graphite and carbon for this purpose is attributable to their inertness towards mercury. This minimizes contamination of the mercury film by a mercury-soluble substrate. The development of the C OTE has made possible the preparation of a transparent mercury electrode by electrodepositing a very thin mercury film onto a C OTE. This Hg-C OTE minimizes the problems of substrate amalgamation which affect other mercury OTEs utilizing platinum (*12*), nickel (*13*), and gold (*14*) as substrates. We report here the preparation and characterization of such a Hg-C OTE and its use in a spectroelectrochemical examination of the mechanism of cysteine oxidation.

EXPERIMENTAL

Apparatus. Carbon film OTEs were prepared commercially (Lebow Company, 1407 Norman Firestone Road, Goleta, Calif. 93017) by evaporating carbon with an electron beam technique onto specially prepared glass and quartz microscope slides according to the procedure described by Mattson and Smith for deposition onto germanium (*7*). Electrodes with a film thickness of 150 to 160 Å were prepared by a single deposition of carbon (A and E in Table I). Electrodes with film thicknesses of 280 to 310 Å were prepared by two separate depositions of ca. 150 Å each. Electrodes were also prepared by deposition onto substrates at 450 °C (A, B, and C) and at room temperature (D and E).

The design and assembly of the optically transparent electrochemical cell has been described (*12*). The potentiostat used for electrochemical experiments was a Princeton Applied Research Model 173 potentiostat–galvanostat with a Model 179 digital coulometer. All potentials were measured vs. a saturated calomel electrode which was isolated from the solution by a thirsty glass plug. Spectra of the C OTEs were recorded on a Cary Model 14 spectrometer. Spectra of *o*-tolidine oxidation were taken with a Harrick Rapid Scanning Spectrometer, Model RSSB (Harrick Scientific Co., Ossining, N.Y.) and recorded on a Houston Instruments 2000 x-y recorder. Transmittance changes at a set wavelength were measured in a spectrometer consisting of a tungsten lamp source, a Schoeffel GM 100 miniature grating monochromator, and an Emitronics #T124 PMT connected to an operational amplifier current to voltage converter. Voltage output was monitored with a Digitec 261 Digital VOM and transmittance-current–potential curves were recorded with a Hewlett-Packard 136A X-Y,Y recorder.

Reagents. The 1.00 mM ferricyanide solution was prepared by dissolving potassium ferricyanide (Allied Chemical) in 1 M KNO_3. The 1.00 mM *o*-tolidine in 0.5 M acetic acid, 1.0 M $HClO_4$ was prepared by dissolving the *o*-tolidine (Aldrich) first in concentrated acetic acid and then diluting almost to volume with distilled water before adding concentrated perchloric acid. Pb^{2+} solutions were prepared by the appropriate dilution of 1000 ppm Fisher atomic absorption standard in 0.5 M KNO_3. The 3 mM mercurous ion solution was prepared by dissolving $HgNO_3 \cdot H_2O$ (Baker Analyzed) in 0.5 M KNO_3. Solutions of cysteine were prepared with L-cysteine hydrochloride hydrate (Aldrich) in 0.1 M $HClO_4$.

Procedure. The carbon film OTE was thoroughly rinsed with 95% ethanol and then with distilled, deionized water immediately before being subjected to five minutes of radiofrequency discharge cleaning (Plasma Cleaner, Harrick Scientific Company, Ossining, N.Y.). The cell was then assembled as previously described (*12*). Deaerated solution was injected into the cell through the SCE port. The SCE, separated from the analyte solution by a thirsty glass plug (Vycor Glass, Corning Glass Company, Corning, N.Y.), was then placed in the cell. The area of electrode exposed to

[1] Present address, Corning Glass Works, Corning, N.Y. 14830.
[2] Present address, Department of Chemistry, Ohio State University, Columbus, Ohio 43210.

Table I. Characteristics of Carbon Film OTEs

Electrode[a]	No. of depositions	Substrate temperature, °C	Carbon film thickness, Å	Carbon film resistance, Ω/□	Absorbance at 540 nm	Cyclic voltammetry ΔE_p, mV[b]
A	1	450	150	1 700	0.472	112
B	2	450	280	1 000	0.625	110
C	2	450	280	1 000	0.602	120
D	2	~25	310	44 000	0.440	540
E	1	~25	160	51 000	0.300	

[a] A, B, D, and E deposited on glass substrate. C deposited on quartz substrate. [b] 1.00 mM ferricyanide, 1.0 M KNO_3. Scan rate = 10 mV s^{-1}.

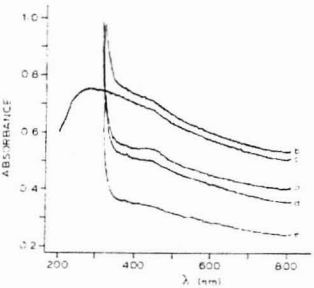

Figure 1. Absorbance spectra for C OTEs prepared by several procedures. See Table I for description of electrodes (A–E)

solution was approximately 0.8 cm^2. Before each new solution was added, the cell was thoroughly rinsed with distilled, deionized water.

The Hg-C OTE was prepared by depositing mercury from a 3 mM $HgNO_3$, 0.5 M KNO_3 solution onto a C OTE. Deposition was accomplished by stepping the potential to −0.7 V vs. SCE for ca. 2 min with the solution unstirred. The cell was then open-circuited and rinsed thoroughly with distilled water.

RESULTS AND DISCUSSION

Carbon OTE. Table I summarizes characteristics of several C OTEs. The electrodes were prepared on both glass microscope slides (electrodes A, B, D, E) and quartz (electrode C) substrates. The effect of substrate temperature during the deposition procedure was evaluated by preparing electrodes with substrates at room temperature (D, E) and at 450 °C (A, B, C). Comparison of the electrical resistance for the various electrodes shows that the resistance decreases as the thickness of the carbon film increases. However, the resistance of the electrodes prepared with the substrate at room temperature is ca. 50 times greater than those with the substrate at 450 °C. Evidently, deposition on a hot substrate is very important for minimizing electrode resistance. The resistances of the electrodes prepared with the hot substrate were 1000 to 1700 Ω/□, depending on the film thickness. This is substantially greater than the resistances of Pt, Au, SnO_2, and InO_2 film OTEs which are typically 5–20 Ω/□ (*1*). The resistances of the electrodes prepared for this study are within a factor of ×2 of the expected resistance for graphite films (490 Ω/□ for a 280-Å film) based on the resistivity of pure graphite.

The optical properties of the C OTEs depended upon film thickness and substrate. Spectra in the ultraviolet–visible range for several electrodes are shown in Figure 1. Electrodes with film thicknesses of 280 Å exhibit an absorbance varying from 0.5 to 0.7 over the optical range of 840 nm to 350 nm. Electrodes with glass substrates absorb strongly below 350 nm, whereas quartz substrates extend the optical range to below 200 nm. This transparency is comparable to that reported for Pt and Au film OTEs (*1*). With a quartz substrate, the C OTE is useable throughout the ultraviolet–visible range.

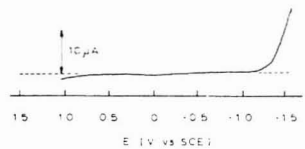

Figure 2. Current-potential curve at the carbon-film OTE; pH 10 carbonate–borate buffer, 0.5 M KNO_3; scan rate 20 mV s^{-1}

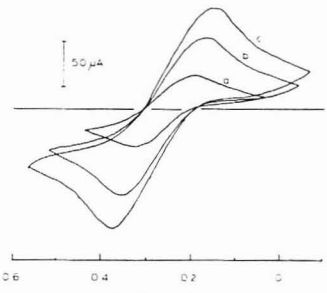

Figure 3. Cyclic voltammograms of 1 mM ferricyanide, 0.1 M KNO_3 at C OTE. Film thickness = 280 Å. Scan rates (*a*) 10 mV s^{-1}, (*b*) 50 mV s^{-1}, (*c*) 100 mV s^{-1}

Observation of the electrode surfaces by scanning electron microscopy revealed a smooth carbon surface with no observable pinholes or irregularities for both the singly and doubly deposited films on substrates at 450 °C.

The electrochemical properties of the carbon OTE were similar to those of bulk graphite electrodes. Figure 2 shows a current–potential curve for a pH 10.0 carbonate–borate buffer. The electrode exhibits low residual current throughout a wide potential window which extends well into both the positive and negative regions. The film was very stable under conditions of repeated potential cycling in aqueous media of varying pH. Mild hydrogen evolution did not disintegrate the film as in the case of Pt OTEs, although vigorous evolution of hydrogen led to separation of the film from the glass substrate around the edges. Generation of oxygen at large positive potentials caused immediate disintegration of the carbon film.

Typical cyclic voltammograms on a C OTE with a 280 Å-thick film for ferricyanide at various scan rates are shown in Figure 3. The voltammograms at slow scan rates are similar to those reported at the graphite electrode (*15*). The cathodic and anodic peak separation (ΔE_p) is greater than the expected 0.059 V, due to the resistance of the carbon film, and increases with faster scan rates because of the larger currents. The $E^{\circ\prime}$

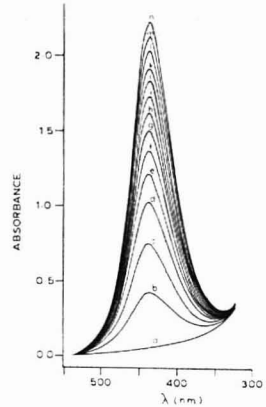

Figure 4. Spectra recorded during oxidation of *o*-tolidine at C OTE (280-Å film) by potential step to +0.8 V vs. SCE in quiescent solution. 1.00 mM *o*-tolidine, 0.5 M acetic acid, 1.0 M $HClO_4$. (*a*) 0, (*b*) 5, (*c*) 10, (*d*–*n*) 10-s intervals

(obtained by averaging the anodic and cathodic peak potentials) of +0.263 V vs. SCE agrees well with that obtained by other workers on bulk graphite (*15*). Values for ΔE_p obtained from ferricyanide voltammograms are shown in Table I for the various electrodes. Comparison of the values for film thicknesses of 150 Å and 280 Å shows only a small improvement for the thicker film. However, the greatly increased resistance of electrode D, which was deposited on room temperature substrates, gives a much larger ΔE_p value.

The utility of the C OTE for spectroelectrochemical measurements was demonstrated with *o*-tolidine, which undergoes a $2e^-$ oxidation to form a yellow product (*16*, *17*). Figure 4 shows a series of spectra recorded through a C OTE during generation of the yellow oxidation product by a potential step to +0.800 V vs. SCE. The optical transparency of the C OTE is sufficiently great that such spectral changes are easily measured. A plot of absorbance (at λ_{max} = 438 nm) vs. $t^{1/2}$ was linear over a range of 5 to >100 s, which indicates a diffusion-controlled oxidation of *o*-tolidine at the C OTE (*1*–*3*). The slope of the plot was 0.19 $s^{-1/2}$. A value for ϵ of 3.7×10^4 M^{-1} cm^{-1}, which was determined for the yellow product by thin-layer spectroelectrochemical techniques (*18*), gives a diffusion coefficient of 2.0×10^{-5} cm^2 s^{-1} for *o*-tolidine. A negative deviation from linearity occurred for times of less than about 4 s. This is attributed to the resistance of the carbon film. Quantitative response for faster times necessitated the use of positive-feedback *iR* compensation.

As illustrated by the results presented above, a stable carbon OTE can be prepared by the procedure described by Mattson and Smith for a carbon–germanium OTE. Optical transparency is sufficient for good spectroelectrochemical measurements in the ultraviolet–visible range. The rather large film resistance presented no difficulty in this characterization; however, it would certainly limit the usefulness of the C OTE in the spectroelectrochemical measurement of fast homogeneous chemical reactions where rapid charging of the electrode is essential (*2*, *3*).

Mercury–Carbon OTE. Transparent mercury electrodes (Hg-C OTE) were prepared by electrodepositing thin mercury films on the carbon OTEs. The best Hg-C OTEs were prepared by deposition at –0.7 V vs. SCE with a solution of Hg_2^{2+} rather than Hg^{2+}. In both cases the transmittance of the OTE decreased as the mercury film was deposited.

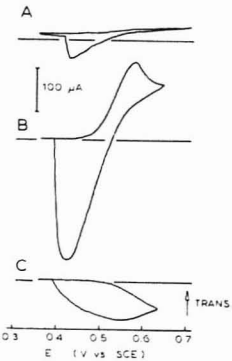

Figure 5. (*A*) Cyclic voltammogram of Pb^{2+} at C OTE. (*B*) Cyclic voltammogram of Pb^{2+} at Hg-C OTE. (*C*) Transmittance–potential behavior at Hg-C OTE during cyclic voltammogram of Pb^{2+}. 2.42 mM Pb^{2+}, pH 4.0 acetate buffer

However, in the case of Hg^{2+} reduction, the transmittance increased when the cell was open-circuited immediately after mercury deposition, indicating dissolution of some of the deposited mercury. This loss of mercury from the film occurred at a diffusion-controlled rate as indicated by linearity of an absorbance–$t^{1/2}$ plot (*1*). The mercury loss is attributed to the following reproportionation (*19*):

$$Hg^0(\text{electrode}) + Hg^{2+}(\text{solution}) \rightleftarrows Hg_2^{2+}(\text{solution}) \quad (1)$$

This reaction is controlled by the rate of diffusion of Hg^{2+} in the plating solution to the electrode surface for reaction with Hg^0. The loss of the mercury film precluded preparation of a satisfactory Hg-C OTE by reduction of Hg^{2+}. Consequently, deposition from a solution of Hg_2^{2+} was used to prepare all Hg-C OTEs used in this study.

The thicknesses of the mercury films on the Hg-C OTEs were typically 15–25 Å. This increased the absorbance of the OTE by only about 0.05 a.u. above the absorbance of the C OTE. Thus, good optical transparency was retained by coating with very thin mercury films.

Examination of the Hg-C OTE surface by reflectance microscopy revealed a mercury deposit existing as droplets, similar to that shown in Figure 2 of reference (*20*). These droplets could not be coalesced by the evolution of hydrogen, a procedure which is successful on bulk platinum (*21*).

The electrochemical characteristics of the Hg-C OTE are similar to those which have been reported for mercury films on bulk carbon and graphite substrates (*20*, *22*). The negative potential range was less than that of pure mercury as a result of the exposed carbon between mercury droplets. The mercury film could be repeatedly stripped off and redeposited with no apparent damage to the carbon film.

The conversion from solid carbon to liquid mercury electrode behavior is evident by comparison of the two cyclic voltammograms for Pb^{2+} in Figure 5. The reduction wave for Pb^{2+} on the carbon OTE is very poorly defined and the Pb stripping wave greatly skewed (Figure 5*A*). By contrast the well-defined voltammogram on the Hg-C OTE (Figure 5*B*) is typical of that obtained on mercury film electrodes used for anodic stripping voltammetry [e.g., curve 1 in Figure 3 of reference (*22*)]. The accumulation of Pb in the mercury droplets could be monitored optically as shown by the transmittance-voltammogram in Figure 5*C*. All of the Pb^0 is removed from the mercury during the positive potential scan

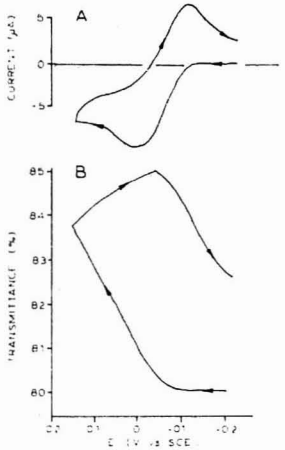

Figure 6. Spectroelectrochemistry of cysteine at Hg-C OTE. 2.00 mM cysteine, 0.1 M $HClO_4$; scan rate 10 mV s^{-1}. (*A*) Cyclic voltammogram. (*B*) Transmittance–potential response of Hg-C OTE during cyclic voltammogram

as evidenced by return of the transmittance to its original value.

The C OTE serves as a good substrate for a transparent mercury film electrode. The inertness of the carbon toward the overlying mercury film eliminates the time-dependent amalgamation of Pt, Ni, and Au substrates which contaminates the mercury with varying amounts of intermetallic compounds such as $PtHg_x$ in the Hg-Pt OTE. The Hg-C OTE is also much more tolerant of hydrogen evolution than is the Hg-Pt OTE. It can be used not only to impart mercury character to the electrode, but also to investigate the participation of mercury itself in an electrochemical reaction as illustrated in the next section.

Cysteine Oxidation at the Mercury–Carbon OTE. The oxidation waves of certain organic and inorganic compounds at mercury involve the oxidation of the electrode itself rather than the compound. An example of this is the oxidation wave for cysteine which has been studied by Kolthoff and Barnum (*23*). At a platinum electrode, cysteine (RSH) undergoes oxidation to form cystine (RSSR) by the following mechanism:

$$2\,RSH \rightleftharpoons RSSR + 2H^+ + 2e^- \qquad (2)$$

However, at the dropping mercury electrode, the oxidation wave occurs at a potential which is 600 mV more negative than on platinum. To account for this large potential shift, the formation of soluble mercurous cysteinate by the following electrode mechanism was proposed:

$$RSH + Hg \rightleftharpoons HgSR + H^+ + e^- \qquad (3)$$

The Hg-C OTE enables the participation of Hg in the oxidation mechanism of cysteine to be optically observed by light passing through the electrode. According to reaction 3, the optical transparency of the Hg-C OTE should increase because of loss of mercury as the electrode potential is positively scanned through the oxidation wave. Since liquid mercury attenuates light throughout the visible range, any visible wavelength is suitable for the optical experiment. Figure 6 shows the current and optical response as the potential is cycled through the oxidation peak and then back through the reduction peak. Indeed, the transmittance of the Hg-C OTE increases during the positive scan in which HgSR is formed and then decreases during the negative scan after the potential for HgSR reduction is reached (ca. −50 mV) and mercury redeposits on the OTE. This directly confirms a mechanism which involves oxidation of the mercury electrode such as the one postulated by Kolthoff and Barnum in Equation 3.

This example illustrates the potential utility of the Hg-C OTE for investigating mechanisms of electrode reactions in which mercury is directly involved. Analogously, the Pt OTE and Au OTE could also be used to observe electrode mechanisms which involve oxidation of these materials.

CONCLUSION

The C OTE and Hg-C OTE are electrodes with good optical transparency, thereby adding to the growing number of OTEs available. The electrode properties are similar to those of bulk graphite electrodes and conventional mercury film electrodes deposited on bulk graphite or carbon substrates, although the resistance is higher. Because of the inertness of the carbon substrate, the Hg-C OTE is in many respects a superior mercury OTE compared to the Hg-Pt, Hg-Ni, and Hg-Au OTEs which are extensively amalgamated with the substrate. The cysteine oxidation illustrates the utility of OTEs for directly observing electrode involvement in a mechanism by optically monitoring the transparency of the electrode itself. This demonstrates a new aspect of OTE applicability which has not previously been utilized. The carbon OTE is potentially useful for spectroelectrochemical studies with chemically modified graphite and carbon electrodes (*24–26*).

ACKNOWLEDGMENT

The authors gratefully acknowledge J. P. Haberman and D. A. Hudson, The Procter and Gamble Company, Cincinnati, Ohio, for scanning electron microscope photographs.

LITERATURE CITED

(1) T. Kuwana and W. R. Heineman, *Acc. Chem. Res.*, **9**, 241 (1976).
(2) N. Winograd and T. Kuwana, in "Electroanalytical Chemistry", Vol. 7, A. J. Bard, Ed., Marcel Dekker, New York, N.Y., 1974.
(3) T. Kuwana, *Ber. Bunsenges. Phys. Chem.*, **77**, 858 (1973).
(4) R. N. Adams, "Electrochemistry at Solid Electrodes", Marcel Dekker, New York, N.Y., 1969.
(5) P. T. Kissinger, *Anal. Chem.*, **46**, 15R (1974).
(6) W. R. Heineman, unpublished results.
(7) J. S. Mattson and C. A. Smith, *Anal. Chem.*, **47**, 1122 (1975).
(8) J. S. Mattson and T. T. Jones, *Anal. Chem.*, **48**, 2164 (1976).
(9) W. R. Matson, D. K. Roe, and D. E. Carritt, *Anal. Chem.*, **37**, 1594 (1965).
(10) T. M. Florence, *J. Electroanal. Chem.*, **27**, 273 (1970).
(11) T. R. Copeland, J. H. Christie, R. A. Osteryoung, and R. K. Skogerboe, *Anal. Chem.*, **45**, 2171 (1973).
(12) W. R. Heineman and T. Kuwana, *Anal. Chem.*, **43**, 1075 (1971); **44**, 1972 (1972).
(13) W. R. Heineman, T. P. DeAngelis, and J. F. Goelz, *Anal. Chem.*, **47**, 1364 (1975).
(14) M. L. Meyer, T. P. DeAngelis, and W. R. Heineman, *Anal. Chem.*, **49**, 602 (1977).
(15) R. Panzer and P. J. Elving, *J. Electrochem. Soc.*, **119**, 864 (1972).
(16) W. N. Hansen, T. Kuwana, and R. A. Osteryoung, *Anal. Chem.*, **38**, 1810 (1966).
(17) R. W. Murray, W. R. Heineman, and G. W. O'Dom, *Anal. Chem.*, **39**, 1666 (1967).
(18) T. P. DeAngelis and W. R. Heineman, *J. Chem. Educ.*, **53**, 594 (1976).
(19) F. A. Cotton and G. Wilkinson, "Advanced Inorganic Chemistry", 3rd ed., Interscience Publishers, New York, N.Y., 1972, p. 509.
(20) M. Stulikova, *J. Electroanal. Chem.*, **48**, 33 (1973).
(21) A. M. Hartley, A. G. Hiebert, and J. A. Cox, *J. Electroanal. Chem.*, **17**, 81 (1968).
(22) Z. Stojek, B. Stepnik, and Z. Kublick, *J. Electroanal. Chem.*, **74**, 277 (1976).
(23) I. M. Kolthoff and C. Barnum, *J. Am. Chem. Soc.*, **62**, 3061 (1940).
(24) B. F. Watkins, J. R. Behling, E. Kariv, and L. L. Miller, *J. Am. Chem. Soc.*, **97**, 3549 (1975).
(25) C. M. Elliott and R. W. Murray, *Anal. Chem.*, **48**, 1247 (1976).
(26) M. Fujihira, A. Tamura, and T. Osa, *Chem. Lett.*, **1977**, 361.

RECEIVED for review December 22, 1976. Accepted May 31, 1977. The authors acknowledge financial support provided by National Science Foundation Grants CHE74-02641 (W.R.H.) and CHE76-04321 (H.B.M.). T.P.D. acknowledges the financial support of the University of Cincinnati Research Council.

Evaluation of a Cesium Primary Ion Source on an Ion Microprobe Mass Spectrometer

Peter Williams* and R. K. Lewis[1]

Materials Research Laboratory, University of Illinois, Urbana, Illinois 61801

Charles A. Evans, Jr.

Materials Research Laboratory and School of Chemical Sciences, University of Illinois, Urbana, Illinois 61801

P. R. Hanley

General Ionex Corp., Ipswich, Massachusetts 01938

A commercially available Cs^+ ion source has been modified for use as the primary ion source on an ion microprobe mass spectrometer. The primary ion current is stable to ~1% over a 1-h period. Up to 1000 h operation is achieved on a single charge of cesium. Current densities of 10 mA cm^{-2} or better are achieved in microfocused spot sizes ranging from 8 μm to 30 μm. Secondary negative ion yields of electronegative species under Cs^+ ion bombardment compare favorably with positive ion yields of electropositive species under O_2^+ ion bombardment. Sputtering rates of Si and GaAs are 2 and 5 times faster respectively than O_2^+ sputtering rates for these substrates. These high sputtering rates facilitate rapid depth profiling analyses. Detection limits have been determined under sample-limited depth profiling conditions for H, C, O, F, and As in Si, and for S in GaAs.

The generation of sputtered ions of solid materials by energetic ion bombardment has become a versatile and sensitive technique for surface and thin film analysis (*1*). Although noble gas primary ions can be used to bombard the sample, it has been known for many years that the yield of positive secondary ions is greatly enhanced by bombardment with electronegative species such as oxygen (*2*, *3*). Duoplasmatron ion sources capable of producing intense oxygen ion beams are now standard on ion microprobes. It has long been known that cesium ion bombardment or the presence of cesium on an ion-bombarded surface leads to the enhancement of negative secondary ion yields (*4*, *5*). Reliable cesium ion sources have been developed in recent years, for space thruster applications (*6*) and, more recently, as components of negative ion sources for particle accelerators (*7*, *8*). A specially designed cesium ion source has recently been operated on an ion microprobe (Applied Research Laboratories IMMA) with very promising results (*9*). We have adapted a commercially available cesium ion source to our ion microprobe (AEI Scientific Apparatus, Manchester, England, Model IM20 (*10*)) in order to evaluate the performance of the source for surface and thin film analysis.

SOURCE DESCRIPTION

The cesium ion source used in this study is based on a part of the "Hiconex" particle accelerator ion source (General Ionex Corp., Ipswich, Mass.). The source, shown schematically in Figure 1, is of the surface ionization type. Cesium metal is vaporized in the stainless steel reservoir which is maintained at ~260 °C, and diffuses via the feed tube to a porous tungsten frit which is maintained at 1100–1200 °C. At this temperature, approximately 99% of the cesium evaporated from the outer surface of the frit is ionized (*11*), and the ionization efficiency is insensitive to small temperature changes. Heat conduction from the frit heater maintains the molybdenum feed tube at a temperature intermediate between those of the reservoir and frit. The frit and frit heater are held by a beam-forming electrode which ensures that the emitting surface is maintained concentric with the axis of the source housing.

The source housing is machined from aluminum and has the approximate dimensions (8-inch diameter by 5 inches deep) of the standard duoplasmatron on the ion microprobe. The Freon cooling system of the duoplasmatron is adequate to cool the cesium source housing. The Freon serves as an electrically insulating heat transfer medium, not as a refrigerant.

A solid stub projects from the reservoir. A hollow copper cooling block is clamped to the stub and is connected to the source housing by $^1/_8$-in. o.d. copper tubing. Heat conduction through the copper tubing to the source housing aids in the temperature regulation of the reservoir. (The source is otherwise very well thermally isolated.) This arrangement ensures that the coolest part of the system is the reservoir which thereby controls the cesium vapor pressure. Freon may be circulated through the cooling block to facilitate rapid shut-down of the source.

For operation on the ion microprobe, it is necessary that the source be floated at +15 to +20 kV relative to ground. Power requirements for the reservoir and frit heater are 40 W and 350 W, respectively. In these preliminary experiments, the source has been satisfactorily powered by unregulated "Variac"-controlled supplies.

ION MICROPROBE MODIFICATIONS

Only one modification to the ion microprobe was required. The "Hiconex" source requires a negative ion suppressor electrode immediately following the ion extraction electrode to suppress negative ions which are sputtered fron apertures in the primary ion optical system. These sputtered negative ions can backstream up the Cs^+ ion beam and rapidly damage the frit by sputtering. It was not convenient to install an additional electrode in the ion microprobe column because no spare electrical feedthroughs were available. Instead, the four primary beam steering plates, which were located in a suitable position to serve as a suppressor, were operated at −600 V relative to ground. This arrangement was entirely satisfactory in protecting the frit from damage. The additional lens action of the steering plate assembly introduced no detectable image aberrations when this arrangement was tested with the standard duoplasmatron ion source.

[1] Present address, Department of Geological and Planetary Sciences, California Institute of Technology, Pasadena, Calif. 91125.

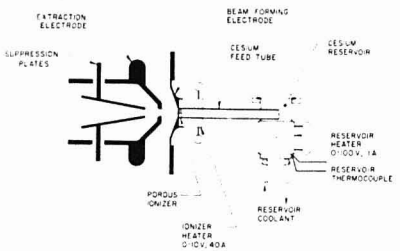

Figure 1. Schematic of cesium ion gun as mounted on AEI IM20 ion microprobe

OPERATION

Typically, the source is loaded with a 5-g charge of cesium. Loading is accomplished in a glove bag containing argon. A sealed glass vial of cesium is heated outside the glove bag to melt the cesium. The vial is then transferred into the glove bag, the seal is broken, and the cesium poured into the reservoir. The reservoir seal is accomplished with a knife-edge flange of the "Conflat" design and a copper gasket. The large frit area allows rapid pump-out of argon trapped in the oven and transfer tube.

The source was originally designed to operate on a horizontal beam line with the transfer tube horizontal and the copper gasket seal at the top of the reservoir away from the molten cesium. Since the IM20 primary ion column is vertical, it is necessary for us to operate the source with the transfer tube vertical and the reservoir on its side, which allows the molten cesium to come into contact with the copper gasket. After several hundred hours of operation, some erosion of the gasket was noted. Copper was found to be plated onto the interior of the reservoir. Since the seal remained intact and since copper does not surface ionize at 1100 °C or poison the ionizer, this erosion poses no contamination problems. However, a new style reservoir is being designed with the gasket reoriented so that it does not contact the liquid cesium. This will eliminate erosion of the gasket.

The source has proved to be remarkably resistant to degradation through exposure to the atmosphere. When the system was vented with argon, the source could be handled in air for an hour or so with no deleterious effect. In addition, after a vacuum accident which vented the system to the atmosphere for 24 h, a useable Cs^+ current could still be obtained after pump down. In the absence of such accidents, a single charge of cesium should last for over 1000 h. When the source was cleaned after several hundred hours of operation, it was estimated that most of the original cesium charge still remained in the reservoir.

Contrary to our expectations, cesium contamination of the primary ion column was almost negligible. The major deleterious effect after several hundred hours of operation with a total Cs^+ current of 1–2 mA was the formation of sputtered metal films inside the extraction electrode assembly. These films eventually flaked off and could short the accelerating gap. When the standard duoplasmatron was reattached to the column and used to produce *negative* oxygen ions, small amounts of cesium on the source mounting flange initially caused excessive field electron emission at −20 kV. This problem disappeared after 1 day.

PRIMARY ION BEAM PERFORMANCE

A freshly cleaned and charged source will deliver ~65 nA into a beam 20 μm in diameter (~20 mA cm^{-2}). Over a period of several hundred hours, a current density of ~10 mA cm^{-2} is routinely attainable. These current densities compare favorably with duoplasmatron performance. Current density is roughly independent of beam size down to the smallest beam diameter used in our instrument (~8 μm). After a 1-h warmup period, current stability is typically better than 1% over an hour. The source is not subject to the high frequency oscillations that can occur in duoplasmatrons and the high thermal inertia of the structure precludes short-term drift. The filament for the frit heater is wound in a bifilar fashion to minimize the production of stray magnetic fields. The 35-A ac heater current produces no detectable 60-cycle modulation of the primary beam position at spot sizes down to 8 μm.

Table I. Elemental Sensitivities under Cs^+ Bombardment[a] (mass analyzed counts/s/nA of Cs^+)

Element (matrix)	Count rate
Si (Si)	9×10^5
As (GaAsP)	1×10^4
As[b] (Si)	2×10^6
P (GaAsP)	4×10^4
P[b] (Si)	3×10^5
H[b] (Si)	8×10^5
O[b] (Si)	7×10^6
C[b] (Si)	4×10^6
S[b] (GaAs)	4×10^6

[a] Normalized to 100 at % concentration. [b] Species present at <1% concentration.

ANALYTICAL PERFORMANCE

Sputtering Performance. When compared with oxygen ion bombardment, cesium ion bombardment at 20-keV impact energy sputters GaAs approximately five times faster and Si about twice as fast. These high sputtering rates result in a valuable reduction in the time required for depth profiling analyses. Cesium ions have a projected range in solid materials of about 60% of that of O_2^+ ions of the same energy. Thus the extent in depth of ion-induced mixing is reduced. Examination in the scanning electron microscope revealed no roughening or cone formation in sputtered Si or GaAs samples. In our instrument, sample charging problems preclude the analysis of insulating samples with positive primary ions.

Secondary Negative Ion Yields. Secondary negative ion count rates have been determined for matrix levels of As and P in GaAsP and Si in Si, for trace levels of H, C, O, P, and As in Si, and for S in GaAs. These count rates are shown in Table I normalized to the respective atomic concentrations. For the matrix level species (Si, P, As) sensitivities were also determined under O_2^+ and Ar^+ bombardment and were found to be, respectively, two and three orders of magnitude lower than yields obtained using Cs^+ bombardment. For comparison, the yield of Fe^+ from iron under O_2^+ bombardment is 8×10^5 counts/sec/nA of O_2^+ (*12*).

Detection Limits. Detection limits in secondary ion mass spectrometry are only infrequently dictated by ion yields. Most often they are dictated by background signals arising from interfering molecular ion species having the same nominal mass as the analytical species (*12*), from adsorption of residual vacuum species such as H, C, and O, or from implantation of primary ion beam species. Under oxygen ion bombardment, a significant number of polymeric oxygen-containing secondary ion species are formed which interfere with heavier species. For example, detection of $^{32}S^-$ is severely hampered by $^{16}O_2^-$, and $^{75}As^-$ detection in silicon is limited by $^{29}Si^{30}Si^{16}O^-$. Although high mass resolving power or energy discrimination (*13*) techniques can sometimes be used to reduce or eliminate the interference signal, the intensity sacrificed constitutes another limitation on detection capability. The use of Cs^+ ion bombardment results not only in high negative ion yields, but also in a significant improvement in the chemistry of the analytical process. The introduction

Table II. Detection Limits for Cs^+ Ion Bombardment (atoms/cm³)

Species (matrix)	Signal limit[a] (background-free)	Background level[b]	Background limit[c]
As (Si)	6×10^{16}	3×10^{15}	
O (Si)	1×10^{16}	4×10^{19}	1×10^{17}
C (Si)	2×10^{17}	4×10^{18}	1×10^{17}
H (Si)	8×10^{17}	4×10^{19}	1×10^{18}
S (GaAs)	2×10^{17}	2×10^{17}	
F (Si)	2×10^{16}	6×10^{16}	

[a] Concentration giving 100 counts (above background) when (30 × 30) μm^2 × 100 Å of sample is sputtered. [b] Concentration which would give a count rate equivalent to the background signal B. [c] Concentration which would give a count rate equivalent to $2\sqrt{B}$.

of oxygen into the sample and the production of oxide polymer ions is avoided. Cesium has a high mass, is monoisotopic, and does not form intense polymeric species with the majority of samples. In most cases, the polymer species that do form are of sufficiently high mass that they do not interfere with the analytical species.

Bulk detection limits are not particularly useful figures in SIMS because the major analytical applications of the technique come in sample-limited situations—in particular depth profiles. We have determined Cs^+ ion bombardment detection limits for a number of elements using our routine depth profiling analysis conditions. These conditions constitute an extreme sample-limited situation. In routine operation, the focussed primary ion beam is rastered over a square region (100 × 100) μm^2. The time taken to complete each "frame" of the raster may be varied, but is generally in the range 4–20 s. During this time, 20–200 Å of sample may be sputtered, depending upon the primary beam current. An electronic aperturing technique is used to ensure that mass analyzed ions of the analytical species are counted only when the primary ion beam is within the central flat region ~(30 × 30) μm^2 of the sputtered crater (*14*). The ions counted during each frame are recorded on a digital printer. For the purposes of this article, we define a detection limit as that concentration which is detectable when a sample volume (100 × 100) μm^2 × 100 Å (corresponding to $\sim 3 \times 10^{-10}$ g of Si) is sputtered and 90% of the sputtered ions are rejected to ensure adequate depth resolution.

Two types of limit can be distinguished.

(1) *Signal Limit.* In the absence of appreciable background signal, the minimum acceptable count rate is taken to be ~100 counts/frame (10% relative standard deviation). The *signal limit* is thus that concentration of the analytical species which produces ~100 counts/frame under the depth profile conditions cited above. Species whose detection limits are of this type include As (in Si) and S (in GaAs).

(2) *Background Limit.* A high background count rate may constitute a detection limit much higher than the signal limit discussed above. Species such as O, C, and H are present in the residual vacuum and can adsorb on the sample surface to produce a background count rate which may mask the signals arising from intrinsic C, O, and H in the sample. The *background limit* is conventionally defined as that concentration of the analytical species which produces a signal equivalent to twice the standard deviation of the background. In pulse-counting detection systems, the standard deviation of the background count rate B is $\sqrt{B}$, so that the background limit to detection is $2\sqrt{B}$.

Detection limits of the two types defined here are given in Table II for six elements: As, C, H, O, F, and S. These limits were determined by performing depth profile analyses on ion-implanted samples. Such samples are well suited for these

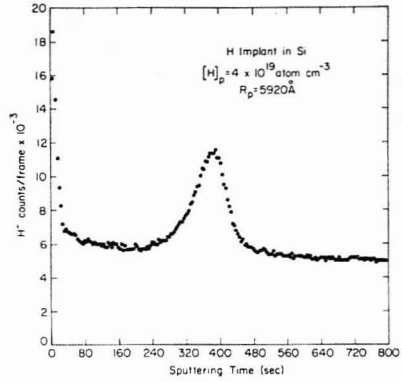

Figure 2. Depth profile of 50-keV H ion implant on Si. Projected range, 5920 Å. Peak H concentration, 4×10^{19} atom cm^{-3}

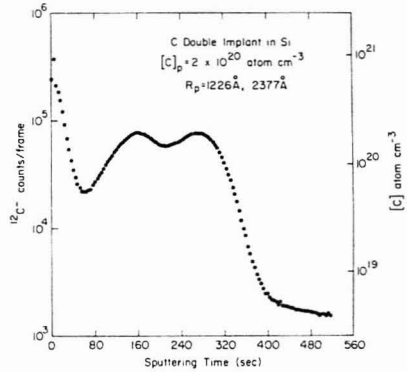

Figure 3. Depth profile of C double implant (55 keV, 110 keV) in Si. Projected range, 1230 Å, 2380 Å. Peak C concentration, 2×10^{20} atom cm^{-3}

determinations for the following reasons: (i) Peak concentrations of ion implanted species can be calculated from tabulated range statistics (*15*). (ii) Observation of the characteristic implant profile (approximately Gaussian) serves as confirmation that the desired analytical species is being monitored. (iii) Gross deviations from the expected Gaussian profile can generally be attributed to instrumental or background limitations. The calculated peak concentration then serves as an internal standard from which the concentration equivalent to the background level may be calculated.

Depth profiles are shown in Figures 2–6 for five implanted species: H, C, O, S, and F. Arsenic depth profiles and detection limits have been discussed in detail elsewhere (*16*). All of the profiles except that of fluorine exhibit a flat "tail" at levels ranging from ~50% of the peak implant signal for hydrogen to ~1% of the peak for sulfur. We estimate that the electronic aperture technique is capable of discriminating by a factor of $\sim 10^3$ against ions sputtered from the peak implant region exposed in the crater wall (*14*). We therefore attribute tails above a level of ~0.1% of the peak count rate to background. The standard deviation of the count rate, B, measured in this region is used to derive a background de-

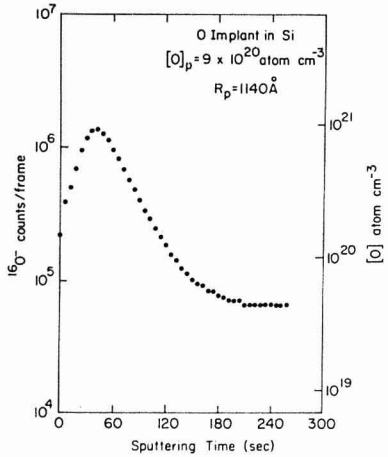

Figure 4. Depth profile of 50-keV O implant in Si. Projected range, 1140 Å. Peak O concentration, 9×10^{20} atom cm^{-3}

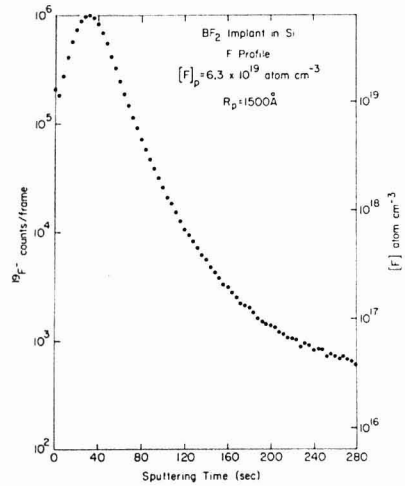

Figure 5. Depth profile of F implant in Si (150-keV BF_2 implant). Projected range, 1500 Å. Peak concentration, 6×10^{19}

tection limit, $2\sqrt{B}$. The fluorine profile differs from the other profiles in that it extends to very low concentration levels and is markedly non-Gaussian (i.e., not parabolic on the semi-log plot). The observed Gaussian shape of the boron profile for this sample (BF_2^+ implant) indicates that the non-Gaussian shape of the fluorine profile is not an instrument-induced artifact. It is possible that the lowest F^- signals accurately reflect implanted fluorine. However, in the absence of confirmation of the profile by an independent technique, we pessimistically designate the tail at $\sim 6 \times 10^{16}$ atom cm^{-3} as background. A fluorine background could arise from the use of HF etchants and the ubiquitous use of Freon in the laboratory.

The concentration equivalents of the background ion count rates are listed in Table II together with the background

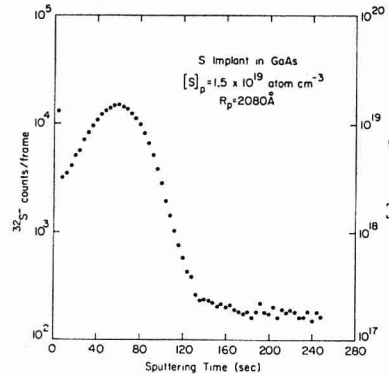

Figure 6. Depth profile of 270-keV S implant in GaAs. Projected range, 2080 Å. Peak concentration, 1.5×10^{19} atom cm^{-3}

detection limits. H and O are clearly present in significant amounts in the sample chamber (ion pumped, liquid nitrogen trapped, pressure 3×10^{-8} Torr). Background signals are quite large for these species but the high ion yields achieved with Cs^+ ion bombardment cause the background signals to have small relative standard deviations. The results of Table II indicate that a sample chamber pressure of $\sim 3 \times 10^{-11}$ Torr would be required to reduce the O and H background to levels equivalent to 1 ppm (6×10^{16} atom cm^{-3}).

The carbon background limit is an order of magnitude lower than those of hydrogen and oxygen, probably reflecting the greater ability of the liquid nitrogen cooled surfaces in the sample chamber to pump ambient carbon-containing species. Intrinsic carbon in the silicon substrate probably contributes to the background level.

Sulfur detection is signal limited at a level equivalent to the background level. That the background signal is due to the sputtering of O_2^- from adsorbed oxygen is demonstrated by its variation with sample chamber pressure and its inverse variation with sputtering rate.

Arsenic is the only one of the species studied which is entirely signal limited. Because background signal was not a limiting factor, it was possible to improve the detection limit to 1×10^{16} atom cm^{-3} by increasing the sample volume consumed to a (250×250) μm^2 crater (*15*).

The cesium source is now in routine use for depth profile analyses of electronegative species. The high sensitivity of the system permits investigation of the behavior of dopant species implanted at low concentrations into minimally damaged samples. Impurity effects can be studied at natural levels without the necessity of doping the sample to artificially high levels for analysis by insensitive techniques. Finally, the system retains the advantages of SIMS: good depth resolution, high speed analyses, and the capability to obtain chemical concentration information from as-received samples.

ACKNOWLEDGMENT

Ion implanted samples for this evaluation were kindly provided by D. Wolford, T. Sigmon, J. C. C. Tsai, K. Vaidyanathan, and D. Meyers. We thank R. Blattner for helpful discussion and V. Deline for experimental assistance.

LITERATURE CITED

(1) C. A. Evans, Jr., *Anal. Chem.*, **47**, 818A (1975).
(2) G. Slodzian and J.-F. Hennequin, *C. R. Hebd. Seances Acad. Sci., Ser. B*, **263**, 1246 (1966).
(3) C. A. Andersen, *Int. J. Mass Spectrom. Ion Phys.*, **2**, 61 (1969).
(4) V. Krohn, *J. Appl. Phys.*, **33**, 3523 (1963).

(5) C. A. Andersen, *Int. J. Mass Spectrom. Ion Phys.*, **3**, 413 (1970).
(6) R. G. Wilson and G. R. Brewer, "Ion Beams", John Wiley, New York, N.Y., 1973.
(7) K. H. Purser, *IEEE Trans. Nucl. Sci.*, **NS-20**, 136 (1973).
(8) R. Middleton, *Nucl. Instrum. Methods*, **122**, 35 (1974).
(9) H. Storms, Vallecitos Nuclear Center, Private communication.
(10) A. E. Banner and B. P. Stimpson, *Vacuum*, **24**, 511 (1975).
(11) Ref. 6, p 29.
(12) P. Williams and C. A. Evans, Jr., *Natl. Bur. Stand. (U.S.), Spec. Publ.*, **427**, 63 (1975).
(13) R. F. K. Herzog, W. P. Poschenrieder, and F. G. Satkiewicz, *Radiat. Eff.*, **18**, 199 (1973).
(14) P. Williams and C. A. Evans, Jr., *Int. J. Mass Spectrom. Ion Phys.*, **22**, 327 (1976).
(15) J. F. Gibbons, W. S. Johnson, and S. W. Mylroie, "Projected Range Statistics", Halsted, New York, N.Y., 1975.
(16) P. Williams and C. A. Evans, Jr., *Appl. Phys. Lett.*, **30**, 559 (1977).

RECEIVED for review March 28, 1977. Accepted May 26, 1977. This work was supported in part by National Science Foundation Grants DMR-76-01058, CHE-74-05745, and CHE-76-03694, and by General Ionex Corporation.

Effect of Matrix Composition on Line Intensity in the Determination of Light Elements in Organic Compounds by X-ray Fluorescence Spectrometry

G. W. Tindall

Tennessee Eastman Company, Division of Eastman Kodak Company, Kingsport, Tennessee 37662

A method is described to calculate the effect of changes in organic composition on the x-ray fluorescent intensity of light elements. The calculation assumes that in these cases excitation is entirely by the monochromatic tube target line. The limitations of this technique were explored using solutions of various elements in solvents. For the case of a light element in an organic matrix, the technique enables standards prepared in one composition to be used to determine the same element in any other known light element composition. This technique is useful in the determination of light elements in organic compounds, especially polymers, where standards preparation is often difficult.

X-ray fluorescence spectrometry is useful for the determination of elements heavier than fluorine in organic chemicals, plastics, and fibers. In most cases, parts per million and greater concentrations of these elements can be determined rapidly and accurately. The major limitation of this technique is the need for standards. The fluorescent intensity measured for an element is a function of both its concentration in a sample and the mass absorption coefficient of that sample. Hence, standards must be prepared in the same organic composition as the samples to be analyzed. When a wide variety of organic compositions needs to be analyzed, it is not practical to prepare standards in this large number of compositions. If the effect of changes in organic composition on fluorescent intensity could be calculated, a standard for some element prepared in one composition could be used to determine this same element in any other composition.

The equation governing fluorescent line intensity is given by:

$$I_i = AC_A \frac{\mu_{A,\lambda_{pri}}}{\mu_{M,\lambda_{pri}} + B\mu_{M,\lambda_i}} \quad (1)$$

where I_i is the fluorescent line intensity for the analyte line measured. A is a constant for a given element and instrument conditions. C_A is the concentration of analyte in the sample. $\mu_{A,\lambda_{pri}}$ is the mass absorption coefficient of the analyte for the wavelength of the primary x-rays. $\mu_{M,\lambda_{pri}}$ is the mass absorption coefficient of the matrix for the wavelength of the primary x-rays. B is a term dependent on the geometry of the spectrometer. (For Siemens spectrometer, this term equals 1.) μ_{M,λ_i} is the mass absorption coefficient of the matrix for the wavelength of the analyte line being measured.

This equation is valid for excitation by monochromatic x-rays (*1*). Since the output of the x-ray tube is not monochromatic, this equation is generally useless for calculating the effects of changes in composition on fluorescent line intensity. However, in certain cases this equation could be useful for calculating matrix effects. The tube most commonly used for the analysis of organic compounds is the chromium target tube. The target lines of this tube account for about 75% of the tube energy, and the energy contribution of the continum at wavelengths longer than the Cr Kα line is insignificant (*2*). The absorption edges of the matrix elements in an organic compound are all of longer wavelength than the Cr Kα line. For the analysis of elements lighter than vanadium, the absorption edge of the analyte is of longer wavelength than the Cr Kα line. In these cases where essentially all excitation results from the monochromatic Cr Kα line, Equation 1 would be used to predict the effect of changes in composition on the fluorescent line intensity of an element. If the effect of composition changes can be calculated, calibration standards prepared in one organic composition can be used to determine the same element in other organic compositions.

As an example, suppose chlorine standards are prepared in methyl alcohol, and we wish to use these standards to determine chlorine in propyl alcohol. The fluorescent line intensity of the methyl alcohol standard is given by Equation 2.

$$I_{Cl,\,MeOH} = AC_{Cl} \frac{\mu_{Cl,\lambda_{Cr\,K\alpha}}}{\mu_{MeOH,\lambda_{Cr\,K\alpha}} + \mu_{MeOH,\lambda_{Cl\,K\alpha}}} \quad (2)$$

The intensity of a propyl alcohol standard of the same concentration is given by Equation 3.

$$I_{Cl,\,PrOH} = AC_{Cl} \frac{\mu_{Cl,\lambda_{Cr\,K\alpha}}}{\mu_{PrOH,\lambda_{Cr\,K\alpha}} + \mu_{PrOH,\lambda_{Cl\,K\alpha}}} \quad (3)$$

Combining these equations yields

$$I_{Cl,\,PrOH} = I_{Cl,\,MeOH} \frac{\mu_{MeOH,\lambda_{Cr\,K\alpha}} + \mu_{MeOH,\lambda_{Cl\,K\alpha}}}{\mu_{PrOH,\lambda_{Cr\,K\alpha}} + \mu_{PrOH,\lambda_{Cl\,K\alpha}}} \quad (4)$$

Table I. Comparison between Measured and Calculated Intensities for 0.5% Chlorine in Solvents

Solvent	$\mu_{M,\,Cr\,K\alpha} + \mu_{M,\,Cl\,K\alpha}$	Measured intensity, $\times 10^{-3}$ counts/s	Calculated intensity, $\times 10^{-3}$ counts/s
Water	270	4.3	
Methanol	202	5.8	5.7
Dimethylformamide	171	6.8	6.8
Propanol	154	7.6	7.5
Methyl isobutyl ketone	145	8.5	8.0
Benzene	123	10.9	9.4
Heptane	112	12.0	10.4

The mass absorption coefficients for the Cr Kα and Cl Kα wavelengths are calculated for the methyl alcohol and propyl alcohol matrices using literature values of mass absorption coefficients for the elements (*1*). Substitution of these values in Equation 4 yields

$$I_{Cl,\,PrOH} = \frac{202}{154} I_{Cl,\,MeOH} \qquad (5)$$

A calibration curve (% chlorine vs. intensity) is prepared from line intensities (measured intensity – background intensity) using the methyl alcohol standards. The slope of this calibration curve is divided by the mass absorption term

$$\mu_{MeOH,\,\lambda_{Cr\,K\alpha}} + \mu_{MeOH,\,\lambda_{Cl\,K\alpha}}/\mu_{PrOH,\,\lambda_{Cr\,K\alpha}} + \mu_{PrOH,\,\lambda_{Cl\,K\alpha}}$$

to yield the slope of the calibration curve for the determination of chlorine in propyl alcohol. Alternatively, the methyl alcohol calibration curve can be prepared by plotting concentration vs. measured intensity. The intercept term for the propyl alcohol curve is estimated by multiplying the intercept term of the methyl alcohol curve by the mass absorption term. Scattered background intensity is approximately inversely proportional to the mass absorption coefficient of the matrix.

EXPERIMENTAL

The usefulness and limitations of using Equation 1 to calculate the effects of changes in composition on line intensity were evaluated using liquid standards. Measurements were made on a Siemens SRS spectrometer using a chromium target tube. Samples were measured in Somar liquid sample cups covered by Somar Labs 0.0005-in. thick polypropylene films.

A 0.5% chlorine standard was prepared in the seven solvents listed in Table I. Lithium chloride was used to prepare the standards in water and methyl alcohol, and dichlorobenzene was used as the standard for the other solvents. The fluorescent intensity of chlorine in each standard and in a blank was measured; the line intensities are given in Table I. From the line intensity measured in water, the predicted line intensity in each other solvent was calculated and is included in Table I.

A 0.5% sulfur standard, as H_2SO_4, was prepared in water containing 0 to 10% sodium as NaOH. The fluorescent intensity of sulfur was measured in each standard, as well as in blanks; the line intensities are given in Table II. From the line intensity measured in water, the predicted line intensity in each other solution was calculated and is included in Table II.

A 0.5% sulfur standard, as H_2SO_4, was prepared in water containing from 0 to 10% bromine as LiBr. The fluorescent intensity of sulfur was measured in each standard and in blanks; the line intensities are given in Table III. From the line intensity measured in water, the line intensity of each other solution was calculated and is included in Table III.

RESULTS AND DISCUSSION

The data in Table I show that the described technique for calculating the effect of changes in composition on line intensity is not exact. In this example, and in general, as the calculated effect gets greater, the error in calculating the effect becomes greater. The worst possible case for organic analysis is illustrated in Table I. The correction between water and heptane is as great a correction as would be encountered for the analysis of organic compounds containing carbon, hydrogen, oxygen, and nitrogen. In practice, standards would not be prepared in water, but in a solvent of intermediate mass; so the errors at each extreme of composition would be minimized.

Table II. Comparison of Measured and Calculated Effect of Sodium on the Fluorescent Intensity of a 0.5% Sulfur Standard in Water

Solution	$\mu_{M,\,Cr\,K\alpha} + \mu_{M,\,S\,K\alpha}$	Measured intensity, $\times 10^{-3}$ counts/s	Calculated intensity, $\times 10^{-3}$ counts/s
0.5% Sulfur	368	4.12	
0.5% Sulfur + 1% sodium	374	4.01	4.01
0.5% Sulfur + 2.5% sodium	388	3.98	3.90
0.5% Sulfur + 5.0% sodium	399	3.83	3.80
0.5% Sulfur + 10% sodium	433	3.55	3.50

Table III. Comparison of Measured and Calculated Effect of Bromine on the Fluorescent Intensity of a 0.5% Sulfur Standard in Water

Solution	$\mu_{M,\,Cr\,K\alpha} + \mu_{M,\,S\,K\alpha}$	Measured intensity, $\times 10^{-3}$ counts/s	Calculated intensity, $\times 10^{-3}$ counts/s
0.5% Sulfur	368	4.21	
0.5% Sulfur + 1% bromine	402	3.95	3.85
0.5% Sulfur + 2.5% bromine	441	3.66	3.51
0.5% Sulfur + 5% bromine	520	3.19	2.98
0.5% Sulfur + 10% bromine	664	2.58	2.33

The measurements and calculations reported in Table I were repeated using the rhodium target tube for excitation. The measured intensities and mass absorption coefficients were, of course, different using the rhodium target tube. But, the fractional change in intensity observed and calculated as a function of composition was nearly identical to that observed and calculated when the chromium target tube was used. This observation is generally valid for any exciting line of shorter wavelength than the absorption edges of matrix and analyte. Hence, it is unnecessary to be concerned about the effects of Kβ or Lβ tube lines. These effects will be the same as those observed and calculated for the Kα and Lα lines.

Another general principle was discovered that applies when using the chromium target tube for excitation. It was found that the fractional increase or decrease in intensity observed or calculated as a result of changing the composition of the organic matrix is the same for titanium, chlorine, sulfur, and phosphorus. We found the line intensity of chlorine is 31% higher in propyl alcohol than in methyl alcohol; and the line intensity of titanium, sulfur, and phosphorus is also 31% higher in propyl alcohol than in methyl alcohol. It is suspected that all elements excited by the chromium target line are similarly affected by matrix changes, but further work is necessary to confirm this hypothesis.

This principle has broad application in the determination of light elements when the composition of the organic matrix is not known. Any internal standard can be used to determine any element, so long as its absorption edges are of longer

wavelength than the target line of the x-ray tube. This principle was used in the determination of chlorine and sulfur at the 0 to 1% level in organic solvent mixtures of unknown composition. Phosphorus was added, as triethyl phosphate, to samples and standards. The ratio of chlorine to phosphorus and sulfur to phosphorus line intensities was used to calculate the amount of chlorine and sulfur in the samples, using chlorine and sulfur standards similarly spiked with the same amount of phosphorus as the samples. Since changes in matrix composition affect all three elements the same, the effects of changes in matrix are compensated.

The data in Table II show how the described technique can be used to calculate the effect of a varying concentration of a light element on the line intensity of a light element. In this case, the calculated and measured intensities agree within experimental error.

The data in Table III show how this technique fails when the matrix contains an element with an absorption edge of shorter wavelength than the target line. In general, the described technique always overestimates the effects of a heavy element. Similarly, the effect of a varying organic composition on an element whose absorption edge occurs at a higher energy than the target line cannot be accurately calculated. In these cases, the target line obviously does not excite the analyte. An estimated effect can be calculated by assuming excitation is by an imaginary monochromatic wavelength that is two-thirds the wavelength of the analyte absorption edge. The error in the calculated effect will be greater in this case than when the analyte is excited by the target line.

The technique for calculating the effect of matrix composition on line intensity described above has been of great value in our laboratory for the determination of light elements in organic compounds, especially organic polymers where standards preparation is often difficult.

ACKNOWLEDGMENT

The author acknowledges the work of Sarah Buchholz, B. H. Collins, and P. L. McConnell, who assisted in the experimental work.

LITERATURE CITED

(1) E. P. Bertin, "Principles and Practice of X-Ray Spectrometric Analysis", 2nd ed., Plenum Press, New York, N.Y., 1975.
(2) J. V. Gilfrich and L. S. Birks, *Anal. Chem.*, **40**, 1077–1080 (1968).

RECEIVED for review April 11, 1977. Accepted May 16, 1977. Paper was presented at the Siemens Logic Controller Conference, Buck Hill Falls, Pa., October 27, 1976.

Propylene Incorporation in 1-Butene Copolymers by Carbon-13 Nuclear Magnetic Resonance Spectrometry

Michael H. Fisch*

Witco Chemical Corporation, P.O. Box 110, Oakland, New Jersey 07436

J. J. Dannenberg

Department of Chemistry, Hunter College, City University of New York, 695 Park Avenue, New York, New York 10021

A method based on ^{13}C nuclear magnetic resonance spectrometry is described whereby standards can be obtained of known propylene content in copolymers with 1-butene. These standards can be used to calibrate the heated cell infrared method for determining propylene content in polybutene.

Numerous methods have been applied to the analysis of 1-butene/α-olefin copolymers, including pyrolysis gas chromatography (*1–3*), differential thermal analysis (*4*), x-ray crystallography (*5*), and melting-point fractionation (*6*). The most widely adopted technique is infrared spectrometry (*5–9*), either using a heated cell to eliminate the effects of crystallinity, or more simply by scanning a film of known thickness and comparing the absorbance to those of standards. For quality control work, infrared is the easiest method to run and the least demanding in equipment. It requires, however, a set of standards for calibration of the instrument used. These standards have in the past been frequently obtained by copolymerization of ^{14}C tagged monomer and radioassay (*10, 11*). This technique, which goes back to the early Italian work (*12, 13*) introduces additional manipulations and the possibility of isotope effects, is time-consuming, and cannot economically be run on a scale approximating production. We wish now to report that satisfactory calibration standards can be drawn from actual production batches and analyzed by ^{13}C NMR.

EXPERIMENTAL

Copolymers were prepared at 65 °C and 150–200 psi in the presence of hydrogen using $(C_2H_5)_2AlCl/TiCl_3$ catalyst. During the reaction, makeup propylene was fed in to keep its concentration fixed. Conversion to copolymer was typically carried to 10–15%.

NMR spectra were measured on representative materials from initial propylene levels of 1.97, 4.05, and 6.91 mol % (Figure 1). Samples were dissolved in deuterochloroform and the spectra measured on a JEOL model PS100 spectrometer.

Since the size of the propylene peaks depended on the level of incorporation, accumulations were arbitrarily continued until the signal to noise ratio was adequate. This required 31 000 scans at the lowest propylene level.

NMR Conditions. $T = 50$ °C. The spectrum width was 5 kHz with 8K data points which corresponds to a computer resolution of 1.2 Hz. The internal lock was deuterium on $CDCl_3$ and the internal standard, $CDCl_3$ solvent. Integrations were performed using standard JEOL/Texas Instrument computer software. The

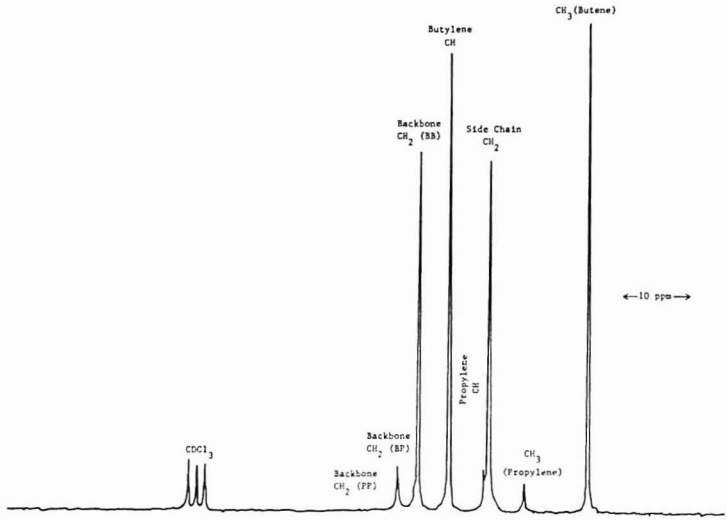

Figure 1. ^{13}C NMR spectrum of a propylene–1-butene copolymer

Table I. Chemical Shifts[a] for Propylene–Butene-1 Copolymer

Assignment	Diads and triads in head-to-tail polymer (cf. Fig. 2)	Lindquist and Adams (*14*)	Carman et al. (*16*)[b]	Calc. (Head-to-Head) Propylene residues head-to-tail only (*14*)	Observed
Propylene CH_3	BPB, BPP, PPP	20.61	21.00	17.13 20.12 17.62	21.4
Backbone CH_2	PP	44.36	45.61	41.42	
Backbone CH_2	BP	41.67	43.27	34.97 32.03 28.84	43.1
Propylene CH	BPB, BPP, PPP	28.38	28.90 28.62	34.99 30.45 32.92	28.2
Butylene CH_3	BBB, BBP, PBP	11.36	11.89	11.36 11.85	10.9
Side Chain CH_2	BBB, BBP, PBP	27.66	28.70	27.66 24.72 27.41	27.5
Backbone CH_2	BB	38.98	40.93	36.04 38.98	39.6
Butylene CH	BBB, BBP, PBP	34.98	35.37 35.09 34.81	34.98 43.66 37.05	34.4
$\sigma = \sqrt{\Sigma d^2/2(N-1)}$		0.55	0.70		

[a] All shifts in parts per million relative to TMS. [b] The epsilon correction (−0.03 ± 0.04) was omitted.

^{13}C frequency was 25.03 MHz. Exponential multiplication of the FID before Fourier Transform induced line broadening of 0.6 Hz.

Normal spectra were taken with 8-μs pulse width (single pulse) corresponding to an approximately 30° flip angle; proton noise decoupled; acquisition time, 0.812 s; and 1.5-s repetition.

Gated decoupled spectra were taken with 20-μs pulse width corresponding to an approximately 75° flip angle; 1-s interval, and 5-s repetition.

DISCUSSION

^{13}C NMR spectra of butene–propylene copolymers were interpreted based on the additivity relations of Lindeman and Adams (*14*), see also (*15*), and of Carman et al. (*16*) (Table I). If one assumes that polymerization is exclusively head-to-tail, there are 18 chemically different carbons, ignoring tacticity (Figure 2). Application of the additivity relationships reduces the number of predicted different chemical shifts to those in Table I (*17*).

For comparison, the calculated shifts for polymer whose propylene component was incorporated in head-to-head fashion are also shown. The observed resonance at 43.1 δ, due to the methylene of the diad BP, occurs slightly less than 2 ppm downfield from that calculated using the Lindeman–

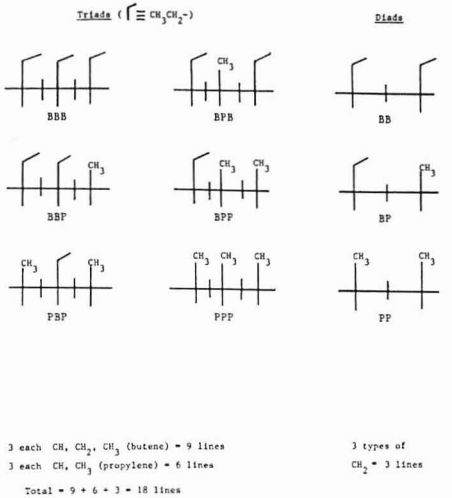

Figure 2. Carbons in head-to-tail random propylene/butene copolymer

Table II. Propylene Incorporation in Propylene-Butene-1 Copolymer

Mol % C_3 in Feed	Mol % C_3 in Copolymer: By Equations 1-3	Mol % C_3 in Copolymer: Corrected[a]
1.97	2.83 ± 0.21	2.91 ± 0.22
4.05	7.80 ± 0.25	8.50 ± 0.27
6.91	11.38 ± 0.56	13.00 ± 0.62

[a] Corrected for probabilistic corrections as outlined in text.

Adams set, which parallels the case of polypropylene itself (observed 46 δ (*18*); calculated 44.4 δ). As easily seen from the Table, agreement between the observed and predicted spectrum for head-to-tail polymer is quite good. Clearly, the head-to-tail random copolymer is consistent with the observed spectra, which is in accord with previous work (*19*, *20*). The simplicity of the spectrum, showing only a single peak for each carbon, suggests that the polymer is highly stereoregular (*21*, *22*). Agreement between experiment and predicted values is satisfactory for either empirical method. The somewhat better fit to the Lindquist–Adams set as opposed to the Carman et al. parameters is not significant.

Propylene residues in the copolymer with 1-butene are believed to be randomly distributed (*19*, *20*). The failure to observe the methylene resonance of the diad PP at ~46 ppm under our conditions is consistent with this conclusion. Even at our highest level of propylene incorporation, the PP diad methylene resonance is predicted to be only 6–7% of that due to the backbone methylene (BP) at 43.1 δ.

Only the area of the methylene from the BP diad was suitable for calculating propylene content. It is the most sensitive to propylene incorporation, since each propylene in a BPB triad gives rise to two such signals, whereas only one propylene methine, and propylene methyl result. The relative methyl area is further reduced because of the nuclear Overhauser effect, and the methine cannot be accurately integrated except as part of the total area with butylene side chain CH_2, from which it is incompletely resolved. Spectra were integrated and the mol % butene was calculated to a first approximation in three different ways (Equations 1–3).

$$\text{Mol \% Butene} = 100\left(\frac{\text{Butylene CH}}{\text{Butylene CH} + {}^1/_2\,\text{Backbone } CH_2\,(\text{PB})}\right) \quad (1)$$

$$\text{Mol \% Butene} = 100\left(\frac{\text{Propylene CH} + \text{Side Chain } CH_2 - {}^1/_2\,\text{Backbone } CH_2\,(\text{PB})}{\text{Propylene CH} + \text{Side Chain } CH_2}\right) \quad (2)$$

$$\text{Mol \% Butene} = 100\left(\frac{\text{Backbone } CH_2\,(\text{BB}) + {}^1/_2\,\text{Backbone } CH_2\,(\text{PB})}{\text{Backbone } CH_2\,(\text{BB}) + \text{Backbone } CH_2\,(\text{PB})}\right) \quad (3)$$

By use of Equations 1–3, all the nonmethyl signals are used in the calculations. The results, which were invariably in reasonable agreement, were averaged from several analyses. Simply taking the relative areas from the carbon spectra and applying Equations 1–3 yields the direct data in Table II which assume all propylenes to be in BPB triads. The corrected propylene levels are then obtained from the following considerations.

The polymer structure is taken to be random from the absence of a detectable methylene from the diad PP, and kinetic considerations (*19*, *20*). Let the (true) mole fraction of propylene be x. Then it can be shown that the proportion of the propylenes with two butenes as neighbors, the triad BPB, will be $(1 - x)^2$; those with two propylenes as neighbors, the triad PPP, will be x^2; and those with one neighbor of each type, PPB will be the rest, $1 - (1 - x)^2 - x^2 = 2x - 2x^2$. Larger blocks are negligible at the levels of incorporation here. Each propylene in the environment BPB contributes two carbons to backbone methylene (PB), but the result is quite different for either of the other arrangements. Per propylene residue, PPB contributes one backbone CH_2(PB) and $^1/_2$ backbone CH_2(PP), whereas PPP adds $^2/_3$ each of backbone CH_2(PP) and backbone CH_2(PB). Correction for the probabilistic considerations and the fact that contributions to the integrated intensity at 43.1 δ are different for PPB, PPP, and BPB, raises the observed values for propylene incorporation to the corrected ones in the last column, the effect being greater as the levels of incorporation are raised.

To estimate the importance of the nuclear Overhauser effect, spectra were run in both the normal Fourier Transform and gated-decoupled modes. Except for the methyl carbons, which were not used in the calculations, the ratios of the integrated carbon resonances were the same within experimental error for both the gated-decoupled and normal modes. Our chosen repetition rate of 5 s meets Levy's recommendation (*23*) that pulse intervals be at least 4–5 times T_1, known to be typically less than 1 s (*24*, *25*).

Although ^{13}C NOEs for solutions of polymers near room temperature are often less than theoretically maximal values (*24*), Schaefer has observed that they are generally invariable from one type of carbon to another within the same polymer (*26*, *27*). Observation of an analogous phenomenon for our system obviated the necessity to record the spectra at a temperature sufficiently elevated to render the NOEs (presumably) maximal and equal. Therefore, we believe that areas obtained from normal noise decoupled spectra at room temperature are adequate for the computations.

A least-square linear plot of mol % C_3 in the feed vs. that in the polymer (corrected) yields a slope of 1.95 ± 0.68 and a correlation coefficient of 0.994 (F statistic 153.7, a 99.35%

value). The derived reactivity ratio for butene, i.e., the reciprocal of the slope, 0.51, is quite reasonable in comparison with the literature value of 0.50 (*28*) reported for a related catalyst system, $Et_3Al/TiCl_3$. However, much more data would be required for a satisfactory measure of this parameter.

These materials were then used in the heated cell infrared method of Tosi et al. (*8*). The absorbances were recorded together with those obtained for a number of blends of polybutene and polypropylene homopolymers. The blends and the standards generate two different lines (Equations 4 and 5 respectively) which, by t test, have significantly different slopes ($t = 2.10$; $t_{0.05,\ 16} = 2.12$). Thus, calibrated standards *are* necessary to carry out the method accurately. Presumably, this is the reason that blends were not used in earlier work on the infrared methods.

$$y(\text{absorbance ratio}) = 1.015x\ (\text{molar ratio P/B}) + 0.244 \quad (4)$$

$$y = 0.798x + 0.240 \quad (5)$$

Coincidentally, the line generated in our work is *not* statistically different from that obtained by Tosi, et al. (*8*), (Equation 6) whereas that for the blends is strikingly so.

$$y = 0.705x + 0.244 \quad (6)$$

where t for slopes of Equations 5 and 6 = 0.89, $t_{0.05,\ 33} = 2.04$, t for slopes of 4 and 6 = 4.49, $t_{0.001,\ 35} = 3.60$.

CONCLUSION

^{13}C NMR is a simple and effective method for determination of propylene incorporation into butene–propylene copolymers. Standards calibrated by this method are suitable for use in simpler plant methods, e.g., IR or DSC.

ACKNOWLEDGMENT

We thank Henry P. Katstra who painstakingly made the infrared measurements, Walter T. Young who prepared the copolymers, and Robert L. Lichter for useful discussions.

LITERATURE CITED

(1) J. C. Verdier and A. Guyot, *Macromol. Chem.*, **175**, 1543 (1974).
(2) E. W. Neumann and H. G. Nadeau, *Anal. Chem.*, **35**, 1454 (1963).
(3) E. M. Barrall, R. S. Porter, and J. F. Johnson, *J. Chromatogr.*, **11**, 177 (1963).
(4) E. M. Barrall, R. S. Porter, and J. F. Johnson, *J. Appl. Polym. Sci.*, **9**, 3061 (1965).
(5) A. Turner Jones, *J. Polym. Sci., Polym. Lett. Ed.*, **3**, 591 (1965).
(6) D. F. Slonaker, R. L. Combs, and H. W. Coover, Jr., *J. Macromol. Sci., Chem.*, **1**, 539 (1967).
(7) T. Huff, C. J. Bushman, and J. W. Cavender, *J. Appl. Polym. Sci.*, **8**, 825 (1964).
(8) C. Tosi, M. P. Lachi, and A. Pinto, *Macromol. Chem.*, **120**, 225 (1968).
(9) N. J. Wegemer, *J. Appl. Polym. Sci.*, **14**, 573 (1970).
(10) J. Lomonte, *J. Polymer Sci., Polym. Lett. Ed.*, **1**, 645 (1963).
(11) J. E. Brown, M. Tryon, and J. Mandel, *Anal. Chem.*, **35**, 2172 (1963).
(12) A. Valvassori and G. Sartori, *Chim. Ind. (Milan)*, **44**, 1091 (1962); *Chem. Abstr.*, **57**, 16824f (1962).
(13) G. Natta, G. Mazzanti, A. Valvassori, and G. Pajaro, *Chim. Ind. (Milan)*, **39**, 733 (1957); *Chem. Abstr.*, **52**, 3729c (1958).
(14) L. P. Lindeman and J. Q. Adams, *Anal. Chem.*, **43**, 1245 (1971).
(15) D. M. Grant and E. G. Paul, *J. Am. Chem. Soc.*, **86**, 2984 (1964).
(16) C. J. Carman, A. R. Tarpley, Jr., and J. H. Goldstein, *Macromolecules*, **6**, 719 (1973).
(17) J. G. Murray, J. Zymonas, E. R. Santee, Jr., and H. J. Harwood, *Polym. Prepr., Am. Chem. Soc., Div. Polym. Chem.*, **14**, 1157 (1973).
(18) L. F. Johnson, F. Heatley, and F. A. Bovey, *Macromolecules*, **3**, 175 (1970).
(19) I. D. Rubin, "Poly(1-Butene)," Gordon and Breach, New York, 1968, Chap. 8.
(20) C. A. Lukach and H. M. Spurlin in "Copolymerization," Vol. 18 of "High Polymers", G. E. Ham, Ed., Interscience, New York, 1964, Chap. IV A.
(21) A. Zambelli, P. Locatelli, G. Bajo, and F. A. Bovey, *Macromolecules*, **8**, 6819 (1975).
(22) A. Zambelli, D. E. Dorman, A. I. R. Brewster, and F. A. Bovey, *Macromolecules*, **6**, 925 (1973).
(23) J. R. Lyerla, Jr., and G. C. Levy in "Topics in NMR Spectroscopy", Vol. 1, G. C. Levy, Ed., Wiley, New York, 1974, p 79.
(24) J. Schaefer and D. F. S. Natusch, *Macromolecules*, **5**, 416 (1972).
(25) J. Schaefer, *Macromolecules*, **5**, 427 (1972).
(26) Identity of NOE for methine and methylene protons at 35 °C has been reported for three homopolymers by J. Schaefer, *Macromolecules*, **6**, 882 (1973).
(27) J. Schaefer in "Topics in NMR Spectroscopy," Vol. 1, G. Levy, Ed., Wiley, New York, 1974, p 149.
(28) I. Hyashi and K. Ono, *Kobunshi Kagaku*, **22**, 446 (1965); *Chem. Abstr.*, **64**, 2174g (1966).

RECEIVED for review October 15, 1976. Accepted May 20, 1977. The funds for the spectrometer were provided in part by NSF Grant No. GP 37025.

Computerized Curve-Fitting to Determine the Equivalence Point in Spectrophotometric Titrations

Scott R. Goode

Department of Chemistry, University of South Carolina, Columbia, South Carolina 29208

A nonlinear least-squares curve-fit is used to determine the equivalence point in spectrophotometric titrations. Titration curves, with a maximum absorbance of 0.4 to 0.8, are calculated under conditions of different equilibrium constants, and signal-to-noise ratios and then fit to a two-parameter model. The equivalence point found is within 2% of the true value as long as the noise is less than 0.008 absorbance unit, even when the titration curve is sufficiently smooth to show no change in slope at the equivalence point. More favorable conditions yield an equivalence point within a few tenths of a percent of the true value.

Volumetric methods are among the most widely-used techniques of chemical analysis. Their popularity is a consequence of their precision, accuracy, and simplicity. The analytical result (location of the equivalence point) is based on a rapid concentration *change*; thus only relative concentrations need be measured. This makes titrations inherently more accurate than methods which require an absolute knowledge of concentration.

The titration curve is a plot of some signal, proportional to analyte concentration as a function of the amount of titrant added. Titration curves have two general forms, sigmoidal and segmented (*1*). An example of the former is the classical, sigmoid-shaped curve which results when pH is plotted during the titration of an acid with a base. The segmented curve is obtained when a parameter which is related linearly to analyte concentration, e.g. absorbance, is corrected for dilution and plotted as a function of titrant added.

The accuracy and precision of the chemical analysis are directly related to the error in locating the equivalence point. When a sigmoidal titration curve is obtained, the inflection

point (maximum slope) is generally used to describe the equivalence point. The inflection point, however, does not always coincide with the equivalence point (*2, 3*) because of dilution effects. The segmented curves, however, do not exhibit this inaccuracy, and the intersection of the two segments coincides with the equivalence point.

This communication will describe several methods to determine the equivalence point of segmented titration curves. The methods include two different computerized curve-fitting procedures and a derivative method. These techniques are applied under conditions with different equilibrium constants and signal-to-noise ratios. The results are compared critically and the methods are analyzed as to their potential utility in a fully-automated titrator.

LOCATION OF THE EQUIVALENCE POINT BY COMPUTERIZED CURVE-FITTING

Nonlinear Curve-fits. The most commonly used model is used to fit experimental data to a *linear* model. An exact equation is available to calculate the slope and intercept which best describe the data (*4*). The "best" fit is the one which minimizes the sum of the squares of the residual (calculated minus experimental). The least-squares fit is not limited to linear equations; a more complex equation can be fit to experimental data, but now an exact solution is generally unavailable, and a numerical one must be used. Parameters are varied in an iterative fashion such that the sum of the squares of the residuals is minimized. Anfalt and Jagner (*5*) suggested that multiparametric curve-fitting should produce the most accurate equivalence point, but did not implement this idea, primarily because of the complexity.

Both sigmoidal and segmented curves are tractable to multiparametric curve-fitting. Gran developed a relatively simple method to linearize the sigmoid-shaped titration curve (*6*). Gran plots exhibit curvature near the equivalence point when the analyte is present in small concentrations or the equilibrium constant of the titration is small. Several researchers (*7–9*) have proposed functions which show less curvature.

Barry and Meites (*10*) used a 3-parameter fit to determine pK_a, the analyte concentration, and activity coefficient in the titration of acetate ion with strong acid. The precision in determining the equivalence point varied between 0.05% to 11% as the concentration of the acetate decreased from 0.002 M to 0.00016 M. They were even able to determine the equivalence point under conditions when an inflection point didn't exist. The authors later included the concentration of the acid as an additional unknown (*11*) and found that the accuracy was improved by a factor of five when compared to titrating with standardized acid and determining the inflection point.

Meloun and Cermak (*12*) performed a 5-parameter fit to a linearized function of a titration which employed a metallochromic indicator. A precision of 0.2% was obtained under favorable conditions. Several investigators (*13, 14*) have used nonlinear least-squares fits to data obtained with ion-specific electrodes. Isbell et al. (*14*) found less error in the curve-fit than in any of the derivative or Gran methods.

McCullough and Meites (*15*) performed a multiparameter fit to a segmented titration curve. They chose to exclude K_{eq} from the adjustable parameters and therefore rejected points in the region of curvature, as well as other outliers. In general, they concluded that it was difficult to produce an accurate and precise value of the equivalence point in a system with instrumental or systematic errors.

Fitting the Data to a Linear Equation. Several authors have determined the best slope and intercept of the two linear segments by a least-squares fit. These data are used to calculate the intersection points. Carr and Onisicki (*16*) determined that the precision of determining the equivalence point was independent of the angle between the segments, but dependent on the difference in slope. They added random noise to simulate a real chemical measurement.

An amperometric titration curve was analyzed by Coenegracht and Duisenberg (*17*). The data were corrected for dilution, but some curvature resulted due to the finite equilibrium constant of the reaction. The precision of the location of the equivalence point was 1% when equilibrium constant-concentration product, $K_{eq}C$, was 100.

A linear least-squares fit was applied to the segments of a spectrophotometric titration by Rosenthal et al. (*18*). They examined the influence of the equilibrium constant and measurement error on the precision of the equivalence point. As the curvature increased (K_{eq} decreases), less of the titration curve fits a linear model, and fewer data points can be used. The noise rejection is obviously poorer under these circumstances, and the precision is about 2% for $K_{eq}C = 20$.

GENERATION OF TITRATION CURVES

Titration curves are generated by numerical computation. The general reaction is

$$S + T \rightarrow P$$

where S is the sample, T the titrant, and P is the product. The equilibrium is described by an equilibrium constant

$$K_{eq} = \frac{[P]}{[S][T]} \tag{1}$$

The titration curve is a plot of absorbance as a function of volume of titrant. The absorption of light is due only to the product so one may conclude

$$A = \epsilon b[P] \tag{2}$$

At any point along the titration curve

$$[S] = C_S - [P] \tag{3}$$

$$[T] = C_T - [P] \tag{4}$$

where C_S and C_T are the analytical concentrations of the sample and titrant.

Equations 1–4 may be combined and solved for absorbance

$$A = \frac{\epsilon b[\alpha + \beta + 1 - \sqrt{(\alpha + \beta + 1)^2 - 4\alpha\beta}}{2K_{eq}} \tag{5}$$

$$\alpha = \frac{K_{eq} V_S C_S}{V_S + V_T} \tag{6}$$

$$\beta = \frac{K_{eq} C_T V_T}{V_S + V_T} \tag{7}$$

where V_S is the volume of the sample as placed in the titration vessel, and V_T is the volume of titrant added at any point.

Titration curves are generated by computation of Equation 5 by a FORTRAN program on an IBM 370/168. Several different conditions, as shown in Table I, were used for the computations. Plots of all curves were performed on a Calcomp flat-bed plotter, interfaced to the computer. In general, 10 mL of 0.01 M sample was titrated with 0.1 M titrant. Two very dissimilar curves, Figures 1 and 2, resulted when the equilibrium constants were 100 and 10^{10}, respectively. All curves would have a maximum value of one absorbance unit if the reaction were complete and dilution effects were negligible.

Inclusion of Noise. There are two major sources of noise in an experimental spectrophotometric titration curve. The spectrophotometric measurement is inherently imprecise, due

Table I. Parameters Used for Titration Curves

Equilibrium constant	$K_{eq} = 10^2$ and 10^{10}
Concentration of sample	$C_S = 0.01$ M
Volume of sample	$V_S = 10.0$ mL
Concentration of titrant	$C_T = 0.10$ M
Equivalence point	$V_{eq} = 1.00$ mL
Molar absorptivity	$\epsilon = 100$ L-mol^{-1} cm^{-1}
Path length	$b = 1.00$ cm
Range of titrant	0 to 2.00 mL
Titrant aliquot	0.001 mL and 0.100 mL
Uncertainty in absorbance	0, 0.001, 0.002, 0.004, 0.008, 0.016 absorbance units
Uncertainty in volume	0, or 0.004 to 0.012 mL (see text)

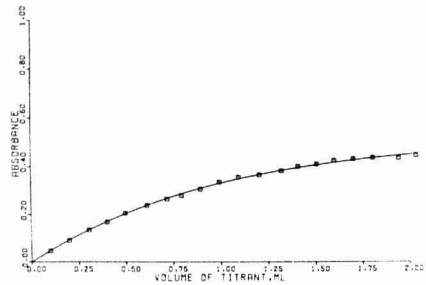

Figure 1. Spectrophotometric titration curve. $K_{eq} = 10^2$, 0.004 absorbance unit of noise. Includes uncertainty in volume. Equivalence point = 1.000 mL. (□) Experimental points. (—) Computer-generated fit

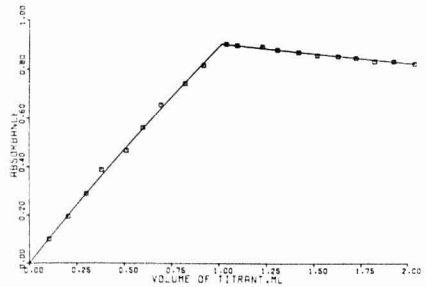

Figure 2. Spectrophotometric titration curve. $K_{eq} = 10^{10}$, 0.004 absorbance unit of noise. Includes uncertainty in volume. Equivalence point = 1.000 mL. (□) Experimental points. (—) Computer-generated fit

to several reasons (*19*). The other major source of noise is the imprecision in the volume measurement. Each is treated below.

Spectrophotometric Noise. Ingle and Crouch (*19*) have shown that the noise sources in a spectrophotometer fall into three major groups. The optimum situation occurs when the dominant noise is source-flicker. This is, indeed, the major noise source in most high-quality modern spectrophotometers except in situations where the light level is low, such as found when small slit widths or when unfavorable wavelengths must be used. This noise is seen as an uncertainty in the absorbance measurement, e.g., 0.30 ± 0.001 absorbance unit, where the magnitude of the uncertainty is independent of the absorbance. The smallest amount of noise included in the calculations is probably more than would be present in a typical spectrophotometer (*20, 21*).

Table II. Precision and Accuracy of Titrant Delivery[a]

Volume read, mL	Volume delivered, mL	Standard deviation, mL
0.100	0.089	0.004
0.200	0.194	0.008
0.300	0.295	0.008
0.500	0.497	0.009
0.700	0.701	0.010
1.000	1.002	0.011
1.500	1.499	0.012
2.000	2.000[b]	0.012

[a] Buret stopped and read every 0.01 mL. [b] Normalized to 2.000.

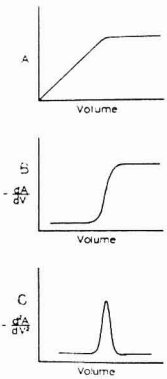

Figure 3. (A) Titration Curve. (B) First derivative plot. (C) Second derivative plot

The IBM-furnished subroutine RANDU (*22*) is used to add a constant amount of noise to the titration curve. Titration curves are calculated and noise of 0.001, 0.002, 0.004, 0.008, and 0.016 absorbance unit are added to each absorbance value. The noise is random, with a mean of zero and a standard deviation of 0.001, 0.002, etc.

Volume Noise. Uncertainty in the volume delivery is more difficult to include. A Radiometer ABU-13 automatic buret (London Company, Westlake, Ohio) was filled with vacuum pump diffusion fluid; aliquots were dispensed and weighed. The buret dispensed 0.100 mL increments, so the data, shown in Table II are the precision of delivering volumes from 0.000 to 0.100, 0.100 to 0.200 mL, etc. These reflect the actual precision obtained in a titration, where an aliquot is delivered, a measurement is made, and another aliquot delivered. The precision in operating between two fixed points is better. The delivery of 1.000 mL has a relative standard deviation of 0.17% if the buret is always started at 0.0 and stopped at 1.000 mL.

Noise corresponding to the values shown in Table II is added to the volume axis, also using RANDU.

EXPERIMENTAL

Ten to twelve titration curves are generated for each different set of experimental conditions. These are stored on magnetic tape for ease of accessibility. Each curve is different, as the noise added is truly random, but with known variance.

The titration curves are analyzed by three procedures. The equivalence point is determined by a derivative method, an extrapolation method, and a nonlinear curve-fit. The accuracy and precision of each method is reported below.

RESULTS

Derivative Method. A representation of the titration curve, first, and second derivative are shown in Figure 3. The

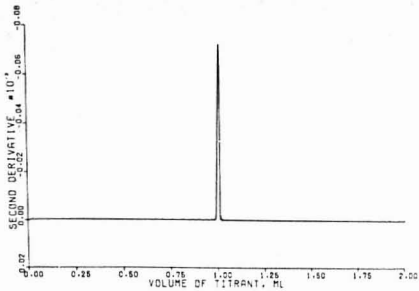

Figure 4. Second derivative plot. $K_{eq} = 10^{10}$. No noise in absorbance measurement

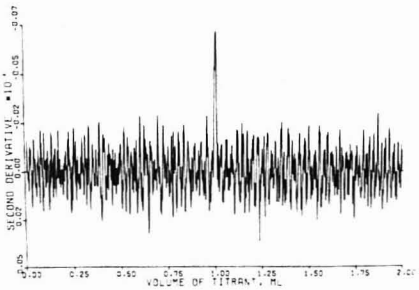

Figure 5. Second derivative plot. $K_{eq} = 10^{10}$, 0.001 absorbance unit of noise

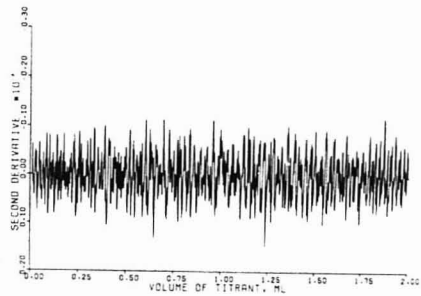

Figure 6. Second derivative plot. $K_{eq} = 10^{10}$, 0.004 absorbance unit of noise

second derivative of the titration curve is calculated using the Savitsky–Golay algorithm (*23*). This method includes a 23-point smooth to improve noise immunity. Titration curves consisted of 2000 points, spaced 0.001 mL apart. This small interval is necessary because the numerical derivative is inherently digital. Thus to obtain a precision of 0.1%, at least 1000 points are needed prior to the equivalence point.

Figures 4, 5, and 6 show the second derivative obtained when 0, 0.001, and 0.004 absorbance unit of noise when $K_{eq} = 10^{10}$ are added to a titration curve obtained. The titration curve with the most noise (0.004 absorbance unit) is shown in Figure 7. One can see that the derivative method cannot be used under conditions of moderate noise.

When the equilibrium constant is small, the titration curve

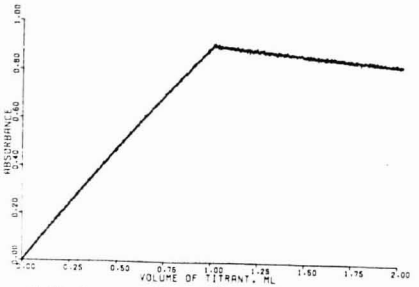

Figure 7. Titration curve. $K_{eq} = 10^{10}$, 0.004 absorbance unit of noise

shows no inflection point, as illustrated in Figure 1. The second derivative has no maximum, and cannot be used to determine the equivalence point.

Under favorable conditions the numerical derivative method always gives the correct answer if there is little or no noise present. Before the derivative is calculated, it is little trouble to have the computer correct for dilution, hence removing the inaccuracy present in an analog or graphical treatment (*1*).

Computation of the derivative has a more fundamental limitation. It requires at least 1000 points to obtain an accuracy of 0.1%. This requirement tends to make the derivative method unwieldy.

Extrapolation Method. The two segments of the titration curve may be corrected for dilution, and fit to two linear equations. The intersection point is calculated to determine the equivalence point. The results of such a study indicate that serious systematic errors arise when the equilibrium constant is small, i.e., Figure 1 cannot be represented as two linear segments. The interval between data points becomes increasingly important as more points are needed if noise is to be rejected. When the equilibrium constant is small, however, only a fraction of the titration curve is described by a linear equation. These results agree with previous reports (*17, 18*).

Nonlinear Least-Squares Fit. The titration is a function of seven parameters: K_{eq}, ϵ, b, C_S, C_T, V_S, and V_T. Of these seven, four are known to the experimenter: the path length, b; the volume of sample, V_S; the concentration of the titrant, C_T; and the volume of titrant added, V_T. The other parameters are described below.

Concentration of Sample. The sample concentration, C_T, is not known, and is to be determined by the titration.

Molar Absorptivity. The molar absorptivity will, in general, not be known. The value is dependent on ionic strength, hence the sample matrix. The nonlinear curve-fit treats ϵ as an unknown.

Equilibrium Constant. The value of the equilibrium constant also is not generally known. The value of the equilibrium constant, however, does not affect the location of the equivalence point, but merely the amount of curvature in the titration curve. Uncertainty in K_{eq} *can* influence the accuracy and precision in calculating the end point, but the equilibrium constant can be determined from the titration of a known amount of sample. Typical results for the determination of K_{eq} and the errors introduced by uncertainty in K_{eq} are shown in a later section.

Even though K_{eq} is generally treated as a known quantity, a three-parameter fit can be employed with K_{eq} as one of the unknowns.

Computational Algorithm. The nonlinear regression of Dye and Nicely (*24*) is used. This algorithm allows the variables, both independent and dependent, to be weighted in accord

Table III. Accuracy and Precision of Nonlinear Curve-Fit

Standard deviation of absorbance	No imprecision in volume: Equivalence point, mL[b]	No imprecision in volume: Standard deviation of equivalence point, mL	Includes imprecision in volume[a]: Equivalence point, mL[b]	Includes imprecision in volume[a]: Standard deviation of equivalence point, mL
Equilibrium constant = 10^{10}				
0.001	1.000	0.001	0.996	0.003
0.002	1.000	0.001		
0.004	1.003	0.003	0.997	0.003
0.008	0.999	0.006		
0.016	1.002	0.01		
Equilibrium constant = 10^{2}				
0.001	1.000	0.014	0.996	0.025
0.002	1.005	0.016		
0.004	0.998	0.042	0.983	0.038
0.008	0.981	0.054		
0.016	0.92	0.17		

[a] See Table II and text. [b] Correct value, 1.000 mL.

Table IV. Influence of K_{eq} on Curve-Fit[a]

K_{eq}	Calculated equivalence point, mL[b]	Standard deviation, mL
102	1.01	0.04
87	0.92	0.05
114	1.05	0.04

[a] Noise is 0.004 absorbance unit; data include imprecision in volume delivery. [b] Correct value, 1.000 mL.

to their experimental variances. This feature was used in all trials.

Twenty data points are fit into Equation 5. The program adjusts ϵ and C_S to minimize the sum of the squares of the differences between the absorbance calculated from ϵ and C_S, and the experimental value.

The nonlinear least-squares fit requires an initial estimate of the variables fitted, ϵ and C_S. The program may not converge if the estimates are poor.

Initial Estimates. The value of the equilibrium constant was found to influence the latitude of the initial estimates. When the curve is smooth (K_{eq} = 100, Figure 1) any value within a factor of 10 of the correct C_S and ϵ allowed the program to converge to proper values. The worst case required 31 iterations, or approximately 3 seconds of CPU time. The sharper curve ($K_{eq} = 10^{10}$, Figure 2) required estimates within a factor of two to converge. Obviously, one can provide better estimates from the sharper curve.

Accuracy and Precision. The results of the curve-fit are shown in Table III. If the noise is 0.004 absorbance unit, or less, the accuracy is better than 0.5% when $K_{eq} = 10^{10}$, and 5% when K_{eq} = 100. The precision is remarkable, especially considering the adverse noise included in the experimental curves. Figures 1 and 2 show the experimental points and the theoretical best fit generated by the computer.

Influence of Equilibrium Constant. When the concentration of the sample, C_S, is known, one may perform a curve-fit to determine K_{eq} and ϵ. Theoretical data for K_{eq} = 100, noise of 0.004 absorbance unit, and noise in the volume delivery were used to obtain an experimental K_{eq}. The value of K_{eq} ranged from 87 to 114, with a mean of 102, and a standard deviation of 10. Since K_{eq} is now known, these values are used to calculate the concentration of the sample in other titration curves. These results are also included in Table IV. The incorrect values of K_{eq} influence location of the calculated equivalence point, but the maximum error is only 8%. These results are quite good considering the magnitude of the noise, lack of knowledge about the chemical system, and small concentration-equilibrium constant product ($C_S K_{eq}$ = 1).

CONCLUSIONS

The nonlinear least-squares fit to a spectrophotometric titration curve is shown to be a superior method to obtain the equivalence point of a spectrophotometric titration. The precision and accuracy vary, according to the amount of noise. If a titration with a large equilibrium constant, and less than 0.004 unit of noise is performed, the equivalence point can be determined to within a few tenths of a percent, and will generally be limited by the precision to which the volume is measured.

When the equilibrium constant is small, the curve-fit may be the only method which is capable of extracting the location of the equivalence point. A titration curve obtained when the equilibrium constant is 100 will provide an answer accurate within 5% as long as the noise is less than 0.01 absorbance unit.

The derivative method and the extrapolation of linear segments do not product acceptable results when the equilibrium constant is small. Additionally, the derivative method also required too many data points to be a good, general-purpose method of locating the equilibrium point.

The nonlinear least-squares fit does require a large computer, but on-line data acquisition is not necessary. The titration curve, 20 pairs of numbers in the cases illustrated here, may be transmitted to a larger computer for analysis at a slightly later time. The data link may be high speed dedicated lines, if the titration data must be analyzed within seconds, or punched cards if overnight computation is acceptable.

One major application of this work is to analyze titration curves obtained under adverse conditions such as low equilibrium constant, poor signal-to-noise ratio, perhaps due to the spectral region involved, and low concentrations of analyte. The nonlinear least-squares fit is seen to provide a good value for the equivalence point under conditions when other techniques fail completely.

ACKNOWLEDGMENT

The author thanks Jethro Matthews, Don Schermer, and David Otto for their help.

LITERATURE CITED

(1) L. Meites and J. A. Goldman, *Anal. Chim. Acta*, **30**, 28 (1964).
(2) L. Meites and J. A. Goldman, *Anal. Chim. Acta*, **29**, 472 (1963); **31**, 297 (1964).
(3) L. Meites and J. A. Goldman, *Anal. Chim. Acta*, **30**, 18 (1964).
(4) D. G. Peters, J. M. Hayes, and G. M. Hieftje, "Chemical Separations and Measurements", W. B. Saunders, Philadelphia, Pa., 1974, p 32 ff.
(5) T. Anfalt and D. Jagner, *Anal. Chim. Acta*, **57**, 165 (1971).
(6) G. Gran, *Analyst (London)*, **77**, 661 (1952).
(7) F. Ingman and E. Still, *Talanta*, **13**, 1431 (1966).
(8) A. Johansson, *Analyst (London)*, **95**, 535 (1970).

(9) D. Midgley and C. McCollum, *Talanta*, **21**, 273 (1974).
(10) D. M. Barry and L. Meites, *Anal. Chim. Acta*, **68**, 432 (1974).
(11) D. M. Barry and L. Meites, *Anal. Chim. Acta*, **69**, 143 (1974).
(12) M. Meloun and J. Cermak, *Talanta*, **23**, 15 (1976).
(13) M. J. D. Brand and G. A. Rechnitz, *Anal. Chem.*, **42**, 1172 (1970).
(14) A. F. Isbell, R. L. Pecsok, R. H. Davies, and J. H. Purnell, *Anal. Chem.*, **45**, 2363 (1973).
(15) J. G. McCullough and L. Meites, *Anal. Chem.*, **47**, 1081 (1975).
(16) P. W. Carr and S. Onisicki, *Anal. Lett.*, **4**, 893 (1971).
(17) P. M. J. Coenegracht and A. J. M. Duisenberg, *Anal. Chim. Acta*, **78**, 183 (1975).
(18) D. Rosenthal, G. Jones, and R. Megargle, *Anal. Chim. Acta*, **53**, 141 (1971).
(19) J. D. Ingle, and S. R. Crouch, *Anal. Chem.*, **44**, 1375 (1972).
(20) L. D. Rothman, S. R. Crouch, and J. D. Ingle, *Anal. Chem.*, **47**, 1226 (1975).
(21) J. D. Ingle, *Anal. Chim. Acta*, **88**, 131 (1977).
(22) "System/360 Scientific Subroutine Package," Version III, GH20-0205-4, 5th ed., IBM Corporation, White Plains, N.Y., 1970, p 77.
(23) A. Savitsky and M. Golay, *Anal. Chem*, **27**, 1627 (1964).
(24) J. L. Dye and V. A. Nicely, *J. Chem. Educ.*, **48**, 433 (1971).

RECEIVED for review February 14, 1977. Accepted June 1, 1977. Acknowledgement is made to the Donors of The Petroleum Research Fund, administered by the American Chemical Society, for partial support of this research.

High Solids Sample Introduction for Flame Atomic Absorption Analysis

R. C. Fry[1] and M. B. Denton*

Department of Chemistry, University of Arizona, Tucson, Arizona 85721

Studies are presented describing direct, clog-free production of high density finely dispersed aerosols from highly complex samples through use of a special nebulizer design based on principles first developed by R. S. Babington. Application of this technique to sample introduction for atomic absorption spectrometry is described for matrices of combined high suspended solids content, increased viscosity, and elevated salt concentration. Cu and Zn are determined in whole blood, urine, seawater, evaporated milk concentrate, and tomato sauce with minimal sample preparation.

Increasingly large numbers of environmental and clinical samples being submitted to analytical laboratories for determination of trace metal constituents make the development of "preparation free" methods of analysis extremely important from the standpoint of cost per analysis, speed, convenience, and freedom from reagent contamination. Atomic absorption spectrometry has been widely applied to samples of complex nature directly (*1*), and indirectly through the use of digestion (*2*) and extraction procedures (*3*). Although such digestion or separation procedures tend to be time consuming and may frequently lead to volatilization loss (*2*) or sample contamination, existing methods often require these steps for a wide variety of samples. The complexity of untreated matrices that may be introduced directly is often limited by nonatomic absorption and vaporization interferences in the case of flameless sampling devices, and by clogging of the capillary orifice and burner slot in the case of conventional burner–nebulizer systems.

Although less sensitive than flameless atomizers, conventional burner–nebulizers have proven to be generally more convenient to operate, lower in cost, capable of introducing a larger number of samples per unit time into the absorption cell, and less susceptible to interferences (*4,5*). These advantages have established the continued use of the capillary pneumatic nebulizer as a principal sample introduction device for analytical atomic spectroscopy. Culver (*6*) has discussed the relative merits of carbon rod and flame techniques and concludes that, although flameless atomizers provide an alternative to nebulizer–burner atomization cells when greater sensitivity and smaller sample size is required, the more convenient flame system should be used whenever possible. Improvement in nebulizer design to allow more complex sampling is therefore highly relevant and desirable.

Development and subsequent characterization of a unique nebulization principle by R. S. Babington (*7*) have resulted in the ability to generate high density, finely dispersed aerosols directly from a variety of extremely complex materials including fuel oil, paints, food products, etc. Possibilities for improved freeze-drying systems, oil burners for home heating, insecticide fogging, etc., applications have been outlined (*8*). A nebulizer based on this principle has been marketed by Owens-Illinois (Toledo, Ohio) and more recently by McGaw Respiratory Therapy (Irvine, Calif.) under the trade names of "HYDROSPHERE" and "MAXI-COOL" for the production of aerosols utilized in respiratory inhalation therapy. This Babington nebulizer has been reported to produce a dense aerosol with a droplet distribution (following considerable aerosol refinement) of median mass diameter at 3.6 μm with 95% of all refined droplets being below 5 μm in diameter (*9*). In view of the spectrochemical importance of droplet size discussed by Alkemade (*10*), it is apparent that this nebulization principle offers great promise as an approach to sample introduction in flame spectrochemical analysis.

A major difference between the Babington nebulization technique and the conventional capillary pneumatic nebulizer arises from the fact that the conventional nebulizer requires the sample to pass through a small ($\approx$0.36 mm) capillary orifice. In contrast, the Babington nebulizer requires that only *gases* pass through an orifice; the relatively unrestricted (2.38 mm) *sample* flow of this system provides the basis for high solids sampling and represents the primary advantage of Babington nebulization as applied to spectrochemical analysis. The upper limit on salt and solids content as well as viscosity of a slurry that may be directly sampled by this technique is determined by the ability of the material to pass through a pumping system. This paper deals with the application of a specially developed nebulizer based on the Babington principle in combination with high solids slot burners to provide direct atomic absorption analysis of highly complex

[1] Present address, Department of Chemistry, Kansas State University, Manhattan, Kan. 66506.

environmental, clinical, and food samples.

EXPERIMENTAL

Apparatus. A single channel, single beam atomic absorption spectrometer similar to most late model commercial designs was constructed with readout in analog and digital form. Both absorbance and %T modes are provided.

Optical components included Jarrell-Ash (Waltham, Mass.) and Varian Techtron (Springvale, Victoria, Australia) hollow cathode lamps (Cd, Cu, Zn, Fe, and H_2), a 1.5-m combination optical rail and bench, a Princeton Applied Research (Princeton, N.J.) optical chopper operating at 312 Hz, Modern Optics (El Monte, Calif.) 150-mm focal length, 51-mm diameter, and 25-mm focal length, 25-mm diameter convex fused silica external intermediate and slit imaging lenses, Heath (Benton Harbor, Mich.) 0.35-m, $f/6.8$ monochromater with 250-nm blazed grating (first order), and a Hamamatsu (Middlesex, N.J.) R212 UH photomultiplier tube. The external optics are positioned to produce hollow cathode images (@ 250 nm) of magnification (1.0) at the center of the slot burner and of reduced magnification (0.125) at the entrance slit of the monochromater.

Electronic components included hollow cathode and photomultiplier power supplies, photo current pre-amplifier, lock-in amplifier, logarithmic amplifier, Data Technology Corp. (Woburn, Mass.) 343 digital voltmeter, and Bausch & Lomb (Rochester, N.Y.) 100-mV VOM-5 strip chart recorder. A standard FET input photocurrent pre-amplifier circuit with variable gain, variable time constant, and current offset was constructed using a Burr Brown (Tucson, Ariz.) 3522L integrated circuit operational amplifier as the basic component. A lock-in amplifier circuit similar in design to that of Horlick (*11*) utilized in the referenceless mode with addition of variable damping was constructed using a Signetics (Sunnyvale, Calif.) 561 phase locked loop, 741 operational amplifiers, and a Teledyne Semiconductor (Mountain View, Calif.) LM208 drift stabilized operational amplifier in the demodulation section as the principal components. The logarithmic amplifier was designed employing an Analog Devices (Norwood, Mass.) 752N temperature compensated logarithmic feedback element and a Signetics 536 operational amplifier according to the suggested circuit supplied by Analog Devices for logarithmic voltage conversion. Overall calibrated readout scales of 0–100% T, 0–2 A, 0–1 A, 0–0.5 A, 0–0.2 A, and 0–0.1 A are provided. The optical and electronic design is generally similar to that of several late model standard commercial instruments.

A high solids single slot air–acetylene burner head similar in design (except for the wider 0.81 mm × 10 cm slot used in this study) to the standard 0.51 mm × 10 cm slot air-acetylene head sold by Varian Instruments, and Instrumentation Laboratory (Lexington, Mass.) Cat. NO. 24036-03 commercial "High Solids" 0.81 mm × 5 cm single slot N_2O–acetylene burner head, and a Jarrell-Ash "Tri flame" 10-cm air–acetylene head were used in these investigations. The two high solids burner heads were found to be desirable for salt, sugar, and solids contents in excess of 5% to prevent clogging and gumming of the slot. Flashback has not occurred to date in the modified high solids air–acetylene design, and the high solids N_2O head sold by Instrumentation Laboratories flashes back only if proper flow rates and flame stoichiometries are not maintained during light-up, operation, and shut-down.

Provision was made at the entrance to the premix chamber for a quick interchange connection allowing press-fit installation of a Varian Techtron variable aspiration rate conventional pneumatic nebulizer with externally adjustable glass bead impactor as well as connection to the modified Babington nebulizer. The smallest restriction in the 29-mm i.d., 48-cm path aerosol refinement and premix chamber is the 15.9-mm flow spoiling restriction. The modified Babington nebulizer (Figure 1) is housed in a 55-mm i.d., 67-mm o.d., cylindrical Plexiglas chamber which is connected to the premix chamber by means of a 33-mm i.d. flexible plastic hose. A 10-mm i.d. exit drain is provided for excess sample and large particle runoff. Nebulizer inserts are held in place by a compression fitting elbow. The nebulizer utilizes a polished 6-mm o.d., 5.5-mm i.d. closed, rounded end, metal tube with a single 0.61-mm orifice located 3 mm below the end of the tube. The 3-mm spherical impactor is mounted on a translational slide to provide gap adjustment externally during aerosol production and

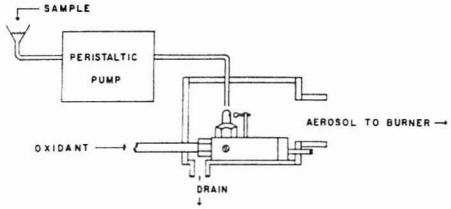

Figure 1. New high solids nebulizer (Babington principle)

flame atomization (optimal gap ~1.4 mm). Sample delivery is accomplished by a Manostat (New York, N.Y.) 72 895-10 peristaltic pump with head and rollers modified to accept 2.38-mm i.d. Tygon tubing. A possible substitute pump would be Cole Parmer–Masterflex (Chicago, Ill.) 7016 pumphead, 7545-10 variable speed pump drive, and 6408-02 tubing or any similar pumping system capable of delivering a steady flow rate of 20–25 mL/min through 2.38-mm i.d. tubing.

Sample is pumped from the tube (located 1 mm above the nebulizer) over the surface of the nebulizer insert forming a film which is interrupted at the point of the orifice by the high velocity exit of oxidant gas. This process serves to generate the aerosol which is then impacted against the small plastic sphere for additional fragmentation of larger droplets. Extremely large non-nebulizable particles simply fall away from the insert and are eventually washed down the drain without having clogged the system. An Eppendorf (Brinkmann Instruments, Westbury, N.Y.) 1000-μL syringe was used to pipet samples conveniently into a glass funnel (60-mm o.d. cone, 6-mm o.d. stem) which is pressed over the input end of the peristaltic pump tubing.

Procedure. Spectral bandwidths between 0.3 nm and 0.6 nm were used for all measurements. Cd, Cu, Zn, and Fe resonance lines at 228.8 nm, 324.7 nm, 213.9 nm, and 248.3 nm, respectively, were used for atomic absorption measurements. Nonatomic absorption measurements were made where necessary using a H_2 continuum hollow cathode. The nonatomic absorbance measurements at 324.7 nm were not affected by the presence of copper at this spectral bandwidth if the solution concentration was less than 100 ppm Cu. All samples were far below this level in the solutions presented to the instrument. The photomultiplier tube was operated at 700 V and, following careful alignment techniques to ensure both beams traversed the same flame profile region, hollow cathode current as well as pre-amplifier gain adjustments were made to match the observed relative emission signal intensity of the continuum source to that of the individual hollow cathodes. A check of the nonatomic absorbance was also made without changing lamps (or alignment) using a nonabsorbing line at 210 nm emitted from the Zn hollow cathode. Nonatomic absorbance did not exceed 0.01 absorbance unit for all samples tested except the 50% $CaCl_2$ sample for which a value of 0.2 A was not exceeded in air–acetylene. Analytically observed flame regions occurred with the center of the beam 6 mm above the burner head.

All direct Babington analyses (with exception of the NBS standard reference material which required dilution of the high levels of Cu and Zn present) were made by the method of minimal dilution standard additions using sample volumes of 1 mL and addition volumes of 10 μL to avoid loss of concentration sensitivity and to demonstrate that these complex sample types can be analyzed in "no-clog" fashion without dilution. Comparison analyses made using the standard Varian nebulizer were carried out following standard (*2*) dry ashing, hot mineral acid digestion of the ash, and final dilution to volume with deionized distilled water. A sample of NBS Orchard Leaves (SRM 1571) was also prepared by this process as a check on the ashing and digestion procedure. In the case of Zn, some of the high concentrations reported were determined without dilution in the Babington nebulizer by sensitivity reduction through shortened path length accomplished by rotation of the slot burner head.

The nebulizer is optimally driven at an oxidant pressure of 50–80 psi. for spectrochemical analysis to yield flow rates between 9 and 12 L/min. The pressure drop occurs across the nebulizer orifice so normal drain and trap collection procedures may be used

Table I. Nebulizer Sensitivities in Air–Acetylene at $Cd_{228.8\ nm}$

Nebulizer	Observed sensitivity	Manufacturers listed sensitivity, (in the commercial instrument)
Modified Babington Nebulizer	0.014 ppm	
Varian Techtron Adjustable Pneumatic Nebulizer	0.010 ppm	0.011 ppm
Jarrell-Ash 810 Pneumatic Nebulizer	0.018 ppm	0.020 ppm
Jarrell-Ash Hetco Pneumatic Nebulizer	0.022 ppm	(0.024 – 0.040 ppm)[a]
Perkin-Elmer Pneumatic Nebulizer		0.025 ppm
Beckman 495 Premix Pneumatic Nebulizer		0.015 ppm

[a] Based on a private communication with Jarrell-Ash personnel.

Table II. Analysis of High Solids Samples

Sample	Zn, ppm		Cu, ppm	
	Direct Babington analysis	Conventional analysis (digest) (Varian nebulizer)	Direct Babington analysis	Conventional analysis (digest) (Varian nebulizer)
Hemolyzed Whole Blood	12.	13.	0.63	0.61
Urine	0.63	0.67	0.062	0.065
Seawater	<0.021	<0.014	0.063	0.069
NBS Orchard Leaves[a] (digest)	24.	27.	13.	11.

[a] NBS certified value: 25 ± 3 ppm Zn and 12 ± 1 ppm Cu for the Orchard Leaves SRM 1571.

for excess sample runoff. The peristaltic pump is normally operated at 20–25 mL/min. One-milliliter samples are pipetted, using an Eppendorf (or similar) microsyringe, into the glass cone yielding a transient signal at the recorder. Larger samples may be used to produce a steady-state signal at the readout if desired, but 1 mL is sufficient to give a transient signal of similar concentration sensitivity and precision. The smaller volume transient sampling method greatly reduces problems associated with burner slot clogging. This transient method of sampling is similar to that discussed for conventional nebulizers by Sebastiani et al. (*12*), by Manning (*13*), and by Berndt and Jackwerth (*14*) except that the sample size is somewhat larger in the high solids Babington system.

RESULTS AND DISCUSSION

Improved Nebulizer Design. Initial evaluation of the Hydrosphere respiratory Babington nebulizer for use in flame analysis demonstrated its ability to produce stable aerosols yielding reasonable spectrochemical sensitivity. This was achieved utilizing gas flow rates compatible with the normal values (8–12 L/min) employed for oxidant gases in conventional atomic absorption burners. Air–acetylene, nitrous oxide–acetylene, and argon–hydrogen–entrained air flames were all supported adequately by this system. Unfortunately, the large solution reservoir and large-scale design of the commercial glass respiratory nebulizer required prohibitively large sample sizes in excess of 500 mL. Subsequent investigations eventually led to development of an improved design involving peristaltic pump sample delivery to the scaled down, geometrically improved metal version of the Babington nebulizer shown in Figure 1. These modifications led to sample sizes of 1 mL making the Babington nebulization principle reasonably applicable for the first time to routine spectrochemical sampling.

Instrument and Nebulizer Performance. Table I summarizes the performance of the improved Babington nebulizer in comparison with several conventional capillary pneumatic nebulizers commonly used for atomic absorption spectrometry. The parameter used for comparison was sensitivity (concentration required to produce 1% absorption) of cadmium measurement at 228.8 nm in a 10-cm air–acetylene flame. Table I demonstrates that the observed sensitivities for the commercial capillary pneumatic nebulizers tested in the instrument constructed for these studies are essentially no different from the values advertised by the manufacturers for the individual nebulizers operating in the corresponding commercial instruments. This indicates that the instrument constructed for these investigations performs at state-of-the-art levels and represents a valid system for nebulizer evaluation.

The data indicate some performance differences between major brands of conventional pneumatic nebulizer; however, the entire range of performance spans only a factor of 2.4 indicating similar aerosol production for the commercially available models of capillary pneumatic nebulizer evaluated in this study. The observed sensitivity for the Babington nebulizer is 0.014 ppm Cd (Table I) which falls well within the same performance range as the commercial pneumatic nebulizers. These results confirm the predicted applicability of the Babington principle to sample introduction for spectrochemical analysis. Although the present "high solids" design of the Babington nebulizer requires more sample (1 mL) than the conventional pneumatic nebulizer (0.1 mL) for high sensitivity transient sampling, the conventional device is rapidly clogged by high solids samples such as whole blood, tomato sauce, etc. These difficult matrices are however readily nebulized by the improved Babington technique. The results summarized in Table I have indicated that this is accomplished without sacrifice in sensitivity (compared with the commercially available pneumatic nebulizers).

Analysis of High Solids Samples. Direct Zn and Cu analyses in air–acetylene of several highly complex samples by the Babington procedure are summarized in Table II. This sample group includes those matrices where the metal is contained entirely in soluble form. A digestion was done on an aliquot of each sample to provide the comparison (conventional nebulizer) analyses listed opposite the Babington results in Table II. Good agreement (within the limits of sample homogeneity) between the procedures is demonstrated by Table II. This indicates the clear feasibility of applying the Babington technique to direct spectrochemical analysis of untreated (except for solids such as the NBS leaf tissue) samples and slurries of increased viscosity, high suspended solids content, and elevated salt content. Salt contents as high as 50% (w/v) or greater are readily accommodated if the solubility is this high. It should be noted that, for quantities ≥1 g of solid sample to be digested, nebulizer tolerance of higher salt contents allows less dilution of the final digest. This results in a higher signal at the instrument and an overall

Table III. Particle Size Effects

Sample	Zn (ppm)			Cu (ppm)			Fe (ppm)		
	Babington[a]	Total[b]	Soluble[c]	Babington	Total	Soluble	Babington	Total	Soluble
(1) Hunt's Tomato Sauce (Suspended particulate size in low millimeter range)	0.62	1.8	0.64	0.55	1.7	0.53			
(2) Carnation Evaporated Milk Concentrate (Suspended particulate size <5 μm)	7.5	7.9	1.6	0.17	0.17	0.11			
(3) Untreated (Babington only) Whole Blood (Suspended particulate size 5–9 μm)	3.9	7.5	0.73	0.69	0.71	0.69	240.	520.	1.5

[a] Untreated whole sample. [b] Digested whole sample. [c] Digested supernatant from centrifuged sample.

sensitivity improvement on the basis of the original solid sample.

Effect of Suspended Particulate Size. Additional sample categories are given in Table III. Comparison analyses in part (1) show that the Babington nebulizer is not affected by the large metal containing pulpy particles found in samples such as tomato sauce. The soluble metal content is determined correctly without sample clogging. Large pulpy particles are simply washed away from the nebulizer insert and removed via the drain by the flowing sample stream. No measurable memory effects are encountered if a portion of distilled water is nebulized between samples. In contrast to the large sized particulate case, part (2) of Table III demonstrates that the direct Babington spectrochemical response to sample suspensions of small metal containing particles (such as milk solids) agrees with the total metal (solids + solution) analysis when the method of additions is employed. The fact that this occurs even though the "add" is made entirely in soluble form substantiates the premise that the smaller milk solid particles are delivered to the burner in a percentage similar to solution droplets, thus yielding a total metal response. The samples in parts (1) and (2) of the table represent particle size extremes for which the Babington procedure agrees with either the total metal or soluble metal content of the sample rather than giving an intermediate response.

The case of intermediate sized suspended particles is summarized in the comparison analyses of part (3) of Table III. Zn and Fe occur in blood plasma (soluble form), but are present in much higher levels in red blood cells. The table indicates that the Babington procedure is measuring a combination of plasma and red cell content of Zn and Fe in fresh (un-hemolyzed) whole blood because the direct Babington result is much higher than the value measured by conventional digestive analysis for plasma alone. The direct Babington results (Zn, Fe), however, fall short of the total Zn and Fe content as measured by digestion procedures. This is readily explained by the larger size (5–9 μm) of intact red blood cells in comparison to the median mass diameter (3.6 μm) of solution aerosol droplets produced by the Babington nebulizer. Aerosol refinement processes in the premix chamber undoubtedly cause these larger cells to be delivered to the burner in a lesser percentage (due to their size and weight) than the droplets produced from blood plasma and the soluble "standard add". This results in a lowered measurement *not corrected* for by the method of additions since the aqueous "add" does not undergo the same percentage droplet selection process in the pre-mix chamber as the red cell metal.

Copper represents a different situation in fresh blood than iron and zinc, because the copper in blood is present primarily in soluble plasma form. Table III, part (3) demonstrates that the Babington nebulizer yields a direct atomic absorption response that is correct in this case even though the sample has not undergone hemolysis (cell rupture).

The Zn result for hemolyzed whole blood (Table II) demonstrates that simple hemolysis facilitates a correct Babington measurement of total Zn content. Hemolysis may be easily induced by standard freeze–thaw, sonication, or osmotic rupture procedures. Elements not contained appreciably by the red cells (such as Cu) can be determined directly in plasma or whole blood without treatment. If metal content of plasma or serum is desired (as is often the case) rather than whole blood, then it is *not* desirable to induce or allow hemolysis to occur especially for elements such as Zn and Fe. In this case, the plasma or serum should be separated as is normally done in conventional analysis, but it may now be analyzed directly by the Babington procedure without further treatment.

Matrix Effects Correctable by the Method of Additions. Although samples of variable viscosity, salt content, and solids content are readily analyzed by the standard addition Babington procedure, these properties may affect the calibration through surface tension and viscosity effects in the nebulizer, variable aerosol refinement in the premix chamber, as well as vaporization and diffusion effects in the flame. No attempt was made to identify the individual contributing sources of the collective matrix effect; it was simply calibrated by the method of additions for all analyses made.

CONCLUSIONS

The overall observations of these investigations are that the modified Babington nebulizer method of sample introduction into flame systems represents a rapid and reliable method of high solids atomization when suspended particle size is taken into consideration, standard addition procedures are utilized, and normal burner–nebulizer sensitivity for a 1-mL sample is adequate for the samples to be analyzed. Untreated samples and slurries containing large quantities of dissolved sugar and salt as well as suspended solids are analyzed directly with only moderate matrix effects that are easily compensated for in a high solids burner system. The unrestricted flow-through nebulizer design provides a system that is convenient to operate and is relatively "clog-free" without any sacrifice in concentration sensitivity. The authors believe that these studies represent the first reported application of the Babington principle of nebulization to spectrochemical analysis.

LITERATURE CITED

(1) H. Koizumi and K. Yasuda, *Anal. Chem.*, **48**, 1178 (1976).
(2) T. T. Gorsuch, *Analyst*, (*London*), **84**, 135 (1959).
(3) J. Y. Hwang, P. A. Ullucci, and S. B. Smith, *Anal. Chem.*, **43**, 1319 (1971).
(4) G. M. Hieftje, T. R. Copeland, D. R. de Olivares, *Anal. Chem.*, **48**, 142R (1976).
(5) D. R. Thomerson and K. C. Thompson, *Chem. Br.*, **11**, 316 (1975).

(6) B. R. Culver, "Analytical Methods for Carbon Rod Atomizers", Varian Techtron Pty. Ltd., Springvale, Vic., Australia, 1975.
(7) R. S. Babington, U.S. Patents 3,421,692; 3,421,699; 3,425,058; 3,425,059, and 3,504,8599
(8) *Popular Science*, May 1973, p 102.
(9) M. Litt and D. E. Swift, *Am. Rev. Respir. Dis.*, **105**, 308 (1972).
(10) C. T. J. Alkemade in "Analytical Flame Spectroscopy", R. Mavrodineaunu, Ed., London, 1970.
(11) G. Horlick and K. R. Betty, *Anal. Chem.*, **47**, 363 (1975).
(12) E. Sebastiani, K. Ohls, and G. Riemer, *Fresenius Z. Anal. Chem.*, **264**, 105 (1973).
(13) D. C. Manning, *At. Absorpt. Newsl.*, **14**, 99 (1975).
(14) H. Berndt and E. Jackwerth, *Spectrochim. Acta, Part B*, 30, 169 (1975).

RECEIVED for review April 12, 1977. Accepted May 13, 1977. This research was supported by the Office of Naval Research and was presented in part at the 1976 Pacific Conference on Chemistry and Spectroscopy (No. 73), Phoenix, Arizona, November 9, 1976.

Comparison of Inorganic Interferences in Atomic Absorption Spectrometric Determination of Arsenic and Selenium

F. D. Pierce* and H. R. Brown[1]

Utah Biomedical Test Laboratory, 520 Wakara Way, Salt Lake City, Utah 84108

A study was undertaken to compare the interfering effects of several selected anions, cations, and acids on routine arsenic and selenium determination by atomic absorption spectrometry. Three sample preparation/sample atomization techniques were employed: manual hydride generation with argon–hydrogen flame atomization, automated hydride generation with heated quartz tube atomization, and graphite furnace atomization. The study showed significant differences in interfering effects observed between the three techniques used.

The use of atomic absorption spectrometry has become the method of choice in analytical laboratories for the routine determination of arsenic and selenium. Determination by direct techniques with air–acetylene or argon–hydrogen flames (*1*) has lost popularity because of the greater sensitivities offered by hydride generation techniques and flameless atomization using graphite tubes. The use of hydrochloric acid and zinc granules for hydride formation has been replaced for the greater part by the use of hydrochloric acid and $NaBH_4$ because of the cleanliness of operation and relative technical ease. Coupling $NaBH_4$ hydride generation and an argon–hydrogen flame has been well-documented (*2–4*). Several papers have dealt with limited potential interference (*3, 5*). The use of a heated quartz tube (*6*) or modifications of a quartz tube (*7*) for arsenic and selenium analysis has grown because of increased sensitivities. Graphite tube atomization has become popular because of its applicability to several cation determinations and has been well-documented for the determination of arsenic and selenium (*8–11*). Analytical interferences to the graphite atomized determination of arsenic and selenium has been documented as well as limited studies comparing graphite techniques to hydride generation techniques (*12–14*).

The work described in this paper is a comprehensive study of inorganic interference to the routine determination of arsenic and selenium utilizing manual hydride generation technique with argon–hydrogen atomization, an automated hydride generation technique with a heated quartz tube atomization (*15, 16*), and a graphite tube atomization technique. The purpose of the experimentation was to document interferences encountered within the routine analytical techniques. Particular focus is placed upon laboratories which routinely handle similar sample matrices and analyze these specimens in a group fashion rather than independently.

[1] Permanent address, Utah State Division of Health, Bureau of Laboratories, 44 Medical Drive, Salt Lake City, Utah 84113

EXPERIMENTAL

Apparatus. Two atomic absorption spectrophotometers were used in this experimental study: an IL 151 and an IL 251 (Instrumentation Laboratories, Incorporated). The data readout was provided by a Dohrmann Model DC 1200R strip chart recorder (Envirotech Corporation). For flameless atomization, an IL 455 Flameless Atomizer was employed. The manual hydride generation was accomplished with an IL hydride generation system. The automated equipment used in the experimentation was comprised of a Technicon II sampler and a Technicon I proportioning pump (Technicon Instrument Corporation).

The automated selenium and arsenic analytical technique used is described in Ref. 15.

Reagents. Analytical regent-grade chemicals were used throughout the experimentation.

Procedure. Aqueous interference test solutions were prepared containing various concentrations of possibly interfering anions, cations, and acids. In the "A" group, the concentrations of Na, K, Ca, Mg, SO_4, and Cl were 3.0 mg/L, 6.0 mg/L, 16.0 mg/L, 33.0 mg/L, 67.0 mg/L, 167 mg/L, and 333 mg/L. The "B" group consisted of Al, Ba, Cd, Cr, Co, Cu, Fe, Pb, Mn, Mo, Ni, Ag, Sr, Sn, V, Zn, SiO_3, Cr_2O_7, MnO_4, VO_3, S_2O_8, NO_3, MoO_4, and PO_4. The interference solutions for these group B anions and cations used were 0.3 mg/L, 0.6 mg/L, 1.6 mg/L, 3.3 mg/L, 6.7 mg/L, 16.7 mg/L, and 33.3 mg/L. The "C" group of interference test solutions contained concentrations of 0.5% (v/v), 1.0%, 1.5%, 2.0%, and 5.0% of hydrochloric acid, nitric acid, and sulfuric acid.

To each interference test solution, an aliquot of selenium or arsenic standard was added to bring the final selenium or arsenic concentration in the interference test solution to 1.0 μg/L, 10.0 μg/L, or 100 μg/L. Aqueous solutions of the selenium and arsenic standards were prepared at concentrations of 10 mg/L using SeO_2 and As_2O_3, respectively.

For use as a control, a portion of each interference test solution, to which no arsenic or selenium standard was added, was analyzed along with a respective spiked interference test solution. The arsenic and selenium analytical results obtained from these control samples were subtracted from the results of their representative spiked interference test solution. The conclusions presented in this paper are based on these corrected analytical results.

The determination of selenium and arsenic utilizing flameless atomization was accompished at the 196.0 nm and the 193.7 nm wavelength, respectively, using background correction mode. The ramp parameters used for arsenic were for drying: 75 °C for 20 s and 225 °C for 20 s; for ashing: 750 °C for 20 s and 1000 °C for 20 s; and for atomization: 2700 °C for 10 s. The ramp parameters used for selenium were for drying: 75 °C for 20 s and

225 °C for 20 s; for ashing: 750 °C for 20 s and 1000 °C for 20 s; and for atomization: 3000 °C for 5 s. Twenty-five μL of solution was used for each atomization, and each interference test solution for flameless atomization for arsenic and selenium was made in a 0.1% $Ni(NO_3)_2$ matrix (*17*, *18*). Optimization of instrumental parameters was accomplished upon the "spiked" specimens. The analyses of the test solutions were accomplished at this optimization as an attempt to approximate a routine sample group analytical run. Standard addition techniques can be used in most cases to acquire accurate analysis of individual specimens but were not investigated within this experimental study as our attention was directed at group analyses.

The analysis of selenium and arsenic utilizing the manual hydride evolution technique utilized a hydrogen–argon flame at the 196.0 nm wavelength for selenium and the 193.7 nm wavelength for arsenic. A 10-mL aliquot of sample was placed in the hydride generator, five mL of concentrated hydrochloric acid was added prior to 1 mL of 1% $NaBH_4$. Peak height and peak area measurements were used to quantitate the generated signal.

The analysis of selenium and arsenic utilizing the automated hydride evolution technique is described in Ref. 15. A heated quartz tube was employed for atomization of selenium and arsenic and quantification at the 196.0 and the 193.7 nm wavelengths, respectively. Hydrochloric acid addition and mixing was accomplished prior to 0.5% $NaBH_4$ addition.

The use of percent analytical suppression or enhancement was chosen for presentation of the experimental results rather than presenting the multitudinous quantitative data. It is from these quantitative results that the suppressions and enhancements given were calculated and represented trends of numerous results rather than isolated findings. Percent analytical suppression or enhancement was calculated as follows:

$$\% \text{ effect} = [\text{Apparent concentration (mg/L) As or Se in spiked sample}]/[\text{Apparent concentration (mg/L) As or Se in blank sample}] \times 100$$

RESULTS AND DISCUSSION

The results of experimental work conducted on the interfering effects of the Group A anions and cations are listed in Table I.

Utilizing the manual hydride evolution technique with an argon–hydrogen flame atomization, no interfering effects were noted at anion and cation concentrations through 333 mg/L for K, Ca, SO_4 or Cl. Mg had a suppressive effect upon both the arsenic and selenium analytical signals as did Na at the higher experimental concentrations.

No interfering effects were found for any of the Group A anions or cations in either the arsenic or selenium analysis utilizing the automated hydride technique with tube atomization. These results, at the 10 μg/L As and Se concentrations, agree with the 1 μg/L As and Se concentration interference effects documented in Ref. 16.

The interfering effects of the Group A anions and cations were notably greater in the case of flameless atomization analysis. In the arsenic determination, signal enhancement was caused by Na, Ca, Mg, and SO_4, while signal suppression was noted in the presence of K and Cl. The enhancive effects noted in the arsenic determination were also confirmed for selenium analytical enhancement in regards to Ca and Mg. K also caused enhancive effects which, for arsenic, were supressive. The suppressive effects noted for arsenic determination were confirmed for Cl. On the other hand, Na and SO_4 depressed selenium and enhanced the arsenic signal.

The Group B experimental results are shown in Table II.

In the experimental study of the Group B interference effects upon arsenic and selenium determination using the manual hydride evolution technique with a hydrogen–argon flame, all tested cations and anions had a suppressive effect. The interfering effects ranged from light suppression of the analytical signal (1–10%) to moderate suppression (11–30%) to massive suppression (31–100%). In the case of arsenic determination at the 10 μg/L concentration, the experimental cations and anions which produced light suppression at a maximum concentration of 33.3 mg/L interferant were Ba, Mo, V, and SiO_3. Those producing moderate suppression to arsenic analysis were Al, Cd, Cr, Fe, Pb, Mn, Se, Zn, NO_3, and PO_4, while the cations and anions producing massive suppression to arsenic were Co, Ca, Ni, Ag, Sn, Cr_2O_7, MnO_4, VO_3, S_2O_8, and MoO_4. Of those producing massive suppression, Ni produced 100% suppression to the determination of arsenic. In the case of selenium determination at the 10 μg/L analyzed concentration utilizing the manual hydride generation technique, the anions and cations which produced a light signal suppression were Ba, V, and SiO_3, while those which produced moderate suppression to selenium were Cr, Mn, Mo, Sr, and PO_4. Most of the cations and anions used in this experimental study produced massive suppression: Al, Cd, Co, Cu, Fe, Pb, Ni, Ag, Sn, Zn, Cr_2O_7, MnO_4, VO_3, S_2O_8, NO_3, and MoO_4. Of these massive suppressors, Cu, Ni, Ag, and Sn produced total signal suppression.

Utilizing the automated hydride technique with quartz tube atomization for arsenic and selenium determination, no analytical interference was noted for any Group B cation used. However, the results using Group B anions show varying interfering effects. No interfering effect was found for SiO_3, NO_3 and PO_4 up to concentrations of 33.3 mg/L. In the determination of arsenic, Cr_2O_7, MnO_4, VO_3, S_2O_8, and MoO_4 produced only moderate suppression (11–30%). No Group B anion used in this study produced massive suppression (31–100%) to the determination of arsenic. The Group B anion effects upon selenium determination showed moderate suppression for concentrations of 33.3 mg/L Cr_2O_7, MnO_4 and S_2O_8; and massive selenium suppression for concentrations 33.3 mg/L VO_3 and MoO_4. No total signal suppression was observed upon a 10 μg/L As or Se signal for any Group B anion at concentrations up to 33.3 mg/L.

The interference effects of Group B anions and cations are notably more complex with the use of flameless atomization in comparison to either manual or automated hydride generation techniques. In arsenic determination, Group B anions and cations at 33.3 mg/L producing light enhancement (0–10%) were Al, Ba, Cr, Co, Pb, Mo, and Cr_2O_7. Those producing moderate enhancement (11–30%) were Fe, Sr, Sn, MnO_4 and NO_3; and those producing massive enhancement (31–100%) were Cu, Mn, Ni, Ag, SiO_3, and S_2O_8. The Group B anions and cations at 33.3 mg/L producing suppressive effects to the determination of arsenic included Cd, V, Zn, VO_3, and MoO_4 producing moderate suppression and PO_4 producing massive suppression. All interfering effects exhibited by Group B anions and cations at the 33.3 mg/L upon selenium determination were suppressive. At 33.3 mg/L interferant concentrations, those anions and cations producing light suppression were Sr and Zn; those producing moderate suppression were Ba, Cd, Cr, Co, Cu, Fe, Pb, Mn, Mo, Ag, Cr_2O_7, VO_3, NO_3, MoO_4, and PO_4; and those producing massive suppression were Al, Ni, Sn, V, SiO_3, MnO_4, and S_2O_8.

The results of experiments conducted to determine the effects of acids in the Group C concentration range are recorded in Table III.

Arsenic and selenium determinations utilizing the manual hydride generation technique and argon–hydrogen flame showed light arsenic suppression and moderate selenium suppression at a 5.0% (v/v) H_2SO_4 concentration. Total suppression of the 10 μg/L arsenic and 10 μg/L selenium signals were noted in HNO_3 concentrations of 1.5% (v/v) or above. No experimentation was done utilizing HCl as it is used for the generation of the hydride.

Utilizing the automated hydride technique and the quartz tube atomization for the determination of arsenic and sele-

Table I. Group A Anions and Cations Interference upon the Determination of Arsenic and Selenium Using Manual Hydride Generation, Automated Hydride Generation and Flameless Atomization

Anions or cations	Method	% effect at concentrations of[a] 3.[b] As	3.[b] Se	6.[b] As	6.[b] Se	16.[b] As	16.[b] Se	33.[b] As	33.[b] Se	67.[b] As	67.[b] Se	167.[b] As	167.[b] Se	333.[b] As	333.[b] Se	333.[c] As	333.[c] Se	333.[d] As	333.[d] Se
Na	Manual	0	0	0	0	0	0	0	0	0	−2	−4	−8	−9	−21	−14	−43	0	−6
	Auto	0	0	0	0	0	0	0	0	0	0	0	0	0	0	0	0	0	0
	Flameless	0	0	0	0	0	0	0	−3	0	−7	+2	−15	+3	−20	+8	−49	0	−10
K	Manual	0	0	0	0	0	0	0	0	0	0	0	0	0	0	0	0	0	0
	Auto	0	0	0	0	0	0	0	0	0	0	0	0	0	0	0	0	0	0
	Flameless	0	0	0	0	0	0	−2	0	−12	0	−19	0	−22	+4	−39	−9	−4	0
Ca	Manual	0	0	0	0	0	0	0	0	0	0	0	0	0	0	0	0	0	0
	Auto	0	0	0	0	0	0	0	0	0	0	0	0	0	0	0	0	0	0
	Flameless	0	0	0	−4	+3	−8	+6	+2	+9	+13	+10	+22	+14	+82	+25	+104	+5	+25
Mg	Manual	0	0	0	0	0	0	0	−2	−5	−6	−8	−12	−21	−19	−36	−37	0	−3
	Auto	0	0	0	0	0	0	0	0	0	0	0	0	0	0	0	0	0	0
	Flameless	0	0	+2	0	+6	0	+11	0	+15	+3	+21	+5	+34	+8	+63	+21	+12	0
SO_4	Manual	0	0	0	0	0	0	0	0	0	0	0	0	0	0	0	0	0	0
	Auto	0	0	0	0	0	0	0	0	0	0	0	0	0	0	0	0	0	0
	Flameless	0	0	0	−2	0	−2	0	−9	+2	−19	+11	−31	+20	−42	+26	−54	0	−18
Cl	Manual	0	0	0	0	0	0	0	0	0	0	0	0	0	0	0	0	0	0
	Auto	0	0	0	0	0	0	0	0	0	0	0	0	0	0	0	0	0	0
	Flameless	0	0	0	0	0	0	0	0	0	−9	−4	−15	−8	−22	−16	−37	0	−4

[a] Interferant concentrations in mg/L. [b] Arsenic and selenium concentration of 10.0 μg/L. [c] Arsenic and selenium concentration of 1.0 μg/L. [d] Arsenic and selenium concentration of 100 μg/L.

Table II. Group B Anions and Cations Interference upon the Determination of Arsenic and Selenium Using Manual Hydride Generation, Automated Hydride Generation, and Flameless Atomization

Anions or cations	Method	% effect of concentrations of:[a] 0.3[b] As	Se	0.6[b] As	Se	1.6[b] As	Se	3.3[b] As	Se	6.7[b] As	Se	16.7[b] As	Se	33.3[b] As	Se	33.3[c] As	Se	33.3[d] As	Se
Al	Manual	0	0	0	0	0	0	−5	−4	−9	−13	−14	−20	−19	−43	−28	−63	−5	−21
	Auto	0	0	0	0	0	0	0	0	0	0	0	0	0	0	0	0	0	0
	Flameless	0	0	0	0	0	0	0	0	0	0	+3	−24	+6	−42	+10	−81	0	−16
Ba	Manual	0	0	0	0	0	0	0	0	−1	0	−6	−4	−9	−7	−13	−11	0	0
	Auto	0	0	0	0	0	0	0	0	0	0	0	0	0	0	0	0	0	0
	Flameless	0	0	0	0	0	0	0	0	0	−3	+2	−7	+6	−14	+11	−17	0	−2
Cd	Manual	0	0	0	0	0	−8	−4	−21	−13	−39	−21	−64	−29	−73	−43	−100	−6	−27
	Auto	0	0	0	0	0	0	0	0	0	0	0	0	0	0	0	0	0	0
	Flameless	0	0	0	0	−2	0	−4	−3	−8	−11	−11	−15	−19	−16	−31	−21	−4	−4
Cr	Manual	0	0	0	0	0	0	−6	−2	−10	−7	−14	−10	−22	−18	−39	−33	−6	−3
	Auto	0	0	0	0	0	0	0	0	0	0	0	0	0	0	0	0	0	0
	Flameless	0	0	0	0	0	0	0	0	0	0	+2	−16	+6	−22	+10	−34	0	0
Co	Manual	0	0	0	−6	−4	−13	−11	−31	−19	−42	−27	−49	−34	−54	−54	−76	−12	−31
	Auto	0	0	0	0	0	0	0	0	0	0	0	0	0	0	0	0	0	0
	Flameless	0	0	0	0	0	0	0	−2	+2	−7	+4	−11	+6	−14	+12	−29	0	−2
Cu	Manual	0	−4	0	−11	−8	−24	−24	−67	−41	−89	−48	−100	−73	−100	−100	−100	−27	−64
	Auto	0	0	0	0	0	0	0	0	0	0	0	0	0	0	0	0	0	0
	Flameless	0	0	0	0	0	0	+2	−3	+13	−9	+27	−11	+62	−16	+120	−31	+3	−3
Fe	Manual	0	0	0	−4	0	−14	−3	−25	−9	−41	−16	−58	−24	−69	−33	−82	−3	−25
	Auto	0	0	0	0	0	0	0	0	0	0	0	0	0	0	0	0	0	0
	Flameless	0	0	0	0	0	0	0	0	0	0	+13	−12	+21	−19	+110	−37	0	0
Pb	Manual	0	0	0	−3	0	−9	−3	−10	−5	−31	−10	−42	−16	−43	−24	−58	−3	−19
	Auto	0	0	0	0	0	0	0	0	0	0	0	0	0	0	0	0	0	0
	Flameless	0	0	0	0	0	−2	0	−9	0	−16	+2	−21	+6	−24	+10	−37	0	−8
Mn	Manual	0	0	0	0	0	0	0	−2	−5	−11	−10	−14	−15	−24	−27	−36	0	−2
	Auto	0	0	0	0	0	0	0	0	0	0	0	0	0	0	0	0	0	0
	Flameless	0	0	0	0	0	0	+7	0	+11	−7	+18	−16	+42	−22	+96	−31	+8	0
Mo	Manual	0	0	0	0	0	0	0	0	−2	−3	−6	−10	−10	−12	−21	−16	0	0
	Auto	0	0	0	0	0	0	0	0	0	0	0	0	0	0	0	0	0	0
	Flameless	0	0	0	0	0	0	0	−2	+3	−6	+4	−13	+8	−22	+16	−31	0	−3
Ni	Manual	0	−4	−12	−13	−34	−37	−53	−82	−71	−100	−82	−100	−100	−100	−100	−100	−50	−80
	Auto	0	0	0	0	0	0	0	0	0	0	0	0	0	0	0	0	0	0
	Flameless	0	0	0	0	0	0	+2	0	+13	−14	+21	−31	+47	−42	+125	−62	0	−2
Ag	Manual	0	−4	0	−21	−4	−64	−16	−94	−23	−100	−38	−100	−47	−100	−63	−100	−16	−96
	Auto	0	0	0	0	0	0	0	0	0	0	0	0	0	0	0	0	0	0
	Flameless	0	0	+2	0	+4	0	+10	−2	+14	−4	+32	−16	+50	−20	+87	+34	+10	−2
Sr	Manual	0	0	0	0	0	−1	−3	−6	−9	−9	−13	−10	−21	−12	−30	−22	−4	−5
	Auto	0	0	0	0	0	0	0	0	0	0	0	0	0	0	0	0	0	0
	Flameless	0	0	0	0	0	0	+2	0	+6	−4	+10	−8	+14	−10	+19	−16	+2	0
Sn	Manual	0	−4	−2	−22	−6	−65	−18	−93	−25	−100	−36	−100	−43	−100	−59	−100	−17	−90
	Auto	0	0	0	0	0	0	0	0	0	0	0	0	0	0	0	0	0	0
	Flameless	0	0	0	0	+2	−4	+4	−8	+11	−14	+18	−21	+26	−42	+42	−63	+4	−8
V	Manual	0	0	0	0	0	0	0	0	0	0	−4	−6	−4	−8	−6	−16	0	0
	Auto	0	0	0	0	0	0	0	0	0	0	0	0	0	0	0	0	0	0
	Flameless	0	0	0	0	0	−4	−2	−11	−5	−24	−7	−31	−16	−40	−22	−52	−2	−10
Zn	Manual	0	0	0	−2	−2	−3	−4	−8	−7	−13	−14	−23	−16	−41	−21	−58	−4	−7
	Auto	0	0	0	0	0	0	0	0	0	0	0	0	0	0	0	0	0	0
	Flameless	0	0	0	0	0	0	0	0	−2	0	−6	−4	−13	−10	−24	−16	0	0
SiO_3	Manual	0	0	0	0	0	0	0	0	0	0	−8	−6	−10	−8	−14	−14	0	0
	Auto	0	0	0	0	0	0	0	0	0	0	0	0	0	0	0	0	0	0
	Flameless	+2	−2	+4	−11	+7	−19	+13	−33	+27	−48	+41	−44	+62	−32	+81	−38	+12	−30
Cr_2O_7	Manual	0	0	−2	−4	−8	−12	−14	−19	−22	−31	−31	−43	−34	−57	−67	−83	−12	−20
	Auto	0	0	0	0	0	0	−4	−11	−15	−17	−20	−25	−23	−29	−40	−40	−5	−10
	Flameless	0	0	0	−2	+2	−2	+2	−6	+2	−8	+4	−17	+8	−21	+13	−43	+2	−5
MnO_4	Manual	0	0	0	0	−2	−6	−8	−10	−21	−17	−24	−31	−37	−47	−62	−83	−9	−10
	Auto	0	0	0	0	0	0	−6	0	−13	−10	−21	−20	−24	−26	−50	−50	−5	−2
	Flameless	0	0	0	−2	0	−8	+4	−17	+7	−28	+11	−32	+13	−37	−27	−56	+4	−16
VO_3	Manual	0	0	0	0	0	−2	−8	−8	−13	−17	−22	−27	−37	−40	−61	−62	−7	−8
	Auto	0	0	0	0	0	0	−5	−6	−8	−14	−16	−20	−21	−36	−50	−60	−4	−5
	Flameless	0	0	0	0	0	0	−2	−4	−2	−8	−9	−14	−16	−21	−38	−43	−2	−4
S_2O_8	Manual	0	0	0	0	−4	−6	−10	−11	−18	−21	−24	−26	−32	−37	−64	−61	−10	−10
	Auto	0	0	0	0	0	−2	0	−6	−2	−11	−6	−17	−12	−22	−50	−40	0	−5
	Flameless	0	0	0	0	+2	−4	+8	−11	+17	−18	+42	−24	+124	−43	+146	−57	+9	−10
NO_3	Manual	0	0	0	0	0	−4	0	−12	−3	−26	−15	−32	−20	−36	−32	−54	0	−21
	Auto	0	0	0	0	0	0	0	0	0	0	0	0	0	0	0	0	0	0
	Flameless	0	0	0	−2	0	−3	0	−9	0	−16	+3	−21	+11	−27	+15	−42	0	−10
MoO_4	Manual	0	0	0	0	0	−2	−6	−8	−13	−18	−22	−37	−37	−43	−63	−64	−6	−9
	Auto	0	0	0	0	0	0	−2	−4	−8	−11	−21	−27	−28	−31	−40	−60	−2	−5
	Flameless	0	0	0	0	0	0	−2	0	−7	−2	−11	−9	−16	−16	−22	−34	−2	0
PO_4	Manual	0	0	0	0	0	−2	−4	−6	−8	−7	−11	−13	−19	−28	−24	−47	−5	−5
	Auto	0	0	0	0	0	0	0	0	0	0	0	0	0	0	0	0	0	0
	Flameless	0	0	−7	0	−19	−4	−30	−8	−43	−12	−64	−16	−89	−21	−100	−40	−30	−7

[a] Interferant concentrations in mg/L. [b] Arsenic and selenium concentration of 10.0 μg/L. [c] Arsenic and selenium concentration of 1.0 μg/L. [d] Arsenic and selenium concentration of 100 μg/L.

Table III. Group C Acids Interference upon the Determination of Arsenic and Selenium Using Manual Hydride Generation, Automated Hydride Generation, and Flameless Atomization

		% effect at concentrations[a]													
		0.5[b]		1.0[b]		1.5[b]		2.0[b]		5.0[b]		5.0[c]		5.0[d]	
Acid	Method	As	Se	As	Se	As	Se	As	Se	As	Se	As	Se	As	Se
HCl	Manual	-	-	-	-	-	-	-	-	-	-	-	-	-	-
	Auto	-	-	-	-	-	-	-	-	-	-	-	-	-	-
	Flameless	−10	−30	−16	−36	−20	−42	−23	−47	−47	−62	−82	−82	−27	−13
HNO_3	Manual	−52	−72	−64	−84	−100	−100	−100	−100	−100	−100	−100	−100	−100	−100
	Auto	0	0	0	0	0	0	−14	−6	−18	−21	−27	−39	0	0
	Flameless	+19	−64	+36	−72	+40	−80	+40	−82	+43	−94	+94	−100	+31	−47
H_2SO_4	Manual	0	0	0	0	−4	−4	−6	−12	−8	−16	−14	−31	−2	+5
	Auto	0	0	0	0	0	0	0	−2	−6	−10	−13	−26	−5	−8
	Flameless	+27	O.S.	+30	O.S.	+33	O.S.	+34	O.S.	+54	O.S.	+106	O.S.	+34	O.S.

[a] Acid concentrations in % (v/v). [b] Arsenic and selenium concentrations of 1.0 μg/L. [c] Arsenic and selenium concentrations of 1.0 μg/L. [d] Arsenic and selenium concentrations of 100. μg/L.

Table IV. Comparison of Observed Detection Limits and Sensitivities

	Manual		Automated		Flameless	
	Arsenic	Selenium	Arsenic	Selenium	Arsenic	Selenium
Absolute:						
sens.[a]	20 pg/mL	30 pg/mL	5 ng	15 ng	20 pg	25 pg
d.l.[b]	10 pg/mL	20 pg/mL	2 ng	4 ng	5 pg	25 pg
Relative:						
sens.[a]	2 μg/L	3 μg/L	0.5 μg/L	1.1 μg/L	0.8 μg/L	1.0 μg/L
d.l.[b]	1 μg/L	2 μg/L	0.2 μg/L	0.4 μg/L	0.2 μg/L	1.0 μg/L

[a] Sensitivity = 1% absorption. [b] Detection limit = 2 × background noise.

nium, H_2SO_4 at a final concentration of 5.0% (v/v) produced only a light suppression (0–10%) on both 10 μg/L signals while HNO_3 at 5.0% (v/v) produced a moderate signal suppression (11–30%). Again, no attempt was made at evaluating HCl interference as it is used in hydride formation.

The interference effects caused by the Group C acids upon the flameless atomization determination of arsenic and selenium were significantly greater. At a final concentration of 5.0% (v/v) HCl, massive suppression of both the μg/L arsenic signal and the 10 μg/L selenium signal was noted. HNO_3 at 5.0% (v/v) produced a massive suppression to the 10 μg/L selenium signal and a massive enhancement to 10 μg/L arsenic signal. The interference effects were studied at H_2SO_4 concentrations as low as 0.5%. Arsenic enhancement was noted as massive for 5.0% (v/v) H_2SO_4.

The purpose of experimenting with three concentrations of arsenic and selenium at the highest interferant concentration was to determine if the interference noted was predictable when the ratio existing between the interferant and the analyte concentrations was known. The possibility of error due to (1) interferant contamination or (2) quantum interference of an interferant due to the interferant concentration alone, was eliminated by the use of blank or control sample subtraction. The matching of interferant concentration with and without an analyte spike and subsequent subtraction of the blank response yielded only interference effects caused by the relationship that existed between the concentrations of interferant and those of the analyte. As shown in Tables I and II, the relationship that exists between the analysis of the 10 μg/L analyte at 33.0 mg/L and the 100 μg/L analyte at 333. mg/L (Group A) as well as the 10 μg/L analyte at 3.3 mg/L and the 100 μg/L analyte at 33.3 mg/L (Group B) interferant concentration discloses a very close correlation in results. Also, the effects of the 1 μg/L analyte concentration are notably greater than those at the 10 μg/L analyte concentration. These findings lead us to believe that the interference effect can be predetermined knowing the interferant's concentration and the resulting quantitative concentration of the analyte.

The detection limits and sensitivites observed in this experimental study for the three techniques of sample preparation/atomization are recorded in Table IV.

CONCLUSIONS

The interferences encountered in this experimental study can be summarized in the following manner:

Interferences Encountered per Technique

Flameless > Manual > Automated

There were much greater interference effects found using the flameless atomization technique than were found using the manual hydride evolution technique, and the automated hydride evolution technique produced the least amount of interfering effects within this experimental study.

The sensitivities offered by these three techniques offer a different form:

Relative Sensitivities Offered per Technique

Automated ≃ Flameless > Manual

The sensitivities offered by the automated hydride evolution technique is approximately equal to those of the flameless atomization technique employed. The manual hydride evolution technique is somewhat less sensitive than the other two techniques.

Using these two parameters, interferences encountered and relative sensitivities offered, the technique which was most advantageous to our laboratory was the automated hydride evolution technique.

ACKNOWLEDGMENT

The authors thank J. H. Nelson for his assistance and advice and the Utah State Division of Health, Bureau of Laboratories for assistance and use of some of the facilities and instrumentation.

LITERATURE CITED

(1) H. L. Kahn and J. E. Schallis, *At. Absorp. Newsl.*, **7**, 5 (1968).
(2) F. J. Fernandez, *At Absorp. Newsl.*, **12**, 93 (1973).

(3) J. Aggett and A. C. Aspell, *Analyst (London)*, **101**, 341 (1976).
(4) J. S. Caldwell, R. J. Lishka, and E. F. McFarren, *J. Am. Water Works Assoc.*, **65**, 731 (1973).
(5) A. E. Smith, *Analyst (London)*, **100**, 300 (1975).
(6) R. C. Chu, G. P. Barron, and P. Q. Baumgarner, *Anal. Chem.*, **44**, 1476 (1972).
(7) D. D. Siemer, P. Koteel, and V. Jariwala, *Anal. Chem.*, **48**, 836 (1976).
(8) R. B. Baird, S. Pourian, and S. M. Gabrielian, *Anal. Chem.*, **44**, 1887 (1972).
(9) P. R. Walsh, J. L. Fasching, and R. A. Duce, *Anal. Chem.*, **48**, 1014 (1976).
(10) G. C. Kunselman and E. A. Huff, *At. Absorp. Newsl.*, **15**, 29 (1976).
(11) P. R. Walsh, J. L. Fasching, and R. A. Duce, *Anal. Chem.*, **48**, 1012 (1976).
(12) B. B. Mesman and T. C. Thomas, *Anal. Lett.*, **8**, (7), 449 (1975).
(13) M. McDaniel, A. D. Shendribar, K. D. Reiszner, and P. W. West, *Anal. Chem.*, **48**, 2240 (1976).
(14) H. Freeman, J. F. Uthe, and B. Flemming, *At. Absorp. Newsl.*, **15**, 49 (1976).
(15) F. D. Pierce, T. C. Lamoreaux, H. R. Brown, and R. S. Fraser, *Appl. Spectrosc.*, **30**, 38 (1976).
(16) F. D. Pierce and H. R. Brown, *Anal. Chem.*, **48**, 693 (1976).
(17) T. D. Martin, J. F. Kopp and R. D. Ediger, *At. Absorp. Newsl.*, **14**, 109 (1975).
(18) J. W. Owens and E. S. Gladney, *At. Absorp. Newsl.*, **15**, 47 (1976).

RECEIVED for review January 31, 1977. Accepted May 19, 1977.

Performance of the Super Modified Simplex

M. W. Routh, P. A. Swartz,[1] and M. B. Denton*

Department of Chemistry, University of Arizona, Tucson, Arizona 85721

A new, improved simplex optimization procedure has been developed which significantly increases the utility, reliability, and efficiency of current state-of-the-art simplicial methods in the presence of random response fluctuations. Comparison of this improved procedure, the Super Modified Simplex (SMS), with several variations of the modified simplex approach utilizing an interactively computer-controlled flame spectrophotometer reveals its inherent superiority in rapidly and efficiently conforming to multidimensional response surface topography. Data are presented which indicate fewer simplices and data points, as well as a reduction in experimental time results when the SMS procedure is employed. Moreover, failure to satisfactorily locate the optimum in the presence of noise due to premature diminuation of the simplex, adherence to false ridges, or inability to accurately home in on the optimum is minimized.

The importance of determining the optimum set of operating conditions for the parameters affecting any given analysis cannot be overemphasized. While the factors involved in analytical procedures such as NMR, mass spectrometry, flame AA, AE, and AF spectrometry, inductively coupled plasma spectrometry, gas chromatography, etc., vary in number, their multi-interdependency often requires increased consideration during the optimization process.

Optimization techniques which employ empirical feedback of results to generate a better approximation to the optimum set of factor levels perhaps best utilize already existing information. Although gradient or steepest ascent (descent) methods successfully predict the direction in which the optimum search should most effectively be directed, the minimum number of experiments required for prediction of the next move and subsequent experimental measurement at the new location ($n + 1$) is somewhat undesirable when the number of variables is large or when the time to perform each of the required experiments becomes important.

Application of the sequential simplex procedure of Spendley and co-workers (*1*) which was later modified by Nelder and Mead (*2*) to optimization problems of a deterministic nature had demonstrated the utility and robustness of the procedure. Further application to the world of chemical analysis (*3–9*) has proved equally useful for a variety of applications.

Unfortunately, until such procedures became more well known to chemists, selection of optimum operating conditions often consisted of a "trial and error" approach, the results of which, although sometimes successful, vary markedly with operator skill and the individual experimental system. Systematic variation of a single factor at a time while holding all remaining factors constant (sectioning) sequentially produces individual optima but can be reliably successful only when the variables are independent of each other. Moreover, convergence on a universal optimim is usually attained very slowly and can often result in a secondary or "false" optimum.

Response surface mapping has proved to be particularly useful in locating optima when only two interdependent variables are involved. One example of response surface mapping is that of the two-dimensional flame profile describing analyte distribution profiles (*10*, *11*) or spectroscopically determined temperature profiles (*12*). This type of response surface determination produces information describing not only the variable coordinates for the optimum but also indicates the nature of the response surface in the domain of interest. Such information, however, is most often acquired at the expense of a large number of experimental measurements rendering the mapping approach cumbersome, difficult to visualize, and virtually prohibitive when the number of variables is increased. Decreasing the number of factor levels for each variable in its respective domain to two results is the basis for the factorial design where the number of experiments required is 2^n, with n defined as the number of experimental variables. Although the factorial design and the related fractional factorial design (generally composed of $^1/_2 \times 2^n$ experiments) require a reasonable number of experiments, some level of prior experience is needed in order to choose the most significant factor levels, information describing behavior near the optimum is relatively scant, and data may often be gathered in regions of little interest to the experimenter. Moreover, if factor levels are not chosen wisely (particularly if the factors are continuous in nature), not only does the domain lying between the two coordinates for each variable remain unexplored, but the response levels for a variable can often indicate that the variable has little or no effect on the experimental response or may actually dictate further optimum searches in a region of the domain far removed from the optimum.

[1] Present address, Hughes Aircraft Co., Tucson, Ariz.

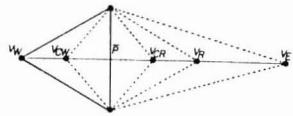

Figure 1. Two-dimensional simplex indicating possible vertex locations in the modified simplex method

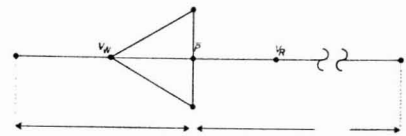

Figure 2. Possible locations for the new vertex on the extended vector joining V_W and V_R in the super modified simplex method

The most attractive attribute of the factorial design (when prior knowledge of the nature of the factors allows them to be judiciously selected) is its ability to indicate which factor areas are of most importance when conducting a more extensive optimum search.

This manuscript contrasts several variations of the Nelder and Mead Modified Simplex (MS) algorithm with an improved version which not only increases the utility, reliability, and efficiency of the simplex method in the presence of random response fluctuations (noise) but also enhances the ability of the procedure to conform rapidly and efficiently to boundary constraints. The utilization of this new approach hereafter referred to as the Super Modified Simplex (SMS) method, with an interactively computer-controlled flame spectrophotometer demonstrates its usefulness and superiority in a stochastic system without alternation of the robustness of the procedure.

DESCRIPTION OF THE MODIFIED SIMPLEX PROCEDURE

The rules of the Modified Simplex (MS) procedure have been described previously (*2, 3*) but will be reviewed briefly here to facilitate comparison with the SMS method.

A simplex is an n-dimensional geometric figure containing $n + 1$ vertices. If each dimension corresponds to a normalized factor domain, each n-coordinate vertex gives rise to a unique response. Replacement of the vertex producing the worst response with a new vertex allows translation of the simplex in n-space toward the set of optimum factor levels. There are four possible relative locations for each move as dictated by Equations 1–4:

$$V_R = \bar{P} + \alpha(\bar{P} - V_W) \qquad \alpha = 1.0 \tag{1}$$

$$V_E = \bar{P} + \gamma(\bar{P} - V_W) \qquad \gamma > 1.0 \tag{2}$$

$$V_{CR} = \bar{P} + \beta(\bar{P} - V_W) \qquad 0 < \beta < 1.0 \tag{3}$$

$$V_{CW} = \bar{P} - \beta(\bar{P} - V_W) \qquad 0 < \beta < 1.0 \tag{4}$$

Using a 2-dimensional simplex as a visual example (see Figure 1), the worst response (V_W) can be replaced by V_R (location of the reflected vertex), V_E (the expanded vertex location), V_{CR} (location of the vertex contracted between V_R and the centroid, $\bar{P}$, of the hyperface calculated without V_W), and V_{CW} (location of the vertex contracted between the centroid and V_W). Nelder and Mead (*2*) showed that the values chosen for α, β, and γ were highly significant with respect to speed and accuracy of convergence and determined the values of 1, $^1/_2$, and 2 for α, β, and γ, respectively, as producing the best compromise.

A failed contraction occurs when the response at either V_{CR} or V_{CW} is worse than the response at V_R or V_W, respectively. Nelder and Mead recommend a "massive contraction" in which each leg of the simplex is contracted to one half its present length toward the vertex producing the best response (V_B), forming a new simplex, $V_BV_N'V_W'$ or $V_BV_N'V_R'$. The responses at the new vertices are then evaluated (requiring n measurements), a new simplex is thus generated, and the optimization process is continued.

Boundary violations are handled by assigning a poor response to the vertex whose location violates the boundary constraint. The new vertex is subsequently located by a C_W contraction midway between the original point and the centroid and the optimization is allowed to continue.

DESCRIPTION OF THE SUPER MODIFIED SIMPLEX PROCEDURE

The Super Modified Simplex (SMS) procedure determines the location of the new vertex in the following way: After determination of the worst response, the responses at the centroid and reflected vertex locations are measured and a second-order polynomial curve is fitted to the responses at V_W, $\bar{P}$, and V_R. Furthermore, the curve is extrapolated beyond V_W and V_R by a percentage of the V_W–V_R vector resulting in two types of curve shapes. In the concave down case, a maximum occurs within the interval. Assuming a maximization process, evaluation of the derivative of the curve reveals the location of the predicted optimum whose response is subsequently evaluated, the new vertex is located at that position, and the optimization process is continued. In the concave up case, a response maximum does not occur within the interval so the extended interval boundary producing the highest predicted response is chosen as the new vertex location, its response is determined, and the optimization is continued. If the response at the predicted extended interval boundary location does not prove to be greater than the response at V_R, V_R may instead be retained as the new vertex and the process continued. The slope at the extended interval boundary may additionally be evaluated dictating the magnitude of the expansion coefficient, i.e., the greater the slope (indicating rapid approach to the optimum location), the smaller the required expansion coefficient and, conversely, the smaller the slope (indicating remoteness from the optimum location), the larger the required expansion coefficient.

If the object of the optimization were to be minimization of the measured response, the procedure of response curve evaluation for concavity up or down would apply simply by testing for concavity up and determining the location of zero slope (minimum response), or concavity down and subsequent location at the extended interval boundary of lowest predicted response.

The SMS procedure thus allows the new vertex the freedom of location at a nearly infinite number of positions (dependent on the resolution of the experimental variables) along the vector joining V_W and V_R plus the extensions of the vector as dictated by the expansion coefficient (see Figure 2). Note, however, that should the predicted optimum response occur at or very near the centroid, location of the new vertex at this point would reduce the dimensionality of the process and would virtually terminate any further progress of the simplex in one or more dimensions. Thus, a small "safety interval" preventing such a move is used to locate the new vertex a percentage of the factor domain away from the centroid. Use of the safety interval is unnecessary when approaching the termination of the optimization search and can easily be eliminated or minimized near the optimum.

Since it is usually desirable that the progress of the simplex proceed as nearly as possible to the boundary constraint whenever such moves are indicated, the SMS procedure incorporates a simple means of accomplishing such moves. The vector connecting V_W and V_R is terminated at the point

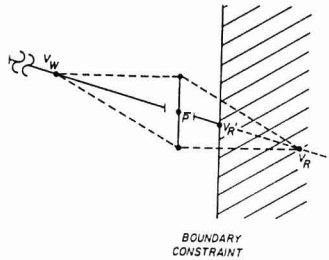

Figure 3. Possible locations for the new vertex after a boundary violation in the super modified simplex method

where the boundary constraint is intersected by the vector and this point is considered an effective V_R (V_R'). The response is then measured at V_R', the second-order polynomial curve is fitted through the responses at V_W, $\bar{P}$, and V_R' and the new vertex location determined. Thus, the new vertex may be located at V_R', i.e., at the boundary constraint or at any other location along the vector as dictated by the general SMS rules (See Figure 3).

EXPERIMENTAL

Reagents. A 1000 μg/mL stock solution of calcium was prepared using analytical reagent grade $CaCO_3$ (Mallinckrodt). A 10 μg/mL solution of calcium was prepared in 1% HNO_3 by diluting an aliquot of the stock solution to the appropriate volume with deionized distilled water and sufficient suprapure HNO_3 (Merck).

Apparatus. The experimental configuration is shown in Figure 4.

A premix laminar flow burner similar in design to that of Gutzler and Denton (*13*) but modified to accept interchangeable burner heads was employed burning a mixture of nitrous oxide and acetylene. The burner is mounted on a dovetail slide (UniSlide, Velmex, Inc., Holcomb, N.Y.) which is affixed perpendicularly to a second dovetail slide providing movement in the plane perpendicular to the angle of acceptance of the monochromator. Stepping motors (Rapid Syn model 34H-599, Computer Devices, Inc., Burlington, Mass.) connected to the dovetail slide screw shafts are driven by a Denco Research, Inc., (Tucson, Ariz.) model SM-2A dual stepper motor control unit (*14*).

Flow rotameters (Dwyer Instruments, Inc., Michigan City, Ind.) and needle valves (NUPRO Co., Cleveland, Ohio) under stepper motor control are used to determine and regulate fuel and oxidant flow rates.

Sample introduction is accomplished with an ultrasonic nebulizer similar to that described in (*15*) with the transducer driven at 1 MHz.

The vertical region viewed by the monochromator (Heath Model EU-700, Heath Co., Benton Harbor, Mich.) is restricted by a 3-mm diameter iris 25 mm in front of the monochromator entrance slit. The horizontal region viewed is limited by a light baffle contained within the monochromator. The monochromator was modified so that the slit and wavelength could also be externally controlled by a second dual stepper motor unit.

Signal detection is accomplished using an RCA 1P28A photomultiplier tube powered by a Heath EU-42A high voltage power supply. The voltage is externally digitally programmed through the use of a 10-bit latch and DAC (Cycon model CY2135, Cycon, Inc., Sunnyvale, Calif.) whose analog output is connected to the analog input provided on the photomultiplier tube power supply module. The output of the PMT is amplified to a suitable voltage level by a specially constructed variable gain current amplifier and digitalized by a 10-bit ADC (Cycon model CY3135).

Interactive control over the experiment and acquisition of digitial data were accomplished by interfacing the DAC and stepper motor controller systems to a Data General Nova 2/10

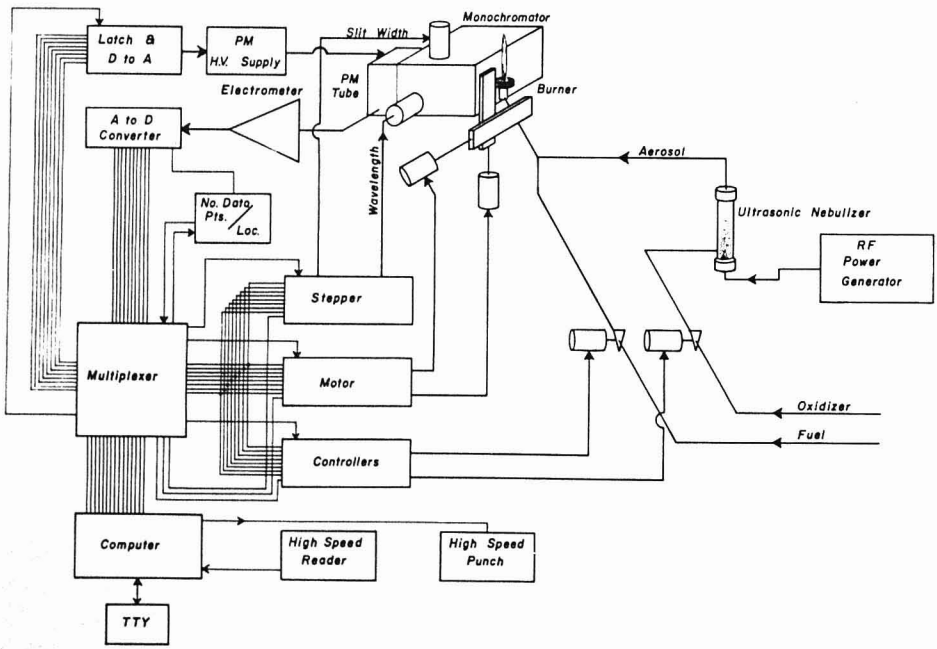

Figure 4. Experimental configuration for studying flame spectrometric processes

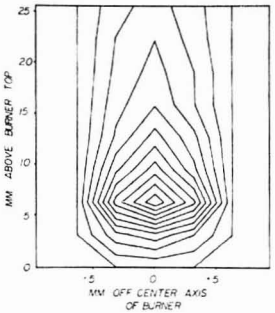

Figure 5. Net calcium emission response surface in the $X-Y$ plane perpendicular to the optical axis

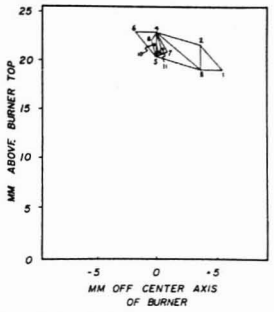

Figure 6. Failure of the modified simplex procedure (MS-1) due to premature simplex contraction

computer (Data General Corp., Southboro, Mass.) equipped with a Xebec model XFD-200 dual drive floppy disk system (Xebec Systems, Inc., Sunnyvale, Calif.) for mass storage. The optimization data are graphically processed utilizing a Tektronix model 4002A graphics terminal (Tektronix, Inc., Beaverton, Oreg.) and Hewlett-Packard model 7200A X-Y plotter (Hewlett-Packard Co., Palo Alto, Calif.).

Procedure. Calcium emission was measured at the 422.7 nm resonance line in the premixed nitrous oxide–acetylene flame. The emission signals were background-corrected by measuring the total signal 10 times at a rate of approximately 4 measurements per second at the wavelength of interest, stepping off the line an amount in excess of the bandpass, and measuring the background emission signal 10 times. High and low responses at each wavelength were discarded, the remaining respective measurements averaged, and the difference was taken as the net emission signal. The maximum net emission was sought as the desired response.

RESULTS AND DISCUSSION

The SMS approach was compared to several versions of the Modified Simplex procedure. Utilization of an exact version of the Nelder and Mead MS algorithm immediately revealed a severe limitation in a stochastic environment. Whenever a spuriously favorable response is encountered, the simplex will shrink and circle about that vertex, immobilizing the simplex progress. In order to avoid excessive retention of such vertices, a response is remeasured after $N + 1$ iterations (*4*) and averaged with the previous response (*3*). Thus, each of the versions subsequently studied included this modification.

Two-dimensional optimizations were first compared utilizing the burner position X and Y parameters for ease of illustration. A net emission response surface was first obtained by acquiring the net background corrected calcium emission signals at each intersection in an 81-point grid (see Figure 5). The optimum emission response is indicated at the center axis of the flame approximately 6 to 7 mm above the burner top.

When the simplex size (each leg typically 10% of its respective domain) and starting location were randomly chosen, the Nelder and Mead procedure with the previously mentioned modification (termed MS-1) often failed to find the true optimum in its search because of premature contraction of the simplex size (see Figure 6). After three successive C_R contractions, replacement of vertex 8 through a C_R contraction produces a failed contraction, dictating shrinkage of the simplex to form simplex 5–10–11. Although massive contractions appear to cause no significant problem when optimizing noise-free functions, failed contractions can often occur when the measured responses have significant noise fluctuations, subsequently dictating shrinkage of the simplex. This limitation becomes particularly acute when the signal gradient is small compared to the relative factor step size. As the simplex contracts in Figure 6 about the line of steepest ascent, the step size becomes too small to evoke a reliable response trend necessary for continued optimization progress ultimately causing the simplex to "run aground". When a large simplex is in the vicinity of the optimum and/or where the gradient is relatively large, a massive contraction becomes more useful in the MS-1 procedure in locating the optimum although n measurements are required to generate the new smaller simplex, thus increasing the time and number of experiments required to reach the optimum. This latter point becomes particularly awkward when higher order optimizations are performed.

Deming (*16*) has suggested that premature simplex contraction may alternately be handled in the following way. When the contracted vertex produces a response that is the worst of the current set of vertices, the second worst vertex may be rejected instead, and subsequently reflected through the centroid followed by continuation of the simplex progress toward the optimum. This treatment (termed MS-2), originally introduced by Spendley et al. (*1*) to avoid stranding the simplex on a narrow ridge or valley in a deterministic environment, was compared with the SMS method. Since the probability of stranding the simplex on a narrow ridge or valley is much more remote when optimizing a random, fluctuating signal, a third treatment (labeled MS-3) proposing continuation of the optimization process without regard to failed contractions was included as a comparative method.

The use of MS-2, through occasional rejection of the second worst vertex, was often found to cause the simplex to move in directions unfavorable to the optimization progress. Although "wrong moves" are generally self-correcting in simplex methods, additional moves are required to resume satisfactory progress and the simplex can often bog down away from the optimum when it becomes relatively small in the presence of noise, as with the MS-1 procedure. Moreover, this attribute becomes unacceptable when wrong moves are translated into undesirable or costly errors, as in industrial processing.

This premature shrinkage of the simplex in one dimension can give the appearance of adherence to a false ridge as shown in Figure 7. Reflection of vertex 5 produces a vertex whose response is worse than those at either 7 or 8, indicating a C_W contraction. Although the response at vertex 9 is worse than that at either 7 or 8, vertex 7 (the second worst response) is rejected instead producing simplex 8–9–10. Simplex 8–10–11 is subsequently formed by a C_W contraction of vertex 9. Again, the new vertex, 11, produces the worst response but vertex 10 is rejected instead to form 8–11–12. Continuation of the process causes the simplex to eventually diminish in size, appearing to lock onto a false ridge substantially removed from the optimum region.

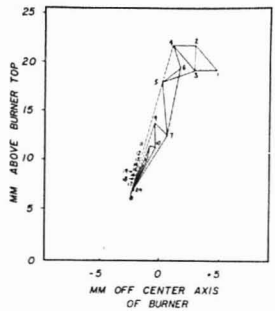

Figure 7. Failure of the modified simplex procedure (MS-2) on a false ridge

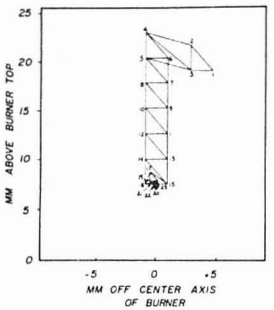

Figure 8. Failure of the modified simplex procedure to quickly contract about and elongate along the line of steepest ascent

Comparison of the MS-3 algorithm in the same 2-dimensional domain indicated no distinct advantage over the MS-1 or MS-2 procedures. Although the MS-3 method seldom prematurely contracted about a false optimum, it correspondingly demonstrated the inability to contract sufficiently quickly, often resulting in 2 or 3 successive contractions of the same vertex. Moreover, the simplex often flip–flops along the line of steepest ascent rather than contracting in the dimension(s) perpendicular and expanding in the dimension(s) parallel to the line of steepest ascent (see Figure 8). This latter attribute is, however, inherent in each of the MS methods and is a limit in the adaptability of the method eliminated by reorientation of the starting simplex.

Beginning at the same location and using the same starting simplex size (see Figure 9), the SMS algorithm is shown to be significantly more efficient in that the desired optimum is found without encountering premature shrinkage, false ridges, or inability to shrink when necessary. Moreover, the path of steepest ascent is readily apparent and closely approached if the centroids of succeeding hyperfaces were connected by a continuous line.

Comparisons of efficiency and accuracy of optimizations in higher dimensionality do not lend themselves easily to the type of graphical illustration shown in Figures 6 through 9. Therefore the data may be alternately plotted as % desired response vs. vertex number. Figure 10 shows the comparative responses obtained at each vertex for a 3-dimensional optimization of the vertical position of the burner (Y) and the flow rates of the fuel and oxidant (acetylene and nitrous oxide, respectively), clearly demonstrating the superiority of the SMS procedure.

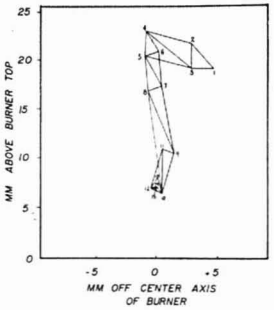

Figure 9. Rapid efficient attainment of the optimum with the super modified simplex procedure

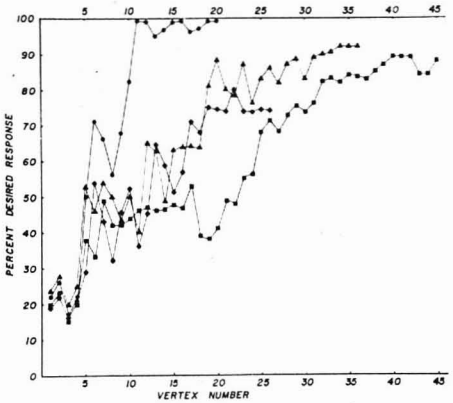

Figure 10. Comparative responses obtained at each vertex for a 3-dimensional optimization demonstrating the superiority of the super modified simplex procedure. (●) = SMS response levels; (■) = MS-1 response levels; (▲) = MS-2 response levels; and (♦) = MS-3 response levels

Similarly, comparisons in four dimensions (X and Y burner position and fuel and oxidant flow rates) reaffirm the superior ability of the SMS procedure to rapidly locate the optimum set of parameter values. The relative responses for the 4-dimensional optimization are compared in Figure 11.

A summary of comparisons in 2, 3, and 4 dimensions is shown in Table I where the relative number of simplices, number of data points, and time required for each type of MS procedure are listed as ratios. In each case, comparisons were made only under equivalent starting conditions and each number represents the mean ratio obtained.

Optimizations were deemed terminated when the coordinates for each vertex differed by less than 2% within each respective domain and the responses obtained at each vertex differed by less than $\pm ts/\sqrt{N-1}$ from the response mean, where t is Student's t for $N = 10$ at the 95% confidence level.

While the Super Modified Simplex requires an average of 72% fewer simplices, it requires an average of only 12% fewer data points to reach termination of the optimization. However, it is interesting to note that an average savings of 21% in required time is accomplished with the SMS procedure, indicating that although the SMS method requires three measurements for prediction of each successive move ($\bar{P}$, V_R, and V_{NEW}) vs. an average of ca. two for each of the

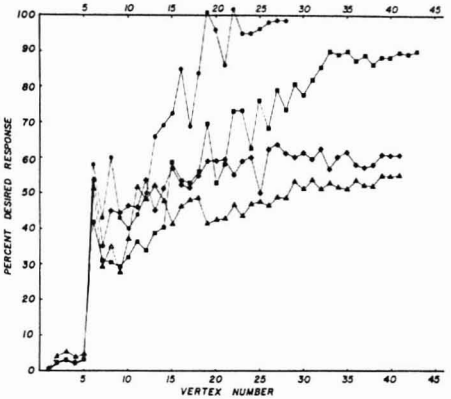

Figure 11. Comparative responses obtained at each vertex for a 4-dimensional optimization demonstrating the superiority of the super modified simplex procedure. (●) = SMS response levels; (■) = MS-1 response levels; (▲) = MS-2 response levels; and (♦) = MS-3 response levels

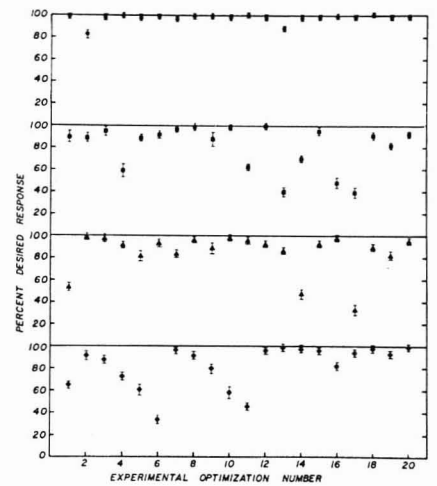

Figure 12. Comparison of the maximum responses obtained with each simplex method for a number of experimental optimizations in 2, 3, and 4 dimensions demonstrating the improved reliability of the super modified simplex procedure. (●) = SMS; (■) = MS-1; (▲) = MS-2; and (♦) = MS-3

MS methods, little time is wasted in moving each time to the centroid. Moreover, while mechanical movement is the rate-limiting step in these optimizations, small movements and the added calculation time do not significantly impede the optimization progress.

Although a clear superiority in efficiency of the SMS procedure is demonstrated in Table I, its impact becomes even more evident when the % desired response is plotted for a number of 2-, 3-, and 4-dimensional optimizations. Figure 12 illustrates the % desired response vs. experimental optimization number for each of the simplex methods compared. Each optimization number corresponds to a different optimization experiment with a unique set of starting parameters

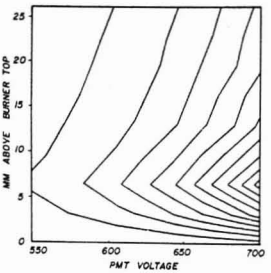

Figure 13. Net calcium emission response surface with respect to vertical location in the flame and photomultiplier tube voltage

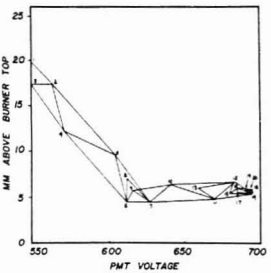

Figure 14. Reluctance of the modified simplex (MS-1) procedure to approach the boundary constraint

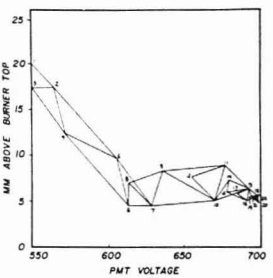

Figure 15. Reluctance of the modified simplex (MS-2) procedure to approach the boundary constraint

common to each simplex method. For example, experimental optimization number 9 corresponds to the same optimization utilizing each simplex method. The vertical bar about the % desired response maximum corresponds to $\pm ts/\sqrt{N-1}$, for $N = 10$ at the 95% confidence level. Thus, while the SMS procedure has been shown to offer a significant advantage in terms of efficiency, its overall reliability in locating the optimum set of conditions clearly demonstrates its superiority.

Comparison of the boundary constraint-handling capabilities of the simplex procedures is easily illustrated with a two-dimensional optimization of vertical burner location (Y) vs. photomultiplier tube voltage. A net calcium emission response surface obtained from an 81-point grid illustrates the response behavior within the domains of interest (see Figure 13), indicating an optimum within the domains at approximately 6 to 7 mm above the burner top at the high boundary of the PMT voltage (710 V). While the MS procedures attain the line of steepest ascent (see Figures 14–16),

Table I. Comparison of the Super Modified Simplex (SMS) Procedure with Various Modified Simplex (MS) Methods[a]

Criterion	Ratio: MS/SMS			
	MS-1	MS-2	MS-3	Avg.
2 Dimensions				
No. of simplices	1.66	1.75	1.61	1.67
No. of data pts	1.19	1.09	1.16	1.15
Time	1.20	1.17	1.19	1.19
3 Dimensions				
No. of simplices	1.72	1.75	1.73	1.73
No. of data pts	1.09	1.15	1.16	1.13
Time	1.25	1.21	1.26	1.24
4 Dimensions				
No. of simplices	1.67	1.58	2.02	1.76
No. of data pts	1.05	1.01	1.19	1.08
Time	1.15	1.18	1.24	1.19
Average				
No. of simplices	1.68	1.69	1.79	
No. of data pts	1.11	1.08	1.17	
Time	1.20	1.19	1.23	

[a] See text for explanation of the MS-1, MS-2, and MS-3 modified simplex procedures.

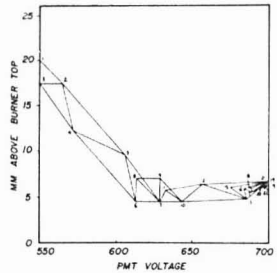

Figure 16. Reluctance of the modified simplex (MS-3) procedure to approach the boundary constraint

they reluctantly approach the boundary constraint by forming C_W contractions whenever the boundary is violated. The SMS procedure not only demonstrates its inherent ability to find the line of steepest ascent but also to rapidly flatten against the boundary constraint (see Figure 17). In each case, the termination criteria are reached after an average of 15% more measurements and 22% more time than with the SMS procedure and the maximum % desired response is 3–10% lower than that achieved with the SMS method.

Adherence to the boundary constraint is of particular importance, whether the constraint is operationally limited or self imposed, when the gradient is large near the boundary constraint. In such cases, for example, a change in the parameter value of only 1% of its relative domain may allow a response improvement of 10% or more.

CONCLUSIONS

The Super Modified Simplex procedure has been found to compare favorably to state-of-the-art Modified Simplex

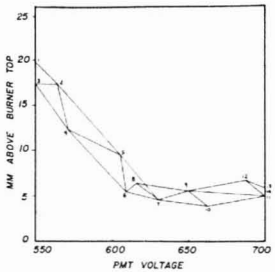

Figure 17. Inherent ability of the super modified simplex procedure to rapidly approach and adhere to a boundary constraint

optimization procedures in systems where there is random fluctuation in the desired response (noise). Although additional calculations are required for the SMS procedure, virtually no delay in the experimental time frame is realized since the time required to change the experimental variables is much greater than the computer's calculation time. As a result of the inherent superiority of the SMS method to rapidly and efficiently conform to response surface topography, a savings in number of simplices, data points, and time required to locate the optimum region is realized. Moreover, failure to find the true optimum in the presence of noise due to premature diminution of the simplex size, adherence to false ridges, and inability to "home in" on the optimum is minimized.

When the study is limited by a boundary constraint, the SMS procedure allows the simplex to elongate along and more rapidly adhere to the constraint if such a parameter value is indicated. This attribute can be of particular significance when the gradient is large near a boundary constraint.

LITERATURE CITED

(1) W. Spendley, G. R. Hext, and F. R. Himsworth, *Technometrics*, **4**, 441 (1962).
(2) J. A. Nelder and R. Mead, *Comput. J.*, **7**, 308 (1965).
(3) S. L. Morgan and S. N. Deming, *Anal. Chem.*, **46**, 1170 (1974).
(4) R. R. Ernst, *Rev. Sci. Instrum.*, **39**, 998 (1968).
(5) S. N. Deming and S. L. Morgan, *Anal. Chem.*, **45**, 278A (1973).
(6) D. E. Long, *Anal. Chim. Acta*, **46**, 193 (1969).
(7) G. L. Ritter, S. R. Lowry, C. L. Wilkins, and T. L. Isenhour, *Anal. Chem.*, **47**, 1951 (1975).
(8) L. R. Parker, Jr., S. L. Morgan, and S. N. Deming, *Appl. Spectrosc.*, **29**, 429 (1975).
(9) E. R. Johnson, C. K. Mann, and T. J. Vickers, *Appl. Spectrosc.*, **30**, 415 (1976).
(10) N. V. Mossholder, V. A. Fassel, and R. N. Kniseley, *Anal. Chem.*, **45**, 1614 (1973).
(11) M. W. Routh and M. B. Denton, *Appl. Spectrosc.*, **30**, 344 (1976).
(12) B. Lewis and G. von Elbe, "Combustion, Flames, and Explosions of Gases", 2nd ed., Academic Press, New York, N.Y., 1961, p 262.
(13) D. E. Gutzler and M. B. Denton, *Anal. Chem.*, **47**, 830 (1975).
(14) M. B. Denton, M. W. Routh, J. D. Mack, and D. B. Swartz, *Am. Lab.*, **8**, 69 (1976).
(15) M. B. Denton and D. B. Swartz, *Rev. Sci. Instrum.*, **45**, 81 (1974).
(16) S. N. Deming, University of Houston, private communication, 1976.

RECEIVED for review December 9, 1976. Accepted May 17, 1977. This investigation was supported in part by the Office of Naval Research.

Determination of pK_a Values of Acid Components in Atmospheric Condensates by Linearization of Segmented Titration Curves

M. D. Seymour, J. W. Clayton, Jr., and Quintus Fernando*

Department of Chemistry and Toxicology Program, University of Arizona, Tucson, Arizona 85721

An iterative calculation has been used to segment and linearize a potentiometric titration curve that was obtained for a mixture of acids. The slopes and *x*-intercepts of the linear plots (modified Gran plots) were used to calculate the acid dissociation constants and the concentrations, respectively, of the acid components in the mixture.

Gran plots (*1, 2*) and various forms of modified Gran plots have been used to locate the equivalence point in a potentiometric titration. This technique of end-point location has found wide application in acid–base titrimetry, particularly in the determination of very weak acids or bases or very dilute solutions of acids or mixtures of weak acids (*3–6*). Improved equations that are applicable to systems containing a monoprotic acid or polyprotic acids have been derived and tested successfully (*7, 8*). Computer programs based on modified Gran plots have been employed to process potentiometric data obtained in the course of the titration of a single acid (*6*) as well as mixtures of acids of nearly equal strengths (*9*). Computer calculations have also been used to determine the accuracy of Gran plots (*10*) and to examine their limitations (*11*).

Almost all of the published work has been concerned with the development of rapid and accurate methods for the analysis of weak acids or mixtures of acids (*12–14*). The use of Gran plots for the determination of acid dissociation constants has attracted relatively little attention (*6, 7, 15, 16*). We report below a method for the determination of the concentrations and pK_a values of the acid components in a mixture of acids. The method is based on the use of modified Gran functions for carrying out the segmentation and linearization of a titration curve. The acid dissociation constants that are calculated from the slopes of the modified Gran plots serve to identify the acids, and their concentrations are given by the intercepts of the Gran plots with the abscissa. The method is of general applicability and can be computerized and used for the analysis of unknown mixtures of acids. The method has been verified by the analysis of synthetic mixtures of acids, that resemble the acid composition of atmospheric condensates, and rainwater samples that were collected in the Tucson area. We have found that most of these samples contain four acid components, one of which is a strong acid.

EXPERIMENTAL

Reagents. A solution of NaOH (50% w/w) was prepared and filtered under nitrogen. Approximately 0.5 mL of the filtered solution was diluted with 1 L of deionized water which had been boiled, and cooled under nitrogen. The NaOH solution was stored in a Teflon lined flask that was vented to the atmosphere through an Ascarite trap and a tube capped with a rubber septum was provided for removal of the NaOH solution. A syringe microburet was filled with the carbonate free NaOH solution and standardized with potassium acid phthalate.

Stock solutions (0.01 M) of $NaHCO_3$ and NH_4Cl were prepared from Analytical Reagent grade chemicals and standardized with the NaOH solution. The $NaHSO_4$ stock solution was prepared from constant boiling H_2SO_4, recrystallized Na_2SO_4, and deionized water. These stock solutions were diluted a hundredfold just before use.

The ionic strength was kept constant, in the course of a titration, with NaCl. A solution of 0.10 M NaCl was prepared in deionized, carbon dioxide-free water and stored under nitrogen. An appropriate volume of the NaCl solution was introduced directly into the titration vessel under nitrogen pressure, thereby preventing the NaCl solution from coming into contact with the carbon dioxide in the atmosphere.

Potentiometric Titrations. All titrations were carried out in a jacketed titration vessel which was maintained at 25 °C. During the titration, nitrogen gas, which was saturated with water vapor, was used to blanket the surface of the solution that was being titrated. Nitrogen gas was not bubbled through the solution during a titration.

The required volume of the stock solution, or a mixture of the stock solutions, was introduced into the titration vessel and diluted with the stock solution of 0.10 M NaCl. The solution was stirred with a magnetic stirrer and any carbon dioxide that was introduced into the solution from the atmosphere was expelled by means of a stream of nitrogen gas presaturated with water vapor. The titration was carried out by placing the tip of the microburet below the surface of the solution in the titration vessel and adding increments of the NaOH solution. A glass-saturated calomel electrode pair, calibrated with NBS buffers at pH 4.01, 6.86, and 9.18, together with an Orion Model 701 Digital pH meter were employed for the pH measurements.

The $NaHCO_3$ stock solution was always added to the diluted solutions in the titration vessel to prevent the localized generation of an excess of carbon dioxide, which occured when concentrated solutions were mixed.

Samples of atmospheric condensates or rainwater were made 0.10 M in NaCl by the addition of solid NaCl to 10 mL of the sample, and the potentiometric titration was carried out as described above.

Derivation of Modified Gran Functions. All titrations were carried out in solutions in which the ionic strength was maintained at a constant value of 0.10 with NaCl. The pH meter readings were converted into hydrogen ion concentrations, $[H^+]$, with the aid of Equations 1 and 2.

$$pH_{measured} = -\log[H^+] - \log y_{H^+} = \frac{E - E'}{\ln 10\, RT/F} \quad (1)$$

$$-\log y_{H^+} = \frac{0.51\, I^{1/2}}{1 + (3.30 \times 10^7)(9.0 \times 10^{-8})I^{1/2}} \quad (2)$$

where y_{H^+} is the activity coefficient of the hydrogen ion; I, the ionic strength of the solution; and the ion size parameter of the hydrogen ion is assumed to be 9.0×10^{-8}. E represents the potential difference in millivolts at 25 °C between the glass electrode and the saturated calomel electrode. E' is a constant if the potential of the saturated calomel electrode and the liquid junction potential remain constant. If the behavior of the glass electrode is Nernstian and the measurements are carried out at 25 °C, $\ln 10\, RT/F$ is a constant and equal to 59.16.

A synthetic mixture of $KHSO_4$, H_2CO_3, and NH_4Cl was prepared by adding an excess of $KHSO_4$ to a mixture of $NaHCO_3$ and NH_4Cl. The total volume of NaOH added at the successive

equivalence points in the neutralization of each of the components, HSO_4^-, H_2CO_3, NH_4^+, and HCO_3^-, is V_{SA}, V', V_{WA}, and V'', respectively. Hence, the acid components in the mixture, HSO_4^-, H_2CO_3, NH_4^+, and HCO_3^- are neutralized by V_{SA}, $(V' - V_{SA})$, $(V_{WA} - V')$ and $(V'' - V_{WA})$ mL of standard NaOH solution. The analytical concentrations, (in moles/L), of each of the acid components, $C_{HSO_4^-}$, $C_{H_2CO_3}$, $C_{NH_4^+}$, and $C_{HCO_3^-}$, are given by the following mass balance equations:

$$C_{HSO_4^-} = \frac{V_{SA}C_B}{(V_0 + V)} = [SO_4^{2-}] = [K^+] \quad (3)$$

(the HSO_4^- concentration is negligibly small because HSO_4^- is considered to be completely dissociated in the solution under consideration).

$$C_{H_2CO_3} = \frac{(V' - V_{SA})C_B}{(V_0 + V)} = [H_2CO_3] + [HCO_3^-] + [CO_3^{2-}] \quad (4)$$

$$C_{HCO_3^-} = \frac{(V'' - V_{WA})C_B}{(V_0 + V)} \quad (5)$$

$$C_{NH_4^+} = \frac{(V_{WA} - V')C_B}{(V_0 + V)} = [NH_4^+] + [NH_3] = [Cl^-] \quad (6)$$

All the terms in square brackets are molar concentrations, C_B the molar concentration, and V the volume of NaOH added. The initial volume of the solution is V_0 and the sodium ion concentration in solution is given by:

$$[Na^+] = \frac{VC_B}{(V_0 + V)} \quad (7)$$

The volume of NaOH required to neutralize the strong acid in solution is V_{SA}, and can be determined experimentally. The electroneutrality condition is:

$$[Na^+] + [K^+] + [NH_4^+] + [H^+] = [OH^-] + 2[SO_4^{2-}] + [HCO_3^-] + 2[CO_3^{2-}] + [Cl^-] \quad (8)$$

Substitution of the mass balance Equations 3-7 in Equation 8 and rearrangement of the terms gives:

$$V_{SA}C_B - VC_B = ([H^+] - [OH^-])(V + V_0) - C_B(V_{WA} - V')\alpha_1^{NH_4^+} - C_B(V' - V_{SA})(\alpha_1^{H_2CO_3} + 2\alpha_2^{H_2CO_3}) \quad (9)$$

i.e.

$$V_{SA}C_B - VC_B = F_{SA} \quad (10)$$

where

$$\alpha_1^{NH_4^+} = \frac{K_{NH_4^+}}{[H^+] + K_{NH_4^+}} \text{ and } (\alpha_1^{H_2CO_3} + 2\alpha_2^{H_2CO_3}) = \frac{K_1[H^+] + 2K_1K_2}{[H^+]^2 + K_1[H^+] + K_1K_2}$$

$K_{NH_4^+}$ represents the acid dissociation constant of NH_4^+ and K_1 and K_2 the successive acid dissociation constants of H_2CO_3. The function F_{SA} is a modified Gran function and a plot of F_{SA} vs. V should give a straight line which has a slope of $-C_B$. The point of intersection of this straight line and the abscissa is $(V_{SA},0)$.

The volume of NaOH required to half-neutralize the H_2CO_3 is $(V' - V_{SA})$, and is determined experimentally with the aid of the modified Gran function F' which is derived as follows: the mass and charge balance Equations 3-8, together with the expression for K_1, the first acid dissociation constant of H_2CO_3 give:

$$\frac{K_1([OH^-] - [H^+])(V + V_0)}{C_B} + K_1\alpha_2^{H_2CO_3}(V' - V_{SA}) - K_1\alpha_0^{NH_4^+}(V_{WA} - V') + K_1[(V' - V_{SA}) + V_{SA} + (V_{WA} - V') - V] = \frac{[H^+]([H^+] - [OH^-])(V + V_0)}{C_B} - [H^+]\,2\alpha_2^{H_2CO_3}(V' - V_{SA}) + [H^+]\alpha_0^{NH_4^+}(V_{WA} - V') + [H^+][V - V_{SA} - (V_{WA} - V')] \quad (11)$$

where $\alpha_0^{NH_4^+} = [H^+]/([H^+] + K_{NH_4^+})$. Rearrangement of this equation gives:

$$K_1V' - K_1V = \frac{([H^+] - [OH^-])(V + V_0)([H^+] + K_1)}{C_B} + [H^+](V - V_{SA}) - \alpha_2^{H_2CO_3}(K_1 + 2[H^+])(V' - V_{SA}) - \alpha_1^{NH_4^+}(K_1 + [H^+])(V_{WA} - V') \quad (12)$$

i.e.,

$$K_1V' - K_1V = F' \quad (13)$$

The linear plot of F' vs. V has a slope, $-K_1$, and an intercept on the x-axis equal to V'.

The volume of NaOH required to neutralize the weak acid, NH_4^+, with an acid dissociation constant of $K_{NH_4^+}$ is $(V_{WA} - V')$, and can be determined by extrapolation of the straight line plot of the modified Gran function F_{WA} vs. V to intersect the abscissa at the point $(V_{WA}, 0)$. The derivation of the function F_{WA} follows the same pattern as before for the derivation of F_{SA} and F', and is given by:

$$K_{NH_4^+} \cdot V_{WA} - K_{NH_4^+} \cdot V = \frac{([H^+] - [OH^-])(V + V_0)([H^+] + K_{NH_4^+})}{C_B} + [H^+](V - V') + (\alpha_0^{H_2CO_3} - \alpha_2^{H_2CO_3})([H^+] + K_{NH_4^+})(V' - V_{SA}) \quad (14)$$

where $\alpha_0^{H_2CO_3} = [H^+]^2/([H^+]^2 + K_1[H^+] + K_1K_2)$.
i.e.,

$$K_{NH_4^+} \cdot V_{WA} - K_{NH_4^+} \cdot V = F_{WA} \quad (15)$$

The slope and the x-intercept of the linear plot can be used to obtain the best estimates of $K_{NH_4^+}$ and V_{WA}, respectively.

In the presence of excess strong acid, it is not necessary to determine a value for V'' because, $(V' - V_{SA}) = (V'' - V_{WA})$.

The experimental determination of V'' from a plot of the modified Gran function F'' vs. V, will serve as a check on the validity of the method for the synthetic sample containing an excess of $KHSO_4$. The function F'' is derived as before and is given by:

$$K_2V'' - K_2V = \frac{([H^+] - [OH^-])(V + V_0)([H^+] + K_2)}{C_B} + [H^+](V - V_{WA}) + \alpha_0^{NH_4^+}([H^+] + K_{NH_4^+})(V_{WA} - V') + \alpha_0^{H_2CO_3}([H^+] + 2K_2)(V'' - V_{WA}) \quad (16)$$

i.e.,

$$K_2V'' - K_2V = F'' \quad (17)$$

Values of K_2 and V'' can be obtained from the slope and x-intercept of the linear plot of F'' vs. V in the region $V_{WA} < V < V''$.

Calculation of Approximate Values of the Gran Functions. The experimental data set that is obtained consists of a series of measured pH values and the corresponding values of V,

Table I. Determination and Identification of the Acid Components in Atmospheric Condensates and Rainwater Samples Collected in Tucson

Acid components	Condensate samples		Rainwater samples	
	No. 35A	No. 36A	No. 141	No. 142
	μmol found in 10 mL			
Strong acid	0.47	0.47	0.10	0.03
NH_4^+	0.91	0.68	0.60	0.65
H_2CO_3	0.23	0.18	0.14	0.19
HCO_3^-	0.19	0.18	0.07	0.15
	Acid dissociation constants found			
NH_4^+	6.25×10^{-10}	7.15×10^{-10}	6.94×10^{-10}	6.25×10^{-10}
H_2CO_3	7.69×10^{-7}	8.33×10^{-7}	3.33×10^{-7}	5.00×10^{-7}
HCO_3^-	1.58×10^{-10}	1.92×10^{-10}	1.72×10^{-10}	1.67×10^{-10}

the volume of NaOH added. The hydrogen ion concentration, $[H^+]$, can be readily calculated for each of the values of $(pH)_{measured}$ from Equations 1 and 2. The first two or three values of $[H^+]$ vs. V are sufficient to give an approximation of the straight line given by Equation 10 in which the values of F_{SA} are calculated by using only the first term on the right hand side of Equation 9. A first estimate of V_{SA} is obtained from the intersection of this straight line and the x-axis. The first two or three values of $V > V_{SA}$ are used next to obtain an approximate straight line given by Equation 13. The first and second terms on the right hand side of Equation 12 are used to calculate an approximate value of the function F'. The value of K_1 in this term can either be ignored, since $K_1 < H^+$ in this region of the titration curve, or a reasonable estimate of K_1 can be used. These approximate values of F' and V are used to establish a straight line that intersects the x-axis at the point $(V', 0)$. Values of $V > V'$ are next used to establish a straight line described by Equation 15, and approximate values of the function F_{WA} are calculated as before, by using the first two terms on the right hand side of Equation 14, either with or without a reasonable estimate of $K_{NH_4^+}$. After the straight line described by Equation 15 is established, and its point of intersection, $(V_{WA}, 0)$, with x-axis is determined, the next several values of $V > V_{WA}$ are used to establish the succeeding straight line given by Equation 17. In this manner the titration curve is divided approximately into four segments from which initial estimates of V_{SA}, V', V_{WA}, V'', K_1, $K_{NH_4^+}$, and K_2 are obtained. These initial estimates are used to refine the modified Gran functions, F_{SA}, F', F_{WA}, and F''.

Refinement of the Modified Gran Functions. At this stage in the calculation, approximate values of V_{SA}, V', V_{WA}, and V'' have been obtained together with initial estimates of K_1, $K_{NH_4^+}$, and K_2 from the slopes of the straight lines given by the approximate Gran functions F', F_{WA}, and F'' vs. V. These initial estimates of the volumes and acid dissociation constants can be refined in the following manner.

In the region $0 < V < V_{SA}$, the function F_{SA} is given by Equation 9. The relative magnitude of each of the three terms on the right hand side of Equation 9 can be estimated and, if necessary, a better value of F_{SA} can be calculated for each value of V. The straight line plot of F_{SA} vs. V should give an improved value of V_{SA} which can be utilized in Equation 12.

For values of V in the region $V_{SA} < V < V'$, the function F' can be calculated with the new value of V_{SA}. The linear plot of F' vs. V in this region will give better values of V' and K_1 which can be used to further refine the functions F' and F_{WA} (Equations 13 and 15).

In the region $V' < V < V_{WA}$, the linear plot of F_{WA} vs. V can be refined to give better values of $K_{NH_4^+}$ and V_{WA} which are in turn employed to refine the function F'' (Equation 17). This method of refinement will ultimately yield four straight lines (Figure 1) from which reliable values of the acid dissociation constants, K_1, $K_{NH_4^+}$, and K_2 and the equivalence volumes V_{SA}, V', V_{WA}, and V'' are obtained.

The above equations are valid for the synthetic samples that contained four acid components, one of which was a strong acid. If any acidic impurities were introduced into the solution, there would be significant deviations from linearity in one or more linear segments. In the analysis of unknown samples of rainwater or atmospheric condensates, the presence of unexpected acidic species will become evident as the segmentation and linearization procedure that is described above is carried out. Simple modifications in the Gran functions that are derived above can be made to take into account the presence of any acidic species that has a pK_a value that is ±0.5 from the pK_a value of another acid that is present in the solution.

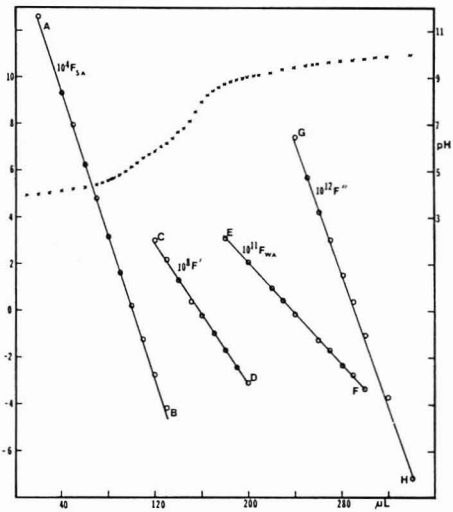

Figure 1. Linearized segments of the titration curve of a mixture of 1.84 μmol HSO_4^-, 1.48 μmol H_2CO_3, and 1.31 μmol NH_4^+ vs. 1.540×10^{-2} M NaOH. F_{SA}, F', F_{WA}, and F'' are the modified Gran functions plotted vs. the volume of NaOH added (in μL). The slopes of F' and F'' give the acid dissociation constants of H_2CO_3 and the slope of F_{WA} gives the acid dissociation constant of NH_4^+. The intersections of these straight lines with the abscissa give the number of μL of NaOH required to neutralize each of the acid components in the mixture

RESULTS AND DISCUSSION

The segmentation and linearization of the titration curve of a synthetic mixture consisting of 1.84 μmol HSO_4^-, 1.48 μmol H_2CO_3, and 1.3 μmol NH_4^+ in a total volume of 10 mL is shown in Figure 1. The initial pH of the solution was 3.89. AB is the best straight line drawn through the experimental points calculated with the aid of Equation 10 in the segment of the titration curve from pH 3.93 to 6.20. The slope of the straight line is C_B, the concentration of the titrant. The straight line AB intersects the x-axis at the point $(V_{SA}, 0)$ and the volume V_{SA} μL corresponds to 1.57 μmol of HSO_4^-. CD

is the linearization of the next segment of the titration curve from pH 5.86 to 9.04 (Equation 13). The slope of CD is 7.66×10^{-7} which compares well with the expected value, 7.76×10^{-7}, the first acid dissociation constant of H_2CO_3 at an ionic strength of 0.10. The intersection of the straight line CD with the x-axis gave a value of $(V' - V_{SA})$ which corresponded to 0.86 μmol of H_2CO_3. The large discrepancy between this value and the expected value of 1.48 is caused by the loss of CO_2 from the solution. This was verified by repeating the determination with the identical initial amounts of HSO_4^-, H_2CO_3, and NH_4^+. In the latter experiment, the solution was allowed to stand in a nitrogen atmosphere for 1 h before the titration was carried out. The value of $(V' - V_{SA})$ obtained in this case corresponded to 0.15 μmol H_2CO_3, which shows that there is a continuous loss of dissolved CO_2 from the solution until an equilibrium concentration is reached.

EF is the linearization of the segment of the titration curve from pH 8.71 to 9.82 (Equation 15). The slope of EF is 5.17×10^{-10} which compares well with the expected value, 5.30×10^{-10}, the acid dissociation constant of NH_4^+ at an ionic strength of 0.10. The intersection of EF with the abscissa gives $(V_{WA} - V')$, which corresponds to 1.39 μmol of NH_4^+. The straight line GH represents the linearization of the segment of the titration curve from pH 9.45 to 10.07 (Equation 17). The slope of GH is 1.4×10^{-10}; the expected value for the second dissociation constant of H_2CO_3 is 1.40×10^{-10} at an ionic strength of 0.10. Again, the number of μmoles the HCO_3^- obtained experimentally (0.79) is much less than the expected value because CO_2 is lost in the course of the titration.

Replicate titrations were carried out to determine the reproducibility of the method. It was found that 1 to 2 μmol of HSO_4^- and NH_4^+ could be determined in 10 mL of solution with a relative standard deviation of 3 to 7%. All four acidic components could be readily identified from the slopes of the modified Gran plots. Weak acids with closely spaced acid dissociation constants, e.g., NH_4^+ and HCO_3^-, can be readily identified.

The method was applied to two samples of atmospheric condensates and two samples of rainwater from Tucson. The condensate samples were collected on the roof of the Atmospheric Sciences building at the University of Arizona. A stainless steel plate cooled below the dew point was used to collect the condensate droplets. The results obtained are summarized in Table I. There was no evidence for the presence of any weak acids other than NH_4^+, H_2CO_3, and HCO_3^-. If any metal ions were present in the rainwater or condensate samples, their tendency to act as Bronsted acids was not detected by this method. Analysis of these samples by atomic absorption spectrophotometry showed that the only detectable cations besides the NH_4^+ and H^+ were K^+ and Ca^{2+} which were present in the 0.02- to 0.07-ppm range. Very little strong acid was found in all the samples; the rainwater contained significantly smaller amounts of strong acid than the condensates. The strong acid can either be HSO_4^- or can be the dissociated protons from HNO_3 or HCl. It is significant that no HSO_3^- was found in these samples. This weak acid species, with an acid dissociation constant of 1.9×10^{-7} at an ionic strength of 0.10 would have affected the determination and identification of the H_2CO_3 species. The concentration of H_2CO_3 in all the samples is approximately equal to the equilibrium value at ambient temperatures (0.1 to 0.2 μmol/10 mL). Therefore, it may be concluded that the concentration of HSO_3^- in these samples is negligibly small. Moreover, we have found that in the titration of synthetic samples containing HSO_3^-, rapid oxidation to HSO_4^- occurs in solution in the presence of dissolved oxygen.

The nature of the strong acid species that is present in rainwater has been a controversial issue for some time. We propose to employ our method in a nonaqueous system to distinguish between the various strong acids that may be present in rainwater.

LITERATURE CITED

(1) G. Gran, *Acta Chem. Scand.*, **4**, 559 (1950).
(2) G. Gran, *Analyst, (London)*, **77**, 661 (1952).
(3) F. Ingman and E. Still, *Talanta*, **13**, 1431 (1966).
(4) A. Johansson, *Analyst*, (London), **95**, 535 (1970).
(5) A. Ivaska, *Talanta*, **21**, 1167 (1974).
(6) A. Ivaska and E. Wanninen, *Anal. Lett.*, **6** (11), 961 (1973).
(7) T. N. Briggs and J. E. Stuehr, *Anal. Chem.*, **46**, 1517 (1974).
(8) D. Midgley and C. McCallum, *Talanta*, **21**, 723 (1974).
(9) F. Ingman, A. Johansson, S. Johansson, and R. Karlson, *Anal. Chim. Acta*, **64**, 113 (1973).
(10) I. Hansson and D. Jagner, *Anal. Chim. Acta*, **65**, 373 (1973).
(11) C. McCallum and D. Midgley, *Anal. Chim. Acta*, **65**, 155 (1973).
(12) A. Ivaska, *Talanta*, **22**, 995 (1975).
(13) C. McCallum and D. Midgley, *Anal. Chim. Acta*, **78**, 171 (1975).
(14) C. McCallum and D. Midgley, *Anal. Chem.*, **48**, 1232 (1976).
(15) A. Ivaska and L. Harju, *Talanta*, **22**, 1051 (1975).
(16) M. D. Seymour and Q. Fernando, *J. Chem. Educ.*, **54**, 225 (1977).

RECEIVED for review April 4, 1977. Accepted June 3, 1977. Work supported by the Engineering Center, Metal Mining Division, Kennecott Copper Corporation, Salt Lake City, Utah.

Composition, Treatment Efficiency, and Environmental Significance of Dye Manufacturing Plant Effluents

Larry M. Games and Ronald A. Hites*

Department of Chemical Engineering, Massachusetts Institute of Technology, Cambridge, Massachusetts 02139

Extraction of the organic compounds from a dye manufacturing plant wastewater with methylene chloride revealed the presence of several chemicals, some of which may be potentially toxic. Qualitative results of composite sampling over a 2.5-month period indicated that grab sampling techniques would have been misleading in assessing environmental impact. Semi-quantitation of the composites from both treated and untreated effluents indicated that some compounds, 1,3,3-trimethyloxindole for example, were actually *increasing* in concentration as a result of reactions occurring during treatment. One of the compounds identified, 5-chloro-3-phenyl-1,2,4-thiadiazole, has been patented as a nematocide and seems to result from an impurity in a raw material. The lack of relevant toxicity data about most of the compounds found in this study emphasizes the need for methods of determining the effects of chronic low level exposures to water pollutants.

Synthetic chemicals associated with various types of industries have been shown to be the cause of tumor formation leading to increased incidence of cancer among industrial workers employed in these operations. A notable, fairly recent example is the clustering of rare liver cancer cases among employees of plants producing or utilizing vinyl chloride. In the late 1800's, dye manufacturing plant employees were found to be victims of increased incidence of bladder cancer, later traced to the use of benzidine and 2-naphthylamine in dye synthesis (*1*). Some dyes, such as Red Dye No. 2, have also been shown to be carcinogenic (*1*). Because of these previous findings concerning the dye industry, and because dye manufacturing in general involves the use of rather complex and sophisticated chemicals of various kinds, we chose a dye manufacturing plant at which to conduct an in-depth study of the types and amounts of synthetic organic compounds being released into the environment.

The only previous study of a dye plant effluent of which we are aware was a rather cursory study done by the EPA (*2*), even though a rather large quantity of dyes are produced annually in the United States, about 3×10^8 lb (*3*). Since some dye intermediates are known to be toxic, an extensive study seemed to be desirable. This report includes (a) an identification and semi-quantitation of the dichloromethane extractable organic compounds present in the dye plant effluent, (b) an assessment of the abatement efficiency of the wastewater treatment plant on the basis of individual compounds versus COD or BOD measurements, and (c), from the analysis of receiving water and sediment samples, an evaluation of the environmental significance or hazard associated with the particular plant studied.

Plant Characteristics and Geography. The geographical layout of the plant is shown in Figure 1. The plant utilizes an average of 3×10^6 gallons/day process water drawn from the fresh water Back River and released after treatment into the brackish water Cooper River which flows directly into the Atlantic Ocean. The flow of the Cooper River is such that the final effluent is diluted by a factor of 10^3; this reduces the concentration of any compound present from 1 ppm to 1 ppb upon release.

The plant wastewater treatment system is shown in Figure 2. Total residence time (by volume) is about 19 days, but in practice, flow patterns can sometimes reduce this to 6 days. The acidic raw effluent is neutralized following the equalization pond and then mechanically stirred in the aeration lagoons to accelerate aerobic biological degradation. Two large settling ponds, which make up ~80% of the total system volume, complete the treatment.

Preliminary studies indicated that the water from the Back River was unpolluted so work was concentrated at the Points A and B, representing the raw and final effluent. Because the dye plant operates in the batch mode, changing product mix often, a complete picture of the effluent could be obtained only by composite sampling. For a $2^1/_2$ month period, composites were collected weekly, sampling over the whole 168-h period on a flow-adjusted basis.

The plant wastewater after treatment is gray in color with no visible suspended matter and no noticeable odor. The reduction of COD and BOD in the treatment plant averages about 70% and 85%, respectively; normal effluent values are 200 mg/L and 60 mg/L. Based on the average COD value, the plant discharges approximately 920 tons of organics yearly.

Identifications. Although many ancillary techniques are used, the heart of the analytical methodology is gas chromatographic mass spectrometry. Since very few of the more complex compounds identified were listed in mass spectral compilations such as the Eight Peak Index (*4*) or the computerized Mass Spectral Search System (*5*), we were forced to rely heavily upon high resolution mass spectrometry, a priori spectral interpretation, synthesis and purchase of standards, and reference material such as the Trade Commission Report (*3*) for identification purposes. The rather secretive nature of the dye industry meant that the mass spectra of many of the compounds found had not been published even though in common use. Although the company involved was very willing to accommodate our work and to aid in sampling, we wish to emphasize that they did not furnish us with any information about their chemical processes. The two exceptions to this were their willingness to confirm the reasonable presence of several of the more complex molecules after identification was complete and to specify the correct isomer in some ambiguous substitution cases.

Substitution patterns are nearly impossible to discern from mass spectrometric data alone without standard spectra for comparison. Even if standards are available, it is not always possible to choose, for instance, between a meta- and para-substituted aromatic ring. As a result, many of the compounds identified in this work, unless we know or have good reason to suspect the substitution pattern, are reported without a specified substituent relationship. In the case of the aromatic amines, this may be particularly important, since *N*-substituted compounds can be inherently more toxic than ring-substituted ones (*1*).

EXPERIMENTAL

Sampling. *Dye Plant.* Preliminary grab samples were collected in 1-gal amber glass bottles with Teflon-lined caps. These

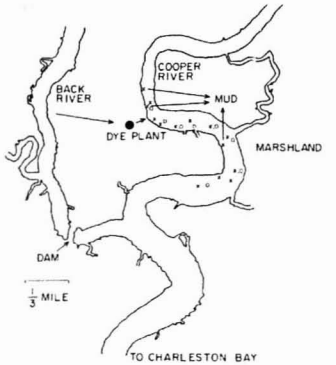

Figure 1. Geographical location of the dye manufacturing plant and locations of the river water (O) and sediment (x) sampling sites

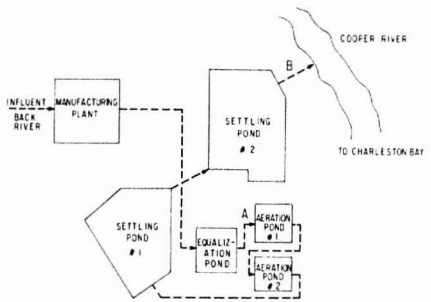

Figure 2. Diagram of the dye manufacturing plant wastewater treatment system. Composite sample collection points are designated A (raw effluent) and B (final effluent)

bottles were carefully pre-cleaned by detergent washing, followed by rinsing in distilled water, nanograde methanol, and nanograde methylene chloride. Samples were preserved during air shipment to the laboratory by the addition of reagent grade HCl to lower the pH to 2 and addition of 250–300 mL of CH_2Cl_2. Addition of the organic solvent also started the extraction.

Composite samples of the raw and final effluent were also collected in pre-cleaned glass bottles. Compositing was done on a variable flow-adjusted basis for the raw effluent and the final effluent.

River Water and Sediment. River water and sediment samples were collected during July 1976, and sampling locations are shown in Figure 1. These locations were chosen (on the basis of local knowledge about current patterns in the area) as places where the effluent stream might pool. Both sets of samples were obtained by a scuba diver operating from a small boat.

The sediment samples were collected using a small, pre-cleaned garden spade. Most of the samples were predominantly mixed grades of sand, two were hard clay, and three contained mostly soft mud, as specified in Figure 1. The samples were placed in acid-cleaned jars and returned to the laboratory within five days where they were frozen until analysis.

River water was collected in 1-gal bottles at or near mid-depth of the river. Workup and preservation was identical to that for the effluent samples.

Extraction. *Water.* The acidic samples were extracted immediately upon arrival at the laboratory. While this extraction should collect all neutral and acidic species, many amines are present in dye plant effluents, so the water was adjusted to pH 10 with reagent grade KOH and a second extraction was carried out to isolate basic species.

Both the acid and base extracts were highly colored, the hue of which changed with each composite sample. Two-dimensional thin-layer chromatography of one of these extracts showed over 50 colored spots which were presumed to be dyes.

Sediment. Approximately 150-g sediment samples were Soxhlet-extracted with 60/40 benzene–methanol. Extraction with other solvents such as methylene chloride or isopropanol/benzene did not appear to improve extraction speed or efficiency. All solvents used were nanograde quality purchased from Mallinckrodt.

For all samples, extracting solvents were removed by distillation at reduced pressure using a commercially available rotary evaporator equipped with Teflon seals. Temperatures were kept at 40 °C or below to minimize sample loss through volatilization during this step.

Analysis. Preliminary gas chromatographic analysis of the sample extracts was done on a 2-mm i.d., $^1/_4$-inch o.d., 6-foot glass column packed with 3% SP-2100 on 80/100 mesh Supelcoport. The column was normally temperature-programmed from 70 to 310 °C at 8°/min in a HP-5730A gas chromatograph equipped with a flame ionization detector.

If preliminary gas chromatographic analysis indicated the presence of a large unresolved "hump" of alkanes, as in most of the sediment samples, open column liquid chromatography with deactivated silica gel (10% water added) was used to separate the alkanes. Elution with hexane removed most of the alkane material, and subsequent elution with benzene and methanol allowed recovery of the dye-plant-derived compounds.

Gas chromatographic mass spectrometry (GC/MS) was done on a HP-5982A quadrupole instrument operated under computer control (HP-2100S) in the continuous scanning mode. The same gas chromatographic column described earlier was utilized. Although the instrument has a dual chemical ionization/electron impact source, all spectra reported here are electron impact spectra obtained at ~70 eV ionization energy.

Because of the complexity of the samples, some of the gas chromatographic analysis was done on high resolution open tubular glass capillary columns. The liquid phase was SE-52, a methyl phenyl silicone; it was coated by a static coating method (*6*) on columns varying in length from 15 to 30 m with inner diameters of approximately 0.27 mm. GC/MS using the capillary column was helpful in many cases to obtain cleaner spectra with less interference from adjacent gas chromatographic peaks.

Since standard spectra of most of the more complex compounds from the dye manufacturing industry were not available, high resolution mass spectrometry was utilized to aid in the identification by providing molecular formulas. Unresolved whole samples were analyzed, and matching of individual peaks in the high resolution mass spectrum to specific compounds was done by use of low resolution mass chromatograms. This technique is obviously useful only when the compound under study has a unique fragment or molecular ion. Data were obtained on a DuPont 21-110B double focusing mass spectrometer located in the laboratory of K. Biemann (*7*).

Selected ion monitoring is a technique which increases mass spectrometric sensitivity by a factor of 10^3 (in some cases) by observing only a limited number of masses rather than the whole spectrum (*8, 9*). The HP-5982A GC/MS system is provided with software to allow monitoring of up to four masses at any given time with variable dwell times. This methodology was used extensively in the studies of the sediment and river water samples, since concentrations of dye-plant-derived compounds were too low to detect by standard GC/MS procedures.

RESULTS AND DISCUSSION

Results of the $2^1/_2$-month compositing study for both the treated and untreated plant effluent are shown in Table I. Structures for a selected group of the compounds listed in Table I are illustrated in Figure 3 and identified by number. Several of these will be discussed in more detail. The numbers in parentheses in Table I refer to the frequency of presence, that is, the number of composite samples in which the particular compounds were found. The concentration range may be somewhat misleading since in some cases only one or two samples contained the compound in question. The number

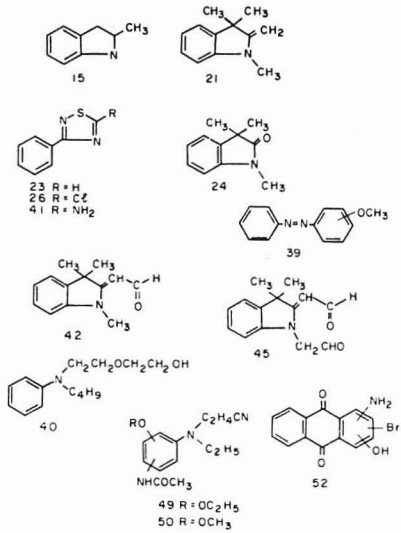

Figure 3. Structures for some of the compounds found in the dye plant wastewater. Numbers refer to compounds as listed in Table I

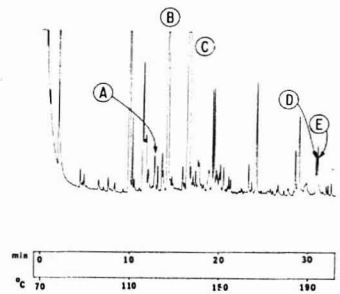

Figure 4. Gas chromatogram of a dye plant final effluent extract run on an SE-52 open tubular glass capillary column: 20 m × 0.26 mm I.d., programmed from 70 to 200 °C at 4°/min. Labeled peaks are (*A*) 1,2,3,3-tetramethylindoline; (*B*) 1,3,3-trimethyl-2-methyleneindoline; (*C*) 1,3,3-trimethyloxindole; (*D*) 5-amino-3-phenyl-1,2,4-thiadiazole; (*E*) 1,3,3-trimethyl-$\Delta^{2,\alpha}$-indolineacetaldehyde

of compounds appearing in low frequency in the composites serves as a justification for relying on the composites and sampling over a fairly long period of time for a plant operating in the batch mode.

Since most of the more complex compounds identified did not have published mass spectra, and thus were not amenable to identification by computer search routines or published mass spectra compilations, it seems useful to discuss for a few examples the general mode of attack in interpreting the spectra.

Figure 4 is the high resolution gas chromatogram from the extract of one of the final effluent composites. Figure 5 contains the mass spectra of peaks labeled *A*, *B*, *C*, and *E* along with structural identifications. Of these compounds, only the oxindole (peak *C*) had a mass spectrum present in the literature (*10*). High resolution mass spectral data confirmed its identification. The molecular formulas of compounds *B*

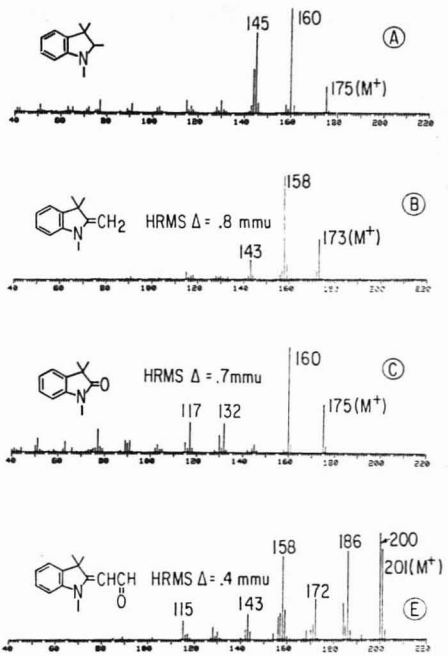

Figure 5. Mass spectra of compounds labeled *A*, *B*, *C*, and *E* in Figure 4. The HRMS Δ refers to the difference in mmass units between the measured exact mass and that calculated from the molecular formula

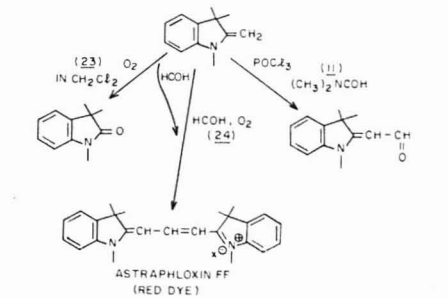

Figure 6. Summary of reactions involving 1,3,3-trimethyl-2-methyleneindoline (*11*, *23*, *24*). The earliest reference to this compound, called Fischer's Base, is found in a paper from 1887 (*25*)

and *E* were obtained from high resolution data, and the structures in Figure 5 were hypothesized by analogy, but positive identification was difficult. A search of the Trade Commission report on synthetic organic chemicals produced in the United States in 1973 (*3*) revealed that compounds *B* and *E* were in fact manufactured by the company which operated the plant we were investigating. A knowledge of mass spectral fragmentation patterns partially confirmed the identification, and purchase of the compound *B*, 1,3,3-trimethyl-2-methyleneindoline (from Aldrich Chemical Co.), enabled a positive identification by mass spectrometry and GC retention time. The indolineacetaldehyde, compound *E*,

Table I. List of Compounds Found in the Composite Samples Collected from the Dye Manufacturing Plant[a]

Compound	Raw wastewater, ppb	Final effluent ppb
1. Chlorobenzene	90-530 (8)[b]	ND[c]
2. Bromoaniline	3 (1)	ND
3. Anisole	37-190 (5)	5-71 (4)
4. Phenol	110-910 (8)	ND
5. Aniline	36-480 (6)	10-96 (7)
6. 4,4-Dimethylpentene	38-420 (8)	ND
7. Dichlorobenzene	90-380 (8)	5-32 (3)
8. Nitrobenzene	15-240 (3)	23 (1)
9. C_1 aniline	54 (1)	8-15 (4)
10. Chloroanilline	ND	7-12 (5)
11. C_2 aniline	7-24 (2)	15-30 (2)
12. C		
12. C_3 aniline	ND	4 (1)
13. Anisidine	29-84 (2)	ND
14. Nitrochlorobenzene	87 (1)	38 (1)
15. 2-Methylindoline[d]	26-400 (4)	28-610 (6)
16. C_4 aniline	95-170 (2)	19-22 (2)
17. Caprolactam	ND	36-150 (2)
18. Methylmethoxyaniline	22-55 (4)	12-40 (5)
19. Dichloroaniline	57 (1)	ND
20. Trimethylindole	ND	13-72 (7)
21. 1,3,3-Trimethyl-2-methylene indoline[d]	320 (1)	3-130 (7)
22. Dibromoaniline	60 (1)	42-66 (2)
23. 3-Phenyl-1,2,4-thiadiazole[d]		
24. 1,3,3-Trimethyloxindole[d]	65-510 (8)	10-3600 (9)
25. Dimethyl phthalate	38-130 (4)	ND
26. 5-Chloro-3-phenyl-1,2,4-thiadiazole[d]	ND	15 (1)
27. Dinitrophenol	400-3200 (8)	42-2700 (5)
28. Dichloronaphthalene	95-180 (2)	ND
29. Bromodiethylaniline	23-120 (3)	43 (1)
30. Bromonitrobenzene	ND	12 (1)
31. Nitroaniline	270 (1)	ND
32. Tribromoaniline	54-87 (3)	5-72 (6)
33. *N*-Hydroxyethyl-*N*-butyl-*p*-bromoaniline	ND	7-34 (2)
34. Bromodinitrobenzene	120 (1)	ND
35. Bromonitroaniline	ND	12-48 (4)
36. *N*-Hydroxyethyl-*N*-butylaniline	36-330 (4)	16-32 (2)
37. 1,3,3-Trimethyloxindole + C_2H_4[e]	ND	27-78 (7)
38. *N*-Hydroxyethyl-*N*-cyanoethyl aniline	ND	68-86 (2)
39. Methoxyazobenzene[d]	ND	52-150 (2)
40. *N*-Butyl-*N*-β-(β-hydroxyethoxy)-ethyl aniline[d]	28-250 (3)	ND
41. 5-Amino-3-phenyl-1,2,4-thiadiazole[d]	5-46 (4)	19-230 (7)
42. 1,3,3-Trimethyl-$\Delta^{2,\alpha}$-indolineacetaldehyde[d]	3-52 (6)	14-440 (7)
43. Anthraquinone	49-110 (6)	ND
44. Bromodinitroaniline	50-120 (5)	8-42 (7)
45. 3,3-Dimethyl-1,$\Delta^{2,\alpha}$-indolinediacetaldehyde[d]	ND	9-460 (4)
46. Hydroxyanthraquinone	ND	5-8 (3)
47. Dihydroxyanthraquinone	ND	5-44 (3)
48. Aminoanthraquinone	69-160 (2)	5-29 (5)
49. *N*-Acetyl-*N'*-ethyl-*N'*-cyanoethyl-ethoxyphenylenediamine[d]	ND	13-44 (4)
50. *N*-Acetyl-*N'*-ethyl-*N'*-cyanoethyl-methoxyphenylenediamine[d]	42 (1)	1.5-220 (6)
51. Hydroxyaminoanthraquinone	ND	1.5-27 (4)
52. Bromoaminohydroxyanthraquinone[d]	170-200 (2)	16-75 (3)
53. Dibromoaminoanthraquinone	92-170 (4)	ND

[a] The raw effluent refers to Point A (Figure 2) and the final effluent to Point B (Figure 2). Where substitutional isomers are designated, they are based, for the most part, on information other than mass spectra interpretation. [b] Number in parentheses refers to the total number of composites in which the compound was found. The raw effluent is based on eight total samples and the final effluent on nine total samples. [c] ND means "not detected". [d] Refers to compounds whose structures are shown in Figure 3. [e] This compound has a similar mass spectrum to 1,3,3-trimethyloxindole, and high resolution mass spectrometry indicated that it has two additional CH_2 units.

was synthesized [for synthetic route, see (*11*) and Figure 6] in our laboratory from *B*, and it had a mass spectrum and GC retention time identical with the unknown. The purchased standard of 1,3,3-trimethyl-2-methyleneindoline contained small quantities of compound *A*, and the similarity of its mass spectrum with that of compound *B*, except for a 2 mass unit shift, led to the assignment of the saturated analogue, 1,2,3,3-tetramethylindoline.

During work with the 1,3,3-trimethyl-2-methyleneindoline, it was noted that colorless standard solutions (in methylene chloride) turned dark red after a short time. Tests indicated that this occurred even in the dark so that no photochemical reaction was taking place. Since this compound has been used extensively in the dye industry, we searched through the literature very carefully for reports of this phenomenon. Figure 6 summarizes the reactions which are apparently occurring. If the red dye is being formed, some methylene donor like formic acid must be present, but we have not pursued the reaction sequence as it occurs in methylene chloride any further. Gas chromatographic and GC/MS analyses clearly show, however, that the indoline is being slowly converted to the oxindole over a period of several days. As will be discussed later, this reaction assumes some importance when considering the efficiency of the waste

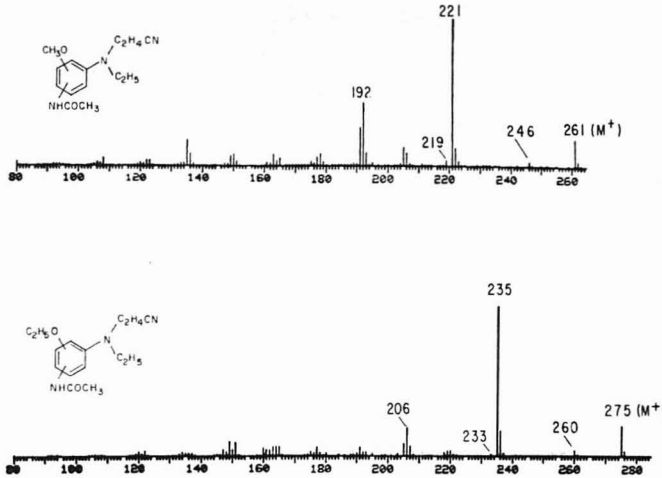

Figure 7. Mass spectra of two related compounds found in the dye plant effluent. These two compounds appear in Table I as entries 49 (bottom) and 50 (top). The ethoxy compound elutes first from an SP-2100 gas chromatographic column

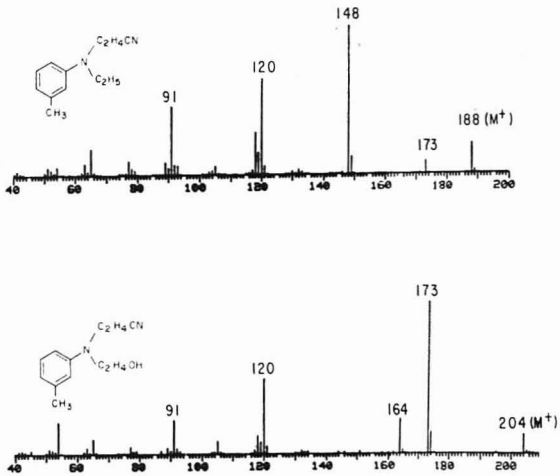

Figure 8. Mass spectra of two standard compounds for comparison to those in Figure 7. The top compound is *N*-ethyl-*N*-cyanoethyl-*m*-toluidine and the bottom is *N*-cyanoethyl-*N*-hydroxyethyl-*m*-toluidine

treatment system presently employed by the dye plant.

The two related mass spectra shown in Figure 7 were even more difficult to interpret. Although high resolution data indicated a molecular formula of $C_{14}H_{19}N_3O_2$ for one and $C_{15}H_{21}N_3O_2$ for the other, thus confirming the interpretation that the compounds differed only by one CH_2 unit, little information that might give an idea about the structures of the two compounds could be found in the literature. The peaks at m/e 221 and 235, respectively, correspond to the loss of CH_2CN from the molecular ions which clearly is more favorable than the loss of methyl, m/e 246 and 260. A small loss of 42 mass units, CH_2CO, also occurs in both compounds, indicating the possible presence of an *N*-acetyl group. Based on such considerations, the structures shown in Figure 7 were assigned by a priori interpretation of the spectra. Confirmation of these structures was not possible by reference to the literature, and synthesis appeared to be a rather involved procedure; thus, the mass spectra of model compounds which had similar structural features and which could be purchased commercially were obtained for comparison purposes.

In particular, the presence of the ethoxy and methoxy groups in the compounds shown in Figure 7 was deduced mainly because OCH_3 and OC_2H_5 were parts of the compounds remaining after mass spectral assignment of the fragment losses observed. However, the presence of *N*-hydroxyethyl groups in two of the other compounds (numbered 33 and 36, Table I) indicated that this particular structural moiety was a common one, and it seemed important to rule out its

Table II. Concentration of Various Individual Compounds in Both the Raw and Final Effluent for Each of the Dates That Composites were Collected.

Date	Aniline		2-Methylindoline		1,3,3-Trimethyloxindole		Dinitrophenol	
	Raw	Final	Raw	Final	Raw	Final	Raw	Final
3/22-3/26	240[a]	—[b]	49	——	160	——	2300	——
3/24-4/3	—[b]	N.D.[c]	——	N.D.	——	340	——	N.D.
4/5-4/9	lost	16	lost	52	lost	300	lost	N.D.
4/19-4/23	160	N.D.	N.D.	140	320	480	1000	120
4/26-4/30	480	10	400	82	510	680	3200	240
5/3-5/7	48	24	26	610	160	3600	2100	2700
5/10-5/14	N.D.	54	N.D.	56	110	660	660	510
5/17-5/21	36	39	N.D.	28	310	740	1400	42
5/24-5/28	370	17	99	N.D.	130	150	400	N.D.
6/1-6/4	N.D.	96	N.D.	N.D.	65	100	600	N.D.

Date	5-Amino-3-phenyl-1,2,4-thiadiazole		1,3,3-Trimethyl-$\Delta^{2,\alpha}$-indolineacetaldehyde		Bromodinitroaniline	
	Raw	Final	Raw	Final	Raw	Final
3/22-3/26	16	——	27	——	69	——
3/24-4/3	——	58	——	57	——	42
4/5-4/9	lost	230	lost	440	lost	38
4/19-4/23	N.D.	33	36	14	110	30
4/26-4/30	N.D.	19	52	14	120	13
5/3-5/7	N.D.	48	N.D.	33	100	30
5/10-5/14	N.D.	42	N.D.	55	N.D.	N.D.
5/17-5/21	46	84	20	16	50	8
5/24-5/28	18	N.D.	18	N.D.	N.D.	15
6/1-6/4	5	N.D.	3	N.D.	N.D.	N.D.

[a] Concentrations in parts per billion. [b] 3/22 to 3/26, only raw composite collected; 3/24 to 4/3, only final composite collected. [c] N.D. means "not detected".

presence. The two standards shown in Figure 8 were purchased (Aldrich Chemical Co.) and analyzed for this purpose. As one can see from the mass spectrum of *N*-hydroxyethyl-*N*-cyanoethyl-*m*-toluidine, competition between loss of CH_2OH (31 mass units) and loss of CH_2CN (40 mass units) clearly favors CH_2OH. Since no fragment corresponding to this loss was present in the mass spectra of the *N*-substituted phenylenediamines (Figure 7), it was ruled out of consideration. The spectrum of the *N*-ethyl-*N*-cyanoethyl-*m*-toluidine, conversely, shows almost exactly the same proportional loss of CH_2CN and CH_3 seen for the phenylenediamines.

Although, for a variety of reasons, we believe the structures we have deduced for these phenylenediamines (see Figure 7) are correct, structural *proof* must await comparison with authentic compounds. In addition, the exact substitution pattern of the three groups around the ring, which cannot be determined from the mass spectra alone, must be fixed based on other spectral, synthetic, or circumstantial data.

Sediment and River Water Samples. Because the sensitivity limits of the standard workup and identification procedures are about 1 ppb for the water samples and because the dilution effect of the river is so large, only a few of the compounds present in the final effluent were expected to be detected by standard gas chromatographic mass spectrometry done on 1-gal river water extracts. In fact, none were detected in this manner. Selected ion monitoring of the predominant mass fragments associated with 1,3,3-trimethyloxindole (m/e 160), dinitrophenol (m/e 184), and 5-amino-3-phenyl-1,2,4-thiadiazole (m/e 177) gave positive results, but only the oxindole appeared to be present in anything but ultra-trace quantities (<10 ppt), even in water samples collected very near the plant outfall. It may be that the dilution effect is an order of magnitude higher than estimated, or that these particular compounds were present in low concentrations on this particular sampling day.

Of the 14 sediment samples collected, only three contained significant quantities of mud (see Figure 1), the others being comprised completely of sand and extremely hard clay. The mud has a much higher absorptive capacity than either the sand or cement-like clay, and samples made up predominantly of this soft mud are much more likely to contain effluent organic compounds. Using selected ion monitoring with a detection limit of about 0.1 ppb, analysis of all but one of the mud samples was negative. Many fatty acids, alkanes, sterols, steranes, and polycyclic aromatic hydrocarbons were present in all of the mud samples; but only the one nearest the outfall, about 25 yards away, contained a small quantity (<1 ppb) of the oxindole. It is quite possible that this small quantity was associated with the water trapped in the mud during collection. The sand and clay sediment samples were nearly devoid of any solvent-extractable organic material, but small quantities of naturally occurring organic material were present.

Treatment Efficiency. Effluent permits issued by the EPA and other government agencies usually specify pounds of COD (or BOD) per pound of product manufactured as the regulated quantity. While these quantities have some relationship to overall organic load, they are not intended to monitor the quantities of specfic compounds being released. This monitoring technique has unfortunately led to the attaching of excess significance to the percent COD(or BOD) reduction that various treatment methods can attain in any given industrial effluent. This is unfortunate because there is very little relationship between potential environmental hazard and COD level when dealing with effluents containing toxic materials. In addition, the reporting of COD reduction levels ignores the extensive and complicated chemistry that can occur in any treatment plant.

The weekly composites collected from the dye plant raw and final effluent over $2^1/_2$ months provide data which comprise a convincing demonstration of the deceptiveness of COD and BOD data. Table II shows the concentrations of several compounds found in each of the samples. The concentration reduction should be compared to values of about 70% for COD reduction and 85% for BOD reduction. As mentioned earlier, the retention time in the treatment system at this plant can vary from 6 to 19 days, which probably

accounts for some of the variation observed in these data and makes it difficult to quantitatively evaluate the treatment efficiency for the individual compounds. Qualitatively, however, the trends are quite clear and lead to some interesting observations. In spite of some anomalies, the concentrations of aniline, bromodinitroaniline, dinitrophenol, and 1,3,3-trimethyl-$\Delta^{2,\alpha}$-indolineacetaldehyde appear to decrease to about the same extent as one would predict from COD data. The 2-methylindoline data are inconclusive. The 1,3,3-trimethyloxindole and 5-amino-3-phenyl-1,2,4-thiadiazole (peak *D* in Figure 4), however, actually *increase* in concentration after passing through the treatment plant.

Because *de novo* synthesis of the thiadiazole and the oxindole in the treatment system is quite unlikely, we conclude that chemical or biological degradation of dye molecules must be causing the observed increase in concentration. Reduction of the azo linkage in the dye shown below during treatment

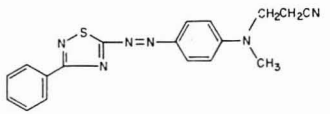

could easily lead to the reappearance of the amino thiadiazole in the final effluent. The situation in the case of the oxindole is somewhat more complex as discussed earlier and illustrated in Figure 6. Oxidative decomposition of Astraphloxin FF or similar dyes could lead to the formation of the oxindole in the treatment plant. In addition, autoxidation of 1,3,3-trimethyl-2-methyleneindoline, as shown in Figure 6, may form the oxindole during treatment as well as during in-plant use. Inspection of Table I, however, indicates that the 1,3,3-trimethyl-2-methyleneindoline is found in only one of the raw effluent samples. This seems to indicate that the indoline is also being formed in the treatment plant, which would suggest that dye decomposition followed by autoxidation is the cause of the oxindole concentration increase. Decomposition of the indoline is undoubtedly also occurring after sample collection but before work-up, and although this may be complicating the analysis, its effect must be minor.

As these data show, it is unwise to ignore the chemical and biological reactions that can take place in a treatment system. Under certain circumtances, the intensive biological activity taking place in a treatment system may be in fact creating an environmental hazard. Measurements of overall organic load such as TOC, BOD, and COD offer no opportunity to address these problems, and it may be desirable to expand the routine methodology used to monitor industrial effluents to include such an assessment.

Environmental and Health Hazards from Dye Plant Effluents. The specific plant being studied in this work probably poses no significant environmental problems from the standpoint of human health. Water from the Cooper River flows directly into the Atlantic Ocean, with no intervening use, for instance, as drinking water. This is mostly a result of the philosophy involved in choosing the particular plant for investigation, since a relatively simple, well-defined situation was desired. The lack of partitioning of dye-plant-derived compounds into the river sediment also mitigates against any environmental effect upon river biota, although we plan to study this question in the future. Since other dye manufacturing operations are not conducted in so favorable a situation, it is important to consider the possible toxicity of the compounds leaving the plant in the effluent.

The one class of compounds in the dye plant effluent about which the most toxicological information is available is the aromatic amine derivatives. A summary of work that has been done on the carcinogenicity of these compounds was recently

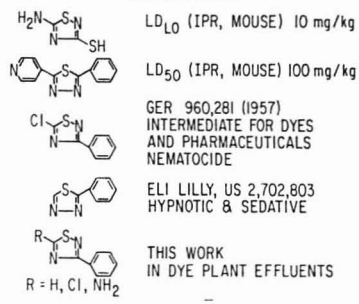

Figure 9. Comparison of thiadiazoles found in the dye plant effluent with metabolically active and toxic compounds. Toxicity data are from the literature (*12*)

published (*1*). Although none of the compounds present here, with exception of aminoanthraquinone (*12*), has been shown to induce tumor formation, several of the amines (including aniline itself, the nitro and dinitroanilines, and the halogenated anilines) are toxic when inhaled or absorbed through the skin in sufficient quantities (*13*).

Several other compounds present in the dye plant effluent are listed as industrial hazards or have exhibited some toxicity under various testing conditions (*12*). These include the nitrobenzenes and, specifically, chloronitrobenzene, a cumulative blood poision (*13*). Also listed are the dinitrophenols, used as insecticides (*14*), which have an LD_{50} for oral ingestion by rats of 30 mg/kg (*12*). The chloroaniline, and by extension possibly the bromoanilines, are fairly toxic, with LD_{50} values of 300 mg/kg for oral ingestion by rats (*13*). Except for these and a few other exceptions, nothing is known about the toxicity of the compounds found in the effluent, and even in these few instances, the data do not really apply to chronic low level exposure.

The 1,2,4-thiadiazoles found in the dye plant effluent are an interesting class of compounds and, in particular, the presence of 5-chloro-3-phenyl-1,2,4-thiadiazole is significant. Figure 9 shows that these compounds may be relatively toxic, and that the chloro derivative has been patented as a nematocide. Consultation with plant personnel provided the information that only the amino compound was utilized as a dye intermediate. Although the 3-phenyl-1,2,4-thiadiazole could be formed by deamination during dye synthesis or by decomposition of a dye molecule, there is no chlorination treatment that could account for the formation of the chloro compound. The 5-chloro-3-phenyl-1,2,4-thiadiazole is apparently an impurity in the amino compound, and although it appears only once in the composite samples, it is present in several grab samples taken over the past year. In this case, the dye plant is unintentionally releasing a compound which may be relatively toxic, and unless the effluent had been monitored for specific compounds, its presence would not have been discovered.

Since industrial raw materials are often impure, the presence of the chlorothiadiazole is undoubtedly not an isolated situation. A second example in this work is the finding of the diacetaldehyde (compound 45 in Table I) which is probably a by-product in the synthesis of 1,3,3-trimethyl-$\Delta^{2,\alpha}$-indolineacetaldehyde. As a result of these findings, one can conclude that it is sometimes very misleading to evaluate the hazards of any individual operation based simply on lists of raw materials and finished products. It is also necessary to consider synthetic routes involved in production of the

intermediates, and also by-products in the synthesis of the final product.

CONCLUSIONS

Several conclusions can be drawn on the basis of these results. Perhaps the most interesting is that high levels of organic compounds in industrial effluents, as evidenced by COD or BOD measurements, do not necessarily reflect a serious environmental hazard, even in a plant producing synthetic organic chemicals. The majority of the organic compounds found in the dye plant effluent are partially water soluble, such as the aniline derivatives, and thus do not accumulate in the river sediments. The effluent runs into a river that is utilized in a manner such that the presence of unusual anthropogenic organic compounds is not particularly worrisome, once they are diluted. We should point out here that our analytical methods discriminate against nonvolatile species, such as the dye molecules themselves. Although low levels of these compounds are present in the wastewater, our techniques do not allow us to identify them and, therefore, we cannot comment on their toxic effect (if any).

The second problem that these data reveal is that dye manufacturing operations utilize and release into the environment many compounds, some of which may be potentially toxic. The identification of the thiadiazoles and a large number of aromatic amine derivatives in this particular dye plant effluent serves to emphasize this potential problem. Treatment systems much more efficient than the one in operation at the plant studied here may be needed at locations where the discharge of such compounds cannot be tolerated.

An area that has received very little attention until recently is the possibility of enhancing the toxicity of industrial and municipal wastewaters during treatment. The discovery of chlorinated hydrocarbons in New Orleans drinking water as a result of chlorination brought this possibility to the attention of both the scientific community and the public at large (*15*, *16*). Even more subtle problems can exist as the result of biological or nonbiological degradation of effluent compounds in a treatment system. Processes somewhat similar to those discussed in a report (*17*) describing retoxification in the human gut (brought about by intestinal bacteria) of polycyclic aromatic hydrocarbons which had been rendered harmless by internal metabolism can be envisioned. The salient point is that the complex mixture of compounds present in an industrial effluent, combined with the high intensity metabolic action possible in a biological treatment system, can lead to complete degradation to harmless products or to partial degradation or alteration to even more hazardous chemicals. Formation of 1,3,3-trimethyloxindole and 5-amino-3-phenyl-1,2,4-thiadiazole are only two examples.

A final point concerns available information about toxicity and the methodology used to determine it. The Toxic Substances List (*12*) is an extensive compilation of compounds suspected or known to be harmful, together with supporting data. Unfortunately, none of the data are applicable to chronic low level exposures without tenuous extrapolation. As a result, application of the data presented here to any discussion of possible environmental hazard is in itself hazardous and subject to much discussion. Direct tests for toxicity or carcinogenicity, which are now available, are slow and extremely expensive. A cheaper bacterial assay relying on the direct correlation of mutagenicity and carcinogenicity has been devised (*18*, *19*), but with known carcinogens it is correct only 80–90% of the time and no dose/response correspondence has been established (*20*, *21*). Human cell culture studies would be preferable, but they have not been brought to the point of routine use (*22*). In the final analysis, it seems that some more direct and rapid screening tests will have to be developed which are applicable to estimation of risk from chronic low level exposure to compounds such as those found in this study.

ACKNOWLEDGMENT

The technical assistance of Mark Manary, John Dillon, and Nathaniel Epstein through the auspices of the Undergraduate Research Opportunities Program at M.I.T. is appreciated The cooperation of the company involved, although anonymous, is also gratefully acknowledged. Without their forebearance, this project would not have been possible.

LITERATURE CITED

(1) C. E. Searle, Ed., "Chemical Carcinogenesis", A.C.S. Monograph 173, American Chemical Society, Washington, D.C., 1976.
(2) E. W. Loy, Jr., D. W. Brown, and J. H. M. Stephenson, "Monitoring the Aquatic Environment for Specific Organic Pollutants", Abstract of Paper Presented at the 167th National Meeting, American Chemical Society, Division of Environmental Chemistry, Los Angeles, Calif., April 1974.
(3) "Synthetic Organic Chemicals, U.S. Production and Sales, 1974", compiled by the United States International Trade Commission, Publication No. 776, U.S. Government Printing Office, Washington, D.C.
(4) "Eight Peak Index of Mass Spectra", Mass Spectrometry Data Centre, AWRE, Reading, R67 4PR, United Kingdom, 1974.
(5) R. S. Heller, G. W. A. Milne, R. J. Feldmann, and S. R. Heller, *J. Chem. Inform. Comput. Sci.*, **16**, 176 (1976).
(6) J. Bouche and M. Verzele, *J. Gas Chromatogr.*, **6**, 501 (1968).
(7) K. Biemann, in "Application of Computer Techniques in Chemical Research", Institute of Petroleum, London, 1972, p 5.
(8) B. S. Middleditch and D. M. Desiderio, *Anal. Chem.*, **45**, 806 (1973).
(9) J. T. Watson, D. R. Pelster, B. J. Sweetman, J. C. Frolich, and J. A. Oates, *Anal. Chem.*, **45**, 2071 (1973).
(10) T. Hino, M. Nakagawa, K. Tsnveoka, and S. Akaboshi, *Chem. Pharm. Bull. (Tokyo)*, **17**, 1651 (1969).
(11) G. F. Smith, *J. Chem. Soc.*, 3842 (1954).
(12) H. E. Christenson, Ed., "Toxic Substances List", U.S. Department of Health, Education, and Welfare, Rockville, Md., 1973.
(13) L. T. Fairhall, "Industrial Toxicology", 2nd ed., Hafner Publishing Co, New York, N.Y., 1969.
(14) W. O. Negherbon, Ed., "Handbook of Toxicology, Volume III—Insecticides", W. B. Saunders Co, Philadelphia, Pa. 1971.
(15) J. J. Rook, *Water Treat. Exam.*, **23**, 234 (1974).
(16) W. H. Glaze, J. E. Henderson IV, and G. Smith, in "Identification and Analysis of Organic Pollutants in Water", L. H. Keith, Ed., Ann Arbor Science Publishers, Inc., Ann Arbor, Mich. 1976, p 247.
(17) A. G. Renwick and B. S. Drasar, *Nature (London)*, **263**, 234 (1976).
(18) J. McCann, E. Choi, E. Yamasaki, and B. N. Ames, *Proc. Natl. Acad. Sci., U.S.A.*, **72**, 5135 (1975).
(19) B. Commoner, in "Identification and Analysis of Organic Pollutants in Water", L. H. Keith, Ed., Ann Arbor Science Publishers, Inc., Ann Arbor, Mich., 1976, p 49.
(20) J. M. McCann, and B. N. Ames, *Proc. Natl. Acad. Sci., U.S.A.*, **73**, 950 (1976).
(21) A. Blum and B. N. Ames, *Science*, **195**, 17 (1977).
(22) W. G. Thilly, J. G. DeLuca, H. Hoppe IV, and B. W. Penman, *Chem.-Biol. Interact.*, **15**, 33 (1976).
(23) R. Robinson, *J. Chem. Soc.*, 586 (1963).
(24) H. Siegrist, *Chimia*, **20**, 295 (1966).
(25) E. Fischer and A. Steche, *Ann. Chem.*, **242**, 353 (1887).

RECEIVED for review February 14, 1977. Accepted May 16, 1977. We are grateful to the Research Applied to National Needs program of the National Science Foundation for support (grant number AEN-7513069).

CORRESPONDENCE

Performance Prediction and Evaluation of Systems for Computer Identification of Spectra

Sir: A wide variety of computer systems for the retrieval and interpretation of unknown spectra, especially mass spectra, have been proposed in recent years (*1–14*). Reliable ways to evaluate these systems are necessary both to develop further improvements and to allow the user to choose the best system for his needs. For tests of such systems it has been common practice to report the proportion of correct answers, with designations such as "reliability" or "% correct". Although the knowledge of this probability is obviously of importance to the user of the system, for the performance evaluation of document retrieval systems it has long been recognized that the "recall", the proportion of possible relevant items retrieved, must also be measured (*15*); "recall" has been utilized in evaluating particular systems for both the retrieval (*5, 13*) and the interpretation (*8, 9, 16*) of mass spectra. Further, it has been pointed out that the observed reliability value is dependent on the proportion of the matching structure in both the tested spectra and the reference file; a modified performance reliability term was proposed which combined the recall value and the proportion of false positive identifications, as neither of these is dependent on the structural composition of the test or reference set (*9*). Recently Wilkins and co-workers (*11*), amplifying theoretical conclusions of Rotter and Varmuza (*10*), have presented a comprehensive approach to the evaluation of pattern recognition systems. It is the purpose of this correspondence to propose a modified approach applicable to both retrieval and interpretation systems, and to recommend criteria for (1) comparing and improving such systems, and (2) evaluating the reliability of a system's predictions for a particular unknown spectrum.

The discussion will be limited to the evaluation of systems for binary classification, the answer of a retrieval system to the question "Is this particular compound (that giving the reference spectrum) present in the unknown?", and of an interpretive system "Is this substructure present in the unknown?". As shown in Table I, four possible results can be found for each "unknown" tested; all four are tabulated and combined into a "figure of merit" in the evaluation scheme of Wilkins and co-workers (*11, 12*). However, for retrieval systems that match unknown spectra against a large data base, the user seldom wishes to know which reference spectra do *not* match that of the unknown; a comprehensive list would be so long that it would be meaningless. Similarly, only predictions of "present" are usually justified for mass spectral interpretive systems, in our opinion (*17*); this was a significant premise in the design of our "Self-Training Interpretive and Retrieval System (STIRS)" (*16*). Functional group information varies widely in its "visibility" in the mass spectrum, in sharp contrast to the behavior found in many other types of spectra. For example, in their infrared spectra both acetone and dimethylaminoacetone show a strong carbonyl stretching frequency characteristic of the keto group. In the mass spectrum of acetone, the acetyl group produces the base (100%) peak at m/e 43, but in the mass spectrum of dimethylaminoacetone this peak is reduced to 5% by the strong fragmentation-directing influence of the amino group. Thus a main reason for selecting a mass spectral interpretive system should be its ability to determine "correct positives", which thus must be determined separately from its ability for "correct negatives". (Prediction of the absence of structures could also be helpful in specific cases, such as functionalities which strongly direct mass spectral fragmentations, and such predictions should also be investigated.)

Table I. Possible Results for a Tested Unkown

Actual	Predicted	Result
Structure present	Present	Correct positive
Structure absent	Present	False positive
Structure present	Absent[a]	False negative
Structure absent	Absent[a]	Correct negative

[a] These predictions are not made for most retrieval systems and for mass spectral interpretive systems such as STIRS.

Considering only cases for which the system has predicted the *presence* of a compound or substructure (first two lines, Table I), its capability will depend both on the probability that it will predict "present" when this is correct (recall, *RC*), and that it will not predict "present" when the structure is absent (false positive, *FP*). These are related as shown in Equations 1 and 2,

$$RC = I_c/P_c \tag{1}$$

$$FP = I_f/P_f \tag{2}$$

where I_c and I_f are the number of correct and false identifications, respectively, and P_c and P_f are the total possible correct and false identifications, respectively ($P_c + P_f = N$, the total number of unknowns tested). (Note that *RC* and *FP* are, in effect, determined by testing with separate data bases which do, and do not, contain the structures sought.) The values of *RC* and *FP* obtained will depend on the strictness of the matching criteria used, for example, the minimum acceptable value of the "Similarity Index" (*3*), "Confidence Value" (*5*), or proportion of matching "K-Nearest Neighbors" (*18*); stricter criteria will improve (lower) the false positives, but degrade the recall. Evaluation should cover a range of RC/FP pairs to allow the user to choose the optimum matching criteria for his particular problem (*5, 13, 15, 18*). [For system performance measurement it would obviously be useful to combine *RC* and *FP* into a single value which is relatively independent of the matching criteria chosen; we proposed (*9*) the relationship $RC/(RC + FP)$ which in practice has caused confusion, and Dromey (*19*) has recently suggested an alternative formulation.] System performance values of *RC* and *FP* should be determined on a statistically large sample of "unknowns" randomly selected from the universe of structures of interest; evaluation should not be carried out with monofunctional compounds if applicability to general types of organic molecules is sought, nor carried out with pure compounds if applicability to mixtures is desired (*5*). Comparison between systems is the most reliable if the same unknowns and reference spectra are used in each evaluation (*18*).

To reiterate, the user's choice of retrieval and interpretive systems should be based on the *RC* and *FP* values the system achieves with unknown spectra representing the universe of unknowns with which the user will deal (*4*). However, when the chosen system is applied to a particular unknown spectrum, the user wants to know, instead, the probability that a prediction of "present" is correct; we will call this the reliability (*RL*) of the prediction (Equation 3).

$$RL = I_c/(I_c + I_f) \quad (3)$$

$$= P_c \cdot RC/(P_c \cdot RC + P_f \cdot FP) \quad (4)$$

Substitution of the above definitions of *RC* and *FP* shows (Equation 4) that the reliability of a prediction depends, in addition, on the occurrence probability of the unknown structure in the reference file, as $P_f = N - P_c$. Obviously if there is no chance that the unknown structure is among those represented in the reference file ($P_c = 0$), *RL* must be zero. On the other hand, the reliability is increased if the proportion of spectra of the unknown compound in the reference file is increased; this has been done by including in the file multiple spectra of the more commonly occurring compounds (*5*), or by limiting the reference file to compounds similar to the unknown (*4*). Consider an application of the "Probability Based Matching (PBM)" system (*5*), assuming that confidence ("K") values of 50 and 100 correspond, respectively, to *RC* values of 55% and 15% and *FP* values of 1/45 000 and 1/1 000 000. An unknown mass spectrum is matched by PBM against a reference file of 25 000 spectra, all of different compounds, but containing a spectrum of the unknown compound (or spectra of the compounds if the unknown is a mixture), and two spectra are retrieved with K values of 50 and 100. For the compound of K = 50, *RL* = 1·55%/(1·55% + 25 000/45 000) = 50%, which can be rationalized as follows. When a spectrum in the file corresponding to a correct answer is matched against the unknown, the recall performance indicates a 55% probability that this correct spectrum will be retrieved with K = 50; because a false positive at the K = 50 level should result once in every 45 000 attempted matches, there is also a 55% probability that this answer found by matching 25 000 spectra is wrong. Thus the 50% reliability results from the fact that the probabilities of right and wrong answers are equal. For the compound of K = 100, *RC* = 15% signifies that in only 15% of attempted matches with a spectrum of the same compound will the two spectra match this well; it does *not* mean that there is only a 15% chance of this being the correct answer. On the contrary, since in only 2.5% ($25\,000/10^6$) of matches giving K = 100 will this be a false answer, the probability that this answer is correct is 86% [*RL* = 1·15%/(1·15% + 0.025)]. Note that the *RL* value of 86% does not correspond to (1 − *FP*); from Equation 4, *RL* approaches 1 − *FP* when half of the reference file are spectra of correct answers ($P_c = P_f$) and *RC* and *RL* approach 100% [because $1/(1 + FP) \sim (1 - FP)$]. If the system is used to report only one answer for each unknown, both P_c and P_f will equal the number of unknowns tested, which is also equal to $I_c + I_f$, and thus $RC = RL = (1 - FP)$. Plots of *RC* vs. *RL* (*5*, *15*), as well as of *RC* vs. *FP* (vide supra), are useful for system evaluations if the composition of test data is sufficiently similar to that of the unknowns.

Although this definition of reliability (Equations 3 and 4) is the same as that used for PBM (*5*), it is not identical with that we used for the STIRS evaluations, $RC/(RC + FP)$ (*9*). The latter was meant, rather, as a measure of system performance, as distinguished from the use here as a measure of the probability that an answer is correct. For future studies we propose to use reliability only as defined by Equations 3 and 4 for interpretive, as well as for retrieval, systems, as described below.

For the evaluation of an interpretive system the basic Equations 1–4 are also applicable, but it should be recognized that a substantially poorer "false positive" performance can be tolerated to achieve comparable levels of reliability. Each substructure sought by the interpretive system can be considered as a reference spectrum against which a match will be sought; pattern recognition studies have employed 60 (*2*), 11 (*12*), and 20 (*18*) substructures, while the STIRS evaluation (*9*) utilized 179 substructures. Thus for the latter an *FP* value only as low as 1/358 is necessary to give a 50% probability that one of these substructures will be selected as a false answer, compared to the *FP* value of 1/50 000 necessary in the PBM example above for a reference file of 25 000 spectra; for the pattern recognition study of 11 substructures (*12*), only *FP* = 1/22 is required. Further, for interpretive systems *RC* performance values are usually determined for the individual substructures, in effect matching the unknown against a file of only one reference spectrum; thus for a statistically meaningful evaluation (to make $P_f > 0$) the test set must contain unknowns which do *not* contain the particular substructure (tests of retrieval systems use unknowns which are present in the file). The proportion of the unknown spectra which contain the substructure under test will affect the observed reliability, in the same way the composition of the reference file affects retrieval reliability (vide supra). As an example consider a substructure such as chloro for which STIRS (*9*, *16*) gives *RC* = 50% at *FP* = 1/100; if for 100 unknown spectra tested, 66 contain Cl then (Equation 4) *RL* = 66·50%/(66·50% + 34·1%) = 99%. If only 6 of the 100 spectra contain Cl, *RL* = 6·50%/(6·50% + 94·1%) = 76%; this drastic reduction in the reliability is not due to a change in the basic capabilities of STIRS, but is only due to the fact that a reduction in the probability that a substructure is present must increase the proportion of identifications which are false positives. If a system such as STIRS is used as an *aid* to the interpreter, however, the poor reliability inherent in the prediction of "rare" substructures is not necessarily a serious problem. For example, although only 6 of 18 806 reference compounds in the STIRS evaluation (*9*) were of azulenes, a 50% recall was achieved at the 1% *FP* level. Thus if STIRS indicates an azulene substructure for an unknown mass spectrum, the interpreter will know that there is a very low probability that this is correct *if* the occurrence probability for azulene in the universe of structures from which the unknown was drawn is 6/18 806, as then *RL* = 6·50%/(6·50% + 18 806·1%) = 1.6%. The presence of azulene will only be worth considering if the interpreter can rationalize a much higher occurrence probability for the particular unknown. Note that this $P_c(P_c + P_f)$ value of 6/18 806 is still larger than values such as 1/25 000 occurring in tests of retrieval systems, again emphasizing the difference in *FP* performance (at a particular *RC* level) required (and achievable) for retrieval in comparison to interpretive systems. The average unknown compound in the STIRS tests (*9*) contained more than five of the 179 substructures; a comparable test of a retrieval system should thus use spectra of mixtures containing five unknown compounds. Similarly, artificially limiting an interpretive system test to the spectra of compounds containing only one functional group (*11*, *12*) will produce a much higher *RC*/*FP* performance (*8*).

Ranking of Predictions. Of course it is more important that a system *performs* well on real unknowns (high *RL* values) rather than that it scores well on tests (optimum *RC* and *FP* values). For most retrieval systems, the ratings of predicted compounds are based on the degree to which the unknown spectrum matches the reference spectrum; to the extent that the data of the nonmatching spectra are randomly distributed over the possible mass and abundance values [PBM (*5*) at-

tempts to do this by weighting these values], this rating should be a measure of the probability that the selected spectrum did not match by the coincidence of its data. Such a rating should thus reflect the "false positives" probability, *not* the reliability. The predictions could be ranked instead by *RL* values derived using Equation 4 from *FP*, *RC*, and estimates of the occurrence probability of the unknown. Alternatively, as mentioned above, the reference file composition could be chosen to reflect the occurrence probability of unknowns by including several different spectra of the same compound for common compounds. Obviously, a retrieval system which must be used in a variety of problems can do little to correct for variations in occurrence probabilities, and the user must weight the system evaluations himself in this regard.

The ranking of substructure predictions in interpretive systems has been based on both *FP* and *RL*. Ratings for STIRS substructure identification should reflect *FP*, as the number of compounds containing the particular substructure in the 15 best matching spectra is weighted for the occurrence probability in the reference file using a random-drawing model (*9*) (if 15 compounds are drawn from the file at random, there would be a substantial probability that two contain chlorine, but very little chance that two would contain azulene). For a K-Nearest Neighbor identification (*6, 18*) requiring two of the three "nearest" compounds to contain the substructure, the chance of a "false positive" for chlorine would obviously be much greater than for azulene, but the chance that an identification of chlorine is correct would also be higher (Equation 4, assuming equivalent *RC* values). In actual use, the rankings of such a system will reflect reliability values only if the occurrence probability of the unknown's substructures are similar to those in the file. On the other hand, use of a system such as STIRS (*9*) with rankings based on *FP* demands that the interpreter rank further the predicted substructures according to his concept of their occurrence probabilities. For a system which provides only a binary ranking of "structure present" or "structure absent" (Table I), the interpreter has little opportunity to modify the results in light of his conception of the occurrence probabilities.

CONCLUSIONS

As a final plea, the potential user of a retrieval or interpretive system deserves to know its basic capabilities, which should be given as a range of *RC*/*FP* pairs determined on a statistically valid sample of unknowns similar to those commonly encountered. The user should also be made to understand to what extent the reported results (especially those ranked by *FP* values) must be further modified to recognize the probability that the prediction is correct. Finally, systems proposed for unknown mass spectra have become so numerous (*7*) that potential users deserve to have direct comparisons based on closely related reference and unknown data (*18*), which for interpretive systems should include a separate evaluation of the capability for indicating the *presence* of substructures (*16, 17*).

ACKNOWLEDGMENT

The author is grateful to R. Venkataraghavan, R. G. Dromey, T. L. Isenhour, and C. L. Wilkins for helpful discussions.

LITERATURE CITED

(1) L. R. Crawford and J. D. Morrison, *Anal. Chem.*, **40**, 1464 (1968).
(2) P. C. Jurs, B. R. Kowalski, T. L. Isenhour, and C. N. Reilley, *Anal. Chem.*, **42**, 1387 (1970).
(3) H. S. Hertz, R. A. Hites, and K. Biemann, *Anal. Chem.*, **43**, 681 (1971).
(4) T. O. Gronneberg, N. A. B. Gray, and G. Eglinton, *Anal. Chem.*, **47**, 415 (1975).
(5) G. M. Pesyna, R. Venkataraghavan, H. E. Dayringer, and F. W. McLafferty, *Anal. Chem.*, **48**, 1362 (1976).
(6) P. C. Jurs and T. L. Isenhour, "Chemical Applications of Pattern Recognition", Wiley-Interscience, New York, 1975.
(7) G. M. Pesyna and F. W. McLafferty in "Determination of Organic Structures by Physical Methods", Vol. 6, F. C. Nachod, J. J. Zuckerman, and E. W. Randall, Ed., Academic Press, New York, 1976.
(8) P. Kent and T. Gäumann, *Helv. Chim. Acta*, **58**, 787 (1975).
(9) H. E. Dayringer, G. M. Pesyna, R. Venkataraghavan, and F. W. McLafferty, *Org. Mass Spectrom.*, **11**, 529 (1976).
(10) H. Rotter and K. Varmuza, *Org. Mass Spectrom.*, **10**, 874 (1975).
(11) L. J. Soltzberg, C. L. Wilkins, S. L. Kaberline, T. F. Lam, and T. R. Brunner, *J. Am. Chem. Soc.*, **98**, 7139 (1976).
(12) T. F. Lam, C. L. Wilkins, T. R. Brunner, L. J. Soltzberg, and S. L. Kaberline, *Anal. Chem.*, **48**, 1768 (1976).
(13) N. A. B. Gray, *Anal. Chem.*, **48**, 1420 (1976).
(14) R. C. Fox, *Anal. Chem.*, **48**, 717 (1976).
(15) G. Salton, "Automatic Information Organization and Retrieval", McGraw-Hill, New York, 1968.
(16) K.-S. Kwok, R. Venkataraghavan, and F. W. McLafferty, *J. Am. Chem. Soc.*, **95**, 4185 (1973).
(17) F. W. McLafferty, "Interpretation of Mass Spectra", Second Edition, Benjamin Addison-Wesley, Reading, Mass., 1973, p 98.
(18) T. L. Isenhour, S. R. Lowry, J. B. Justice, Jr., F. W. McLafferty, H. E. Dayringer, and R. Venkataraghavan, *Anal. Chem.*, submitted.
(19) R. G. Dromey, Research School of Chemistry, The Australian National University, Canberra, A.C.T. 2600, Private Communication, February 1977.

F. W. McLafferty

Department of Chemistry
Cornell University
Ithaca, N.Y. 14853

RECEIVED for review February 4, 1977. Accepted May 2, 1977. The author thanks the Environmental Protection Agency (grant R804509) for generous financial support.

Factor Analysis of the Mass Spectra of Oligodeoxyribonucleotides

Sir: Factor analysis (*1*) is a multivariate analysis technique that can be used to identify similar patterns of variation in data variables. Several applications of factor analytic techniques to the interpretation of mass spectral data have recently appeared in the chemical literature (*2–5*). The purpose of those studies was to determine which approaches would be most useful for studying mass spectral data and to apply these approaches to low resolution mass spectral data of organic compounds. Rozett and Petersen (*2–4*) have studied the low resolution mass spectra of the 22 isomers of molecular formula $C_{10}H_{14}$. They have identified factors related to the structures of the isomers and have used these factors to classify the isomers according to structural similarities. Justice and Isenhour (*5*) have studied 630 low resolution mass spectra of compounds with composition $C_{2-10}H_{2-22}O_{0-4}N_{0-2}$ and have identified factors related to the seven functional groups represented in the data set.

We have used factor analytic techniques to study the low resolution mass spectra obtained from intact underivatized oligodeoxyribonucleotides. The purpose of these studies was to identify structural information that was contained in the mass spectra of these compounds (Table I) that would be useful for analysis of unknown compounds. That is, we would like to obtain information related to the presence or absence of a given nucleoside, the relative numbers of the different nucleosides, or the sequence of the nucleosides in a compound.

Details of the data collection process and a description of the computer facilities used in these studies are given elsewhere (*6, 7*). The intensities of 32 ions from the mass spectra were used. These ions were selected based on previous mass spectral studies of nucleosides and nucleotides (*6, 8*). The ions selected to be representative of the presence of each nucleoside are listed in Table II.

Since no calibration factor was obtained with the mass spectra and since the absolute intensities of the ions varied considerably from compound to compound, two relative measures of the ion intensities were used. They were: normalization of the individual ion intensities to the sum of the intensities for selected subsets of the ions, and ratios of ion intensities.

Identification of Nucleosides Present. To determine the presence or absence of a particular nucleoside in a compound, the normalized-to-sum intensities of the ions representative of that nucleoside were used. A separate Q-type (*1, 2*) principal components analysis, using covariance about the origin as the dispersion matrix, was used to establish the presence or absence of each nucleoside in a compound. Each principal components analysis included all the oligonucleotides listed in Table I. For each analysis, only the eight ions (Table II) derived from the nucleoside whose presence or absence was to be established were used. Figure 1 demonstrates the results obtained for the analysis of the adenosine ions. The first factor represents the presence of adenosine in a compound as indicated by the high loadings for all the compounds that contain adenosine. The second factor represents the absence of adenosine in a compound as indicated by the high loadings for the compounds that do not contain adenosine. Similar results were obtained from the analyses of the normalized-to-sum ions for the other three nucleosides.

A Q-type principal components analysis was also performed using all 32 ions (Table II) normalized to their sum. Again, all the oligonucleotides were used and covariance about the origin was used as the dispersion matrix. Twenty factors were found, with the first four accounting for approximately 99% of the variance. Rotation of these four factors according to the varimax criterion (*1, 2*) indicated that each factor was representative of one of the four nucleosides. However, the loadings on each factor could not be used to reliably establish the presence or absence of the nucleosides represented by each factor in compounds that contained more than one type of nucleoside. The ability of the loadings on each factor to establish the presence or absence of the nucleosides generally decreased as the number of different types of nucleosides in a compound increased. This was because the normalized intensities of the ions for each nucleoside depended on the intensities of the ions for all the nucleosides in a compound when the ions for all the nucleosides were used.

Table I. Compounds Used in These Studies[a]

pApC	pTpTpApA	pTpG	pTpCpG
pCpA	pApG	pCpC	pCpTpT
$(pApC)_2$	pGpA	pGpG	pCpTpTpT
$(pCpA)_2$	pCpG	pTpT	GpCpA
$(pCpA)_2$	pGpC	pApA	pApApApC
pApT	pCpT	pApGpA	ApTpGpC
pTpA	pTpC	$(pApGpA)_2$	pApTpGpCpApT
$(pTpA)_2$	pGpT	pApTpC	pCpGpApTpGpC

[a] A represents adenosine, C represents cytidine, T represents thymidine, G represents guanosine, and p represents the 3′ to 5′ phosphate linkage between adjacent nucleosides.

Table II. Selected Ions (*m/e*) Listed According to Nucleoside

Adenosine	Guanosine	Thymidine	Cytidine
108	109	126	122
119	151	181	125
120	176	206	162
135	188	225	191
172	231	243	192
186	268	257	228
252	282	258	242
295	311	286	271

Determination of Nucleoside Ratios. Information as to the relative numbers of the different nucleosides in a compound should be contained in the ion intensities for each nucleoside. The best features to describe this information are ratios of the ion intensities for different nucleosides. Analyses using ratio features were performed to determine if this information was contained in the mass spectra.

All the compounds in our data set that contained both adenosine and thymidine and all the compounds that contained both cytidine and guanosine had the same relative numbers of the two nucleosides. The compounds that contained the other pairs of nucleosides (adenosine–cytidine, thymidine–cytidine, adenosine–guanosine, and thymidine–guanosine) had different relative numbers of the two nucleosides and were used in these analyses.

Feature selection was performed by an R-type (*1, 2*) analysis, using covariance about the origin as the dispersion matrix, of the normalized-to-sum ions for each nucleoside for all compounds that did not contain that nucleoside. Those ions were retained that accounted for less than 1% of the total variance. Thus, those ions represented the nucleoside of interest with a minimal contribution from the other nucleosides. Ratios of the selected ions were formed for each pair of nucleosides with the ions for a given nucleoside always in either the numerator or denominator to keep the "sense" of the ratios the same. The ratios are listed in Table III.

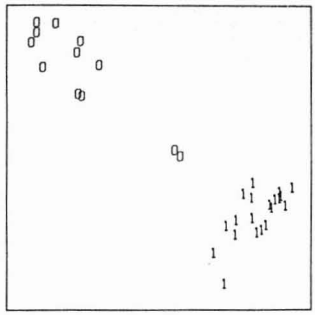

Figure 1. Two-dimensional plot of the loadings on the first two factors resulting from Q-analysis of the normalized-to-sum adenosine ions for compounds containing adenosine (class 1) and compounds not containing adenosine (class 0)

Table III. Ratios of Ions Selected by R-analysis

Nucleoside pair	Ratios of ions (m/e)
Adenosine-cytidine	172/191, 172/192, 172/271, 186/191, 186/192, 186/271, 252/191, 252/192, 252/271, 295/191, 295/192, 295/271
Thymidine-cytidine	225/191, 225/192, 225/271, 286/191, 286/192, 286/271
Adenosine-guanosine	172/188, 172/231, 172/268, 172/282, 186/188, 186/231, 186/268, 186/282, 252/188, 252/231, 252/268, 252/282, 295/188, 295/231, 295/268, 295/282
Thymidine-guanosine	225/188, 225/231, 225/268, 225/282, 286/188, 286/231, 286/268, 286/282

Q-type analyses of the compounds containing a given pair of nucleosides, using covariance about the origin for the dispersion matrix, for the ratios listed in Table III were performed. The relative loadings for the different compounds on the principal factor resulting from each analysis are listed in Table IV according to the nucleoside pairs. The loadings for the compounds containing both adenosine and cytidine and the compounds containing thymidine and cytidine give a semiquantitative estimate of the relative numbers of the two nucleosides present in a compound. The results for the compounds containing guanosine were not as good. A possible reason for this is discussed below. Other feature selection methods were applied in an attempt to identify ratios that would yield better results. No other feature combinations were found that yielded better results.

Sequence Analysis. Pattern recognition techniques have been successfully applied to the sequence analysis of dinucleotide isomers (*6, 7*). The features found useful for the sequence analysis of the dinucleotides were not useful for analysis of longer chain compounds. This was not suprising since the spectra of the oligonucleotides were much more complex because of the presence of more than two types of nucleosides and multiple residues of a given nucleoside. The factor analyses of the normalized-to-sum ions for each nucleoside indicated that any variation in the fragmentation patterns for the nucleosides, that were related to the position of the nucleoside in the compound, were less than the experimental variations in the data and could not be detected by factor analysis of the normalized-to-sum ions for each nucleoside. Thus, we were not able to obtain sequence information for compounds larger than dinucleotides.

CONCLUSIONS

The factor analysis studies reported here have produced promising results. Although the presence or absence of a nucleoside can be determined by the presence or absence of a few of the most intense ions for that nucleoside, the capability of factor analysis for reliable computerized determination of the presence or absence of a nucleoside has been demonstrated. The factor analyses have also indicated that information related to the relative numbers of nucleosides in a compound may be present in the mass spectra of oligonucleotides.

The fact that only a semiquantitative estimate of the relative numbers of nucleosides in a compound was obtained was probably due to the limited resolution of the data col-

Table IV. Relative Loadings on the Principal Factors Resulting from Q-analyses with the Ratios Listed in Table III. The Loadings Are Relative to the Average of the Loadings for the Compounds That Have a Nucleoside Ratio of 1

Adenosine-cytidine

Compound	Nucleoside ratio (A/C)	Relative loading
pApC	1	0.85
$(pApC)_2$	1	1.1
pCpA	1	1.2
$(pCpA)_2$	1	0.5
$(pCpA)_4$	1	0.75
pApTpC	1	1.1
GpCpA	1	0.96
pApApApC	3	4.0
ApTpGpC	1	1.5
pApTpGpCpApT	2	3.1
pCpGpApTpGpC	0.5	0.66

Thymidine-cytidine

Compound	Nucleoside ratio (T/C)	Relative loading
pCpT	1	0.95
pTpC	1	0.64
pApTpC	1	0.56
pTpCpG	1	1.3
pCpTpT	2	1.5
pCpTpTpT	3	5.0
ApTpGpC	1	1.5
pApTpGpCpApT	2	3.4
pCpGpApTpGpC	0.5	0.79

Thymidine-guanosine

Compound	Nucleoside ratio (T/G)	Relative loading
pGpT	1	1.8
pTpG	1	0.93
pTpCpG	1	0.44
ApTpGpC	1	0.86
pApTpGpCpApT	2	1.6
pCpGpApTpGpC	0.5	0.44

Adenosine-guanosine

Compound	Nucleoside ratio (A/G)	Relative loading
pApG	1	0.99
pGpA	1	1.6
pApGpA	2	0.35
$(pApGpA)_2$	2	0.88
GpCpA	1	0.43
ApTpGpC	1	0.94
pApTpGpCpApT	2	1.2
pCpGpApTpGpC	0.5	0.35

lection process. Visual inspection of the spectra for those compounds that deviated the most from the expected relationships indicated that these spectra were generally less intense than those obtained for the compounds that showed the expected relationships. This was most noticeable for guanosine because it yields the least intense spectra of the four nucleosides. Since adenosine and cytidine yield the most intense spectra, the results of analyses involving these nucleosides came closest to the expected results.

While the results reported here cannot be considered conclusive because of the limited data set studied and the limited resolution of the data collection process, we feel that they are sufficiently encouraging to warrant further studies with a larger and better defined data set, and that we have demonstrated a useful approach for the factor analysis of complex data sets.

LITERATURE CITED

(1) R. J. Rummel, "Applied Factor Analysis", Northwestern University Press, Evanston, Ill., 1970.
(2) R. W. Rozett and E. M. Petersen, *Anal. Chem.*, **47**, 1301 (1975).
(3) R. W. Rozett and E. M. Petersen, *Anal. Chem.*, **47**, 2377 (1975).
(4) R. W. Rozett and E. M. Petersen, *Anal. Chem.*, **48**, 817 (1976).
(5) J. B. Justice, Jr., and T. L. Isenhour, *Anal. Chem.*, **47**, 2286 (1975).
(6) J. L. Wiebers and J. A. Shapiro, *Biochemistry*, **16**, 1044 (1977).
(7) D. R. Burgard, S. P. Perone, and J. L. Wiebers, *Biochemistry*, **16**, 1051 (1977).
(8) J. A. McCloskey in "Basic Principles in Nucleic Acid Chemistry", Vol. I, P.O.P. Ts'o, Ed., Academic Press, New York, N.Y., 1974, Chapter 3.

D. R. Burgard
S. P. Perone*

Department of Chemistry
Purdue University
West Lafayette, Indiana 47907

J. L. Wiebers

Department of Biological Sciences
Purdue University
West Lafayette, Indiana 47907

RECEIVED for review April 25, 1977. Accepted June 6, 1977. This work supported by NSF grant No. MPS74-12762, the Office of Naval Research, and NSF grant No. PCM76-21554.

Atomic Spectrochemical Measurements with a Fourier Transform Spectrometer

Sir: In a preliminary report, we discussed the potential application of Fourier transform spectrochemical instrumentation to atomic spectral measurements (*1*). Since that time we have further developed our experimental system in order to improve our measurement capability in the visible and ultraviolet spectral regions. The Michelson interferometer that we have designed and built for application to Fourier transform spectroscopy has three optical inputs; a He-Ne laser, a white light (tungsten bulb) source, and the spectral signal of interest. Laser fringe referencing is used to sequence digitization and to control the velocity of the moving mirror using a phase-locked loop. The mirror drive system consists of an electromechanically driven mirror supported by an air bearing. The mirror movement is repetitive and both the scan rate and length can easily be set or altered. With control signals derived from the white light interferogram and the laser fringes, signal interferograms can be precisely time averaged. This system uses a unique "pretrigger" approach that allows acquisition of any desired number of signal interferogram data points both before and after the zero path difference position. We did not have this last feature when the data were acquired for Ref. 1. This meant that only "one sided" interferograms could be acquired with *no* points acquired before the central fringe of the signal interferogram. This made it essentially impossible to reliably phase correct spectra. With our present ability to acquire full double sided interferograms, i.e., an equal number of points on either side of the zero path difference position, excellent spectra can be calculated without using any phase correction procedures, i.e., by calculating the amplitude spectrum. As will be seen, this makes a considerable improvement in the quality of the spectra that can be measured with our system. In addition the interferometer is now interfaced to a larger computer (PDP 11/10) which is presently capable of 4 k transforms (floating point FORTRAN). This has allowed us to more fully use the designed resolution capability of the interferometer. Our previous maximum transform size was 512 points.

The flame (Air-C_2H_2) emission spectrum of Li, K, Rb, and Cs as measured using our Fourier transform spectrometer with four different sampling rates is shown in Figure 1. A Si photodiode was used as the detector. These spectra were calculated from 512-point double-sided interferograms (i.e., 256 points each side of zero path difference) and 50 scans were taken of each interferogram. The solution used to obtain the spectra shown in Figure 1 contained about 250 ppm of each element.

In addition to illustrating the marked improvement in spectrum quality arising from the acquisition and processing of double-sided interferograms, this series of spectra also provides an excellent illustration of the utility of aliasing in providing optimized resolution and spectral coverage with a limited transform size. Since we use the standard He–Ne reference laser, the basic sampling interval for the interferometer system is 0.6328 μm. This means that the shortest wavelength of light that can be properly sampled without aliasing is 1.266 μm (7901 cm^{-1}). In order to measure the major emission lines of Cs, Rb, K, and Li in the near-IR (See Table IV of Ref. 1) without aliasing, a bandwidth of 15 803 cm^{-1} is necessary. This can be achieved with our measurement system by frequency doubling the laser fringe signal using phase-locked loop techniques (*2*) to provide a sampling interval of 0.3164 μm. However, with a 512-point transform limit the potassium and rubidium doublets cannot be resolved. This is shown in Figure 1a. The numbers (6, 7, 8) shown below the spectral peaks refer to spectral regions associated with the +4 sampling rate (see Table III of Ref. 1). The arrows indicate the direction of increasing wavenumbers.

Using a 0.6328-μm sampling interval (Figure 1b), resolution is doubled and the spectral information is aliased. With a sampling interval of 1.266 μm (Figure 1c), the potassium doublet is resolved and the cesium lines have aliased into the potassium-rubidium region and in the last spectrum (Figure 1d) measured with the 2.532-μm sampling interval, all lines are well resolved and all three regions overlap via aliasing. It is clear from this series of spectra that aliasing can be used to advantage in optimizing spectral coverage and resolution when making Fourier transform spectrochemical measurements.

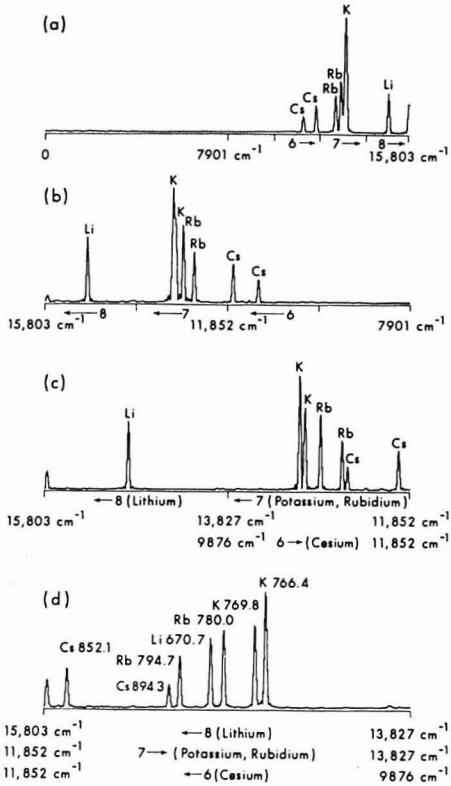

Figure 1. Flame emission spectrum of Cs, Rb, K, and Li measured with sampling intervals of (a) 0.3164 μm, (b) 0.6328 μm, (c) 1.2656 μm, and (d) 2.5312 μm. The wavelengths in Figure 1d are given in nm

The spectrum shown in Figure 1d should be compared to that shown in Figure 6 of Ref. 1 to note the improvement in quality as a result of measuring a double sided interferogram. It should also be pointed out that since the spectrum shown in Figure 6 of Ref. 1 was calculated from a 512-point one-sided interferogram (2.532-μm sampling interval), it has a theoretical resolution of 8 cm^{-1} as compared to 16 cm^{-1} (both triangularly apodized) for the spectrum shown in Figure 1d. At 770.0 nm, a resolution of 16 cm^{-1} corresponds to 0.95 nm.

These data clearly indicate that acquisition and processing of double-sided interferograms significantly improve the spectral quality of line emission spectra measured with a Fourier transform spectrometer. The phase correction procedures utilized in mid-IR Fourier transform spectroscopy are designed primarily for absorption spectra measured using broad band sources and are not particularly effective with line emission spectra. During a recent visit to our department, J. C. Polanyi (*3*) indicated that he had experienced similar difficulties in phase correcting infrared line emission spectra (infrared chemiluminescence) measured with a Fourier transform spectrometer, as has Griffiths (*4*) in the measurement of CO emission spectra. Finally, one might think that the phase correction procedures utilized in Fourier

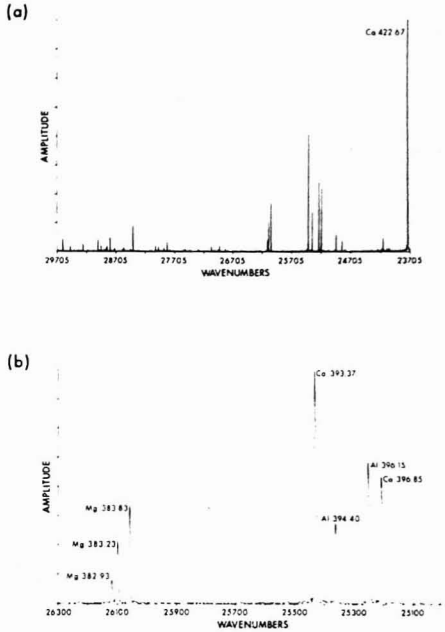

Figure 2. (a) Spectrum of a Mg-Al-Ca hollow cathode lamp from 31 604 to 23 703 cm^{-1} (316.4 to 421.9 nm) as measured with Fourier transform spectrometer. (b) Expanded plot of 26 300 to 25 000 cm^{-1} region. The wavelengths are given in nm

transform NMR (*5*, *6*) might be applicable to the interferograms shown in Ref. 1. We made some attempt to use these procedures but found that each aliased region required a different phase angle making it next to impossible to phase correct a spectrum such as that shown in Figure 6 of Ref. 1.

Some results obtained using the larger data system are shown in Figure 2. The source was a Mg-Al-Ca hollow cathode lamp (Ne filler gas) and the detector was a 1P28 photomultiplier tube. The spectrum shown in Figure 2 was calculated from a 4096-point double-sided interferogram (Gaussian apodization) sampled at 0.6328-μm intervals. Fifty interferograms were time averaged resulting in an observation time of about 50 s. The spectral bandpass of the system was limited with a Corning 7-59 filter primarily to 31 604–23 703 cm^{-1} (316.4 to 421.9 nm) [region 4 of Table I in Ref. 1] with some aliasing in from region 3 possible. The theoretical resolution was about 8 cm^{-1} which is equivalent to 0.1 nm in the center of this region.

While the complete 4096-point spectrum is too detailed to adequately show on a journal page, we have included a plot of 3000 points of the spectrum in Figure 2a to give the reader a feel for the spectral range simultaneously measured using region 4. It should be noted that the Ca 422.67 nm line is actually aliased into this region from region 3 (See Table I in Ref. 1). The region from 26 300 to 25 000 cm^{-1} (621 points) is shown expanded in Figure 2a. Note that the two magnesium lines at 382.93 and 383.23 nm ($\Delta\lambda$ = 0.3 nm) are resolved to the baseline. The calculated wavelengths of these lines taken from four independently measured spectra are listed in Table I along with the literature values. These data indicate that both precise and accurate wavelength measurements can be

Table I. Line Wavelengths Calculated from Spectra Measured with Fourier Transform Spectrometer

Literature values, nm		Experimental values, nm			
		1	2	3	4
Mg	382.93	382.88	382.88	382.88	382.88
Mg	383.23	383.16	383.16	383.16	383.16
Mg	383.83	383.76	383.76	383.79	383.76
Al	394.40	394.33	394.36	394.36	394.33
Al	396.15	396.10	396.10	396.10	396.07
Ca	393.37	393.31	393.31	393.31	393.31
Ca	396.85	396.77	396.77	396.80	396.77

made with our present Fourier transform spectrometer in this spectral region. At most, only one point jitter (0.03 nm) is observed and all wavelengths are accurate to 0.07 nm or better.

Further studies on the application of Fourier transform spectrochemical instrumentation to atomic spectrochemical measurements are continuing in our laboratory. These studies include the assessment of the simultaneous multielement analysis capability of our system (both qualitative and quantitative) utilizing flame, dc arc, and ICP sources.

LITERATURE CITED

(1) Gary Horlick and W. K. Yuen, *Anal. Chem.*, **47**, 775A (1975).
(2) H. V. Malmstadt, C. G. Enke, S. R. Crouch, and G. Horlick, "Optimization of Electronic Measurements", W. A. Benjamin, Menlo Park, Calif., 1974, p 67.
(3) J. C. Polanyi, Department of Chemistry, University of Toronto, Toronto, Ontario, private communication.
(4) P. R. Griffiths, Pittsburgh Conference on Analytical Chemistry and Applied Spectroscopy, Cleveland, Ohio, Paper No. 440 (1977).
(5) "Nicolet 1080 System for FT-NMR", Nicolet Instrument Corporation, 5225 Verona Road, Madison, Wisc. 53711.
(6) J. W. Cooper, "The Minicomputer in the Laboratory", John Wiley, New York, 1977, p 301.

W. K. Yuen
Gary Horlick*

Department of Chemistry
University of Alberta
Edmonton, Alberta, Canada T6G 2G2

RECEIVED for review March 22, 1977. Accepted May 11, 1977.

Stoichiometry of Nitrogen Dioxide Determination in Triethanolamine Trapping Solution

Sir: Nitrogen dioxide may be determined in air by a variation of the Saltzman method (*1*) in which the trapping solution is 0.1 N triethanolamine (TEA) in water (*2*). Several workers have proposed differing stoichiometries for the formation of nitrite ion in this trapping solution (*2, 3*) based on the results of analyses of prepared atmospheres containing NO_2 in low concentrations. However, the mechanism for the reaction has not been established. The absence of mechanistic hypotheses for this important reaction renders the elucidation of a trapping mechanism at relatively high NO_2 concentrations important in providing a starting point for investigation of the stoichiometry at low NO_2 concentrations. The present investigation was conducted on the reaction of gram quantities of NO_2 with equivalent amounts of TEA. In aqueous solution, equimolar amounts of nitrite and triethanolammonium nitrate were formed. When the reaction was run in methylene chloride with the exclusion of water, a precipitate having properties consistent with formulation as a nitroso ammonium salt could be observed. On the basis of these results, the following scheme is proposed for the reaction of equivalent amounts of NO_2 and TEA in an aqueous solution:

$$2NO_2 \rightleftharpoons N_2O_4$$

$$N_2O_4 + (HOCH_2CH_2)_3N \longrightarrow (HOCH_2CH_2)_3NNO^+NO_3^-$$

$$(HOCH_2CH_2)_3NNO^+NO_3^- + H_2O \longrightarrow (HOCH_2CH_2)_3NH^+NO_3^- + HNO_2$$

I II

This reaction path requires a stoichiometric factor of 0.5 for the conversion of gaseous NO_2 to nitrite ion.

RESULTS AND DISCUSSION

Reaction of a slight excess of TEA in distilled water with a measured amount of NO_2 yielded 96% of the theoretical amount of nitrite based on the proposed reaction scheme. In addition, 83% of the theoretical amount of recrystalized II could be recovered from the aqueous solution. Since no characterization of II could be found in the literature, its structure was established by satisfactory elemental analysis, molecular weight determination by freezing point depression, NMR (Figure 1), IR (Figure 2), and UV (Figure 3).

When TEA was reacted with NO_2 at −5 °C in CH_2Cl_2 under nitrogen with the exclusion of water, a white precipitate I, different from II, formed immediately on addition of NO_2. Compound I melted over a range (60–67 °C) with decomposition and vigorous evolution of gas. The qualitative UV spectrum obtained in methanol from freshly isolated I was different from the spectra of II, NO_2, or $NaNO_2$ in methanol (Figure 3). Gradual decomposition with evolution of gas occurred during warming to room temperature under both vacuum and a nitrogen atmosphere.

Attempts to isolate I for elemental analysis were unsuccessful; however, its behavior is consistent with formulation as a nitroso ammonium salt. Under neutral or alkaline conditions the nitroso salt would be expected to yield nitrite on hydrolysis (*4, 5*). Although isolation of I followed by reaction with water gave a nitrite yield of only 54%, immediate reaction with water in situ resulted in a nitrite yield of 86% based on the proposed reaction scheme. Formation of II and appearance of nitrogen dioxide above the solid when I was exposed to moist air can be accounted for by hydrolysis of I to yield nitrous acid which subsequently decomposes to nitric oxide and nitrogen dioxide. Also, in accordance with the results expected for a nitroso ammonium intermediate, compound II could be recovered without recrystallization in 97% yield when the NO_2 addition was run in methylene chloride in the presence of one equivalent of water.

The formation of I from NO_2 is in accord with a number of observations in the literature. Spectroscopic evidence indicates that nitrogen dioxide in equilibrium with dinitrogen tetroxide may exist to some extent as a tautomer that can be formulated as nitrosyl nitrate (*6*). Consistent with this finding, dinitrogen tetroxide appears to heterolyze in solution to NO^+ and NO_3^- (*7, 8*), which in the presence of TEA would be expected to lead to I.

Reactions of primary and secondary amines with potential NO^+ donors appear from kinetic considerations to proceed

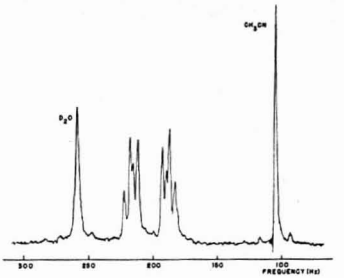

Figure 1. 60-MHz NMR of compound II

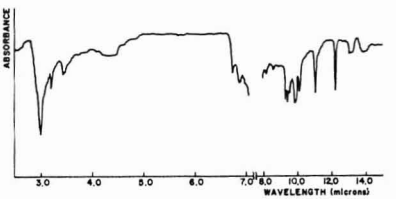

Figure 2. IR of compound II. Range 2.5–7 μm, fluorolube mull; range 8–14 μm, Nujol mull

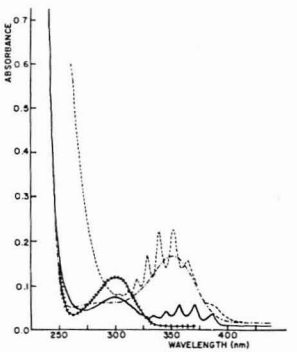

Figure 3. UV spectra in methanol. (——) compound I, (•••) nitrite ion, (—) nitrogen dioxide, and (+++) compound II

via nitroso ammonium salts analogous to I (*9–11*). Additionally, reaction of several tertiary amines with $NOBF_4$ (*5*) and NO_2 (*12*) at low temperature yielded precipitates with properties similar to I and consistent with nitroso ammonium salts.

The proposed scheme for the trapping of high concentrations of NO_2 by aqueous TEA solution is supported by data (*3*) on the analysis of dynamically prepared concentrations of NO_2 in air. Data from Ref. 3, regrouped and presented in Table I, show that for NO_2 concentrations above 10 ppm the stoichiometric factor is ~0.5. However, the factor appears to increase with decreasing NO_2 concentration. A number of investigators have examined the question of a similar concentration effect for the stoichiometric factor of the Saltzman reaction (*13–15*) and have arrived at conflicting conclusions. In the case of the Saltzman determination the question of predominance among competing mechanisms has been raised (*15*), but evidence to support specific hypotheses is lacking.

Table I. Results of Analyses of Dynamically Prepared Concentrations of Nitrogen Dioxide Based on Data from Ref. 3

Nominal NO_2 concn, ppm	No. of determinations	Av. stoichiometric factor found	$\pm\sigma$
3.3–3.5	9	0.73	0.05
6.6–6.7	3	0.61	0.03
10.6–10.8	4	0.56	0.06
Grand total	16	0.67	0.10

Likewise, there is at this time no evidence to support an explanation for the trend in the stoichiometric factor observed in Table I for the TEA reaction. However, the proposed reaction scheme with the stoichiometric factor 0.5 appears to hold for air concentrations of NO_2 >10 ppm.

EXPERIMENTAL

Reagents. Sodium nitrite, Mallinckrodt reagent grade, was assayed by adding excess $KMnO_4$ and back-titrating with ferrous ammonium sulfate (*16*) and found to be 99.3% pure. Methylene chloride, Fisher reagent grade, was distilled from $CaCl_2$ for dry reactions. TEA, Fisher reagent grade, was used as received for reactions run in water. For water-free reactions, the TEA was evacuated in a desiccator containing P_2O_5 for 48 h at 10^{-2} mm and then vacuum distilled (bp 135–140 °C, 10^{-2}mm). Nitrogen dioxide, Matheson Gas Products 99.5% pure, was passed through P_2O_5 before use.

Nitrite Determinations. Nitrite yields were determined colorimetrically by the diazo coupling of *N*-(1-naphthyl) ethylene diamine and sulfanilamide (*2*) using solutions of assayed sodium nitrite as standards.

Reaction of TEA and NO_2 in Aqueous Solution. (a) A 500-mL round bottom flask with stopcock adaptor having a total volume of 527 mL, was evacuated to 10^{-2} mm and filled to atmospheric pressure with NO_2. At room temperature (23 °C) and atmospheric pressure with 82% dimerization of NO_2, this volume corresponds to 19.6 mmol N_2O_4. With the stopcock closed, the NO_2/N_2O_4 was condensed to a white solid by placing the bottom of the reaction flask in crushed dry ice and a solution of 5 g TEA (33.5 mmol) in 150 mL distilled water added through the stopcock by suction resulting from the vacuum created on condensation of the NO_2. The reaction mixture was rinsed into a 500-mL volumetric flask and made up to volume with additional distilled water. This stock solution was further diluted 500:1 for nitrite determination. Average yield of four runs: 96%.

(b) This reaction was also run at room temperature by adding 500 mL of NO_2/N_2O_4 gas by syringe to a stirred solution of 4.5 g TEA in 250 mL distilled water, resulting in a nitrite yield of 86%. Repetition of the reaction with the removal of the water on a rotary evaporator, followed by two recrystallizations from MeOH-$CHCl_3$ yielded 3.29 g (83%) of II, mp 78–80 °C.

Compound II was recrystallized from MeOH-$CHCl_3$ five times and evacuated at 10^{-2} mm overnight for elemental analysis. Calculated for $C_6H_{16}N_2O_6$: C, 33.96%; H, 7.55%; O, 45.28%; N, 13.21%. Found: C, 33.93%; H, 7.52%; O, 45.19%; N, 13.06%. The molecular weight determined by freezing point depression in water was 210 ± 3 compared to the expected value of 212. The NMR (D_2O) consisted of two A_2B_2 multiplets in 1:1 ratio centered at 83 Hz and 111 Hz downfield from CH_3CN (Figure 1). The IR (fluorolube) showed bands at 3.00, 3.20, 3.45, 6.45, and 6.80 μm. In Nujol, additional bands occurred at 9.30, 9.40, 9.85, 10.1, and 12.2 μm (Figure 2). The UV (MeOH) had $\lambda_{max}(\epsilon)$ at 297 mm (9.5).

Yield of Nitrate Salt in CH_2Cl_2. Reaction (a) was carried out with a solution of 5 g TEA in 150 mL CH_2Cl_2 to which 0.4 mL distilled water (1 equiv) had been added. The precipitate was collected on a fritted filter, rinsed with CH_2Cl_2 and evacuated at 10^{-2} mm to constant weight, yielding 4.03 g (97%) of the crystalline nitrate, mp 73–76 °C undepressed by II.

Nitrite Yield from I in Situ. Reaction (a) was run with the exclusion of water, adding via syringe a solution of 5 g dry TEA

in 30 mL CH_2Cl_2 distilled from $CaCl_2$ under nitrogen. The precipitate was allowed to warm to 0 °C and then quenched with 100 mL distilled water. After decanting the water from the CH_2Cl_2 into a 500-mL volumetric flask, 100 mL 0.1N NaOH was added to the reaction flask, and the CH_2Cl_2 evaporated at room temperature on a rotary evaporator. The NaOH solution was added to the volumetric flask and the nitrite determination performed as described above, giving a yield of 86%.

Attempted Isolation of Nitrosoammonium Salt. Five grams of dried TEA were distilled into a 500-mL 3-neck flask equipped with a Teflon stir bar and a three-way stopcock adaptor. After distilling in 100 mL CH_2Cl_2 from $CaCl_2$ under nitrogen, an inlet for NO_2 was fitted to one neck and the reaction flask cooled to −5 °C in an ice-brine bath under positive nitrogen pressure. Approximately 500 mL NO_2/N_2O_4 passed through P_2O_5 was metered via a rotameter into the stirred reaction mixture. After the addition had been completed, the reaction mixture was held at −5 °C for 10 min and then the CH_2Cl_2 was filtered off with nitrogen pressure through a frit placed on one neck. At this point, the formation of bubbles in the precipitate indicated some decomposition. No attempt was made to characterize decomposition products. The reaction flask was briefly evacuated to remove traces of CH_2Cl_2 and transferred to a glove box under nitrogen where an aliquot was weighed out for determination of nitrite (best yield of three reactions, 54%). A qualitative UV in dry methanol was also taken at this juncture.

ACKNOWLEDGMENT

The author thanks O. Grubner and G. Dudek for helpful discussions and the Chemistry Department of Harvard University for use of their NMR spectrometer.

LITERATURE CITED

(1) B. E. Saltzman, *Anal. Chem.*, **26**, 1949 (1954).
(2) D. A. Levaggi, W. Siu, and M. Feldstein, *J. Air Pollut. Control Assoc.*, **23**, 30 (1973).
(3) J. H. Blacker, *Am. Ind. Hyg. Assoc. J.*, **34**, 390 (1973).
(4) W. Lijinsky, L. Keefer, E. Conrad and R. Van de Bogart, *J. Natl. Cancer Inst.*, **49**, 1239 (1972).
(5) P. A. S. Smith and R. N. Loeppky, *J. Am. Chem. Soc.*, **89**, 1147 (1967).
(6) H. A. Bent, *Inorg. Chem.*, **2**, 747 (1963).
(7) C. C. Addison, W. Karcher and H. Hecht, "Chemistry in Nonaqueous Ionizing Solvents," Vol. III, Pergammon Press, New York, 1967, pp 3–75.
(8) F. A. Cotton and G. Wilkinson "Advanced Inorganic Chemistry, a Comprehensive Text," 3rd ed., Interscience, New York, 1972, pp 357–359.
(9) S. Patai, "The Chemistry of the Amino Group," Interscience, New York, 1968, pp 305–320.
(10) B. C. Challis and J. H. Ridd, *Proc. Chem. Soc. (London)*, 245 (1960).
(11) E. D. Hughes and J. H. Ridd, *J. Chem. Soc.*, 82 (1958).
(12) A. E. Comyns, *J. Chem. Soc.*, 1557 (1955).
(13) F. P. Scaringelli, E. Rosenberg, and K. A. Rehme, *Environ. Sci. Technol.*, **4**, 924 (1970).
(14) H. J. Cercelius and W. Forweg, *Staub-Reinholt. Luft*, **30**, 23 (1970).
(15) H. Hartkamp and G. Nitz, *Staub-Reinholt Luft*, **34**, 340 (1974).
(16) J. Rosin, "Reagent Chemicals and Standards," 5th ed., D. Van Nostrand Co., Inc., Princeton, N.J., 1967, p 471.

Avram Gold

Occupational Health Program
Harvard School of Public Health
665 Huntington Avenue
Boston, Massachusetts 02115

RECEIVED for review December 22, 1976. Accepted May 4, 1977. Supported by NIOSH Grant OH00369-05 and Center Grant (ES 00002) from the National Institute of Environmental Health Sciences.

AIDS FOR ANALYTICAL CHEMISTS

Modified Inductively Coupled Plasma Arrangement for Easy Ignition and Low Gas Consumption

John L. Genna and Ramon M. Barnes*

Department of Chemistry, University of Massachusetts, Amherst, Massachusetts 01003

Charly D. Allemand

Jarrell-Ash Division, Fisher Scientific Company, Waltham, Massachusetts 02154

Since the initial description by Reed (*1*) of a practical inductively coupled plasma (ICP) discharge and the independent realization of its potential as an analytical tool by Greenfield et al. (*2*), and Wendt and Fassel (*3*), developments of the ICP discharge as a spectrochemical source have intensified (*4*, *5*).

Design of an ICP arrangement specifically for totally automated, unmanned operation with low coolant gas consumption and ease of ignition emphasized optimization of plasma tube geometry in the region near the induction coil (*6*). The resulting successful configuration required precise machined dimensions obtainable with material like boron nitride but not with quartz. This note describes a simple modification of the gas flow injection region which is readily achieved with conventional materials such as quartz and which promotes the formation of closed loops of ionized gas to ease discharge ignition. This modification also provides reduced coolant gas consumption.

In popular ICP arrangements (*7–11*), total argon flows reach approximately 11 to 30 L/min with the major portion used in the outer tube (Figure 1) annulus to prevent the outer quartz confinement walls from overheating. In high-power level ICP discharges, high nitrogen flows in the outer annulus provides effective cooling and low background levels (*11*, *12*).

Reed recognized the importance of tangential coolant gas introduction for vortex stabilization (*1*). Although laminar (*3*) and other arrangements have been explored (*13*), tangential gas introduction is popular and effective. Stabilization is attributed to production of a low pressure region along the central axis of the tubes by the swirling gas flow near the confinement wall (*1*). This low pressure allows increased amounts of countercurrent gas flow.

The low pressure produced by the tangential introduction of gas is a function of the mass flow rates, but, more importantly, the gas velocity. In cylindrical coordinates, the gas velocity comprises the following three components (Figure 1): a radial (V_r), an axial (V_z), and angular or swirl (V_θ) component. The swirl velocity travels parallel to the circular torch walls and is critical in the stabilization of the discharge. Control of the swirl component is essential in the improvements described here.

To increase the argon flow countercurrent to the main flow, the low-pressure regions in the discharge must be increased. These low-pressure regions may be created, in turn, by the

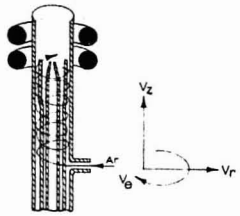

Figure 1. Illustration of coolant gas flow in a plasma torch and its three gas velocity components

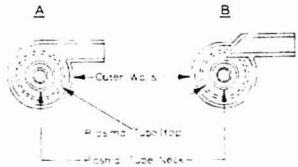

Figure 2. Comparison of plasma torch side arm geometries. Top view of conventional torch (A) and modified torch (B)

swirl or vortex flow which results from the tangential introduction of the coolant flow. In practice, the swirl velocity is determined by the position and shape of the gas inlet. Conventional torch configurations have gas inlets as shown in Figure 2A. Through modifications of the gas inlet, the swirl velocity can be controlled which results in improved discharge performance.

EXPERIMENTAL

To increase the swirl velocity, the gas inlet was modified to form a directional nozzle which protrudes into the annular space of the quartz ICP torch as shown in Figure 2B.

Conventional geometries were compared with the modified arrangement on two different ICP systems. The first system is a commercial configuration employing a crystal controlled RF generator and a multichannel spectrometer, and the second system is a research instrument using a free running generator (*14*). Table I gives the operating conditions used in the commercial system for these experiments.

Pressure measurements employed a water-cooled Pitot tube (*15*) and a capacitive pressure transducer (*16*).

RESULTS AND DISCUSSION

Modification of the gas inlet in the form of a nozzle results in two significant effects in the operation of the ICP. First, the ease of initiation is improved substantially, and seldom does a distorted discharge occur as in conventional configurations. Secondly, the discharge can be operated at a coolant flow 30 to 40% lower than conventional arrangements. Under similar conditions, the conventional arrangement rapidly heats and the outer tube in the coil region melts.

The discharge produced when the modified gas inlet geometry is employed is quite stable and can be operated for long periods without damage to the inner or outer quartz walls.

The effect of the modified gas inlet arrangement on coolant flow during plasma operation was tested with two totally different ICP systems. For both systems, the usual operating flow of coolant gas and that required with the modified gas inlet were compared employing the same plasma torch. With the commercial instrument normally operated at a coolant flow of 18 L/min and forward power of 1.2 kW, the coolant flow was reduced to 12 L/min using the modified torch. At lower flow rates, the silicon emission signal increased to unacceptable values. The usual minimum coolant flow with this system is 11 L/min. Employing the research instrument with generator output of 1.2 kW (~780 W in the discharge)

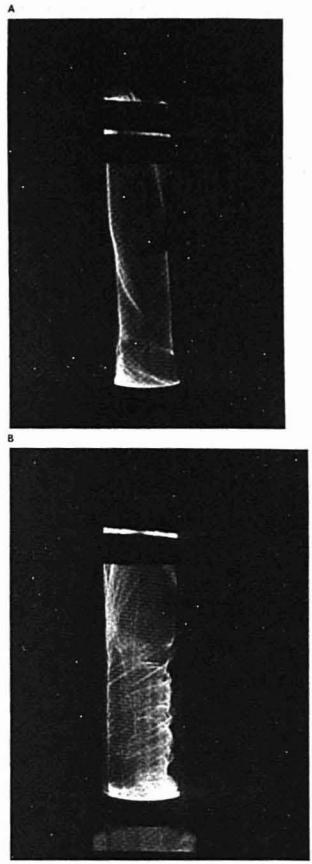

Figure 3. Photographs of plasma torch during initiation of the discharge showing swirling ionized argon; conventional torch (A) and modified torch (B)

and 10 L/min coolant gas flow used routinely, the coolant flow was reduced to 5 L/min. At a flow of 3.5 L/min, the quartz softened and the discharge became unstable. With the conventional torch, the same effects occurred in the research system at approximately 8 L/min. Flow differences between the two ICP systems using the same torch result from peculiarities of coil geometry and coupling efficiency.

Several preliminary experiments were conducted to explore the phenomena which allowed the reduction in flow and to establish whether or not the excitation conditions of the discharge changed significantly. These include photography during discharge initiation, direct pressure measurements, and determination of powers of detection. Measurements of excitation temperatures, electron and particle density, and gas velocity fields are currently under way.

Observation of the pathways of ionized gas during initiation of the discharge, commonly called filaments, provides visual indication of significant differences in swirl for the two gas inlet geometries. In Figure 3, the gas appears to travel in closed loops with reduced pitch and higher velocity with the

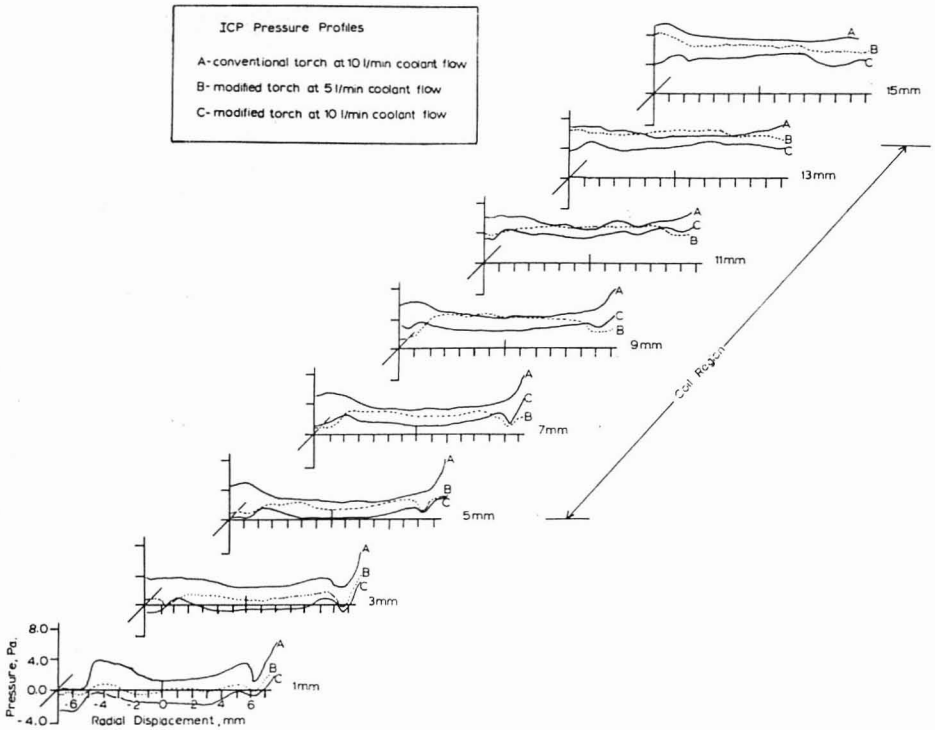

Figure 4. Axial pressure (V_z) profiles for conventional plasma torch at 10 L/min coolant flow (A), modified plasma torch at 5 L/min coolant flow (B), and modified plasma torch at 10 L/min coolant flow (C). Center of the tube is located at 0 mm on the radial displacement scale. Axial position is given relative to the top of the plasma tube

Table I. Operating Conditions

Jarrell-Ash Plasma Atomcomp	
Power Forward	1.2 kW
Reverse	0 W
Coolant flow (conventional torch)	18 L/min
Coolant flow (modified torch)	12 L/min
Plasma flow	<0.5 L/min
Central flow	0.5 L/min
Nebulizer	Cross Flow Pneumatic
Nebulizer uptake	1.35 L/min
Spectrometer	Jarrell-Ash Atomcomp (Model 96-975)
Entrance slit height	3 mm
Entrance slit width	25 μm
Exit slit width	50 μm
External magnification	3.5 X
Height of observation zone above coil	20 mm
Coil	4 turns $^3/_{16}$-inch o.d. copper tube

modified inlet geometry than with the conventional arrangement.

Pressures measured at the gas inlet permit calculation of the swirl velocity V_θ for both arrangements. In the conventional torch, the swirl velocity is 3.5 m/s; whereas, with the injection nozzle, the velocity is greater than 38 m/s. In contrast, the axial velocity V_z remained essentially the same at approximately 10 m/s. The higher swirl velocity is consistent with the visually observed coolant gas pathways when the nozzle is present.

In order to obtain a high V_θ but maintain the same V_z, the gas must travel a longer path as it moves through the annular zone between the outer confinement wall and the inner coaxial wall. To accomplish this, the number of closed loops the gas travels for a given length must increase, and the distance between each loop must decrease. This increases the gas contact area with the outer wall which results in improved heat exchange and cooler confinement walls.

The same effect is also responsible for the improvement in the initiation of the discharge. In order to generate an ICP discharge, an initial supply of electrons and ions must be produced. This is normally accomplished by ionizing the argon gas momentarily with a Tesla coil. The electrons and ions travel into the coil region where energy is coupled to them from the induction coil. Although the mass flow in the modified torch remains the same or is even somewhat reduced near the outer confinement, the electron and ion density is higher than in the common torch, thus increasing the probability of the formation of a closed loop during initiation. This effect is especially important in the coil region where closed loops lead to inductive coupling, and initiation of the discharge.

Table II. Detection Limits (ng/mL)[a]

Element	λ, nm	Conventional	Modified
Al	396.1	5.7	12.0
B	249.8	2.0	1.5
Ba	455.4	0.37	0.6
Ca	422.7	1.8	3.1
Cd	226.5	7.0	7.4
Cr	267.7	4.5	9.8
Cu	324.7	1.5	4.0
Fe	259.9	3.8	4.7
K	766.5	37.0	40.0
Mn	293.3	7.4	13.0
Mo	386.4	15.0	25.0
Pb	220.3	22.0	74.0
Sb	206.8	36.0	70.0
Si	251.6	11.0	7.9
Sn	189.9	82.0	61.0
Ti	334.9	1.4	3.0
V	309.3	2.8	2.6

[a] All solutions made up in distilled H_2O @ 5% HNO_3.

Pressures were measured spatially in the discharge for different coolant gas flows for the conventional and modified arrangements. The results for the conventional torch with 10 L/min coolant flow, and the modified torch with 10 L/min and 5 L/min flow are plotted in Figure 4. With the modified arrangement, substantially lower pressures are recorded than with the conventional geometry. When operated at 5 L/min, the modified configuration gives a pressure profile which approaches that of the conventional torch at 10 L/min. Apparently this decrease in pressure promotes an increase in the recirculation of argon in and around the discharge. This recirculation presumably provides a more efficient use of argon present within the discharge region. When coupled with improved cooling efficiency of the confinement walls, the modified geometry allows the discharge to be operated at reduced flow rates without seriously damaging the torch.

To determine whether the analytical performance of the modified arrangement is comparable to that of the conventional ICP torch, detection limits were obtained under compromise conditions and compared to those previously obtained with a conventional torch. Table II shows those values obtained in the two cases using the commercial system. The detection limit is defined as that concentration which would give a signal which is two times the standard deviation of the background.

Although the two sets of detection limits were obtained on separate days, operating conditions were otherwise constant. The values are within a factor of about 3 of each other.

Studies are under way to establish parameters such as electron densities and gas velocity distributions for the modified torch. In addition, various alternative geometries which result in similar ICP properties are being investigated.

ACKNOWLEDGMENT

We appreciate the assistance of Charles Wohlers in making the detection limit measurements.

LITERATURE CITED

(1) T. B. Reed, *J. Appl. Phys.*, **32**, 821 (1961).
(2) S. Greenfield, I. Ll. Jones, and C. T. Berry, *Analyst (London)*, **89**, 713 (1964).
(3) V. A. Fassel and R. H. Wendt, *Anal. Chem.*, **37**, 920 (1965).
(4) S. Greenfield, H. McD. McGeachin, and P. B. Smith, *Talanta*, **23**, 1 (1976).
(5) P. W. J. M. Boumans and F. J. de Boer, *Proc. Anal. Div. Chem. Soc.*, **12**, 140 (1975).
(6) C. D. Allemand and R. M. Barnes, submitted to *Appl. Spectrosc.*
(7) S. Greenfield, U.S. Patent No. 3,467,471, Sept. 16, 1969.
(8) R. H. Scott, V. A. Fassel, R. N. Kniseley, and D. F. Nixon, *Anal. Chem.*, **46**, 75(1974).
(9) V. A. Fassel and R. N. Kniseley, *Anal. Chem.*, **46**, 1155A (1974).
(10) P. W. J. M. Boumans and F. J. de Boer, *Spectrochim. Acta., Part B*, **307**, 309 (1975).
(11) S. Greenfield, I. Ll. Jones, C. T. Berry, and L. G. Bunch, *Proc. Soc. Anal. Chem.*, **2**, 111 (1975).
(12) S. Greenfield, I. Ll. Jones, H. McD. McGeachin, and P. B. Smith, *Anal. Chim. Acta*, **74**, 225 (1975).
(13) P. A. Huska and C. W. Clump, *Ind. Eng. Chem., Process Des. Dev.*, **6**, 238 (1967).
(14) R. M. Barnes, and R. G. Schleicher, *Anal. Chem.*, **47**, 724 (1975).
(15) R. M. Barnes and S. Nikdel, *Appl. Spectrosc.*, **29**, 477 (1975).
(16) D. J. Curran and J. L. Driscoll, *Anal. Chem.*, **38**, 1746 (1966).

RECEIVED for review February 4, 1977. Accepted May 2, 1977. This research is supported by a grant from the Alcoa Foundation.

Evaluation of Tetraphenylporphinatozinc(II) as a Stable Standard for Porphyrin Determinations by Fluorescence Spectrometry

David K. Lavallee* and James T. Norelius

Department of Chemistry, Colorado State University, Fort Collins, Colorado, 80523

Promising techniques for the determination of protoporphyrin concentrations by fluorescence spectroscopy for use in the diagnosis of lead intoxication, iron deficiency, and porphyrias have recently been developed (*1–6*). Lamola et al. have demonstrated that the zinc complex of protoporphyrin IX is the prevalent form of non-heme protoporphyrin in erythrocytes of patients suffering from lead intoxication or iron deficiency anemia (*7*). Their group has developed a convenient method for determination of protoporphinatozinc(II) which utilizes a broad bandpass excitation and emission fluorometer that is adequately calibrated by use of a rhodamine dye standard. Most techniques that are presently employed in determining protoporphyrin concentrations involve extraction followed by fluorometric determination of free protoporphyrin which is not bound to a metal ion (*1*). Many laboratories find these techniques quite satisfactory and will likely continue to use them. These methods would be improved, however, by better standards.

Uroporphyrins I and III and coproporphyrins I and III are determined in the urine as indicators of porphyrias and a number of metabolic disorders (*8, 9*). A rapid separation procedure based on anion-exchange resin adsorption and elution has been reported by Sobel et al. (*10*). In this case also, better standards would be helpful.

The limitations of standards which are commonly employed for porphyrin determinations are instability of some compounds, differences in the excitation and emission characteristics of others, and high costs. Protoporphyrin IX itself decomposes rapidly and is unsuitable for routine use (*11*). In the use of coproporphyrin I as a standard, the coproporphyrin I solution is checked daily against a reference standard of protoporphinatozinc(II) (Porphyrin Products, Logan, Utah) which is claimed to be stable for only a few hours by the supplier. The cost of such porphyrin standards is on the order of $20/10-mg vial of coproporphyrin and $15 for a 5-μg vial of protoporphinatozinc(II). The cost of tetraphenylporphi-

natozinc(II), on the other hand, is only $25/g.

Although stable dyes such as rhodamine or quinine sulfate dihydrate are adequate for calibrating broad bandpass filter instruments, they are not as suitable for use as standards in calibrating instruments equipped with excitation and emission monochromators. For these instruments, it is better to use standards with excitation and emission maxima and bandwidths that are as close as possible to the substance being analyzed. Similar spectral characteristics allow for rapid "trouble shooting" and selection of correct instrument settings, both of which can be important when an instrument is used for different analyses or by different operators.

We have evaluated a stable, commercially available, inexpensive compound, *meso*-tetraphenylporphinatozinc(II), as a suitable calibration standard for determinations of protoporphyrin IX, protoporphinatozinc(II), coproporphyrins and uroporphyrins.

EXPERIMENTAL

Reagents. Tetraphenylporphinatozinc(II) was prepared by adding zinc chloride (Fisher Certified reagent grade) to tetraphenylporphine (prepared by the method of Adler et al. (*12*)) in refluxing dimethylformamide, according to the procedure of Adler et al. (*13*). Upon cooling, deep purple crystals of the desired product form. The crystals were washed and dried and identified by their characteristic visible absorption spectrum (*14*). This compound may be obtained in high purity (>98%, as shown by the comparison of molar absorptivity with published values (*14*) and from a single band on an alumina column) from Strem Chemical Company (P.O. Box 212, Danvers, Mass.). Protoporphinatozinc(II), protoporphyrin IX, uroporphyrin III, and coproporphyrin I were obtained from Porphyrin Products, Inc., Logan, Utah.

Solvents were distilled according to standard procedures (*15*). We have found that a useful solvent for the use of ZnTPP as a standard is bis(methoxyethyl) ether (diglyme) which may be used without distillation if reagent grade material (Aldrich Chemical Company, Milwaukee, Wis.) is obtained.

Of the various solvents which are suitable for dissolving ZnTPP without quenching its fluorescence at room temperature, three were chosen for evaluation. A major consideration was miscibility with water, since this property would allow application of ZnTPP as an internal standard if desired. Any of the three solvents—acetonitrile, dimethylformamide, and diglyme—could be used. Diglyme is less volatile than acetonitrile, precluding evaporation losses from a standard solution in day-to-day usage, and it does not show appreciable fluorescence background in the region of interest as found for dimethylformamide. Diglyme is also much less toxic than the other two solvents, being similar in effect to ethylene glycol which is only significantly hazardous by ingestion.

Apparatus. An Aminco-Bowman corrected spectrofluorometer, (SPF125, American Instrument Company, 8030 Georgia Avenue, Silver Spring, Md. 20910) with Hamatsu R818 photomultiplier tube, thermostated with a Lauda K-2/R circulating bath, was used for all fluorescence measurements. The emission quantum corrected mode was used. An excitation slit of 2 mm (11-nm bandpass) and an emission slit of 0.5 mm (2.25-nm bandpass) were employed. Acceptable results (linearity over the same concentration range, average deviation of less than 5%, etc.) are obtained for a variety of slit widths and in standard as well as corrected modes.

Procedures. Weighed samples of tetraphenylporphinatozinc(II), (ZnTPP), from the commercial source and from our preparations were dissolved in various solvents and fluorescence spectra were obtained. Either source of material gave the same results within normal reproducibility. After cursory examination of several water-miscible solvents, diglyme was chosen for extensive study. Spectra were recorded at 11.0 ± 0.1 °C, 18.0 ± 0.1 °C and 30.0 ± 0.1 °C. Fluorescence measurements were generally repeated twice daily on samples tested for longevity. Between runs, the samples were stored at room temperature in glass vessels covered with aluminum foil. No special precautions concerning moisture or temperature control were necessary.

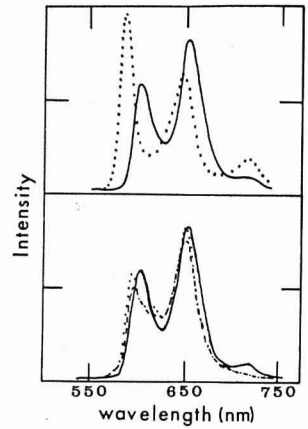

Figure 1. Upper fluorescence spectra are tetraphenylporphinatozinc(II) (4.36×10^{-7} M in diglyme, λ_{ex} 424 nm (—), and protoporphyrin IX (4.45×10^{-7} M in dilute blood (400:1) at pH 6.0) (· · ·). Lower spectra are tetraphenylporphinatozinc(II) (—), uroporphyrin dication (4.16×10^{-7} M is 1.0 M HCl (· · ·), and coproporphyrin dication (4.89×10^{-7} M in 0.1 M HCl (- - -). The protoporphinatozinc(II) spectrum is very similar to these spectra also. All spectra were taken in the emission quantum corrected mode

The quantum yield for ZnTPP was determined for comparison with the literature value (*16*). Protoporphinatozinc(II), protoporphyrin IX, uroporphyrin III, and coproporphyrin I were used for determining quantum yields. To obtain the quantum yield, the absorbance spectrum was measured on a Cary 14 spectrophotometer and integrated in the region defined by the bandpass of the excitation slit (e.g., with an excitation wavelength setting of 424 nm and a 2-mm slit which has an 11-nm bandpass, the absorbance from 418.5 to 429.5 nm was integrated). Excitation quantum correction, which compensates for the different number of photons emitted by the xenon lamp at different wavelengths, was used to obtain a relative corrected excitation spectrum from which an absorbance correction was obtained. The fluorescence intensity was obtained in the emission quantum corrected mode. The quantum yield was determined by dividing the integrated emission intensity by the corrected absorbance and comparing with the corresponding ratio for a substance of known quantum yield, tetraphenylporphyrin in air saturated benzene at 25 °C (*17*). The quantum yield measurements were performed using solutions well within the linear range of emission intensity vs. concentration for each compound.

RESULTS AND DISCUSSION

Calibration Standard. The fluorescence of tetraphenylporphinatozinc(II) provides an excellent standard for the determination of protoporphinatozinc(II) (ZnTPP) by the method of Lamola et al. (*6*). We find essentially the same positions for ZnTPP in diglyme—an excitation maximum of 424 nm and emission maxima of 600 and 652 nm. The bandwidths are very similar also (Table I, Figure 1). Peak widths at half-height for comparable intensities are within 15% of each other for ZnTPP and ZnPRP, and, in fact, for protoporphyrin IX also. Thus, the instrument response for ZnTPP and ZnPRP should be as similar as can be expected for different compounds. Use of ZnTPP for instrument calibration in protoporphyrin IX determination is not quite as good since the excitation and emission maxima for PRP are slightly different from those of ZnTPP. The excitation maximum for PRP in blood is 397 nm while emission maxima are at 624 and 687 nm. Better agreement is obtained if acid is added to give the diprotonated form of PRP which has an

Table I. Quantum Yields and Relative Intensities

Compound	Quantum yield[a]	Concn	Peak characteristics				
			λ_{ex}, nm	λ_{em}, nm	Band width at half height, nm[b]	Observed intensity[c]	Rel intensity
Tetraphenylporphinatozinc(II)	0.031[d]	4.4×10^{-7}	424	653	13	4.19	1.00
ZnTPP in diglyme at 25 °C				600	13	2.90	0.69
In benzene at 25 °C	0.033[e]						
Protoporphinatozinc(II)	0.047	4.5×10^{-7}	424	650	13	3.15	0.76
ZnPRP				587[f]	7	4.75	1.14
In whole blood at 25 °C[g]							
Protoporphyrin IX	0.070	4.7×10^{-7}	410	624	14	7.80	1.74
PRP				687	6	3.00	0.67
In whole blood at 25 °C[g]							
Coproporphyrin I dication	0.054	6.5×10^{-7}	404	650	13	13.53	2.19
Copro I				595	8	9.09	1.47
In 0.1 M HCl at 25 °C							
Uroporphyrin III dication	0.051	2.1×10^{-7}	410	650	13	5.80	2.90
Uro III				583	8	3.49	1.75
In 1.0 M HCl at 25 °C							

[a] The quantum yield for integrated emission from 500 to 750 nm, using the equation $Q_u = Q_s [(FA_u)(A_s)(n_u)^2]/[(FA_s)(A_u)(n_s)^2]$ where Q is the quantum yield, FA is the integrated emission, A is the integrated corrected absorbance and n is the refractive index of the solvent. [b] Using deconvolution of Gaussian peaks. [c] Note that quantum yield depends also on integrated absorbance as well as fluorescence intensity. Thus the lower emissions of protoporphyrin IX and protoporphinatozinc(II) relative to coproporphyrin and uroporphyrin are compensated for by their lower absorbances. [d] This work. [e] Reference 14. [f] Observed by Lamola et al. at 594 nm (Ref. 6) for the species incorporated into hemoglobin rather than free in solution. [g] Diluted 400:1, NH_3/NH_4Cl buffer, pH 6.5.

excitation maximum at 412 nm and emission maxima at 612 and 670 nm. For use with monochromator equipped fluorometers, a change of the excitation wavelength is recommended. The broader bandpass of interference filter instruments should allow use of ZnTPP as a standard for PRP dication without filter changes, although this has not been verified.

The forms of coproporphyrins and uroporphyrins obtained by the separation technique of Sobel et al. (*10*) are diprotonated porphyrin (dication) due to the acidic solutions used for eluting the porphyrins from the anion-exchange column. The excitation maximum of coproporphyrin dication is 404 nm and the emission maxima are 595 and 650 nm, while for uroporphyrins, the excitation maximum is 410 nm and the emission maxima are 583 and 650 nm in the eluent solutions. Thus, ZnTPP is also a good calibrating standard for these determinations. It is interesting to note that we have found the emission intensities of the dications to be more reproducible and linear over a wider range than the intensities of the neutral porphyrins. Thus, in the determination of coproporphyrins and uroporphyrins by other separation techniques, it would be advisable to acidify the solution (pH 3 or less) and determine the porphyrins as the diprotonated species.

For a calibration curve in the concentration range 6.40×10^{-9} M to 1.00×10^{-6} M (4.3 to 680 μg/L), the average deviation from the curve was 2.2% in the emission quantum corrected mode and 1.4% in the standard mode. Thirty samples at eight concentrations were observed over a period of two weeks from dissolution to obtain these results. In the concentration range 1.60×10^{-8} M to 1.60×10^{-7} M, the calibration curve is nearly linear, with a standard deviation (for 16 points, corrected mode) of 3.7% from a straight line vs. 2.8% for the standard deviation from the mean at each concentration (4 independent points at each of 4 concentrations). The slope of the straight line segment is 0.88 in both corrected and standard modes.

To provide a comparison of accuracy with the commercial standard, protoporphinatozinc(II) (Porphyrin Products, Logan, Utah), eight 250-μL aliquots of a 1.04×10^{-4} M solution (17 μg) of ZnTPP in dichloromethane were evaporated in test tubes. Several days later 5.00 mL of diglyme was added to each test tube. The fluorescence intensity readings (corrected and standard modes) had a standard deviation of 2.0%. Commercial protoporphinatozinc(II) standards gave comparable results (2.5% std. dev.), with proper aging (20 to 60 min). The major advantage of the ZnTPP standard in terms of accuracy is that the ZnTPP standard solutions are stable for weeks whereas the ZnPRP solutions begin to show variable readings after a few hours. In addition, the ZnTPP standard requires only reagent grade diglyme as a solvent whereas a six-component solvent is used for ZnPRP dissolution.

The temperature dependence of the fluorescence intensity of ZnTPP is not severe. Independent measurements of the same stock solution at temperatures which encompass maximum normal ranges of laboratory temperature (11–30 °C, 52–86 °F) gave relative intensities of 10.4 ± 0.1 (11 °C), 9.8 ± 0.1 (18 °C), and 9.0 ± 0.1 (30 °C) in the standard mode and 49.5 ± 0.3 (11 °C), 47.5 ± 0.2 (18 °C), and 44.6 ± 0.2 (30 °C) in the corrected mode where average deviations have been indicated.

Table I indicates the quantum yields determined for tetraphenylporphinatozinc(II), protoporphinatozinc(II), protoporphyrin IX, and dication forms of uroporphyrin III and coproporphyrin I, and the relative intensities at the wavelength of maximum emission.

Internal Standard. In addition to evaluation of ZnTPP as a calibration standard, its stability as an internal standard is reported. Tetraphenylporphinatozinc(II) is not water soluble. At the concentrations for which it is useful as an internal standard (10^{-9} to 10^{-6} M, the concentration of natural porphyrins), however, it is soluble in 1:1 water/diglyme solutions. The fluorescence intensities of protoporphyrin IX, protoporphinatozinc(II), coproporphyrin dication, and uroporphyrin dication are essentially the same in water/diglyme solutions as in the aqueous solutions which result from techniques presently employed. Solutions in solvents which are used in protoporphyrin determination methods, ethanol, ethyl acetate, and acetone, were also diluted with diglyme without showing significant spectral changes (except, of course, the lowering of intensities proportional to the dilution factor).

The recommended procedure for use of ZnTPP as an internal standard is to: (1) determine the intensities of known concentrations of the porphyrin to be analyzed and of ZnTPP,

or tetraphenylporphyrin cation, as appropriate, in the solvent system to be used, (2) dilute the appropriate solution to be used for the porphyrin determination 1:1 with diglyme and record the fluorescence spectrum, (3) add a known volume of a stock solution of ZnTPP in diglyme (for example, $^1/_{10}$ of the total volume of the sample), and (4) use the intensity increase and the analytical curve for the standard stock solution to calculate the concentration of porphyrin in the sample.

For the determination of protoporphyrin IX in the ethanol extract of the procedure recommended by Hanna et al. (*1*), a sample calculation is:

$$\underset{\substack{\text{dilution}\\\text{with}\\\text{diglyme}}}{2} \times \underset{\substack{\text{standard}\\\text{solutions}}}{\frac{I_{\text{ZnTPP}}}{I_{\text{PRP}}}} \times \frac{I_{\text{PRP}}\ \text{(sample)}}{I_{\text{ZnTPP}}\ \text{(internal standard)}}$$

$$\times \underset{\substack{\text{dilution}\\\text{with standard}}}{1.1} \times \frac{[\text{ZnTPP}]}{11} = [\text{PRP}]$$

$$2 \times \frac{1.00}{0.76} \times \frac{1.89}{3.81} \times 1.1 \times \frac{4.4 \times 10^{-6}}{11}$$

$$= 5.7 \times 10^{-7}\ \text{M}\ (32\ \mu\text{g}/100\ \text{mL})$$

The ratio for the standard solutions need be determined only once for the instrument and can then be applied for these determinations. The term [ZnTPP]/11 is the concentration of ZnTPP in the standard stock solution divided by the dilution of the standard as it is added to the sample solution. For the example calculated above, the emission intensities at 650 nm with excitation at 425 nm were used. The results of the internal standard method give protoporphyrin concentrations accurately with a standard deviation of the determination of 2.0%.

In acidic solutions, the ZnTPP used as an internal standard is instantaneously converted to the tetraphenylporphyrin dication. This species has an excitation maximum at 445 nm and an emission maximum at 687 nm. The emission intensity is linear (slope = 1.00, standard deviation = 1%) over the range of 5×10^{-9} to 10^{-6} M. In using this species as an internal standard, the excitation wavelength is changed on recording the fluorescence spectra of the standard solution with and without internal standard. The emission intensity of the standard at 687 nm is used in the calculation. This method is applicable to coproporphyrin and uroporphyrin determination by the method of Sobel et al. (*10*) and protoporphyrin in ethyl acetate/acetic acid or acidified acetone extracts (*5*).

LITERATURE CITED

(1) T. L. Hanna, D. N. Dietzler, C. H. Smith, S. Gupta, and H. S. Zarkowsky, *Clin. Chem.* (*Winston-Salem, N.C.*), **22**, 161 (1976).
(2) S. Granich, S. Sassa, J. L. Granich, R. O. Lavere, and A. Kappas, *Proc. Natl. Acad. Sci.*, U.S.A., **69**, 2381 (1972).
(3) L. P. Kammholz, L. G. Thatcher, F. M. Blodgett, and T. A. Good, *Pediatrics*, **50**, 625 (1972).
(4) S. Piomelli, *J. Lab. Clin. Med.*, **81**, 932 (1973).
(5) J. J. Chisholm, C. W. Hastings, and D. K. K. Cheung, *Biochem. Media*, **9**, 113 (1974).
(6) A. A. Lamola, M. Joselow, and T. Yamane, *Clin. Chem.* (*Winston-Salem, N.C.*), **21**, 93 (1975).
(7) A. A. Lamola, and T. Yamane, *Science*, **186**, 936 (1974).
(8) L. Heilmeyer, "Disturbances in Heme Synthesis", C. C Thomas Publishing Co., New York, N.Y., 1963.
(9) A. Goldberg and C. Rimington, "Diseases of Porphyrin Metabolism", C. C Thomas Publishing Co., Springfield, Ill., 1962.
(10) C. Sobel, C. Cano, and R. E. Thiers, *Clin. Chem.* (*Winston-Salem, N.C.*), **20**, 1397 (1974).
(11) J. J. Chisholm, Jr. and D. H. Brown, *Clin. Chem.* (*Winston-Salem, N.C.*), **21**, 1669 (1975).
(12) A. D. Adler, F. R. Longo, J. D. Finarelli, J. Goldmacher, J. Assour, and L. Korsakoff, *J. Org. Chem.*, **32**, 476 (1967).
(13) A. A. Adler, F. R. Longo, F. Kampers, and J. Kino, *J. Inorg. Nucl. Chem.*, **32**, 2443 (1970).
(14) J. R. Miller and G. D. Dorough, *J. Am. Chem. Soc.*, **74**, 3977 (1952).
(15) D. P. Perrin, W. L. F. Armarego, and D. R. Perrin, "Purification of Laboratory Chemicals", Pergamon Press, London, 1966.
(16) D. J. Quimby and F. R. Longo, *J. Am. Chem. Soc.*, **97**, 5111 (1975).
(17) P. G. Seybold and M. Gouterman, *J. Mol. Spectrosc.*, **31**, 1 (1969).

RECEIVED for review December 10, 1976. Accepted May 17, 1977. Research was carried out as part of a study of photophorimetric analysis of porphyrins in blood and urine, supported by the National Institute of Environmental Health Sciences Grant No. ES-00987-01.

Low Capacity Codes for Mass Spectra Based on Statistical Moments

C. P. Anese and J. A. Richards*

Department of Electrical Engineering, James Cook University of North Queensland, Townsville, Queensland 4811, Australia

Attention has been given recently to the development of low capacity codes for the mass spectrum owing to the high degree of redundancy present in this form of analytical data. This work has been directed principally towards low capacity storage of spectral libraries and, to a lesser extent, to low capacity transmission of spectral information over communications channels. Wangen et al. (*1*) and Gotch (*2–4*) have investigated the usefulness of spectra coded by noting simply the absence or presence of a peak below or above a predetermined slicing level, resulting in a spectral code numerically equal in bits (binary digits) to the mass range considered significant. Crawford and Morrison (*5*) and Knock et al. (*6*) have considered the properties of a code in which spectra are represented by a number of their strongest peaks. In a variant of this, other investigators (*6, 7*) have discussed coding schemes in which the N most intense peaks in consecutive 14 amu spectral windows are adopted as the signature of the spectrum. By correlating mass positions Wangen, Woodward, and Isenhour (*1*) produced a further spectral code, with significantly reduced redundancy, leading to both 80- and 48-bit code lengths; these gave acceptable performance when tested in library searching procedures for spectral identification.

In this paper, a code based upon statistical moments of the spectrum is proposed and discussed. While retaining uniqueness comparable to that of the above codes, its length (i.e., bits/spectrum) is significantly smaller, recommending its use in situations demanding low capacity.

SPECTRAL SIGNATURES BASED UPON STATISTICS

Since the mass spectrum is a discrete probability distribution, it is natural to consider the significance of moments in describing its essential features. Indeed, for distributions of this type it is possible to exhibit *all* properties of the spectrum in terms of its moments, or functions of its moments; a collection of low order moments is adequate to define the gross features of a distribution, although very high order moments may be necessary to define details. Since the primary concern of this investigation is the preservation of the uniqueness of a spectrum after coding, and not the re-

Table I. Observed Ranges of Statistics in 1500 Spectra, Bit Allocations, and Subsequent Ranges and Precisions of Statistics Allowable

Statistic	Observed range		Bits allocated	Allowable range		
	Min	Max		Min	Max	Increment
Mean	23	425	9	1	512	1
Standard deviation	8	326	9	1	512	1
Skewness	−5.4	7.5	8	−12.7	12.8	0.1
Kurtosis	4	1.3×10^7	8	0	2550	10

production of the original distribution of peak intensities, a set of low order moments can be considered sufficient as a discriminating spectral signature. This is supported by results to follow.

If the mean of the spectrum is defined, in the usual way, as

$$\mu = \sum_i f_i x_i / \sum_i f_i$$

where the x_i are mass positions and the f_i are the corresponding intensities, then the kth central moment is defined by

$$m_k = \sum_i (x_i - \mu)^k f_i / \sum_i f_i$$

Rather than use moments directly, spectral *statistics* can be generated. In addition to the mean, only three are of interest here, these being the standard deviation, $\sigma = \sqrt{m_2}$; the skewness, $s = m_3/\sigma^3$; and the kurtosis, $k = m_4/\sigma^4$.

It is appropriate to remark that Bender et al. (8) have also adopted moments, however in their case to precondition mass spectral data in pattern classification approaches to recognition.

EXPERIMENTAL

A set of 1500 spectra from the MSDC collection was chosen to evaluate the effectiveness of using mean, standard deviation, skewness, and kurtosis as a spectral code. To establish ranges of significance, the data set was searched for maximum and minimum values of each statistic. From this information and from an arbitrarily but sensibly chosen precision, the number of bits necessary to represent the complete range and precision of a particular statistic was chosen. This is summarized in Table I where it will be observed that the maximum value of kurtosis is very high. As a result, this was restricted to an upper limit, with higher values truncated to the limit. By allocating 9 bits each to mean and standard deviation, and 8 bits each to skewness and kurtosis, a 34-bit spectral code results. The 1500 spectra in the data set were so encoded and searched for subsequent matching pairs. Only 8 were found, representing 0.53% of the complete set. In practice it would be desirable to have a code length of 32 bits since this is a common computer word length and is an integral multiple of minicomputer and microprocessor word lengths. Therefore, the range over which mean and standard deviation are specified was lowered by allocating only 8 bits to each of those parameters also. This permitted values only up to 256 to be used in those parameters (again higher values were truncated to that limit). In the data set only 4% of means and 1% of standard deviations exceeded 256 so that the effect of such a restriction is not severe. When the 1500 spectra were scanned again, only 9 matching pairs were found (0.60%). These results should be compared to those given by other coding procedures. Such a comparison (based upon results given by previous investigators) is depicted in Table II where the success of the 32-bit spectral statistics code in delineating spectra is seen to be better than all others, apart from one-bit encoding using a 1% slicing level. That code however is four times longer than the statistics code and yet is only marginally better in delineation.

It can be shown (9) that the maximum accuracy in peak heights necessary to generate the 32-bit statistics code, to the precisions implicit in the bit allocation, is 0.3%, and that on the average only a 1% precision in peak height is required. These are within the capabilities of present magnetic and, in some cases, quadrupole mass spectrometers.

Table II. Comparison of Properties of Spectral Codes

Code	Mass range, amu	Code length bits	No. of matching groups expressed as % of the total sample
Statistics μ, σ, s, k	Entire	32	0.60%
One peak in each 14-amu window (4)	6-453	128	0.83%
One-bit encoding (2) (slicing level = 1% of base peak)	13-140	128	0.46%
One-bit encoding (1) (slicing level = 0.1% of base peak)		352	0.83%
One-bit encoding with correlation of mass positions (1)			
(80 channels)		80	1.23%
(48 channels)		48	3.11%

NEAREST NEIGHBOR LIBRARY SEARCHING

For a coding procedure to be viable, it is necessary that it permit successful spectral identification in the face of experimental and related errors. A technique which enhances the usefulness of codes in this situation is that in which the kth nearest neighbors to the unknown are searched for (1, 3). This method utilizes a measure of the difference between unknown and library coded spectra with the kth nearest neighbors to the unknown being selected from the library if their difference measures are the kth smallest.

Since four spectral statistics contribute to the code adopted herein, the relative significance of each was determined in order to provide weighting constants for the nearest neighbor algorithm. Significance was determined on the basis of the success of each statistic *individually* in distinguishing spectra in the data set. The percentages of matching spectra in such a test were found to be in the ratios 1:2:5:5 for mean:standard deviation:skewness:kurtosis. Therefore weights of 1, 0.5, 0.2, and 0.2 were adopted in library searching.

The search algorithm required computing the relative difference in each statistic for the unknown and a library spectrum. These differences were weighted according to the above prescription and summed to produce a measure of mismatch. The procedure was repeated for each library spectrum and, e.g., the five spectra corresponding to the five smallest values of the mismatch measure or index were selected as the five nearest neighbors and listed in order of increasing mismatch index. A typical result is shown in Table III, where it will be seen that the nearest neighbors are isomers and homologues. In producing this, each statistic for a library of 1000 spectra was stored to one order of magnitude greater precision than the unknown, principally to permit the nearest neighbors to be listed in order of likelihood. Otherwise a number of zero mismatch indices (exact matches) were obtained, permitting no ordering. While this implies an additional 16 bits per spectrum for each library entry, it does illustrate the performance of library searching based upon the four statistics when experimental rounding or errors are present, or differences in precision are available, since *the*

Table III. Example of Nearest Neighbor Library Searching Based upon Statistics Code

Unknown ($C_6H_{14}O$)
Mean = 50
Standard deviation = 17
Skewness = 0.3
Kurtosis = 220

The 5 nearest neighbors are:

	Mismatch index	Mean	Std dev	Skewness	Kurtosis
$C_6H_{14}O$	0.04	49.5	17.0	0.26	220
$C_7H_{16}O$	0.09	50.3	17.9	0.26	188
$C_8H_{18}O$	0.14	51.6	17.8	0.41	214
$C_4H_{10}O$	0.18	53.1	18.4	0.40	212
$C_7H_{16}O$	0.18	47.3	15.6	0.37	258

unknown was retained in its 32-bit format. With the library spectra also in 32-bit form, the unknown was still listed as one of the first 5 nearest neighbors, illustrating that entire 32-bit coding (library and unknowns) should generally be useful in library searching procedures of this type. The performance of the search routine was still creditable when further larger errors were introduced into the unknown. For example, when the standard deviation of $C_6H_{14}O$ was altered by 15% and the kurtosis by 10%, the correct compound was cited as the second nearest neighbor. It is also worth noting that, when weighting factors were not used, the correct compound was suggested as the third most likely neighbor. Finally, library searching using the statistics code performs well in terms of delineation from isomers and homologues. In some cases where the first neighbor listed was not the correct compound, the unknown was in the top two or three; the compounds ranked higher were almost always its isomers, with extremely similar mismatch indices. While one-bit encoding is generally not successful in separating isomers (*1*), the code used in this investigation was found to have a high success rate in doing so. Thirty-seven of the forty compounds used as unknowns were correctly listed as the first neighbor, even though isomers existed in the library.

CONCLUSIONS

In devising coding techniques to reduce redundancy, it is important to ensure that the essential information of a spectrum is not lost—i.e., it is important that the degree of uniqueness of encoded spectra be similar to that of full spectra. Certainly the results of this study imply that little spectral information is sacrificed in the coding method used even though the ultimate code length is only 32 bits. An accompanying advantage in choosing moments or moment-derived statistics is that errors in the determination of peak intensities will not be amplified in the code. Rather the accuracy of the moments will be of comparable order to that of the spectrum. On the other hand, errors in peak position could propagate larger moment errors, for which reason the technique is more suited to low resolution spectra in which all peaks are constrained to occur at integral mass numbers.

Clearly other codes based upon spectral statistics could be invented. For example it is possible to construct a reliable code based upon just mean and kurtosis, resulting in a greatly reduced code word length (20 bits) with reasonable discrimination (~1%). However the accuracy required in each of those parameters requires peak height precisions which are not practicable. Allocation of 8 bits to each of the four statistics is a compromise which does not place undue demands on the performance of a mass spectrometer and yet which yields very satisfactory results.

ACKNOWLEDGMENT

The authors thank A. Griffiths of the Department of Electrical Engineering, James Cook University of North Queensland, for useful discussions on some aspects of this work.

LITERATURE CITED

(1) L. E. Wangen, W. S. Woodward, and T. L. Isenhour, *Anal. Chem.*, **43**, 1605–1614 (1971).
(2) S. L. Grotch, *Anal. Chem.*, **42**, 1214–1222 (1970).
(3) S. L. Grotch, *Anal. Chem.*, **43**, 1362–1370 (1971).
(4) S. L. Grotch, *Anal. Chem.*, **45**, 2–6 (1973).
(5) L. Crawford and J. Morrison, *Anal. Chem.*, **40**, 1464–1469 (1968).
(6) B. A. Knock, I. C. Smith, D. E. Wright, R. G. Ridley, and W. Kelly, *Anal. Chem.*, **42**, 1516–1520 (1970).
(7) H. Hertz, R. Hites, and K. Biemann, *Anal. Chem.*, **43**, 681–691 (1971).
(8) C. F. Bender, H. D. Shepherd, and B. R. Kowalski, *Anal. Chem.*, **45**, 617–618 (1973).
(9) C. P. Anese, B.E. Thesis, James Cook University of North Queensland, Townsville, Australia, 1976.

RECEIVED for review December 30, 1976. Accepted April 19, 1977.

Teflon Powders for Near Infrared Spectra of Hydrides

Tryggvi Emilsson and Vakula S. Srinivasan*

Department of Chemistry, Bowling Green State University, Bowling Green, Ohio 43403

Obtaining spectra in the near infrared region (1 μm to 3.5 μm) is usually difficult because of interference from water (OH stretch). One resorts to potassium bromide pellet with protective windows or heavy water solutions under very dry conditions. We would like to report here the use of Teflon (DuPont) as a pressable matrix, for the spectra in this region.

Teflon powders have been used for making strongly water repelling electrodes with great integrity and mechanical stability (*1*). These powders are now available commercially, and they can be used very easily for mixing and molding. We used both Teflon 7A and 7C, obtained from E. I. du Pont de Nemours and Company, Wilmington, Del., in our experiments. The spectra were run on Beckman Acta IV and Perkin-Elmer Model 337. The pellets were made by weighing 100 mg of Teflon and pressing in a dye of $^3/_8$-inch diameter at a pressure of 12 tons, under vacuum. In Figure 1(a), the background spectrum of a pellet is shown. One could see that the material is transparent in the near IR region, with increasing scattering as the wavelength decreased.

In Figures 1(b) and 1(c) are shown the spectra of lithium aluminum hydride and sodium cyanoborohydride with the pellets made with very small quantities of each. The metal-hydrogen stretch (2) is dominant over the background. The stability of the pellets to moisture was clearly demonstrated

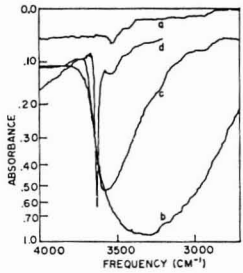

Figure 1. Infrared Spectra of Teflon pellets of various compositions. (a) Background spectrum of pellet. (b) Spectrum of lithium aluminum hydride in Teflon. (c) Spectrum of sodium cyanoborohydride in Teflon. (d) Spectrum of calcium hydroxide in Teflon

by the fact that when the pellet containing $LiAlH_4$ was placed in distilled water, except for very small initial bubbling on the surface, the pellet stayed intact. The spectrum shown in Figure 1(b) was exactly reproduced. The broadening of the spectra may be due to trace moisture entering the system prior to pressing, with water molecules coordinating to the metal. For reference we have shown the spectrum of $Ca(OH)_2$ in Teflon to locate the OH stretch.

We believe that this approach is a valuable analytical aid for the analysis of hydrides. With the future moving toward hydrogen storage, analysis of the hydride will play an important role. Further, obtaining near IR spectra of intervalence charge-transfer complexes is easier with Teflon than with D_2O.

ACKNOWLEDGMENT

The receipt of samples of Teflon powders from E. I. du Pont de Nemours and Company, Wilmington, Del. is gratefully acknowledged.

LITERATURE CITED

(1) L. K. Klatt, D. R. Connell, and R. E. Adams, *Anal. Chem.*, **47**, 2470 (1975).
(2) K. Nakamoto, "Infrared Spectra of Inorganic and Coordination Compounds", 2nd ed., Wiley-Interscience, New York, N.Y., 1970.

RECEIVED for review March 14, 1977. Accepted May 11, 1977. Support for T.E. from the National Science Foundation, Grant GP-43645, is acknowledged.

Modification of Pulse Polarograph for Rapid Scanning and Its Use with Stationary Electrodes

KeriLyn C. Burrows, Mark P. Brindle, and Michael C. Hughes*

Department of Chemistry, Lehigh University, Seeley G. Mudd Building #6, Bethlehem, Pennsylvania 18015

Since its introduction by Parry and Osteryoung (*1*, *2*), differential pulse polarography (DPP) at the dropping mercury electrode (DME) has become a widely employed technique for trace analysis of ionic and molecular species at concentrations of about 1 part per million and higher (*3–6*). On the other hand, differential pulse voltammetry (DPV) at stationary electrodes has until very recently been largely overlooked.

Christian (*7*) first reported that DPV at the hanging mercury drop electrode (HMDE) showed current behavior similar to that reported by Parry and Osteryoung for DPP at the DME. Keller and Osteryoung have derived equations for DPV at stationary electrodes for both reversible and irreversible systems (*8*), and Rifkin and Evans have published equations for reversible systems which include the effects of prior pulses on the concentration of the electroactive species in the diffusion layer (*9*, *10*). Rifkin and Evans also demonstrated the analytical utility of DPV at platinum electrodes for analysis of sub-part per million concentrations of organic compounds. In both cases where theoretical equations were presented, the authors assumed a computer generated excitation function which is different from that generated by commercially available instrumentation.

Blutstein and Bond (*11*) have applied a rapid sweep differential pulse function to the DME. They utilized a commercially available polarographic analyzer whose circuit was modified to generate shorter pulse intervals and more rapid current response than are normally available on the instrument. While good sensitivity was obtained, the increase in the electrode area during the course of the experiment made a considerable contribution to dc faradaic and double-layer capacitance background currents, and distorted baselines became a significant problem at low analyte concentrations.

The principal practical advantage of DPV at stationary electrodes is that much shorter pulse intervals (time between successive pulse applications) may be employed, since the pulse intervals are no longer tied to the drop time of a DME. The use of shorter pulse intervals produces currents that are higher than those obtainable at the DME, and at the same time permits the use of much higher scan rates than can be used at the DME.

We are reporting here a set of simple and inexpensive modifications which can be made on a commercially available instrument to realize the enhanced analytical capabilities of DPV at stationary electrodes. The instrument is evaluated for the measurement of several metal ions at the HMDE; using the current readout of the instrument with no special data processing, accurate determinations are possible in the 25-ppb range, and detection limits of a few ppb are indicated. The voltammetric behavior of reversible and irreversible systems (in the dc polarographic sense) is briefly compared and the results indicate that the method may also be useful in the study of electrode kinetics. Dillard and Hanck (*12*) have recently reported on the application of DPP at the DME to the measurement of electrode kinetic parameters.

EXPERIMENTAL

A Princeton Applied Research Corporation Model 174 Polarographic Analyzer was modified as shown in Figure 1. The modifications made pulse intervals ("drop times") of 0.1 and 0.2 s available in addition to the normal 0.5, 1, 2, and 5-s intervals and also reduced the time constant of the current processing and readout circuitry from a measured value of about 500 ms to about 5 ms. A more complex time constant modification for the PARC 174 has recently been described by Abel et al. (*13*).

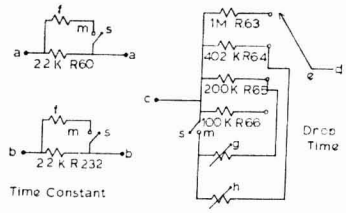

Figure 1. Schematic circuit modifications of PARC 174. (a) Current sample and hold circuit, (b) differential sample and hold circuit, (c) to clock input, (d) to +15 V dc, (e) drop time rotary switch, (f) matched 200-Ω resistors, (g) 50-K potentiometer, (h) 100-K potentiometer, (s) switch position for standard operation, (m) switch position for modified operation. Resistor numbers as on PARC 174 schematic

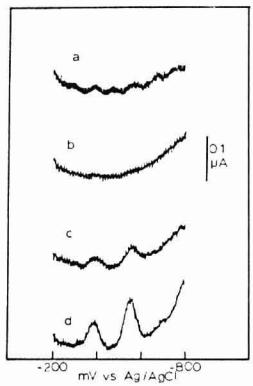

Figure 2. Differential pulse voltammograms of 0.5 M acetate buffer. (a) Potentiometer out of adjustment, (b) potentiometer adjusted for minimal noise, (c) 25 ppb Pb, Cd added, (d) 100 ppb Pb, Cd added. t = 0.1 s, ΔE = −50 mV, ν = −20 mV/s, 5-ms time constant, 0.3-s filter

In the PARC Model 174, the drop time circuitry is keyed to zero crossing of line frequency (multiples of 16.7 ms) to minimize noise. Substitution of resistors into this circuit permits various pulse intervals to be used. For intervals of 0.5 s and greater, 5% resistors suffice, but shorter intervals require more precise adjustment. If the resistor value is not optimum, synchronization to line frequency is lost, and, at high current sensitivity, a beat is observed in the current response as in Figure 2a. When the potentiometers in the 0.1 and 0.2-s circuits are properly adjusted, a very low background of random noise results, as in Figure 2b.

Voltammograms were recorded on a Hewlett-Packard Moseley Model 7001-A X-Y recorder. A standard H-cell was used, with saturated NaCl silver–silver chloride reference and platinum counter electrodes. The working electrode was a micrometer-type HMDE (PARC No. 9323); a standard electrode area of 1.5×10^{-2} cm^2 (determined by linear sweep voltammetry of Cd^{2+} in 0.1 M KCl) was used. Additions of microliter quantities of standard solutions were made using Eppendorf micropipets or Finnpipette variable micropipets.

All chemicals for the studies of the variation of instrument response with varying instrumental parameters were reagent grade, used as received. The detection limit studies used 0.5 M sodium acetate–acetic acid buffer (pH 4.5) pre-electrolyzed at a mercury pool cathode for 48 h at −1.3 V vs. SCE. A PARC Model 9500 electrolyte purification apparatus and Wenking Model 66 TS 10 potentiostat were used. The buffer was stored in a pre-cleaned linear polyethylene bottle. Standard metal ion solutions (100 ppm) were prepared daily from 1000 ppm atomic absorption standards ($CdCl_2$ and $Pb(NO_3)_2$ were dried and dissolved in 1 M HNO_3 made from J. T. Baker "Ultrex" HNO_3 and distilled water. Pure Cu and Zn metal were dissolved in "Ultrex" HNO_3 and brought to 1 M with distilled water. (Distilled water was distilled from glass, followed by quartz sub-boiling distillation.) High purity nitrogen saturated with water was used for deaeration.

Table I. Variation of Peak Current with Scan Rate[a]

Scan rate, mV/s	Peak current, μA	
	Cd	Ni
−2	9.02	4.89
−5	8.70	6.99
−10	8.43	9.04
−20	8.55	11.31
−50	8.74	15.92

[a] t = 0.2 s, ΔE = −25 mV, C = 1 mM, time constant = 5 ms.

RESULTS AND DISCUSSION

To a first approximation, peak DPV current as a function of potential is given by Parry and Osteryoung's original equation (2):

$$\Delta i_p = \frac{nFAC_0{}^*D_0{}^{1/2}}{(\pi\delta)^{1/2}}\left[\frac{1-\sigma}{1+\sigma}\right] \quad (1)$$

where $\sigma = \exp[(nF/2RT)\Delta E]$, ΔE is the pulse amplitude (in volts) and δ is the pulse width (in seconds); the other terms have their usual significance. Equations more directly applicable to DPV have been reported (*8–10*), but, as mentioned earlier, they are all based on computer generated stepping potential functions.

Investigation of the effects of varying instrumental parameters on current response was carried out on the reversible system Cd^{2+}/Cd^0 in 1 M $NaClO_4$ (*14*) and the irreversible system Ni^{2+}/Ni^0 in 0.1 M KCl (*15*). Solutions were approximately 1 mM in metal ion.

Effect of Pulse Amplitude, ΔE. The behavior of the cadmium system agrees well with Equation 1. The nickel system gives a much lower slope than predicted, apparently because of irreversibility. The current corresponding to a −100-mV pulse is anomalously high for the nickel system, behavior which is also observed in DPP at the DME (*16*). Plots of peak potential vs. pulse amplitude are linear and conform to the equation (2)

$$E_p = E_{1/2} - \frac{\Delta E}{2} \quad (2)$$

Half-wave potentials calculated from this equation using experimental E_p values are slightly cathodic of those obtained from dc polarography, behavior which has been noted by Christian (*7*) and Christie et al. (*17*), and which has generally been attributed to an instrumental artifact of the PARC 174.

Effect of Pulse Interval, t. Rifkin and Evans (*9*) have reported the sole previous study of the effects of pulse interval in relation to pulse width, showing that peak current is essentially constant when the pulse interval (t) exceeds three times the pulse width. Blutstein and Bond (*11*) noted a pulse interval effect, but did not attempt to quantify it. Our limited data (Figure 3) agree with Rifkin and Evans' results for the cadmium system, showing enhanced peak currents at reduced pulse intervals (pulse width is fixed at 57 ms). In contrast, the peak currents of the nickel system appear to be completely independent of the pulse interval–pulse width relationship. Figure 3 also shows the effects of the reduced instrumental time constant on measured peak currents.

Effect of Scan Rate. Rifkin and Evans (*10*) found little effect of a varying stepping potential between pulses on calculated peak currents. They did not report on experimental

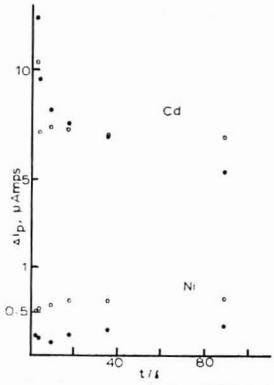

Figure 3. Variation of peak current with pulse interval factor. (●) 500-ms time constant. (○) 5-ms time constant, $\Delta E = -25$ mV, $\nu = -1$ mV/s. Note scale change at 1 μA

verification of this behavior. The present data (Table I), taken using pulses applied on a continuously changing potential, verify Rifkin and Evans' (*10*) predictions for the Cd^{2+}/Cd^{0} system at scan rates above 5 mV/s. At slower scan rates, nondiffusive transport during the course of the experiment undoubtedly contributes to the slightly higher peak currents observed. For the Ni^{2+}/Ni^{0} system, a very definite dependence of peak current on scan rate is observed, which appears to be related to the irreversible nature of the system. We are presently working on a more detailed experimental and theoretical study of this behavior.

Effect of Time Constants. Reducing the instrumental time constant shows an effect primarily at scan rates above 10 mV/s, where data taken in the reduced time constant mode show better agreement with theoretical predictions, as would be expected.

Detection Limits. Copper, lead, cadmium, and zinc were determined individually by DPV at the HMDE with $t = 0.1$ s and 5 ms time constant in an acetate buffer of pH 4.5. Two instrumental settings were used: $\Delta E = 25$ mV, $\nu = -50$ mV/s and $\Delta E = -50$ mV, $\nu = -20$ mV/s. Because of the high current sensitivity (0.1 to 0.5 μA/in.) the 0.3-s low pass filter of the PARC 174 was employed. Use of the second pair of settings roughly doubled the current sensitivity; this is due in part to the increased pulse amplitude. In general, these curves were smoother and easier to read.

Peak heights were measured from an interpolated baseline. Copper and zinc are both located on sloping baselines, Cu on the mercury oxidation wave and Zn on the hydrogen ion reduction wave. These two showed a bit more scatter than Pb and Cd, but all four metals gave linear current vs. concentration plots from 25 to 500 ppb, summarized in Table II. Equal concentrations of Pb and Cd were also determined simultaneously (Table III). Although the sensitivities were decreased by roughly 30%, 25 ppb were easily discerned (Figure 2c).

These results indicate that commercial polarographs such as the PARC 174 may be easily modified to perform comparably to more sophisticated computer-based systems. The required modifications described here extend detection limits by increasing current sensitivity, and by reducing the instrumental time constant to permit the use of higher scan rates. Gradual changes in response characteristics as the reversibility of the electrochemical system decreases may prove useful in studies of electrode kinetics, as well.

Further instrument modifications are being studied at the present time which will make the instrument more flexible in the choice of the excitation function. The application of this instrument to both analyses and the study of electrode and solution kinetics will be reported in the future.

Table II. Peak Current vs. Concentration Data, Individual Ions[a]

Metal	Sensitivity, nA/ppb	Background, nA	Detection limit, ppb[b]
Cu	0.32	−0.3	2
Pb	0.07	0.8	23
Cd	0.13	1.0	15
Zn	0.18	0.8	9

[a] pH 4.5, acetic acid-acetate buffer, $t = 0.1$ s, $\Delta E = 50$ mV, $\nu = 20$ mV/s, time constant = 5 ms. All correlation coefficients 0.99+. [b] Current twice background level.

Table III. Simultaneous Determination of Pb and Cd[a]

Metal	Sensitivity, nA/ppb	Background, nA	Detection limit, ppb
Pb	0.051	−0.8	31
Cd	0.092	0.5	11

[a] Conditions as in Table II, except correlation coefficients, 0.97.

ACKNOWLEDGMENT

The authors thank Barry Yeakel for making the circuit modifications described and for many helpful discussions.

LITERATURE CITED

(1) E. P. Parry and R. A. Osteryoung, *Anal. Chem.*, **36**, 1366 (1964).
(2) E. P. Parry and R. A. Osteryoung, *Anal. Chem.*, **37**, 1634 (1965).
(3) AN-111, -117, Princeton Applied Research Corporation, Princeton, N.J. (1972).
(4) J. G. Osteryoung and R. A. Osteryoung, *Am. Lab.*, **4**, (July), 8 (1972).
(5) J. Lindquist and S. M. Farroha, *Analyst (London)*, **100**, 377 (1975).
(6) K. Hasabe and J. Osteryoung, *Anal. Chem.*, **47**, 2412 (1975).
(7) G. D. Christian, *J. Electroanal. Chem.*, **22**, 333 (1969).
(8) H. E. Keller and R. A. Osteryoung, *Anal. Chem.*, **43**, 342 (1971).
(9) S. C. Rifkin and D. H. Evans, *Anal. Chem.*, **48**, 1616 (1976).
(10) S. C. Rifkin and D. H. Evans, *Anal. Chem.*, **48**, 2174 (1976).
(11) H. Blutstein and A. M. Bond, *Anal. Chem.*, **48**, 248 (1976).
(12) J. W. Dillard and K. W. Hanck, *Anal. Chem.*, **48**, 218 (1976).
(13) R. H. Abel, J. H. Christie, L. L. Jackson, J. G. Osteryoung, and R. A. Osteryoung, *Chem. Instrum.*, **7**, 123 (1976).
(14) G. C. Barker, R. L. Faircloth, and A. W. Gardner, *Nature (London)*, **181**, 247 (1959).
(15) L. Meites, "Polarographic Techniques", John Wiley-Interscience, New York, N.Y., 1965, Chapter 4.
(16) K. C. Burrows and M. C. Hughes, unpublished data.
(17) J. H. Christie, J. Osteryoung, and R. A. Osteryoung, *Anal. Chem.*, **45**, 210 (1973).

RECEIVED for review January 27, 1977. Accepted May 12, 1977. Portions of this paper have been presented at the 7th Northeast Regional Meeting of the American Chemical Society, Albany, N.Y., August 1976, and at the 11th Middle Atlantic Regional Meeting of the American Chemical Society, Newark, Del., April 1977. The authors also thank the donors of the Petroleum Research Fund, administered by the American Chemical Society (PRF 9186-65), for the partial support of this research.

Dynamically Refreshable Computer Display Controller with Vertical Line Generator for Mass Spectrometry Applications

Philip S. Berger[1] and William F. Holmes*

Department of Biological Chemistry, Division of Biology and Biomedical Sciences, Washington University, St. Louis, Missouri 63110

Laboratory computer systems frequently include a graphic display terminal to monitor instrument performance and to review and process data previously collected. Mass spectrometry applications benefit greatly from graphic terminals, since large numbers of mass spectra are generated. A typical low resolution mass spectrometer with gas chromatographic inlet may be scanned over the full mass range at intervals of 3 to 5 s, generating many hundreds of spectra during a single analysis. Quantitative analyses or capillary column separations may require scans as frequently as once per second. Low resolution mass spectra are commonly represented as bar graphs, with the abscissa representing integer mass values, and the ordinate representing the intensities of the ions. Each vertical bar corresponds to the summed intensities of all ions with the same nominal integer mass. The bar graph representation has its limitations, however, since it is difficult to show clearly and accurately the entire mass spectrum on one graph of reasonable size. The mass scale must extend out to the molecular ion yet still be readable at unit mass resolution. The intensity scale must represent ions over a size range of 1–1000 or more. A number of strategems have been used to expand the size of mass spectrum bar graphs, such as breaking the mass scale into several parts, or magnifying the intensity scale at the high mass end where the ions usually have smaller relative intensities. A more flexible method for examining mass spectra is provided by graphic display terminals, since a portion of the spectrum can be expanded in either the mass or intensity scales for a detailed view.

A graphic display terminal for mass spectrometry applications is most effective when the user can work with the spectra in a highly interactive manner, expanding scales, shifting mass ranges, and quickly examining groups of spectra collected in sequence. The spectra are often complicated, so that a fast writing rate and good resolution are important. The graph should be carefully labeled so that individual ions can be easily located, and the spectrum as a whole identified. In practice, storage oscilloscopes are often used to display these graphs. They offer flicker-free displays at moderate resolution, and do not require computer processor time or memory storage to maintain the display, once it has been written. However storage oscilloscopes are rather costly, and they have a slow response time. The entire display must be cleared and rewritten whenever a change requires removal of any part of the display. For example, clearing the screen of the commonly used Tektronix 4010 terminal takes 700 ms (*1*), and new points or intensity bars can be written no faster than 150 per second with the standard serial interface, far from ideal for interactive examination of complex spectra.

Ordinary display oscilloscopes must be continually refreshed by writing the display at a rate of 30 times per second or more to prevent flicker. Maintaining the display requires both data storage and data processing time, which may place a heavy burden on the central computer. These functions may be transferred partially or completely to the display terminal by including an independent memory and display generating hardware. High speed display oscilloscope terminals with hardware character and vector generators are quite expensive however. Video monitors offer a relatively low cost alternative. The entire display is considered as a matrix of points, with the intensity of each point stored in a memory and read in synchrony with the video scan (*2, 3*). However the resolution of the video monitor is somewhat limiting, and memory costs may be even more so, since memory size will increase as the square of the linear point density on the video screen. Multiple intensity levels also require more memory; even two levels of intensity will double the memory size required.

The constraints imposed by cost, resolution, and response time when using commercially available graphic terminals led us to design a relatively inexpensive refreshable display system with enough resolution and speed for high quality displays of mass spectrometer data. The display is part of a computer system designed and programmed for mass spectrometry applications (*4*), five of which are currently in use at the Washington University School of Medicine. The display system consists of a controller containing hardware for generating characters and vertical bars attached to a simple display oscilloscope with x, y, and z inputs. The choice of the oscilloscope is not critical. We have used both Tektronix 602 and 604 Display Monitors, and the electronics are adjustable so that other x, y, z type displays can be used.

GENERAL CHARACTERISTICS

A simplified block diagram of the display system is shown in Figure 1. The controller has been designed to work with the Computer Automation Alpha LSI-2 and LSI-3 computers, but the interface signals are quite straightforward. There are 8 address lines, 3 input control lines, 12 input data lines, and 1 output status line. Five of the address lines (not shown) are used to select the controller; the other three select the function that the controller is to perform. Data, such as an x or y position, character code, or vertical bar height are presented on the 12 data lines simultaneously with the corresponding function on the address lines. The actual transfer is clocked by one of two control lines (not shown) generated by the corresponding computer instruction. A third control line is used to request the READY/BUSY status of the READY/BUSY flipflop in the controller, which can be switched onto the output status line. This flipflop is set to BUSY by the controller when the DISPLAY CHARACTER or DISPLAY VERTICAL BAR functions are initiated, since these operations in general take considerably longer than a typical computer instruction.

The controller contains five basic registers, X, Y, Y BAR/CHARACTER CODE, INCREMENT SIZE, and INTENSITY. The X and Y registers contain the position of any point, character, or vertical bar displayed on the oscilloscope. X and Y can be specified to 12 bits, 1 part in 4096, ensuring that the display resolution will not be limited by the controller. The dual purpose Y BAR/CHARACTER CODE register contains either the height of the vertical bar to be displayed, or a 6-bit ACSII character code. The vertical bar height is specified to 12 bits, and can have either a positive or negative value. The X and Y registers specify the position of the base end of a vertical bar during a bar display, and the lower left corner of a character during a character display.

The INCREMENT SIZE and INTENSITY registers are loaded together when the SET INTENSITY AND INCREMENT SIZE function is presented to the controller. Characters and vertical bars are both displayed as a set of closely spaced points. The INCREMENT SIZE register determines how far apart these points are separated, thus controlling the size of the characters, and the point density of vertical bars. This register is 4 bits wide, specifying 16 increment sizes. The INTENSITY register is 2 bits

[1]Present address, Teknivent Corp., 9261 Old Bonhomme Road, St. Louis, Mo. 63132.

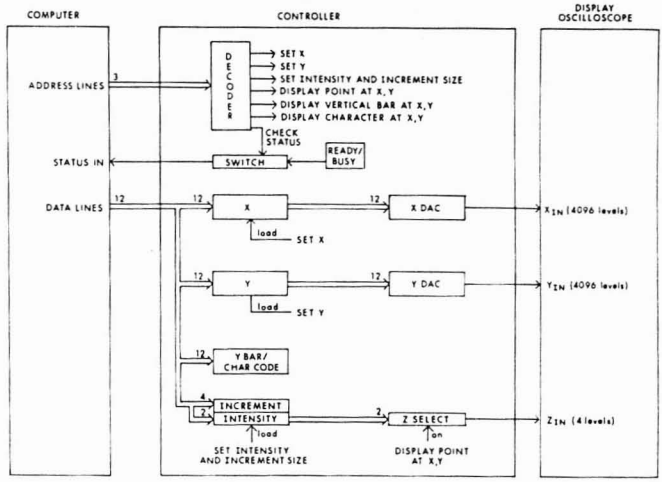

Figure 1. Block diagram of the display controller, showing its relationship to the computer and the display oscilloscope. Broad arrows indicate digital data lines. The number of lines is shown. Digital control signals and analog signals are shown as single width arrows (→)

wide, allowing 4 levels of intensity to be displayed. This register is decoded at the Z SELECT site to a 4-level analog voltage connected to the z input of the display oscilloscope. A shunt transistor biases the z input off until a point is actually displayed.

The digital x and y values in the display controller go to 12 bit digital to analog converters (DACs, Datel Model DAC-I12B) which are connected by drivers to the x and y inputs of the display oscilloscope chosen. In the simplest case, displaying a single point, the inputs to the DACs come directly from the X and Y registers. These converters have a settling time of 150 ns; thus the display response time is normally limited by the controller logic or the oscilloscope. The x and y drivers can cover a range from 0 to 2.5 V, which is sufficient to drive Tektronix 602 and 604 Display Monitors, and the larger Hewlett-Packard 1310A. Since the internal timing of the controller can be slowed down to accommodate the response times of slower display devices, the controller should be able to drive any oscilloscope with x, y, and z inputs by minor changes in the voltage ranges.

DETAILED DESCRIPTION

Displaying a Point. The procedure for displaying a point can be seen by examining Figure 1. The x position of the point is specified by loading a 12-bit binary value into the X register. This is done by presenting the SET X function on the address lines while the binary value of x is presented on the data lines. The y position is loaded into the Y register in the same manner using the SET Y function. The point is actually displayed by issuing the DISPLAY POINT AT X,Y function, which transfers information from the controller to the display oscilloscope. The X and Y registers are gated to the X and Y DACs, respectively, and converted to analog x and y voltages leading to the oscilloscope. After a short delay to allow the oscilloscope electronics to settle, the shunt transistor in the Z SELECT circuit is turned off, allowing the analog z level specified by the INTENSITY register to pass to the z input of the oscilloscope, causing a point display at x,y. The settling time and the on-time of the display are both adjustable, so that these times can be matched to the display oscilloscope specifications. Displaying a point at x,y is a basic component of the more complex vertical bar and character displays. The X and Y registers are still used to hold the primary positions of the vertical bar and character, but secondary registers are required to generate the changes in X or Y that are needed to display these forms.

Displaying a Vertical Bar. The data flow diagram for displaying a vertical bar is shown in Figure 2. The base of the bar is specified by the X and Y registers, which must be preset by the SET X and SET Y functions. These registers are not changed during the display. The display sequence is initiated by the DISPLAY VERTICAL BAR AT X,Y function which is presented on the address lines along with the signed height of the vertical bar on the data lines. The bar height is loaded into the Y BAR/CHARACTER CODE register through SWITCH 1 which is later used to switch decremented values of Y BAR back into this register as the display progresses. The Y BAR SIGN flipflop is also set positive or negative, and the READY/BUSY flipflop set to BUSY. The contents of registers Y and Y BAR are then added together and sent through SWITCH 2 to the Y DAC, and a point is displayed at the position x, $y + y$ bar. A control loop is now started which repetitively subtracts (or adds if the vertical bar is negative) the current INCREMENT value from the Y BAR register, loading the revised value through SWITCH 1 back into the Y BAR register. The contents of registers Y and Y BAR are added and displayed as before. When the value of Y BAR changes sign, SWITCH 2 is flipped so that the contents of the Y register are sent to the Y DAC, displaying the final point at x,y, the base of the vertical bar. Thus both ends of the vertical bar are specified with 12-bit accuracy, even though the interior points of the bar have a resolution equal to the INCREMENT size. The total display time will depend on the number of points, which is equal to 1 plus the bar height divided by the increment size, allowing increased display speed at the cost of a grainier appearance to the line. During the vertical bar display, the READY/BUSY flipflop is set to BUSY, and the CHECK STATUS function can be used to switch the BUSY status onto the output status line. No other functions are valid until the flipflop becomes READY again.

Displaying a Character. Characters are displayed by standard scanning techniques using a ROM chip (Signetics N8228I-CD162) holding 64 standard ASCII characters stored as 8×8 arrays of data (Figure 3). The position of the lower left corner of the character is determined by the contents of the X and Y registers. The Y register remains unchanged after a character is displayed, but the X register is increased by 10 INCREMENT values, which is the correct position for displaying a new character. Thus a series of DISPLAY CHARACTER AT X,Y functions will result in the display of a line of characters. When this function is presented, the 6-bit ASCII code is simultaneously presented on the data lines and loaded into the Y BAR/CHARACTER CODE register, where it is used to address the appropriate dot matrix pattern in the ROM. The

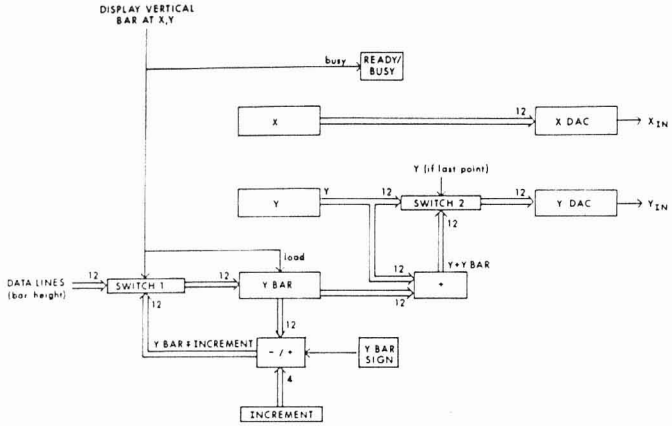

Figure 2. Data flow diagram for displaying a vertical bar

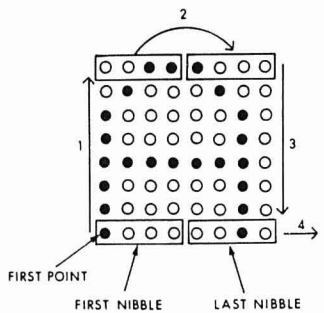

Figure 3. Diagram showing how a character pattern stored in a ROM is scanned and displayed. Black circles (●) indicate points that are displayed. The arrows show the order of scanning and the corresponding displacements in the *x* and *y* positions

READY/BUSY flipflop is also set to BUSY. The scanning procedure for displaying the character can be seen in Figure 3, which shows the pattern for the letter "A". The character dots are read as bits from the ROM 4 at a time (a nibble) and loaded into a shift register, starting at the lower left nibble. The bits are shifted and tested one by one as the X register is simultaneously increased by the INCREMENT value using a temporary register. If the dot value is 1, a point is displayed. If the dot value is 0, the point display cycle (oscilloscope settling time plus on-time) is skipped, speeding up the total character display time. After each 4-bit nibble scan is complete, the *x* value is restored to the original X register value and the Y register increased by the INCREMENT value. This process is repeated until the top left nibble of the character is scanned. Then the X register is increased by 4 INCREMENT values and the process continues as before except the INCREMENT value is now subtracted from the Y register. When the last nibble in the lower right corner is scanned, the X register is set for the next character position and the READY/BUSY flipflop set to READY.

The relative character size is determined by the INCREMENT value. The smaller the characters, the more that will fit on a full scale line. The smallest INCREMENT value will allow 102 characters/line, but the resolution of the display oscilloscope is usually the limiting factor.

DISCUSSION

The display controller has worked very effectively with our mass spectrometry systems. It is fast enough so that real time displays of mass spectra during data acquisition are not seriously degraded. Computer overhead can be reduced up to 80% for vertical bars and 90% for characters, compared with point by point generation using software. Using the Tektronix 604 Display Monitor, the maximum practical display time is 2 μs per point, for single points as well as for points displayed in vertical bars or character patterns. Allowing 3 μs per point gives rounder dots and simplifies the procedure for adjusting the controller timing. With this oscilloscope, a size three INCREMENT value is the smallest one suitable for reading the characters easily; this size allows 34 characters/line, displayed on a 5-inch width face.

Parts for the controller cost about $350, much of this for the two DACs and a ±15-V power supply. The logic portions of the controller have been implemented on a 7.5 × 17 inch printed circuit card containing 83 integrated circuits. The DACs and power supply are mounted in a separate small box connected by a cable to the card. The circuit logic drawings and a detailed circuit description are available for construction purposes.

ACKNOWLEDGMENT

The authors thank Gary Appel for technical assistance during the design and construction of the controller.

LITERATURE CITED

(1) "Tektronix 4010 and 4010-1 Maintenance Manual", Part No. 070-1183-00, Tektronix Inc., Beaverton, Ore. (1972).
(2) G. L. Brezler, *Proc. Twenty-Third Annu. Conf. Mass Spectrom.*, 259 (1975).
(3) H. J. Skov, L. Kryger, and D. Jagner, *Anal. Chem.*, **48**, 933 (1976).
(4) P. S. Berger, P. D. Norberg, and W. F. Holmes, Ref. 2, p 507.

RECEIVED for review February 24, 1977. Accepted May 12, 1977. This work was supported by National Institutes of Health Grants No. RR 00396 and RR 00954.

High-Speed, High-Purity Extraction Apparatus

Walter A. Aue,* Marek M. Daniewski,[1] Jürgen Müller, and John P. Laba

Chemistry Department, Dalhousie University, Halifax, Nova Scotia, Canada

In the production of bonded phases in general, and ultrathin polymer layers (*1*) in particular, the synthesized materials have to be exhaustively extracted to remove any nonbonded material. In our experience this generally takes a long time, e.g., from one to a few weeks in a regular soxhlet. To cut down on this time, we switched to soxhlets which extract at the boiling point temperature of the solvent (Kontes Model K585100). Frequent use was also made of Goldfish apparatus (Fisher Laboratory Supplies), where the extraction proceeds at boiling point temperatures and the solvent returns to the flask continuously, rather than batchwise as in a soxhlet.

The latter apparatus worked quite well for bonded layer synthesis; it was also extensively used for an entirely different purpose, namely, sample extraction for pesticide residue analysis. Extraction times could be cut to about $^1/_4$ of those necessary with the regular soxhlet. However, some problems remained.

First, a still higher flow was desirable. Second, an all-glass apparatus was considered superior for reasons of purity and inertness. And third, one would want certain extractions to be conducted under nitrogen and/or at high temperatures.

To meet these requirements we designed a simple, versatile extractor. Several models with different capacities, flow-rates, etc., were made, which had the following features in common: first, use of Clearseal joints (Wheaton Scientific, Millville, N.J.) to obtain a leak-tight, high-purity system free from lubricants; second, direct flow (comparable to column chromatograph) of the condensed solvent, at or close to boiling-point temperature, through the sample; third, a built-in thermal insulation, such that a predominant fraction of the evaporated and condensed solvent actually flowed through the material to be extracted, and high-boiling solvents could be used if desirable.

RESULTS AND DISCUSSION

Figures 1 and 2 show self-explanatory blueprints of two extractor units (together with more or less conventional boiling flasks and reflux condensors); the main difference between them being that in the first the extraction thimble is an integral part of the extractor; in the second, it is built to be easily inserted and removed.

The advantage of the first model is that it can be easily scaled up (our largest model held a half-liter sample) and that dimensions are not critical. The advantage of the second is that a greater number of thimbles, if desired of very small volume and of different frit porosities, can be inexpensively made and used with the same extractor body. Most of our experiences were obtained on the first extractor type, but should in general be applicable to the second as well. They were as follows.

First, because of the short extraction time and the use of nitrogen (which also obviates the sometimes detrimental use of boiling stones), any decomposition of labile materials is kept to a minimum. The volume of the solvent flask is easily varied, usually depending on whether the extracted material or the extract is of interest.

Second, high-boiling solvents can be used; e.g., a hexadecane (bp = 287 C°) extraction under (oxygen-free) nitrogen poses no difficulties.

Third, the apparatus is fairly simple to make and fairly easy to clean to high-purity standards (especially important in the case of pesticide residue analysis). Customary safety precautions should be taken though in regard to the high-vacuum jacket, e.g., by applying a polymer coat.

Fourth, the apparatus (especially the one shown in Figure 2) can become difficult to run with solvent mixtures such as the familiar "hexanes" used in pesticide residue analysis,

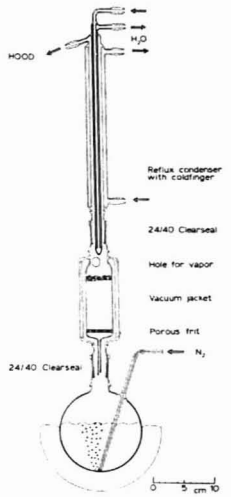

Figure 1. Extraction apparatus with built-in thimble

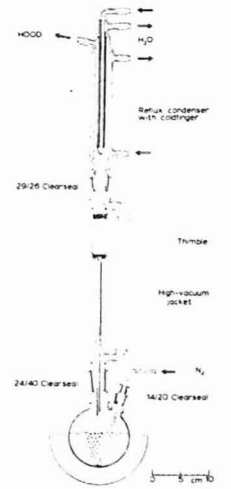

Figure 2. Extraction apparatus with removable thimble

[1] Present address, Polish Academy of Science, Warsaw, Poland.

because lower-boiling fractions may disrupt the sample packed inside the thimble. A neat solvent is definitely preferable.

Fifth, the extractor shown in Figure 1 can take all the solvent vaporized from a 1-L flask by a 500 W thermowell at full power; provided the frit is not too fine and the material above offers no unusual flow resistance.

In the case of the removable thimble apparatus (Figure 2), this proviso is even more important since the frit area is limited. Rapid flow through the thimble is aided by hydrostatic pull through the long stem. In order for this effect to work well, the stem has to be a few degrees lower than the boiling point of the solvent, and this has to be taken into account in choosing the dimensions of this part of the extractor.

Rapid liquid flow implies an enormous flow of vapor, and the openings in the apparatus which allow the vapor to pass through have to be rather large or liquid can build up in the condensor, especially when the thimble fills to the brim. In Figure 1, the same opening for the vapor would also serve to accommodate liquid overflow (which, however, never occurred with the materials we were extracting). If a large overflow should be encountered due to unusual flow resistance in the thimble, a second, slightly lower-placed opening on the opposite side would be desirable.

The overflow problem is potentially more acute in the removable thimble version and has been taken care of by essentially separating vapor flow from solvent flow in the critical area.

If high flows are to be achieved, the reflux condensor obviously must be capable of handling them. Shown in Figures 1 and 2 are two constructions which we have used, with equal cross-sections of upward and downward flow in the coldfinger, and two water flows in parallel through the (high-resistance) coldfinger and the (low-resistance) outer jacket. They worked to our satisfaction; however, some types of commercial condensors might have served equally well.

The obvious application of the described extractors is not the routine experiment but the unusual type of extraction, which calls for high speed, high purity, and possibly high temperature. Under these circumstances they have performed extremely well.

LITERATURE CITED

(1) W. A. Aue, C. R. Hastings, and S. Kapila, *Anal. Chem.*, **45**, 725 (1973).

RECEIVED for review March 7, 1977. Accepted April 4, 1977. This study was supported by NRC Grant A-9604, AC Grant EMR-7401 and DRB Grant 9502-04.

Laboratory Real Time Clock Featuring Computer, Experiment, and Manual Interaction

Robert L. Veazey and Timothy A. Nieman*

School of Chemical Sciences, University of Illinois, Urbana, Illinois 61801

Laboratory instruments often require a precise, highly stable time base for operation. Many experiments, particularly those which use a computer system for control and data acquisition, require this same degree of precision and stability, plus the flexibility of a timer with a widely variable period. A crystal controlled oscillator with digital counting circuitry is the only means for obtaining this combination of stability and flexibility. With the advent of microcomputers for control of instrumentation, many labs are faced with major changes in their computer systems. It is awkward and time-consuming to redesign a clock system with every major instrumentation change.

This report describes a flexible clock designed and used in our laboratory which meets the criteria of high stability and adaptability, and which has several desirable functions and a unique interaction capability. Many laboratory clocks, the so-called mainframe clocks, are completely dedicated to computer-only interaction; other peripheral type clocks are devoted to one particular instrument (*1*). The design of our general lab clock allows computer interaction as with a mainframe clock and experimental interaction as with the peripheral clock, as well as manual interaction for setting clock parameters and for initialization. None of the control sources are restricted: every clock function can be controlled from any of the controlling elements. Output information is provided as to the status of the clock, independent of the controlling element. The design we describe here is advantageous in that the interaction is versatile enough that the clock will function with any computer-experiment setup.

GENERAL CIRCUIT DESCRIPTION

A block diagram of the clock showing the important interactions is shown in Figure 1. The clock is really a dual clock designed around a pair of MOS technology counter time-base chips (Mostek 5009P). A 10^6-Hz crystal controlled oscillator which is accurate to 1 ppm controls the chip internal oscillator circuit. As the diagram of Figure 1 shows, the two independent clocks (PG Time Base and DM Time Base) use the same crystal. The oscillator output connection of one time base (DM) allows synchronous oscillation of the second time base (PG) using the external oscillator provision of the second chip. Note that the two clock circuits are synchronous in their base frequency dependence on the same crystal, however the output frequencies are chosen independently, as are all other functions. Each clock chip has internal synchronous dividers which can be externally selected to provide frequency division ranges from 1 to 36×10^8: nine division ranges from 1 to 10^8 are used in the clock design. The time base chips have reset provisions to reset the internal counters to their highest or lowest states: these functions are used to ensure that clock initialization commands do not produce an initial timing error.

The clock is designed so that one of the two clock oscillators, designated the Decade Marker (DM), is used merely as a decade time base and as such does not have some functions available with the other clock oscillator (designated the programmable clock, PG). The PG clock has an additional four decade counter chain (Presettable Counter) external to the actual clock chip. The 74192 BCD counters used have the capabilities of bidirectional counting, clear, and preset; these capabilities are the basis for the various counting functions available with the PG clock. The use of two independent time bases in the design is an important feature of the system. For example, using the decade marker and the programmable clock together, an experiment can be designed in which data are taken in every DM period until the PG clock overflows. The PG clock thus frees the processor from the burden of counting repeated clock interrupts for timing and, since the PG clock is designed to operate independently of

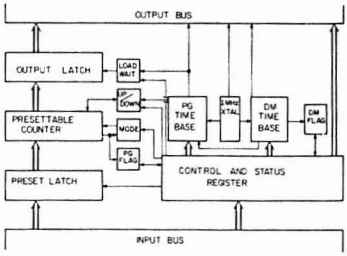

Figure 1. Block diagram of clock

any computer software, errors caused by computer cycle time are reduced.

Our present design uses BCD counters in order to make human interaction easy: the thumbwheel data input switches and the LED readouts display decimal. The computer then carries out the BCD-to-binary conversions in software, or the conversions could be done in hardware interface circuitry. It is possible to operate the main clock in straight binary by replacing the 74192 decimal counters with pin-compatable 74193 binary counters, which also will extend the counter range. If this substitution is made, the manual counter input and output circuitry will yield erroneous data, unless a mental or hardwired number base conversion is made.

As mentioned in the introduction, control of the clock can be under manual, computer, or experimental control or a combination of these sources. The input must thus allow access to all possible controllable functions; likewise, the output bus must be able to indicate the actual state of the functions being controlled. This is accomplished by requiring that all input control signals be negative pulses from open-collector type gates, and by designing all clock state functions other than reset commands to be latched on the main clock board (at the Preset Latch and the Control and Status Register). The latches allow the state of any function to be read out at any time. There are 15 control lines input and 9 status lines output. Our design uses 16 data lines but this can be modified up or down depending on the required range and resolution.

FUNCTIONS

Frequency Selection. The frequencies of the PG and DM clocks are chosen individually by loading the input latches (in the Control and Status Register) to the Mostek clock chips. Binary input of the numbers 0 through 8 allows increasing decade division of the primary frequency to provide frequencies of 10^6 through 10^{-2} Hz.

Count Direction. The external PG counters can count up or down. This selection is latched at the main clock board and, through a 3 NAND gate circuit, controls which input to the counters is active.

Preset. The four counters external to the PG clock can be preset to an initial value, thus having the advantage of variable modulus counting. This initial value is held in four 7475 four-bit latches, and upon command can be loaded into the counters. With the preset, a wide variety of nondecade time bases can be obtained, using the overflow bit as the timer. When using the preset, one normally counts down from the preset number. The preset number for a desired frequency is the period, with the time base set accordingly. Four decimal digit accuracy (or 16 binary bits) in the period is available, but use of all digits is not required.

Mode. The mode selection governs the action taken when the external PG counters overflow. In the *Clear* mode, upon overflow the counters simply are reset to zero and resume

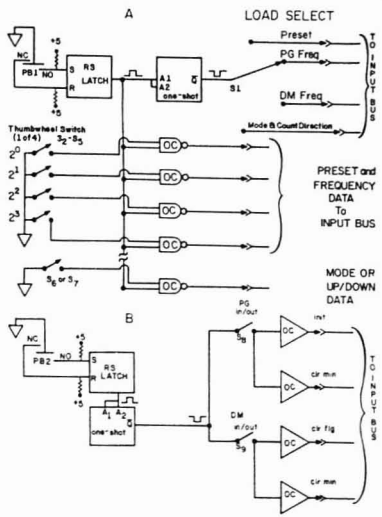

Figure 2. Diagram of (A) manual data loader and (B) reset control

counting. In the *Set* mode, overflow causes the counter to load the number in the preset latches before counting is resumed. This allows repetition of nondecade periods. By changing the preset number between overflows, an aperiodic time base can be generated using the *Set* mode. An aperiodic time base is useful in kinetics, as in studies of an exponentially decreasing function where data must be taken rapidly during the initial decay, and much more slowly as time progresses.

Flags. Flags are provided with the PG and DM clocks to signal overflow. In normal use, the overflow signal is used to initiate a task at the computer or experiment: the initiation is acknowledged by clearing the flag. If acknowledgement is not received before the next overflow, an error flag is set. The overflow flag changes state at a frequency one-half that of the clock if the clear function is not used, thus providing an extended choice of time base.

Reset Max and Reset Min. The 5009P clock chips have provision to reset their internal counters to their maximum (*Reset Max*) or minimum (*Reset Min*) states. To avoid an initial error in the clock period upon initialization, *Reset Min* is strobed when the clock is started. *Reset Max* provides a negative going pulse on the next clock pulse following the strobe (10^{-6} s).

Initialize. A timing task for the PG clock is normally begun using the *Initialize* command. This instruction synchronizes clearing of the PG flags, strobing of the PG *Reset Min*, and resetting of the external PG counters as prescribed by the *Mode*.

Read. When the PG clock is used as an event timer, the *Read* command loads the Output Latch from the Presettable Counter. The latch then contains the number of PG time base periods which have passed since the *Initialization* of the clock. A wait circuit (Load Wait) at the latch command is used to ensure that the counter is not latched during a counter ripple carry.

Manual Control. Manual control of the clock is accomplished via the front panel switches (see Figure 2). The rotary load select switch S1 (Figure 2A) selects the function to be controlled, and the chosen command is given upon pushing the *Load* pushbutton, PB1. The rotary switch has

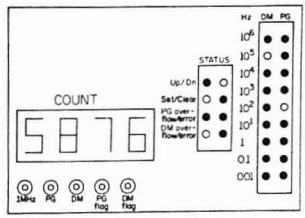

Figure 3. Front panel display showing frequency LEDs (DM frequency = 10^5 Hz, PG frequency = 10^2 Hz), status display (count is *Down*, mode is *Set*, PG flag is *Clear*, and DM overflow is *Set*), count output (5876), and banana jack outputs

positions for: (1) loading the PG counter preset, (2) setting the PG frequency, (3) setting the DM frequency, and (4) setting the PG conditions of *Mode* and *Count Direction*. BCD thumbwheel switches S2–S5 provide the data for frequency and preset controls, and spst switches S6 and S7 provide *Mode* and *Count Direction* data. The circuit design is such that all control data are presented to the main clock at once, but only the data chosen by the load select is accepted.

As mentioned previously, each function is controllable through the input bus. In manual control, however, it is not possible to initialize both DM and PG clocks and to clear all flags synchronously using the individual functions, so a *Start* function unique to the manual control system joins these functions under control of PB2 and switches S8 and S9 (Figure 2B). The switches are to select whether the PG or DM clock is to be started, or both simultaneously. Pushing the *Start* pushbutton carries out the reset operation for the chosen clock(s).

The front panel (Figure 3) has a visual output of the clock states, showing the count in the output latch through four 7 segment LEDs. (A circuit similar to that of Figure 2B is provided for manual updating of the output latch.) The frequency for each clock is shown by the *on* state of one of nine LEDs per clock. PG status of *Count Direction*, *Mode*, and PG and DM flag states are also indicated by individual LEDs. The front panel also provides convenient banana jack outlets for some important signals: 1-MHz oscillator, PG clock out, DM clock out, and PG and DM overflow flag signals can be accessed through the front panel.

CONCLUSION

The lab clock described can provide considerable flexibility in choice of timer–computer–experiment interactions. The input bus and control design is not dedicated to a specific computer, but can be easily interfaced to any computer or microprocessor. The basic design for the heart of the clock is not unique, but is based on previous designs (largely unpublished) for computer mainframe clocks (*2–4*). It is the versatility of interaction which makes our clock unique and which amplifies its utility.

The provision for human interaction is a step forward in clock design, not backward. In laboratories involved in development of new instrumentation, manual intervention is often highly desirable, especially during initial stages of development or during testing. Our design allows manual control and observation of every clock function.

Experimental interaction allows things not possible with operation of mainframe clocks—for example 1-μs and 10-μs time scales are useless on a mainframe clock because of computer cycle time considerations. Most experiments, however, make direct use of the *Start* and *Stop* commands, and thus the high frequency selections can be used advantageously. If the experiment is sufficiently complex, data lines can also be controlled by the experiment.

With a total parts cost including power supply of approximately $300, the circuit described is within the budget of any laboratory. Detailed circuit diagrams are available from the authors.

LITERATURE CITED

(1) B. K. Hahn and C. G. Enke, *Anal. Chem.*, **45**, 651A (1973).
(2) B. K. Hahn, Ph.D. thesis, Michigan State University, East Lansing, Mich., 1974.
(3) E. J. Darland, Ph.D. thesis, Michigan State University, East Lansing, Mich., 1977.
(4) T. Last, Ph.D. thesis, Michigan State University, East Lansing, Mich., 1977.

RECEIVED for review March 11, 1977. Accepted May 9, 1977. This work was supported, in part, by a grant from Research Corporation.

Unheated External Column and Inlet Modification of a Gas Chromatograph for Phosphine Determinations

Jerry R. Bean[1]* and Robert E. White[2]

U.S. Fish & Wildlife Service, Wildlife Research Center, Denver, Colorado 80225

The gas chromatographic detection and measurement of phosphine (PH_3) due to hydrolized zinc phosphide (Zn_3P_2) has been carried out in this laboratory for a number of years, serially using the methods of the Food and Drug Administration (*1*), Robinson (2), Hilton (*3*), and Okuno (*4*). A recent modification to the gas chromatograph used in three of these procedures has increased its utility as a dual-detector instrument (flame photometric and microcoulometric). Before this modification, the column oven temperature was lowered from 190 °C to about 40 °C for phosphine analyses which precluded the use of the columns in the microcoulometric system for chlorinated hydrocarbon analysis and the flame photometric detector columns for other organophosphorous insecticide detection. This drastic temperature change frequently resulted in leaks (especially with glass columns) due to expansion and contraction of ferrules used to seal the columns at the column inlet, long waits for instrument equilibration, and inability to utilize both detectors concurrently. By simply adding another injection inlet and a 6-mm × 46-cm aluminum column outside the column oven, the phosphine measurements can still be made while column oven temperatures for microcoulometry and flame photometric detection of the commonly occurring insecticides are maintained.

MODIFICATIONS

The gas chromatograph used in our laboratory is a Microtek MT-220 (Tracor Instruments, Austin, Texas) with two detectors and four columns in a common oven. Two column

[1]Present address, U.S. Fish & Wildlife Service, 238 E. Dillon St., Pocatello, Idaho 83201.
[2]Present address, International Joint Commission, 100 Ouellette Avenue, Windsor, Ontario, Canada N9A 6T3.

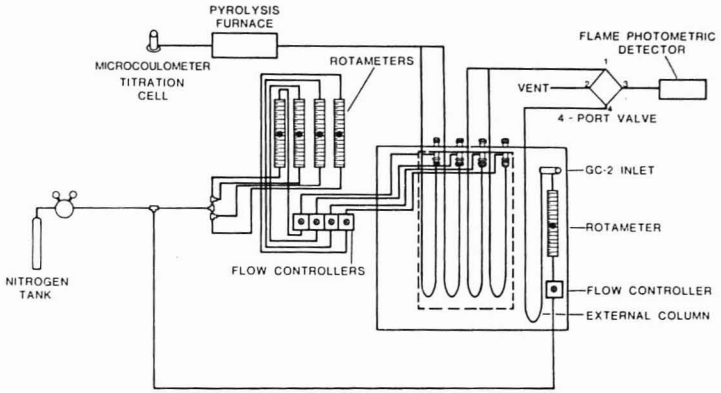

Figure 1. Carrier flow arrangement after modification

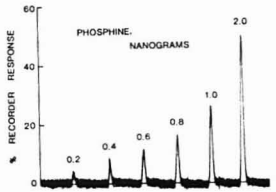

Figure 2. Phosphine chromatogram obtained with 6-mm × 46 cm aluminum column packed with Chromosorb 102

effluents are attached through a combiner to a Dohrmann pyrolysis furnace and microcoulometer system terminating at a titration cell. This system is used oxidatively for the detection of chlorinated hydrocarbons. The other two column effluents (before modification) were not combined but each was attached to a separate port of high temperature, four-port valve. The third port was used as a vent to atmosphere and the fourth connected to the flame photometric detector. The valve helped select the column to be used in the analysis and vent solvent which could extinguish the flame in the detector.

The diagram in Figure 1 shows the carrier flow arrangement after the modification. In modifying, we combined the heated column effluents going to the flame photometric detector and attached this combiner to the four-port valve. The second and third ports were left vented to atmosphere and attached to the detector, respectively. The fourth port was attached to another column which is the major modification described here.

A tee was placed in the carrier gas (nitrogen) line to the instrument and connected in series with $^1/_8$-inch copper tubing to a rotameter and a flow controller. The rotameter and controller were attached to an external panel beside the instrument's column oven. An injection port from another instrument (Beckman model GC-2) was then attached to this panel and the inlet line connected to the controller. This injection port was attached to and provided support for a chromatographic column placed in the space between the column oven and the external panel. The fourth port of the four-port valve was then connected to this column.

When the heated columns to the flame detector are needed, the flow in the ambient temperature column is vented with the 4-way valve. Selection of one heated column over another is accomplished by reducing flow to one and increasing it appropriately to the other. Since column temperatures for microcoulometric and flame photometric detection are similar, as we use them, no conflict of use occurs and these systems now can be used simultaneously.

DISCUSSION

Figure 2 illustrates a phosphine chromatogram obtained with a 6-mm × 46-cm aluminum column packed with Chromosorb 102.

Phosphine will successfully chromatograph at ambient temperatures. This allows us to have a fifth column outside the heated oven with an unheated inlet and utilize two detectors concurrently without costly time interruptions. This modification should be feasible for most other models of gas chromatographs. When analyzing compounds like phosphine that can be readily detected and chromatographed without heating, such an addition can provide more efficient instrument use.

LITERATURE CITED

(1) Hazleton Labs, Inc., in "U.S. Food and Drug Administration, Pesticide Analytical Manual", Vol. 11, Pesticides Reg. Sec. 120.235 Aluminum Phosphide Method A, 1968.
(2) W. H. Robison and H. W. Hilton, *J. Agric. Food Chem.*, **19**, 875–878 (1971).
(3) H. W. Hilton and W. H. Robison, *J. Agric. Food Chem.*, **20**, 1209–1213 (1972).
(4) I. Okuno, R. A. Wilson, and R. E. White, *Bull. Environ. Contam. Toxicol.*, **13**, 392–396 (1975).

RECEIVED for review April 15, 1977. Accepted June 6, 1977.

Optically Transparent Vitreous Carbon Electrode

V. E. Norvell and Gleb Mamantov*

Department of Chemistry, University of Tennessee, Knoxville, Tennessee 37916

Development of optically transparent electrodes (OTEs) for simultaneous spectroscopic and electrochemical studies (*1*), particularly of electrochemically generated reactants (*2*), has received considerable attention. A special type of OTE, the optically transparent thin-layer electrode (OTTLE) has been especially useful in such studies because the small cell volume of a typical OTTLE allows complete electrolysis of the thin-layer solution within a short period of time (*2, 3*). OTTLEs have proved to be useful for determining values of $E^{\circ\prime}$ and n for several complex biological redox systems (*2*).

Thus far, UV–visible spectroelectrochemistry using OTEs has involved the use of an electrode consisting either of a film of metal or metal oxide on a transparent substrate, or a metal wire mesh minigrid held between two optical windows (*2*). OTEs based on a germanium plate (*4, 5*) or carbon film (*6, 7*) have been reported for IR studies.

The recent development of reticulated vitreous carbon (RVC) (*8*) has made possible the construction of an OTE with an RVC electrode. The structure of RVC allows the RVC-OTE to exhibit many of the characteristics of an OTTLE, even though the volume of solution electrolyzed is 10–20 times greater than for a typical minigrid OTTLE. The fabrication and evaluation of the RVC-OTE are discussed in this paper.

EXPERIMENTAL

Construction of the RVC-OTE. RVC (trademark of Chemotronics) with porosity of 100 pores per inch (ppi) was obtained from Chemotronics International, Inc., Ann Arbor, Mich. This material was cut into slices of approximate dimensions 2 cm × 4.5 cm with thicknesses ranging from 0.8 to 1.2 mm for use as electrodes. Electrical contact to the RVC was made in the following manner: a fine Cu wire was threaded through a corner of the electrode and folded over to secure it; Liquid Organic Silver No.9167 (Englehard Industries, East Newark, N.J.) was then applied to the surrounding area and the organic portion burned away leaving a silver coating; this was repeated several times until a sturdy contact was achieved.

The OTE was assembled by sealing the RVC electrode between two clean microscope slides with epoxy in a configuration similar to that suggested by DeAngelis and Heineman (*3*). The RVC was positioned a few mm from the bottom of the slides and extended about 1 cm beyond the slides on each side. To prevent accidental breakage of the RVC at the edge of the slides, the whole exposed portion of the electrode, including the silvered contact region, was coated with epoxy. The Teflon spacers used by DeAngelis and Heineman (*3*) were not necessary here since the thickness of the cell was determined by the thickness of the RVC slice.

A small diameter Teflon tube was connected to the top of the cell to allow solution to be drawn into the cell with a syringe. To dislodge air bubbles from the RVC electrode, it was necessary to draw solution above the top of the electrode and then "pump" the solution up and down rapidly. Purging the OTE with nitrogen before filling helped minimize this problem. Small residual bubbles that remained in the electrode after this procedure did not affect the operation of the OTE. The solution level was maintained above the top of the electrode by clamping the filling tube.

Cells constructed according to the above procedure had volumes of 400 to 550 μL depending on the thickness of the electrode. These volumes were determined by coulometry with a standard solution of $K_3Fe(CN)_6$ using the calculation procedure given by DeAngelis and Heineman (*3*). Cell thicknesses were calibrated by comparing the absorbance of a $KMnO_4$ solution in the OTE with the absorbance of the same solution in a 1.0-cm cuvette with a 0.9-cm spacer.

Apparatus. Cyclic voltammetry was performed with a PAR 173/179 Potentiostat/Coulometer and a PAR 175 Universal Programmer. The PAR 173/179 instrument was also used for coulometry. Spectra were recorded with a Bausch and Lomb Spectronic 505 spectrophotometer. All potentials were measured vs. the saturated calomel electrode.

Reagents. Standard ACS grade reagents and deionized water were used for all solutions without further purification.

RESULTS AND DISCUSSION

The RVC-OTE is unique among OTEs because of the composition and special structure of the electrode material. RVC is a glasslike carbon with a porous structure having a free void volume of about 97% and a surface area of about 65 cm^2/cm^3 (*8*). An electrode of substantial surface area can thus be made from a relatively small piece of RVC. RVC-OTEs of the dimensions given above have surface areas ranging from 30 to 40 cm^2 (based on the calibrated cell thickness). This compares to a surface area for a typical minigrid OTTLE of 1–2 cm^2 (*9, 10*). When RVC is cut into thin slices, its light transmittance is comparable to that of wire mesh minigrids (13%–45% for 100 ppi RVC 1.2 mm to 0.5 mm thick) and is essentially constant over the entire UV–visible spectrum.

The three-dimensional structure of RVC allows the RVC-OTE to behave in a fashion similar to a minigrid OTTLE, i.e., electrochemical equilibrium is rapidly achieved and electrolysis of the solution in the immediate vicinity of the electrode can be carried out to completion within a short period of time with diffusion as the sole means of mass transport. This is because most of the solution in the vicinity of the electrode is actually *inside* the electrode, so that each electroactive entity has a relatively short diffusional path to the electrode surface. This behavior is illustrated by the chronocoulogram shown in Figure 1. A standard solution of $K_3Fe(CN)_6$ was reduced by stepping the potential of the RVC-OTE from 0.6 V to 0.0 V at time $t = 0$. The charge is seen to increase rapidly, finally leveling off to a constant value, Q_T, when complete electrolysis has been achieved. By subtracting the background, Q_B, the cell volume and approximate thickness can be calculated (*3*). The background correction was determined with a solution of the supporting electrolyte, and was typically 2 to 8% of the total charge (Table I). The results of coulometry were very reproducible both in the shape of the chronocoulogram and the total charge required for complete electrolysis (Table I).

The cyclic voltammetric behavior of the RVC-OTE (Figure 2) is very similar to that of a minigrid OTTLE (*3*). The important feature to note here is the rapid drop in current to near zero following the peak in both scan directions. This is an indication of complete electrolysis of the electroactive species (*3*). The measured values of i_{p_a} and i_{p_c} are identical, indicating complete retention of the electroactive material within the small cell volume. Diffusion into the bulk solution is negligible.

The RVC-OTE has been applied to the spectroelectrochemistry of *o*-tolidine (*11*) and MnO_4^- (*12, 13*), and the results are illustrated in Figures 3 and 4. These spectra were obtained by applying a potential at which only the reduced form was present (MnO_4^- was converted to MnO_4^{2-} by the reaction $4MnO_4^- + 4OH^- \rightarrow 4MnO_4^{2-} + O_2 + 2H_2O$), then applying potential steps to generate the oxidized form. The current was allowed to decay for two or three minutes to background level before each spectrum was recorded. For both *o*-tolidine and permanganate, the same sets of spectra were obtained

Table I. Coulometric Data Reproducibility for the RVC-OTE[a]

RVC-OTE No. 1[b]		RVC-OTE No. 2[c]	
Q_T	Q_B	Q_T	Q_B
0.1630	0.0125	0.2164	0.0043
0.1617	0.0122	0.2167	0.0043
0.1638	0.0126	0.2160	0.0043
0.1655	0.0147	0.2162	0.0031
0.1635 ± 0.0016	0.0130 ± 0.0011	0.2163 ± 0.0003	0.0040 ± 0.0006

[a] Solution: 4.0×10^{-3} M $K_3Fe(CN)_6$ in 1.0 M KCl. Potential stepped from 0.6 V to 0.0 V. [b] Cell volume: ~400 μL, cell thickness: ~0.92 mm. [c] Cell volume: ~550 μL, cell thickness: ~1.20 mm.

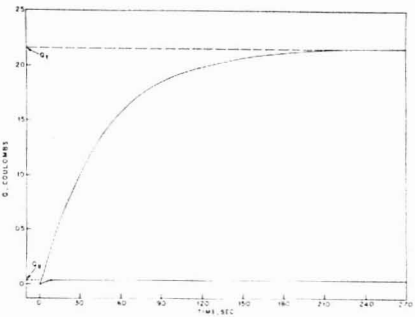

Figure 1. RVC-OTE chronocoulogram of 4.05×10^{-3} M $K_3Fe(CN)_6$ in 1.0 M KCl. Potential stepped from 0.6 V to 0.0 V at $t = 0$. Cell volume: ~550 μL. Cell thickness: ~1.2 mm

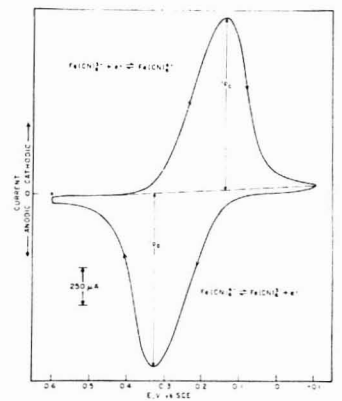

Figure 2. RVC-OTE cyclic voltammogram of 4.05×10^{-3} M $K_3Fe(CN)_6$ in 1.0 M KCl. Scan rate: 1 mV/s. Cell volume: ~550 μL. Cell thickness: ~1.2 mm

when starting with the oxidized form and reducing stepwise. The limited transmittance of the OTE was corrected for by placing in the reference beam of the spectrophotometer a piece of RVC of a thickness similar to that used in the OTE.

The RVC-OTE has several characteristics which overcome some of the disadvantages of wire minigrid or metal oxide OTEs, while combining the advantages of both of these types of electrodes. Because RVC is a rather chemically inert matrix of vitreous carbon, strongly acidic or basic solutions, or strongly oxidizing or reducing solutions have little or no effect on the operation of the electrode. The electrode is also electrochemically unreactive, exhibiting a usable potential

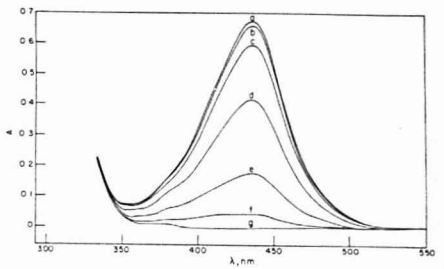

Figure 3. RVC-OTE spectra of 1.0×10^{-4} M *o*-tolidine in 0.05 M acetic acid and 0.1 M perchloric acid, for different values of applied potential: (*a*) 0.700, (*b*) 0.580, (*c*) 0.560, (*d*) 0.540, (*e*) 0.520, (*f*) 0.500, (*g*) 0.400 V vs. SCE. Cell thickness: ~0.92 mm, transmittance: 22%

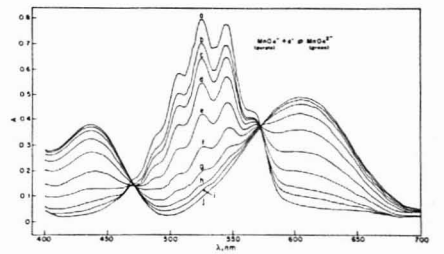

Figure 4. RVC-OTE spectra of 3.0×10^{-3} M MnO_4^- in 4.0 M KOH, for different values of applied potential: (*a*) 0.550, (*b*) 0.400, (*c*) 0.380, (*d*) 0.360, (*e*) 0.340, (*f*) 0.320, (*g*) 0.300, (*h*) 0.280, (*i*) 0.260, (*j*) 0.150 V vs. SCE. Cell thickness: ~0.92 mm, transmittance: 22%

range extending from about 1.2 V to −1.0 V at pH 7. These limits represent a current density of approximately 5 $\mu A/cm^2$ of electrode surface area. This range is comparable to that of a tin oxide or indium oxide OTE, whereas the range of a metal film or wire minigrid OTE is more restricted (*2*). The spectral characteristics of the RVC-OTE, on the other hand, are very similar to those of a wire minigrid OTE, i.e., practically constant transmission over the UV–visible spectrum (*2*). This is in contrast to the widely varying transmission of metal film or metal oxide OTEs (*2*). The RVC-OTE thus combines the electrochemical advantages of metal oxide electrodes with the spectroscopic advantages of the minigrid OTE.

Preliminary experiments have indicated that it may be possible to extend the negative potential limit of the RVC-OTE by deposition of a mercury film onto the RVC surface. This procedure has been successfully applied to Pt film OTEs (*14*) and nickel (*10*) and gold (*15*) minigrid OTEs. Our success with this technique has been limited because of poor Hg film formation; however, a smooth mercury coating has been

achieved by depositing mercury on nickel-plated RVC (*16*).

The use of the RVC-OTE for IR spectroelectrochemistry in aqueous solutions has been considered, but the thickness of the electrode (see below) would appear to make direct IR transmission spectroscopy difficult. Internal reflectance spectroscopy appears to be more promising. A cell of the type used by Laser and Ariel (*17*), in which the internal reflection element is surrounded by an OTE, could be easily constructed with an RVC electrode.

Bulk RVC is available in various porosities, and can easily be cut into any desired shape. The choice of several porosities allows control over the optical characteristics as well as the surface area-to-volume ratio of any particular electrode. The minimum thickness to which RVC can be cut (thus the maximum optical transmittance) is dependent on the porosity. We have found the minimum thickness for 100 ppi RVC to be about 0.5 mm. RVC is also very inexpensive. A complete OTE can be made with less than $0.15 worth of material.

In conclusion, we have demonstrated that the RVC-OTE is a versatile new optically transparent electrode which has properties unlike any previously reported OTE. We feel that the RVC-OTE, or modifications thereof, will be applicable to a number of spectroelectrochemical studies, particularly in nonaqueous or corrosive solutions at elevated temperatures, e.g., molten salt systems.

LITERATURE CITED

(1) T. Kuwana, *Ber. Bunsenges. Phys. Chem.*, **77**, 858 (1973), and references therein.
(2) T. Kuwana and W. R. Heineman, *Acc. Chem. Res.*, **9**, 241 (1976), and references therein.
(3) T. P. DeAngelis and W. R. Heineman, *J. Chem. Educ.*, **53**, 594 (1976).
(4) H. B. Mark, Jr., and B. S. Pons, *Anal. Chem.*, **38**, 119 (1966).
(5) D. R. Tallant and D. H. Evans, *Anal. Chem.*, **41**, 835 (1969).
(6) J. S. Mattson and C. A. Smith, *Anal. Chem.*, **47**, 1122 (1975).
(7) J. S. Mattson and T. T. Jones, *Anal. Chem.*, **48**, 2164 (1976).
(8) Bulletin No. 176, Chemotronics International, Inc., Ann Arbor, Mich.
(9) W. R. Heineman, J. N. Burnett, and R. W. Murray, *Anal. Chem.*, **40**, 1970 (1968).
(10) W. R. Heineman, T. P. DeAngelis and J. F. Goelz, *Anal. Chem.*, **47**, 1364 (1975).
(11) R. W. Murray, W. R. Heineman, and G. W. O'Dom, *Anal. Chem.*, **39**, 1666 (1967).
(12) D. B. Freeman, Ph.D. Dissertation, University of Tennessee, Knoxville, Tenn., 1971.
(13) D. B. Freeman and G. Mamantov, *Electrochim. Acta*, **21**, 257 (1976).
(14) W. R. Heineman and T. Kuwana, *Anal. Chem.*, **43**, 1075 (1971); **44**, 1972 (1972).
(15) M. L. Meyer, T. P. DeAngelis, and W. R. Heineman, *Anal. Chem.*, **49**, 602 (1977).
(16) W. A. Rice and C. H. Franklin, Chemotronics International, Inc., Ann Arbor, Mich., private communication.
(17) D. Laser and M. Ariel, *J. Electroanal. Chem.*, **41**, 381 (1973).

RECEIVED for review April 22, 1977. Accepted May 27, 1977. We would like to acknowledge the support by the Energy Research and Development Administration under Contract E(40-1)-5053.

Author Index

Allemand, C. D. 1450
Anese, C. P. 1456
Ataman, O. Y. 1331
Aue, W. A. 1465

Barnes, R. M. 1450
Bartholomew, J. C. 1290
Bean, J. R. 1468
Berger, P. S. 1462
Berti, M. 1313
Birke, R. L. 1380
Boulton, R. B. 1297
Breitenbach, L. P. 1346
Bresseleers, C. M. 1326
Brindle, M. P. 1459
Brown, H. R. 1417
Burgard, D. R. 1444
Burrows, K. C. 1459
Buso, G. 1313

Chen, H-F. 1357
Clayton, J. W. 1429
Colautti, P. 1313
Covington, A. K. 1363
Crowe, H. R. 1353

Dale, A. D. 1311
Dalrymple-Alford, P. 1390
Daniewski, M. M. 1465
Dannenberg, J. J. 1405
DeAngelis, T. P. 1395
Denton, M. B. 1413, 1422
DePalma, R. A. 1376

Emilsson, T. 1458
Evans, C. A., Jr. 1399
Ewan, G. T. 1297

Fernando, Q. 1429
Ferra, M. I. A. 1363
Fisch, M. H. 1405
Fry, R. C. 1413

Games, L. M. 1433
Gaylor, V. F. 1386
Genna, J. L. 1450
Gold, A. 1448
Goldberg, I. B. 1353
Goode, S. R. 1408
Goto, M. 1390

Hanley, P. R. 1399
Heineman, W. R. 1395
Hites, R. A. 1433
Holmes, W. F. 1462
Horlick, G. 1446
Hughes, M. C. 1459
Hurst, R. W. 1395

Ishizuka, T. 1339

Jadamec, J. R. 1316

Kuwana, T. 1348

Laba, J. P. 1465
Lavallee, D. K. 1453
Lewis, R. K. 1399
Lin, C-H. 1357
Little, C. J. 1311

McDonald, D. C. 1336
McLafferty, F. W. 1441
Maker, P. D. 1346
Mamantov, G. 1470
Mark, H. B., Jr. 1331, 1343, 1395
Marten, T. R. 1311
Mattson, J. S. 1395
Millard, M. M. 1290
Moore, W. M. 1386
Moschini, G. 1313
Muller, J. 1465

Nieman, T. A. 1322, 1466
Niki, H. 1346
Norelius, J. T. 1453
Norvell, V. E. 1470
Nowak, R. J. 1343

Oldham, K. B. 1390
Ord, D. A. 1311

Patriarche, G. J. 1343
Perone, S. P. 1369, 1376, 1444
Petersen, B. A. 1304
Pierce, F. D. 1417

Richards, J. A. 1456
Routh, M. W. 1422

Saner, W. A. 1316
Savage, C. M. 1346
Seymour, M. D. 1429
Srinivasan, V. S. 1458
Stieg, S. 1322
Stievano, B. M. 1313
Sunahara, H. 1339
Swartz, P. A. 1422
Szentrimay, R. A. 1348

Talmi, Y. 1316
Thomas, Q. V. 1369, 1376
Tindall, G. W. 1403
Tregnaghi, C. 1313

Uwamino, Y. 1339

Vanderborght, B. M. 1326
Van Grieken, R. E. 1326
Veazey, R. L. 1466
Vire, J-C 1343
Vouros, P. 1304

Wagner, C. D. 1282
White, R. E. 1468
Wiebers, J. L. 1444
Williams, P. 1399

Yacynych, A. M. 1395
Youssefi, M. 1380
Yuen, W. K. 1446

Future Articles

Spectroscopic System for the Study of Fluorescent Lanthanide Probe Ions in Solids

M. P. Miller, D. R. Tallant, F. J. Gustafson, and J. C. Wright

Determination of Phosphorus in Milk Powders by Optical Emission Spectrometry with a High Frequency Inductively-Coupled Argon Plasma Source

A. M. Gunn, G. F. Kirkbright, and L. N. Opheim

Laser Two-Photon Excited Fluorescence Detection for High Pressure Liquid Chromatography

M. J. Sepaniak and E. S. Yeung

Qualitative Analysis of Thin Gallium Nitride Films with Secondary Ion Mass Spectrometry

J. E. Andrews, A. P. Duhamel, and M. A. Littlejohn

Determination of Acid POH Groups of Hydrolysis-Susceptible Esters of Phosphorous Acid

R. Siegfried

Reaction-Rate Method for the Determination of Hydrocortisone

R. M. Oteiza, D. L. Krottinger, M. S. McCracken, and H. V. Malmstadt

Sampling Error in Ion Microprobe Analysis

G. J. Scilla and G. H. Morrison

Generation of Nitrosamines for Gas Chromatographic Analysis via Direct Injection

D. J. Freed and A. M. Mujsce

Phase-Selective Fundamental and Second Harmonic Alternating Current Voltammetry Bismuth(III) and Lead(II) at a Continuously Mercury-Coated Rotating Platinum Disk Electrode

N. Kanzaki, Y. Kanzaki, and S. Bruckenstein

Trace Chloride Determination by Rate Controlled Coulometric Titration

M. J. Zetlmeisl and D. F. Laurence

Determination of Intact Oxazepam by Electron Capture Gas Chromatography after an Extractive Alkylation Reaction

J. Vessman and M. Johansson

Enhancement of Emission by Potassium Chloride in the Low-Pressure Microwave-Induced Plasma Emission Spectrometer

I. Atsuya, H. Kawaguchi, C. Veillon, and B. L. Vallee

Study of the Steady-State Current at Tubular Electrodes in the Micromolar Concentration Region

W. J. Blaedel and D. G. Iverson

Colorimetric Determination of Hippuric Acid in Urine and Liver Homogenate

S. Ohmori, M. Ikeda, S. Kira, and M. Ogata

Sample pick-up, pipetting, tip ejection... On the new Eppendorf® Pipettes, a single button does it all.

New shape.

The new Eppendorf System 4700 Pipettes fit your hand perfectly. A finger rest at the top provides positive support during use, prevents rolling off the workbench when laid down. Slimmer nose cone allows entry into narrow test tubes. Available in 30 fixed-volume sizes from 1 to 1,000 µl.

New built-in tip ejector.

On System 4700 Pipettes, the same button used for filling and pipetting also ejects the tip. All functions are controlled by depressing a button through a series of clear, distinct positive stops, without changing grip position. The new models require less force to operate, reducing fatigue during repetitive sampling.

New multi-volume models.

Same size, similar accuracy and tip ejector feature as fixed-volume models, but a partial twist of the operating button adjusts the pipettes for any of 3 different volumes. Ratchet-type stops assure positive engagement of desired setting and prevents accidental change of volume. Choice of 6 models: 10/20/25 µl, 20/25/50 µl, 50/75/100 µl, 100/200/250 µl, 200/300/500 µl, and 500/750/1,000 µl.

New tray-mounted tips.

New Eppendorf Disposable Pipette Tips (yellow and blue) are available in bags of 50 loose tips, or in boxes of 100 tray-mounted tips for convenient "hands off" tip mounting. Two boxes fit into the new modular Eppendorf Pipette Stand.

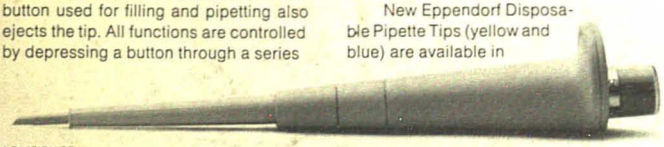

New modular pipette stand.

Basic rack module holds up to 4 pipettes and tips (loose or tray-mounted) in a plastic storage box with removable, hinged cover. Interlocking "add on" rack modules expand pipette holding capacity to 8, 12, 16, etc.

For an informative brochure on the Eppendorf Pipetting System, write: Eppendorf Division, Brinkmann Instruments, Cantiague Road, Westbury, N.Y. 11590. In Canada: 50 Galaxy Boulevard, Rexdale (Toronto), Ont.

A DIVISION OF BRINKMANN

Eppendorf Pipetting System

CIRCLE 16 ON READER SERVICE CARD

-4 MAR 2520